# PYROPHOSPHATES AND POLYPHOSPHATES IN PLANTS AND MICROORGANISMS

EDITED BY: Jose Roman Perez-Castineira, Roberto Docampo, Tatsuhiro Ezawa and Aurelio Serrano

PUBLISHED IN: Frontiers in Plant Science, Frontiers in Molecular Biosciences and Frontiers in Microbiology

frontiers Research Topics

# frontiers



ISSN 1664-8714
ISBN 978-2-88966-810-6
DOI 10.3389/978-2-88966-810-6

## About Frontiers

Frontiers is more than just an open-access publisher of scholarly articles: it is a pioneering approach to the world of academia, radically improving the way scholarly research is managed. The grand vision of Frontiers is a world where all people have an equal opportunity to seek, share and generate knowledge. Frontiers provides immediate and permanent online open access to all its publications, but this alone is not enough to realize our grand goals.

## Frontiers Journal Series

The Frontiers Journal Series is a multi-tier and interdisciplinary set of open-access, online journals, promising a paradigm shift from the current review, selection and dissemination processes in academic publishing. All Frontiers journals are driven by researchers for researchers; therefore, they constitute a service to the scholarly community. At the same time, the Frontiers Journal Series operates on a revolutionary invention, the tiered publishing system, initially addressing specific communities of scholars, and gradually climbing up to broader public understanding, thus serving the interests of the lay society, too.

## Dedication to Quality

Each Frontiers article is a landmark of the highest quality, thanks to genuinely collaborative interactions between authors and review editors, who include some of the world's best academicians. Research must be certified by peers before entering a stream of knowledge that may eventually reach the public - and shape society; therefore, Frontiers only applies the most rigorous and unbiased reviews.
Frontiers revolutionizes research publishing by freely delivering the most outstanding research, evaluated with no bias from both the academic and social point of view. By applying the most advanced information technologies, Frontiers is catapulting scholarly publishing into a new generation.

## What are Frontiers Research Topics?

Frontiers Research Topics are very popular trademarks of the Frontiers Journals Series: they are collections of at least ten articles, all centered on a particular subject. With their unique mix of varied contributions from Original Research to Review Articles, Frontiers Research Topics unify the most influential researchers, the latest key findings and historical advances in a hot research area! Find out more on how to host your own Frontiers Research Topic or contribute to one as an author by contacting the Frontiers Editorial Office: frontiersin.org/about/contact

# PYROPHOSPHATES AND POLYPHOSPHATES IN PLANTS AND MICROORGANISMS

Topic Editors:
**Jose Roman Perez-Castineira,** Sevilla University, Spain
**Roberto Docampo,** University of Georgia, United States
**Tatsuhiro Ezawa,** Hokkaido University, Japan
**Aurelio Serrano,** Institute of Plant Biochemistry and Photosynthesis (IBVF), Spain

**Citation:** Perez-Castineira, J. R., Docampo, R., Ezawa, T., Serrano, A., eds. (2021). Pyrophosphates and Polyphosphates in Plants and Microorganisms. Lausanne: Frontiers Media SA. doi: 10.3389/978-2-88966-810-6

# Table of Contents

frontiers in Plant Science

EDITORIAL
published: 26 March 2021
doi: 10.3389/fpls.2021.653416

# Editorial: Pyrophosphates and Polyphosphates in Plants and Microorganisms

*José R. Pérez-Castiñeira[1]*, Roberto Docampo[2], Tatsuhiro Ezawa[3] and Aurelio Serrano[1]*

[1] *Instituto de Bioquímica Vegetal y Fotosíntesis, Universidad de Sevilla-CSIC, Sevilla, Spain,* [2] *Department of Cellular Biology and Center for Tropical and Emerging Global Diseases, University of Georgia, Athens, GA, United States,* [3] *Graduate School of Agriculture, Hokkaido University, Sapporo, Japan*

**Keywords: pyrophosphate, polyphosphates, phosphate metabolism, PPI, polyP**

## Editorial on the Research Topic

## Pyrophosphates and Polyphosphates in Plants and Microorganisms

Phosphorus is the fifth most abundant chemical element in living cells. Microorganisms and plants take up phosphorus as dissolved (ortho)phosphate (Pi), that is often limited due to the formation of sparingly soluble complexes in soil; on the other hand, overapplication of phosphate fertilizer generally leads to the problems of eutrophication (diCenzo et al., 2017). Phosphorus usually occurs *in vivo* as free Pi or forming esters or diesters in metabolites and macromolecules. Protein phosphorylation also controls major metabolic pathways and cell division cycle (Li et al., 2016). Phosphate anion can react with another, releasing a molecule of water and producing a dimer, **pyrophosphate** (PPi, $P_2O_7^{4-}$). More Pi residues may be added to PPi by means of this linkage, known as a "phosphoanhydride bond," thus producing **polyphosphate** (polyP). Hydrolysis of phosphoanhydride bonds is thermodynamically favorable and kinetically slow, consequently, PPi and polyP are used for energy transfer and storage in many organisms. PPi and polyP also participate in metabolites like nucleoside triphosphate, inositol pyrophosphate, or activated isoprene.

PPi is produced from ATP in many reactions, such as protein, RNA and DNA biosynthesis. Removal of PPi by hydrolysis allows the shifting of anabolic reactions toward biosynthesis, thus regulating biosynthetic fluxes and allowing recycling of Pi by incorporating it to ADP to form ATP. This links PPi metabolism with the control of the cellular energy status. PPi hydrolysis can be coupled to $H^+$ or $Na^+$-translocation across biological membranes by the membrane-bound $H^+$-translocating and $Na^+$-translocating inorganic pyrophosphatases ($H^+$-PPases and $Na^+$-PPases), respectively. $H^+$-PPases occur in all members of the eukaryotic green evolutionary lineage (from unicellular algae to higher plants), as well as some protists, eubacteria and archaea, while $Na^+$-PPases have been identified in some archaea, eubacteria and marine photosynthetic protists. These proteins establish a transmembrane electrochemical gradient, a useful form of biological energy, which might be crucial to overcome stress situations (Serrano et al., 2007). PPi also participates in inositol pyrophosphates (PP-InsPs), a group of signaling molecules found in fungi, plants and animals, involved in the control of Pi homeostasis by interacting with the so-called SPX domains of certain proteins (Shears, 2015; Wild et al., 2016).

Phosphate is stored in different forms depending on organisms and tissues: protists (free-living and parasitic) and fungi store polyP mostly in acidocalcisomes and vacuoles, respectively (Docampo et al., 2005), whereas plants store Pi and inositol phosphates in vacuoles or inclusion bodies of vegetative tissues and seeds, respectively, although phytic acid and other Pi-containing metabolites also seem to be involved (Yang et al., 2017).

OPEN ACCESS

***Edited by:***
*Massuo Jorge Kato, University of São Paulo, Brazil*

***Reviewed by:***
*Masami Yokota Hirai, RIKEN Center for Sustainable Resource Science (CSRS), Japan*

****Correspondence:***
*José R. Pérez-Castiñeira*
*jroman@us.es*

***Specialty section:***
*This article was submitted to Plant Metabolism and Chemodiversity, a section of the journal Frontiers in Plant Science*

***Received:*** *14 January 2021*
***Accepted:*** *01 March 2021*
***Published:*** *26 March 2021*

***Citation:***
*Pérez-Castiñeira JR, Docampo R, Ezawa T and Serrano A (2021) Editorial: Pyrophosphates and Polyphosphates in Plants and Microorganisms. Front. Plant Sci. 12:653416. doi: 10.3389/fpls.2021.653416*

Living organisms must finely regulate Pi uptake, incorporation to biomolecules, storage, and mobilization and PPi and polyP are known to be implicated in this regulation, although many aspects remain to be established. Consequently, the metabolism of PPi and polyP in plants and microorganisms has major agricultural and environmental implications, due to the role that these organisms play in the biogeochemical cycle of phosphorus.

The ten articles included in this Research Topic will certainly contribute to the knowledge of the biological importance of PPi and polyP in microorganisms and plants. In a review article, Sanz-Luque et al. summarized the information available on metabolism, storage, and function of polyP in photosynthetic microbes (algae and cyanobacteria) and their potential use in bioremediation. In a similar context, the review article of Baker et al. specifically focused on the molecular and genetic aspects of PolyP production in the context of wastewater remediation by microalgae. Austin and Mayer highlighted the advances in understanding the mechanisms of cellular Pi homeostasis maintained through the INPHORS signaling pathway in yeast. In another review article, Holmes et al. summarized recent structural and functional studies on $H^+$- and $Na^+$-PPases (mPPases) catalytic and cation pumping mechanisms supporting a complex catalytic cycle involving inter-subunit communication and ion channel motions, which opens new perspectives for their modification as agro-technological and clinical targets. In connection with this topic, the opinion article of Baykov presents a revised interpretation of the energy coupling mechanism involved in oxidative and photo phosphorylation based on recent structural and functional data on mPPases, the simplest and most primitive primary ion pumps known so far.

Two articles reporting experiments carried out with the model organism *Arabidopsis thaliana* illustrate the detrimental effects of alterations in the PPi metabolism in plants. Gunji et al. have shown that vacuolar $H^+$-PPase plays a key role in PPi homeostasis and plant morphogenesis, so that an excess of PPi restrains cell morphogenesis and alters organ flatness by collapsing lipid and gluconeogenic metabolisms. The article of Fukuda et al. reported that vacuolar $H^+$-PPase and cytosolic soluble PPases act in concert to finely regulate PPi homeostasis, so that lack of these pyrophosphatases causes fatal morphological defects in early stages of plant development. In another article Regmi et al. have proven that overexpression of *Arabidopsis* vacuolar $H^+$-PPase (AVP1) in wheat (*Triticum aestivum*) plants improves biomass yield and photosynthate partitioning, a biotechnological strategy that could help to improve crop productivity. In this regard, the article of Pérez-Castiñeira and Serrano demonstrate that mPPases primarily act by hydrolyzing cytosolic PPi when expressed in yeast, and that the *Arabidopsis* vacuolar $H^+$-PPase AVP1 is more susceptible to $Na^+$ inhibition than the archaeal $Na^+$-PPase MVP both *in vivo* and *in vitro*; based on this experimental evidence the use of $Na^+$-PPases as biotechnological tools to generate salt-tolerant plants is proposed. Finally, Terashima et al. describe a novel and straightforward method for screening and isolation of polyP accumulating bacteria from complex microbial communities, by using DAPI staining and fluorescence-activated cell sorting.

In conclusion, this collection of themed articles enriches our knowledge on the biological functions of inorganic phosphate polymers, reinforcing the relevance of futures studies aimed to agrotechnological and biomedical applications.

## AUTHOR CONTRIBUTIONS

All authors listed have made a substantial, direct and intellectual contribution to the work, and approved it for publication.

## REFERENCES

diCenzo, G. C., Sharthiya, H., Nanda, A., Zamani, M., and Finan, T. M. (2017). PhoU allows rapid adaptation to high phosphate concentrations by modulating PstSCAB transport rate in *Sinorhizobium meliloti*. *J. Bacteriol.* 199, e00143–e00117. doi: 10.1128/JB.00143-17

Docampo, R., de Souza, W., Miranda, K., Rohloff, P., and Moreno, S. N. (2005). Acidocalcisomes - conserved from bacteria to man. *Nat. Rev. Microbiol.* 3, 251–261. doi: 10.1038/nrmicro1097

Li, Y., Jia, R., Al-Mahamedh, H. H., Xu, D., and Gu, T. (2016). Enhanced biocide mitigation of field biofilm consortia by a mixture of D-Amino acids. *Front. Microbiol.* 7:896. doi: 10.3389/fmicb.2016.00896

Serrano, A., Pérez-Castiñeira, J. R., Baltscheffsky, M., and Baltscheffsky, H. (2007). H+-PPases: yesterday, today and tomorrow. *IUBMB Life* 59,7 6–83. doi: 10.1080/15216540701258132

Shears, S. B. (2015). Inositol pyrophosphates: why so many phosphates? *Adv. Biol. Regul.* 57, 203–216. doi: 10.1016/j.jbior.2014.09.015

Wild, R., Gerasimaite, R., Jung, J. Y., Truffault, V., Pavlovic, I., Schmidt, A., et al. (2016). Control of eukaryotic phosphate homeostasis by inositol polyphosphate sensor domains. *Science* 352, 986–990. doi: 10.1126/science.aad9858

Yang, S.-Y., Huang, T. K., Kuo, H. F., and Chiou, T. J. (2017). Role of vacuoles in phosphorus storage and remobilization. *J. Exp. Bot.* 12, 3045–3055. doi: 10.1093/jxb/erw481

**Conflict of Interest:** The authors declare that the research was conducted in the absence of any commercial or financial relationships that could be construed as a potential conflict of interest.

frontiers in Molecular Biosciences

REVIEW
published: 22 November 2019
doi: 10.3389/fmolb.2019.00132

# The Function of Membrane Integral Pyrophosphatases From Whole Organism to Single Molecule

*Alexandra O. M. Holmes*[1], *Antreas C. Kalli*[2] *and Adrian Goldman*[1,3]*

[1] School of Biomedical Sciences and Astbury Centre for Structural Molecular Biology, University of Leeds, Leeds, United Kingdom, [2] Leeds Institute of Cardiovascular and Metabolic Medicine and Astbury Centre for Structural Biology, University of Leeds, Leeds, United Kingdom, [3] Research Program in Molecular and Integrative Biosciences, University of Helsinki, Helsinki, Finland

Membrane integral pyrophosphatases (mPPases) are responsible for the hydrolysis of pyrophosphate. This enzymatic mechanism is coupled to the pumping of $H^+$ or $Na^+$ across membranes in a process that can be $K^+$ dependent or independent. Understanding the movements and dynamics throughout the mPPase catalytic cycle is important, as this knowledge is essential for improving or impeding protein function. mPPases have been shown to play a crucial role in plant maturation and abiotic stress tolerance, and so have the potential to be engineered to improve plant survival, with implications for global food security. mPPases are also selectively toxic drug targets, which could be pharmacologically modulated to reduce the virulence of common human pathogens. The last few years have seen the publication of many new insights into the function and structure of mPPases. In particular, there is a new body of evidence that the catalytic cycle is more complex than originally proposed. There are structural and functional data supporting a mechanism involving half-of-the-sites reactivity, inter-subunit communication, and exit channel motions. A more advanced and in-depth understanding of mPPases has begun to be uncovered, leaving the field of research with multiple interesting avenues for further exploration and investigation.

**Keywords: membrane-integral pyrophosphatases, human pathogens, plants, structural biology, molecular mechanism, membrane proteins, hydrolysis, ion pumping**

OPEN ACCESS

***Edited by:***
*Andrea Mozzarelli, University of Parma, Italy*

***Reviewed by:***
*Alexander Baykov, Lomonosov Moscow State University, Russia*
*Cesare Indiveri, University of Calabria, Italy*

***Correspondence:**
*Adrian Goldman*
*a.goldman@leeds.ac.uk*

***Specialty section:***
*This article was submitted to Structural Biology, a section of the journal Frontiers in Molecular Biosciences*

***Received:*** *28 August 2019*
***Accepted:*** *08 November 2019*
***Published:*** *22 November 2019*

***Citation:***
*Holmes AOM, Kalli AC and Goldman A (2019) The Function of Membrane Integral Pyrophosphatases From Whole Organism to Single Molecule. Front. Mol. Biosci. 6:132. doi: 10.3389/fmolb.2019.00132*

## INTRODUCTION

Pyrophosphatases (PPases) are enzymes responsible for the reversible hydrolysis of the phosphoanhydride bond in pyrophosphate ($PP_i$) to two inorganic phosphate molecules (Kajander et al., 2013). PPases are subcategorized into three separate protein families; Family I, Family II, and membrane-integral pyrophosphatases (mPPases). Families I and II are evolutionarily unrelated soluble proteins. Despite their common enzymatic activity, mPPases are vastly different to the other PPase families. Firstly, the architecture and sequence of these protein families are unrelated. Ignoring the oligomeric structure, a single subunit of both Family I and mPPases consists of a single domain, while Family II PPases have two domains per subunit. mPPases are the only family that is embedded in the membrane: they have 15-17 transmembrane helices (TMH) per 70-81 kDa subunit (Kellosalo et al., 2012; Lin et al., 2012). Secondly, mPPases have only been reported as homodimers,

whereas Family I PPases can form other oligomeric arrangements (Kankare et al., 1996; Kellosalo et al., 2012; Lin et al., 2012; Li et al., 2016; Tsai et al., 2019; Vidilaseris et al., 2019). Family I and II PPases are only responsible for removing excess waste $PP_i$ from the cytoplasm, while mPPases are primary ion pumps: they couple hydrolysis to movement of $H^+$ and/or $Na^+$ across a membrane (Kajander et al., 2013) and thus generate a membrane potential, which contributes to a number of cellular functions, such as acidocalcisome and vacuole regulation and energization (Shah et al., 2016). The catalytic activities of these protein families differ by orders of magnitude. The mPPases are the slowest as they can only hydrolyze ≈ 10 $PP_i$ molecules per second, followed by Family I, which can hydrolyze ≈ 200 molecules per second, and Family II which can hydrolyze ≈ 2,000 per second (Kajander et al., 2013).

mPPases are less abundant than soluble PPases but still occur in all kingdoms of life except fungi and multicellular animals (Kajander et al., 2013). In eukaryotes, they are localized in the membranes of organelles, such as the Golgi apparatus (Mitsuda et al., 2001), plant vacuoles (Gaxiola et al., 2007), or the acidocalcisomes of protists (Moreno and Docampo, 2009). They are also present in the inner cellular membrane of bacteria such as *Bacteroides vulgatus* (Luoto et al., 2013a). mPPases have been found to play a role in stress tolerance and plant maturation. Finally, mPPases promote energy efficiency and survival in numerous human pathogens, making them clinically relevant as potential drug targets (Luoto et al., 2011; Shah et al., 2016).

This evolutionarily ancient family evolved through a gene triplication; they thus consist of three structurally-conserved splayed 4-helix bundles made up of TMH 3-6, 9-12, and 13-16 (Au et al., 2006; Kajander et al., 2013) arranged with ∼3-fold symmetry perpendicular to the membrane plane. The bundles are structurally highly similar with RMSD/$C_\alpha$ values of 2.1–2.9 Å between them (Kellosalo et al., 2012) and also have 23.6–26.1% sequence identity (Kellosalo et al., 2012). Phylogenic analysis suggests that hydrolysis of $PP_i$ to provide energy may have occurred prior to the adoption of ATP as the universal energy currency (Baltscheffsky et al., 1999). Therefore, mPPases may have been the first enzymes to couple phosphoanhydride bond formation/hydrolysis to chemiosmotic potential. Since the initial discovery of mPPase in *Rhodospirillum rubrum*, seven different mPPase subfamilies have been discovered (**Table 1**) (Luoto et al., 2011, 2015; Tsai et al., 2014). In brief, the different mPPases are subdivided into two main groups: (i) $K^+$ independent, which pump protons ($H^+$-PPases) and can be regulated by $Na^+$, and (ii) $K^+$ dependent, which can function in the absence of $K^+$, but require $K^+$ for maximal activity. Of these, there are $H^+$-PPases, $Na^+$ pumping ($Na^+$-PPase), and dual $Na^+/H^+$ pumping ($Na^+/H^+$-PPase) PPases (Kajander et al., 2013). Sequence analysis suggests that the first mPPases were $Na^+$-PPases, and that $H^+$-PPases evolved from these four independent times (Baykov et al., 2013). Additionally, it is likely that the evolution of $Na^+/H^+$-PPases occurred separately to the $H^+$-PPases (Luoto et al., 2013b).

This review encompasses our current knowledge of mPPase function, including their evolution, role in whole organisms, and their structure and mechanism on the molecular level. We also suggest avenues for future exploration.

# FUNCTION AND RELEVANCE

## Plants

Under physiological conditions in plants, $H^+$-PPases are predominantly localized to the tonoplast membrane surrounding the vacuole (Segami et al., 2014) and make up 10% of its protein components (Segami et al., 2018a). The vacuole possesses multiple functions that require the large-scale movement of molecules across its membrane. The required membrane potential is generated by the vacuolar ATPase complex (V-ATPase) in combination with $H^+$-PPases (Kriegel et al., 2015). There is some controversy over the delineation of the roles of these proton pumps, as a V-ATPase knock-out strain was able to properly maintain acidification of the vacuole and normal function (Krebs et al., 2010). However, a more recent study suggested that lack of V-ATPase could not be compensated for by increased mPPase activity (Kriegel et al., 2015). The general consensus is that the role of $H^+$-PPase in stress tolerance is to replace V-ATPase activity when ATP levels are low (Maeshima, 2000), but this does not fully address the roles of the proton pumps under normal conditions.

$H^+$-PPases are important in plant maturation (Li et al., 2005) because they remove $PP_i$ from the cytoplasm (Ferjani et al., 2011; Asaoka et al., 2016). $PP_i$ is the by-product of many different cellular processes, including the biosynthesis of protein, RNA and, importantly for plants, cellulose (Maeshima, 2000). Removing the excess $PP_i$ following these reactions is critical for driving these processes. Additionally, $PP_i$ has a modulatory role as a biochemical intermediate of a number of enzymes (Heinonen, 2001), so tight control of its cytoplasmic availability is essential for normal cellular function. mPPase over-expression in *Arabidopsis thaliana* resulted in increased cell division and hyperplasia of different organs, in particular the leaves. In contrast, knock-out mutants, and RNA interference studies showed severely disrupted root and shoot development. Each of these were linked to increased or decreased trafficking of the phytohormone auxin, which is known to mediate organogenesis (Li et al., 2005), suggesting a role for $H^+$-PPases in auxin regulation.

This role in auxin regulation was further highlighted in studies of transgenic plants over-expressing $H^+$-PPase genes. Multiple studies have shown that increased polar auxin transport upon mPPase over-expression is closely related to improved root development under stress conditions (Li et al., 2005; Park et al., 2005; Pasapula et al., 2011; Zhang et al., 2011). This plays a role in drought resistance, as the larger root system provides enhanced water absorption (Zhang et al., 2011). In addition to the increased root biomass mechanism, the effect of $H^+$-PPase over-expression on vacuolar function improved tolerance of drought and salinity. The increased electrochemical gradient may drive uptake of ions into the vacuole, producing an increase in osmotic potential and stimulating water uptake (Park et al., 2005; Brini et al., 2006; Zhao et al., 2006; Pasapula et al., 2011; Zhang et al., 2011). Further evidence of the potential of mPPases to improve crop tolerance to

**TABLE 1 |** mPPase subfamily classification.

| Cation Pumping Specificity | Monovalent Cation Dependence | Semi-Conserved Glutamate Location | Regulation | Hypothesized Sodium Binding Sites | Example | References |
|---|---|---|---|---|---|---|
| $H^+$ | $K^+$ | 6.57 | – | – | *Vigna radiata* | Tsai et al., 2014 |
| | | 6.53 | – | – | *Carboxydothermus hydrogenoformans* | Tsai et al., 2014 |
| | | 5.43 | – | – | *Flavobacterium johnsoniae* | Tsai et al., 2014 |
| | - | 6.53 | $Na^+$ and $K^+$ | Inhibitory | *Chlorobium limicola* | Luoto et al., 2015 |
| | | | – | – | *Pyrobaculum aerophilum* | Luoto et al., 2011 |
| $Na^+$ | $K^+$ and $Na^+$ | 6.53 | – | Activating and Inhibitory | *Thermotoga maritima* | Tsai et al., 2014 |
| $Na^+$ and $H^+$ | $K^+$ and $Na^+$ | 6.53 | – | Activating | *Bacteroides vulgatus* | Tsai et al., 2014 |

suboptimal conditions were the reports of increased chlorophyll content, photosynthesis, leaf water content and fiber yield, with decreased cell membrane damage in transgenic cotton plants, as compared to wild-type under low water and high salt conditions (Lv et al., 2009; Pasapula et al., 2011). Interestingly, these effects may not be predominantly due to the proton pumping activity of the vacuolar mPPases. One study saw a *Vr*-PPase mutant lacking proton pumping activity, but retaining hydrolysis, was sufficient to rescue the stunted knock-out phenotypes (Asaoka et al., 2016). In addition to this, an *A. thaliana* plant $H^+$-PPase knockout saw no heterotrophic growth following germination, but this phenotype was rescued by soluble PPase expression, suggesting that effective $PP_i$ clearance is the primary function of $H^+$-PPases during postgerminative growth in *Planta* (Ferjani et al., 2011). It is not clear why this is the case, as all plant cells express soluble Family I PPases at concentrations that should be sufficient to clear the pyrophosphate generated. An explanation could be that the soluble and mPPases function cooperatively (Segami et al., 2018b). In this model, the $H^+$-PPase functions as the major cytosolic $PP_i$-hydrolysis enzyme and the soluble PPases contribute to preventing accumulation to toxic levels, which would explain how soluble PPase expression was able to somewhat compensate for mPPase loss in the aforementioned study (Ferjani et al., 2011).

## Human Pathogens

### Protozoan Pathogens

A number of major human diseases are caused by protozoan parasites, for example, malaria (*Plasmodium ssp.*), toxoplasmosis (*Toxoplasma gondii*), trypanosomiasis (*Trypanosome spp.*), and leishmaniasis (*Leishmania spp.*) (Shah et al., 2016). These diseases each have a high prevalence and risk of fatality (Büscher et al., 2017; World Health Organization, 2018) or association with other diseases. For example, toxoplasmosis has been suggested to be associated with a number of conditions, such as psychiatric, neurological, and neoplastic disorders (Torgerson and Mastroiacovo, 2013; Flegr et al., 2014). In addition to this, several protozoan strains responsible for malaria and trypanosomiasis have emerged that are resistant to most of the current treatment regimes (Büscher et al., 2017; World Health Organization, 2018). Therefore, there is a demand for novel therapeutics for these tropical diseases.

The protozoan parasite life cycle typically involves transitions between vectors and hosts and intracellular to extracellular environments, which means the protozoan cell must survive and adapt to several different conditions (Crompton et al., 2014). In terms of mPPase function, the most relevant change to overcome is the difference in osmotic pressure the cells experience in these different environments. The main protozoan mechanism for adjusting internal osmotic pressure involves the acidocalcisome (Docampo et al., 2013), where mPPases are localized in protozoa (Scott et al., 1998; Marchesini et al., 2000). This is a small acidic compartment where numerous ions are stored, including polyphosphate, which the parasite hydrolyses or synthesizes in response to osmotic stress and to release energy (Ruiz et al., 2001). The low pH of the acidocalcisome is crucial for its function, as loss of acidity can lead to a 10-fold decrease in stored polyphosphate levels (Lemercier et al., 2002), resulting in reduced capability to respond to osmotic changes. In addition to the effects on polyphosphate storage, there are detrimental effects on intracellular pH regulation, growth rate and final cell density (Lemercier et al., 2002), suggesting that the loss of mPPases has more widespread effects than just reduced osmotic regulation.

As mPPase function in protozoa is highly important, mPPases are a validated target for pharmacological intervention. Knock-down and knock-out studies in *Trypanosoma brucei* (Lemercier et al., 2002) *T. gondii* (Liu et al., 2014), and *P. falciparum* (Zhang et al., 2018) have demonstrated that mPPases are required for maintaining acidocalcisome acidification, parasitic virulence and *in vitro* asexual bloodstage growth. Additionally, mPPase-inhibiting bisphosphonate derivatives retarded intracellular proliferation of *T. gondii* with no effect on host cells (Rodrigues et al., 2000).

### Bacterial Pathogens

The most relevant mPPase-expressing bacterial genus to human health are *Bacteroides spp.*, especially *B. vulgatus*

**TABLE 2 |** Published mPPase structures.

| Species | Ligand[a] | Ions[a] | Conformation | Mutation | PDB | Resolution (Å) | Noteworthy | References |
|---|---|---|---|---|---|---|---|---|
| *Vigna radiata* | IDP | 5 $Mg^{2+}$ $K^{+}$ | Symmetrical IDP-Bound | – | 4A01 | 2.35 | First mPPase Structure | Lin et al., 2012 |
| | $PO_4$ | 2 $Mg^{2+}$ | Relaxed Product Bound | – | 5GPJ | 3.5 | | Li et al., 2016 |
| | 2 $PO_4$ | 5 $Mg^{2+}$ $K^{+}$ | Product Bound | – | 6AFS | 2.3 | Demonstrated Exit Channel Width Affects Function | Tsai et al., 2019 |
| | | | | $E^{6.57}Q$ | 6AFT | 2.5 | | |
| | | | | $L^{12.64}M$ | 6AFU | 2.8 | | |
| | | | | $L^{12.64}K$ | 6AFV | 2.7 | | |
| | | | | $T^{5.36}D$ | 6AFW | 2.2 | | |
| | | | | $E^{5.33}A$ | 6AFX | 2.3 | | |
| | | | | $E^{5.33}S$ | 6AFY | 2.4 | | |
| | | | | $E^{5.33}H$ | 6AFZ | 2.5 | | |
| *Thermotoga maritima* | - | $Mg^{2+}$ $Ca^{2+}$ | Resting | – | 4AV3 | 2.6 | | Kellosalo et al., 2012 |
| | 2 $PO_4$ | 4 $Mg^{2+}$ $K^{+}$ | Product Bound | – | 4AV6 | 4.0 | | Kellosalo et al., 2012 |
| | IDP | 5 $Mg^{2+}$ $Na^{+}$ | Symmetrical IDP-Bound | – | 5LZQ | 3.5 | | Li et al., 2016 |
| | $WO_4$ | 2 $Mg^{2+}$ | Relaxed Product Bound | – | 5LZR | 4.0 | | Li et al., 2016 |
| | 2 ATC[b] IDP | 5 $Mg^{2+}$ $Na^{+}$ | Locked | – | 6QXA | 3.7 | Asymmetrical Structure Allosteric Inhibitor | Vidilaseris et al., 2019 |

[a] *The number of ligands or ions per subunit.*
[b] *Only bound to one of the subunits.*
*IDP, imidodiphosphate; ATC, N-[(2-amino-6-benzthiazolyl)methlyl]-1H-indole-2-carboxamide.*

and *Bacteroides fragilis* (Luoto et al., 2013a), which form a mutualistic relationship with healthy individuals as part of the gastrointestinal microflora (Wexler, 2007). However, outside this environment, they can cause bacteremia (presence of bacteria in the blood), intra-abdominal sepsis, appendicitis, gynecological, and skin infections, endocarditis, septic arthritis, and abscesses in tissues including the brain and female urogenital tract (Wexler, 2007). This is a major threat to human health, as *Bacteroides* reportedly have the highest resistance rates of all anaerobic pathogens (Wexler, 2007), and an associated mortality rate of over 19%, rising to 60% in untreated cases (Goldstein, 1996).

Bacterial mPPases are primarily found in species that exist under conditions of low-energy stress, such as the obligate anaerobes *Bacteroides* and deep-sea organisms (*Thermotoga maritima* and *Pyrobaculum aerophilum*) (Luoto et al., 2011). In these situations, mPPases may be essential to increasing energy efficiency and promoting survival. mPPases have also been shown to confer greater resistance to other stress conditions. One study revealed that expression of transgenic plant mPPases in *Escherichia coli* and *Saccharomyces cerevisiae* resulted in improved tolerance to heat, hydrogen peroxide and high salinity (Yoon et al., 2013). Therefore, we speculate that inhibiting mPPase activity could have effects on bacterial viability in response to stressors, similar to the effects seen in protozoan parasites and plants.

# STRUCTURE AND MECHANISM

## Structural Overview

There are now several structures of mPPases (**Table 2**). In the current structures, each subunit of the homodimeric mPPase is formed by 16 TMH, which form two concentric rings (**Figure 1A**) surrounding the four catalytic regions: the hydrolytic center, the coupling funnel, the ion gate and the exit channel (**Figure 1C**) (Kellosalo et al., 2012; Lin et al., 2012; Li et al., 2016). The protein subunit-subunit interface is maintained by hydrophobic interactions and hydrogen bonds between residues on TMH 10 ($I/R^{10.33}$,$N^{10.42}$, $S^{10.45}$, $K^{10.49}$), 13 ($L^{13.19}$, $L/V^{13.21}$, $N^{13.22}$, $M/V^{13.23}$, $I^{13.33}$, $Y^{13.40}$, $S^{13.48}$, $G^{13.54}$, $E^{13.59}$, $R^{13.62}$), and 15 ($S^{15.45}$, $Q^{15.48}$) (Shah et al., 2016). Here, we use the Ballesteros and Weinstein numbering system, first introduced for GPCRs, so that all functional residues have the same index ($Residue^{helixnumber.offset}$) (Ballesteros and Weinstein, 1995), and which we adopted for mPPases (Tsai et al., 2014). In this system, each residue is assigned two numbers, one indicating the TMH and the other to describe its offset from a well-conserved residue close to the middle of the TMH (assigned position 50), as shown in **Table 3**. For example, K415 from *Tm*-PPase, is on TMH10 and is one before the conserved S416 and is thus designated $K^{10.49}$.

The inner ring is composed of six TMH (Baltscheffsky et al., 1999; Moreno and Docampo, 2009; Luoto et al., 2013a; Tsai et al., 2014, 2019; Vidilaseris et al., 2019) and the outer ring

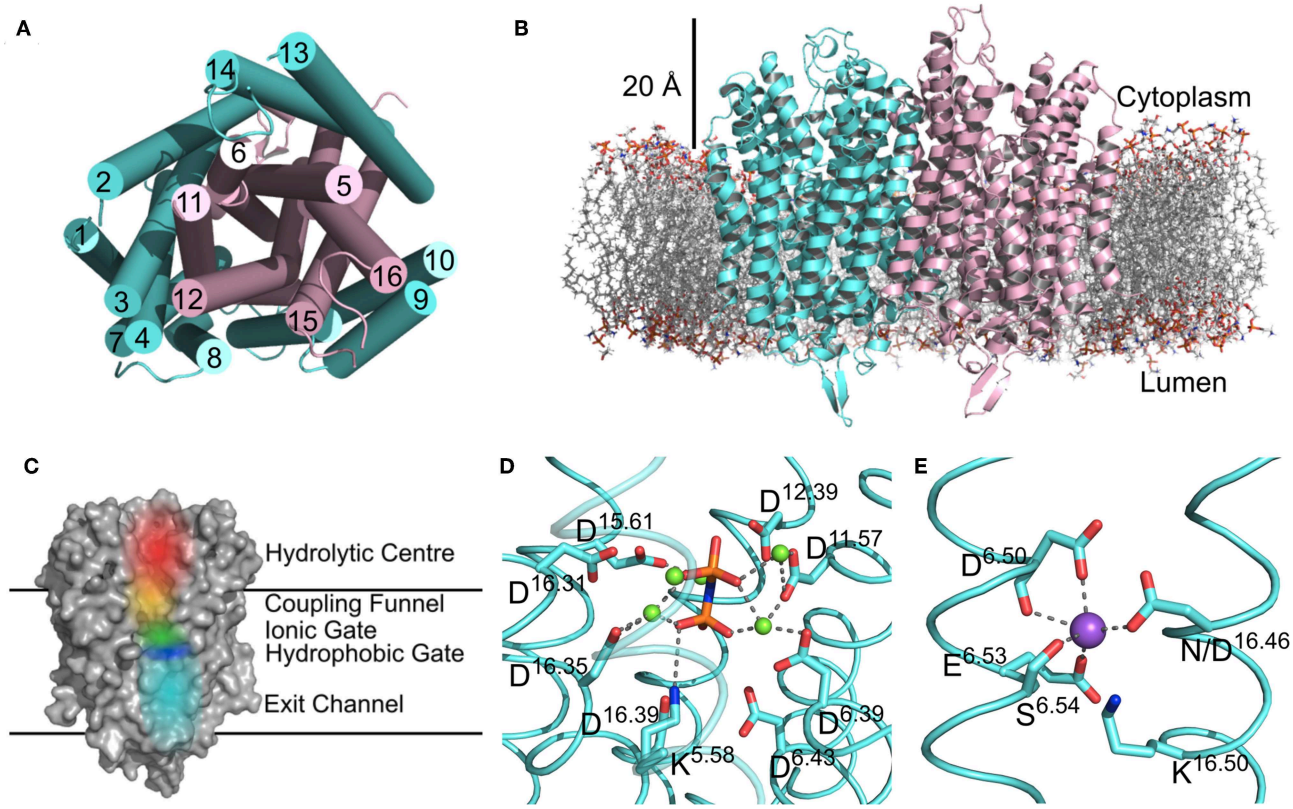


**FIGURE 1 |** Structural Features of mPPases. **(A)** The concentric ring arrangement of the 16 helices in one mPPase subunit, as viewed from the cytoplasmic side. **(B)** The dimeric protein and its positioning in the lipid bilayer viewed from the membrane plane. The mPPase subunits are colored cyan and pink. **(C)** A surface view of one mPPase subunit with each of the catalytic regions colored (red, hydrolytic center; yellow, coupling funnel; green, ionic gate; dark blue, hydrophobic gate; light blue, exit channel). The coordination of **(D)** IDP and $Mg^{2+}$ (green spheres) in the hydrolytic center and **(E)** of $Na^{+}$ (purple sphere) at the ionic gate. Figures generated using PyMol (DeLano, 2002) and the IDP-bound *Tm*-PPase structure (PBD: 5LZQ) (Li et al., 2016).

is composed of the remaining 10 (**Figure 1A**) (Kellosalo et al., 2012; Lin et al., 2012; Li et al., 2016). A large hydrophilic region extends about 20 Å into the cytoplasm (**Figure 1B**). This region has a hydrolytic center, which is lined with highly conserved negative ($D^{5.61}$, $D^{5.65}$, $E^{5.76}$, $D^{5.77}$, $D^{6.35}$, $D^{6.39}$, $D^{6.43}$, $D^{11.57}$, $D^{15.61}$, $D^{16.31}$, $D^{16.35}$, $D^{16.39}$), positive ($K^{5.58}$, $K^{15.64}$, $K^{16.38}$) and polar ($N^{12.53}$) residues that are involved in substrate binding through both direct interactions and *via* coordination of $Mg^{2+}$ and water (**Figure 1D**). The hydrolytic center is followed by the coupling funnel, which is comprised of an ionic network between TMH 5-6 ($R^{5.50}$, $K^{5.58}$, $D^{6.39}$, $D^{6.50}$), 11-12 ($D^{11.50}$, $K^{12.50}$) and 16 ($K^{16.38}$, $D^{16.39}$). Below this is the ionic gate, which is situated in the center of the membrane and where the cation is bound prior to pumping (**Figure 1E**). This region is made up of charged and hydrophilic residues ($S^{5.43}$, $D^{6.50}$, $E/S^{6.53}$, $S^{6.54}$, $E^{6.57}$, $D^{16.46}$, $K^{16.50}$). The hydrophobic gate located near the ionic gate and is formed by semi-conserved non-polar residues on TMH 5, 6, 12, and 16. Mutations of residues near the ionic and hydrophobic gates ($I^{12.54}$, $L^{12.64}$, $D^{16.46}$, $V^{16.54}$, $L^{16.57}$) to alanine decouple the enzyme so that mPPase can hydrolyze $PP_i$ but does not pump, suggesting these regions are also essential for the coupling of hydrolysis to pumping (Asaoka et al., 2014). Finally, the residues of the exit channel are not highly conserved between mPPases. However, allosteric inhibitor binding to this region in one *Tm*-PPase subunit is nonetheless associated with a "locked" conformation (Vidilaseris et al., 2019) and exit channel width has been implicated in coupling hydrolysis and pumping (Tsai et al., 2019), thereby illustrating the importance of conformational changes in this region during the catalytic cycle.

## Structural Differences Between Subfamilies

### Cation Specificity

Mutagenesis and structural studies showed that the residues $E^{6.53/6.57}$, $S^{6.54}$, and $D/N^{16.46}$ are involved in cation binding and pumping specificity (Asaoka et al., 2014; Li et al., 2016). The main residue regulating cation specificity is the semi-conserved glutamate on TMH6. Movement of this glutamate down one helical turn from $E^{6.53}$ to $E^{6.57}$ converts a $Na^{+}$-PPase to a $H^{+}$-PPase by destroying the $Na^{+}$ binding site in the substrate bound state (Li et al., 2016). However, the reverse mutation does not yield a $Na^{+}$-PPase, indicating that the factors dictating cation specificity are more complex than solely the location of a single residue.

**TABLE 3 |** Ballesteros and weinstein numbering for mPPases.

| TMH | Signifier | % Sequence Identity | Residue in *Tm*-PPase | Residue in *Vr*-PPase | Residue in *Pa*-PPase |
|---|---|---|---|---|---|
| 1 | 1.50 | 38.1 | F17 | F25 | Y20 |
| 2 | 2.50 | 27.6 | K55 | K94 | R58 |
| 3 | 3.50 | 99.5 | S87 | S153 | S96 |
| 4 | 4.50 | 92.9 | G130 | G194 | G138 |
| 5 | 5.50 | 86.4 | R191 | R242 | R182 |
| 5-6 Border[a] | 5.77 | 99.9 | D218 | D269 | D210 |
| 5-6 Border[b] | 6.26 | 96.2 | D219 | D270 | D211 |
| 6 | 6.50 | 99.7 | D243 | D294 | D235 |
| 7 | 7.50 | 46.3 | G297 | G334 | A271 |
| 8 | 8.50 | 75.8 | L321 | L361 | L296 |
| 9 | 9.50 | 91.1 | G369 | G411 | G333 |
| 10 | 10.50 | 84.3 | S416 | S458 | S380 |
| 11 | 11.50 | 98.1 | D458 | D500 | D439 |
| 12 | 12.50 | 99.7 | K499 | K541 | K480 |
| 13 | 13.50 | 99.4 | V566 | V597 | V554 |
| 14 | 14.50 | 79 | M611 | M642 | F599 |
| 15 | 15.50 | 94 | A649 | A680 | S637 |
| 16 | 16.50 | 94.5 | K707 | K742 | K691 |

[a] *The last TMH5 residue.*
[b] *The first TMH6 residue.*

## $K^+$ Dependence and Independence

Mutation of $A^{12.46}$ to lysine in the active site converts a $K^+$-dependent enzyme to an independent enzyme (Belogurov and Lahti, 2002). Modeling this mutation suggested that the $NH_3^+$ group of the lysine sidechain functionally replaces the $K^+$ ion at physiological $PP_i$ concentrations (Kellosalo et al., 2012; Lin et al., 2012). A systematic analysis of the potassium ion binding site or active site lysine ($K^+/K^{12.46}$ catalytic center) across all mPPase subfamilies revealed that the lysine contributed to, but was not essential, for the activity of $K^+$ independent mPPases, as the activity was restored at high $K^+$ concentrations when mutated (Artukka et al., 2018). This suggests that $K^{12.46}$ masks a $K^+$ binding site, but there appear to be larger-scale differences between the two classes than just the identity of $A/K^{12.46}$ in the active site (see Inter-subunit Communication).

## $Na^+$ Regulatory Sites

The difference between $Na^+$- or $H^+$-PPases and $Na^+/H^+$-PPases was unclear prior to the discovery of $Na^+$ and $K^+$ regulated $H^+$-PPases (Luoto et al., 2015). These are a subfamily of $K^+$ independent $H^+$-PPases, in which low $K^+$ concentrations enhance $H^+$ transport but higher $Na^+$ and $K^+$ concentrations inhibit ion pumping and hydrolysis. This led to the hypothesis that there are two possible $Na^+$ binding sites; one in the ion conductance channel associated with activation of the mPPase, and the other located away from the conductance channel conferring inhibition of $H^+$ conductance, to which $K^+$ can bind with low affinity. This fits with the reports of $H^+$ translocation by $Na^+$-PPases in sub-physiological sodium concentrations (Luoto et al., 2013a), suggesting that loss of the second inhibitory site led to the evolution of the $Na^+/H^+$-PPases.

## Mechanism of Pumping and Hydrolysis

Three mechanisms have been proposed for mPPase pumping and hydrolysis: (i) pumping occurs upon binding of substrate and prior to hydrolysis in a "binding change" type mechanism (Kellosalo et al., 2012), (ii) the proton released upon hydrolysis triggers release of the ions at the ion gate *via* a Grotthus type mechanism (Lin et al., 2012), and (iii) the hydrolysis-generated proton is directly transported in a "direct-coupling" mechanism (Baykov et al., 2013). This first mechanism assumes that the nucleophilic proton may not be involved in pumping, whereas the second and third propose that the hydrolysis-generated proton is the one pumped, thereby assuming hydrolysis precedes cation-pumping. However, neither the second nor the third mechanisms account for $Na^+$ transport (Kajander et al., 2013), except for potentially *via* a "billiard-type" model in the third, where the $Na^+$ is pushed into the exit channel by the nucleophilic water proton (Baykov et al., 2013). In our opinion, models in which hydrolysis precedes cation pumping do not conform with the studies of non-hydrolysable substrate analogs [IDP and methylene diphosphonate (MEDP)] binding to *Vr*-PPase (Li et al., 2016; Shah et al., 2017) resulting in a single ion turnover event.

The "binding change" mechanism unifies both sodium and proton pumping, and is supported by studies indicating that charge transfer—and so presumably ion pumping—does not require hydrolysis (Li et al., 2016; Shah et al., 2017) and so presumably precedes it in the full catalytic cycle. In this model (**Figure 2**), the substrate binds to the hydrolytic center, which is then closed to the cytoplasm by ordering of the 5-6 loop and movement of TMHs 11-12 and 15-16 toward the center of the coupling funnel (**Figure 2A**a,b). During these conformational changes, a cation is pumped out from the ionic

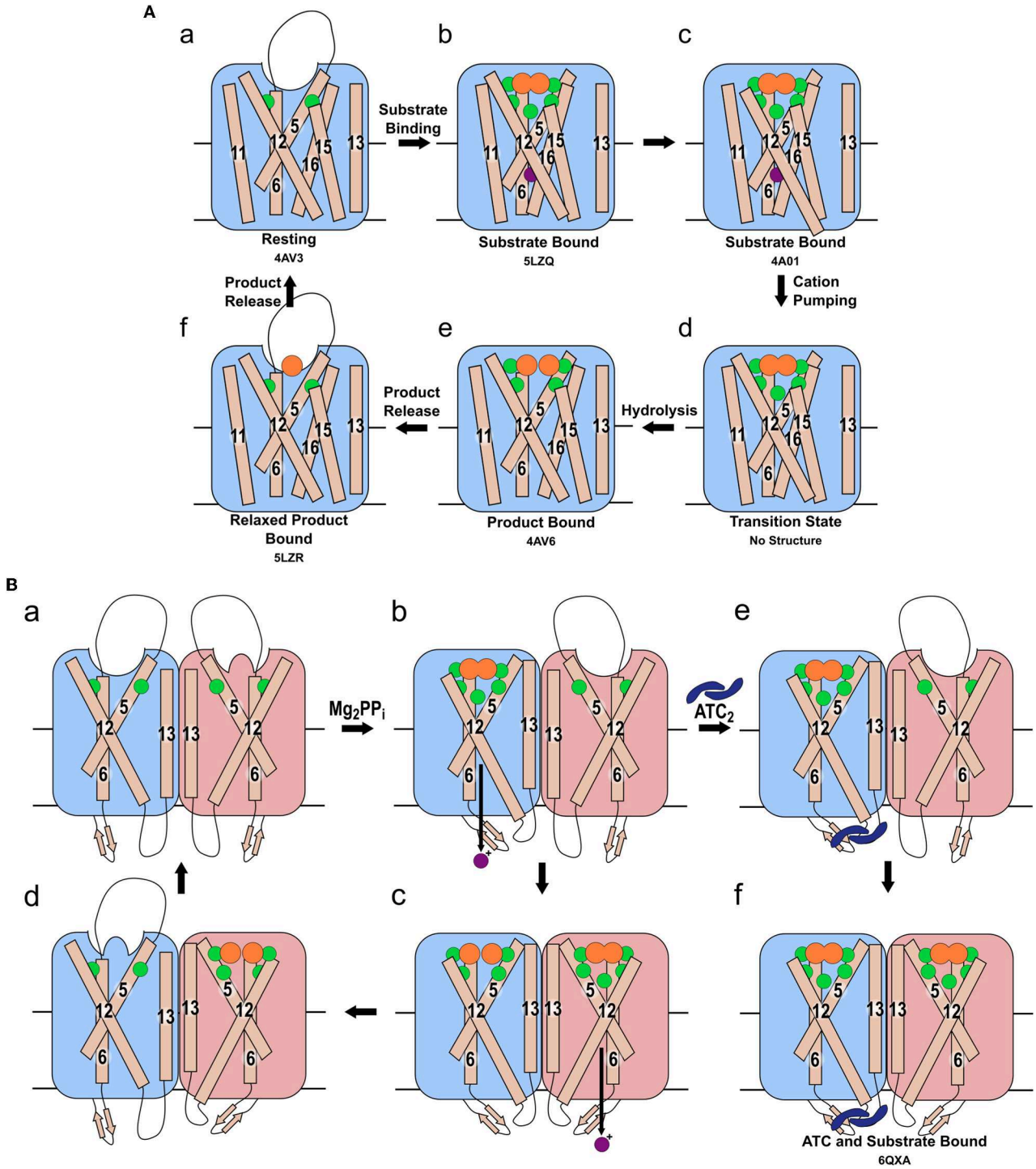


**FIGURE 2 |** Mechanism of pumping and hydrolysis. **(A)** "Binding change" mechanism. In the resting state (a), a cation may be present, but its position has not been revealed structurally. When substrate binds, the hydrolytic center is occluded by movement of the 5-6 loop and of TMH 11-12 and 15-16, and a cation localizes to the ionic gate (b). The cation is then pumped (c) and TMH 12 resumes its original position (d). Hydrolysis then occurs (e). Prior to the sequential release of the product $P_i$, the 5-6 loop, TMH 11-12 and 15-16 relax to their resting positions (f). **(B)** The proposed asymmetric cycle of the mPPase dimer. One site is capable of binding $PP_i$, while the other is distorted (a). Upon binding of one $PP_i$ molecule and ion pumping, the other site undergoes a conformational change, triggered by the movement of TMH13, to increase its affinity for $PP_i$ (b). The second $PP_i$ molecule binds and the second cation is pumped, while the first $PP_i$ is hydrolyzed (c). Upon release of the resulting $P_i$, this active site is distorted to reduce affinity for $PP_i$ whilst the second bound $PP_i$ undergoes hydrolysis (d). States (e,f): the proposed result of allosteric inhibitor ATC binding to the mPPase. The dimer is trapped in a state unable to hydrolyze $PP_i$, but capable of binding one (e) or two (f) $PP_i$. (Green spheres: $Mg^{2+}$, purple spheres: cation for pumping, orange spheres: $PP_i$ or $PO_4$, blue dimeric shape: ATC). PDB IDs for structurally defined states are listed beneath the relevant image.

gate (**Figure 2A**c,d). The increase in overall negative charge in this region leads to downwards movement of TMH 12 by 2 Å and an associated bend of TMH11, as observed structurally (**Figure 2A**b,c) (Kellosalo et al., 2012; Lin et al., 2012; Li et al., 2016). This causes deprotonation of the aspartate pair $D^{6.43}$ and $D^{16.39}$, which activates the water nucleophile leading to hydrolysis (**Figure 2A**d,e) (Kajander et al., 2013). This process has been demonstrated to be independent of cation pumping in exit channel mutants (Asaoka et al., 2014). These mutations were initially proposed to alter the position and angle of their helices and thereby uncouple the reactions (Asaoka et al., 2014). However, more recent structural characterization of exit channel and hydrophobic gate mutants indicate that this uncoupling appear to be due to widening of the exit channel (Tsai et al., 2019), potentially allowing ion back-flow.

## Asymmetry and Inter-subunit Communication

The events occurring in each mPPase subunit during pumping and hydrolysis are relatively well-understood (see above), but recent studies have provided evidence of asymmetry and subunit interdependence. Firstly, the role of the $K^+/K^{12.46}$ catalytic center in inter-subunit communication, as inferred from the effects of excess substrate was published (Artukka et al., 2018) (see Inter-subunit Communication). Shortly after this, the first structural evidence of asymmetry, further functional evidence, and a putative mechanism involving both subunits were reported (Vidilaseris et al., 2019). The earliest reports of subunit interdependence were in the 1990s in a series of studies utilizing radiation-induced damage to identify the functional unit size of mPPases (Wu et al., 1991; Sarafian et al., 1992; Tzeng et al., 1996). Several of these showed that one impaired subunit conferred compromised function to the unaffected subunit (see Inter-subunit Communication).

### Functional Asymmetry

Vidilaseris et al. (2019) reported that binding of the first substrate increased the affinity of the second subunit to $PP_i$. They also observed that the binding of first substrate molecule potentiated binding of the second. This suggests *positive* co-operativity for substrate binding, and thus they proposed the following mechanism (**Figure 2B**a): the first substrate binds to the first subunit leading to cation translocation in this subunit (**Figure 2B**b), this causes conformational changes in the second subunit to optimize $PP_i$ binding. Following the binding of the second substrate molecule, hydrolysis occurs in the first subunit and ion pumping in the second (**Figure 2B**c). This then allows hydrolysis in the second subunit and product release (**Figure 2B**d). However, the same study (Vidilaseris et al., 2019) also reported a 20-fold decrease in the maximal rate of hydrolysis when both subunits bind substrate, which does not appear to fit with their proposed asymmetric mechanism.

In contrast, Artukka et al. (2018) reported a *decrease* in affinity for $PP_i$ at the second subunit following substrate binding to the first. The binding of fluorescein 5'-isothiocyanate (FITC) to a lysine believed to be in the catalytic center ($K^{12.50}$) also decreases the affinity for FITC in the second subunit (Yang et al., 2000), providing further support for an allosteric mechanism. Binding at the first site thus presumably distorts the active site in the second subunit, reducing its affinity for $PP_i$/FITC. Negative co-operativity for substrate binding is highly relevant, because excess substrate inhibits hydrolysis in all wild-type mesophilic mPPases studied so far (Artukka et al., 2018), so excess substrate may play a role in proton pumping inhibition (Luoto et al., 2015). As there is no evidence of an alternative $PP_i$ binding site, and the hydrolytic center and coupling funnel could not accommodate further $PP_i$ molecules, the inhibition must be a result of substrate binding to the second subunit. This would only be possible in excess substrate concentrations, due to the decreased affinity at the second site. Similar to Vidilaseris et al. (2019), this study also saw a 3–16-fold decrease in maximal velocity of hydrolysis in both subunits upon binding of the second substrate. This again supports the model in which excess substrate inhibits hydrolysis through binding at this second site, thus suggesting that at moderate $PP_i$ concentrations only one subunit operates at any given time. The direct implication of this is that the symmetrical IDP bound structures are potentially not mechanistically relevant at typical $PP_i$ concentrations, but a possible artifact of the 4 mM minimum IDP concentration during crystallization (Lin et al., 2012; Li et al., 2016). These papers by Artukka et al. (2018) and Vidilaseris et al. (2019) are the first two definitive studies of possible asymmetry: further data are needed to understand fully the mechanism involving both subunits.

What could explain the inconsistencies between these two studies? Firstly, one study investigated thermophilic protein in an assay at 71°C (Vidilaseris et al., 2019), whereas, the other used mesophilic protein at 30°C (Artukka et al., 2018). The behavior could indicate different properties between thermo- and mesophilic proteins, or different activities at different temperatures. Secondly, one study was performed with purified protein in detergent micelles (Vidilaseris et al., 2019) and the other used unpurified protein in inner membrane vesicles (Artukka et al., 2018). This could suggest that the lipid environment of the enzyme could be involved in regulating the dimeric interface, a concept for which there is increasing evidence (Gupta et al., 2017; Pyle et al., 2018).

### Structural Asymmetry

Kinetic and structural studies showed that the non-phosphorous allosteric inhibitor *N*-[(2-amino-6-benzothiazolyl)methyl]-1*H*-indole-2-carboxamide (ATC) binds as a dimer to one of the subunits in *Tm*-PPase (Vidilaseris et al., 2019) (**Figure 3A**) thereby trapping an asymmetric structure, with RMSD/$C_\alpha$ values reaching 1.6 Å for some of the loops vs. a highest RMSD/$C_\alpha$ of 0.5 Å for the equivalent loops in the symmetrical IDP-bound structure (PDB: 5LZQ). The ATC dimer bound *via* the β1-2 loop (Q268, K269, Q277), loop 8-9 (Q348, D351, V352), and loop 12-13 (G528, P530, P531) (*Tm*-PPase numbering) (**Figure 3B**). The chief difference between the 5LZQ and 6QXA structures is the presence of ATC in the crystals. Due to the ATC, the β1-2 loop moves closer to loop 12-13 and away from the dimer interface to an angle similar to that seen in the resting and product bound structures, indicating closure of the exit channel. Loop 12-13 also experienced some slight movements, but TMH12 still

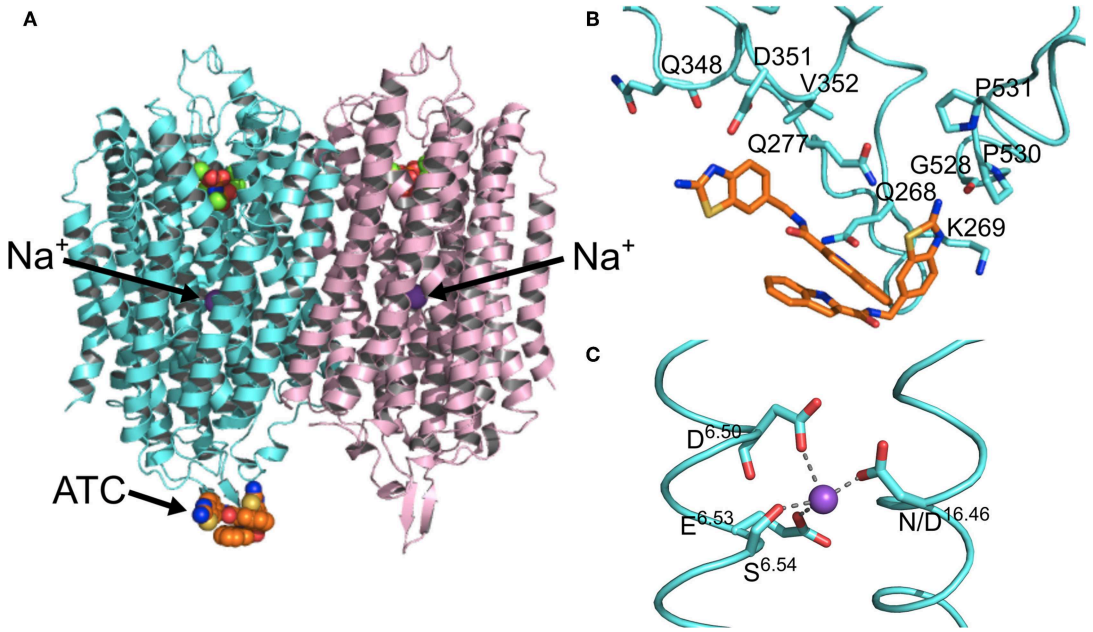


**FIGURE 3 |** Structural asymmetry. **(A)** The location of the ATC molecule (orange spheres) and the $Na^+$ ion (purple sphere) in the mPPase dimer. **(B)** The binding of the two ATC molecules (orange sticks) to the β1-2 loop, loop 8-9, and loop 12-13, with the interacting residues shown at sticks *(Tm*-PPase numbering). **(C)** The tetracoordination of $Na^+$ (purple sphere) at the ionic gate. (PDB: 6QXA) (Vidilaseris et al., 2019).

moves downwards by about 2 Å compared to the resting state. In addition, the coordination of $Na^+$ at the ionic gate changes from pentacoordination to tetracoordination and the ion is displaced by about 1.2 Å from the IDP-only structure (**Figure 3C**). Thus, the ATC-bound subunit appears to be trapped in a closed exit channel state and cannot perform hydrolysis, and the unbound subunit cannot undergo its catalytic cycle, due to the ATC-bound subunit restricting its motions (**Figure 2B**e,f).

### Inter-subunit Communication

Artukka et al. (2018) demonstrated that the wild-type $K^+/K^{12.46}$ center was important for inter-subunit communication. Substrate inhibition only occurred in $K^+$ independent mPPases when the native $K^{12.46}$ residue was present. In the $K^{12.46}A$ substituted enzymes there was no inhibition. Similarly, $K^+$ dependent mPPases were not inhibited by excess $PP_i$ unless $K^+$ was present, even in $A^{12.46}K$ substituted enzymes. Consequently, this suggests the lysine and potassium ion are unable to perfectly replace each other, despite the findings of previous modeling studies (Kellosalo et al., 2012). This is further evidence that inter-subunit communication in response to excess $PP_i$ is modulated by the native $K^+/K^{12.46}$ center, as its presence is required for excess substrate inhibition.

The recent asymmetrical ATC structure (see above) demonstrated direct linkage of TMH 12 to the dimer interface (Vidilaseris et al., 2019). Vidilaseris et al. suggest that, in the presence of $K^+$, the movement of TMH 12 upon substrate binding to one subunit induces conformational changes in the dimer interface, which are then propagated to the other subunit. Moreover, when residues close to $A^{12.46}$ were mutated to alanine, proton pumping and hydrolysis were uncoupled (Asaoka et al., 2014). This may be because this region is implicated in inter-subunit communication for cation translocation at normal $PP_i$ levels, and thus when it is mutated, cation pumping ceased. This is further supported by the fact that mPPases are dimers, even though all the required catalytic domains are contained within a single monomer.

Early studies of the functional unit size of mPPases demonstrated that mPPases had to be functional dimers for cation pumping (Sarafian et al., 1992) but a single catalytic subunit was sufficient for hydrolysis (Sarafian et al., 1992; Tzeng et al., 1996). Although these studies were limited by the utilization of radiation-induced destruction, a technique which damages the entire molecule, not just specific sites (Kempner, 1993), they are still relevant when interpreting more recent evidence of subunit interdependence.

## CONCLUSION AND FUTURE OUTLOOK

mPPases represent an important area of research, due to their essential functions in plants and human parasites. These functions make the enzymes both clinically and agriculturally relevant targets for modification. They are validated drug targets against a number of human diseases, and there is a wealth of evidence that manipulation of these proteins in plants can improve their tolerance to environmental stressors. An essential part of developing these modulation strategies is understanding the mPPase catalytic and cation pumping mechanism on a molecular level. Despite the recent structural and functional studies (Artukka et al., 2018; Vidilaseris et al., 2019), the mechanism involving both protein subunits remains elusive. To elucidate their full mechanism, further studies that couple time-resolved experimental techniques with molecular dynamics simulations are required.

## AUTHOR CONTRIBUTIONS

AH, AG, and AK: conceptualization, writing-review, and editing. AG and AK: funding acquisition and supervision. AH: investigation and writing-original draft preparation.

## FUNDING

This work was supported by a BBSRC DTP fellowship (BB/M011151/1) (to AH) and grants from the BBSRC (BB/M023281/1) and the Academy of Finland (1286429) (to AG). AK was supported by a Springboard Award from the Academy of Medical Sciences (GB) and the Wellcome Trust (SBF002\1031).

## ACKNOWLEDGMENTS

We thank Dr. Steven Harborne for reading an early version of this manuscript, and the members of the Goldman group for sharing unpublished results.

## REFERENCES

Artukka, E., Luoto, H. H., Baykov, A. A., Lahti, R., and Malinen, A. M. (2018). Role of the potassium/lysine cationic center in catalysis and functional asymmetry in membrane-bound pyrophosphatases. *Biochem. J.* 475, 1141–1158. doi: 10.1042/BCJ20180071

Asaoka, M., Segami, S., and Maeshima, M. (2014). Identification of the critical residues for the function of vacuolar $H^+$-pyrophosphatase by mutational analysis based on the 3D structure. *J. Biochem.* 156, 333–344. doi: 10.1093/jb/mvu046

Asaoka, M. M., Segami, S., Ferjani, A., and Maeshima, M. (2016). Contribution of PPi-hydrolyzing function of vacuolar $H^+$-pyrophosphatase in vegetative growth of arabidopsis: evidenced by expression of uncoupling mutated enzymes. *Front. Plant Sci.* 7, 1–12. doi: 10.3389/fpls.2016.00415

Au, K. M., Barabote, R. D., Hu, K. Y., and Saier, M. H. (2006). Evolutionary appearance of $H^+$-translocating pyrophosphatases. *Microbiology* 152, 1243–1247. doi: 10.1099/mic.0.28581-0

Ballesteros, J. A., and Weinstein, H. (1995). Integrated methods for the construction of three-dimensional models and computational probing of structure-function relations in g protein-coupled receptors. *Methods Neurosci.* 25, 366–428. doi: 10.1016/S1043-9471(05)80049-7

Baltscheffsky, M., Schultz, A., and Baltscheffsky, H. (1999). $H^+$-proton-pumping inorganic pyrophosphatase: a tightly membrane-bound family. *FEBS Lett.* 452, 121–127. doi: 10.1016/S0014-5793(99)00617-1

Baykov, A. A., Malinen, A. M., Luoto, H. H., and Lahti, R. (2013). Pyrophosphate-fueled $Na^+$ and $H^+$ transport in prokaryotes. *Microbiol. Mol. Biol. Rev.* 77, 267–276. doi: 10.1128/MMBR.00003-13

Belogurov, G. A., and Lahti, R. (2002). A lysine substitute for $K^+$: A460K mutation eliminates $K^+$ dependence in $H^+$-pyrophosphatase of *Carboxydothermus hydrogenoformans*. *J. Biol. Chem.* 277, 49651–49654. doi: 10.1074/jbc.M210341200

Brini, F., Hanin, M., Mezghani, I., Berkowitz, G. A., and Masmoudi, K. (2006). Overexpression of wheat $Na^+/H^+$ antiporter TNHX1 and $H^+$-pyrophosphatase TVP1 improve salt- and drought-stress Tolerance in *Arabidopsis thaliana* plants. *J. Exp. Bot.* 8, 301–308. doi: 10.1093/jxb/erl251

Büscher, P., Cecchi, G., Jamonneau, V., and Priotto, G. (2017). Human African trypanosomiasis. *Lancet* 390, 2397–2409. doi: 10.1016/S0140-6736(17)31510-6

Crompton, P. D., Moebius, J., Portugal, S., Waisberg, M., Hart, G., Garver, L. S., et al. (2014). Malaria immunity in man and mosquito: insights into unsolved mysteries of a deadly infectious disease. *Annu. Rev. Immunol.* 32, 157–187. doi: 10.1146/annurev-immunol-032713-120220

DeLano, W. (2002). Pymol: an open-source molecular graphics tool. *CCP4 Newsl Protein Crystallogr* 40.

Docampo, R., Jimenez, V., Lander, N., Li, Z. H., and Niyogi, S. (2013). New insights into roles of acidocalcisomes and contractile vacuole complex in osmoregulation in protists. *Int. Rev. Cell Mol. Biol.* 305, 69–113. doi: 10.1016/B978-0-12-407695-2.00002-0

Ferjani, A., Segami, S., Horiguchi, G., Muto, Y., Maeshima, M., and Tsukaya, H. (2011). Keep an eye on $PP_i$: the vacuolar-Type $H^+$-pyrophosphatase regulates postgerminative development in Arabidopsis. *Plant Cell.* 23, 2895–2908. doi: 10.1105/tpc.111.085415

Flegr, J., Prandota, J., Sovičková, M., and Israili, Z. H. (2014). Toxoplasmosis – a global threat. correlation of latent toxoplasmosis with specific disease burden in a set of 88 countries. *PLoS ONE* 9:e90203. doi: 10.1371/journal.pone.0090203

Gaxiola, R. A., Palmgren, M. G., and Schumacher, K. (2007). Plant proton pumps. *FEBS Lett.* 581, 2204–2214. doi: 10.1016/j.febslet.2007.03.050

Goldstein, E. J. (1996). Anaerobic bacteremia. *Clin. Infect. Dis.* 23, S97–101. doi: 10.1093/clinids/23.Supplement_1.S97

Gupta, K., Donlan, J. A. C., Hopper, J. T. S., Uzdavinys, P., Landreh, M., Struwe, W. B., et al. (2017). Robinson. The role of interfacial lipids in stabilizing membrane protein oligomers. *Nature* 541, 421–424. doi: 10.1038/nature 20820

Heinonen, J. K. (2001). *Biological Role of Inorganic Pyrophosphate*. Boston, MA: Springer US. doi: 10.1007/978-1-4615-1433-6

Kajander, T., Kellosalo, J., and Goldman, A. (2013). Inorganic pyrophosphatases: one substrate, three mechanisms. *FEBS Lett.* 587, 1863–1869. doi: 10.1016/j.febslet.2013.05.003

Kankare, J., Salminen, T., Lahti, R., Cooperman, B. S., Baykov, A. A., and Goldman, A. (1996). Sructure of *Escherichia coli* inorganic pyrophosphatase at 2.2 Å resolution. *Acta Crystallogr Sect D Biol Crystallogr.* 52, 551–563. doi: 10.1107/S0907444996000376

Kellosalo, J., Kajander, T., Kogan, K., Pokharel, K., and Goldman, A. (2012). The structure and catalytic cycle of a sodium-pumping pyrophosphatase. *Science* 337, 473–476. doi: 10.1126/science.1222505

Kempner, E. S. (1993). Damage to proteins due to the direct action of ionizing radiation. *Q. Rev. Biophys.* 26, 27–48. doi: 10.1017/S0033583500003954

Krebs, M., Beyhl, D., Gorlich, E., Al-Rasheid, K. A. S., Marten, I., Stierhof, Y. D., et al. (2010). Arabidopsis V-ATPase activity at the tonoplast is required for efficient nutrient storage but not for sodium accumulation. *Proc. Natl. Acad. Sci. U.S.A.* 107, 3251–3256. doi: 10.1073/pnas.0913035107

Kriegel, A., Andrés, Z., Medzihradszky, A., Krüger, F., Scholl, S., Delang, S., et al. (2015). Job sharing in the endomembrane system: vacuolar acidification requires the combined activity of V-ATPase and V-PPase. *Plant Cell* 27, 3383–3396. doi: 10.1105/tpc.15.00733

Lemercier, G., Dutoya, S., Luo, S., Ruiz, F. A., Rodrigues, C. O., Baltz, T., et al. (2002). A vacuolar-type $H^+$-pyrophosphatase governs maintenance of functional acidocalcisomes and growth of the insect and mammalian forms of *Trypanosoma brucei*. *J. Biol. Chem.* 277, 37369–37376. doi: 10.1074/jbc.M204744200

Li, J., Yang, H., Peer, W. A., Richter, G., Blakeslee, J., Bandyopadhyay, A., et al. (2005). Arabidopsis $H^+$-PPase AVP1 regulates auxin-mediated organ development. Science 310, 121–125. doi: 10.1126/science.1115711

Li, K. M., Wilkinson, C., Kellosalo, J., Tsai, J. Y., Kajander, T., Jeuken, L. J., et al. (2016). Membrane pyrophosphatases from *Thermotoga maritima* and *Vigna radiata* suggest a conserved coupling mechanism. *Nat. Commun.* 7:13596. doi: 10.1038/ncomms13596

Lin, S. M., Tsai, J. Y., Hsiao, C. D., Huang, Y. T., Chiu, C. L., Liu, M. H., et al. (2012). Crystal structure of a membrane-embedded $H^+$-translocating pyrophosphatase. *Nature* 484, 399–403. doi: 10.1038/nature10963

Liu, J., Pace, D., Dou, Z., King, T. P., Guidot, D., Li, Z. H., et al. (2014). A vacuolar-$H^+$-pyrophosphatase (TgVP1) is required for microneme secretion, host cell invasion, and extracellular survival of *Toxoplasma gondii*. *Mol. Microbiol.* 93, 698–712. doi: 10.1111/mmi.12685

Luoto, H. H., Baykov, A. A., Lahti, R., and Malinen, A. M. (2013b). Membrane-integral pyrophosphatase subfamily capable of translocating both $Na^+$ and $H^+$. *Proc. Natl. Acad. Sci. U.S.A.* 110, 1255–1260. doi: 10.1073/pnas.1217816110

Luoto, H. H., Belogurov, G. A., Baykov, A. A., Lahti, R., and Malinen, A. M. (2011). $Na^+$-translocating membrane pyrophosphatases are

widespread in the microbial world and evolutionarily precede $H^+$-translocating pyrophosphatases. *J. Biol. Chem.* 286, 21633–21642. doi: 10.1074/jbc.M111.244483

Luoto, H. H., Nordbo, E., Baykov, A. A., Lahti, R., and Malinen, A. M. (2013a). Membrane $Na^+$-pyrophosphatases can transport protons at low sodium concentrations. *J. Biol. Chem.* 288, 35126–35137. doi: 10.1074/jbc.M113.510909

Luoto, H. H., Nordbo, E., Malinen, A. M., Baykov, A. A., and Lahti, R. (2015). Evolutionarily divergent, $Na^+$-regulated $H^+$-transporting membrane-bound pyrophosphatases. *Biochem. J.* 467, 281–291. doi: 10.1042/BJ20141434

Lv, S. L., Lian, L. J., Tao, P. L., Li, Z. X., Zhang, K. W., and Zhang, J. R. (2009). Overexpression of *Thellungiella halophila* $H^+$-PPase (TsVP) in cotton enhances drought stress resistance of plants. *Planta* 229, 899–910. doi: 10.1007/s00425-008-0880-4

Maeshima, M. (2000). Vacuolar $H^+$ pyrophosphatase. *Biochim. Biophys. Acta* 1465, 37–51. doi: 10.1016/S0005-2736(00)00130-9

Marchesini, N., Luo, S., Rodrigues, C. O., Moreno, S. N., and Docampo, R. (2000). Acidocalcisomes and a vacuolar $H^+$-pyrophosphatase in malaria parasites. *Biochem. J.* 347, 243–253. doi: 10.1042/bj3470243

Mitsuda, N., Enami, K., Nakata, M., Takeyasu, K., and Sato, M. H. (2001). Novel type *Arabidopsis thaliana* $H^+$-PPase is localized to the golgi apparatus. *FEBS Lett.* 488, 29–33. doi: 10.1016/S0014-5793(00)02400-5

Moreno, S. N., and Docampo, R. (2009). The role of acidocalcisomes in parasitic protists. *J. Eukaryot. Microbiol.* 56, 208–213. doi: 10.1111/j.1550-7408.2009.00404.x

Park, S., Li, J., Pittman, J. K., Berkowitz, G. A., Yang, H., Undurraga, S., et al. (2005). Up-regulation of a $H^+$-pyrophosphatase ($H^+$-PPase) as a strategy to engineer drought-resistant crop plants. *Proc. Natl. Acad. Sci. U.S.A.* 102, 18830–18835. doi: 10.1073/pnas.0509512102

Pasapula, V., Shen, G., Kuppu, S., Paez-Valencia, J., Mendoza, M., Hou, P., et al. (2011). Expression of an arabidopsis vacuolar $H^+$-pyrophosphatase Gene (AVP1) in cotton improves drought- and salt tolerance and increases fibre yield in the field conditions. *Plant Biotechnol. J.* 9, 88–99. doi: 10.1111/j.1467-7652.2010.00535.x

Pyle, E., Kalli, A. C., Amillis, S., Hall, Z., Lau, A. M., Hanyaloglu, A. C., et al. (2018). Structural lipids enable the formation of functional oligomers of the eukaryotic purine symporter UapA. *Cell Chem. Biol.* 25, 840–848. doi: 10.1016/j.chembiol.2018.03.011

Rodrigues, C. O., Scott, D. A., Bailey, B. N., De Souza, W., Benchimol, M., Moreno, B., et al. (2000). Vacuolar proton pyrophosphatase activity and pyrophosphate ($PP_i$) in *Toxoplasma gondii* as possible chemotherapeutic targets. *Biochem. J.* 349, 737–745. doi: 10.1042/bj3490737

Ruiz, F. A., Rodrigues, C. O., and Docampo, R. (2001). Rapid changes in polyphosphate content within acidocalcisomes in response to cell growth, differentiation, and environmental stress in *Trypanosoma cruzi*. *J. Biol. Chem.* 276, 26114–26121. doi: 10.1074/jbc.M102402200

Sarafian, V., Potier, M., and Poole, R. J. (1992). Radiation-inactivation analysis of vacuolar $H^+$-ATPase and $H^+$-pyrophosphatase from *Beta-Vulgaris* L.: functional sizes for substrate hydrolysis and for $H^+$ transport. *Biochem. J.* 283, 493–497. doi: 10.1042/bj2830493

Scott, D. A., de Souza, W., Benchimol, M., Zhong, L., Lu, H. G., Moreno, S. N., et al. (1998). Presence of a plant-like proton-pumping pyrophosphatase in acidocalcisomes of *Trypanosoma cruzi*. *J. Biol. Chem.* 273, 22151–22158. doi: 10.1074/jbc.273.34.22151

Segami, S., Asaoka, M., Kinoshita, S., Fukuda, M., Nakanishi, Y., and Maeshima, M. (2018a). Biochemical, structural and physiological characteristics of vacuolar $H^+$-pyrophosphatase. *Plant Cell Physiol.* 59, 1300–1308. doi: 10.1093/pcp/pcy054

Segami, S., Makino, S., Miyake, A., Asaoka, M., and Maeshima, M. (2014). Dynamics of vacuoles and $H^+$-pyrophosphatase visualized by monomeric green fluorescent protein in arabidopsis: artifactual bulbs and native intravacuolar spherical structures. *Plant Cell* 26, 3416–3434. doi: 10.1105/tpc.114.127571

Segami, S., Tomoyama, T., Sakamoto, S., Gunji, S., Fukuda, M., Kinoshita, S., et al. (2018b). Vacuolar $H^+$-pyrophosphatase and cytosolic soluble pyrophosphatases cooperatively regulate pyrophosphate levels in *Arabidopsis thaliana*. *Plant Cell* 30, 1040–1061. doi: 10.1105/tpc.17.00911

Shah, N., Vidilaseris, K., Xhaard, H., and Goldman, A. (2016). Integral membrane pyrophosphatases: a novel drug target for human pathogens? *AIMS Biophys.* 3, 171–194. doi: 10.3934/biophy.2016.1.171

Shah, N. R., Wilkinson, C., Harborne, S. P., Turku, A., Li, K. M., Sun, Y. J., et al. (2017). Insights into the mechanism of membrane pyrophosphatases by combining experiment and computer simulation. *Struct. Dyn.* 4, 1–12. doi: 10.1063/1.4978038

Torgerson, P. R., and Mastroiacovo, P. (2013). The global burden of congenital toxoplasmosis: a systematic review. *Bull. World Health Organ.* 91, 501–508. doi: 10.2471/BLT.12.111732

Tsai, J. Y., Kellosalo, J., Sun, Y. J., and Goldman, A. (2014). Proton/sodium pumping pyrophosphatases: the last of the primary ion pumps. *Curr. Opin. Struct. Biol.* 27, 38–47. doi: 10.1016/j.sbi.2014.03.007

Tsai, J. Y., Tang, K. Z., Li, K. M., Hsu, B. L., Chiang, Y. W., Goldman, A., et al. (2019). Roles of the hydrophobic gate and exit channel in *Vigna radiata* pyrophosphatase ion translocation. *J. Mol. Biol.* 431, 1619–1632. doi: 10.1016/j.jmb.2019.03.009

Tzeng, C. M., Yang, C. Y., Yang, S. J., Jiang, S. S., Kuo, S. Y., Hung, S. H., et al. (1996). Subunit structure of vacuolar proton-pyrophosphatase as determined by radiation inactivation. *Biochem. J.* 316, 143–147. doi: 10.1042/bj3160143

Vidilaseris, K., Kiriazis, A., Turku, A., Khattab, A., Johansson, N. G., Leino, T. O., et al. (2019). Asymmetry in catalysis by *Thermotoga maritima* membrane-bound pyrophosphatase demonstrated by a nonphosphorus allosteric inhibitor. *Sci. Adv.* 5:eaav7574. doi: 10.1126/sciadv.aav7574

Wexler, H. M. (2007). Bacteroides: the good, the bad, and the nitty-gritty. *Clin. Microbiol. Rev.* 20, 593–621. doi: 10.1128/CMR.00008-07

World Health Organization (2018). *Global Malaria Programme*. World Malaria Report 2017.

Wu, J. J., Ma, J. T., and Pan, R. L. (1991). Functional size analysis of pyrophosphatase from *Rhodospirillum rubrum* determined by radiation inactivation. *FEBS Lett.* 283, 57–60. doi: 10.1016/0014-5793(91)80552-E

Yang, S. J., Jiang, S. S., Van, R. C., Hsiao, Y. Y., and Pan, R. (2000). A lysine residue involved in the inhibition of vacuolar $H^+$-pyrophosphatase by fluorescein 5'-isothiocyanate. *Biochim. Biophys. Acta* 1460, 375–383. doi: 10.1016/S0005-2728(00)00203-6

Yoon, H. S., Kim, S. Y., and Kim, I. S. (2013). Stress response of plant $H^+$-PPase-expressing transgenic *Escherichia coli* and *Saccharomyces cerevisiae*: a potentially useful mechanism for the development of stress-tolerant organisms. *J. Appl. Genet.* 54, 129–133. doi: 10.1007/s13353-012-0117-x

Zhang, H., Shen, G., Kuppu, S., Gaxiola, R., and Payton, P. (2011). Creating drought- and salt-tolerant cotton by overexpressing a vacuolar pyrophosphatase gene. *Plant Signal. Behav.* 6, 861–863. doi: 10.4161/psb.6.6.15223

Zhang, M., Wang, C., Otto, T. D., Oberstaller, J., Liao, X., Adapa, S. R., et al. (2018). Uncovering the essential genes of the human malaria parasite *Plasmodium falciparum* by saturation mutagenesis. *Science* 360:eaap7847. doi: 10.1126/science.aap7847

Zhao, F. Y., Zhang, X. J., Li, P. H., Zhao, Y. X., and Zhang, H. (2006). Co-expression of the *Suaeda salsa* SsNHX1 and arabidopsis AVP1 confer greater salt tolerance to transgenic rice than the single SsNHX1. *Mol. Breed.* 17, 341–353. doi: 10.1007/s11032-006-9005-6

**Conflict of Interest:** The authors declare that the research was conducted in the absence of any commercial or financial relationships that could be construed as a potential conflict of interest.

frontiers in Plant Science

OPINION
published: 14 February 2020
doi: 10.3389/fpls.2020.00107

# Energy Coupling in Cation-Pumping Pyrophosphatase—Back to Mitchell

*Alexander A. Baykov* *

*Belozersky Institute of Physico-Chemical Biology, Lomonosov Moscow State University, Moscow, Russia*

**Keywords: membrane pyrophosphatase, $H^+$ pumping, $Na^+$ pumping, energy coupling, Mitchell, pyrophosphate**

> *"Scientists frequently debate theories".*
> Douglas Allchin

## INTRODUCTION

Those of a certain age may remember (and their younger colleagues can read) accounts of the vivid debate in the 1970s surrounding the coupling mechanism involved in oxidative and photo phosphorylation. By that time, Mitchell's chemiosmotic hypothesis had already gained credence, and the debated issue was how a transmembrane $H^+$ potential difference drives ATP synthesis by F-type ATP synthases. The major mechanisms that were considered assumed that the membrane ($F_o$) and peripheral ($F_1$) parts were functionally connected in different ways. Peter Mitchell proposed a "direct coupling" mechanism in which protons are translocated through $F_o$ into the catalytic site of $F_1$, where they participate directly in ADP phosphorylation and form water as the second product (Mitchell, 1974). Paul Boyer, the proponent of the main competing mechanism, advocated an "indirect coupling" mechanism (successively termed "alternating site", "binding change", or "rotational") that implied that protons transfer their energy to the catalytic site indirectly, *via* distant conformational strain (Boyer, 1997). The debate was resolved in favor of Boyer's mechanism when it became clear that the alternative mechanism is inconsistent with $H^+$/ATP stoichiometry and, finally, when the three-dimensional structure of the F-ATPase was determined (Abrahams et al., 1994).

Now, after several decades, the problem of energy coupling is being revisited in connection with membrane pyrophosphatases (mPPases), ancient transporters that couple $H^+$ and $Na^+$ transport across biological membranes in plant vacuoles and bacteria to pyrophosphate hydrolysis. mPPases are functional analogs of F-type ATPases and similarly catalyze a direct attack of a water molecule on a phosphorus atom without formation of a phosphorylated intermediate. However, mPPases have a much simpler structure; each of the two identical subunits of mPPase consists of 15–17 transmembrane α-helices, and six of them form the catalytic site on the cytosolic side. $H^+$-transporting mPPases ($H^+$-PPases) have been known since 1966 (Baltscheffsky et al., 1966; Serrano et al., 2007) and are recognized as contributors to plant stress resistance (Yang et al., 2014). More recent studies have identified an evolutionarily related prokaryotic $Na^+$-transporting mPPase lineage ($Na^+$-PPases) that can pump both $H^+$ and $Na^+$ (Malinen et al., 2007; Luoto et al., 2013a; Luoto et al., 2013b). mPPase studies have been further boosted by publication in 2012 of the three-dimensional structures of the $H^+$-

OPEN ACCESS

***Edited by:***
*Jose Roman Perez-Castineira, University of Seville, Spain*

***Reviewed by:***
*Rosa Laura Lopez-Marques, University of Copenhagen, Denmark*

***Correspondence:**
*Alexander A. Baykov*
*baykov@belozersky.msu.ru*

***Specialty section:***
*This article was submitted to Plant Metabolism and Chemodiversity, a section of the journal Frontiers in Plant Science*

***Received:*** *23 December 2019*
***Accepted:*** *24 January 2020*
***Published:*** *14 February 2020*

***Citation:***
*Baykov AA (2020) Energy Coupling in Cation-Pumping Pyrophosphatase—Back to Mitchell. Front. Plant Sci. 11:107. doi: 10.3389/fpls.2020.00107*

transporting mPPase from *Vigna radiata* (Lin et al., 2012) (**Figure 1A**) and the $Na^+$-transporting mPPase from *Thermotoga maritima* (Kellosalo et al., 2012). Two mechanisms to explain coupling between $PP_i$ hydrolysis and $H^+$ ($Na^+$) pumping, proposed based on these structures, differ principally in the order of hydrolysis and transport events and the role of the proton released by the attacking water nucleophile.

This short treatise on mPPases has three principal purposes. One is to reconsider the available functional data on $H^+$-

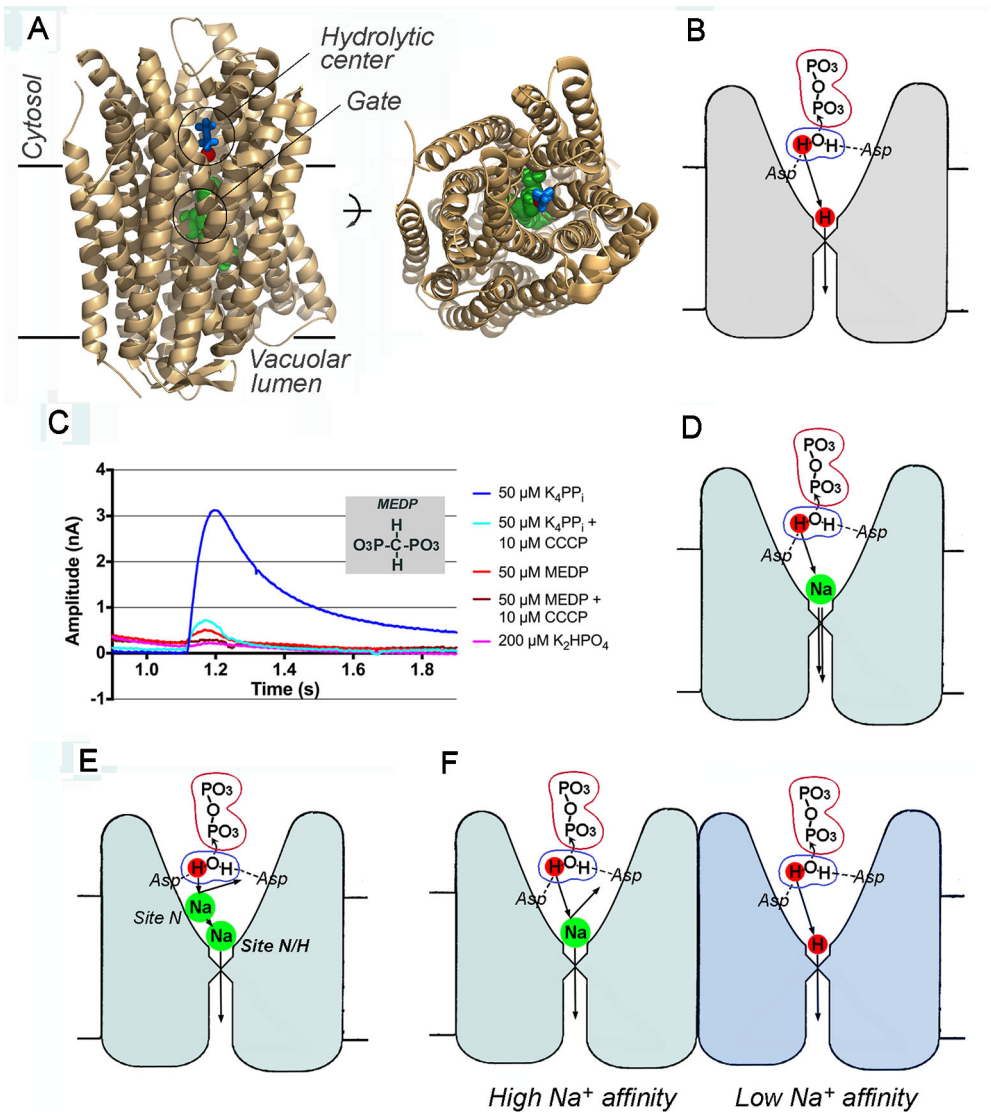


**FIGURE 1 |** Membrane pyrophosphatase as an $H^+$ and $Na^+$ transporter. **(A)** Two views of a subunit of *V. radiata* homodimeric $H^+$-pyrophosphatase, showing elements of the transport machinery [PDB code: 4A01; Lin et al., 2012)]. The image on the right is a top view from the cytosolic side. Blue sticks, imidodiphosphate; red sphere, water nucleophile (the oxygen atom); green spheres, three gate-forming residues (Arg242, Asp294, and Lys 742); imidodiphosphate-liganded $Mg^{2+}$, and $K^+$ ions are not shown. Created with PyMOL (The PyMOL Molecular Graphics System, Version 1.5.0.4, Schrodinger, LLC). **(B)** Mitchell-type coupling of $PP_i$ hydrolysis with $H^+$ transport in a single subunit. The ions (atoms) directly involved in the transport process are marked by colored circles. Two aspartate residues (Asp287 and Asp731 in *V. radiata* mPPase) coordinate and activate the nucleophilic water molecule during its attack on $PP_i$. **(C)** Electrometric traces of *V. radiata* pyrophosphatase-loaded liposomes obtained with a Nanion SURFE$^2$R N1 instrument. Currents were recorded following the addition of $K_4PP_i$, methylene diphosphonate (MEDP), and $K_2HPO_4$ in the absence and presence of the protonophore CCCP (carbonyl cyanide *m*-chlorophenyl hydrazone). This panel was reproduced with permission from Shah et al. (2017). **(D)** A billiard-type mechanism of $Na^+$ transport at a low $Na^+$ concentration. The nucleophile-generated $H^+$ pushes out the gate-bound $Na^+$ (coordinated by Asp243, Glu246, and Asp703 carboxylates in *T. maritima* mPPase; Li et al., 2016) and passes the gate itself in the same or successive turnover. **(E)** Inhibition of $Na^+$ transport by a $Na^+$ ion bound at a low-affinity transitory site N. The identities of the residues forming it are yet unknown. **(F)** An alternative mechanism of concurrent $Na^+$ and $H^+$ transport by different subunits of dimeric $Na^+$-PPase. In this mechanism, excess $Na^+$ will inhibit $H^+$ transport by binding to the pump-loading site of the right subunit, which exhibits a much lower affinity to $Na^+$ (strong negative cooperativity).

transporting mPPases that favor Mitchell's direct coupling mechanism. The second is to recapitulate modifications to this mechanism to explain $Na^+$ transport. And the third is to raise the possibility that mPPases additionally employ elements of Boyer's conformational coupling mechanism.

## PROPOSED COUPLING MECHANISMS OF $H^+$-TRANSPORTING mPPASE—PROS AND CONS

The first coupling mechanism, proposed by Lin et al. (2012) (**Figure 1B**), was essentially an adaptation of Mitchell's hypothesis to mPPases. In the mPPase structure, the presumed water nucleophile is located near the conductance channel, such that the proton released from the attacking water molecule can move to the channel and along it *via* Grotthuss shuttling through a water wire. This proton is thus in the right place at the right time to create high local acidity that drives proton translocation to the other side of the membrane. The mechanism suggested by Lin et al. (2012) therefore assumes that $H^+$ transport follows or occurs concurrently with $PP_i$ hydrolysis. This mechanism is consistent with the experimentally determined $H^+/PP_i$ coupling ratio of 1 for mPPases (Segami et al., 2018) and, further, predicts that medium $H^+$ ions should not compete with the transported $H^+$ ion.

An alternative hypothesis (Kellosalo et al., 2012) suggested instead that the transported $H^+$ ion passes the gate as a result of $PP_i$ binding and that $PP_i$ hydrolysis is only required to prepare the transport machinery for the next transport/hydrolysis cycle. This mechanism, named "binding change" (not to be confused with Boyer's "binding change" for $F_oF_1$-ATPase), does not ascribe any specific role to the proton released from the nucleophilic water molecule. Operation of this mechanism in reverse was proposed to explain $PP_i$ synthesis by plant mPPases (Regmi et al., 2016).

The proton released by the nucleophilic water is thus the key player in the mechanism of Lin et al., whereas the alternative mechanism ascribes no role to the proton in question, other than being dispersed in the medium. The possibility that this proton is transported in the mechanism of Kellosalo et al. seems unlikely because this would unrealistically presume that the nucleophilic water is converted into a hydroxide ion by means of its coordination to two aspartates. This is reminiscent of the abandoned "charge relay" hypothesis in serine proteases, which assumed similar $H^+$ abstraction from a serine hydroxyl (Hedstrom, 2002). Instead, the two aspartates that coordinate the nucleophilic water in mPPases are involved in general acid/base catalysis, as is the case in aspartic proteases (Meek, 1998). Notably, the available structures of several mPPase species formed during the catalytic cycle do not differentiate between these mechanisms, because the reaction intermediates that these structures mimic are common to both mechanisms.

To support the "binding change" hypothesis, Li et al. (2016) and Shah et al. (2017) used a modification of a previously described electrometric assay (Kondrashin et al., 1980) to measure charge movement across the membrane of *V. radiata* mPPase-loaded liposomes in response to non-hydrolyzable $PP_i$ analogs (imidodiphosphate and methylene diphosphonate). They indeed observed a small signal of the appropriate sign and interpreted it as an indication that substrate binding alone suffices to transport $H^+$ ions across the membrane (**Figure 1C**). However, the authors inexplicably ignored their own observation that $PP_i$ produced a 10-times greater signal compared with its analogs (**Figure 1C**), despite similar affinities for mPPase (Baykov et al., 1993). Importantly, the $PP_i$ signal arose from a single rather than multiple turnover(s). Indeed, the time required to build up the electrometric signal upon addition of $PP_i$ (or its analog) to mPPase-containing liposomes was slightly less than 0.1 s (**Figure 1C**), which is sufficient for only one turnover, based on the turnover number for a purified *V. radiata* mPPase molecule of 11.5 $s^{-1}$ (Segami et al., 2018). In summary, a complete turnover produced a 10-times greater electrometric signal compared to that produced by $PP_i$ analog (and seemingly $PP_i$) binding. Had the transport event preceded hydrolysis, the signals would have been equal unless the transport stoichiometries for the two ligands differ 10-fold—a far-fetched and unlikely scenario. Putting things right side up, the electrometric data strongly support the notion that cation transport is associated with hydrolysis and/or product release, not substrate-binding step in a single turnover.

The low size of the electrometric signals generated by $PP_i$ analogs is consistent with charge crossing only part of the membrane thickness (Skulachev et al., 2013), for example, by analog-induced binding of additional $Mg^{2+}$ or $H^+$ ions to the active site (the effect of CCCP in **Figure 1C** does not discriminate between primarily transported cations). Alternatively, charged amino acid residues may change their positions in the membrane during the conformational change induced by analog binding (Hsu et al., 2015; Li et al., 2016).

## BILLIARD-TYPE HYPOTHESIS OF $Na^+$ TRANSPORT

Although $Na^+$-PPases are not found in plants, their study may provide important insights into plant $H^+$-PPases because $Na^+$-PPases are structurally very similar to $H^+$-PPases and can pump both $H^+$ and $Na^+$ at low (<5 mM) $Na^+$ concentrations. The major difference of $Na^+$-PPase is the presence of a glutamate residue in the gate that forms a $Na^+$-binding site (Kellosalo et al., 2012).

Because $Na^+$, unlike the transported $H^+$, is not a reaction product and comes from the medium, $Na^+$ pumping should employ a different mechanism. The billiard-type hypothesis (Baykov et al., 2013), a logical extension of the mechanism of Lin et al. (2012), posits that the proton released by the nucleophilic water is the major driving force for $Na^+$ transport (**Figure 1D**). This proton is assumed to push a bound $Na^+$ ion into the ion conductance channel and, at low $Na^+$ concentrations, enter the channel itself in place of $Na^+$. Notably, neither this nor any other mPPase mechanism found in literature assumes a "one-jump" transfer of cation through the

membrane. The particular $H^+$ or $Na^+$ ion that enters the conductance channel in each turnover exits the channel after *n* turnovers, where *n* is the number of cation-binding sites the cation occupies on its way along the channel. However, a consideration of the pathways through which the cations pass the conductance channel and ionic gate and the associated conformational changes are outside the scope of this article.

The interplay between $H^+$ and $Na^+$ on their way to the ionic gate appears to involve two cation-binding sites ("N/H" and "N") in $Na^+$-PPases, as indicated by the $Na^+$ dependencies of the $H^+$- and $Na^+$-transporting activities and the effects of substitutions in gate residues (Luoto et al., 2013b). According to these analyses, the pump loading site N/H is associated with the gate and can bind both $Na^+$ and $H^+$. Its binding constant for $Na^+$ lies in the sub-millimolar range, and its occupancy by $Na^+$ is required for enzymatic activity. The crystal structure of *T. maritima* $Na^+$-PPase (Li et al., 2016) did reveal a gate-bound $Na^+$ ion. The other, site N, binds $Na^+$ in the millimolar range and presumably acts as a transitory $Na^+$-binding site and a filter for $H^+$ in the channel (**Figure 1E**). The $Na^+$ ion that occupies site N at high $Na^+$ concentrations physically or electrostatically disallows $H^+$ passage, explaining why dual $Na^+$ and $H^+$ specificity is observed with most $Na^+$-PPases only at low $Na^+$ levels (Luoto et al., 2013b). A similar explanation assuming two $Na^+$-binding sites was proposed by Holmes et al. (2019).

An alternative possibility is that $Na^+$ and $H^+$ transport are carried out by different subunits of dimeric $Na^+$-PPase binding $Na^+$ at a single site per subunit in a negatively cooperative manner because of dimer asymmetry (Artukka et al., 2018; Vidilaseris et al., 2019) (**Figure 1F**). In this mechanism, $Na^+$ could inhibit $H^+$ transport by occupying both pump-loading sites, resembling the effect of high substrate concentration on enzymatic activity (Artukka et al., 2018).

The "pumping-before-hydrolysis" mechanism of Kellosalo et al. (2012) does not differentiate between $H^+$ and $Na^+$ and suggests a similar pumping mechanism for both. If, as we saw above, the electrometric data rule out the hypothesis that the transport event precedes substrate hydrolysis in the case of $H^+$ pumping, this mechanism is similarly unlikely to operate in $Na^+$ pumping. This conclusion is supported by the presence of gate-bound $Na^+$ in the complex of TmPPase with imidodiphosphate (Li et al., 2016), but not in the complex with $P_i$ (Kellosalo et al., 2012). Similar electrometric measurements with $Na^+$-PPases would aid in testing this aspect of the billiard-type mechanism.

## CONCLUSIONS AND PERSPECTIVES

The available data thus indicate that $H^+$-PPases operate *via* Mitchell's direct coupling mechanism. But this is only the first milestone in this exciting journey. Recent kinetic data (Artukka et al., 2018) suggest that active sites undergo oscillations between active and inactive conformations during catalysis, a phenomenon resembling the anchor mechanism in watches, and reflecting structural data (Vidilaseris et al., 2019) indicating asymmetrical binding of an allosteric inhibitor to two subunits. This may mean that mPPases combine two mechanisms of energy coupling—Mitchell's direct coupling and Boyer's conformational coupling (its "alternating sites" version), which were antagonists in the debate over $F_oF_1$-ATPase—in one protein.

The interplay between $H^+$ and $Na^+$ transport activities is another unresolved aspect of mPPase functioning, especially in $Na^+$, $H^+$-PPases, the group of $Na^+$-PPases that pump both $Na^+$ and $H^+$ at physiological $Na^+$ concentrations and, apparently, co-transport both cations in each catalytic cycle (Luoto et al., 2013a). This is thermodynamically permitted in membranes that generate low or moderate electrochemical potential gradients, like those in fermentative bacteria.

Paul Boyer called $F_oF_1$-ATPase a "splendid molecular machine" (Boyer, 1997). This characterization is fully applicable to its predecessor, mPPase, which combines a deceptively simple structure with evolutionary diversity and a multifaceted transport mechanism.

## AUTHOR CONTRIBUTIONS

The author confirms being the sole contributor of this work and has approved it for publication.

## FUNDING

This work was supported by a grant from the Russian Science Foundation (research project 19-14-00063).

## ACKNOWLEDGMENTS

I thank Alexander Bogachev and Anssi Malinen for discussions.

## REFERENCES

Abrahams, J. P., Leslie, A. G. W., Lutter, R., and Walker, J. E. (1994). Structure at 2.8 Å resolution of $F_1$-ATPase from bovine heart mitochondria. *Nature* 370, 621–628. doi: 10.1038/370621a0

Artukka, E., Luoto, H. H., Baykov, A. A., Lahti, R., and Malinen, A. M. (2018). Role of the potassium/lysine cationic center in catalysis and functional asymmetry in membrane-bound pyrophosphatases. *Biochem. J.* 475, 1141–1158. doi: 10.1042/BCJ20180071

Baltscheffsky, H., Von Stedingk, L. V., Heldt, H. W., and Klingenberg, M. (1966). Inorganic pyrophosphate: formation in bacterial photophosphorylation. *Science* 153, 1120–1122. doi: 10.1126/science.153.3740.1120

Baykov, A. A., Dubnova, E. B., Bakuleva, N. P., Evtushenko, O. A., Zhen, R.-G., and Rea, P. A. (1993). Differential sensitivity of membrane-associated pyrophosphatases to inhibition by diphosphonates and fluoride deliniates two classes of enzyme. *FEBS Lett.* 2, 199–202. doi: 10.1016/0014-5793(93)80169-U

Baykov, A. A., Malinen, A. M., Luoto, H. H., and Lahti, R. (2013). Pyrophosphate-fueled $Na^+$ and $H^+$ transport in prokaryotes. *MMBR* 77, 267–276. doi: 10.1128/MMBR.00003-13

Boyer, P. D. (1997). The ATP synthase—a splendid molecular machine. *Annu. Rev. Biochem.* 66, 717–749. doi: 10.1146/annurev.biochem.66.1.717

Hedstrom, L. (2002). Serine protease mechanism and specificity. *Chem. Rev.* 102, 4501–4523. doi: 10.1021/cr000033x

Holmes, A. O. M., Kalli, A. C., and Goldman, A. (2019). The function of membrane integral pyrophosphatases from whole organism to single molecule. *Front. Mol. Biosci.* 6, 132. doi: 10.3389/fmolb.2019.00132

Hsu, S.-H., Lo, Y.-Y., Liu, T.-H., Pan, Y.-J., Huang, Y.-T., Sun, Y.-J., et al. (2015). Substrate-induced changes in domain interaction of vacuolar $H^+$-pyrophosphatase. *J. Biol. Chem.* 290, 1197–1209. doi: 10.1074/jbc.M114.568139

Kellosalo, J., Kajander, T., Kogan, K., Pokharel, K., and Goldman, A. (2012). The structure and catalytic cycle of a sodium-pumping pyrophosphatase. *Science* 337, 473–476. doi: 10.1126/science.1222505

Kondrashin, A. A., Remennikov, V. G., Samuilov, V. D., and Skulachev, V. P. (1980). Reconstitution of biological molecular generators of electric current. Inorganic pyrophosphatase. *Eur. J. Biochem.* 113, 219–222. doi: 10.1111/j.1432-1033.1980.tb06159.x

Li, K. M., Wilkinson, C., Kellosalo, J., Tsai, J. Y., Kajander, T., Jeuken, L. J. C., et al. (2016). Membrane pyrophosphatases from *Thermotoga maritima* and *Vigna radiata* suggest a conserved coupling mechanism. *Nat. Commun.* 7, 1–11. doi: 10.1038/ncomms13596

Lin, S. M., Tsai, J. Y., Hsiao, C. D., Huang, Y. T., Chiu, C. L., Liu, M. H., et al. (2012). Crystal structure of a membrane-embedded $H^+$-translocating pyrophosphatase. *Nature* 484, 399–403. doi: 10.1038/nature10963

Luoto, H., Baykov, A. A., Lahti, R., and Malinen, A. M. (2013a). Membrane-integral pyrophosphatase subfamily capable of translocating both $Na^+$ and $H^+$. *Proc. Natl. Acad. Sci. U. S. A.* 110, 1255–1260. doi: 10.1073/pnas.1217816110

Luoto, H. H., Nordbo, E., Baykov, A. A., Lahti, R., and Malinen, A. M. (2013b). Membrane $Na^+$-pyrophosphatases can transport protons at low sodium concentrations. *J. Biol. Chem.* 288, 35489–35499. doi: 10.1074/jbc.M113.510909

Malinen, A. M., Belogurov, G. A., Baykov, A. A., and Lahti, R. (2007). $Na^+$-pyrophosphatase: a novel primary sodium pump. *Biochemistry* 46, 8872–8878. doi: 10.1021/bi700564b

Meek, T. D. (1998). "Catalytic mechanisms of the aspartic proteases," in *Comprehensive Biological Catalysis*, vol. 1 . Eds. M. Sinnott (San Diego: Academic Press), 327–344.

Mitchell, P. (1974). A chemiosmotic molecular mechanism for proton translocating adenosine triphosphatase. *FEBS Lett.* 43, 189–194. doi: 10.1016/0014-5793(74)80997-X

Regmi, K. C., Pizzio, G. A., and Gaxiola, R. A. (2016). Structural basis for the reversibility of proton pyrophosphatase. *Plant Signaling Behav.* 11 (10), e1231294. doi: 10.1080/15592324.2016.1231294

Segami, S., Asaoka, M., Kinoshita, S., Fukuda, M., Nakanishi, Y., and Maeshima, M. (2018). Biochemical, structural and physiological characteristics of vacuolar $H^+$-pyrophosphatase. *Plant Cell Physiol.* 59, 1300–1308 doi: 10.1093/pcp/pcy054

Serrano, A., Pérez-Castiñeira, J. R., Baltscheffsky, M., and Baltscheffsky, H. (2007). $H^+$-PPases: yesterday, today and tomorrow. *IUBMB Life* 59, 76–83. doi: 10.1080/15216540701258132

Shah, N. R., Wilkinson, C., Harborne, S. P. D., Turku, A., Li, K. M., Sun, Y. J., et al. (2017). Insights into the mechanism of membrane pyrophosphatases by combining experiment and computer simulation. *Struct. Dyn.* 4, 032105. doi: 10.1063/1.4978038

Skulachev, V. P., Bogachev, A. V., and Kasparinsky, F. O. (2013). *Principles of Bioenergetics* (Heidelberg, New York, Dordrecht, London: Springer), 47–50. doi: 10.1007/978-3-642-33430-6

Vidilaseris, K., Kiriazis, A., Turku, A., Khattab, A., Johansson, N. G., Leino, T. O., et al. (2019). Asymmetry in catalysis by *Thermotoga maritima* membrane bound pyrophosphatase demonstrated by a nonphosphorus allosteric inhibitor. *Sci. Adv.* 5, eaav7574. doi: 10.1126/sciadv.aav7574

Yang, H., Zhang, X., Gaxiola, R. A., Xu, G., Peer, W. A., and Murphy, A. S. (2014). Over-expression of the Arabidopsis proton-pyrophosphatase AVP1 enhances transplant survival, root mass, and fruit development under limiting phosphorus conditions. *J. Exp. Bot.* 65, 3045–3053. doi: 10.1093/jxb/eru149

**Conflict of Interest:** The author declares that the research was conducted in the absence of any commercial or financial relationships that could be construed as a potential conflict of interest.

frontiers in Plant Science

ORIGINAL RESEARCH
published: 21 February 2020
doi: 10.3389/fpls.2020.00031

# Excess Pyrophosphate Restrains Pavement Cell Morphogenesis and Alters Organ Flatness in *Arabidopsis thaliana*

*Shizuka Gunji*[1], *Yoshihisa Oda*[2,3], *Hisako Takigawa-Imamura*[4], *Hirokazu Tsukaya*[5] *and Ali Ferjani*[1,6*†]

[1] United Graduate School of Education, Tokyo Gakugei University, Tokyo, Japan, [2] Department of Gene Function and Phenomics, National Institute of Genetics, Mishima, Japan, [3] Department of Genetics, The Graduate University for Advanced Studies, SOKENDAI, Mishima, Japan, [4] Department of Anatomy and Cell Biology, Graduate School of Medical Sciences, Kyushu University, Fukuoka, Japan, [5] Department of Biological Sciences, Graduate School of Science, The University of Tokyo, Tokyo, Japan, [6] Department of Biology, Tokyo Gakugei University, Tokyo, Japan

OPEN ACCESS

**Edited by:**
Jose Roman Perez-Castineira, University of Seville, Spain

**Reviewed by:**
Takumi Higaki, Kumamoto University, Japan
Olivier Hamant, École Normale Supérieure de Lyon, France

***Correspondence:**
Ali Ferjani
ferjani@u-gakugei.ac.jp

**†Present address:**
Ali Ferjani, Department of Life Sciences, Graduate School of Arts and Sciences, University of Tokyo, Tokyo, Japan

**Specialty section:**
This article was submitted to Plant Metabolism and Chemodiversity, a section of the journal Frontiers in Plant Science

**Received:** 26 November 2019
**Accepted:** 13 January 2020
**Published:** 21 February 2020

**Citation:**
Gunji S, Oda Y, Takigawa-Imamura H, Tsukaya H and Ferjani A (2020) Excess Pyrophosphate Restrains Pavement Cell Morphogenesis and Alters Organ Flatness in Arabidopsis thaliana. Front. Plant Sci. 11:31. doi: 10.3389/fpls.2020.00031

In *Arabidopsis thaliana*, the vacuolar proton-pumping pyrophosphatase ($H^+$-PPase) is highly expressed in young tissues, which consume large amounts of energy in the form of nucleoside triphosphates and produce pyrophosphate (PPi) as a byproduct. We reported that excess PPi in the $H^+$-PPase loss-of-function *fugu5* mutant severely compromised gluconeogenesis from seed storage lipids, arrested cell division in cotyledonary palisade tissue, and triggered compensated cell enlargement; this phenotype was recovered upon sucrose supply. Thus, we provided evidence that the hydrolysis of inhibitory PPi, rather than vacuolar acidification, is the major contribution of $H^+$-PPase during seedling establishment. Here, examination of the epidermis revealed that *fugu5* pavement cells exhibited defective puzzle-cell formation. Importantly, removal of PPi from *fugu5* background by the yeast cytosolic PPase IPP1, in *fugu5-1 AVP1*$_{pro}$*::IPP1* transgenic lines, restored the phenotypic aberrations of *fugu5* pavement cells. Surprisingly, pavement cells in mutants with defects in gluconeogenesis (*pck1-2*) or the glyoxylate cycle (*icl-2*; *mls-2*) showed no phenotypic alteration, indicating that reduced sucrose production from seed storage lipids is not the cause of *fugu5* epidermal phenotype. *fugu5* had oblong cotyledons similar to those of *angustifolia-1* (*an-1*), whose leaf pavement cells display an abnormal arrangement of cortical microtubules (MTs). To gain insight into the genetic interaction between ANGUSTIFOLIA and $H^+$-PPase in pavement cell differentiation, *an-1 fugu5-1* was analyzed. Surprisingly, epidermis developmental defects were synergistically enhanced in the double mutant. In fact, *an-1 fugu5-1* pavement cells showed a striking three-dimensional growth phenotype on both abaxial and adaxial sides of cotyledons, which was recovered by hydrolysis of PPi in *an-1 fugu5-1 AVP1*$_{pro}$*::IPP1*. Live imaging revealed that cortical MTs exhibited a reduced velocity, were slightly fragmented and sparse in the above lines compared to the WT. Consistently, addition of PPi *in vitro* led to a dose-dependent delay of tubulin polymerization, thus supporting a link between PPi and MT dynamics. Moreover, mathematical simulation of three-dimensional growth based on

cotyledon proximo-distal and medio-lateral phenotypic quantification implicated restricted cotyledon expansion along the medio-lateral axis in the crinkled surface of *an-1 fugu5-1*. Together, our data suggest that PPi homeostasis is a prerequisite for proper pavement cell morphogenesis, epidermal growth and development, and organ flattening.

**Keywords: *Arabidopsis thaliana*, $H^+$-PPase, *fugu5* mutant, PPi, pavement cells**

## INTRODUCTION

Although housekeeping enzymes have been characterized in detail, molecular lesions in such genes are often associated with lethality, hampering assessment of the mechanism of their *in vivo* roles beyond housekeeping activities. For example, 3-phosphoglycerate dehydrogenase (PHGDH) catalyzes the first step of L-serine biosynthesis in animals (Klomp et al., 2000). PHGDH deficiency causes a disorder of L-serine biosynthesis that is characterized by congenital microcephaly, psychomotor retardation, and seizures (Klomp et al., 2000). Although L-serine is a non-essential amino acid, studies on patients with Neu-Laxova syndrome have suggested a fundamental role for PHGDH activity in metabolism, development, and function of the human central nervous system (Klomp et al., 2000). Moreover, several recent reports have indicated that some of these housekeeping enzymes perform a variety of other functions, such as acting as virulence factors for pathogens (Pancholi and Chhatwal, 2003; and references therein).

All above-ground organs of plants emerge at the shoot apical meristem (SAM). Plant leaves play a central role not only in capturing light for photosynthesis but also by sensing the environmental signals that are integrated to enable optimal growth. These functions are accomplished independently and cooperatively by the different cell types on the surface or embedded within plant leaf tissues. Leaf primordia evolve at the flanks of the SAM and undergo a phase of cell proliferation followed by cell differentiation (Donnelly et al., 1999; Ferjani et al., 2007). Proliferating cells are characterized by an active metabolism, whereby they consume large amounts of energy in the form of nucleoside triphosphates (NTPs). Simultaneously, in nearly 200 different metabolic reactions (Heinonen, 2001)—including DNA replication, amino acid activation, and protein and cell wall biosynthesis—they produce pyrophosphate (PPi). PPi is a toxic molecule that if not immediately hydrolyzed by soluble-type pyrophosphatases (sPPases) and/or membrane-bound pyrophosphatases ($H^+$-PPases) (Ferjani et al., 2014; Segami et al., 2018), irreversibly arrests the above metabolic reaction.

Most studies of the physiological function(s) of PPi-hydrolyzing enzymes, which can be viewed as housekeeping enzymes, and the impact of excess PPi *in vivo*, have been unsuccessful (Ferjani et al., 2014). Indeed, the importance of PPi-homeostasis in development is evidenced by the many reports in several organisms. For example, decreased expression of *ppa*, encoding *E. coli* sPPase, raised the PPi level and arrested growth (Chen et al., 1990). Similarly, the cytosolic PPase IPP1 is essential for cell viability in *Saccharomyces cerevisiae* (Lundin et al., 1991). Moreover, the *Caenorhabditis elegans* sPPase *pyp-1* null mutant, displayed gross defects in intestinal morphology and function and was arrested at early larval stages (Ko et al., 2007).

The importance of PPi homeostasis in plant growth and development in *Arabidopsis thaliana* (Arabidopsis, hereafter) has been intensively investigated using *fugu5* mutants, harboring a molecular lesion in the vacuolar-type $H^+$-PPase. For instance, we demonstrated that the $H^+$-PPase is the major PPase in Arabidopsis (Ferjani et al., 2011; Ferjani et al., 2014; Asaoka et al., 2016; Segami et al., 2018). Failure to hydrolyze PPi led to developmental defects at the organism, organ, tissue, and cellular levels. Indeed, the *fugu5* mutant plants display retarded post-germinative growth and exhibit oblong-shaped cotyledons and compensation in their palisade tissue, such as excessive cell expansion triggered by decreased cell proliferation (Ferjani et al., 2007; Ferjani et al., 2008; Ferjani et al., 2011; Ferjani et al., 2012). In addition, gluconeogenesis, the process that produces sucrose (Suc) from triacylglycerol (TAG) in seed storage lipids, is partially suppressed in *fugu5* mutants (Ferjani et al., 2011; Takahashi et al., 2017).

Comparative metabolomics using capillary electrophoresis time-of-flight mass spectrometry (CE-TOF MS) combined with the mathematical theory structural sensitivity analysis unambiguously demonstrated that UDP-Glc pyrophosphorylase (UGPase) is the major target of the inhibitory effect of PPi *in vivo* (Ferjani et al., 2018). Moreover, stomatal closure delay and patterning defects in the *fugu5* background are specifically triggered by excess PPi within guard cells (Asaoka et al., 2019). Notably, specific removal of PPi by the expression of yeast sPPase IPP1 rescued all of the above developmental and metabolic defects. Therefore, most developmental defects triggered by excess PPi can be regarded as the result of metabolic defects, pointing to the importance of metabolic regulation in organogenesis. Despite being produced in all plant cells, the developmental and metabolic targets of PPi are unexpectedly specific, challenging the established concept of the role of housekeeping enzymes (Horiguchi et al., 2012; Tsukaya et al., 2013). Notably, the constitutive expression of $H^+$-PPase promotes growth of plants confronted by a variety of abiotic stresses, rendering this enzyme of great interest to crop breeders (Wang et al., 2016; Schilling et al., 2017).

Epidermal pavement cells in Arabidopsis leaves grow into jigsaw shapes. However, why and how plants make such interlocking puzzle-shaped cells remains under investigation. Several proteins of the Rho guanidine triphosphatase (GTPase) of plants (ROP) family play a key role in shaping pavement cells. Pavement cell morphogenesis is regulated by the signaling of two ROP-mediated pathways with opposing effects on cell expansion

(Fu et al., 2005). In fact, ROP2 activates RIC4 to promote lobe formation (actin) and ROP6 activates RIC1 to promote neck formation (MTs/cellulose) (Fu et al., 2005). Perturbation of the ROP/RIC pathways result in defective puzzle cell formation (Fu et al., 2002; Fu et al., 2005; Fu et al., 2009; Xu et al., 2010; Lin et al., 2013). The phytohormone auxin was proposed to act as an extracellular communication signal, provided that a lobe in one pavement cell is connected to the neck of its neighbor (Fu et al., 2005; Xu et al., 2010; Li et al., 2011; Lin et al., 2015), but this is still debated. The countersignaling of the above two pathways explains the interdigitating separation of the lobing and indenting domains of the cell cortex during the formation of interlocking puzzle-shaped cells. While the above studies unveiled key players in pavement cell patterning, the impact of metabolic regulation on this process is unclear.

Here, we propose PPi homeostasis as a key factor in puzzle cell patterning. We found that while excess PPi ions reduced the complexity of pavement cells, this recovered upon PPi hydrolysis but not Suc supply. Both *in vivo* live imaging of MTs and *in vitro* assays of tubulin polymerization indicated that the inhibitory effect of PPi within pavement cells could be in part explained by aberrant MT dynamics. Finally, excess PPi in the *angustifolia-1* (*an-1*) mutant background led to organs with wavy surfaces and three-dimensional (3D) protrusions, to which a computational model revealed that restriction of cotyledon expansion along the medio-lateral axis is a major contributor. Taken together, our findings suggest that excess PPi has different effects in different leaf tissues, namely the palisade and epidermis.

# MATERIALS AND METHODS

## Plant Materials and Growth Conditions

The wild type (WT) used in this study was Columbia-0 (Col-0), and all other mutants and transgenic lines were in the Col-0 background. The three independent loss-of-function mutant alleles of $H^+$-PPase used in this study, namely *fugu5-1*, *fugu5-2*, and *fugu5-3* have been all previously characterized (Ferjani et al., 2011; Fukuda et al., 2016). In addition, two previously described independent transgenic lines expressing yeast-soluble PPase IPP1 in the *fugu5-1* mutant background (*fugu5-1 AVP1*$_{pro}$*::IPP1*#8-3 and *fugu5-1 AVP1*$_{pro}$*::IPP1*#17-3) were used (Ferjani et al., 2011; Fukuda et al., 2016). Seeds of *icl-2*, *mls-2*, and *pck1-2* mutant lines, which have all been previously characterized in (Eastmond et al., 2000; Cornah et al., 2004; Penfield et al., 2004), respectively, were a kind gift from Professor Ian Graham (The University of York, UK). Seeds were sown on rockwool (Nitto Boseki), watered daily with 0.5 g $L^{-1}$ Hyponex solution and grown under a 16/8 h light/dark cycle with white light from fluorescent lamps at approximately 50 μmol $m^{-2}$ $s^{-1}$ and 22°C. Sterilized seeds were sown on Suc-free Murashige and Skoog (MS) medium (Wako Pure Chemical) or MS medium with 2% (w/v) Suc where indicated, and solidified using 0.2% to 0.5% (w/v) gellan gum (Murashige and Skoog, 1962) to determine the effect of medium composition on phenotype. After sowing the seeds, the MS plates were stored at 4°C in the dark for 3 days. Next, the seedlings were grown in the light (as indicated above) for the indicated periods of time.

## Mutant Genotyping and Double-Mutant Generation

*fugu5-1* was used as a representative mutant allele of $H^+$-PPase (Ferjani et al., 2011). dCAPS primers with one mismatch (fugu5-1-FW: 5′-CAGGCTGGTGTATCAGAGCAT-3′ and fugu5-1-RV: 5′-GACTCAACAGCCATGAGCTT-3′) were used for *fugu5-1* genotyping. PCR amplification followed by *Sph*I digestion was used to distinguish between the WT (134 bp + 18 bp fragments) and *fugu5-1* mutant (152 bp fragment). *icl-2*, *mls-2*, and *pck1-2* were genotyped as described previously (Eastmond et al., 2000; Cornah et al., 2004; Penfield et al., 2004). *fugu5-1*, *icl-2*, *mls-2*, and *pck1-2* plants were crossed with *an-1* mutant, which has been previously characterized (Kim et al., 2002; Minamisawa et al., 2011), to generate double mutants, and the genotypes of the $F_2$ plants were checked using the above PCR-based markers.

## Morphological Observations and Cellular Phenotypic Analyses

Photographs of the gross plant phenotypes at 10 days after sowing (DAS) were obtained using a stereoscopic microscope (M165FC; Leica Microsystems) connected to a charge-coupled device (CCD) camera (DFC300FX; Leica Microsystems) and those at 21 DAS were obtained using a digital camera (D5000 Nikkor lens AF-S Micro Nikkor 60 mm; Nikon). Leaves were fixed in formalin/acetic acid/alcohol and cleared with chloral solution (200 g of chloral hydrate, 20 g of glycerol, and 50 mL of deionized water) to measure leaf area and cell number, as described previously (Tsuge et al., 1996). Whole leaves were observed using a stereoscopic microscope equipped with a CCD camera. Leaf palisade tissue cells were observed and photographed under a light microscope (DM-2500; Leica Microsystems) equipped with Nomarski differential interference contrast optics and a CCD camera. Cell size was determined as mean palisade cell area, determined from a paradermal view, as described previously (Ferjani et al., 2011).

## Observation and Quantitative Analysis of Epidermal Cells

For scanning electron microscopy (SEM), cotyledons were dissected from plants at the indicated growth stages. Samples were fixed overnight in formalin–acetic acid–alcohol (FAA; 4% formalin, 5% acetic acid, and 50% ethanol) at room temperature. The fixed specimens were dehydrated in an ethanol series [50%, 60%, 70%, 80%, 90%, 95%, 99.5%, and 100% (v/v); 60 min per step] and stored overnight in 100% (v/v) ethanol at room temperature. The ethanol was replaced with 3-methylbutyl acetate and the samples were dried in a critical-point dryer (JCPD-5; JEOL), sputter-coated with platinum–palladium using an anion sputter (JFC-1100; JEOL), and examined under an S-3400N SEM (Hitachi), as described previously (Maeda et al., 2014). SEM images of the adaxial side of cotyledons were used to quantify pavement cell complexity. The area and perimeter of

individual pavement cells (25 cells from one cotyledon; six cotyledons total) were measured using ImageJ (version 1.63), and their complexity was quantified by calculating the undulation index (UI) (Thomas et al., 2003) using the following equation (Kürschner, 1997):

$$UI = \frac{P}{2\pi\sqrt{A/\pi}} \quad (1)$$

where UI (dimensionless) is the undulation index, $P$ (μm) is the cell perimeter, and $A$ ($\mu m^2$) is the cell area. Note that increased undulation index means increased pavement cell complexity, and *vice versa*.

## Histological Cross-Sections

For histological cross-sections, cotyledons were dissected (as indicated above), fixed overnight in FAA at room temperature, dehydrated in a graded series of ethanol [50%, 60%, 70%, 80%, 90%, and 95% (v/v); 30 min per step], and stored overnight in 99.5% (v/v) ethanol at room temperature. Next, fixed specimens were embedded in Technovit resin (Kulzer and Co.) according to the manufacturer's instructions and sectioned using a microtome (RM2125 RTS; Leica Microsystems). The sections were stained with toluidine blue and photographed under a microscope (BX-50; Olympus).

## Tubulin Polymerization Assay *in Vitro*

Tubulin polymerization was induced in a solution of 5 mg/mL porcine tubulin (T240, Cytoskeleton, Inc.), 80 mM piperazine-N, N′-bis(2-ethanesulfonic acid) (PIPES), 1 mM ethylene glycol-bis (β-aminoethyl ether)-N,N,N′,N′-tetraacetic acid, 2 mM $MgCl_2$, 10% glycerol, 1 mM GTP, and 0, 1, 5, or 10 mM sodium pyrophosphate tetrabasic decahydrate (Sigma). The 20 μL reaction mixture was transferred into a 384 microplate (#242757, Thermo Scientific), and the absorption at 350 nm was measured every 30 s for 40 min at 37°C using a Multiskan FC plate reader (Thermo Scientific).

## Inhibitor Treatment

Seedlings were grown on Suc-free half-strength MS agar containing 2.3 g/L MS salt mix, 0.5 mg/L nicotinic acid, 0.1 mg/L thiamine HCl, 0.5 mg/L pyridoxine HCl, 0.1 g/L myo-Inositol, and 2 mg/L glycine (pH 5.8) at 22°C under constant light. Four-day-old seedlings were transferred into water containing 2 μM oryzalin (Wako) and incubated at 22°C in the dark for 2 h.

## Confocal Microscopy of Cortical MTs

The epidermis of the cotyledon was observed under an inverted fluorescence microscope (IX83-ZDC, Olympus) fitted with a confocal unit (CSU-W1, Yokogawa), an EM-CCD camera (iXon3-888, Andor), an UPLANSAPO 60× water-immersion objective (NA = 1.20, Olympus), and laser lines set at 488 and 561 nm. Images were acquired using MetaMorph software (Molecular Devices).

## Image Analysis for the Quantification of MT Dynamics

To quantify MT length and density, $z$-stack images at 2 μm intervals were acquired and analyzed using ImageJ software (https://imagej.nih.gov/ij/). The image stacks were projected to single images by maximum intensity projection. A 50 × 50-pixel region was collected from each cell and denoised using the Subtract background (5-pixel diameter) and Despeckle commands. Next, MT regions were extracted and converted to binary images using the Ridge detection plug-in (Steger, 1998). The total area and mean length of MTs were determined using the Analyze particle function.

To quantify the MT growth rate, time-lapse images at 5 s intervals were acquired and analyzed using ImageJ software. To extract the growing region of MTs, the three-frame shifted time-lapse images were subtracted from the original time-lapse images. The subtracted images were denoised by a Gaussian filter ($\sigma = 1$). The trajectory of MT growing regions was analyzed using the TrackMate plugin (Tinevez et al., 2016). The MT growing regions were detected using a LoG detector and filtered by a mean intensity filter. Tracking of MT growing regions was performed using Simple LAP tracker with the Track duration and Track displacement filters. Values of estimated blob diameter, linking max distance, gap-closing max distance, and gap-closing max frame gap were set at 10, 8, 8, 2, respectively.

## Mechanical Buckling Model

We constructed a two-dimensional model in which cell shapes were represented by particles of different sizes with interaction forces. **Figure S10A** shows a schematic representation of the initial geometry of the model, with a reduced number of particles for simplicity. Mesophyll cells are represented by green particles. Pavement and guard cells are shown as pairs of particles in blue and red, respectively, in the initial geometry. An oval covering a pair of particles was defined as the shape of the epidermal cell, as depicted in **Figure 7**.

It was assumed that each particle interacts with its adjacent neighbors. The interaction force was described as follows:

$$\mathbf{F}_{i,j}^{int} = k^{int} f\left(\frac{d_{i,j}}{d_{i,j}^0}\right) \frac{(\mathbf{x}_i - \mathbf{x}_j)}{|\mathbf{x}_i - \mathbf{x}_j|}$$
$$f(\xi) = \begin{cases} \xi^{\lambda} + c\ \xi^{-\lambda} - 1 - c & \text{for } 0 < \xi \leq 1 \\ \lambda(1-c)(\xi - 1) & \text{for } \xi > 1 \end{cases}, \quad (2)$$

where $\mathbf{F}_{i,j}^{int}$ is the force working on the $i$-th particle caused by the interaction between the $i$-th and $j$-th particles. The parameter $k^{int}$ defines the strength of the particle interaction, and $c$ and $\lambda$ determine its dependence on the particle distance. The vector $\mathbf{x}_i$ is a non-dimensional position vector of the center of the $i$-th particle. The distance between the $i$-th and $j$-th particles was calculated as $d_{i,j} = |\mathbf{x}_i - \mathbf{x}_j|$, and its optimal value was defined as $d_{i,j}^0 = r_i + r_j$, where $r_i$ is the radius of the $i$-th particle. The function $f(d_{i,j}/d_{i,j}^0)$ takes positive and negative values when $d_{i,j}/d_{i,j}^0 < 1$ and $d_{i,j}/d_{i,j}^0 > 1$, which correspond to repulsive and

attractive interactions, respectively (**Figure S10B**). The links of adjacent neighbors were determined from the initial geometry and were sustained throughout the calculation. Exceptionally, the guard cells were assumed not to bind to any mesophyll cells. It was also assumed that close approach of cells not defined as adjacent neighbors exerts a repulsive force as follows:

$$\mathbf{F}_{i,j}^{rep} = k^{rep} g\left(\frac{d_{i,j}}{d_{i,j}^{0}}\right)\frac{(\mathbf{x}_i - \mathbf{x}_j)}{|\mathbf{x}_i - \mathbf{x}_j|}$$
$$g(\xi) = \begin{cases} \xi^{\lambda} + c\ \xi^{-\lambda} - 1 - c & \text{for } 0 < \xi \leq 1 \\ 0 & \text{for } \xi > 1. \end{cases} \quad (3)$$

The radii of mesophyll-representing particles were assumed to have a continuous uniform distribution on the interval (0.7, 1.3). Cellular growth was described by increasing the radius of particles by 28% in 40,000 time-steps. The radii of guard cell-representing particles were set at $r_i$= 0.2 and maintained constant.

The pavement cell was represented by two particles of initial radius $r_i$= 0.3. Growth of the pavement cells was described as extension of these cells at constant height (**Figure S10D**). For that purpose, a new particle of radius $r_i$= 0.03 was inserted in the middle of the cell (between two particles) at time $t$ = 1. The radii of new particles were gradually increased to 0.3 in 40,000 time-steps.

The epidermal layer, which is described as the sequence of particles representing pavement and guard cells, was assumed to have bending rigidity to express the smooth surface of the leaf (**Figure S10C**). The force caused by the bending rigidity was introduced as follows:

$$\mathbf{F}_i^{bend} = k^{bend}\left(\frac{\theta_i - \theta_{i-1}}{d_{i,i-1}}\mathbf{n}_{i-1,i} + \frac{\theta_i - \theta_{i+1}}{d_{i,i+1}}\mathbf{n}_{i,i+1}\right), \quad (4)$$

where $\theta_i$ is the angle between the vectors $\mathbf{x}_i$-$\mathbf{x}_{i-1}$ and $\mathbf{x}_{i+1}$-$\mathbf{x}_i$, $k^{bend}$ defines the strength, and $\mathbf{n}_{i-1,i}$ is the unit vector normal to the vector $\mathbf{x}_i$-$\mathbf{x}_{i-1}$ ($\pi$/2-rotation).

Taken together, the sum of the force contributing to movement of the $i$-th particle was assigned as follows:

$$\mathbf{F}_i = \sum_j \mathbf{F}_{i,j}^{int} + \sum_j \mathbf{F}_{i,j}^{rep} + \mathbf{F}_i^{bend}. \quad (5)$$

The motion of the particle was described as follows:

$$\mathbf{x}_i^{t+1} = \mathbf{x}_i^{t} + \gamma^{-1}\mathbf{F}_i \Delta t + \mathbf{z}, \quad (6)$$

where $\gamma^{-1}\boldsymbol{F}_i$ corresponds to the velocity of the $i$-th particle, $\gamma$ corresponds to the friction coefficient, and $t$ represents the time step. The random vector $\mathbf{z}$ was introduced to prevent accidental generation of a gap between particles in the numerical simulations.

The positions of the particles at both ends of the epidermal layer were independent from Eq. (5). The tissue width was controlled by moving the particles outward (WT) or by fixing them at their initial positions (*an-1 fugu5-1* mutant). For the WT, the tissue width was increased by 28% in 40,000 time-steps.

The development of particle behaviors was calculated using C ++. In this study, $c$ = 1.63, $\lambda$ = 2, $k^{rep}$ = 30, $k^{bend}$ = 25, and $\gamma$= 20. Interactions among mesophyll particles were dependent on $k^{int}$ = 30, that between mesophyll and pavement particles on $k^{int}$ = 20, and among epidermal particles on $k^{int}$ = 70.

## Statistical Analysis

To quantify pavement cell phenotype, data from at least five cotyledons (>115 pavement cells) were used to calculate the undulation index, and the values were subjected to statistical analyses using tow-tailed Student's $t$ test with Bonferroni correction, or ANOVA with Tukey's honestly significant difference (HSD) test, KaleidaGraph ver. 4.1.4. To quantify pavement cell neck width and lobe length, 825 measurements from five cotyledons were averaged and the values were subjected to statistical analyses using Student's $t$ test. To quantify MTs length and density, data from 120 pavement cells were averaged and the values were subjected to statistical analyses using ANOVA with Scheffe test. Finally, to quantify the growth rate of cortical MTs, data from 30 cells (80 < MTs/cell) were averaged and subjected to statistical analyses using ANOVA with Scheffe test.

# RESULTS

## Excess PPi Reduced Pavement Cell Complexity

*fugu5* mutants show a strong phenotype in their cotyledons, and so were used as model organs. The adaxial side of mature cotyledons was investigated by SEM, which revealed that pavement cells are less complex in the *fugu5* mutant compared to the WT (**Figures 1A–I**). Quantification of lobe height and neck width revealed that *fugu5-1* has shallower lobes and wider necks than the WT (**Figures 1J, K**). Consistently, the UI in all three *fugu5* alleles was inferior to that of the WT (**Figure 1L**). Importantly, all *fugu5* phenotypes recovered in the *fugu5-1 AVP1*$_{pro}$*::IPP1* lines, in which PPi was specifically removed from the *fugu5* background (**Figures 1A–I, L**).

We reported that there are fewer and larger palisade tissue cells in *fugu5*, the so-called compensation phenotype (Ferjani et al., 2007; Ferjani et al., 2008; Ferjani et al., 2011). Excess PPi inhibits gluconeogenesis during seedling establishment, and compensation is complemented by hydrolyzing PPi or exogenous Suc supply (Ferjani et al., 2011; Ferjani et al., 2012). Unexpectedly, Suc supply did not restore the shape of pavement cells in *fugu5* (**Figures 1M–R**). Together, these results suggest that excess PPi exerts different effects on the palisade and epidermis.

## Excess PPi Altered Pavement Cell Size and Distribution

To gain insight into the effect of excess PPi on pavement cells, SEM images of the adaxial side of the cotyledon were traced and color-coded based on their size (**Figure 2**). WT pavement cells were not only more complex but also significantly larger than those of the *fugu5* mutants (**Figures 2A–D, G**). In addition, small pavement cells in *fugu5* mutants tended to form small clusters with stomata on the adaxial side of cotyledons (compare **Figure**

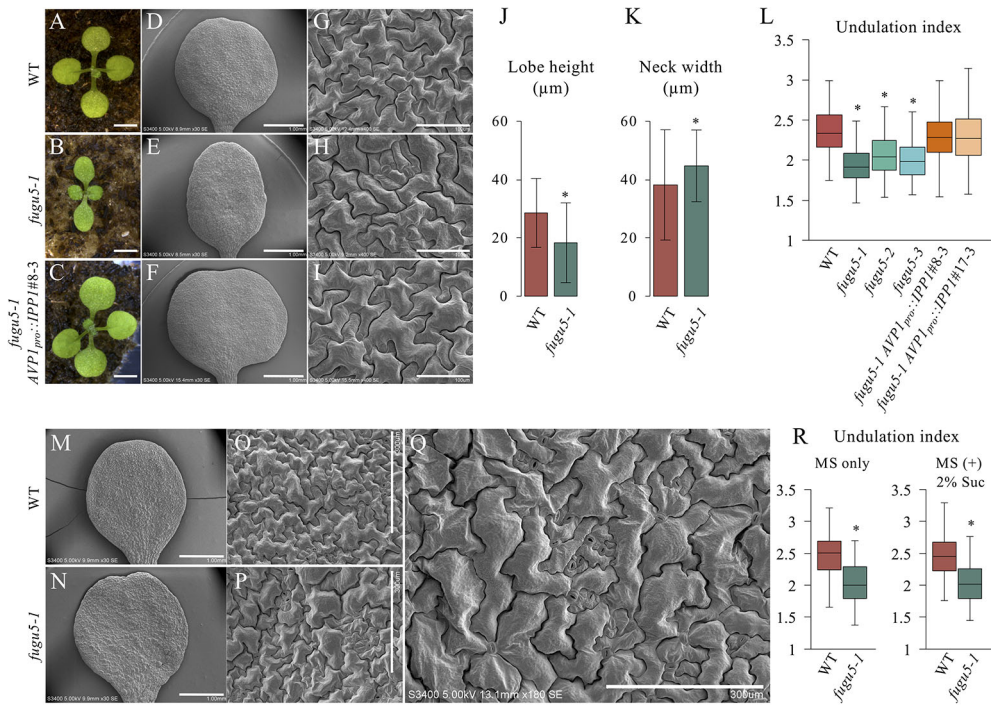


**FIGURE 1 |** Analysis of adaxial pavement cell phenotype. **(A–C)** Photographs of seedlings of the indicated genotypes at 14 DAS. Scale bar, 2 mm. **(D–F)** SEM images of the adaxial side of cotyledons at 25 DAS. Scale bar, 1 mm. **(G–I)** Magnified SEM images of pavement cells on the adaxial side of cotyledons. Scale bar, 100 μm. **(J)** Average neck width and lobe length **(K)** of pavement cells ($n$ = 825 measurements of five cotyledons). Data are means ± standard deviation (SD) at $P < 6.6 \times 10^{-57}$ (lobe), $P < 1.0 \times 10^{-16}$ (neck) between the WT and *fugu5-1* (two-tailed Student's $t$ test). **(L)** Undulation index ($n$ = 150 pavement cells, taken from six cotyledons). Data are means ± SD. Asterisk represents a significant difference at $P < 1.6 \times 10^{-16}$ compared to the WT (two-tailed Student's $t$ test, Bonferroni correction). **(M, N)** SEM images of WT and *fugu5-1* cotyledons, respectively, grown for 20 DAS on MS plates containing 2% sucrose. Scale bar, 1 mm. **(O, P)** SEM images of adaxial side pavement cells of the WT and *fugu5-1* mutant, respectively. Scale bar, 300 μm. **(Q)** Magnified SEM image of *fugu5-1* adaxial pavement cells. Scale bar, 300 μm. **(R)** Undulation index ($n$ = 125 pavement cells from at least five cotyledons). Data are means ± SD. Asterisk represents a significant difference between the two genotypes at $P < 1.0 \times 10^{-20}$ (two-tailed Student's $t$ test). DAS, days after sowing. Suc, sucrose.

**2A** to **Figures 2B–D**). Consistently, stomatal distribution was aberrant in all *fugu5* mutant alleles, in violation of the one-cell-spacing rule (**Figures 2B–D**; see also Asaoka et al., 2019). Pavement cell size and complexity and the stomatal distribution recovered when PPi was specifically removed from the *fugu5-1 AVP1*$_{pro}$*::IPP1*#8-3 and *fugu5-1 AVP1*$_{pro}$*::IPP1*#17-3 lines (**Figures 2E–G**).

## Cotyledon Development and Pavement Cell Phenotype Are Synergistically Enhanced in *an-1 fugu5-1*

ANGUSTIFOLIA (AN) is the sole homolog of CtBP/BARS in Arabidopsis. The CtBP/BARS protein family has diverse functions, intercellular localization, and developmental role in a wide range of land plants (Kim et al., 2002; Minamisawa et al., 2011; Furuya et al., 2018; Hashida et al., 2019). AN regulates the width of Arabidopsis leaves by controlling the polar elongation of leaf cells. In fact, the *an-1* mutant displayed an abnormal arrangement of cortical MTs in leaf cells, which accounted for its abnormal cell shape (Kim et al., 2002). Therefore, AN might regulate the polarity of cell growth by controlling the arrangement of cortical MTs (Kim et al., 2002). The AN-DYRKP complex reportedly regulates the alignment of actin filaments during centripetal nuclear positioning in leaf cells (Iwabuchi et al., 2019). Interestingly, the typical oblong cotyledons of *fugu5-1* mutants are reminiscent of the *an-1* mutant (Kim et al., 2002; Minamisawa et al., 2011). Thus, to gain insight into the genetic interaction between AN and $H^+$-PPase, we constructed *an-1 fugu5-1* double mutants and analyzed their pavement cell phenotype (**Figure 3**). Surprisingly, the *an-1 fugu5-1* double mutants displayed a drastic phenotype, consisting of extremely narrow cotyledons and a wavy epidermis (**Figures 3A–D**). SEM of the adaxial side of *an-1 fugu5-1* cotyledons revealed 3D protrusions whereby twisted pavement cells lifted a stoma (**Figures 3E–J**). In addition, histological cross sections confirmed the above SEM observations and further showed that the wavy-epidermis phenotype occurred on both sides of cotyledons (**Figures 3K–N**; **Figure S1**). Magnified images of histological cross sections confirmed that a pair of guard cells was indeed lifted atop the protruding pavement cells (**Figures 3O, P**).

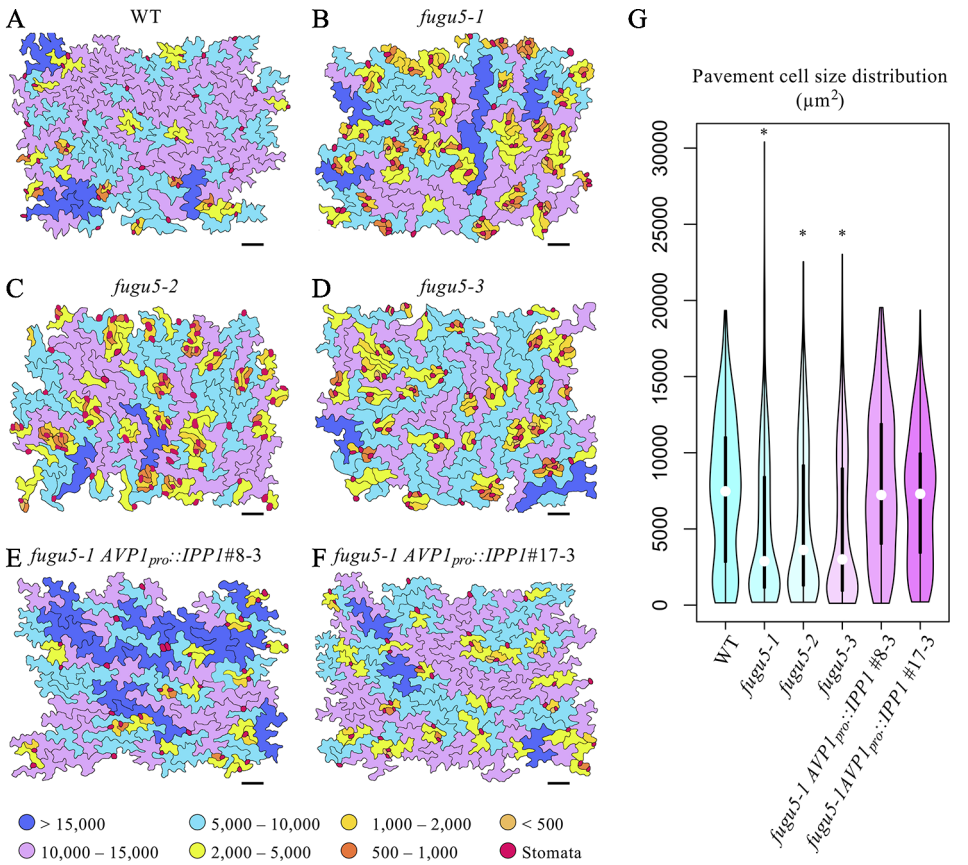


**FIGURE 2 |** Distribution of pavement cell size. **(A–F)** SEM images of adaxial side pavement cells of the cotyledons of WT, *fugu5-1*, *fugu5-2*, *fugu5-3*, *fugu5-1 AVP1*$_{pro}$*::IPP1*#8-3, and *fugu5-1 AVP1*$_{pro}$*::IPP1*#17-3, respectively. Scale bar, 100 μm. Cells were traced and color-coded based on their size (μm$^2$, see color scale chart). Note that the *fugu5* mutants have a disturbed stomatal one-cell-spacing rule. **(G)** Violin plot showing pavement cell size distribution ($n$ > 200 pavement cells from three cotyledons). Data are means ± SD. Asterisk represents a significant difference compared to the WT at $P$ < 0.0001 (ANOVA with Tukey HSD test, KaleidaGraph ver. 4.1.4).

## Cotyledon Expansion Is Severely Restricted Along the Mediolateral Axis in *an-1 fugu5-1*

Based on the above results, we examined the gross morphological phenotype of *an-1 fugu5-1* to evaluate the wavy-epidermis phenotype. We performed a quantitative time-course analysis of various morphological features of cotyledons at three distinct developmental stages. The leaf index (LI = the ratio of leaf blade length to leaf blade width) values indicated that while WT cotyledons were nearly spherical (LI ≒ 0.9–1), those of *fugu5-1* were slightly longer than wide (LI ≒ 1.2), *an-1* were more elongated than *fugu5-1* (LI = 1.3–1.5), and *an-1 fugu5-1* were the most elongated (LI = 1.3–1.7) (**Figure 4A**). The differences among the above genotypes were small at early stages of cotyledon development (5 DAS), but greater at later stages (15 and 25 DAS). Quantification of cotyledon area, length, and width confirmed that *an-1 fugu5-1* cotyledon expansion along the medio-lateral axis was arrested at 15 DAS or earlier (**Figures 4B–D**).

To determine the timing of emergence of the 3D-growth phenotype, whole *an-1 fugu5-1* seedlings were collected at 5 and 10 DAS, fixed, and prepared for SEM. The 3D-growth phenotype was not visible at 5 DAS on the adaxial side of cotyledons (**Figure S2A**). However, at 10 DAS, the adaxial side of *an-1 fugu5-1* cotyledons displayed a wavy texture, typical 3D growth not evident in the parental lines (**Figures S2B, S3**, and **S4**). Together, the above results indicated that the drastic developmental defects in *an-1 fugu5-1* occur at an early post-germinative developmental stage, and that they are enhanced as organ maturation progresses.

## Defects in Pavement Cell Differentiation Are Specifically Triggered by Excess PPi

As mentioned above, while exogenous supply of Suc rescued the *fugu5* palisade tissue phenotype, epidermis developmental defects did not recover unless PPi was specifically removed, such as in the *fugu5-1 AVP1*$_{pro}$*::IPP1*#8-3 and *fugu5-1 AVP1*$_{pro}$*::IPP1*#17-3 lines (**Figure 1**). Consistently, Suc availability did not

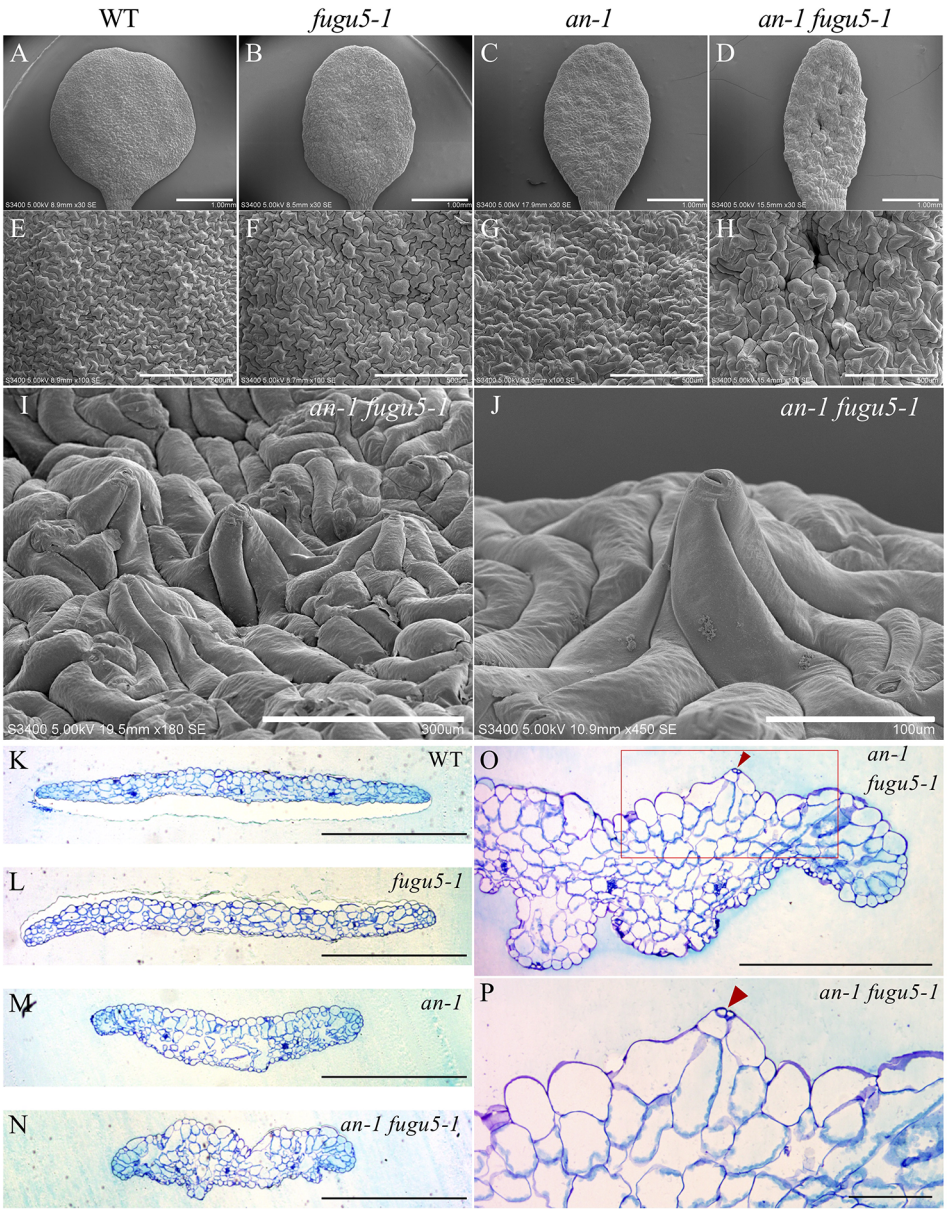


**FIGURE 3 |** Observation of adaxial epidermis developmental defects in *an-1 fugu5-1*. **(A–D)** SEM images of the adaxial side of the cotyledon of the WT, *fugu5-1*, *an-1*, and *an-1 fugu5-1*, respectively, at 25 DAS. Scale bar, 1 mm. **(E–H)** SEM images of the adaxial side pavement cells of the WT, *fugu5-1*, *an-1*, and *an-1 fugu5-1*, respectively. Scale bar, 500 µm. **(I, J)** SEM images of the adaxial side of the cotyledon of *an-1 fugu5-1* showing developmental defects of pavement cells. Scale bar, 300 µm **(I)**, 100 µm **(J)**. **(K–N)** Histological cross sections of the WT and *fugu5-1*, *an-1*, and *an-1 fugu5-1* mutant cotyledons at 25 DAS. Samples were stained with toluidine blue. Scale bar, 1 mm. **(O, P)** Magnified cross-sectional images of *an-1 fugu5-1*. Scale bar, 500 µm. **(O)** Aberrant pavement cells in *an-1 fugu5-1* (red box in (O)), are magnified in **(P)**. Scale bar, 100 µm. Red arrowheads indicate stomata.

affect the *an-1 fugu5-1* phenotypes, as indicated by the formation of 3D protrusions on the adaxial side of *an-1 fugu5-1* grown for 20 days on MS medium containing 2% Suc (**Figures S5, S6**). We previously reported that mutants with defects in gluconeogenesis (*pck1-2*) or the glyoxylate cycle (*icl-2*; *mls-2*), produced less Suc from TAG and exhibited compensation in their cotyledons that recovered upon Suc supply (Takahashi et al., 2017). This led to the conclusion that lowered Suc production, but not excess PPi, is necessary to trigger compensation in palisade tissue (Takahashi et al., 2017). However, the epidermal cells of the above mutant lines were not examined.

The pavement cells of *icl-2*, *mls-2*, and *pck1-2* were indistinguishable from the WT in terms of their UI values (**Figures S7A–G**). Next, we constructed *an-1 icl-2*, *an-1 mls-2*, and *an-1 pck1-2* mutants and evaluated their pavement cell phenotypes. Importantly, while these double mutants displayed

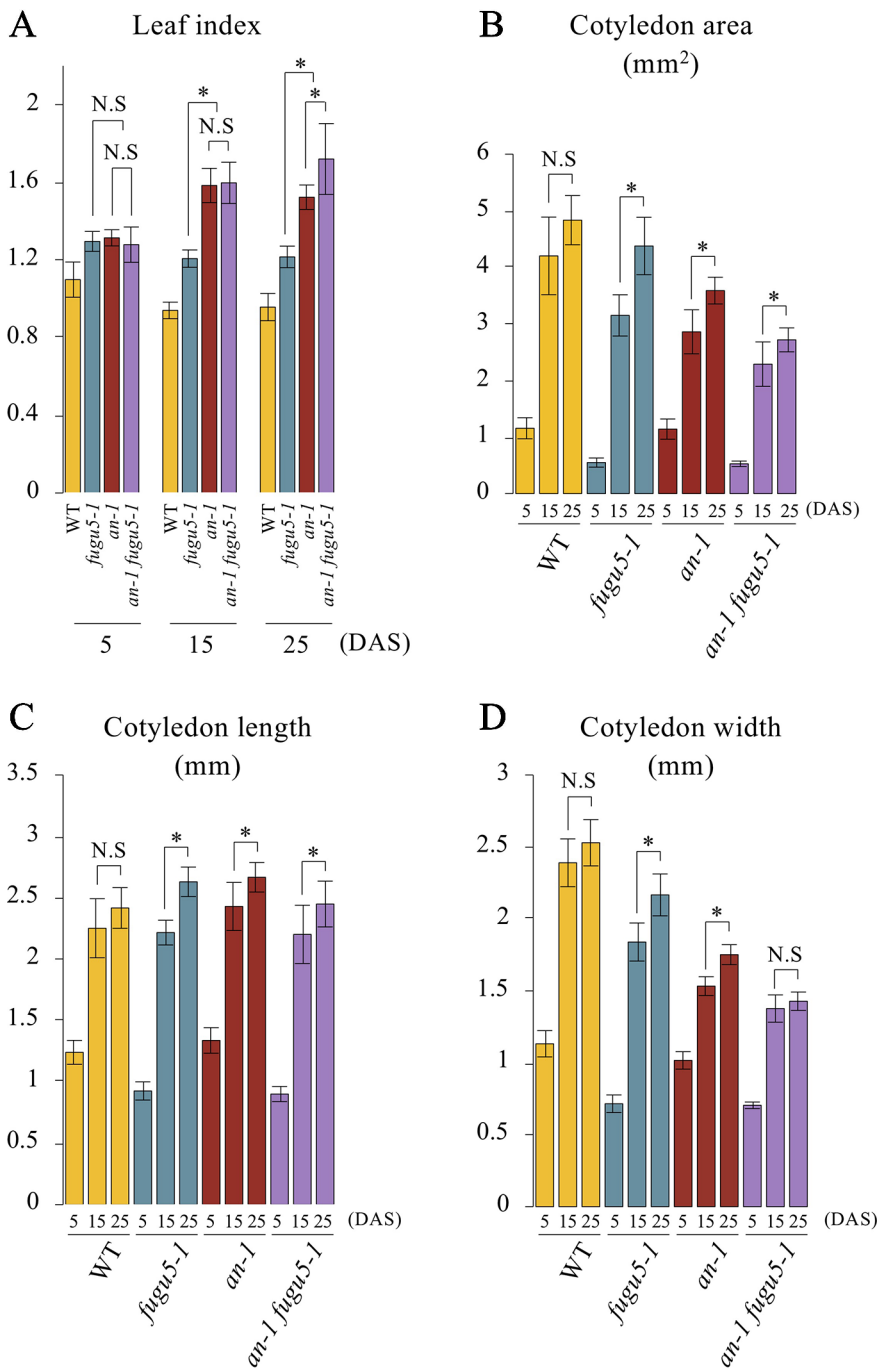


**FIGURE 4 |** Quantitative time-course analysis of cotyledon morphological phenotypes. **(A)** Leaf index was determined for the WT, *fugu5-1*, *an-1*, and *an-1 fugu5-1* at the indicated growth stages. **(B)** The cotyledon area was determined for each genotype at the indicated growth stages. **(C, D)** The cotyledon length and width were determined for each genotype at the indicated growth stages. Values were calculated from SEM images of a time-course analysis of each genotype (**Figure S4**). Data are means ± SD (WT, *fugu5-1*, *an-1*: $n = 6$; *an-1 fugu5-1*: $n = 5$). Asterisk represents a significant difference between genotypes at $P < 0.05$ (two-tailed Student's *t* test). DAS, days after sowing. N.S, not significant.

a severely reduced cotyledon width reminiscent of *an-1 fugu5-1*, they did not exhibit 3D protrusions (**Figures S7H–M**). In addition, the UI values of the above double mutants were comparable to that of *an-1* (**Figure S7N**). Together, these results confirmed that compensation in palisade tissue is due to Suc deficit, while the pavement cell patterning defects, including 3D protrusions, are PPi-dependent. If so, removal of PPi from the *an-1 fugu5-1* double mutant background would be

sufficient to suppress the 3D protrusions. As expected, phenotypic analysis of *an-1 fugu5-1 AVP1$_{pro}$::IPP1*#8-3 confirmed that PPi removal was indeed necessary and sufficient for restoring pavement cell patterning, which mimicked that of the *an-1* single mutant (**Figures 5A–F**). Quantification of the UI further supported these findings (**Figure 5G**).

## The H$^+$-PPase Promotes MT Growth and Genetically Interacts With *AN* in MT Dynamics

Given the axial role of MTs in the control of pavement cell morphogenesis (Fu et al., 2005), the above observations suggested that PPi affects MT dynamics. Thus, we investigated the role of MTs in the regulation of cell morphology in our system. First, we investigated MTs in the epidermis of cotyledons of the *fugu5-1*, *an-1*, and *an-1 fugu5-1* mutants. To observe MTs in living cotyledon epidermis, we crossed *UBQ10::EYFP-TUB6* plants (Sugiyama et al., 2017) with *fugu5-1*, *an-1*, and *an-1 fugu5-1* mutant plants and obtained homozygotes harboring *UBQ10::EYFP-TUB6*. In the pavement cells of young cotyledons from the *fugu5-1*, *an-1*, and *an-1 fugu5-1* mutants, cortical MTs were normally organized and indistinguishable from those in WT cells (**Figure 6A**). To examine the properties of MTs in these mutants, we treated the seedlings with 2 μM oryzalin, which is not sufficient to disrupt cortical MTs in WT plants. As expected, cortical MTs were intact in WT plants even after oryzalin treatment (**Figure 6A**). By contrast, in *fugu5-1*, *an-1*, and *an-1 fugu5-1* pavement cells, cortical MTs were slightly fragmented and sparse (**Figure 6A**). Indeed, the mean length of cortical MTs in *fugu5-1*, *an-1*, and *an-1 fugu5-1* cells was shorter than in WT cells (**Figure 6B**). The mean MT length was shortest in *an-1 fugu5-1* cells (**Figure 6B**). The density of cortical MTs, calculated as the area of EYFP-TUB6-positive pixels, was also lower in *an-1*, and markedly lower in *an-1 fugu5-1* cells, than in WT cells (**Figure 6C**). These results suggested that cortical MTs are more unstable in *fugu5-1* and in *an-1* cells than in WT cells and that genetic interactions of *FUGU5* and *AN* influence MT stability.

We next investigated the dynamics of cortical MTs in young pavement cells. Cortical MTs exhibit growth, shrink, rescue, catastrophe, and stop (Shaw et al., 2003). However, due to the high density of cortical MTs in young cotyledons, we could not analyze the dynamics of MTs. Instead, we examined the net growth rate of cortical MTs by subtracting the time-shifted images from the time-lapse images and capturing the track of their growth (**Movie S1**). Next, we quantified the net growth rate (velocity) of cortical MTs (**Figure 6D**). MT growth rate was slightly lower in *fugu5-1* cells and markedly lower in *an-1 fugu5-1* cells than in WT, again suggesting that *FUGU5* promotes MT growth and genetically interacts with *AN* to influence MT dynamics.

Because *fugu5-1* cells accumulate a high level of PPi in the cytosol (Ferjani et al., 2011), we reasoned that MT dynamics might be directly affected by excess PPi ions in *fugu5-1* mutants. To

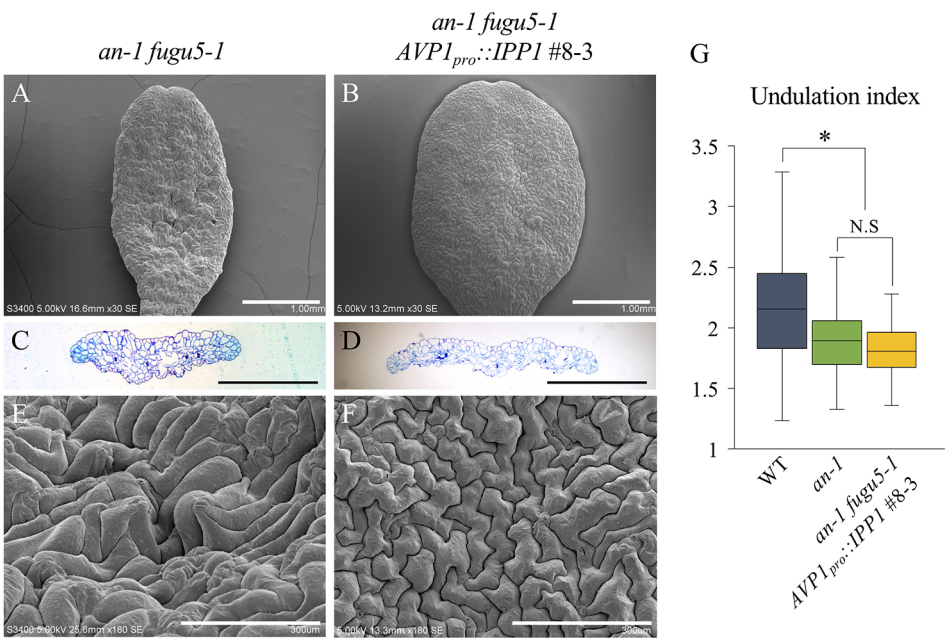


**FIGURE 5 |** Expression of *IPP1* rescued *an-1 fugu5-1* developmental defects. **(A, B)** SEM images of the adaxial side of cotyledons of *an-1 fugu5-1* and *an-1 fugu5-1 AVP1$_{pro}$::IPP1* #8-3 at 25 DAS. Scale bar, 1 mm. **(C, D)** Cotyledon histological cross sections of *an-1 fugu5-1* and *an-1 fugu5-1 AVP1$_{pro}$::IPP1* #8-3 at 25 DAS. Scale bar, 1 mm. **(E, F)** Magnified SEM images of the adaxial side of cotyledons of *an-1 fugu5-1* and *an-1 fugu5-1 AVP1$_{pro}$::IPP1* #8-3 at 25 DAS. Note that *an-1 fugu5-1* developmental defects of the epidermis were recovered by expression of *IPP1*. Scale bar, 300 μm. **(G)** Undulation index of pavement cells ($n$ = 115 pavement cells from at least four cotyledons). Data are means ± SD. Asterisk represents a significant difference compared to the WT at $P < 0.0001$ (ANOVA with Tukey HSD test, KaleidaGraph ver. 4.1.4). DAS, days after sowing. N.S, not significant.

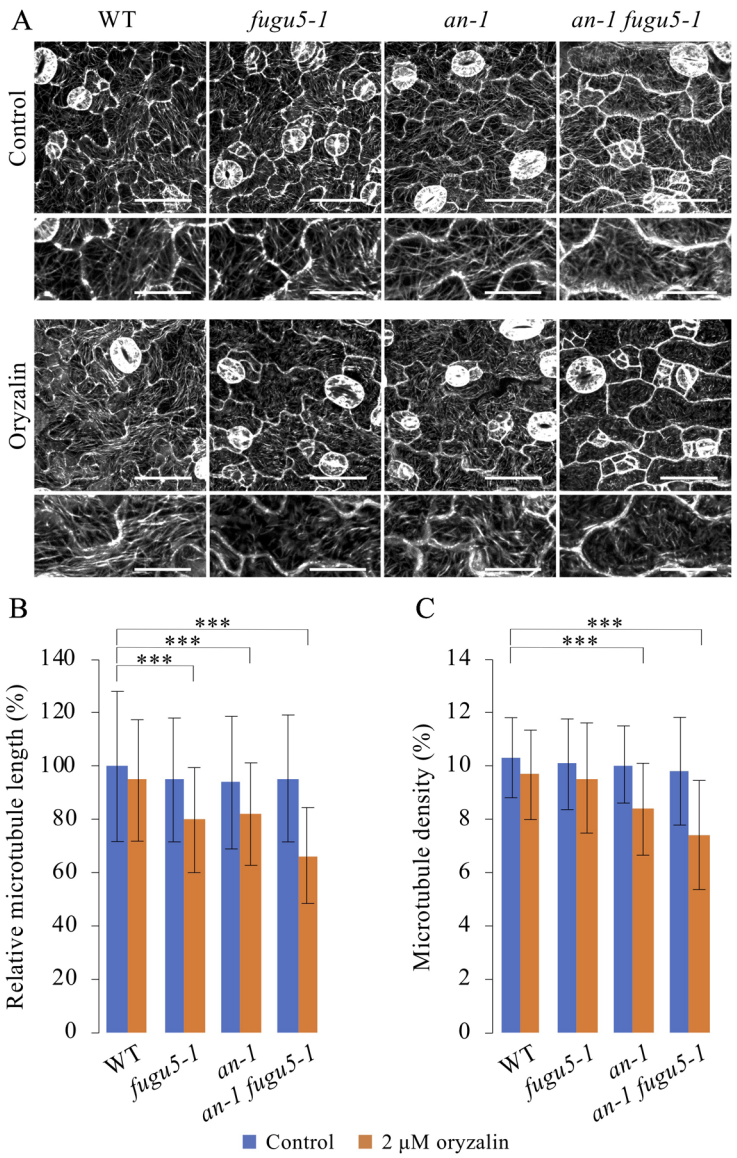


**D**

| Genotype | Velocity ( Mean ± SD, nm $s^{-1}$) |
|---|---|
| WT | 84.8 ± 3.1 |
| *fugu5-1* | 81.5 ± 3.8 *** |
| *an-1* | 85.7 ± 3.1 |
| *an-1 fugu5-1* | 76.2 ± 3.2 *** |

**FIGURE 6 |** Effect of oryzalin on cortical microtubule dynamics in pavement cells. **(A)** Cortical microtubules in the cotyledon epidermis of WT, *fugu5-1*, *an-1*, and *an-1 fugu5-1* plants expressing *UBQ10::EYFP-TUB6*. Four-day-old seedlings were observed without (control) or after 2 h of treatment with 2 µM oryzalin (oryzalin). Bars, 50 µm. 200%-magnified close-ups are shown below each image. Bars, 25 µm. **(B, C)** Microtubule length **(B)** and density **(C)** of the cotyledon epidermis. Data are means ± SD (***$P < 0.001$, ANOVA with Scheffe test, $n = 120$ cells). **(D)** Growth rate of cortical microtubules in the cotyledon epidermis of WT, *fugu5-1*, *an-1*, and *an-1 fugu5-1* plants expressing *UBQ10::EYFP-TUB6*. Measurements were performed on 5-day-old seedlings. Data are means ± SD [***$P < 0.01$ to WT, ANOVA with Scheffe test, $n = 30$ cells (80 < MTs/cell)].

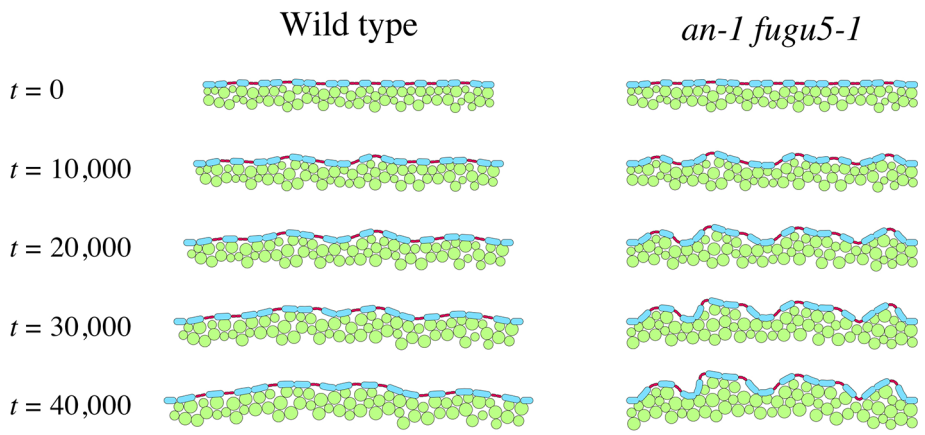


**FIGURE 7 |** Effect of medio-lateral growth limitation on the epidermis. Computational model describing tissue growth of the WT (left panel) and the *an-1 fugu5-1* double mutant (right panel). Green circles denote mesophyll cells, and blue and red ovals represent pavement and guard cells, respectively. Mesophyll and pavement cells increased in size over time. The tissue width increased over time in the WT but remained constant in the *an-1 fugu5-1* double mutant.

assess this possibility, we examined the tubulin polymerization rate *in vitro* in the presence of 1, 5, and 10 mM PPi (**Figure S8**). Consistently, addition of PPi led to a dose-dependent delay of tubulin polymerization (**Figure S8**). Thus, PPi at higher than physiological concentrations may directly interfere with MT dynamics by inhibiting their polymerization (Weiner et al., 1987; Heinonen, 2001). We also noticed that reduced pavement cell complexity and stomatal patterning defects were evident at 4 DAS (**Figure S9**).

## Three-Dimensional Protrusions in *an-1 fugu5-1* Are Caused by Mechanical Buckling Between Adjacent Pavement Cells

To examine the possibility that mechanical buckling of the epidermis generates the undulation seen in *an-1 fugu5-1*, a computational model of the mechanical interaction between cells was developed (**Figure S10**). We applied a model framework in which cells were represented by particles that grow and crowd each other, followed by a change in tissue shape (Takigawa-Imamura et al., 2015; Higaki et al., 2017). In this study, the cross-sectional structure of a part of the upper surface of a cotyledon was considered in a 2D space. The model comprised pavement cells, guard cells, and mesophyll cells, which were assigned abstract round shapes for simplicity (**Figure S10**). Repulsive interaction was assumed between cells to prevent overlaps, and an attractive interaction was assumed so that cell-cell connections were sustained (**Figure S10B**). The epidermal layer was assumed to have bending stiffness. To describe the smooth surface of the cotyledon, the restoring force due to bending stiffness was introduced along the sequence of pavement and guard cells (**Figure S10C**). The growth of mesophyll cells was described by increasing their diameter. The growth of pavement cells was described as horizontal extension at constant height (**Figure S10D**). Guard cell growth was omitted because the change in guard cell width is considered to be limited. In the model guard cells were distinguished from pavement cells in that they were not attached to the mesophyll and are less tall.

**Figure 7** shows tissue growth described using the model (**Movie S2** and **S3**). We assumed that tissue width increases gradually in the WT, whereas it is constant in *an-1 fugu5-1* based on our observations (**Figure 4D**). The computational simulation showed that undulations of the epidermis emerged in *an-1 fugu5-1* but not in the WT as the pavement cells expanded (**Figure 7**), demonstrating that coordination between the growth orientation of the mesophyll and the expansion of the epidermis significantly affects tissue shape. Notably, peaks of undulating epidermis were mostly at the sites of guard cells, suggesting that attachment to the mesophyll suppresses mechanical buckling at the sites of pavement cells.

# DISCUSSION

Cell differentiation is a focus of investigation, given the fundamental role of specialized cell types in the execution of vital functions at the cell, tissue, organ, and organismal levels. Although key transcription factors orchestrate cell fate at the transcriptional level, metabolism has also been proposed to be vital in cell differentiation. We evaluated the link between the role of $H^+$-PPase in PPi homeostasis and its impact on plant development. Here, we present several lines of evidence on the role of metabolism in this process, with emphasis on PPi homeostasis and its multifaceted impact on developmental regulation of plant leaves, tissues, and cells.

## The Pleiotropic, Yet Specific, Targets of PPi in Arabidopsis

PPi is a metabolic byproduct (Heinonen, 2001), whose accumulation at high levels in cells of all kingdoms has been reported not only to inhibit anabolic reactions but also to cause lethality in extreme cases (Ferjani et al., 2011; Ferjani et al., 2014;

Segami et al., 2018). Indeed, the $H^+$-PPase loss-of-function *fugu5* mutants of Arabidopsis exhibit a pleiotropic phenotype, as they fail to reactivate cell cycling in cotyledonary palisade tissue following seed imbibition due to inhibition of gluconeogenesis from seed-stored TAG (Ferjani et al., 2011). The lack of Suc, the sole source of energy in the form of NTPs at a critical stage of the plant life cycle, triggered cellular phenotypes (compensation) and reduced hypocotyl elongation, both of which can be interpreted as metabolism-related developmental defects (Ferjani et al., 2011; Katano et al., 2016; Takahashi et al., 2017). Indeed, the addition of Suc exogenously, or the removal of PPi, restored the above phenotypes.

Moreover, excess PPi in guard cells inhibited stomatal closure, likely by perturbing its metabolism and/or omitting its responsiveness to the phytohormone abscisic acid (Asaoka et al., 2019). Therefore, PPi exerts an inhibitory effect on specific targets within different cell types. In other words, the function of $H^+$-PPase, the major PPi-hydrolyzing enzyme in plant cells (Ferjani et al., 2014; Segami et al., 2018), goes beyond housekeeping, and the breadth and specificity of its contribution warrants investigation.

## Excess PPi Within Pavement Cells Reduces Their Size and Complexity

Given that PPi is produced in all plant cell types, particularly those with an active metabolism, we extended our investigation to the epidermis, a major tissue that wraps the whole plant body. Pavement cells in *fugu5* were less complex in shape, which was not recovered by exogenous Suc supply. This finding suggested that the reduced pavement cell complexity in *fugu5* is not a result of reduced Suc production (due to inhibited gluconeogenesis) but is triggered by excess PPi. In support of this interpretation, pavement cell complexity was restored when PPi was specifically hydrolyzed by the soluble PPase IPP1 in the *fugu5* background (**Figure 1L**). Moreover, pavement cells were as complex as the WT even in mutants with defects in gluconeogenesis (*pck1-2*) or the glyoxylate cycle (*icl-2* and *mls-2*), all of which exhibited severely reduced TAG-Suc conversion during seedling establishment (**Figure S7G**; Takahashi et al., 2017). Taken together, the above results indicated that excess PPi targets likely differ even among adjacent leaf tissues, namely the epidermis and the palisade tissues. We recently reported that UGPase is the major target of the inhibitory effect of excess PPi *in vivo* (Ferjani et al., 2018). At this stage, while the partial inhibition of UGPase activity is the trigger of compensated cell enlargement (CCE) in palisade tissue cells, this metabolic step is not critical for the formation of interlocking puzzle-shaped pavement cells in epidermal tissue. Finally, given that pavement cells were significantly smaller in the *fugu5* mutants, this indicates that CCE does not occur in the epidermis and that the reduced UI could be a result of restricted cell growth (**Figure 2G**).

## Potential Effect of Excess PPi on MT Dynamics

In plant leaves PPi is located predominantly in the cytosol at 0.2–0.3 mM (Weiner et al., 1987; Heinonen, 2001). We reported previously that the PPi level in *fugu5* was ~ 2.5-fold higher than in the WT (Ferjani et al., 2011), which is roughly estimated to be 0.5–0.75 mM. In this study, PPi at 1–10 mM reduced the tubulin polymerization rate in a concentration-dependent manner *in vitro* (**Figure S8**); these concentrations are higher than those reported *in vivo*. To address this discrepancy, we live imaged cortical MTs in the *fugu5* background. Based on the UI values, we expected to find clear differences in the arrangement of cortical MTs and/or their dynamics. However, the relative MT length and density were unexpectedly comparable between *fugu5* and the WT. By contrast, following oryzalin treatment at low concentrations, *fugu5* cortical MTs were slightly fragmented (reduced relative MT length) and sparse (reduced relative MT density), while the WT MTs were intact. Therefore, the increase in the PPi level in *fugu5* did not affect the arrangement but interfered with MT dynamics *in vivo*. This was supported by the fact that reduced MT length, density, and growth rate (velocity) in *fugu5* were significantly enhanced in *an-1 fugu5*. Together, the above results suggest that FUGU5 promotes MT growth and that it genetically interacts with AN to influence MT dynamics. However, the mechanism underlying this interaction is unclear and should be the focus of future research.

As mentioned above, several proteins of the ROP family together with the plant hormone auxin have been proposed to play a key role in shaping pavement cells, in which MT dynamics are of central importance. So, what are the implications of the above observations on *fugu5* MTs within the cell? MT polymerization rates *in vivo* are approximately 5- to 10-fold higher than those measured using purified tubulin *in vitro* (Cassimeris, 1993). Provided that the excess PPi level in *fugu5* partially inhibits gluconeogenesis and *de novo* protein synthesis *in vivo* (Ferjani et al., 2011), MT-associated proteins or other factors could be targets of suppression by PPi, even at concentrations lower than those used in the *in vitro* assay. If true, this would provide a plausible explanation for the *in vivo versus in vitro* discrepancy, but more research on the effects of PPi on MT-associated proteins is needed to resolve this issue.

## Perturbation of Leaf Flatness Due to Mechanical Buckling Between Adjacent Pavement Cells

Striking phenotypic similarities exist between *an-1* and *fugu5-1* mutant cotyledons. In fact, both single mutants exhibited oblong cotyledons, yet this phenotypic trait is controlled by different mechanisms. *fugu5-1* cotyledons are oblong because the cell number along their medio-lateral axis does not increase during postembryonic development (Ferjani et al., 2011). By contrast, *an-1* cotyledons are oblong due to restricted polar cell expansion along their medio-lateral axis and are thick due to excessive elongation of mesophyll cells along the adaxial-abaxial axis (Kim et al., 2002; Minamisawa et al., 2011). Here, pavement cell phenotyping revealed that in addition to the above similarities at the organ level, these two mutants shared a decreased complexity of pavement cells. Henceforth, *an-1 fugu5-1* double mutants were analyzed to evaluate whether their genetic interaction influences pavement cells.

Interestingly, live imaging of MTs revealed that their dynamics in *an-1 fugu5-1* are more severely affected than their respective

parental lines (**Figure 6**). The most striking phenotype of *an-1 fugu5-1* cotyledons was their wavy surface, enhanced thickness (**Figure 3**), and higher cell density per unit length (**Figure S11**). The wavy surface was restored upon PPi removal in *an-1 fugu5-1 AVP1$_{pro}$::IPP1*#8-3, which had notably wider cotyledons (**Figure 5**). Therefore, alleviation of the restricted organ expansion along the medio-lateral axis is sufficient to re-establish the smooth organ surface. Consistent with this, in our computational model, restriction of organ widening alone reproduced the 3D-protruding cells and the wavy surface characteristic of *an-1 fugu5-1*. The above interpretation highlights the loss of growth coordination along two major axes and the consequences on organ global morphology, yet it does not take into account the individual and/or local response of pavement cells. Hence, the twisting of pavement cells observed around stomata (**Figure 3J**) may reflect a mechanical conflict between guard cells and pavement cells, whereby MTs responsiveness to stress is different (Hervieux et al., 2017). Although single mutations in various genes reportedly disrupt leaf flattening, the combination of *an-1* and *fugu5-1* mutations indicated that this important trait can be altered by severely restricting cell proliferation and expansion along the leaf medio-lateral axis, adding to our knowledge of the genetic regulation of this important trait.

Taken together, our results provide valuable information on the effect of the accumulation of unhydrolyzed PPi on plant development *in vivo*. While PPi quantification and visualization are challenging (Gdula et al., 1998; Heinonen, 2001; and references therein), excess PPi resulted in visible phenotypes, such as compensation in the palisade tissue and defects in epidermal cell differentiation. Henceforth, we will focus on verifying how PPi exerts differential effects on different cell types, and whether the PPi concentration varies among plant tissues and cell types. Ultimately, we aim to identify key cellular components and/or critical metabolic steps, an important topic considering the universality of PPi homeostasis in all kingdoms of life.

## DATA AVAILABILITY STATEMENT

The raw data supporting the conclusions of this article will be made available by the authors, without undue reservation, to any qualified researcher.

## AUTHOR CONTRIBUTIONS

SG performed the experiments, analyzed the data, and wrote the article. YO performed live imaging of MT dynamics, and analyzed the data. HT-I performed computational modeling of the mechanical buckling, and analyzed the data. HT directed and funded the study. AF conceived the project, designed and funded the study, and wrote the paper with input from all co-authors. All authors read and approved the final manuscript.

## FUNDING

This work was supported by the Ministry of Education, Culture, Sports, Science and Technology of Japan [Grant-in-Aid for Encouragement of Young Scientists (B) (21770036 to AF); Grant-in-Aid for Scientific Research (B) (16H04803 to AF; 18H02469 to YO); Grant-in-Aid for Scientific Research on Innovative Areas (25113002 to AF and HT; 16H06280 and 19H05677 to YO); Grant-in-Aid for Scientific Research on Innovative Areas (18H05487 to AF); Grant-in-Aid for Scientific Research on Innovative Areas (19H05672 to HT); Grant-in-Aid for Scientific Research (C) (26520207 to HT-I)]; BIO-NEXT project from Okazaki Institute for Integrative Bioscience (KK and HT); and The Naito Foundation.

## ACKNOWLEDGMENTS

We thank Prof. Ian Graham (The University of York) and Dr. Alison Gilday (The University of York) for providing *icl-2*, *mls-2* and *pck1-2* mutant seeds. We thank Dr. Yuki Sugiyama (The University of Tokyo/National Institute of Genetics) for providing *UBQ10::EYFP-TUB6* line seeds. We thank Prof. Seisuke Kimura (Kyoto Sangyo University), Dr. Hokuto Nakayama (Kyoto Sangyo University), for their great support while starting up histological cross-sectioning protocols. We thank Dr. Akitoshi Iwamoto (Tokyo Gakugei University) for his expert advices on scanning electron microscopy while starting up this project. We also thank Dr. Kensuke Kawade (NIBB/Exploratory Research Center on Life and Living Systems (ExCELLS)) for his critical reading of the manuscript.

## SUPPLEMENTARY MATERIAL

The Supplementary Material for this article can be found online at: https://www.frontiersin.org/articles/10.3389/fpls.2020.00031/full#supplementary-material

## REFERENCES

Asaoka, M., Segami, S., Ferjani, A., and Maeshima, M. (2016). Contribution of PPi-hydrolyzing function of vacuolar $H^+$-pyrophosphatase in vegetative growth of *Arabidopsis*: evidenced by expression of uncoupling mutated enzymes. *Front. Plant Sci.* 7, 415. doi: 10.3389/fpls.2016.00415

Asaoka, M., Inoue, S. I., Gunji, S., Kinoshita, T., Maeshima, M., Tsukaya, H., et al. (2019). Excess pyrophosphate within guard cells delays stomatal closure. *Plant Cell Physiol.* 60, 875–887. doi: 10.1093/pcp/pcz002

Cassimeris, L. (1993). Regulation of microtubule dynamic instability. *Cell Motil. Cytoskeleton* 26, 275–281. doi: 10.1002/cm.970260402

Chen, J., Brevet, A., Fromant, M., Lévêque, F., Schmitter, J. M., Blanquet, S., et al. (1990). Pyrophosphatase is essential for growth of *Escherichia coli*. *J. Bacteriol.* 172, 5686–5689. doi: 10.1128/JB.172.10.5686-5689.1990

Cornah, J. E., Germain, V., Ward, J. L., Beale, M. H., and Smith, S. M. (2004). Lipid utilization, gluconeogenesis, and seedling growth in *Arabidopsis* mutants lacking the glyoxylate cycle enzyme malate synthase. *J. Biol. Chem.* 279, 42916–42923. doi: 10.1074/jbc.M407380200

Donnelly, P. M., Bonetta, D., Tsukaya, H., Dengler, R. E., and Dengler, N. G. (1999). Cell cycling and cell enlargement in developing leaves of *Arabidopsis*. *Dev. Biol.* 215, 407–419. doi: 10.1006/dbio.1999.9443

Eastmond, P. J., Germain, V., Lange, P. R., Bryce, J. H., Smith, S. M., and Graham, I. A. (2000). Postgerminative growth and lipid catabolism in oilseeds lacking the glyoxylate cycle. *Proc. Natl. Acad. Sci. U.S.A.* 97, 5669–5674. doi: 10.1073/pnas.97.10.5669

Ferjani, A., Horiguchi, G., Yano, S., and Tsukaya, H. (2007). Analysis of leaf development in *fugu* mutants of *Arabidopsis* reveals three compensation modes that modulate cell expansion in determinate organs. *Plant Physiol.* 144, 989–999. doi: 10.1104/pp.107.099325

Ferjani, A., Yano, S., Horiguchi, G., and Tsukaya, H. (2008). *Control of leaf morphogenesis by long- and short-distance signaling: Differentiation of leaves into sun or shade types and compensated cell enlargement. Plant Cell Monographs: Plant Growth Signaling*. Eds. L. Bögre and G. T. S. Beemster (Springer-Verlag Berlin Heidelberg), 47–62. doi: 10.1007/7089_2007_148

Ferjani, A., Segami, S., Horiguchi, G., Muto, Y., Maeshima, M., and Tsukaya, H. (2011). Keep an eye on PPi: the vacuolar-type $H^+$-pyrophosphatase regulates postgerminative development in *Arabidopsis*. *Plant Cell* 2, 2895–2908. doi: 10.1105/tpc.111.085415

Ferjani, A., Segami, S., Horiguchi, G., Sakata, A., Maeshima, M., and Tsukaya, H. (2012). Regulation of pyrophosphate levels by $H^+$-PPase is central for proper resumption of early plant development. *Plant Signal. Behav.* 7, 38–42. doi: 10.4161/psb.7.1.18573

Ferjani, A., Segami, S., Asaoka, M., and Maeshima, M. (2014). "Regulation of PPi levels through vacuolar membrane $H^+$-pyrophosphatase," in *Progress in Botany*, vol. 75 . Eds. U. Lüttge, W. Beyschlag and J. Cushman (Heidelberg: Springer-Verlag), 145–166. doi: 10.1007/978-3-642-38797-5_5

Ferjani, A., Kawade, K., Asaoka, M., Oikawa, A., Okada, T., Mochizuki, A., et al. (2018). Pyrophosphate inhibits gluconeogenesis by restricting UDP-glucose formation. *In vivo. Sci. Rep.* 8, 14696. doi: 10.1038/s41598-018-32894-1

Fu, Y., Li, H., and Yang, Z. (2002). The ROP2 GTPase controls the formation of cortical fine F-actin and the early phase of directional cell expansion during *Arabidopsis* organogenesis. *Plant Cell* 14, 777–794. doi: 10.1105/tpc.001537

Fu, Y., Gu, Y., Zheng, Z., Wasteneys, G., and Yang, Z. (2005). *Arabidopsis* interdigitating cell growth requires two antagonistic pathways with opposing action on cell morphogenesis. *Cell* 120, 687–700. doi: 10.1016/j.cell.2004.12.026

Fu, Y., Xu, T., Zhu, L., Wen, M., and Yang, Z. (2009). A ROP GTPase signaling pathway controls cortical microtubule ordering and cell expansion in *Arabidopsis*. *Curr. Biol.* 19, 1827–1832. doi: 10.1016/j.cub.2009.08.052

Fukuda, M., Segami, S., Tomoyama, T., Asaoka, M., Nakanishi, Y., Gunji, S., et al. (2016). Lack of $H^+$-pyrophosphatase prompts developmental damage in *Arabidopsis* leaves on ammonia-free culture medium. *Front. Plant Sci.* 7, 819. doi: 10.3389/fpls.2016.00819

Furuya, T., Hattori, K., Kimori, Y., Ishida, S., Nishihama, R., Kohchi, T., et al. (2018). ANGUSTIFOLIA contributes to the regulation of three-dimensional morphogenesis in the liverwort *Marchantia polymorpha*. *Development* 145 (18), dev161398. doi: 10.1242/dev.161398

Gdula, D. A., Sandaltzopoulos, R., Tsukiyama, T., Ossipow, V., and Wu, C. (1998). Inorganic pyrophosphatase is a component of the *Drosophila* nucleosome remodeling factor complex. *Genes Dev.* 12, 3206–3216. doi: 10.1101/gad.12.20.3206

Hashida, Y., Takeuchi, K., Abiru, T., Yabe, N., Nagase, H., Hattori, K., et al. (2019). Two *ANGUSTIFOLIA* genes regulate gametophore and sporophyte development in *Physcomitrella patens*. *Plant J.* doi: 10.1111/tpj.14592

Heinonen, J. K. (2001). *Biological Role of Inorganic Pyrophosphate* (London: Kluwer Academic Publishers). doi: 10.1007/978-1-4615-1433-6

Hervieux, N., Tsugawa, S., Fruleux, A., Dumond, M., Routier-Kierzkowska, A. L., Komatsuzaki, T., et al. (2017). Mechanical shielding of rapidly growing cells buffers growth heterogeneity and contributes to organ shape reproducibility. *Curr. Biol.* 27, 3468–3479. doi: 10.1016/j.cub.2017.10.033

Higaki, T., Takigawa-Imamura, H., Akita, K., Kutsuna, N., Kobayashi, R., Hasezawa, S., et al. (2017). Exogenous cellulase switches cell interdigitation to cell elongation in an RIC1-dependent manner in *Arabidopsis thaliana* cotyledon pavement cells. *Plant Cell Physiol.* 58, 106–119. doi: 10.1093/pcp/pcw183

Horiguchi, G., Van Lijsebettens, M., Candela, H., Micol, J. L., and Tsukaya, H. (2012). Ribosomes and translation in plant developmental control. *Plant Sci.*, 191–192, 24–34. doi: 10.1016/j.plantsci.2012.04.008

Iwabuchi, K., Ohnishi, H., Tamura, K., Fukao, Y., Furuya, T., Hattori, K., et al. (2019). ANGUSTIFOLIA regulates actin filament alignment for nuclear positioning in leaves. *Plant Physiol.* 179, 233–247. doi: 10.1104/pp.18.01150

Kürschner, W. M. (1997). The anatomical diversity of recent and fossil leaves of the durmast oak (*Quercus petraea* Lieblein/*Q. pseudocastanea* Goeppert)—implications for their use as biosensors of palaeoatmospheric $CO_2$ levels. *Rev. Palaeobot. Palynol.* 96, 1–30. doi: 10.1016/S0034-6667(96)00051-6

Katano, M., Takahashi, K., Hirano, T., Kazama, Y., Abe, T., Tsukaya, H., et al. (2016). Suppressor screen and phenotype analyses revealed an emerging role of the monofunctional peroxisomal enoyl-CoA hydratase 2 in compensated cell enlargement. *Front. Plant Sci.* 7, 132. doi: 10.3389/fpls.2016.00132

Kim, G. T., Shoda, K., Tsuge, T., Cho, K. H., Uchimiya, H., Yokoyama, R., et al. (2002). The *ANGUSTIFOLIA* gene of *Arabidopsis*, a plant *CtBP* gene, regulates leaf-cell expansion, the arrangement of cortical microtubules in leaf cells and expression of a gene involved in cell-wall formation. *EMBO J.* 21, 1267–1279. doi: 10.1093/emboj/21.6.1267

Klomp, L. W., de Koning, T. J., Malingré, H. E., van Beurden, E. A., Brink, M., Opdam, F. L., et al. (2000). Molecular characterization of 3-phosphoglycerate dehydrogenase deficiency–a neurometabolic disorder associated with reduced L-serine biosynthesis. *Am. J. Hum. Genet.* 67, 1389–1399. doi: 10.1086/316886

Ko, K. M., Lee, W., Yu, J. R., and Ahnn, J. (2007). PYP-1, inorganic pyrophosphatase, is required for larval development and intestinal function in *C. elegans*. *FEBS Lett.* 581, 5445–5453. doi: 10.1016/j.febslet.2007.10.047

Li, H., Lin, D., Dhonukshe, P., Nagawa, S., Chen, D., Friml, J., et al. (2011). Phosphorylation switch modulates the interdigitated pattern of PIN1 localization and cell expansion in *Arabidopsis* leaf epidermis. *Cell Res.* 21, 970–978. doi: 10.1038/cr.2011.49

Lin, D., Cao, L., Zhou, Z., Zhu, L., Ehrhardt, D., Yang, Z., et al. (2013). Rho GTPase signaling activates microtubule severing to promote microtubule ordering in *Arabidopsis*. *Curr. Biol.* 23, 290–297. doi: 10.1016/j.cub.2013.01.022

Lin, D., Ren, H., and Fu, Y. (2015). ROP GTPase-mediated auxin signaling regulates pavement cell interdigitation in *Arabidopsis thaliana*. *J. Integr. Plant Biol.* 57, 31–39. doi: 10.1111/jipb.12281

Lundin, M., Baltscheffsky, H., and Ronne, H. (1991). Yeast *PPA2* gene encodes a mitochondrial inorganic pyrophosphatase that is essential for mitochondrial function. *J. Biol. Chem.* 266, 12168–12172.

Maeda, S., Gunji, S., Hanai, K., Hirano, T., Kazama, Y., Ohbayashi, I., et al. (2014). The conflict between cell proliferation and expansion primarily affects stem organogenesis in *Arabidopsis*. *Plant Cell Physiol.* 55, 1994–2007. doi: 10.1093/pcp/pcu131

Minamisawa, N., Sato, M., Cho, K. H., Ueno, H., Takechi, K., Kajikawa, M., et al. (2011). ANGUSTIFOLIA, a plant homolog of CtBP/BARS, functions outside the nucleus. *Plant J.* 68, 788–799. doi: 10.1111/j.1365-313X.2011.04731.x

Murashige, T., and Skoog, F. (1962). A revised medium for rapid growth and bioassays with tobacco tissue cultures. *Physiol. Plant* 15, 473–497. doi: 10.1111/j.1399-3054.1962.tb08052.x

Pancholi, V., and Chhatwal, G. S. (2003). Housekeeping enzymes as virulence factors for pathogens. *Int. J. Med. Microbiol.* 293, 391–401. doi: 10.1078/1438-4221-00283

Penfield, S., Rylott, E. L., Gilday, A. D., Graham, S., Larson, T. R., and Graham, I. A. (2004). Reserve mobilization in the *Arabidopsis* endosperm fuels hypocotyl elongation in the dark, is independent of abscisic acid, and requires PHOSPHOENOLPYRUVATE CARBOXYKINASE1. *Plant Cell* 16, 2705–2718. doi: 10.1105/tpc.104.024711

Schilling, R. K., Tester, M., Marschner, P., Plett, D. C., and Roy, S. J. (2017). AVP1: One Protein, Many Roles. *Trends Plant Sci.* 22, 154–162. doi: 10.1016/j.tplants.2016.11.012

Segami, S., Tomoyama, T., Sakamoto, S., Gunji, S., Fukuda, M., Kinoshita, S., et al. (2018). Vacuolar $H^+$-pyrophosphatase and cytosolic soluble pyrophosphatases cooperatively regulate pyrophosphate levels in *Arabidopsis thaliana*. *Plant Cell* 30, 1040–1061. doi: 10.1105/tpc.17.00911

Shaw, S. L., Kamyar, R., and Ehrhardt, D. W. (2003). Sustained microtubule treadmilling in *Arabidopsis* cortical arrays. *Science* 300, 1715–1718. doi: 10.1126/science.1083529

Steger, C. (1998). An unbiased detector of curvilinear structures. *IEEE Trans. Pattern Anal. Mach. Intell.* 20, pp.113–pp.125. doi: 10.1109/34.659930

Sugiyama, Y., Wakazaki, M., Toyooka, K., Fukuda, H., and Oda, Y. (2017). A novel plasma membrane-anchored protein regulates xylem cell-wall deposition

through microtubule-dependent lateral inhibition of Rho GTPase domains. *Curr. Biol.* 27, 2522–2528. doi: 10.1016/j.cub.2017.06.059

Takahashi, K., Morimoto, R., Tabeta, H., Asaoka, M., Ishida, M., Maeshima, M., et al. (2017). Compensated cell enlargement in *fugu5* is specifically triggered by lowered sucrose production from seed storage lipids. *Plant Cell Physiol.* 58, 668–678. doi: 10.1093/pcp/pcx021

Takigawa-Imamura, H., Morita, R., Iwaki, T., Tsuji, T., and Yoshikawa, K. (2015). Tooth germ invagination from cell-cell interaction: Working hypothesis on mechanical instability. *J. Theor. Biol.* 382, 284–291. doi: 10.1016/j.jtbi.2015.07.006

Thomas, P. W., Woodward, F. I., and Quick, W. P. (2003). Systematic irradiance signalling in tobacco. *New Phytol.* 161, 193–198. doi: 10.1046/j.1469-8137.2003.00954.x

Tinevez, J. Y., Perry, N., Schindelin, J., Hoopes, G. M., Reynolds, G. D., Laplantine, E., et al. (2016). TrackMate: An open and extensible platform for single-particle tracking. *Methods* 115, 80–90. doi: 10.1016/j.ymeth.2016.09.016

Tsuge, T., Tsukaya, H., and Uchimiya, H. (1996). Two independent and polarized processes of cell elongation regulate leaf blade expansion in *Arabidopsis thaliana* (L.) Heynh. *Development* 122, 1589–1600.

Tsukaya, H., Byrne, M. E., Horiguchi, G., Sugiyama, M., Van Lijsebettens, M., and Lenhard, M. (2013). How do 'housekeeping' genes control organogenesis?–Unexpected new findings on the role of housekeeping genes in cell and organ differentiation. *J. Plant Res.* 126, 3–15. doi: 10.1007/s10265-012-0518-2

Wang, X., Wang, H., Liu, S., Ferjani, A., Li, J., Yan, J., et al. (2016). Genetic variation in *ZmVPP1* contributes to drought tolerance in maize seedlings. *Nat. Genet.* 48, 1233–1241. doi: 10.1038/ng.3636

Weiner, H., Stitt, M., and Heldt, H. W. (1987). Subcellular compartmentation of pyrophosphate and alkaline pyrophosphatase in leaves. *Biochim. Biophys. Acta* 893, 13–21. doi: 10.1016/0005-2728(87)90143-5

Xu, T., Wen, M., Nagawa, S., Fu, Y., Chen, J. G., Wu, M. J., et al. (2010). Cell surface- and rho GTPase-based auxin signaling controls cellular interdigitation in *Arabidopsis*. *Cell* 143, 99–110. doi: 10.1016/j.cell.2010.09.003

**Conflict of Interest:** The authors declare that the research was conducted in the absence of any commercial or financial relationships that could be construed as a potential conflict of interest.

frontiers in Plant Science

ORIGINAL RESEARCH
published: 17 March 2020
doi: 10.3389/fpls.2020.00273

# Improved Yield and Photosynthate Partitioning in AVP1 Expressing Wheat (*Triticum aestivum*) Plants

*Kamesh C. Regmi[1†], Kalenahalli Yogendra[2†], Júlia Gomes Farias[1], Lin Li[1], Raju Kandel[1], Umesh P. Yadav[3], Shengbo Sha[2], Christine Trittermann[2], Laura Short[2], Jessey George[2], John Evers[3], Darren Plett[2], Brian G. Ayre[3], Stuart John Roy[2*] and Roberto A. Gaxiola[1*]*

[1] School of Life Sciences, Arizona State University, Tempe, AZ, United States, [2] Australian Centre for Plant Functional Genomics, The University of Adelaide, Adelaide, SA, Australia, [3] Department of Biological Sciences, BioDiscovery Institute, University of North Texas, Denton, TX, United States

OPEN ACCESS

**Edited by:**
Jose Roman Perez-Castineira, University of Seville, Spain

**Reviewed by:**
Ramón Serrano, Universitat Politècnica de València, Spain
Eduardo Blumwald, University of California, Davis, United States

***Correspondence:**
Stuart John Roy
stuart.roy@adelaide.edu.au
Roberto A. Gaxiola
roberto.gaxiola@asu.edu

[†] These authors have contributed equally to this work

**Specialty section:**
This article was submitted to Plant Metabolism and Chemodiversity, a section of the journal Frontiers in Plant Science

**Received:** 22 November 2019
**Accepted:** 21 February 2020
**Published:** 17 March 2020

**Citation:**
Regmi KC, Yogendra K, Gomes Farias J, Li L, Kandel R, Yadav UP, Sha S, Trittermann C, Short L, George J, Evers J, Plett D, Ayre BG, Roy SJ and Gaxiola RA (2020) Improved Yield and Photosynthate Partitioning in AVP1 Expressing Wheat (Triticum aestivum) Plants. Front. Plant Sci. 11:273. doi: 10.3389/fpls.2020.00273

A fundamental factor to improve crop productivity involves the optimization of reduced carbon translocation from source to sink tissues. Here, we present data consistent with the positive effect that the expression of the *Arabidopsis thaliana* $H^+$-PPase (*AVP1*) has on reduced carbon partitioning and yield increases in wheat. Immunohistochemical localization of $H^+$-PPases (TaVP) in spring wheat Bobwhite L. revealed the presence of this conserved enzyme in wheat vasculature and sink tissues. Of note, immunogold imaging showed a plasma membrane localization of TaVP in sieve element- companion cell complexes of Bobwhite source leaves. These data together with the distribution patterns of a fluorescent tracer and [U$^{14}$C]-sucrose are consistent with an apoplasmic phloem-loading model in wheat. Interestingly, $^{14}$C-labeling experiments provided evidence for enhanced carbon partitioning between shoots and roots, and between flag leaves and milk stage kernels in AVP1 expressing Bobwhite lines. In keeping, there is a significant yield improvement triggered by the expression of *AVP1* in these lines. Green house and field grown transgenic wheat expressing *AVP1* also produced higher grain yield and number of seeds per plant, and exhibited an increase in root biomass when compared to null segregants. Another agriculturally desirable phenotype showed by AVP1 Bobwhite plants is a robust establishment of seedlings.

**Keywords: wheat (*Triticum aestivum*), $H^+$-PPase (proton pyrophosphatase), reduced carbon partition, yield, PPi metabolism**

## INTRODUCTION

According to the Food and Agriculture Organization of the United Nations, wheat (*Triticum aestivum* L.) is the largest primary commodity in the world, cultivated on more land area than any other commercial crop (~220 Mha) with global production of over 700 million tons, a total global annual export value of close to US$50 billion, and accounts for a fifth of our total available dietary calories[1]. Given that plant productivity is dependent on how organic carbon and other nutrients are acquired and partitioned (Khadilkar et al., 2015), it is imperative that we mechanistically dissect this complex process in important crops like wheat, and identify rate-limiting steps to improve yield (Ainsworth and Bush, 2010; Braun et al., 2013; Dasgupta et al., 2014; Yadav et al., 2015).

[1] http://www.fao.org/faostat/en/#data

The synthesis of primary photosynthate, sucrose (Suc), in wheat starts with carbon fixation into triose phosphates in the photoautotrophic mesophyll cells in source leaves. It is then either transiently stored in chloroplasts and vacuoles, or is transported via the phloem to heterotrophic sink tissues and/or used as the substrate for starch reserves in the grain endosperm (Trethewey and Smith, 2000; Bahaji et al., 2014; Griffiths et al., 2016; Kumar et al., 2018). Wheat leaf blades have the characteristic parallel venation pattern of a monocot, with intermediate and small sized veins, together called the minor veins, constituting the collection phloem that channel into the major veins or the transport phloem (Fritz et al., 1983; Russell and Evert, 1985). Transfer of the photoassimilate from the collection phloem to the transport phloem occurs via the transverse veins that connect adjacent parallel veins (Kuo et al., 1972). None of the monocots studied thus far have intermediary cells in the phloem that are typical of plants that employ the polymer trapping mechanism (Esau, 1969; Rennie and Turgeon, 2009; Turgeon, 2010; Braun et al., 2013). Early anatomical (Kuo et al., 1974) and micro-autoradiography studies (Altus and Canny, 1982, 1985) suggested a passive symplasmic path for sucrose loading in wheat source leaves.

However, more recent studies implicate an active apoplasmic phloem loading strategy in wheat leaves. In a eudicot like arabidopsis, the role of Group 2 SUT proteins in apoplasmic loading is well-established (Truernit and Sauer, 1995; Stadler and Sauer, 1996; Bürkle et al., 1998; Wright et al., 2003; Srivastava et al., 2008; Ayre, 2011). Aoki et al. (2002) isolated three single-copy homeologous sucrose symporter genes *TaSUT1A*, *1B*, and *1D*, encoding 98% identical proteins, and later found that while the *TaSUT1* encoded transcripts were localized in the companion cells in source leaves, the *TaSUT1* epitopes localized to the plasma membrane of sieve elements in large, intermediate, and minor veins in source leaves (Aoki et al., 2004). Furthermore, upon feeding symplasmic tracer dye 6-Carboxyfluorescein diacetate, Aoki et al. (2002) also found that the sieve element companion cell (SE-CC) complexes of minor veins in source leaves were symplasmically isolated, suggesting a predominantly apoplasmic phloem loading strategy in wheat.

The consensus model for apoplasmic phloem loading in wheat would therefore hold that, sucrose first passively diffuses via plasmodesmata from the mesophyll cells (Giaquinta, 1983) to the phloem parenchyma cells through intervening layers of bundle sheath and mestome sheath cells (Kuo et al., 1974). Next, SWEET proteins, with 59 putative members identified in the wheat genome (Gao et al., 2018), facilitate the efflux of sucrose from the phloem parenchyma cells into the apoplasmic space (Chen et al., 2010, 2012) prior to being imported into the CCs by Sucrose/$H^+$ symporters encoded by *TaSUT1* (Aoki et al., 2002). The proton motive force (pmf) required for this symport is provided by plasma membrane (PM)-localized P-type ATPases (DeWitt and Sussman, 1995), the ATP for whose operation is expected to be supplied by the oxidation of some of the symported Suc hydrolyzed via the PPi-dependent Sucrose Synthase (SUS) pathway (Geigenberger et al., 1993; Nolte and Koch, 1993; Lerchl et al., 1995; Gaxiola et al., 2012, 2016b; Khadilkar et al., 2015; Pizzio et al., 2015), where source of PPi has been proposed to be a PM-localized type I $H^+$-PPase functioning as a PPi Synthase (Gaxiola et al., 2012; Pizzio et al., 2015; Scholz-Starke et al., 2019). It is worth emphasizing that there is no report in the literature providing data regarding the type I $H^+$-PPase localization in wheat.

Type I $H^+$-PPases are found to be ubiquitously expressed, with highest levels observed in the collection, transport, and unloading phloem as well as sink tissues (Mitsuda et al., 2001; Li et al., 2005; Paez-Valencia et al., 2011; Segami et al., 2014; Khadilkar et al., 2015; Kriegel et al., 2015; Pizzio et al., 2015; Regmi et al., 2015). In active sink tissues, the type I $H^+$-PPases at the tonoplast are hypothesized to hydrolyze PPi – a byproduct of numerous anabolic reactions – to drive these biosynthetic reactions forward, while simultaneously using the free energy of PPi hydrolysis to energize the rapidly expanding vacuoles (Shiratake et al., 1997; Maeshima, 2000; Heinonen, 2001; Viotti et al., 2013; Regmi et al., 2015). Increased abundance and or activity in these tissues is expected to have a positive effect in sink strength by favoring biosynthetic reactions (Gaxiola et al., 2016b).

Under a favorable proton gradient, as is found in the phloem apoplasmic interface, a PM-localized type I $H^+$-PPase (Long et al., 1995; Ratajczak et al., 1999; Langhans et al., 2001; Paez-Valencia et al., 2011; Regmi et al., 2015) has been proposed on thermodynamic (Davies et al., 1997) and structural grounds (Regmi et al., 2016), to function in reverse as a PPi-synthase (Khadilkar et al., 2015; Pizzio et al., 2015). In fact, the bidirectionality of plant membrane-bound type I $H^+$-PPases has been shown \y (Scholz-Starke et al., 2019) and suggested biochemically (Façanha and de Meis, 1998; Marsh et al., 2000).

In contrast to arabidopsis, whose type I $H^+$-PPase is encoded by a single copy gene, *Arabidopsis thaliana* $H^+$-PPase (*AVP1*), the hexaploid wheat genome harbors three phylogenetically distinct gene paralogs encoding $H^+$-PPases – *TaVP1, TaVP2*, and *TaVP3* – identified through extensive expressed sequence tag (EST) data mining and mapped to homoeologous chromosome groups 1 and 7 (Wang et al., 2009). The amino acid alignment of the consensus polypeptides encoded by these paralogs against 23 type I $H^+$-PPase orthologous sequences from barley, maize, rice, sorghum, tobacco and arabidopsis showed high sequence homology, including that of a highly conserved $D(X)_7KXE$ motif (Wang et al., 2009). More importantly, Wang et al. (2009) used RT-PCR and dbEST surveys to examine the tissue-specific expression levels of the *TaVP*-specific transcripts and found that *TaVP3* was only expressed in developing seeds (Wang et al., 2009). *TaVP2* was found to be primarily expressed in shoot tissues, including 10-days-old seedling leaves, flag leaves, inflorescences, and uppermost internodes, but not in germinating seeds (Wang et al., 2009). *TaVP1*, which is phylogenetically more similar to *TaVP2* than *TaVP3*, was expressed more broadly, including germinating seeds, and particularly at the highest level in roots (Wang et al., 2009).

Given the versatility of type I $H^+$-PPases and their utility as powerful yet simple biotechnological tools (Gaxiola et al., 2012, 2016a; Schilling et al., 2017, and references therein), we constitutively expressed *AVP1* under the control of a maize *Ubiquitin* (*UBI*) promoter in the spring wheat cultivar Bobwhite L., to understand its role in carbon partitioning. An immunohistochemical survey of various tissues showed that the

wheat $H^+$-PPase orthologs – TaVPs – depicted basal expression in all tissues, with maximal localization levels in the sink tissues, and the collection, transport, and unloading phloem. Using $^{14}CO_2$ labeling, it was found that vegetative wheat plants partition most of the photosynthates to heterotrophic roots during the dark period, and that the delivery into roots of *UBI:AVP1* transgenic lines was prolonged in the dark period compared to controls. Moreover, during the reproductive phase, $^{14}CO_2$ labeling of the terminal source flag leaves showed that the transgenic lines accumulated more $^{14}C$ signal in the kernels. We found that TaVPs were localized in vacuoles of the scutellar epithelial cells and at the plasma membrane of SE-CC complexes using immunogold labeling. The implications of this vacuolar localization are discussed. Overall, we show evidence consistent with the expression of AVP1 augmenting carbon partitioning from source to sinks in wheat plants by either empowering the flux of carbon via phloem loading and transport, or by strengthening the sinks, which ultimately translates into improved yield.

# MATERIALS AND METHODS

## Generation of Transgenic Wheat Expressing *AVP1*

The coding sequence of *AVP1* (At1g15690) was amplified from the *Arabidopsis thaliana* ecotype Col-0 cDNA and ligated into a *pENTR/D-TOPO* (Invitrogen, Carlsbad, CA, United States) entry vector. The cloned insert verified by sequencing and then subcloned into the *pMDC32* plant transformation vector (Curtis and Grossniklaus, 2003) using the Gateway LR recombination reaction (Invitrogen, Carlsbad, CA, United States). Transgenic wheat cv. Bob white expressing *pUBI:AtAVP1* was developed by biolistic transformation (Sanford et al., 1995; Vasil and Vasil, 2006). Wheat calli were developed from immature embryos (1.0–1.5 mm in length, semitransparent) and were used for bombardment. Microprojectile bombardment was performed using the Biolistic PDS-1000/He Particle Delivery System (Bio-Rad, Hercules, CA, United States). Genes of interest and selectable markers are present as intact plasmids or DNA fragments and used to coat the microprojectiles prior to shooting (Kovalchuk et al., 2009). A total of 29 independent transgenic calli were initially transformed, from which 11 independent lines were regenerated. Regenerated plants were transplanted into soil and grown under normal greenhouse conditions using standard agronomic practices to maturity. Two independent lines which showed one transgene copy number and a stable phenotype were characterized further. From the above process, an AVP1 Null line was selected as a control. AVP1 transgene copy number (**Supplementary Figure S1C**) and expression level were determined by qPCR (**Supplementary Figure S1D**).

## Total Protein Extraction

Approximately 300 mg of wheat leaves were immediately ground into a fine powder with liquid $N_2$ and transferred in approximately 200 μL aliquots to screw-cap Eppendorf tubes. To each tube, 1 mL of 10% (v/v) trichloroacetic acid in −20°C acetone was added, and proteins were allowed to precipitate overnight at −20°C. The samples were centrifuged at 10000 *g* for 30 min at 4°C, followed by removal of the supernatant. The pellet was washed with −20°C acetone containing 0·07% β-mercaptoethanol, vortexed and centrifuged at 10000 *g* for 10 min at 4°C. The washing, vortexing, and centrifugation steps were repeated four more times. After the final centrifugation step, the supernatant was removed and the pellet dried in a tabletop vacuum for approximately 30 min. Total protein was solubilized by adding Laemmli's buffer to the pellet. Half of the samples were boiled in a water bath for better mobility and separation of membrane proteins on SDS–PAGE. Prior to storage at −80°C, the mixture was vortexed, and centrifuged at 5000 *g* for 5 min at 4°C three times.

## Western Blot

The solubilized protein extracts from wheat leaves were then run on a 10% SDS–polyacrylamide gel, transferred to a PVDF membrane, blocked with 5% (w/v) non-fat dry milk in Tris–buffered saline with 0·01% Tween-20 (TBST) and probed with 1:1000 dilution of polyclonal sera generated against $H^+$-PPase specific CTKAADVGADLVGKIE motif overnight at 4°C. After washing in TBST, the membrane was developed using a Bio-rad Alkaline Phosphatase Immun-Blot® Colorimetric Assay kit (Bio-Rad Inc., United States[2]) according to the manufacturer's instructions.

## Genotyping and Expression Profiling of Transgenic Lines

Plants were genotyped by PCR to confirm the presence/absence of *AVP1*. Genomic DNA was isolated using CTAB (cetyl trimethylammonium bromide) method (Porebski et al., 1997). Oligos were designed from the open reading frame and used in PCR reaction (**Supplementary Table S1**). The PCR cycling condition is followed by initial denaturation at 98°C–5 min (1 cycle), denaturation at 98°C–5 s, annealing at 65°C–30 s & extension at 72°C–1 min (a total of 34 cycle), and final extension at 72°C–10 min (1 cycle). PCR positive lines were identified after running 1% agarose gel (**Supplementary Figure S1A**).

Total RNA was extracted from leaf tissue using TRIzol reagent (Invitrogen) and a Direct-zol RNA MiniPrep Kit (Zymo Research, CA, United States) with an on-column DNase treatment. A 2.0 μg aliquot of purified RNA was used for cDNA synthesis using a High-Capacity cDNA Reverse Transcription Kit (Applied Biosystems, Victoria, Australia) and random oligo primers supplied in the kit (**Supplementary Figure S1B**). The expression of *AVP1*, as well as the control gene *TaGAPDH* (EU022331), were determined using Quantitative real-time PCR with gene specific primers (**Supplementary Table S1**). Quantitative real-time PCR was performed with KAPA SYBR® Fast qRT-PCR kit Master Mix (Kapa Biosystems, Wilmington, United States) and amplification was monitored in real-time on a QuantStudioTM 6 Flex Real-Time PCR System (Applied Biosystems, Foster City, United States). Reference gene stability was assessed with the geNorm function of

[2]www.bio-rad.com

qBASE + software using default settings (Hellemans et al., 2007). Gene expression relative to the control gene was calculated (**Supplementary Figures S1 C,D**) using equation from Hellemans et al. (2007). Values are means of 3–5 biological replicates and 3 technical replicates.

## Growth Chamber Conditions

Seeds of *AVP1 Null*, *AVP1-1* and *AVP1-2* were soaked in 30% (v/v) commercial bleach with 0.01% Tween-20 for 5 min, washed several times with water, imbibed in water for 8 h, sown on moist filter paper pads in petri dishes, and incubated at room temperature in the dark for 2 days for germination. The germinated seeds were directly sown on Sunshine® potting mix in pots or on Turface® artificial soil in 50mL falcon tubes and grown in growth room under 12: 12: light: dark regime. The composition of the liquid fertilizer used to nourish the plants was obtained from Shavrukov et al. (2012). Photoperiod of the chamber was set up as 12 h light/12 h dark at 25°C (EGC C6 Environmental Growth Chambers), providing the light of intensity 80 μmol $m^{-2}$ $s^{-1}$ photosynthetic photon flux.

## Light Microscopy and Immunohistochemistry

Source leaves, leaf sheaths, flag leaves, crown roots, peduncle, spikelets, and basal rachis were excised from *AVP1 Null*, *AVP1-1*, and *AVP1-2* plants. The tissues excised processed for paraplast embedding, sectioning, and immunolabeling with anti-AVP1 rabbit polyclonal antibodies according to Regmi et al. (2015). For semi-quantitative immunohistochemistry on source leaves, the 3-3′-Diaminobenzidine development time was kept at 30s for both control and transgenic lines. Images were acquired with either a Zeiss Axioskop or Nikon Eclipe E600 (Keck Bioimaging Center, ASU) light microscope.

## High-Pressure Freezing, Immunogold Labeling, and Transmission Electron Microscopy

*Arabidopsis thaliana* $H^+$-PPase *Null* seeds were germinated for 2 days under sterile conditions, dissected under 150 mM sucrose to expose the scutellar epidermis, and along with *AVP1 Null* source leaves were high-pressure frozen, freeze-substituted, embedded in LR White, ultrathin sectioned, immunogold labeled with anti-AVP1 polyclonal antibody, and imaged according to Regmi et al. (2015). Quantification of gold labeling comparing the number of 10 nm gold particles at either the PM of SEs or CCs, or the vacuoles of CCs from nine independent micrographs from three independently grown plants was done through *post hoc* pairwise comparisons using Tukey HSD.

## Pulse Chase Experiment With $^{14}CO_2$ on 10-Days-Old Bobwhite and Transgenic Seedlings

Approximately 4 h into the photoperiod, 48 10-days-old wheat seedlings (12 per Bobwhite and each transgenic line, i.e., 3 plants per line per time point) were placed in a large transparent acrylic box under a halogen lamp emitting 80 μmol $m^{-2}$ $s^{-1}$ photosynthetic photon flux. A 1-h pulse of $^{14}CO_2$ (80 μCi total $^{14}C$ activity) was supplied to the box by mixing radioactive $NaH^{14}CO_3$ (specific activity: 56 mCi/mmol, concentration: 2.0 mCi/mL; MP Biomedicals, LLC) with 80% (v/v) lactic acid. Samples for radioactivity measurement (shoot and root) were weighed and collected in 20 ml scintillation vials contained 3 ml 80%(v/v) methanol. After incubating in methanol for 3 days, 0.5 mL commercial bleach (6.0% Sodium Hypochlorite) was added to each vial and incubated for 1 day. Next, 17.5 ml ECOLUME()$^{TM}$ liquid scintillation cocktail (MP Biomedicals, LLC) was added to each vial to determine the $^{14}C$ radioactivity of the solution fractions. Samples were incubated at room temperature with agitation at 50 rpm for all the incubation steps. Disintegrations per minute (DPM) was read by Beckman Multi-Purpose Scintillation Counter Ls6500 with a counting time of 2 min as described in Yadav et al. (2017). Any tissue harvesting in the dark period were performed under a green light source. The experiment was run twice independently – and 3 plants per line per time point were used. The experiment was run twice independently – and 3 plants per line per time point were used.

## Flag Leaf $^{14}CO_2$ Labeling

Approximately 4 h into the photoperiod, the flag leaves from *AVP1 Null* and transgenic lines (Zadoks stage 75) from the main shoot were individually sealed in large transparent zip-lock bags under a halogen lamp emitting 80 μmol $m^{-2}$ $s^{-1}$ photosynthetic photon flux. 3 days later, 8 seeds from apical, central, and basal parts of the spikelet, and five disks ∼6mm from central part of flag leaf, and two 1.5 cm peduncle pieces from each half were measured for $^{14}C$ activity in using the protocol described in Yadav et al. (2019). $n$ = 5 plants for *AVP1 Null*, 4 plants per transgenic line.

## Evaluating Grain Set Index

The distribution of floret fertility within each spike of the main culm was mapped from the apex of the spike to the base, according to Rawson et al. (1996). Spikes were harvested during the milk stage. Established CMU (Chiang Mai University) (Rerkasem et al., 1989) and the LAC (Lumle Agricultural Research Centre) methods (Sthapit, 1988) were used to calculate the grain set index for the assessment of spike fertility:

CMU GSI (%) = (C/20) × 100, where C is the number of grains per primary and secondary floret of ten central spikelet. $n$ = 3 plants per line.

LAC GSI (%) = B × 100/A, where A is the number of competent florets per spike, and B is the number of grains per spike. $n$ = 4 plants per line.

The spikelets were analyzed as diagrammed in **Supplementary Figure S2 C**. Naming of florets within the spikelets followed (González et al., 2003).

## Evaluating Wheat Seed Germination and Post-germinative Growth

Three wheat lines (*AVP1 Null*, *AVP1-1,* and *AVP1-2*) were evaluated from seed germination until early seedling stage (96 h).

Seeds were surface sterilized, imbibed in sterile water for 24 h in the dark, and 20 seeds per line were placed in petri dishes in the dark for 24 h. After this period, three seedlings per line were dissected to measure total fresh weight and fresh weights of coleoptile and root at 48, 72, 80, and 96 h after hydration, in addition to imaging 2 seedlings per line with a Nikon D5100 camera. At 80 h, root hairs on seminal roots were imaged using an Olympus SZX7 stereo microscope.

## Evaluation of Transgenic Wheat Under Greenhouse Conditions

Evenly sized seeds of transgenic and null segregant plants were imbibed in reverse osmosis (RO) water at room temperature for 4 h. Seeds were then placed in the dark at 4 °C for 3 days prior to transplanting into pots (diameter 150 mm and height of 150 mm). Pots were filled with a 2.0 L of cocopeat soil (South Australian Research and Development Institute (SARDI), Adelaide, Australia). Plants were grown in The Plant Accelerator (Australian Plant Phenomics Facility, University of Adelaide, Australia, latitude: −34.971353 & longitude: 138.639933) using standard agronomic practices for water management, as well as fertilizer and disease treatments. The plants were grown under natural light conditions, in a temperature-controlled greenhouse with a 22 °C daytime and 15 °C night temperatures. Measurements of plant yield data including, grain yield per plant, number of seeds per plant, head number and thousand-grain weight were taken at the time of harvesting. Phenotypic data was statistically analyzed using a one-way ANOVA and Dunnett's test in PRISM 7 for Windows ver. 7.00 (Graphpad Software Inc., CA, United States) to determine means that were significantly different at a probability level of $P \leq 0.05$.

## Evaluation of Transgenic Wheat Under Field Conditions

*Arabidopsis thaliana* $H^+$-PPase transgenic wheat lines were grown under field trials at Glenthorne Farm, South Australia (Lat −35.056933°, Long 135.556251°). Two independent transformation events expressing *AVP1* (*AVP1-1,* and *AVP1-2* $T_5$ generation) and AVP1 null segregates were sown. Plants were sown at a depth of 3 cm in 1 m × 0.7 M plots. Transgenic lines were sown in the middle two rows of the plot, with the outer plot rows a non-transgenic barley, cv Fielder, buffer to reduce edge effects and to stop pollen flow to neighboring plots. The barley cultivar Fielder was sown across the top and bottom of the plot (20 cm in width) to mitigate edge effects and to reduce pollen flow between the plots. An 8 cm gap was left between each plot, with a 50 cm gap left between every 5th plot to allow access. Plots were sown in a randomized block design and bird-netting placed over the trial to avoid damaged caused by birds.

Planting took place on the 25th of May 2017. High Phosophate Super Phosphate (RICHGRO, Jandakot, Western Australia, Australia) and Soluble Nitrogen Urea (RICHGRO) were applied at germination (2 weeks after sowing) at a rate of 50g $m^2$ and 20g $m^2$, respectively. Snail bait (Blitzem Snail & Slug Pellets, Yates, Auckland, New Zealand) was also applied at a rate of 5 g $m^2$. Irrigation was supplied by rainfall, with 435 mm of rain in the growing season. At 4 weeks, establishment counts were taken of the plots. The development of the plants was observed weekly until grain harvest. Harvesting of the plant material took place on the 11th and 12th of December 2017. At harvest, total plant biomass, tiller number, the grain number, head number and grain yield per plant were recorded. $n = 15$ independent plants per line.

## Root Morphology Analysis of Transgenic Wheat Lines

Wheat transgenic lines, *AVP1* and null plants were grown in 2.5 L standard pots (150mm diameter, 190mm height) contains 2.0L Profile Porous Ceramic (PPC) Greens Grade soil (Profile Products LLC, Buffalo Grove, IL, United States) with 10 g of Osmocote (Scotts Australia Pty Ltd., Bella Vista, NSW, Australia) and watered with aqueous liquid fertilizer (1 g/L) (FertPro Australia Pty Ltd., Dinmore, QLD, Australia) every 10 days after germination. The transgenic and null wheat lines were sampled at either 3 or 6 weeks after sowing for root morphology analysis or for root biomass, respectively. Scanning of root material was found to accurately measure root length up to 3 weeks of growth (Data not shown). At three weeks, the soil was carefully removed from the plant's root and root diameter, length, number, surface area and volume determined using a flatbed scanner (Epson, EU-88, Suwa, Japan) and RootGraph image analysis system (Cai et al., 2015). The imaging parameters used were as follows: image resolution: 600 dpi; image type: gray level; width (cm): 30; length (cm): 40 (Melino et al., 2015). After 6 weeks, roots were removed from the soil by gentle washing, dried in an oven at 80°C for 72 h, and dry weight determined. $n = 5$ independent plants per line.

# RESULTS

## Immunohistochemical Localization of $H^+$-PPases in Various Wheat Tissues

In both eudicot arabidopsis and monocot rice, $H^+$-PPases are basally expressed in all tissues, but also localized at both the sink tissues like root and shoot apical meristems (RAM and SAM, respectively), leaf primordia, and the phloem in source leaves (Li et al., 2005; Regmi et al., 2015). In view of this, we conducted a comparative study to examine the tissue-specific localization pattern of the TaVPs (*Triticum aestivum* vacuolar $H^+$-PPases) in various wheat tissues. Previously characterized antiserum (Li et al., 2005; Park et al., 2005) generated against the highly conserved CTKAADVGADLVGKIE motif (Rea et al., 1992) in $H^+$-PPases was used in this experiment, that showed a distinct band at the expected size (∼80 kDa) when immunoblotted against the total protein extracted from wheat seedlings (**Figure 1A**). Of note, higher molecular weight protein aggregates are recognized by the antibody if samples are not boiled. Consistent with previous outcomes (Li et al., 2005; Regmi et al., 2015), we found that TaVPs were localized in either the actively growing sink tissues or in the vasculature (**Figure 1**). Specifically, active sink tissues of wheat such as the SAM (**Figure 1D**, asterisk), leaf primordia (**Figure 1D**, arrows), lateral root primordium (**Figure 1H**), displayed the strongest

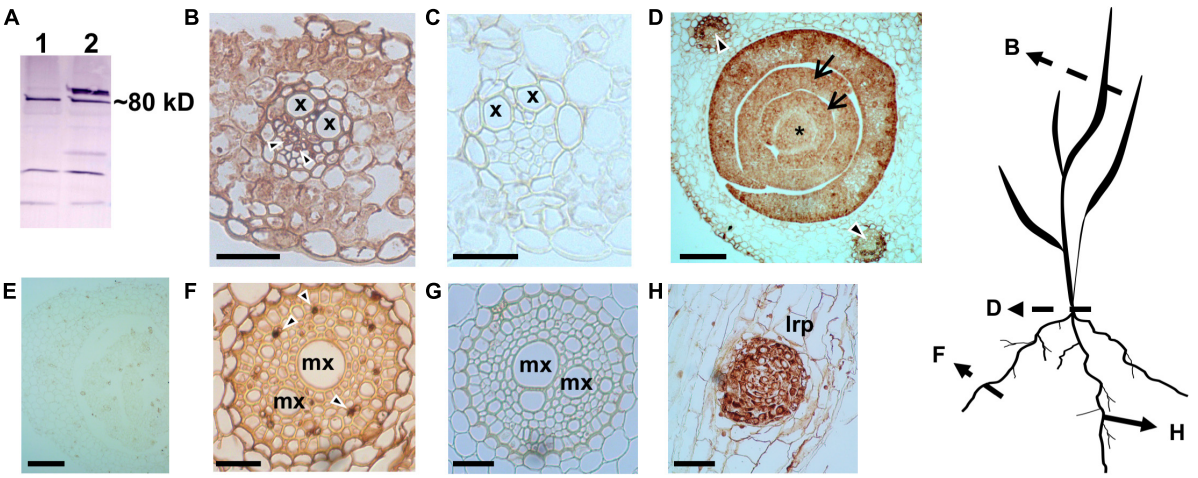


**FIGURE 1 |** Immunohistochemical localization of wheat $H^+$-PPase orthologs TaVPs in vascular and sink tissues of seedlings. **(A)** Western blot of total protein extracts from *AVP1 Null* seedlings. Lanes 1 and 2 correspond to boiled and non-boiled samples, respectively. **(B)** Transverse section of a source leaf vasculature shows a distinct immunohistochemical reaction in the phloem (arrowheads). **(C)** Pre-immune control of panel **(B)**. **(D)** Transverse section of an *AVP1 Null* seedling shows a distinct immunohistochemical reaction in the shoot apical meristem (*), leaf primordia (arrows), and vascular tissues of mature leaves (arrowheads). **(E)** Pre-immune control of panel **(D)**. **(F)** Transverse section through a root shows immunohistochemical reaction at the phloem cells (arrowheads). **(G)** Pre-immune control of panel **(F)**. **(H)** Immunohistochemical reaction at a lateral root primordium. Scale bars: **(B,C)** 50 μm; **(D,E)** 100 μm; **(F,G)** 25 μm; **(H)** 10 μm. x, xylem; mx, metaxylem; lrp, lateral root primordium. Silhouette diagram of a wheat seedling showing localization of the different sections.

signal. The TaVPs were also prominently localized in the phloem cells of the vascular bundles of the leaf sheath of a growing seedling (**Figure 1D**, arrowheads), in the vascular tissues of source leaves (**Figure 1B**, arrowheads), and in vascular elements of the stele (**Figure 1F**, arrowheads). Representative negative controls using pre-immune serum (**Figures 1C,E,G**) showed that the immunohistochemical signals observed in various wheat tissues were TaVP-specific.

## $H^+$-PPases and Apoplasmic Phloem Loading in Wheat Source Leaves

In monocot species like wheat, phloem loading occurs in the minor and intermediate veins; whereas transport out of the leaf occurs in the large lateral veins. Transfer of the photoassimilate from the collection phloem to the transport phloem within the large veins occurs via the transverse veins that connect adjacent parallel veins (Kuo et al., 1972). In wheat source leaf minor veins, a photosynthetic bundle sheath layer (arrowhead; **Figure 2A**) concentrically surrounds 2 – 3 layers of non-photosynthetic mestome sheath cells (arrows; **Figure 2A**) as described previously (Kuo et al., 1974). It has been shown that the fluorescent tracer dye (5)6-carboxyfluorescein diacetate (CFDA) trafficked exclusively via the parallel vascular strands of wheat source leaves (Aoki et al., 2002). Furthermore, [$U^{14}C$]-sucrose infiltrated strips of wheat source leaves showed that the radiolabel was predominantly localized in the parallel veins of the leaf (Yadav et al., 2019), as expected from apoplasmically phloem loading species. Based on previous results (Paez-Valencia et al., 2011; Regmi et al., 2015), and in the positive $H^+$-PPase immunohistochemical reaction shown in vascular tissues (**Figures 1B,D,F**) we proceeded to document the actual membrane of $H^+$-PPase residence in wheat vasculature. We used immunogold labeling in high-pressure frozen Bobwhite source leaf samples and found that the TaVPs are localized at the PM in the sieve element companion cell (SE-CC) complexes (**Figures 2B,C**), while negative controls performed with the pre-immune serum showed that the observed immunogold labeling was TaVP-specific (**Figures 2D,E**). Of note, quantification data comparing tonoplast vs. PM gold particles from nine independent micrographs showed that the distribution of TaVPs was preferentially at the PM of SEs and CCs (**Figure 2F**).

The transgenic wheat lines generated by transforming immature wheat embryos with *pUBI:AVP1* construct were verified for expression of *AVP1* with Q-PCR (**Supplementary Figure S1D**) and genotyped with specific primers (**Supplementary Figures S1A,B** and **Supplementary Table S1**). We further proceeded to ascertain that the *pUBI:AVP1* transgenic wheat lines had higher levels of $H^+$-PPase in the source leaves, and upon immunolocalization and development of the 3,3′-diaminonezidine (DAB) signal for 17 s, found that the *AVP1.1* and *AVP1.2* transgenic lines had visibly stronger signal in both mesophyll cells (**Figures 2H,I**) and vasculature (black arrowheads, **Figures 2H,I**) than the control *AVP1 Null* leaf sections (**Figure 2G**). The pre-immune serum (**Figure 2J**) showed that the immunohistochemical signals observed were TaVP-specific.

## Enhanced Photosynthate Partitioning to the Heterotrophic Roots in *AVP1* Expressing Vegetative Wheat Plants

To monitor reduced carbon transport from source leaves into sink organs in the vegetative stages of wheat plants, we $^{14}CO_2$

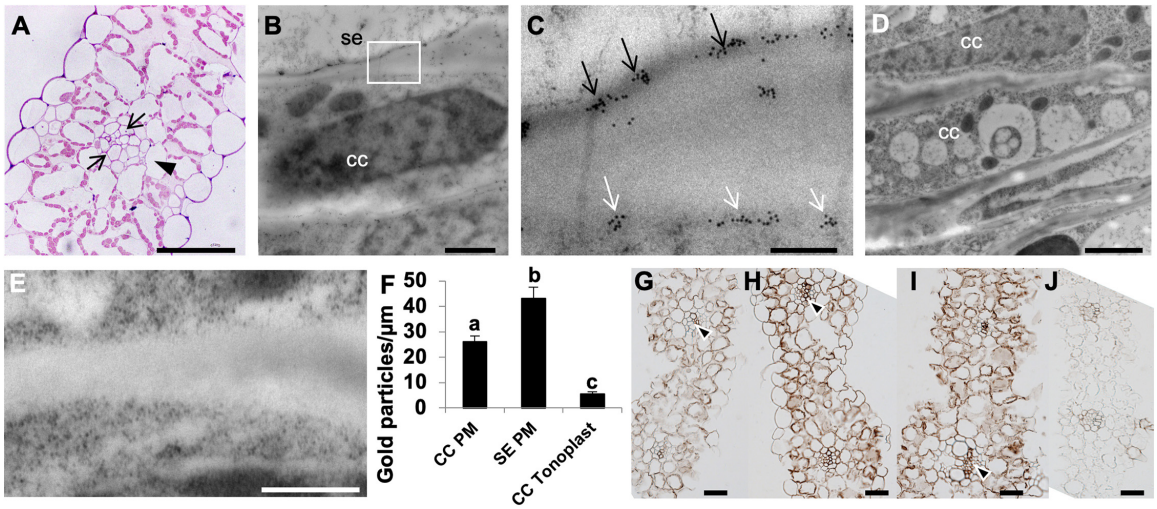


**FIGURE 2 |** Apoplasmic phloem loading in wheat source leaves, and ultrastructural localization of H+-PPases. **(A)** A toluidine blue stained 500 nm semi-thin transverse section of wheat source leaf minor vein showing a layer of bundle sheath cell (arrowhead) surrounding two layers of non-photosynthetic mestome sheath cells (arrows). **(B)** Representative electron micrograph showing immunogold labeling of a longitudinal ultrathin section through a sieve element companion cell (SE-CC) complex in high-pressure frozen wheat source leaf. **(C)** Boxed inset from the panel (**B**; white box) showing distinct plasma membrane localization of anti-rabbit IgG conjugated to 10 nm gold particles in both companion cells (CC) and sieve elements (SE) (arrows). **(D,E)** Pre-immune serum negative control showing a lack of immunogold labeling. **(F)** Quantification of gold labeling comparing the number of 10 nm gold particles at either the PM of SEs or CCs, or the vacuoles of CCs from nine independent micrographs from three independently grown plants. Statistically significant differences were found in the distribution of TPV-specific gold label per μm of SE PM, CC PM and CC V ($F_{2,75}$ = 51.12; $P$ < 0·0001). It was inferred from *post hoc* pairwise comparisons using Tukey HSD that the mean number of gold particles per μm of SE PM (mean = 43.19, s.e. = 4.31) was significantly different from the mean number of gold particles per μm of CC PM (mean = 26.14, s.e. = 2.25), and the mean number of gold particles per μm of CC PM was also significantly different from the number of gold particles per μm of CC V (mean = 5.54, s.e. = 0.82). **(G–J)** Immunolocalization of H+-PPases in the source leaves of *AVP1 Null* **(G)**, *AVP1.1* **(H)**, *AVP1.2* **(I)**, and pre-immune serum negative control **(J)**. Distinct reaction in collection phloem is indicated by arrowheads. Scale bars: **(A)** 100 μm, **(B)** 10 μm, **(C)** 1 μm, **(D)** 5 μm; **(E)** 50 0nm, and **(G–J)** 50 μm.

labeled 10-days old *AVP1 Null* seedlings (i.e., Zadoks scale 13 developmental stage). It has been suggested before that plant mobilize transitory starch in the shoots to heterotrophic roots during the dark period (Gibon et al., 2004; Smith and Stitt, 2007). 10-day old seedlings were labeled at 10:00 AM for 60 min with $^{14}CO_2$, and $^{14}C$ transport into heterotrophic roots was measured by scintillation counting at 12:00 PM (mid-day; peak of light period), 6:00 PM (onset of dark period), 12:00 AM (peak of dark period), and 6:00 AM (onset of light period) time points. As shown in **Figure 3A**, there is an increase in radiolabel in the heterotrophic roots during the dark period with a concomitant decrease in radiolabel in the shoots, suggesting that the majority of photosynthate flux from source to sink in vegetative wheat plants occurs during the night. Upon comparing, radiolabel levels in the roots of *AVP1 Null* and transgenic lines (**Figure 3A**), it is noteworthy that the accumulation of photosynthates in *AVP1 Null* roots reaches a peak between 6 PM and 12 AM before decreasing between 12 AM and 6 AM. In contrast, both transgenic lines continued to accumulate more label throughout the dark period (i.e., between 6 PM – 6 AM; **Figure 3A**), despite the fact that the shoot, root, and total fresh weight of *AVP1 Null*, *AVP1* transgenic seedlings were not statistically significant at the 95% confidence interval (**Table 1**). Of note, monitoring root growth of *AVP1 Null* and *AVP1* transgenic plants grown under optimal conditions in greenhouse indicated that *AVP1* transgenic lines developed statistically significant longer roots (45–75%) (**Figure 3D**). Furthermore, a positive tendency, not statistically significant, regarding root biomass (30−35% higher) in both transgenic lines when compared to *AVP1 Nulls* is evident (**Figures 3B,C**).

## $^{14}CO_2$ Label Supplied From the Source Flag Leaf Into Milk Stage Kernels

While roots and young leaves are the primary sinks during the vegetative stage of a plant's life cycle, the reproductive organs are the major sinks as plants enter the reproductive phase. During grain filling in C3 cereals like wheat, the terminal flag leaf has long been considered the primary source of photoassimilates to the kernels (Evans and Rawson, 1970; Evans, 1975; Araus and Tapia, 1987). We tested if *AVP1* expressing lines would show increased accumulation of photosynthates supplied from the flag leaf into kernels.

To further document H+-PPase presence in flag leaf and reproductive tissues we immunohistochemically localized TaVPs in the flag leaf and the peduncle of *AVP1 Null* plants, at Zadoks stage 59 (**Figures 4A–F**). Transverse sections showed clear localization of TaVPs in the vascular tissues of both the flag leaf and the peduncle (**Figures 4A,E** arrowheads) and sub-epidermal storage parenchyma cells in the peduncle (**Figures 4B,C** arrowheads). Negative controls performed with pre-immune serum showed that the observed signal was TaVP-specific (**Figures 4D,F**). We then compared whether the milk kernel sinks (at Zadoks stage 75) of *AVP1-1* and *AVP1-2* lines

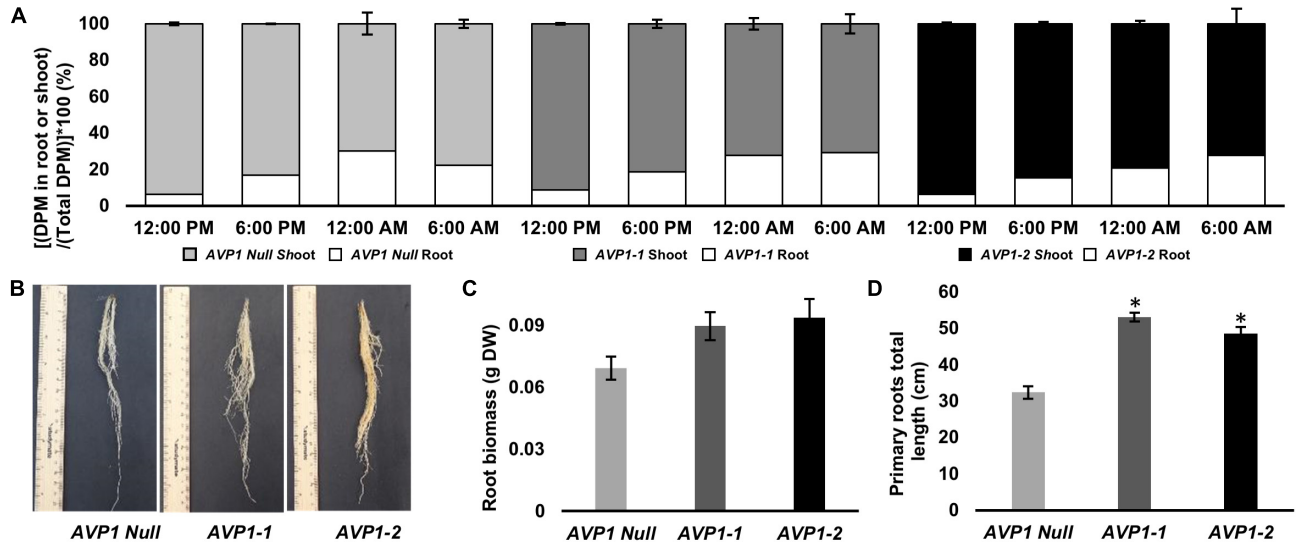


**FIGURE 3 |** Carbon partitioning between the photoautotrophic shoot and heterotrophic root of 10-days old wheat seedlings. **(A)** Long-distance transport from the shoot to root in *AVP1 Null, AVP1-1* and *AVP1-2* plants using $^{14}CO2$ over light and dark periods. *n* = 3 plants per time point, per experiment, results from two independent experiments; error bars represent standard error of the mean. DPM, Disintegrations per minute. **(B)** Root growth of transgenic wheat plants expressing AVP1 under optimal growth conditions at 6 weeks after sowing. **(C)** Root biomass at 3 weeks after sowing. **(D)** Primary roots total length at 3 weeks after sowing. Plants from two independent AVP1 transformation events were grown in an inorganic kiln-fired porus ceramic matrix for three weeks prior to their root system being imaged using an Epson flatbed scanner before root mass was dried at 80°C oven for 4 days and the weight recorded. Results are the mean ± SE (*n* = 5 independent plants). Significant differences between transgenic and null plants using Dunnett's multiple comparison test: $^*P < 0.05$.

**TABLE 1 |** Shoot and root biomass (fresh weight) of 10-days old *AVP1 Null* and overexpressing transgenic lines (Zadoks scale 13) used for $^{14}CO_2$ labeling.

| | AVP1 Null | AVP1-1 | AVP1-2 |
|---|---|---|---|
| **Shoot biomass (mg)** | 233.67 (±8.97) | 257.15 (±11.85) | 235.70 (±8.84) |
| **Root biomass (mg)** | 130.80 (±9.88) | 157.12 (±11.23) | 136.86 (±11.16) |
| **Total biomass (mg)** | 364.48 (±18.43) | 414.27 (±21.93) | 372.56 (±19.35) |

*Standard error of the mean is reported in parentheses; n = 24 plants per line.*

accumulated more $^{14}C$ relative to *AVP1 Null* by labeling the source flag leaves with $^{14}CO_2$, and quantified $^{14}C$-associated label accumulated into the milk kernels. Label accumulation in the milk stage kernels of *AVP1-1* and *AVP1-2* was about 36% and 26% higher than in *AVP1 Null*, respectively (**Figure 4G**).

We then followed *AVP1 Null*, *AVP1-1* and *AVP1-2* lines to maturity under growth chamber conditions and harvested the seeds to determine yield (i.e., seeds per plant, or grams of seeds per plant, or 1000 kernel weight). Under these conditions *AVP1-1* and *AVP1-2 lines* produced significantly more seeds per plant, 53.4 and 91.4%, respectively, than *AVP1 Null* (**Table 2**). Furthermore, the mean weight of total seeds per plant was about 36.4 and 109.1% higher in *AVP1-1* and *AVP1-2* lines than in *AVP1 Null,* respectively (**Table 2**). Of note, the 1000 kernel weight averages were similar among all the plants (**Table 2**).

Considering that yield and seed set are determined at the flowering stage with kernel abortion being a significant limiting factor, we also conducted an analysis of floret fertility among all lines using established methods. Using both, Lumle Agricultural Research Centre (LAC) and Chiang Mai University (CMU) method for quantifying grain set index (Sthapit, 1988; Rerkasem et al., 1989), it was found that the transgenic lines had significantly more fertile florets per spike than *AVP1 Null* (**Figure 4H** and **Suppplementary Figure S2C**).

## H+-PPases in Wheat Are Localized in the Scutellar Epithelial Cells of Germinating Wheat Seeds

Morphologically, it is apparent that the highly metabolically active scutellar epithelial cells have a single large nucleus, are highly vacuolated, and have numerous mitochondria that are distributed throughout the cytoplasm (**Supplementary Figure S3**). Previous studies have implicated H+-PPases in the germination of arabidopsis and barley seeds (Swanson and Jones, 1996; Ferjani et al., 2011). Hence, we immunohistochemically localized TaVPs in germinating wheat seeds 3 days after imbibition. H+-PPases were localized at the scutellar epithelial cells (**Figure 5A**) and in the aleurone cells (**Figure 5E**). Parallel negative controls with pre-immune sera (**Figures 5B,F**) showed that the signal in **Figures 5A,E** were TaVP-specific. To document if there is a possible connection between TaVP of scutellar epithelial cells and aleurone cells with the Sucrose Synthase (SUS) pathway proposed by the studies of Aoki and Perata (Perata et al., 1997; Aoki et al., 2006), we proceeded to immunolocalize SUS in the scutellar epithelial and aleurone cells. SUS orthologs were localized in

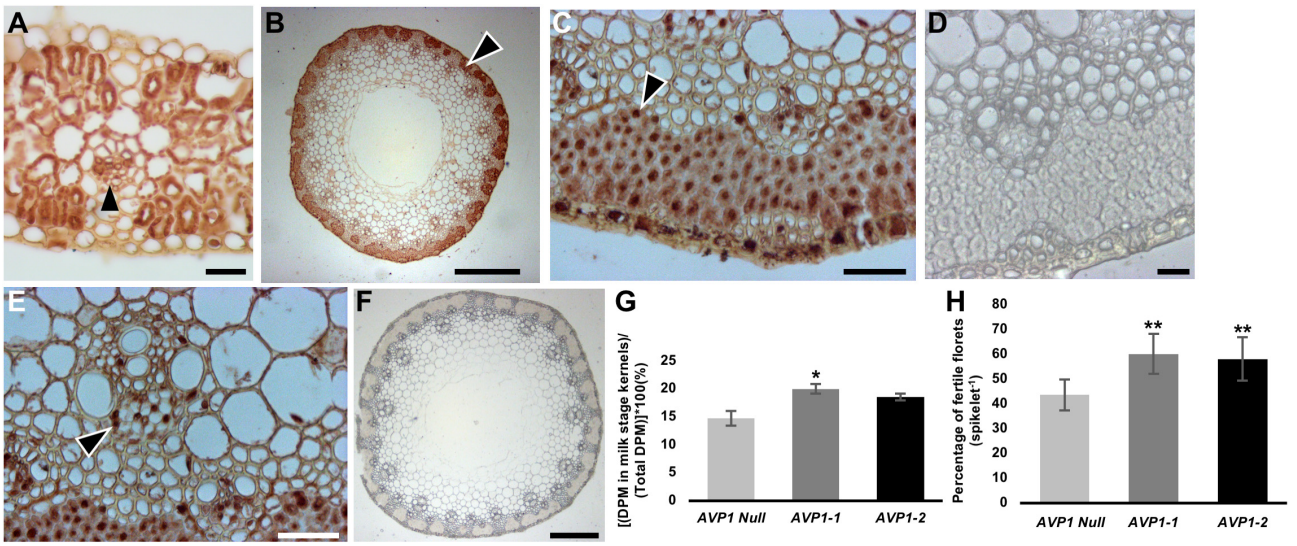


**FIGURE 4 |** Transport of photoassimilates from flag leaves to filling stage grains in wheat plants. **(A)** Immunohistochemical localization of $H^+$-PPases in transverse section of *AVP1 Null* flag leaf. Arrow head highlight immunohistochemical reaction in a minor vein. **(B–F)** Transverse section through an *AVP1 Null* peduncle shows distinct brown 3,3′-diaminobenzidine precipitate at the sub-epidermal storage parenchyma cells, arrowhead **(B–C)**, and phloem cells in vascular tissues (**E**; arrowhead). **(D,F)** Pre-immune serum negative controls of peduncle transverse sections. Scale bars: **(A)** 200 μm, **(B)** 200 μm, **(C,E)** 25 μm, **(D)** 25 μm, and **(F)** 200 μm. **(G)** Transport of $^{14}C$-label into milk-stage kernels after $^{14}CO_2$ labeling of the flag leaves of *AVP1 Null, AVP1-1* and *AVP1-2*. $n = 5$ plants for *AVP1 Null*, 4 plants per transgenic line. Error bars represent standard error of the mean. Significant differences from the *AVP1 Null* are based on Student's *t*-test. * indicates $P < 0.05$. **(H)** Quantification of floret fertility within each spike of the main culm of *AVP1 Null* and transgenic lines by the LAC grain set index method. $n = 4$ plants per line. Error bars represent standard error of the mean. Significant differences from the AVP1 Null are based on Student's *t*-test. ** indicates $P < 0.01$. LAC, Lumle Agricultural Research Centre.

**TABLE 2 |** Seed yield parameters from AVP1 Null and transgenic lines grown in growth-chamber, as indicated. Standard error reported in parentheses; $n = 4$ plants per line.

| | AVP1 Null | AVP1-1 | AVP1-2 |
|---|---|---|---|
| **Mean yield per plant (g)** | 3.84 (±0.94) | 5.24 (±0.83)* | 8.03 (±0.92)* |
| **Total number of seeds per plant** | 169.50 (±45.66) | 260.00 (±41.54)* | 324.50 (±41.68)* |
| **1000 kernel weight (g)** | 23.03 (±1.61) | 20.17 (±1.81) | 24.94 (±1.89) |

*Significant differences from the AVP1 Null plants are based on Student's t-test. * indicates $P < 0.05$.*

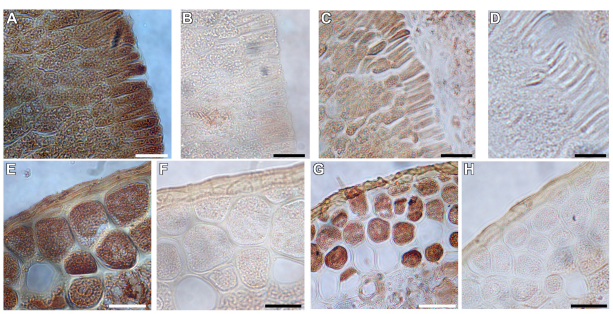


**FIGURE 5 |** Immunohistochemical localization of $H^+$-PPases and Sucrose Synthase in germinating *AVP1 Null* wheat seeds three days after imbibition. **(A,E)** Phase-contrast micrographs showing immunolocalization of $H^+$-PPases in longitudinal sections of scutellar epithelial **(A)** and aleurone **(E)** cells. **(B,F)** Pre-immune control of panels **(A)** and **(E)**, respectively. **(C,G)** Phase-contrast micrographs showing distinct localization of Sucrose Synthase in the scutellar epithelial cells **(C)** and aleurone **(G)**. **(D,H)** Pre-immune control of panels **(C)** and **(G)**, respectively. Scale bars: **(A–H)** 10 μm.

both types of cells in germinating wheat seeds 3 days after imbibition (**Figures 5C,G**). Negative controls performed by omitting the primary antibody showed no SUS-associated signal (**Figures 5D,H**).

## Enhanced Post-germinative Growth in AVP1 Expressing Wheat

The conspicuous of localization of TaVPs and SUS in the scutellar epithelial cells and the hypoxic conditions characteristic of this tissue suggest an interplay of both enzymes likely in carbohydrate catabolism (Primo et al., 2019). To test if the expression of the arabidopsis AVP1 could affect wheat seedling development, we measured the fresh weights of the embryonic shoot (coleoptile) and root (radicle) of *AVP1 Null*, *AVP1-1* and *AVP1-2* lines imbibed and grown in the dark for 48, 72, 80, and 96 h. It was found that at the first two time points (48 and 72 h) the only line that showed a positive tendency of post-germinative growth advantage was *AVP1-1* (**Figures 6A,C**). Interestingly, the other transgenic line, *AVP1-2*, picked up its growth pace at 80 and 96 h and obtained by the end of the experiment about 34%

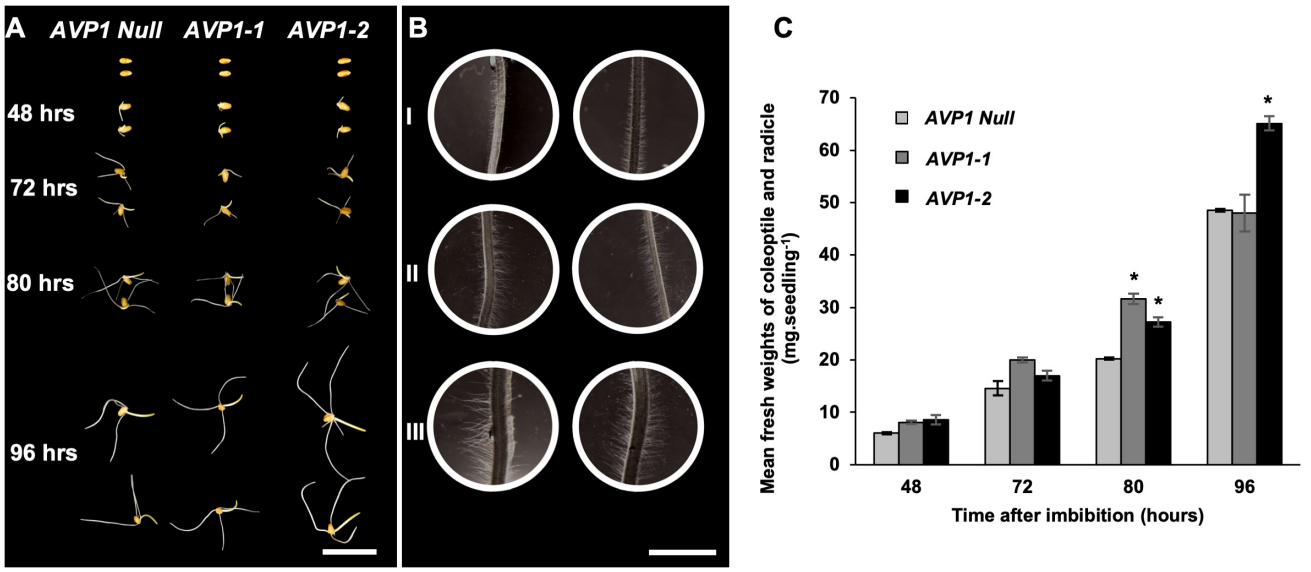


**FIGURE 6 |** Germination of seeds and post-germinative growth of wheat seedlings in the dark. **(A)** Representative images of wheat seeds and seedlings from *AVP1 Null* and transgenic lines (*AVP1-1* and *AVP1-2*) imbibed and grown in the dark for 48, 72, 80, and 96 h. Scale bar: 2 cm. **(B)** Light micrographs of differentiation zones of seminal roots at 80 h of post-germinative growth (see A). I = *AVP1 Null,* II and III = *AVP1-1* and *AVP1-2*, respectively. Scale bar: 2 mm. **(C)** Comparative mean fresh weights of the coleoptiles and radicles from *AVP1 Null*, *AVP1-1* and *AVP1-2* lines grown in the dark (see panel **A**). $n = 3$ per line per time point. Error bars represent standard error of the mean. Significant differences from the *AVP1 Null* are based on Student's *t*-test. * indicates $P < 0.05$.

biomass increases compared to *AVP1 Null*. Additionally, upon closer examination of the material, it was also found that at 80 h, the root hairs of the differentiation zones of the seminal roots of all transgenic lines had visibly longer and denser root hairs compared to that of *AVP1 Null* (**Figures 6B**, I – III).

## Transgenic Wheat Expressing *AVP1* Has Increased Shoot Biomass and Grain Yield Under Greenhouse and Field Conditions

Phenotypic evaluation of the transgenic wheat expressing *AVP1* and null segregants were conducted in greenhouse and field under optimal growth conditions. In greenhouse, transgenic plants expressing *AVP1* were larger (20–80%; **Figure 7A**), had increased leaf number (28%; **Figure 7B**) and had the capability to enhance grain yield per plant by 28–62% compared with null segregants (**Figure 7C**). *AVP1-2* lines had the greatest increase in grain yield per plant (62%), followed by *AVP1-1* (28%) lines. The enhanced grain yield in *AVP1* lines was accompanied by an increase in number of seeds per plant (10–42%; **Figure 7D**). The transgenic lines also flowered 7–8 days before the *AVP1* nulls (**Supplementary Figure S2D**).

In GM field trials, increase in shoot biomass (2–10%; **Figure 7E**), number of leaves (7–10%; **Figure 7F**) and grain yield per plant (18–20%; **Figure 7G**) was observed for *AVP1* expressing wheat lines compared to null segregants. Furthermore, *AVP1* transgenic lines had an increase in the number of seeds per plant (8–17%; **Figure 7H**). The relationship between flag leaf weight and grain yield from greenhouse grown lines was investigated (**Figures 7I,J** and **Supplementary Figure S4**), no relationship was found.

# DISCUSSION

Maximizing the photosynthetic capacity of plants could be considered the ideal way to increase plant productivity; yet, photosynthesis is inhibited by its own products (Kottapalli et al., 2018). Strategies to circumvent this bottleneck include enhancing phloem loading/transport capacity and/or empowering the sinks (Ainsworth and Bush, 2010; Braun et al., 2013; Yadav et al., 2015). $H^+$-PPases have been implicated in regulating reduced carbon transport and sink strength (Gaxiola et al., 2012, 2016b; Schilling et al., 2017). In order to test if genetic manipulation of this enzyme in wheat can improve photosynthate partitioning and yield, we expressed *AVP1* in spring wheat Bobwhite L. under the control of a maize Ubiquitin (*UBI*) promoter (**Supplementary Figures S1A–D**).

In this study, we first established the tissue localization pattern of $H^+$-PPases encoded in the wheat genome – TaVPs – using antibody generated against the 100% conserved epitope CTKAADVGADLVGKIE (Rea et al., 1992). Higher molecular weight aggregates present in non-boiled samples suggest that $H^+$-PPases may interact *in vivo* with other proteins (**Figure 1A**). As shown in other plants (Paez-Valencia et al., 2011; Segami et al., 2014; Regmi et al., 2015) $H^+$-PPases showed basal expression in most cells and maximal localization signal in sink tissues (**Figures 1D,H**) and collection (**Figures 1B–D**, **2G–J**, **4A**), and transport phloem (**Figures 1F**, **4E**).

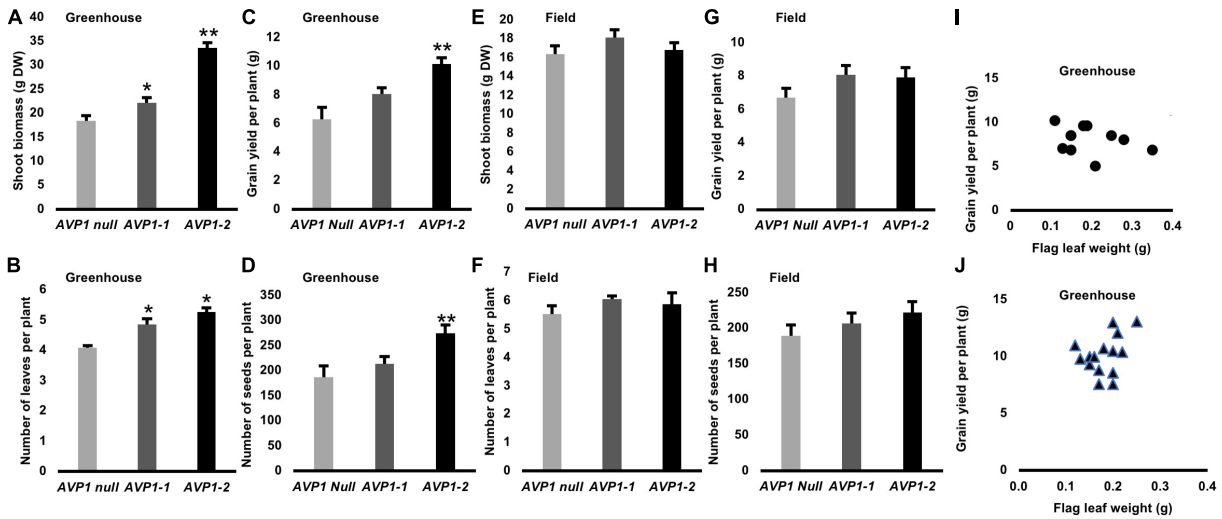


**FIGURE 7 |** Shoot growth and yield attributes of transgenic wheat plants expressing *AVP1* under optimal growth conditions in green house and field: **(A,E)** shoot biomass (g DW), **(B,F)** Number of leaves per plant **(C,G)** Grain yield per plant, **(D,H)** Number of seeds per plant. Two independent single gene transformation events analyzed, along with the respective null segregants, which had segregated from each of the lines at the $T_1$ stage. Results are the mean ± SE ($n$ = 15 independent plants per line). Significant differences between transgenic and null plants using Dunnett's multiple comparison test: $^*P < 0.05$ and $^{**}P < 0.01$. **(I)** Relationship between flag leaf weight (g) and grain yield per plant (g) of transgenic wheat plants expressing AVP1 under optimal growth conditions in green house. Two independent single gene transformation events analyzed [*AVP1-1* marked as circles, $n$ = 10 independent plants **(I)** and *AVP1-2* marked as triangles, $n$ = 13 independent plants **(J)**], which had segregated from each of the lines at the $T_1$ stage. Person correlation coefficient ($r$ = 0.3113) was calculated with two tailed $P$-values and 95% confidence interval.

TaVPases were localized in the vascular tissues (**Figures 1B,D,F**, **2G–I**, **4A,E**) suggesting that in wheat these enzymes could be involved in photosynthate partition (Regmi et al., 2015). Reports of symplasmic fluorescent tracer (5)6-Carboxyfluorescein diacetate (CFDA) and [U$^{14}$C]-sucrose localized in the vascular bundles of wheat source leaves are consistent with apoplasmic loading (**Figure 2C**; Aoki et al., 2002; Yadav et al., 2019). Unlike actively dividing cells where H$^+$-PPases are localized at the tonoplast (Maeshima and Yoshida, 1989; Maeshima, 2000; Heinonen, 2001; Regmi et al., 2015), H$^+$-PPases have been shown to be localized at the plasma membrane (PM) in the sieve element companion cell (SE-CC) complexes of apoplasmic loaders like arabidopsis (Paez-Valencia et al., 2011), rice (Regmi et al., 2015), and ricinus (Long et al., 1995; Langhans et al., 2001). In agreement, TaVP-specific immunogold labeling was found to be at the PM of SE-CC complexes (**Figures 2B,C**).

The model postulated by Gaxiola et al. (2012) proposed that PM-localized H$^+$-PPases in SE-CC complexes work as PPi synthases and favor the SUS-mediated hydrolysis of Suc. Given that the evidence pointed to wheat being an apoplasmic phloem loader and that wheat H$^+$-PPase orthologs were distinctly localized at the PM of SE-CC complexes (**Figures 2B,C**) together with the fact that immunohistochemical reactions in the transgenic lines are consistent with augmented presence of H$^+$-PPase in collection phloem (**Figures 2G–I** arrow heads), we tested if the constitutive expression of *AVP1* in wheat could affect carbon flux from source to sink (Gaxiola et al., 2012; Khadilkar et al., 2015). $^{14}CO_2$ labeling of vegetative 10-days old *AVP1 Null* seedlings showed that more than 50% of the root $^{14}$C label was transported from the shoots to the roots during the dark period with peak transport attained at midnight before declining by the onset of the light period (**Figure 3A**). In contrast, the constitutively *AVP1* expressing lines *AVP1-1* and *AVP1-2* continued to transport $^{14}$C label to the roots throughout the dark period (**Figure 3A**). This behavior suggests that in transgenic wheat the constitutive expression of type I H$^+$-PPases is instrumental in prolonging the transport of reduced carbon from source to sink. Of note, we cannot rule out that in transgenic *AVP1* plants, H$^+$-PPase expression could not only influence the loading/transport of reduced carbon from the source, but also confer increased sink strength by favoring biosynthetic reactions (Gaxiola et al., 2016b).

Beyond the vegetative phase of wheat, the most important source-sink relationship occurs during the reproductive stage. The majority of photoassimilates destined for phloem unloading via the peduncle (uppermost stem internode) into developing sink kernels are synthesized in the terminal flag leaf blade (Evans and Rawson, 1970; Evans, 1975; Araus and Tapia, 1987). Upon immunohistochemical labeling, it was found that TaVPs were localized in the vascular tissues of the flag leaf and the peduncle (**Figures 4A,E** arrow heads). In addition to the vascular tissues, a conspicuous localization of TaVPs in the sub-epidermal storage parenchyma cells in the peduncle, known to store simple and complex carbohydrates (Scofield et al., 2009), was evident (**Figures 4B,C** arrow heads). Currently, we cannot provide any clear role for TaVP presence in the sub-epidermal storage parenchyma cells, and further research is needed to clarify this point.

We labeled the terminal flag leaf blades with $^{14}CO_2$ and assessed whether the transgenic lines accumulated more $^{14}$C label

in the milk stage kernels than Bobwhite. As shown in **Figure 4G**, kernels from *AVP1-1* and *AVP1-2* accrued 36% and 26% more $^{14}C$ label on average compared to *AVP1 Null*. Here too, it is clear that increased abundance of $H^+$-PPase augments carbon partition from source to sinks. Interestingly, *AVP1-1* and *AVP1-2* lines generated more grains per plant – 260 ± 41.5 and 324 ± 41.7, respectively – than *AVP1 Null* (169.5 ± 45.7) lines (**Table 2**) when grown in growth chamber. Seeds constitute the primary yield component of crops like wheat and the yield per plant is directly contingent on sink strength and sucrose supply from the source leaves (Xu et al., 2012). Therefore, it can be plausibly inferred from our data that the transgenic lines not only have increased $^{14}C$ transport into both the roots and kernels (**Figures 3B**, **4G**), but also presumably have stronger sinks. Interestingly, the *AVP1* expressing lines did not show any correlation between flag leaf weight and seed production (**Figures 7I,J** and **Supplementary Figure S4**). The lack of correlation further indicates that the effect of the $H^+$-PPase in carbon partition is more due to its role in transport and or sink strength rather than its direct effects on photosynthesis.

Final seed set is also determined at the flowering stage with kernel abortion via programed cell death causing major losses in yield (Boyer and McLaughlin, 2006). Our finding that the *AVP1 Null* and transgenic lines had statistically similar number of spikes per plant (**Supplementary Figure S2A**), yet the transgenic lines outperformed the *AVP1 Null* in terms of seeds produced per plant, suggests that there is a lower rate of kernel abortion in the transgenic lines. In keeping, the quantification of grain set index showed ∼38 to 33% more fertile florets per spike in the *AVP1-1* and *AVP1-2* lines, respectively, compared to the *AVP1 Null* (**Figure 4H** and **Supplementary Figure S2C**). However, the role of $H^+$-PPases in the mechanism underlying this phenotype is unclear and needs further detailed investigation.

From earlier studies, the role of $H^+$-PPases was found not only to be limited to maintaining PPi homeostasis in meristematic and phloem tissues (Maeshima, 2000; Pizzio et al., 2015), but also in germinating arabidopsis seeds (Ferjani et al., 2011) and in the aleurone cells of barley seeds (Wisniewski and Rogowsky, 2004). Given the role $H^+$-PPases play in sucrose partitioning between source and sinks (Li et al., 2005; Khadilkar et al., 2015; Pizzio et al., 2015), it is considered important to study their role in germinating wheat seeds (Schilling et al., 2017) where the early heterotrophic growth of the embryonic shoots (coleoptile) and roots (radicle) is driven by the endosperm starch (Edelman et al., 1959; Aoki et al., 2006). The immunolocalization data of *TaVP* and *TaSUS* in the scutellar epithelial cells (**Figures 5A,C**) suggests a possible connection between *TaVP* and the Sucrose Synthase (SUS) pathway proposed by the studies of Aoki and Perata (Perata et al., 1997; Aoki et al., 2006). It is possible to speculate that the $H^+$-PPases could be instrumental in scavenging cytosolic pyrophosphate, thereby promoting the synthesis of sucrose via the PPi-sensitive Sucrose Synthase pathway (Ferjani et al., 2011).

We measured the fresh weights of the embryonic shoots (coleoptile) and roots (radicle) of *AVP1 Null*, *AVP1-1*, and *AVP1-2* lines, and found that over a period of 96 h of etiolated post-germinative growth, the transgenic line *AVP1-2* outperformed the *AVP1 Null* by 34% (**Figures 6A,C**). Interestingly, seeds from the *AVP1-1* did not attain significantly different germinative growth when compared to *AVP1 Nulls*, however, they did develop larger and denser root hairs similar to those of *AVP1-2* seedlings (**Figure 6B**). An enhanced post-germinative growth of wheat seedlings in the *AVP1-2* line relative to *AVP1 Nulls* might facilitate early phases of wheat seedling establishment. Given that successful seedling establishment is the first critical step for crop production (Finch-Savage and Bassel, 2015), it would be important to test whether these results from AVP1 expressing lines translate to more realistic field conditions. Additionally, upon closer examination during the same experiment, it was also found that the root hairs of the differentiation zones of the seminal roots in all *AVP1* transgenic lines were visibly longer and denser when compared to that of *AVP1 Nulls* (**Figure 6B**, I – III). Root hairs increase the absorptive surface area of the roots and are implicated in rhizosphere-mediated phosphorus nutrition of plants (Itoh and Barber, 1983; Schjørring and Nielsen, 1987; Föhse et al., 1991; Caradus, 1994). More pertinently, *AVP1* expression in diverse plants including arabidopsis, tomato, and rice induced enhanced phosphorus nutrition under phosphorus-limiting conditions (Yang et al., 2014). Whether this phenotype is conserved in *AVP1* expressing wheat lines merits further investigation.

The transgenic wheat lines expressing *AVP1* were evaluated in green house and field under optimal growth conditions to verify whether increased photosynthate partitioning from source flag leaf to filling grains results in improved yield or not. In this study, *AVP1* expressing wheat plants produced greater shoot biomass associated with an increase leaf number compared to null segregants (**Figure 7**). In addition, *AVP1* expressing wheat produced a greater root system and had a significantly higher grain yield. The enhanced grain yield in *AVP1* lines was accompanied by an increase in the number of seeds per plant. Our results are consistent with our work on barley (Schilling et al., 2014), supporting that *AVP1*-expression could lead to increase in shoot biomass and grain yield under non-saline conditions. Other studies have also shown that *AVP1* (or *AVP1* ortholog) expressing plants generated larger shoot biomass and/or yield compared to plants without this gene in non-saline conditions (Yang et al., 2007; Lv et al., 2008; Li et al., 2010; Vercruyssen et al., 2011; Gouiaa et al., 2012) but as this has not been the main focus of their work and so little commentary has been made on these results. Evidence that is more recent suggests that vacuolar $H^+$-PPases have other roles, including the acquisition and partitioning of organic carbon and other nutrients between the different organs of the plant body (Gaxiola et al., 2001, 2016b; Ferjani et al., 2011; Ferjani and Maeshima, 2016; Schilling et al., 2017). Furthermore, our study suggests that the upregulation of the $H^+$-PPase localized to the plasma membrane of SE–CC complexes increases the PPi supply facilitating sucrose loading and transport from source to sink tissues (Gaxiola et al., 2012, 2016b; Khadilkar et al., 2015), which possibly explain the improved grain yield of transgenic wheat expressing *AVP1*. However, we cannot rule out that the upregulation of the $H^+$-PPase in sinks could also enhanced sink strength by favoring biosynthetic reactions

(Gaxiola et al., 2016b). Generation of transgenic plants carrying source and sink specific AVP1 expression cassettes could help to understand the specific role of $H^+$-PPase in carbon partition.

## CONCLUSION

As reported in evolutionarily divergent plants including physcomitrella (Regmi et al., 2017), arabidopsis (Paez-Valencia et al., 2011; Viotti et al., 2013), and rice (Regmi et al., 2015), $H^+$-PPase orthologs in wheat show dual membrane localization; with distinct PM localization in the SE-CC complexes of source leaf minor veins. *AVP1* expressing wheat plants in the vegetative stage had improved photosynthate transport from source leaves to roots. These transgenic wheat lines also showed increased photosynthate partitioning from the source flag leaf to filling grains resulting in improved yield – increasing seeds produced per plant – suggesting more efficient transport and/or stronger sinks. It would be important to generate tissue specific chimeras to test if the augmented reduced carbon translocation requires $H^+$-PPase expression either at the source and/or at the sinks. Interestingly, an enhanced post-germinative growth of wheat seedlings in the *AVP1-1* line relative to *AVP1 Null* was evident. This early advantage can facilitate the crucial phase of wheat seedling establishment, a key agriculturally desirable phenotype. It is shown that the expression of *AVP1* in wheat improves the grain yield when grown in green house and field conditions under optimal growing conditions. Furthermore, the enhanced yield of the plants was accompanied by increase in number of seeds, shoot biomass, tillers and enhanced root growth in both controlled and/or field environments.

## DATA AVAILABILITY STATEMENT

The raw data supporting the conclusions of this article will be made available by the authors, without undue reservation, to any qualified researcher.

## AUTHOR CONTRIBUTIONS

SR and RG conceived the research plans. KR, JGF, and LL performed most of the lab experiments. DP made the constructs. KY transformed the plants, screened for transgenic lines, and performed real-time PCR experiments and all glasshouse and field data acquisition. SS performed the root phenotyping. CT, LS, and JG designed and managed the Adelaide greenhouse and field trials. RK genotyped the plants. UY, JGF, and BA performed the radioactive sucrose infiltration assays, and helped develop the $^{14}CO_2$ labeling experiments. KR and RG wrote the manuscript. All authors reviewed and approved the final version of the manuscript.

## FUNDING

This work was performed as part of an International Wheat Yield Partnership project awarded to SR and RG, funded through a USDA grant # 59-0210-6-003 and a NSF IOS grant # 1557890 to RG, and a GRDC grant ACP0009 to SR.

## ACKNOWLEDGMENTS

We would like to thank Mr. David Lowry at the Electron Microscopy Bio-imaging Facility at the School of Life Sciences (ASU) for his assistance with high-pressure freezing, and Dr. Debra P. Baluch at the Keck Bio-imaging Facility and Dr. Robert W. Roberson at the School of Life Sciences for access to the light microscopy facility. KR and RG would like to thank Dr. Karen E. Koch at the University of Florida for generously gifting us with the Sucrose Synthase antibody.

## SUPPLEMENTARY MATERIAL

The Supplementary Material for this article can be found online at: https://www.frontiersin.org/articles/10.3389/fpls.2020.00273/full#supplementary-material

**FIGURE S1 |** Molecular evaluation of *AVP1* expressing transgenic wheat plants. **(A)** Genotyping for the presence or absence of AVP1 using polymerase chain reaction (PCR) with AVP1-specific primers and TaGAPDH specific primers (internal control). **(B)** Expression analysis of AVP1 using reverse transcription PCR (RT-PCR) with AVP1-specific and TaGAPDH-specific primers (internal control) for transgenic wheat expressing AVP1 and null segregants. Lane WT is wildtype wheat plant, lanes 1, 2 and 3 (AVP1-1) & 4, 5 and 6 (AVP1-2) are transgenic wheat plants, lanes 7, 8 and 9 are null segregants and lane (–) is a negative control (water). **(C)** Transgene copy numbers in *AVP1*-transgenic wheat plants estimated by Q-PCR. **(D)** Relative expression of *AVP1* gene of transgenic wheat expressing *AVP1* compared to null segregants. Expression data displayed as normalized relative quantity (NRQ) for two independent single gene transformation events. Values are means of 3–5 biological replicates and three technical replicates. Error bars represent standard error of the mean.

**FIGURE S2 |** Differences in reproductive tissue development between AVP1 Null and transgenic lines. **(A)** The number of spikes produced by AVP1 Null and transgenic lines. $n = 4$ plants per line. No significant differences at the 95% confidence interval were found. *AVP1-Null* = 3.00 ± 1.41; *AVP1-1* = 3.75 ± 0.50; and *AVP1-2* = 3.5 ± 0.58. **(B)** Schematic diagram illustrating spikelets' positions within the spike as well as the florets' positions that were evaluated in the floret fertility study. **(C)** Quantification of floret fertility within each spike of the main culm of AVP1 Null and transgenic lines by the CMU grain set index method. $n = 3$ plants per line with grains of 20 florets of the 10 central spikelets evaluated. Significant differences from the AVP1 Null are based on Student's *t*-test.* indicates $P < 0.05$. Error bars represent standard error of the mean. **(D)** Flowering time of transgenic wheat expressing AVP1 compared to null segregants. Flowering data are the mean ± SE ($n = 15$ independent plants per line). Significant differences between transgenic and null plants using Dunnett's multiple comparison test: $^*P < 0.05$ and $^{**}P < 0.01$.

**FIGURE S3 |** Ultrastructural morphology of high-pressure frozen wheat scutellar epithelial cells two days after imbibition. The cells have prominent nuclei (n), are elongated and highly vacuolated (v) with numerous mitochondria (m) interspersed throughout the cytoplasm.

**FIGURE S4 |** Relationship between flag leaf weight (g) and grain yield per plant (g) of transgenic wheat plants expressing AVP1 under optimal growth conditions in green house. Null segregants (AVP1 Null marked as square, $n = 12$ independent plants), which segregated from each of the lines at the $T_1$ stage. Person correlation coefficient ($r = 0.3113$) was calculated with two tailed P values and 95% confidence interval.

**TABLE S1 |** List of primers used for genotyping and quantifying expression in *AVP1*, *AVP1-2* lines.

## REFERENCES


Ainsworth, E. A., and Bush, D. R. (2010). Carbohydrate export from the leaf-A highly regulated process and target to enhance photosynthesis and productivity. *Plant Physiol.* 155, 64–69. doi: 10.1104/pp.110.167684

Altus, D., and Canny, M. (1982). Loading of assimilates in wheat leaves. I. The specialization of vein types for separate activities. *Funct. Plant Biol.* 9, 571–581.

Altus, D., and Canny, M. (1985). Loading of assimilates in wheat leaves. II. The path from chloroplast to vein. *Plant Cell Environ.* 8, 275–285. doi: 10.1111/j.1365-3040.1985.tb01400.x

Aoki, N., Scofield, G., Wang, X.-D., Patrick, J., Offler, C., and Furbank, R. (2004). Expression and localisation analysis of the wheat sucrose transporter TaSUT1 in vegetative tissues. *Planta* 219, 176–184. doi: 10.1007/s00425-004-1232-7

Aoki, N., Scofield, G. N., Wang, X.-D., Offler, C. E., Patrick, J. W., and Furbank, R. T. (2006). Pathway of sugar transport in germinating wheat seeds. *Plant Physiol.* 141, 1255–1263. doi: 10.1104/pp.106.082719

Aoki, N., Whitfeld, P., Hoeren, F., Scofield, G., Newell, K., Patrick, J., et al. (2002). Three sucrose transporter genes are expressed in the developing grain of hexaploid wheat. *Plant Mol. Biol.* 50, 453–462.

Araus, J. L., and Tapia, L. (1987). Photosynthetic gas exchange characteristics of wheat flag leaf blades and sheaths during grain filling: the case of a spring crop grown under Mediterranean climate conditions. *Plant Physiol.* 85, 667–673. doi: 10.1104/pp.85.3.667

Ayre, B. G. (2011). Membrane-transport systems for sucrose in relation to whole-plant carbon partitioning. *Mol. Plant* 4, 377–394. doi: 10.1093/mp/ssr014

Bahaji, A., Li, J., Sánchez-López, ÁM., Baroja-Fernández, E., Muñoz, F. J., Ovecka, M., et al. (2014). Starch biosynthesis, its regulation and biotechnological approaches to improve crop yields. *Biotechnol. Adv.* 32, 87–106. doi: 10.1016/j.biotechadv.2013.06.006

Boyer, J. S., and McLaughlin, J. E. (2006). Functional reversion to identify controlling genes in multigenic responses: analysis of floral abortion. *J. Exp. Bot.* 58, 267–277. doi: 10.1093/jxb/erl177

Braun, D. M., Wang, L., and Ruan, Y.-L. (2013). Understanding and manipulating sucrose phloem loading, unloading, metabolism, and signalling to enhance crop yield and food security. *J. Exp. Bot.* 65, 1713–1735. doi: 10.1093/jxb/ert416

Bürkle, L., Hibberd, J. M., Quick, W. P., Kühn, C., Hirner, B., and Frommer, W. B. (1998). The H+-sucrose cotransporter NtSUT1 is essential for sugar export from tobacco leaves. *Plant Physiol.* 118, 59–68. doi: 10.1104/pp.118.1.59

Cai, J., Zeng, Z., Connor, J. N., Huang, C. Y., Melino, V., Kumar, P., et al. (2015). RootGraph: a graphic optimization tool for automated image analysis of plant roots. *J. Exp. Bot.* 66, 6551–6562. doi: 10.1093/jxb/erv359

Caradus, J. (1994). Selection for improved adaptation of white clover to low phosphorus and acid soils. *Euphytica* 77, 243–250. doi: 10.1007/bf02262637

Chen, L.-Q., Hou, B.-H., Lalonde, S., Takanaga, H., Hartung, M. L., Qu, X.-Q., et al. (2010). Sugar transporters for intercellular exchange and nutrition of pathogens. *Nature* 468, 527–532. doi: 10.1038/nature09606

Chen, L.-Q., Qu, X.-Q., Hou, B.-H., Sosso, D., Osorio, S., Fernie, A. R., et al. (2012). Sucrose efflux mediated by SWEET proteins as a key step for phloem transport. *Science* 335, 207–211. doi: 10.1126/science.1213351

Curtis, M. D., and Grossniklaus, U. (2003). A gateway cloning vector set for high-throughput functional analysis of genes in planta. *Plant Physiol.* 133, 462–469. doi: 10.1104/pp.103.027979

Dasgupta, K., Khadilkar, A., Sulpice, R., Pant, B., Scheible, W.-R., Fisahn, J., et al. (2014). Expression of sucrose transporter cDNAs specifically in companion cells enhances phloem loading and long-distance transport of sucrose, but leads to an inhibition of growth and the perception of a phosphate limitation. *Plant Physiol.* 165, 715–731. doi: 10.1104/pp.114.238410

Davies, J. M., Darley, C. P., and Sanders, D. (1997). Energetics of the plasma membrane pyrophosphatase. *Trends Plant Sci.* 2, 9–10. doi: 10.1016/s1360-1385(97)82732-x

DeWitt, N. D., and Sussman, M. R. (1995). Immunocytological localization of an epitope-tagged plasma membrane proton pump (H (+)-ATPase) in phloem companion cells. *Plant Cell* 7, 2053–2067. doi: 10.1105/tpc.7.12.2053

Edelman, J., Shibko, S., and Keys, A. (1959). The role of the scutellum of cereal seedlings in the synthesis and transport of sucrose. *J. Exp. Bot.* 10, 178–189. doi: 10.1093/jxb/10.2.178

Esau, K. (1969). *The Phloem. Encyclopedia of Plant Anatomy*. Berlin: Gebrüder Borntraegger.

Evans, L., and Rawson, H. M. (1970). Photosynthesis and respiration by the flag leaf and components of the ear during grain development in wheat. *Aust. J. Biol. Sci.* 23, 245–254.

Evans, L. T. (ed.) (1975). *Crop Physiology: Some Case Histories*. Cambridge: Cambridge University Press.

Façanha, A. R., and de Meis, L. (1998). Reversibility of H+-ATPase and H+-pyrophosphatase in tonoplast vesicles from maize coleoptiles and seeds. *Plant Physiol.* 116, 1487–1495. doi: 10.1104/pp.116.4.1487

Ferjani, A., and Maeshima, M. (2016). Multiple facets of H+-pyrophosphatase and related enzymes. *Front. Plant Sci.* 7:1265. doi: 10.3389/fpls.2016.01265

Ferjani, A., Segami, S., Horiguchi, G., Muto, Y., Maeshima, M., and Tsukaya, H. (2011). Keep an eye on PPi: the vacuolar-type H+-pyrophosphatase regulates postgerminative development in *Arabidopsis*. *Plant Cell* 23, 2895–2908. doi: 10.1105/tpc.111.085415

Finch-Savage, W. E., and Bassel, G. W. (2015). Seed vigour and crop establishment: extending performance beyond adaptation. *J. Exp. Bot.* 67, 567–591. doi: 10.1093/jxb/erv490

Föhse, D., Claassen, N., and Jungk, A. (1991). Phosphorus efficiency of plants. *Plant Soil* 132, 261–272.

Fritz, E., Evert, R. F., and Heyser, W. (1983). Microautoradiographic studies of phloem loading and transport in the leaf of *Zea mays* L. *Planta* 159, 193–206. doi: 10.1007/BF00397525

Gao, Y., Wang, Z. Y., Kumar, V., Xu, X. F., Zhu, X. F., Li, T. Y., et al. (2018). Genome-wide identification of the SWEET gene family in wheat. *Gene* 642, 284–292. doi: 10.1016/j.gene.2017.11.044

Gaxiola, R. A., Li, J., Undurraga, S., Dang, L. M., Allen, G. J., Alper, S. L., et al. (2001). Drought-and salt-tolerant plants result from overexpression of the AVP1 H+-pump. *Proc. Natl. Acad. Sci. U.S.A.* 98, 11444–11449. doi: 10.1073/pnas.191389398

Gaxiola, R. A., Regmi, K., and Hirschi, K. D. (2016a). Moving on up: H+-PPase mediated crop improvement. *Trends Biotechnol.* 34, 347–349. doi: 10.1016/j.tibtech.2015.12.016

Gaxiola, R. A., Regmi, K., Paez-Valencia, J., Pizzio, G., and Zhang, S. (2016b). Plant H+-PPases: reversible enzymes with contrasting functions dependent on membrane environment. *Mol. Plant* 9, 317–319. doi: 10.1016/j.molp.2015.09.008

Gaxiola, R. A., Sanchez, C. A., Paez-Valencia, J., Ayre, B. G., and Elser, J. J. (2012). Genetic manipulation of a "vacuolar" H+-PPase: from salt tolerance to yield enhancement under phosphorus-deficient soils. *Plant Physiol.* 159, 3–11. doi: 10.1104/pp.112.195701

Geigenberger, P., Langenberger, S., Wilke, I., Heineke, D., Heldt, H. W., and Stitt, M. (1993). Sucrose is metabolised by sucrose synthase and glycolysis within the phloem complex of *Ricinus communis* L. seedlings. *Planta* 190, 446–453.

Giaquinta, R. T. (1983). Phloem loading of sucrose. *Annu. Rev. Plant Physiol.* 34, 347–387. doi: 10.1146/annurev.pp.34.060183.002023

Gibon, Y., Bläsing, O. E., Palacios−Rojas, N., Pankovic, D., Hendriks, J. H., Fisahn, J., et al. (2004). Adjustment of diurnal starch turnover to short days: depletion of sugar during the night leads to a temporary inhibition of carbohydrate utilization, accumulation of sugars and post−translational activation of ADP−glucose pyrophosphorylase in the following light period. *Plant J.* 39, 847–862. doi: 10.1111/j.1365-313x.2004.02173.x

González, F. G., Slafer, G. A., and Miralles, D. J. (2003). Floret development and spike growth as affected by photoperiod during stem elongation in wheat. *Field Crops Res.* 81, 29–38. doi: 10.1016/s0378-4290(02)00196-x

Gouiaa, S., Khoudi, H., Leidi, E. O., Pardo, J. M., and Masmoudi, K. (2012). Expression of wheat Na+/H+ antiporter TNHXS1 and H+-pyrophosphatase TVP1 genes in tobacco from a bicistronic transcriptional unit improves salt tolerance. *Plant Mol. Biol.* 79, 137–155. doi: 10.1007/s11103-012-9901-6

Griffiths, C. A., Paul, M. J., and Foyer, C. H. (2016). Metabolite transport and associated sugar signalling systems underpinning source/sink interactions. *Biochim. Biophys. Acta* 1857, 1715–1725. doi: 10.1016/j.bbabio.2016.07.007

Heinonen, J. K. (2001). *Biological Role of Inorganic Pyrophosphate*. New York, NY: Springer Science & Business Media.

Hellemans, J., Mortier, G., De Paepe, A., Speleman, F., and Vandesompele, J. (2007). qBase relative quantification framework and software for management and automated analysis of real-time quantitative PCR data. *Genome Biol.* 8:R19.

Itoh, S., and Barber, S. (1983). Phosphorus uptake by six plant species as related to root hairs 1. *Agron. J.* 75, 457–461. doi: 10.2134/agronj1983.00021962007500030010x

Khadilkar, A. S., Yadav, U. P., Salazar, C., Shulaev, V., Paez-Valencia, J., Pizzio, G. A., et al. (2015). Constitutive and companion cell-specific overexpression of AVP1, encoding a proton-pumping pyrophosphatase, enhances biomass accumulation, phloem loading and long-distance transport. *Plant Physiol.* 170, 401–414. doi: 10.1104/pp.15.01409

Kottapalli, J., David-Schwartz, R., Khamaisi, B., Brandsma, D., Lugassi, N., Egbaria, A., et al. (2018). Sucrose-induced stomatal closure is conserved across evolution. *PLoS One* 13:e0205359. doi: 10.1371/journal.pone.0205359

Kovalchuk, N., Smith, J., Pallotta, M., Singh, R., Ismagul, A., Eliby, S., et al. (2009). Characterization of the wheat endosperm transfer cell-specific protein TaPR60. *Plant Mol. Biol.* 71, 81–98. doi: 10.1007/s11103-009-9510-1

Kriegel, A., Andrés, Z., Medzihradszky, A., Krüger, F., Scholl, S., Delang, S., et al. (2015). Job sharing in the endomembrane system: vacuolar acidification requires the combined activity of V-ATPase and V-PPase. *Plant Cell* 27, 3383–3396. doi: 10.1105/tpc.15.00733

Kumar, R., Mukherjee, S., and Ayele, B. T. (2018). Molecular aspects of sucrose transport and its metabolism to starch during seed development in wheat: a comprehensive review. *Biotechnol. Adv.* 36, 954–967. doi: 10.1016/j.biotechadv.2018.02.015

Kuo, J., O'brien, T., and Canny, M. (1974). Pit-field distribution, plasmodesmatal frequency, and assimilate flux in the mestome sheath cells of wheat leaves. *Planta* 121, 97–118. doi: 10.1007/BF00388750

Kuo, J., O'brien, T., and Zee, S. (1972). The transverse veins of the wheat leaf. *Aust. J. Biol. Sci.* 25, 721–738.

Langhans, M., Ratajczak, R., Lützelschwab, M., Michalke, W., Wächter, R., Fischer-Schliebs, E., et al. (2001). Immunolocalization of plasma-membrane H+-ATPase and tonoplast-type pyrophosphatase in the plasma membrane of the sieve element-companion cell complex in the stem of *Ricinus communis* L. *Planta* 213, 11–19. doi: 10.1007/s004250000475

Lerchl, J., Geigenberger, P., Stitt, M., and Sonnewald, U. (1995). Impaired photoassimilate partitioning caused by phloem-specific removal of pyrophosphate can be complemented by a phloem-specific cytosolic yeast-derived invertase in transgenic plants. *Plant Cell* 7, 259–270. doi: 10.1105/tpc.7.3.259

Li, J., Yang, H., Peer, W. A., Richter, G., Blakeslee, J., Bandyopadhyay, A., et al. (2005). *Arabidopsis* H+-PPase AVP1 regulates auxin-mediated organ development. *Science* 310, 121–125. doi: 10.1126/science.1115711

Li, Z., Baldwin, C. M., Hu, Q., Liu, H., and Luo, H. (2010). Heterologous expression of *Arabidopsis* H+−pyrophosphatase enhances salt tolerance in transgenic creeping bentgrass (*Agrostis stolonifera* L.). *Plant Cell Environ.* 33, 272–289. doi: 10.1111/j.1365-3040.2009.02080.x

Long, A., Williams, L. E., Nelson, S., and Hall, J. (1995). Localization of membrane pyrophosphatase activity in *Ricinus communis* seedlings. *J. Plant Physiol.* 146, 629–638. doi: 10.1016/s0176-1617(11)81925-5

Lv, S., Zhang, K., Gao, Q., Lian, L., Song, Y., and Zhang, J. (2008). Overexpression of an H+-PPase gene from *Thellungiella halophila* in cotton enhances salt tolerance and improves growth and photosynthetic performance. *Plant Cell Physiol.* 49, 1150–1164. doi: 10.1093/pcp/pcn090

Maeshima, M. (2000). Vacuolar H+-pyrophosphatase. *Biochim. Biophys. Acta* 1465, 37–51. doi: 10.1016/s0005-2736(00)00130-9

Maeshima, M., and Yoshida, S. (1989). Purification and properties of vacuolar membrane proton-translocating inorganic pyrophosphatase from mung bean. *J. Biol. Chem.* 264, 20068–20073.

Marsh, K., Gonzalez, P., and Echeverría, E. (2000). PPi formation by reversal of the Tonoplast-bound H+-pyrophosphatase from Valencia'Orange Juice Cells. *J. Am. Soc. Hortic. Sci.* 125, 420–424. doi: 10.21273/jashs.125.4.420

Melino, V. J., Fiene, G., Enju, A., Cai, J., Buchner, P., and Heuer, S. (2015). Genetic diversity for root plasticity and nitrogen uptake in wheat seedlings. *Funct. Plant Biol.* 42, 942–956.

Mitsuda, N., Takeyasu, K., and Sato, M. H. (2001). Pollen-specific regulation of vacuolar H+-PPase expression by multiple cis-acting elements. *Plant Mol. Biol.* 46, 185–192.

Nolte, K. D., and Koch, K. E. (1993). Companion-cell specific localization of sucrose synthase in zones of phloem loading and unloading. *Plant Physiol.* 101, 899–905. doi: 10.1104/pp.101.3.899

Paez-Valencia, J., Patron-Soberano, A., Rodriguez-Leviz, A., Sanchez-Lares, J., Sanchez-Gomez, C., Valencia-Mayoral, P., et al. (2011). Plasma membrane localization of the type I H+-PPase AVP1 in sieve element–companion cell complexes from *Arabidopsis thaliana*. *Plant Sci.* 181, 23–30. doi: 10.1016/j.plantsci.2011.03.008

Park, S., Li, J., Pittman, J. K., Berkowitz, G. A., Yang, H., Undurraga, S., et al. (2005). Up-regulation of a H+-pyrophosphatase (H+-PPase) as a strategy to engineer drought-resistant crop plants. *Proc. Natl. Acad. Sci. U.S.A.* 102, 18830–18835. doi: 10.1073/pnas.0509512102

Perata, P., Guglielminetti, L., and Alpi, A. (1997). Mobilization of endosperm reserves in cereal seeds under anoxia. *Ann. Bot.* 79, 49–56. doi: 10.1105/tpc.113.121939

Pizzio, G. A., Paez-Valencia, J., Khadilkar, A. S., Regmi, K. C., Patron-Soberano, A., Zhang, S., et al. (2015). *Arabidopsis* proton-pumping pyrophosphatase AVP1 expresses strongly in phloem where it is required for PPi metabolism and photosynthate partitioning. *Plant Physiol.* 167, 1541–1553. doi: 10.1104/pp.114.254342

Porebski, S., Bailey, L. G., and Baum, B. R. (1997). Modification of a CTAB DNA extraction protocol for plants containing high polysaccharide, and polyphenol components. *Plant Mol. Biol. Rep.* 15, 8–15. doi: 10.1007/bf02772108

Primo, C., Pizzio, G. A., Yang, J., Gaxiola, R. A., Scholz-Starke, J., and Hirschi, K. D. (2019). Plant proton pumping pyrophosphatase: the potential for its pyrophosphate synthesis activity to modulate plant growth. *Plant Biol. (Stuttg.)* 21, 989–996. doi: 10.1111/plb.13007

Ratajczak, R., Hinz, G., and Robinson, D. G. (1999). Localization of pyrophosphatase in membranes of cauliflower inflorescence cells. *Planta* 208, 205–211. doi: 10.1007/s004250050551

Rawson, H., Zajac, M., and Noppakoonwong, R. (1996). "Effects of temperature, light and humidity during the phase encompassing pollen meiosis on floret fertility in wheat," in *Proceedings of the Sterility in Wheat in Subtropical Asia; Extent, Causes and Solutions*, eds H. M. Rawson, and K. D. Subedi, (Canberra, ACT: Australian Centre for International Agricultural Research), 78–84.

Rea, P. A., Britten, C. J., and Sarafian, V. (1992). Common identity of substrate binding subunit of vacuolar h-translocating inorganic pyrophosphatase of higher plant cells. *Plant Physiol.* 100, 723–732. doi: 10.1104/pp.100.2.723

Regmi, K. C., Li, L., and Gaxiola, R. A. (2017). Alternate modes of photosynthate transport in the alternating generations of *Physcomitrella patens*. *Front. Plant Sci.* 8:1956. doi: 10.3389/fpls.2017.01956

Regmi, K. C., Pizzio, G. A., and Gaxiola, R. A. (2016). Structural basis for the reversibility of proton pyrophosphatase. *Plant Signal. Behav.* 11, 257–268.

Regmi, K. C., Zhang, S., and Gaxiola, R. A. (2015). Apoplasmic loading in the rice phloem supported by the presence of sucrose synthase and plasma membrane-localized proton pyrophosphatase. *Ann. Bot.* 117, 257–268. doi: 10.1093/aob/mcv174

Rennie, E. A., and Turgeon, R. (2009). A comprehensive picture of phloem loading strategies. *Proc. Natl. Acad. Sci. U.S.A.* 106, 14162–14167. doi: 10.1073/pnas.0902279106

Rerkasem, B., Saunders, D., and Dell, B. (1989). Grain set failure andboron deficiency in wheat in Thailand. *J. Agric. (Chiang Mai University)* 5, 1–10.

Russell, S. H., and Evert, R. F. (1985). Leaf vasculature in *Zea mays* L. *Planta* 164, 448–458. doi: 10.1007/BF00395960

Sanford, J., Smith, F., and Russell, J. (1995). "Optimizing the biolistic process for different biological applications," in *Recombinant DNA Methodology II*, ed. R. Wu, (San Diego, CA: Acadamic Press), 485–511. doi: 10.1016/b978-0-12-765561-1.50038-2

Schilling, R. K., Marschner, P., Shavrukov, Y., Berger, B., Tester, M., Roy, S. J., et al. (2014). Expression of the *Arabidopsis* vacuolar H+−pyrophosphatase gene (AVP1) improves the shoot biomass of transgenic barley and increases grain yield in a saline field. *Plant Biotechnol. J.* 12, 378–386. doi: 10.1111/pbi.12145

Schilling, R. K., Tester, M., Marschner, P., Plett, D. C., and Roy, S. J. (2017). AVP1: one protein, many roles. *Trends Plant Sci.* 22, 154–162. doi: 10.1016/j.tplants.2016.11.012

Schjørring, J. K., and Nielsen, N. E. (1987). Root length and phosphorus uptake by four barley cultivars grown under moderate deficiency of phosphorus in field experiments. *J. Plant Nutr.* 10, 1289–1295. doi: 10.1080/01904168709363658

Scholz-Starke, J., Primo, C., Yang, J., Kandel, R., Gaxiola, R. A., and Hirschi, K. D. (2019). The flip side of the *Arabidopsis* type I proton-pumping pyrophosphatase (AVP1): Using a transmembrane H+ gradient to synthesize pyrophosphate. *J. Biol. Chem.* 294, 1290–1299. doi: 10.1074/jbc.RA118.006315

Scofield, G. N., Ruuska, S. A., Aoki, N., Lewis, D. C., Tabe, L. M., and Jenkins, C. L. (2009). Starch storage in the stems of wheat plants: localization and temporal changes. *Ann. Bot.* 103, 859–868. doi: 10.1093/aob/mcp010

Segami, S., Makino, S., Miyake, A., Asaoka, M., and Maeshima, M. (2014). Dynamics of vacuoles and H+-pyrophosphatase visualized by monomeric green fluorescent protein in *Arabidopsis*: artifactual bulbs and native intravacuolar spherical structures. *The Plant Cell* 26, 3416–3434. doi: 10.1105/tpc.114.127571

Shavrukov, Y., Genc, Y., and Hayes, J. (2012). "The use of hydroponics in abiotic stress tolerance research," in *Hydroponics-A Standard Methodology for Plant Biological Researches*, ed. T. Asao, (Rijeka: InTech).

Shiratake, K., Kanayama, Y., Maeshima, M., and Yamaki, S. (1997). Changes in H+-pumps and a tonoplast intrinsic protein of vacuolar membranes during the development of pear fruit. *Plant Cell Physiol.* 38, 1039–1045. doi: 10.1093/oxfordjournals.pcp.a029269

Smith, A. M., and Stitt, M. (2007). Coordination of carbon supply and plant growth. *Plant Cell Environ.* 30, 1126–1149. doi: 10.1111/j.1365-3040.2007.01708.x

Srivastava, A. C., Ganesan, S., Ismail, I. O., and Ayre, B. G. (2008). Functional characterization of the *Arabidopsis* AtSUC2 sucrose/H+ symporter by tissue-specific complementation reveals an essential role in phloem loading but not in long-distance transport. *Plant Physiol.* 148, 200–211. doi: 10.1104/pp.108.124776

Stadler, R., and Sauer, N. (1996). The *Arabidopsis thaliana* AtSUC2 gene is specifically expressed in companion cells. *Bot. Acta* 109, 299–306. doi: 10.1111/j.1438-8677.1996.tb00577.x

Sthapit, B. (1988). *Studies on Wheat Sterility Problem in the Hills, Tar and Tarai of Nepal.* Technical Report No. 16/88. Lumle: Lumle Agricultural Research Centre.

Swanson, S. J., and Jones, R. L. (1996). Gibberellic acid induces vacuolar acidification in barley aleurone. *Plant Cell* 8, 2211–2221. doi: 10.1105/tpc.8.12.2211

Trethewey, R. N., and Smith, A. M. (2000). "Starch metabolism in leaves," in *Photosynthesis: Physiology and Metabolism*, eds R. C. Leegood, T. D. Sharkey, and S. von Caemmerer, (Dordrecht: Wolters Kluwer), 205–231. doi: 10.1007/0-306-48137-5_9

Truernit, E., and Sauer, N. (1995). The promoter of the *Arabidopsis* thaliana SUC2 sucrose-H+ symporter gene directs expression of β-glucuronidase to the phloem: evidence for phloem loading and unloading by SUC2. *Planta* 196, 564–570.

Turgeon, R. (2010). The role of phloem loading reconsidered. *Plant Physiol.* 152, 1817–1823. doi: 10.1104/pp.110.153023

Vasil, I. K., and Vasil, V. (2006). Transformation of wheat via particle bombardment. *Methods Mol. Biol.* 318, 273–283.

Vercruyssen, L., Gonzalez, N., Werner, T., Schmülling, T., and Inzé, D. (2011). Combining enhanced root and shoot growth reveals cross talk between pathways that control plant organ size in *Arabidopsis*. *Plant Physiol.* 155, 1339–1352. doi: 10.1104/pp.110.167049

Viotti, C., Krüger, F., Krebs, M., Neubert, C., Fink, F., Lupanga, U., et al. (2013). The endoplasmic reticulum is the main membrane source for biogenesis of the lytic vacuole in *Arabidopsis*. *Plant Cell* 25, 3434–3449. doi: 10.1105/tpc.113.114827

Wang, Y., Xu, H., Zhang, G., Zhu, H., Zhang, L., Zhang, Z., et al. (2009). Expression and responses to dehydration and salinity stresses of V-PPase gene members in wheat. *J. Genet. Genomics* 36, 711–720. doi: 10.1016/S1673-8527(08)60164-2

Wisniewski, J.-P., and Rogowsky, P. M. (2004). Vacuolar H+-translocating inorganic pyrophosphatase (Vpp1) marks partial aleurone cell fate in cereal endosperm development. *Plant Mol. Biol.* 56, 325–337. doi: 10.1007/s11103-004-3414-x

Wright, K. M., Roberts, A. G., Martens, H. J., Sauer, N., and Oparka, K. J. (2003). Structural and functional vein maturation in developing tobacco leaves in relation to AtSUC2 promoter activity. *Plant Physiol.* 131, 1555–1565. doi: 10.1104/pp.102.016022

Xu, S.-M., Brill, E., Llewellyn, D. J., Furbank, R. T., and Ruan, Y.-L. (2012). Overexpression of a potato sucrose synthase gene in cotton accelerates leaf expansion, reduces seed abortion, and enhances fiber production. *Mol. Plant* 5, 430–441. doi: 10.1093/mp/ssr090

Yadav, U. P., Ayre, B. G., and Bush, D. R. (2015). Transgenic approaches to altering carbon and nitrogen partitioning in whole plants: assessing the potential to improve crop yields and nutritional quality. *Front. Plant Sci.* 6:275. doi: 10.3389/fpls.2015.00275

Yadav, U. P., Khadilkar, A. S., Shaikh, M. A., Turgeon, R., and Ayre, B. G. (2017). Quantifying the capacity of phloem loading in leaf disks with [14 C] sucrose. *Bio Protoc* 7:e2658.

Yadav, U. P., Shaikh, M. A., Evers, J., Regmi, K. C., Gaxiola, R. A., and Ayre, B. G. (2019). Assessing long-distance carbon partitioning from photosynthetic source leaves to heterotrophic sink organs with photoassimilated [$^{14}$C] $CO_2$. *Methods Mol. Biol.* 223–233. doi: 10.1007/978-1-4939-9562-2_19

Yang, H., Knapp, J., Koirala, P., Rajagopal, D., Peer, W. A., Silbart, L. K., et al. (2007). Enhanced phosphorus nutrition in monocots and dicots over−expressing a phosphorus−responsive type I H+−pyrophosphatase. *Plant Biotechnol. J.* 5, 735–745. doi: 10.1111/j.1467-7652.2007.00281.x

Yang, H., Zhang, X., Gaxiola, R. A., Xu, G., Peer, W. A., and Murphy, A. S. (2014). Over-expression of the *Arabidopsis* proton-pyrophosphatase AVP1 enhances transplant survival, root mass, and fruit development under limiting phosphorus conditions. *J. Exp. Bot.* 65, 3045–3053. doi: 10.1093/jxb/eru149

**Conflict of Interest:** The authors declare that the research was conducted in the absence of any commercial or financial relationships that could be construed as a potential conflict of interest.

frontiers in Microbiology

ORIGINAL RESEARCH
published: 30 April 2020
doi: 10.3389/fmicb.2020.00793

# Rapid Enrichment and Isolation of Polyphosphate-Accumulating Organisms Through 4'6-Diamidino-2-Phenylindole (DAPI) Staining With Fluorescence-Activated Cell Sorting (FACS)

*Mia Terashima*[1,2], *Yoichi Kamagata*[1,2,3] *and Souichiro Kato*[1,2]*

[1] Bioproduction Research Institute, National Institute of Advanced Industrial Science and Technology (AIST), Sapporo, Japan, [2] Division of Applied Bioscience, Graduate School of Agriculture, Hokkaido University, Sapporo, Japan, [3] Bioproduction Research Institute, National Institute of Advanced Industrial Science and Technology (AIST), Tsukuba, Japan

OPEN ACCESS

**Edited by:**
*Tatsuhiro Ezawa, Hokkaido University, Japan*

**Reviewed by:**
*Karim Benzerara, Centre National de la Recherche Scientifique (CNRS), France*
*Homayoun Fathollahzadeh, University of Toronto, Canada*

***Correspondence:**
*Souichiro Kato*
*s.katou@aist.go.jp*

**Specialty section:**
*This article was submitted to Microbiological Chemistry and Geomicrobiology, a section of the journal Frontiers in Microbiology*

**Received:** *26 January 2020*
**Accepted:** *02 April 2020*
**Published:** *30 April 2020*

**Citation:**
*Terashima M, Kamagata Y and Kato S (2020) Rapid Enrichment and Isolation of Polyphosphate-Accumulating Organisms Through 4'6-Diamidino-2-Phenylindole (DAPI) Staining With Fluorescence-Activated Cell Sorting (FACS). Front. Microbiol. 11:793. doi: 10.3389/fmicb.2020.00793*

Screening for bacteria with abilities to accumulate valuable intracellular compounds from an environmental community is difficult and requires strategic methods. Combining the experimental procedure for phenotyping living cells in a microbial community with the cell recovery necessary for further cultivation will allow for an efficient initial screening process. In this study, we developed a strategy for the isolation of polyphosphate-accumulating organisms (PAOs) by combining (i) nontoxic fluorescence staining of polyphosphate granules in viable microbial cells and (ii) fluorescence-activated cell sorting (FACS) for the rapid detection and collection of target cells. To implement this screening approach, cells from wastewater sludge samples were stained with 4'6-diamidino-2-phenylindole (DAPI) to target cells with high polyphosphate (polyP) accumulation. We found a staining procedure (10 μg/ml of DAPI for 30 min) that can visualize polyP granules while maintaining viability for the majority of the cells (>60%). The polyP positive cells were recovered by FACS, purified by colony isolation and phylogenetically identified by 16S rRNA gene sequencing. Follow-up analysis confirmed that these isolates accumulate polyP, indicating that DAPI can be implemented in staining living cells and FACS can effectively and rapidly screen and isolate individual cells from a complex microbial community.

**Keywords: Polyphosphate-accumulating organisms, flow cytometry, wastewater sludge, bacteria isolation, DAPI**

## INTRODUCTION

The genetic and metabolic diversity of microbial species provide a wealth of possibilities for biotechnological applications. Currently, highly effective isolation methods are largely based on selection by growth capabilities. For example, hydrocarbon-degrading bacteria can be enriched and isolated by using selection media with hydrocarbons as a sole carbon source (Head et al., 2006; Yakimov et al., 2007). In contrast, selectively isolating microorganisms that accumulate desirable

intracellular compounds, such as high-valued organic chemicals or environmental pollutants (such as heavy metals), can be challenging, as these organisms may not grow rapidly or may not grow in a unique environment that can be utilized as a selection parameter or selective pressure.

Advances in omics approaches such as single-cell genomics have resulted in the identification of industrially interesting bacteria (Gawad et al., 2016; Rinke, 2018). However, the isolation of microorganisms that accumulate valuable compounds is often a result of laborious individual strain screening, hypothesis-driven isolation methods, or by chance discovery. Persistent screenings of bacterial isolates from seaweed led to the identification of a strain capable of polyhydroxyalkanoates (PHA) production from starch, after investigation of numerous strains for PHA accumulation (Han et al., 2014). Identification of a dominant phylotype *Dechloromonas* in a wastewater treatment plant using 16S rRNA sequencing followed by screening for bacterial strains allowed the isolation of polyphosphate-accumulating strains (Terashima et al., 2016). In one study, enrichment of butanol-tolerant strains led to the identification of a bacterium in the family *Erysipelotrichaceae* that accumulates large amounts of long-chain free fatty acids, with capabilities of retaining these acids under starvation conditions (Katayama et al., 2014). In order to avoid laborious screening of single strains during targeted isolation endeavors, establishing a method to initially enrich for strains showing promising characteristics directly from a mixed population would vastly accelerate the downstream screening process. However, methods to analyze accumulation of specific compounds in individual living cells from a community, followed by recovery and isolation, are still limited.

In this study, we propose a strategy for the isolation of polyphosphate-accumulating organisms (PAOs) by coupling (i) specific staining of an intracellular accumulate without compromising cell viability, and (ii) rapid detection and sorting of target cells by using fluorescence-activated cell sorting (FACS), for which wastewater sludge samples were utilized. During wastewater processing, the removal of phosphate is enhanced by taking advantage of some microorganisms that uptake more phosphate than necessary for growth, leading to the accumulation of polyphosphates (polyP) as an intracellular storage compound (Mino et al., 1998). The use of PAOs in wastewater treatment is a sustainable and economical process and provides a renewable source of phosphate (Yuan et al., 2012). However, many knowledge of PAOs are based on microbial community analyses and not on single strains (Lanham et al., 2018; Nielsen et al., 2019). Although *in situ* data is crucial in identifying and characterizing PAOs, isolating and culturing PAOs will allow for more in-depth experiments. For this reason, our approach focuses on the isolation and cultivation of candidate PAOs from a wastewater sample using fluorescent staining and FACS. The stain 4'6-diamidino-2-phenylindole (DAPI) is frequently used to visualize cellular polyP granules, as it emits a green-yellow fluorescence, which is distinct from the blue fluorescence emitted from DAPI-stained DNA (Tijssen et al., 1982; Streichan et al., 1990; Aschar-Sobbi et al., 2008; Omelon et al., 2009; Schlagenhauf et al., 2016; Correa Deza et al., 2017; Voronkov and Sinetova, 2019). DAPI-staining coupled with fluorescent in situ hybridization followed by microscopy and flow cytometry have been frequently used for fingerprinting and identification of PAOs in various environments (Kong et al., 2005; Günther et al., 2009). However, there have been no reports for the application of DAPI-staining for the isolation of PAOs, since DAPI-staining, which is often accompanied by cell fixation, has been considered to compromise cell viability.

FACS enables rapid screens, with capabilities of analyzing thousands of cells per second. For example, FACS has been utilized for the characterization of microbial community structures and the assessment of live/dead cells from environmental samples (Emerson et al., 2017; Van Nevel et al., 2017; Perera et al., 2019). FACS has also been used in combination with heterologously expressed fluorescent proteins as markers to screen for NADPH-dependent enzymes, phenol-degrading enzymes, amino acid production enzymes and metabolite-responsive transcriptional regulatory proteins (Uchiyama et al., 2005; Uchiyama and Miyazaki, 2013; van Rossum et al., 2013; Eggeling et al., 2015; Mahr et al., 2015; Meier et al., 2016; Bott and Eggeling, 2017; Emerson et al., 2017; Van Nevel et al., 2017; Frei et al., 2018; Ngara and Zhang, 2018; Perera et al., 2019). However, there are only a few studies that utilize FACS for isolation of novel microorganisms from environments. Zengler et al. (2002) achieved isolating viable strains by encapsulating single cells in gel microdroplets and collecting those showing growth by microcolony formation using flow cytometry. Kalyuzhnaya et al. also sorted metabolically active cells using a redox-sensing probe, targeting and successfully isolating methanotrophs (Kalyuzhnaya et al., 2008). However, the targets in these studies were simply active microorganisms and there are currently no reports of application of FACS for the isolation of microorganisms that accumulate a valuable intracellular product, including polyP.

In this study, we developed a rapid method using DAPI staining and FACS for the isolation of PAOs from a complex microbial community. We examined the viability of the cells after DAPI staining and determined a condition that allows for the majority of stained cells remain alive, enabling effective isolation of PAOs after FACS-based phenotype screening.

# MATERIALS AND METHODS

## Sample Collection and Culture Growth Conditions

The sludge sample utilized for flow cytometry was collected from the oxidation ditch wastewater treatment plant (WWTP) in Okishima, Omihachiman, Shiga prefecture, Japan during the aerobic phase (Terashima et al., 2016). In short, the sludge receives domestic wastewater and is operated with a repetitive cycle of 4 h aerobic ($>0.5$ mg $L^{-1}$ dissolved oxygen) and 6 h anaerobic phases ($<0.5$ mg $L^{-1}$ dissolved oxygen). The annual average of biological oxygen demand in the influent/effluent is $167 \pm 93/5.0 \pm 1.2$ mg $L^{--1}$. The total nitrogen and total phosphorus in the influent/effluent are $28.8 \pm 6.2/4.3 \pm 1.8$ mg $L^{--1}$ and $3.9 \pm 1.6/0.6 \pm 0.2$ mg $L^{--1}$,

respectively. The influent wastewater pH was 6.7–7.7 (average 7.1) and the effluent wastewater pH was 7.0–7.6 (average 7.4). The plant is located outside with no temperature controls and sampling was conducted when the water temperature was approximately 20°C. In order to allow sufficient time for phosphate uptake, sludge samples were pre-cultured under aerobic conditions at 25°C for by inoculating 4 ml of sludge samples into 8 ml of acetate medium and cultured for 4 h prior to FACS analyses. Sodium acetate was added to the medium because most PAOs prefer short chain fatty acids as a growth substrate (Shen and Zhou, 2016). For the growth medium, sodium acetate was added to a final concentration of 10 mM to the basal media [pH 7, containing per liter of distilled water: 1 g of $NH_4Cl$, 0.1 g of $MgCl_2{\cdot}6H_2O$, 0.08 g of $CaCl_2{\cdot}6H_2O$, 0.6 g of NaCl, 2.72 g $KH_2PO_4$, 7.16 g $Na_2HPO_4{\cdot}12H_2O$, 0.1 g of yeast extract, and 10 ml each of vitamin solution and trace metal solution (Kato et al., 2016)].

## Microscopic Observation of Intracellular PolyP Using DAPI Stain

PolyP and DNA were visualized using fluorescent dye DAPI. 1 ml of sludge samples or individual strains were collected by centrifugation (8,000 g, 5 min) and resuspended in 1 ml of phosphate-buffered saline (PBS) solution and stained for 30 min with DAPI (10 μg/ml final concentration). Cells were imaged using a DMI 4000B Leica fluorescence microscope with a 340–380 nm excitation filter and 425 LP emission filter. Both polyP and lipid inclusions are known to emit in the 450–650 nm range when excited at 360 nm, but lipid inclusions can be easily distinguished from polyP, as their fluorescence intensity is much lower and rapidly fades within seconds (Streichan et al., 1990; Serafim et al., 2002; Seviour et al., 2008; Mesquita et al., 2013). Therefore, all images photographed were exposed to excitation light for at least 1 min before imaging in order to detect consistent, long-lasting bright green-yellow fluorescence from polyP.

## Recovery Test After DAPI Staining

For the viability test after DAPI staining, overnight *E. coli* (strain K-12) cultures and the sludge cultures grown for 4 h as well as for 24 h were utilized. Each sample consisted of three biological replicates and cells were grown in acetate-containing medium as described above. DAPI staining was performed in PBS buffer, as described above, and unstained controls were processed in parallel. After staining, serial dilutions of cells were plated out onto acetate-containing agar plates and incubated at 25°C. Recovered colonies were counted (minimum ∼100 colonies per plate) after 2 days for the *E. coli*-containing plates and after 4 days for the sludge-containing plates. Percent recoveries were determined by dividing the colony numbers of stained sample to the numbers from the unstained control.

## FACS Enrichment of PolyP-Containing Cells

After 4 h of growth in acetate media, cells were vortexed (3 times, 1 min) to break apart cell clumps and filtered through a 40°μm sieve and spun at 8,000 g for 5 min. Cells were resuspended in phosphate-buffered saline (PBS) solution and stained with DAPI and immediately processed by a BD FACS Aria II for sorting. For FACS, a forward scatter threshold of 800 was used and DNA was monitored using a 355 nm UV excitation laser and emission filter of 425–475 nm. PolyP fluorescence was monitored using 405 nm violet laser with an emission filter of 585–625 nm. The voltages used for the forward scatter, DNA and polyp lasers were 277, 515, and 588, respectively. Cells were sorted at a rate of approximately 5,000 cells/s. 1,2% of the cells that showed highest polyP fluorescence relative to the DNA fluorescence were collected by drawing a FACS collection gate and named "PolyP" fraction. As a control, all types of cells detected by FACS regardless of polyP fluorescence intensity were also collected as the "all events" fraction. Over half a million cells were collected (1,2 ml was collected at a concentration of $0.5 \times 10^6$ cells/ml) for each sample and a fraction of the collected cells were plated out onto acetate medium agar plates for recovery (replicates of suspension containing 1,000 cells, 100 cells, and 10 cells were plated out). After 4 days of incubation at 25°C, colonies were randomly picked and transferred to clean plates for further analysis.

## Identification of Colonies Recovered After FACS by 16S rRNA Gene Sequencing

The picked colonies were identified via colony-PCR and 16S rRNA gene fragment sequencing. PCR amplification was performed with 27F and U533R primers as described previously (Kato et al., 2010, 2016). PCR products were sequenced at the Biomedical Center of TAKARA Bio Inc with the Applied Biosystems 3730xl DNA Analyzer. The ∼500 bp 16S rRNA gene fragment sequence of each colony analyzed were classified to phylotypes with a cut-off value of 97% sequence identity using BLASTClust (Altschul et al., 1997). The phylotypes were phylogenetically classified with the Classifier program in the Ribosomal Database Project (Wang et al., 2007) and were compared to sequences in the GenBank nucleotide sequence database using the BLAST program (Altschul et al., 1997).

## Accession Numbers

The nucleotide sequence data obtained in this study have been submitted to GenBank database under Accession Nos. LC198009–LC198038.

# RESULTS AND DISCUSSION

## Sludge Samples Contain PolyP-Accumulating Strains and Cells Remain Viable After PolyP Staining by DAPI

PolyP-accumulation is known to occur under aerobic conditions (Mino et al., 1998). In order to allow for sufficient polyP

accumulation prior to DAPI staining, we cultured the sludge samples in phosphate-rich acetate-containing medium under aerobic conditions for 4 h. The presence of polyP-accumulating cells was initially confirmed using microscopy of sludge samples grown overnight and stained with DAPI. DAPI concentration of 1 μg/ml was too low to clearly visualize polyP granules (data not shown), but at a concentration of 10 μg/ml, clear green-yellow fluorescence stemming from polyP granules could be observed (**Figure 1A**). Additionally, the effect of DAPI staining on cell viability was investigated by plating stained cells on agar plates. Tests using *E. coli* showed that 70% of cells remained viable and formed colonies on plates after staining with 10 μg/ml DAPI for 30 min (**Figure 1B**). Higher DAPI concentration (100 μg/ml) was also tested in preliminary experiments, which decreased the recovery rate of the cells by approximately half. For the sludge samples, 60–75% of cells retained growth capabilities after 10 μg/ml DAPI staining, showing no significant differences to recovery rates observed for *E. coli* (**Figure 1B**). These results suggest that DAPI concentration at 10 μg/ml is optimal for polyP detection without compromising cell viability.

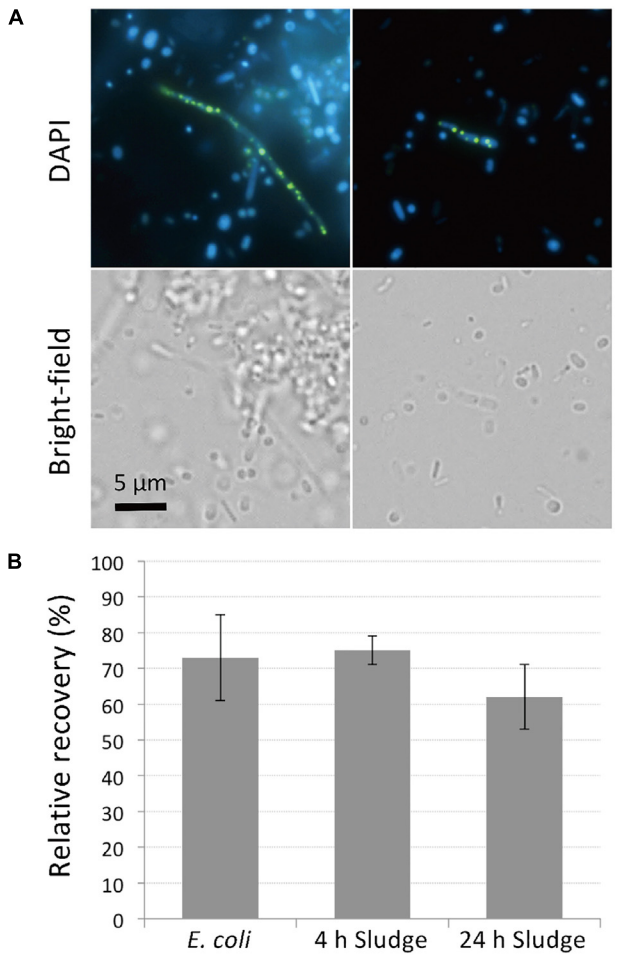


**FIGURE 1 |** DAPI stains DNA and polyP while maintaining cell viability. **(A)** DAPI-stained images of sludge sample. Top panels show fluorescence images using DAPI filter and bottom panels show bright-field images. DNA emits a blue fluorescence and polyP emits green-yellow fluorescence. **(B)** Most cells recover and generate colonies after DAPI staining. Recovery rates were compared between DAPI-stained and unstained cells by colony counting. Here, the relative recovery rates (% recovery of DAPI-stained cells relative to unstained cells) are shown. Error bars indicate standard deviations of three replicate experiments.

## FACS Enrichment and Recovery of PolyP-Accumulating Cells

The sludge sample was pre-cultured for 4 h, stained with DAPI, and subjected FACS analysis to enrich polyP-accumulating strains. The sludge sample showed a linear distribution between DNA fluorescence and polyP fluorescence (**Figure 2**). In order to avoid simply collecting large cells based only on high polyP fluorescence signal, cells that showed increased polyP fluorescence relative to the DNA fluorescence were collected. The collection gate was drawn diagonally to encompasses the 1,2% of cells deviating from the linear distribution due to increased polyP fluorescence relative to the DNA signal. These cells in the "polyP" gate were designated as polyP-positive cells and collected, along with collecting all cells ("all events") as a control, and plated onto acetate medium agar plates. After 2 days, around 30–40% of cells generated colonies on the plates relative to the cells plated out according to numbers obtained from the FACS count. Colonies were identified using colony PCR and 16S rRNA gene fragment sequencing. For the polyP-positive samples, a total of 107 colonies, and for the control samples, 106 colonies

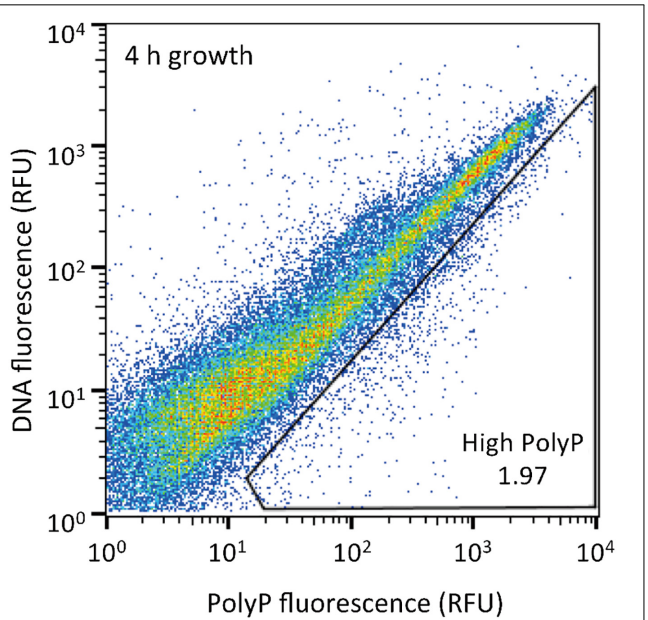


**FIGURE 2 |** Sludge samples after 4 h of growth in acetate media were stained with DAPI and the top 1,2% of cells with increased green-yellow polyP fluorescence relative to DNA fluorescence were isolated. 10,000 cells are plotted on each graph and the gate drawn onto each plot was used to isolate high polyP cells. The number in the gate represents the % of cells within the gate. RFU, relative fluorescence units.

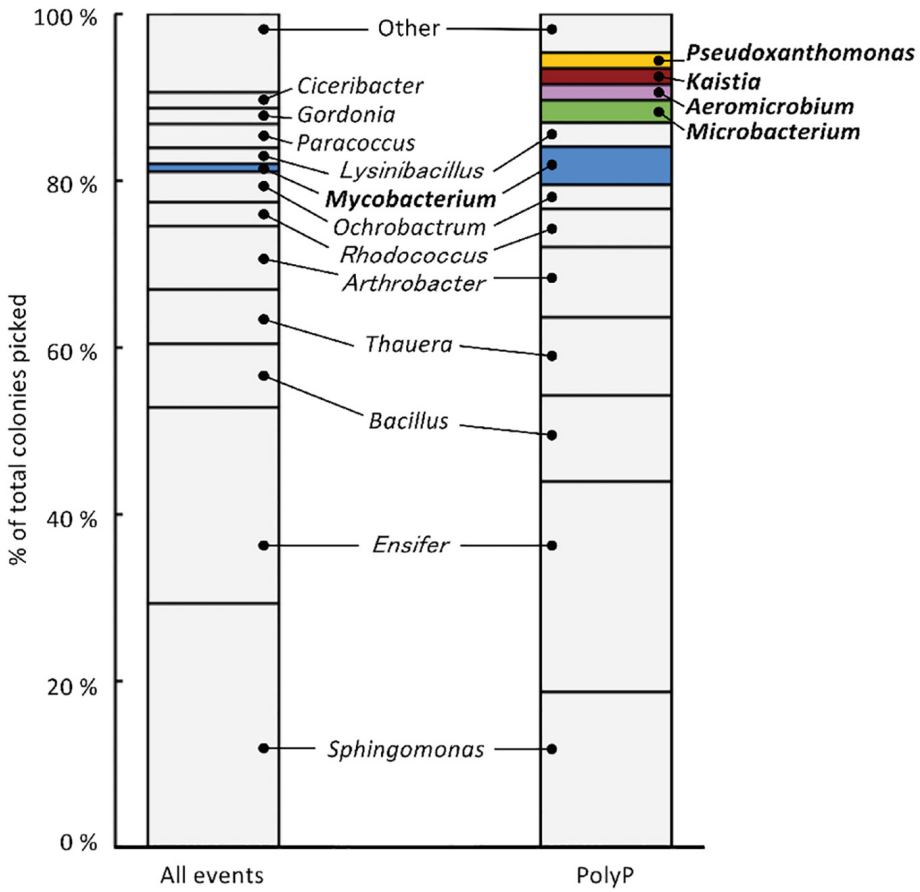


**FIGURE 3 |** 213 isolates were analyzed using 16S rRNA gene sequencing, resulting in the identification of 27 phylotypes (with a cut-off value of >97 %). "All events" indicate control fraction collected by FACS containing all cells and "PolyP" indicates strains collected from the fraction of cells showing high green-yellow fluorescence. Phylotypes that are colored in the graph were three-fold or more enriched in the polyP samples or were exclusively identified in the enrichment fraction by two or more colonies.

were sequenced. Among 213 total colonies analyzed, 27 different phylotypes (with cut off value of >97% identity) were identified (**Figure 3** and **Supplementary Table S1**).

Strains that are candidates for high polyP accumulation were identified by comparing the number of colonies identified for each phylotype between the polyP-positive sample from the "polyP" sort fraction and the "all events" control sample. This approach was taken in order to identify phylotypes that are actually enriched in the "polyP" fraction instead of the distribution tail of a particular phylotype that happened to fall into the sorting gate. Five phylotypes showed a three-fold or more enrichment in the number of colonies in the polyP-positive sample (with a minimum of two isolates), and within these five enriched phylotypes, four were exclusively identified in the polyP-positive samples (**Figure 3**). These five phylotypes stem from the phyla *Actinobacteria*, *Alphaproteobacteria*, and *Gammaproteobacteria* and are classified into genera *Aeromicrobium* (2 colonies in "PolyP"), *Microbacterium* (3 colonies in "PolyP"), *Mycobacterium* (1 colony in "All" and 5 colonies in "PolyP"), *Kaistia* (2 colonies in "PolyP"), and *Pseudoxanthomonas* (2 colonies in "PolyP") (**Supplementary Table S1**). Each of the genus is represented by a single OTU.

## FACS-Enriched Phylotypes Show Consistent PolyP Accumulating Phenotype

The five isolates (*Aeromicrobium* sp. SA_22, *Microbacterium* sp. SA_19, *Mycobacterium* sp. SA_18, *Kaistia* sp. SA_07 and *Pseudoxanthomonas* sp. SA_14) that were enriched in the polyP-positive population were cultured and re-stained with DAPI and observed using a fluorescence microscope (**Figures 4A–E**). As a control, we also imaged *Paracoccus* sp. SA_04, which was absent from the colonies recovered from the "polyP" sort, but was present in the "all events" FACS sort of the sludge samples (this strain made up ∼3% of the population in the "all events" FACS control sort, but was 0% in the "polyP" enrichment sort) (**Figure 4F**). For cells enriched in the "polyP" fraction, microscopy clearly indicated the presence of intracellular granules emitting green-yellow fluorescence (**Figure 4A–E**). All of these isolates were rod or coccus-shaped and contained one or

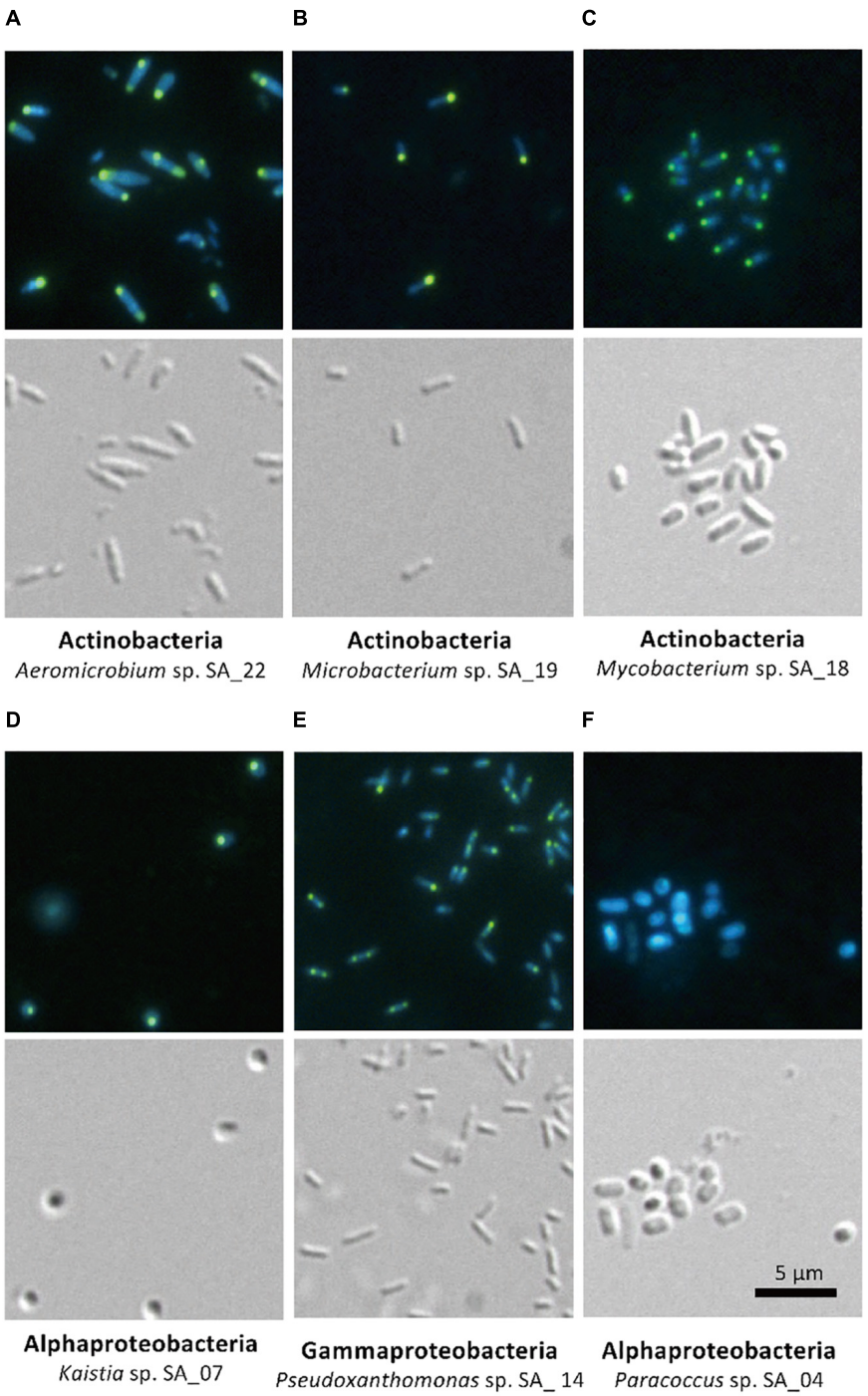


**FIGURE 4 |** Microscopy of FACS-isolated strains. The top panel for each strain shows DAPI-stained cells and the bottom panel shows differential interference image. Each set of picture is labeled below with the phylum and the strain name. **(A–E)** Strains enriched in the high-polyP sort. **(F)** *Paracoccus* strain, not detected in the high-polyP fraction after 4 h cultivation.

two large polyphosphate granule(s) in the majority of the cells. On the other hand, the *Paracoccus* sp. SA_04 did not show green-yellow fluorescence (**Figure 4F**). These results indicate that by isolating the upper 1,2% of high polyP fluorescing cells by FACS, we were able to enrich for isolates capable of polyP accumulation.

The enrichment and isolation of polyP-accumulating phylotypes from wastewater microbial community inoculated in acetate-medium contained bacteria in the phyla *Actinobacteria*, and subphyla *Gammaproteobacteria* and *Alphaproteobacteria* (**Figure 3**). Culture-independent approaches have identified

*Betaproteobacteria* related to the group *Rhodocyclus* as being dominant PAOs in many activated sludge systems, as well as members from the *Gammaproteobacteria* and a variety of *Actinobacteria* (Hesselmann et al., 1999; Kong et al., 2005; Seviour et al., 2008; He and McMahon, 2011; Kawakoshi et al., 2012; Nguyen et al., 2012, 2015; Mielczarek et al., 2013; Nielsen et al., 2019). However, it is important to note phylogenic closeness does not necessarily indicate polyP accumulation, as a close relative to a PAO *Candidatus* Accumulibacter phosphatis, a member of the order *Rhodocyclus*, does not accumulate polyP in situ (Albertsen et al., 2016). Members of *Alphaproteobacteria* have been identified in activated sludge systems in many studies, but have not been described to accumulate substantial polyP, (Wong et al., 2004; Beer et al., 2006; Ahn et al., 2007; Zhang et al., 2012; Liao et al., 2013). They may play a role in wastewater phosphate removal, as *Alphaproteobacteria Rhodospirillum rubrum* and *Agrobacterium tumefaciens* are known to accumulate polyP in acidocalcisomes, and members of the *Magnetococcaceae* family also have been found to accumulate high levels of polyP (Seufferheld et al., 2004; Rivas-Lamelo et al., 2017; Kulakovskaya et al., 2019). This, along with our results, further demonstrates the wide phylogenic span of polyP accumulation.

## Concluding Remarks

In this study, we targeted polyP-accumulating bacteria from a wastewater microbial community in order to implement FACS enrichment of living cells as an initial step for phenotype screening of cells accumulating valuable intracellular products. We demonstrated that ∼70% of cells remain viable after DAPI staining, allowing for the phenotype screening and the isolation of polyP-accumulating strains through a single method using FACS. The phylogenies of the isolated colonies were confirmed by 16S rRNA sequencing and colony abundance of each phylotypes was used to identify the PAOs enriched in the polyP-positive fractions. The polyP accumulating capabilities were confirmed by follow-up microscopy. The strains enriched in the polyP sort consistently accumulated large polyP granules. This FACS-based approach allowed for an efficient screening process by identifying promising candidates that led to the successful isolation of PAOs. Further optimization of this method and growth conditions will enable the isolation of a more extensive group of PAOs, including those that were not recovered in our study due to unfavorable growth conditions, sensitivity to DAPI staining or FACS. Comparative genomics on the isolated phylotypes will also further shed light on the polyP metabolism of the isolates. For future endeavors, this approach can not only be adapted to various environmental and wastewater samples for further isolation of PAOs, but also for other phenotype-based screens, such as using non-lethal lipophilic stains (ex. Nile Red) to stain for lipid or PHA accumulation (Lee et al., 2013; Terashima et al., 2015). Furthermore, this approach is not limited to environmental samples, but can be utilized to screen a variety of heterogeneous pool of cells, such mutant isolation after random mutagenesis on a single strain for gene-phenotype linkage analyses.

## DATA AVAILABILITY STATEMENT

The datasets generated for this study can be found in the GenBank database (Accession Nos. LC198009–LC198038).

## AUTHOR CONTRIBUTIONS

MT, YK, and SK designed the research and analyzed the data. MT conducted the experiments and wrote the manuscript with input from all authors.

## FUNDING

This work was supported by the Institute of Fermentation, Osaka.

## ACKNOWLEDGMENTS

The sludge sample and the information regarding the oxidation ditch WWTP was generously provided by Hiyoshi Corporation. We thank the open facility at the Institute for Genetic Medicine at Hokkaido University for use of flow cytometer.

## SUPPLEMENTARY MATERIAL

The Supplementary Material for this article can be found online at: https://www.frontiersin.org/articles/10.3389/fmicb.2020.00793/full#supplementary-material

## REFERENCES

Ahn, J., Schroeder, S., Beer, M., McIlroy, S., Bayly, R. C., May, J. W., et al. (2007). Ecology of the microbial community removing phosphate from wastewater under continuously aerobic conditions in a sequencing batch reactor. *Appl. Environ. Microbiol.* 73, 2257–2270. doi: 10.1128/aem.02080-06

Albertsen, M., McIlroy, S. J., Stokholm-Bjerregaard, M., Karst, S. M., and Nielsen, P. H. (2016). "Candidatus propionivibrio aalborgensis": a novel glycogen accumulating organism abundant in full-scale enhanced biological phosphorus removal plants. *Front. Microbiol.* 7:1033. doi: 10.3389/fmicb.2016.01033

Altschul, S. F., Madden, T. L., Schaffer, A. A., Zhang, J., Zhang, Z., Miller, W., et al. (1997). Gapped BLAST and PSI-BLAST: a new generation of protein database search programs. *Nucleic Acids Res.* 25, 3389–3402.

Aschar-Sobbi, R., Abramov, A. Y., Diao, C., Kargacin, M. E., Kargacin, G. J., French, R. J., et al. (2008). High sensitivity, quantitative measurements of polyphosphate using a new DAPI-Based approach. *J. Fluoresc.* 18, 859–866. doi: 10.1007/s10895-008-0315-4

Beer, M., Stratton, H. M., Griffiths, P. C., and Seviour, R. J. (2006). Which are the polyphosphate accumulating organisms in full-scale activated sludge enhanced biological phosphate removal systems in Australia? *J. Appl. Microbiol.* 100, 233–243. doi: 10.1111/j.1365-2672.2005.02784.x

Bott, M., and Eggeling, L. (2017). Novel technologies for optimal strain breeding. *Adv. Biochem. Eng. Biotechnol.* 159, 227–254. doi: 10.1007/10_2016_33

Correa Deza, M. A., Grillo-Puertas, M., Salva, S., Rapisarda, V. A., Gerez, C. L., and Font de Valdez, G. (2017). Inorganic salts and intracellular polyphosphate inclusions play a role in the thermotolerance of the immunobiotic *Lactobacillus rhamnosus* CRL 1505. *PLoS One* 12:e0179242. doi: 10.1371/journal.pone.0179242

Eggeling, L., Bott, M., and Marienhagen, J. (2015). Novel screening methods–biosensors. *Curr. Opin. Biotechnol.* 35, 30–36. doi: 10.1016/j.copbio.2014.12.021

Emerson, J. B., Adams, R. I., Roman, C. M. B., Brooks, B., Coil, D. A., Dahlhausen, K., et al. (2017). Schrodinger's microbes: tools for distinguishing the living from the dead in microbial ecosystems. *Microbiome* 5:86. doi: 10.1186/s40168-017-0285-3

Frei, C. S., Qian, S., and Cirino, P. C. (2018). New engineered phenolic biosensors based on the AraC regulatory protein. *Protein Eng. Des. Sel.* 31, 213–220. doi: 10.1093/protein/gzy024

Gawad, C., Koh, W., and Quake, S. R. (2016). Single-cell genome sequencing: current state of the science. *Nat. Rev. Genet.* 17, 175–188. doi: 10.1038/nrg.2015.16

Günther, S., Trutnau, M., Kleinsteuber, S., Hause, G., Bley, T., Roske, I., et al. (2009). Dynamics of polyphosphate-accumulating bacteria in wastewater treatment plant microbial communities detected via DAPI (4',6'-diamidino-2-phenylindole) and tetracycline labeling. *Appl. Environ. Microbiol.* 75, 2111–2121. doi: 10.1128/aem.01540-08

Han, X., Satoh, Y., Kuriki, Y., Seino, T., Fujita, S., Suda, T., et al. (2014). Polyhydroxyalkanoate production by a novel bacterium Massilia sp. *UMI*-21 isolated from seaweed, and molecular cloning of its polyhydroxyalkanoate synthase gene. *J. Biosci. Bioeng.* 118, 514–519. doi: 10.1016/j.jbiosc.2014.04.022

He, S. M., and McMahon, K. D. (2011). Microbiology of 'Candidatus Accumulibacter' in activated sludge. *Microb. Biotechnol.* 4, 603–619. doi: 10.1111/j.1751-7915.2011.00248.x

Head, I. M., Jones, D. M., and Roling, W. F. (2006). Marine microorganisms make a meal of oil. *Nat. Rev. Microbiol.* 4, 173–182. doi: 10.1038/nrmicro1348

Hesselmann, R. P. X., Werlen, C., Hahn, D., van der Meer, J. R., and Zehnder, A. J. B. (1999). Enrichment, phylogenetic analysis and detection of a bacterium that performs enhanced biological phosphate removal in activated sludge. *Syst. Appl. Microbiol.* 22, 454–465. doi: 10.1016/s0723-2020(99)80055-1

Kalyuzhnaya, M. G., Lidstrom, M. E., and Chistoserdova, L. (2008). Real-time detection of actively metabolizing microbes by redox sensing as applied to methylotroph populations in Lake Washington. *ISME J.* 2, 696–706. doi: 10.1038/ismej.2008.32

Katayama, T., Kanno, M., Morita, N., Hori, T., Narihiro, T., Mitani, Y., et al. (2014). an oleaginous bacterium that intrinsically accumulates long-chain free fatty acids in its cytoplasm. *Appl. Environ. Microbiol.* 80, 1126–1131. doi: 10.1128/aem.03056-13

Kato, S., Goya, E., Tanaka, M., Kitagawa, W., Kikuchi, Y., Asano, K., et al. (2016). Enrichment and isolation of Flavobacterium strains with tolerance to high concentrations of cesium ion. *Sci. Rep.* 6:20041. doi: 10.1038/srep20041

Kato, S., Nakamura, R., Kai, F., Watanabe, K., and Hashimoto, K. (2010). Respiratory interactions of soil bacteria with (semi)conductive iron-oxide minerals. *Environ. Microbiol.* 12, 3114–3123. doi: 10.1111/j.1462-2920.2010.02284.x

Kawakoshi, A., Nakazawa, H., Fukada, J., Sasagawa, M., Katano, Y., Nakamura, S., et al. (2012). Deciphering the genome of polyphosphate accumulating actinobacterium *Microlunatus phosphovorus*. *DNA Res.* 19, 383–394. doi: 10.1093/dnares/dss020

Kong, Y. H., Nielsen, J. L., and Nielsen, P. H. (2005). Identity and ecophysiology of uncultured actinobacterial polyphosphate-accumulating organisms in full-scale enhanced biological phosphorus removal plants. *Appl. Environ. Microbiol.* 71, 4076–4085. doi: 10.1128/aem.71.7.4076-4085.2005

Kulakovskaya, T., Zvonarev, A., Laurinavichius, K., Khokhlova, G., and Vainshtein, M. (2019). Effect of Fe on inorganic polyphosphate level in autotrophic and heterotrophic cells of *Rhodospirillum rubrum*. *Arch. Microbiol.* 201, 1307–1312. doi: 10.1007/s00203-019-01697-x

Lanham, A. B., Oehmen, A., Carvalho, G., Saunders, A. M., Nielsen, P. H., and Reis, M. A. M. (2018). Denitrification activity of polyphosphate accumulating organisms (PAOs) in full-scale wastewater treatment plants. *Water Sci. Technol.* 78, 2449–2458. doi: 10.2166/wst.2018.517

Lee, J. H., Lee, S. H., Yim, S. S., Kang, K. H., Lee, S. Y., Park, S. J., et al. (2013). Quantified high-throughput screening of *Escherichia coli* producing poly(3-hydroxybutyrate) based on FACS. *Appl. Biochem. Biotechnol.* 170, 1767–1779. doi: 10.1007/s12010-013-0311-2

Liao, R. H., Shen, K., Li, A. M., Shi, P., Li, Y., Shin, Q. Q., et al. (2013). High-nitrate wastewater treatment in an expanded granular sludge bed reactor and microbial diversity using 454 pyrosequencing analysis. *Bioresour. Technol.* 134, 190–197. doi: 10.1016/j.biortech.2012.12.057

Mahr, R., Gatgens, C., Gatgens, J., Polen, T., Kalinowski, J., and Frunzke, J. (2015). Biosensor-driven adaptive laboratory evolution of l-valine production in *Corynebacterium glutamicum*. *Metab. Eng.* 32, 184–194. doi: 10.1016/j.ymben.2015.09.017

Meier, M. J., Paterson, E. S., and Lambert, I. B. (2016). Use of substrate-induced gene expression in metagenomic analysis of an aromatic hydrocarbon-contaminated soil. *Appl. Environ. Microbiol.* 82, 897–909. doi: 10.1128/aem.03306-15

Mesquita, D. P., Amaral, A. L., and Ferreira, E. C. (2013). Activated sludge characterization through microscopy: a review on quantitative image analysis and chemometric techniques. *Anal. Chim. Acta* 802, 14–28. doi: 10.1016/j.aca.2013.09.016

Mielczarek, A. T., Nguyen, H. T. T., Nielsen, J. L., and Nielsen, P. H. (2013). Population dynamics of bacteria involved in enhanced biological phosphorus removal in Danish wastewater treatment plants. *Water Res.* 47, 1529–1544. doi: 10.1016/j.watres.2012.12.003

Mino, T., Van Loosdrecht, M. C. M., and Heijnen, J. J. (1998). Microbiology and biochemistry of the enhanced biological phosphate removal process. *Water Res.* 32, 3193–3207. doi: 10.1016/s0043-1354(98)00129-8

Ngara, T. R., and Zhang, H. (2018). Recent advances in function-based metagenomic screening. *Genomics Proteomics Bioinform.* 16, 405–415. doi: 10.1016/j.gpb.2018.01.002

Nguyen, H. T. T., Kristiansen, R., Vestergaard, M., Wimmer, R., and Nielsen, P. H. (2015). Intracellular accumulation of glycine in polyphosphate-accumulating organisms in activated sludge, a novel storage mechanism under dynamic anaerobic-aerobic conditions. *Appl. Environ. Microbiol.* 81, 4809–4818. doi: 10.1128/aem.01012-15

Nguyen, H. T. T., Nielsen, J. L., and Nielsen, P. H. (2012). Candidatus Halomonas phosphatis', a novel polyphosphate-accumulating organism in full-scale enhanced biological phosphorus removal plants. *Environ. Microbiol.* 14, 2826–2837. doi: 10.1111/j.1462-2920.2012.02826.x

Nielsen, P. H., McIlroy, S. J., Albertsen, M., and Nierychlo, M. (2019). Re-evaluating the microbiology of the enhanced biological phosphorus removal process. *Curr. Opin. Biotechnol.* 57, 111–118. doi: 10.1016/j.copbio.2019.03.008

Omelon, S., Georgiou, J., Henneman, Z. J., Wise, L. M., Sukhu, B., Hunt, T., et al. (2009). Control of vertebrate skeletal mineralization by polyphosphates. *PLoS One* 4:e0005634. doi: 10.1371/journal.pone.0005634

Perera, I. A., Abinandan, S., Subashchandrabose, S. R., Venkateswarlu, K., Naidu, R., and Megharaj, M. (2019). Advances in the technologies for studying consortia of bacteria and cyanobacteria/microalgae in wastewaters. *Crit. Rev. Biotechnol.* 39, 709–731. doi: 10.1080/07388551.2019.1597828

Rinke, C. (2018). Single-cell genomics of microbial dark matter. *Methods Mol. Biol.* 1849, 99–111. doi: 10.1007/978-1-4939-8728-3_7

Rivas-Lamelo, S., Benzerara, K., Lefèvre, C. T., Monteil, C. L., Jézéquel, D., Menguy, N., et al. (2017). Magnetotactic bacteria as a new model for P sequestration in the ferruginous lake pavin. *Geochem. Perspect. Lett.* 5, 35–41. doi: 10.7185/geochemlet.1743

Schlagenhauf, A., Pohl, S., Haidl, H., Leschnik, B., Gallistl, S., and Muntean, W. (2016). Non-enzymatic quantification of polyphosphate levels in platelet lysates and releasates. *J. Pharm. Biomed. Anal.* 131, 1–5. doi: 10.1016/j.jpba.2016.08.005

Serafim, L. S., Lemos, P. C., Levantesi, C., Tandoi, V., Santos, H., and Reis, M. A. M. (2002). Methods for detection and visualization of intracellular polymers stored by polyphosphate-accumulating microorganisms. *J. Microbiol. Methods* 51, 1–18. doi: 10.1016/s0167-7012(02)00056-8

Seufferheld, M., Lea, C. R., Vieira, M., Oldfield, E., and Docampo, R. (2004). The H(+)-pyrophosphatase of *Rhodospirillum rubrum* is predominantly located in polyphosphate-rich acidocalcisomes. *J. Biol. Chem.* 279, 51193–51202. doi: 10.1074/jbc.m406099200

Seviour, R. J., Kragelund, C., Kong, Y. H., Eales, K., Nielsen, J. L., and Nielsen, P. H. (2008). Ecophysiology of the Actinobacteria in activated sludge systems. *Antonie Van Leeuwenhoek* 94, 21–33. doi: 10.1007/s10482-008-9226-2

Shen, N., and Zhou, Y. (2016). Enhanced biological phosphorus removal with different carbon sources. *Appl. Microbiol. Biotechnol.* 100, 4735–4745. doi: 10.1007/s00253-016-7518-4

Streichan, M., Golecki, J. R., and Schon, G. (1990). Polyphosphate-accumulating bacteria from sewage plants with different processes for biological phosphorus removal. *FEMS Microbiol. Ecol.* 73, 113–124. doi: 10.1111/j.1574-6968.1990.tb03931.x

Terashima, M., Freeman, E. S., Jinkerson, R. E., and Jonikas, M. C. (2015). A fluorescence-activated cell sorting-based strategy for rapid isolation of high-lipid *Chlamydomonas mutants*. *Plant J.* 81, 147–159. doi: 10.1111/tpj.12682

Terashima, M., Yama, A., Sato, M., Yumoto, I., Kamagata, Y., and Kato, S. (2016). Culture-dependent and -independent identification of polyphosphate-accumulating *Dechloromonas* spp. predominating in a full-scale oxidation ditch wastewater treatment plant. *Microbes Environ.* 31, 449–455. doi: 10.1264/jsme2.ME16097

Tijssen, J. P. F., Beekes, H. W., and Vansteveninck, J. (1982). Localization of polyphosphates in saccharomyces-fragilis, as revealed by 4',6-Diamidino-2-phenylindole fluorescence. *Biochim. Biophys. Acta* 721, 394–398. doi: 10.1016/0167-4889(82)90094-5

Uchiyama, T., Abe, T., Ikemura, T., and Watanabe, K. (2005). Substrate-induced gene-expression screening of environmental metagenome libraries for isolation of catabolic genes. *Nat. Biotechnol.* 23, 88–93. doi: 10.1038/nbt1048

Uchiyama, T., and Miyazaki, K. (2013). Metagenomic screening for aromatic compound-responsive transcriptional regulators. *PLoS One* 8:e75795. doi: 10.1371/journal.pone.0075795

Van Nevel, S., Koetzsch, S., Proctor, C. R., Besmer, M. D., Prest, E. I., Vrouwenvelder, J. S., et al. (2017). Flow cytometric bacterial cell counts challenge conventional heterotrophic plate counts for routine microbiological drinking water monitoring. *Water Res.* 113, 191–206. doi: 10.1016/j.watres.2017.01.065

van Rossum, T., Kengen, S. W., and van der Oost, J. (2013). Reporter-based screening and selection of enzymes. *FEBS J.* 280, 2979–2996. doi: 10.1111/febs.12281

Voronkov, A., and Sinetova, M. (2019). Polyphosphate accumulation dynamics in a population of *Synechocystis* sp. PCC 6803 cells under phosphate overplus. *Protoplasma* 256, 1153–1164. doi: 10.1007/s00709-019-01374-2

Wang, Q., Garrity, G. M., Tiedje, J. M., and Cole, J. R. (2007). Naive Bayesian classifier for rapid assignment of rRNA sequences into the new bacterial taxonomy. *Appl. Environ. Microbiol.* 73, 5261–5267. doi: 10.1128/aem.00062-07

Wong, M. T., Tan, F. M., Ng, W. J., and Liu, W. T. (2004). Identification and occurrence of tetrad-forming Alphaproteobacteria in anaerobic-aerobic activated sludge processes. *Microbiol. SGM* 150, 3741–3748. doi: 10.1099/mic.0.27291-0

Yakimov, M. M., Timmis, K. N., and Golyshin, P. N. (2007). Obligate oil-degrading marine bacteria. *Curr. Opin. Biotechnol.* 18, 257–266. doi: 10.1016/j.copbio.2007.04.006

Yuan, Z., Pratt, S., and Batstone, D. J. (2012). Phosphorus recovery from wastewater through microbial processes. *Curr. Opin. Biotechnol.* 23, 878–883. doi: 10.1016/j.copbio.2012.08.001

Zengler, K., Toledo, G., Rappe, M., Elkins, J., Mathur, E. J., Short, J. M., et al. (2002). Cultivating the uncultured. *Proc. Natl. Acad. Sci. U.S.A.* 99, 15681–15686. doi: 10.1073/pnas.252630999

Zhang, T., Shao, M. F., and Ye, L. (2012). 454 Pyrosequencing reveals bacterial diversity of activated sludge from 14 sewage treatment plants. *ISME J.* 6, 1137–1147. doi: 10.1038/ismej.2011.188

**Conflict of Interest:** The authors declare that the research was conducted in the absence of any commercial or financial relationships that could be construed as a potential conflict of interest.

The handling editor declared a shared affiliation with the authors.

frontiers in Plant Science

ORIGINAL RESEARCH
published: 26 May 2020
doi: 10.3389/fpls.2020.00655

# Lack of Vacuolar $H^+$-Pyrophosphatase and Cytosolic Pyrophosphatases Causes Fatal Developmental Defects in *Arabidopsis thaliana*

*Mayu Fukuda[1], Marika Mieda[1], Ryosuke Sato[1], Satoru Kinoshita[1], Takaaki Tomoyama[1], Ali Ferjani[2], Masayoshi Maeshima[1,3]* and Shoji Segami[1,4]**

[1] Laboratory of Cell Dynamics, Graduate School of Bioagricultural Sciences, Nagoya University, Nagoya, Japan, [2] Department of Biology, Tokyo Gakugei University, Tokyo, Japan, [3] Graduate School of Bioscience and Biotechnology, Chubu University, Kasugai, Japan, [4] National Institute for Basic Biology, Okazaki, Japan

OPEN ACCESS

**Edited by:**
*Aurelio Serrano, Universidad de Sevilla and Consejo Superior de Investigaciones Científicas (CSIC), Spain*

**Reviewed by:**
*Julio Paez Valencia, University of Wisconsin-Madison, United States*
*Agustín Hernández, Federal University of São Carlos, Brazil*
*Evenilton Pessoa Costa, State University of the North Fluminense Darcy Ribeiro, Brazil*

***Correspondence:**
*Masayoshi Maeshima*
*maeshima@agr.nagoya-u.ac.jp; maeshima@isc.chubu.ac.jp*
*Shoji Segami*
*segami@nibb.ac.jp*

**Specialty section:**
*This article was submitted to Plant Metabolism and Chemodiversity, a section of the journal Frontiers in Plant Science*

**Received:** *21 February 2020*
**Accepted:** *28 April 2020*
**Published:** *26 May 2020*

**Citation:**
*Fukuda M, Mieda M, Sato R, Kinoshita S, Tomoyama T, Ferjani A, Maeshima M and Segami S (2020) Lack of Vacuolar $H^+$-Pyrophosphatase and Cytosolic Pyrophosphatases Causes Fatal Developmental Defects in Arabidopsis thaliana. Front. Plant Sci. 11:655. doi: 10.3389/fpls.2020.00655*

The cytosolic level of inorganic pyrophosphate (PPi) is finely regulated, with PPi hydrolyzed primarily by the vacuolar $H^+$-pyrophosphatase ($H^+$-PPase, VHP1/FUGU5/AVP1) and secondarily by five cytosolic soluble pyrophosphatases (sPPases; PPa1–PPa5) in *Arabidopsis thaliana*. Loss-of-function mutants of $H^+$-PPase (*fugu5*s) have been reported to show atrophic phenotypes in their rosette leaves when nitrate is the sole nitrogen source in the culture medium. For this phenotype, two questions remain unanswered: why does atrophy depend on physical contact between shoots and the medium, and how does ammonium prevent such atrophy. To understand the mechanism driving this phenotype, we analyzed the growth and phenotypes of mutants on ammonium-free medium in detail. *fugu5-1* showed cuticle defects, cell swelling, reduced β-glucan levels, and vein malformation in the leaves, suggesting cell wall weakening and cell lethality. Based on the observation in the double mutants *fugu5-1 ppa1* and *fugu5-1 ppa4* of more severe atrophy compared to *fugu5-1*, the nitrogen-dependent phenotype might be linked to PPi metabolism. To elucidate the role of ammonium in this process, we examined the fluctuations of sPPase mRNA levels and the possibility of alternative PPi-removing factors, such as other types of pyrophosphatase. First, we found that both the protein and mRNA levels of sPPases were unaffected by the nitrogen source. Second, to assess the influence of other PPi-removing factors, we examined the phenotypes of triple knockout mutants of $H^+$-PPase and two sPPases on ammonium-containing medium. Both *fugu5 ppa1 ppa2* and *fugu5 ppa1 ppa4* had nearly lethal embryonic phenotypes, with the survivors showing striking dwarfism and abnormal morphology. Moreover, *fugu5 ppa1*$^{+/-}$ *ppa4* showed severe atrophy at the leaf margins. The other triple mutants, *fugu5 ppa1 ppa5* and *fugu5 ppa2 ppa4*, exhibited death of root hairs and were nearly sterile due to deformed pistils, respectively, even when grown on standard medium. Together,

these results suggest that $H^+$-PPase and sPPases act in concert to maintain PPi homeostasis, that the existence of other PPi removers is unlikely, and that ammonium may suppress the production of PPi during nitrogen metabolism rather than stimulating PPi hydrolysis.

**Keywords: *Arabidopsis thaliana*, cell wall, leaf atrophy, nitrogen nutrient, pyrophosphate, pyrophosphatase**

## INTRODUCTION

Vacuolar $H^+$-translocating inorganic pyrophosphatase ($H^+$-PPase; gene, VHP1) has two physiological roles: hydrolysis of PPi in the cytosol and active translocation of protons into plant vacuoles. PPi is generated as a byproduct of the synthesis of macromolecules, such as DNA, RNA, proteins, and polysaccharides (Stitt, 1998; Maeshima, 2000; Heinonen, 2001). Excessive accumulation of PPi in the cytosol suppresses macromolecule biosynthesis based on the law of mass action. On the other hand, several bi-directional enzymes involved in glycolysis, including pyrophosphate-dependent phosphofructokinase (PFP), UGPase, and pyruvate phosphate dikinase (PPDK) can both utilize and produce PPi (Hajirezaei et al., 1993; Heinonen, 2001; Park et al., 2010; Chastain et al., 2011). Thus, sufficient PPi is also essential for metabolic activities in plant cells. In addition to scavenging PPi, $H^+$-PPase acts as a proton pump along with vacuolar $H^+$-ATPase to maintain acidic pH within the vacuolar lumen, which occupies the largest volume within plant cells (Maeshima and Yoshida, 1989; Nakanishi et al., 2003). In most young tissues of plants, $H^+$-PPase accounts for 10% of vacuolar membrane proteins by weight (Maeshima, 2001). Therefore, loss of $H^+$-PPase activity is expected to markedly suppress plant growth. Surprisingly, the loss of $H^+$-PPase function had a relatively mild phenotypic effects. A T-DNA insertion $H^+$-PPase knockout mutant *vhp1-1* of *Arabidopsis thaliana* (*A. thaliana*) and amino acid exchange and deletion mutants of $H^+$-PPase (*fugu5*s) showed abnormal cotyledon shape, with fewer and larger cells, when seedlings were grown in the absence of sucrose (Ferjani et al., 2011), as well as a mild suppression of plant growth (Asaoka et al., 2016), and delayed stomatal closure (Asaoka et al., 2019). Very recently, excess PPi has been reported to limit cotyledon pavement cell morphogenesis and to alter cotyledon flatness (Gunji et al., 2020). On the contrary, V-ATPase knockout mutant *vha-a2 vha-a3* showed severer growth defect and higher vacuolar pH than *fugu5*, suggesting that V-ATPase is the primary vacuolar proton pump (Krebs et al., 2010; Kriegel et al., 2015). Although another $H^+$-PPase knockout mutant allele *avp1-1* (Li et al., 2005) displayed severe auxin-related growth defects, Kriegel et al. (2015) unambiguously demonstrated that *avp1-1* growth defects are due to a secondary T-DNA insertion in ARF-GEF GNOM gene, which is essential for PIN cycling. Few other studies suggested that $H^+$-PPase can act as PPi synthase, providing PPi to sucrose oxidation pathway to energize sucrose loading into phloem (Pizzio et al., 2015; Khadilkar et al., 2016; Scholz-Starke et al., 2019).

The oblong shape of *fugu5* cotyledons recovered upon the addition of sucrose to the growth medium, as this phenotype was triggered by lowered sucrose production from seed storage lipids (Takahashi et al., 2017). Previous research into metabolite changes in *fugu5* seedlings using capillary electrophoresis time-of-flight mass spectrometry (CE-TOF-MS) and mathematical analysis revealed that UGPase is the major target of PPi's inhibitory effect on gluconeogenesis, which ultimately leads to reduced sucrose production (Ferjani et al., 2018). In addition, double knockout mutants of $H^+$-PPase and cytosolic soluble PPase (sPPase) exhibited marked changes in morphology and metabolites, including defect of cell wall components and excessive accumulation of starch, while sPPase quadruple mutants displayed a normal phenotype (Segami et al., 2018). Thus, $H^+$-PPase has a greater impact on PPi homeostasis than that of sPPases.

Some non-plant species such as the purple photosynthetic bacterium *Rhodospirillum rubrum*, parasitic protozoa, *Streptomyces*, hyperthermophilic bacteria, and *Agrobacterium* possess $H^+$-PPases (Baltscheffsky et al., 1999; Maeshima, 2000; Pérez-Castiñeira et al., 2001; Seufferheld et al., 2003; Hirono et al., 2007). In organisms without $H^+$-PPase, such as *Escherichia coli* and *Saccharomyces cerevisiae*, loss of sPPase causes growth arrest and cell death due to hyperaccumulation of PPi (Chen et al., 1990; Serrano-Bueno et al., 2013) which were rescued by genetic complementation with $H^+$-PPase (Pérez-Castiñeira et al., 2002). However, no lethal phenotype has been reported in plants to date. Other PPases such as PPi-dependent phosphofructokinase (Stitt, 1998; Amthor et al., 2019) may contribute to PPi hydrolysis in plants. In this study, we prepared multiple knockout mutants of $H^+$-PPase and sPPase(s) to identify lethal conditions in plants and to evaluate the physiological contributions of four cytosolic soluble PPases (PPa1, PPa2, PPa4, and PPa5).

Recently, growth of *fugu5* and *vhp1* was found to be severely suppressed and cell death was observed at the basal region of the true leaves when grown on ammonium-free medium (Fukuda et al., 2016), which is commonly used for hydroponics. The phenotype was rescued either by addition of ammonium to the growth medium at more than 1 mM or genetic insertion of the yeast sPPase IPP1, indicating that excessive accumulation of PPi causes the observed phenotypic effects (Fukuda et al., 2016). Based on these observations, we explored the changes in the tissues of mutant lines grown under these specific conditions. In this study, we found that deletion of both $H^+$-PPase and

**Abbreviations:** DAG, days after germination; DAP, days after pollination; $H^+$-PPase, $H^+$-translocating pyrophosphatase; PFP, PPi-dependent phosphofructokinase; PPDK, pyruvate orthophosphate dikinase; PPi, inorganic pyrophosphate; sPPase, soluble inorganic pyrophosphatase; UGPase, UDP-glucose pyrophosphorylase.

sPPase resulted in marked changes in the morphology and construction of cells and tissues, cell surface components, cell death rate, and development of plants, even in those grown on standard growth medium. These results reveal the importance of PPi homeostasis for nitrogen metabolism and amino acid biosynthesis as well as macromolecule and sucrose biosynthesis in plants. Here, we discuss the biochemical and physiological effects of excessive PPi on cell morphology and cell fate, with consideration of macromolecule biosynthesis and differences in nitrogen assimilation between roots and shoots.

# MATERIALS AND METHODS

## Plant Materials and Growth Conditions

*A. thaliana* (accession Columbia-0; hereafter referred to as wild type, WT) seeds, which were provided by the RIKEN BioResource Center (Tsukuba, Japan), were surface-sterilized, placed in the dark at 4°C for 2 days and then sown on plates of 0.5× Murashige-Skoog (MS) medium containing 2.5 mM MES-KOH (pH 5.7), 1% (w/v) sucrose, and 0.6% gellan gum (0.5× MS plates) at 22°C under long-day conditions (light/dark regime of 16 h/8 h, cool-white lamps, 90 μmol/$m^2$ s). In addition to WT, two loss-of-function mutant alleles of $H^+$-PPase (Ferjani et al., 2007, 2011), also in the Columbia-0 background, were characterized under the same conditions. The PPa5-GFP which expresses cfSGFP2-tagged PPa5 under the control of its own promoter, the loss-of-function mutants of cytosolic soluble PPase (*ppa1*, *ppa2*, *ppa4*, and *ppa5*) and double mutants (*ppa1 ppa5*, *fugu5 ppa1*, *fugu5 ppa2*, *fugu5 ppa4*, and *fugu5 ppa5*) were prepared as described previously (Segami et al., 2018). Triple mutants (*fugu5 ppa1 ppa2*, *fugu5 ppa1 ppa4*, *fugu5 ppa1 ppa5*, and *fugu5 ppa2 ppa4*) were prepared through crossing of the corresponding mutant lines.

Molecular Genetics Research Laboratory (MGRL) culture medium and a modified form of it supplemented with $NH_4^+$ ($MGRL^{Am}$) were prepared for examination of the effects of the $NO_3^-$ and $NH_4^+$ ions on plant growth. Basal MGRL medium for gel plates contained 1.5 mM $NaH_2PO_4$, 0.26 mM $Na_2HPO_4$, 1.5 mM $MgSO_4$, 2.0 mM $Ca(NO_3)_2$, 3.0 mM $KNO_3$, 12 μM Fe(III)-EDTA, 10 μM $MnSO_4$, 30 μM $H_3BO_3$, 1.0 μM $ZnSO_4$, 1.0 μM $CuSO_4$, 24 nM $(NH_4)_6Mo_7O_{24}$, 130 nM $CoCl_2$, 2% sucrose, and 0.4% gellan gum (Fujiwara et al., 1992; Naito et al., 1994). $MGRL^{Am}$ medium contained 3.0 mM $NH_4Cl$ and 3.0 mM KCl instead of 3.0 mM $KNO_3$, and thus contained 4 mM $NO_3^-$ and 3 mM $NH_4^+$ as the sole nitrogen sources. Medium pH of MGRL and $MGRL^{Am}$ were adjusted to 5.8.

## Morphological Observations

Whole plants were observed and photographed using an EOS D60 (Canon) or EOS Kiss X7 digital camera (Canon) and a stereoscopic microscope (SZ61; Olympus) equipped with a CCD camera (DP50, Olympus or DSX500, Olympus). Embryos were cleared using Hoyer's solution (Feng and Ma, 2017) and observed with a BX51 upright microscope (Olympus) equipped with a CCD camera (DP72, Olympus).

For observation of leaf veins, 10-, 15-, and 20-day-old leaves were fixed in a solution (ethanol:acetate = 3:1) at room temperature. The fixed specimens were washed in an ethanol series (70%, 50%, 30%, and 15%) and rinsed with ClearSee (10% xylitol, 15% sodium deoxycholate, and 25% urea) (Kurihara et al., 2015).

To observe the cross sections of rosette leaves, leaf samples including the leaf margin were cut to a size of 2 × 2 mm with a razor. Both ends of the leaves were sliced to allow the fixative solution to permeate well into the sample, and then the samples were immersed in a fixative solution (3% glutaraldehyde, and 50 mM Na-Pi, pH 7.0) and degassed thoroughly. The samples were embedded in 5% agar and sliced to 40 μm thickness with a microtome (VT 1200 s, Leica).

## Scanning Electron Microscopy (SEM)

Leaves were dissected from 10- and 20-DAG plants. They were mounted on a stub with adhesive carbon tape, and then transferred directly to a specimen chamber of the low-vacuum SEM (TM3030, Hitachi). Leaf epidermal cells were observed at 0–4°C, under low-vacuum conditions (30∼50 Pa).

## Confocal Laser Scanning Microscopy (CLSM)

Confocal laser scanning microscopy (CLSM) observations were conducted with an upright FV1000-D confocal laser scanning microscope (Olympus). For fluorescein diacetate (FDA) and propidium iodide (PI) staining, samples were soaked in dye solution containing 5 μg/ml FDA, 10 μg/ml PI, and 100 mM sorbitol. After 1 min, the samples were observed via CLSM. For calcofluor white staining, samples were fixed in 4% paraformaldehyde in phosphate-buffered saline (PBS) for 60 min under a vacuum at room temperature. The fixed tissues were washed twice for 1 min in PBS and cleared with ClearSee (Kurihara et al., 2015). The cleared samples were stained with 0.1% calcofluor white in ClearSee solution for 60 min and then washed with ClearSee solution for 30 min. The stained samples were observed via CLSM. UPLSAPO10X or UPLSAPO60XW (Olympus) was used as the objective lens. The excitation wavelength and transmission range for emission were 473 nm and 485 to 560 nm for FDA and green fluorescent protein (GFP), 559 nm and 617 to 717 nm for PI, and 405 nm and 425 to 475 nm for calcofluor white.

## Immunoblotting

Preparation of the soluble fraction from *A. thaliana* plants and immunoblotting were conducted as described previously (Segami et al., 2018). To detect PPa isozymes, a peptide-specific antibody for *A. thaliana* PPa1–PPa5 (C+MPMIDQGEKDDKII) was used.

## Toluidine Blue Staining

Whole plants grown on plate medium were stained with 0.1% toluidine blue for 2 min. After washing three times with distilled water, leaves were observed via a stereomicroscope (SZ61, Olympus).

## Image Analysis

Image analysis of leaf surface, leaf vein and area quantification was performed using an ImageJ Fiji (Schindelin et al., 2012).

For quantification of the leaf areole density, in brief, the vessel patterns were traced manually, and subjected to "Analyze Particles" function to extract total areole area. Areole total area was divided by total leaf area. The obtained quotient was shown as an indicator of the leaf vein continuity.

For calculation of undulation index (UI), the cell perimeter and cell area of pavement cells were measured on SEM images (3∼7 leaves per one sample, more than 15 cells from one leaf). The complexity of the pavement cells was quantified by calculating the UI (Thomas et al., 2003) using the following equation (Kürschner, 1997):

$$UI = \frac{P}{2\pi\sqrt{A/\pi}}$$

where *UI* (dimensionless) is the undulation index, *P* (μm) is the cell perimeter, and *A* ($\mu m^2$) is the cell area.

Quantification of leaf and seed area was performed using an ImageJ macro, as shown in **Supplementary Figure 8**. In brief, to select the desired area, Color Thresholder 2.0.0-rc-69/1.52p software was used. Then, the auto-generated macro code constructed by Color Thresholder was pasted into the macro at the indicated line.

# RESULTS

## Morphological Phenotypes of Leaf of *fugu5*

In *fugu5*, dead cells were observed in a highly proliferative region, namely the petiole-blade junction, of leaves grown on MGRL (Fukuda et al., 2016). To investigate further morphological changes in the other regions, we carefully observed the leaf veins, tissue construction of palisade mesophyll, and cell arrangement of the epidermis of true leaves. The first true leaves of 10-day-old plants grown on MGRL plates or plates with modified MGRL medium supplemented with 3 mM $NH_4Cl$ ($MGRL^{Am}$) were fixed with a solution of ethanol and acetate, and then treated with ClearSee to visualize leaf veins. Normal networks of leaf veins were observed in WT grown on either MGRL or $MGRL^{Am}$ plates (**Figures 1A,B**). In contrast, *fugu5-1* and *fugu5-3* leaves, particularly in the distal leaf region, did not form the normal network of veins when grown on MGRL plates (**Figures 1C,E**, arrows). This defect was clearly rescued when *fugu5-1* and *fugu5-3* was cultivated on $MGRL^{Am}$ (**Figures 1D,F**). Statistical analysis of the images using the quotient of the areole area and total leaf area values confirm that *fugu5s* grown on MGRL had abnormal networks of leaf veins, in other word, networks with low leaf vein continuity (**Figure 1G**).

Next, we observed cross sections of true leaves to investigate tissue construction. Generally, leaf mesophyll tissue is composed of four to five layers of cells of similar size. In 20-day-old plants, leaves from WT grown on both MGRL and $MGRL^{Am}$ and *fugu5-1* grown on $MGRL^{Am}$ showed the normal arrangement of cells of regular size (**Figures 2A,D,E**). In *fugu5-1* leaves, the alignment of cells (cell layers) was irregular and cell size was variable (**Figures 2B,C**). Furthermore, several large cells were present in the pavement cells of *fugu5-1* grown on MGRL (**Figure 2B**, arrowhead). *fugu5-1 ppa1* and *fugu5-1 ppa4* plants grown on $MGRL^{Am}$ showed severe phenotypic effects, including cell swelling and abnormal cell alignment (**Supplementary Figure 1**), suggesting that PPi accumulation caused cell swelling in leaves. Notably, *fugu5-1 ppa1* grown on MGRL showed cell death in the adaxial side of the leaf, while *fugu5-1 ppa4* showed cell death in the leaf margins (**Supplementary Figure 1**).

To detect morphological differences in pavement cells of 20-day-old leaves, SEM analysis was performed. Pavement cells usually exhibit puzzle-cell formation, but very recently Gunji et al. (2020) reported that the complexity of cotyledon pavement cells was reduced by PPi accumulation via inhibiting microtubule dynamics. On both MGRL and $MGRL^{Am}$, WT leaves showed normal pavement cell structure (**Figures 2F,G**). However, *fugu5-1* grown on MGRL showed obviously simplified cells (**Figure 2H**), while *fugu5-1* grown on $MGRL^{Am}$ showed puzzle-cell formation (**Figure 2I**), suggesting ammonium deficient conditions likely increased PPi level in pavement cells. Statistical analysis of UI, which indicates the degree of cell structure complexity, confirmed the above observations (**Figure 2J**).

To check whether nitrogen content was affected by *fugu5* mutation, ammonium and nitrate contents were analyzed in plant shoots. For ammonium content, there was no significant difference between the WT and *fugu5-1*, although shoots grown on $MGRL^{Am}$ accumulated twice more ammonium than MGRL in 10-DAG plants (**Supplementary Figure 2A**). On the other hands, in 10-DAG plants, there was no large difference in nitrate content except a little decrease in the WT grown on $MGRL^{Am}$ (**Supplementary Figure 2C**). In 20-DAG plants grown on $MGRL^{Am}$, both the WT and *fugu5-1* consumed ammonium and nitrate (**Supplementary Figures 2B,D**). Together, these results imply that there were no large differences between WT and *fugu5-1* in nitrogen usage.

## Defects in the Cell Wall and Cuticle Layer of Mutant Leaf Epidermis

In roots, *fugu5-1 ppa1* showed cell swelling, which was likely caused by decreased cellulose and root tip burst due to hypotonic treatment (Segami et al., 2018). Previously, we reported that contact of leaves with the culture medium was closely related to the occurrence of leaf atrophy (Fukuda et al., 2016). Therefore, we estimated that cell death in *fugu5* leaves on MGRL is caused by extracellular abiotic stresses.

To check for deficiencies of cell wall components, we stained 10-day-old leaves with calcofluor white, a fluorescent dye that binds to β-glucan (Anderson et al., 2010), and observed the epidermal cells at leaf margins with CLSM (**Figure 3**). *fugu5-1* grown on MGRL showed a strong decrease in the fluorescence signal and *fugu5-1* grown on $MGRL^{Am}$ showed a mild decrease in signal intensity compared with WT grown on both MGRL and $MGRL^{Am}$. The double mutants *fugu5-1 ppa1* and *fugu5-1 ppa4*, particularly the former, which exhibited a severe leaf phenotype (**Supplementary Figure 1**), also showed markedly low signals. These results suggest a relationship between the β-glucan content and mechanical strength of the cell wall.

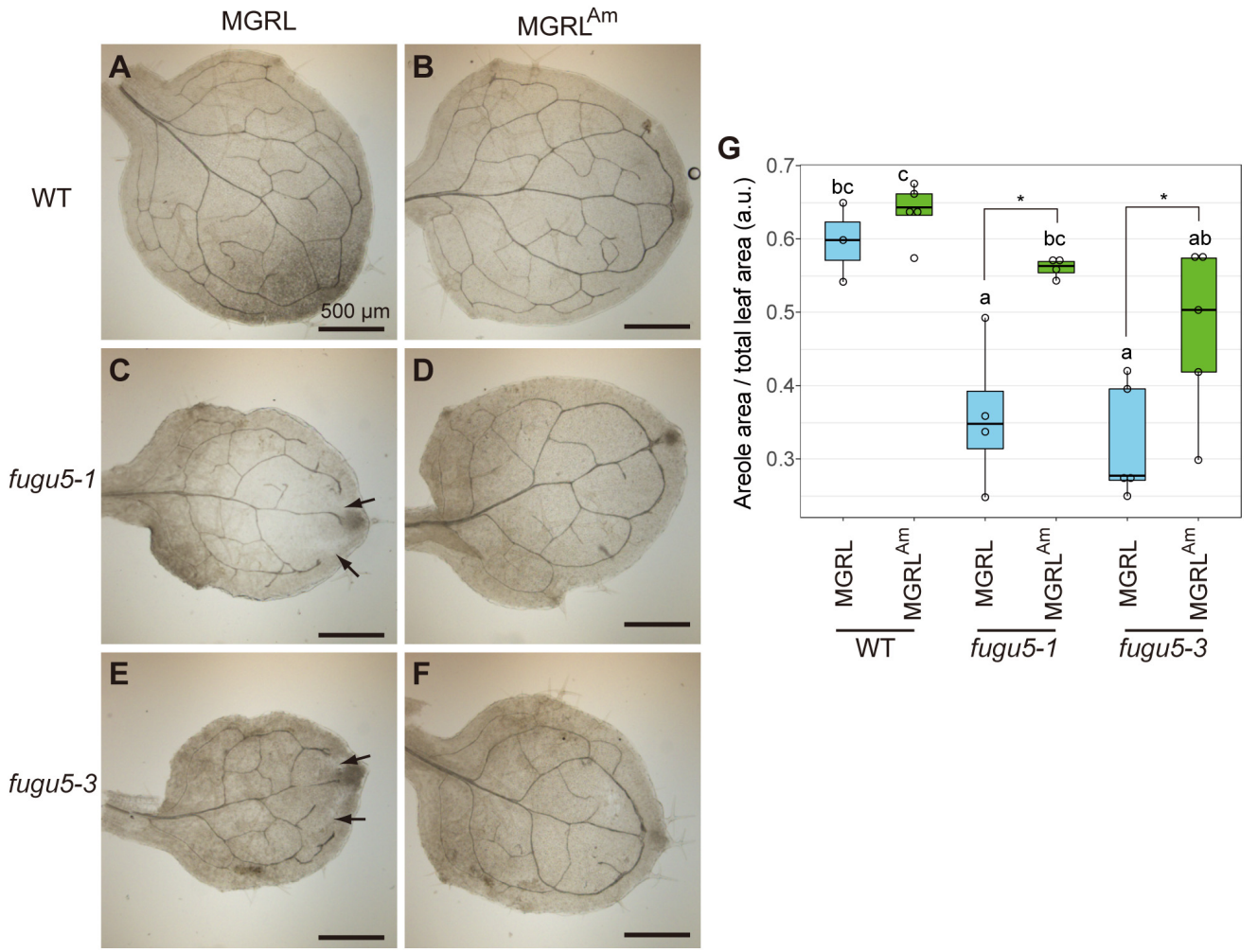


**FIGURE 1 |** Phenotype of leaf veins of *fugu5* grown on MGRL culture medium. WT, *fugu5-1* and *fugu5-3* were grown on MGRL or MGRL$^{Am}$ plates for 10 days. The first rosette leaves were collected and fixed for observation. Leaves of **(A)** WT, **(C)** *fugu5-1* and **(E)** *fugu5-3* grown on an MGRL plates and leaves of **(B)** WT, **(D)** *fugu5-1* and **(F)** *fugu5-3* grown on an MGRL$^{Am}$ plates were photographed. Scale bars = 500 μm. Arrows indicate unconnected veins in *fugu5*. **(G)** Areole density. Different letters above each bar indicate statistically significant differences ($P < 0.05$, Tukey's HSD test), and asterisks indicate statistically significant differences (*$P < 0.05$, Welch two sample *t*-test).

Generally, the surface of plant shoot tissues is covered with a thin hydrophobic layer called the cuticle (Fich et al., 2016). The cuticle prevents water loss from the leaf surface and entry of water and solutes. The cuticle is a multilayered structure composed of waxes and related hydrocarbons deposited on the leaf epidermis. To examine the integrity of the cuticles of WT and *fugu5* leaves, fresh leaves were stained with toluidine blue, which is a water-soluble dye with high affinity for acidic components. If the leaf surface lacks a cuticle layer, the dye would stain the cells (Tanaka et al., 2004). WT leaves grown on both plate media did not stain (**Figures 4A,B**). In contrast, *fugu5-1* leaves grown on MGRL stained moderately (10-day-old seedling; **Figure 4A**) or strongly at the rim of basal region (20-day-old; **Figure 4B**), which coincides with the atrophic region. These results indicate that the epidermal cells of *fugu5-1* are unable to synthesize the components to generate adequate cuticles.

## Double Mutants Grown in Ammonium-Free Medium Exhibit Severe Growth Defects

Leaf atrophy in *fugu5-1* depends on other factors, such as contact of leaves with the medium surface and agar concentration (i.e., medium hardiness) (Fukuda et al., 2016). Therefore, the observed phenotypes varied among independent experiments. Additionally, we found striking leaf atrophy in *fugu5-1 ppa1* and *fugu5-1 ppa4* plants grown on MGRL. These mutants are known to show a weak leaf atrophy phenotype when grown in half-strength MS, which contains 10 mM ammonium (Segami et al., 2018). All individuals of the double mutants failed to fully expand leaves when grown on MGRL (**Figures 5A,B**). This phenotype was stable, and the variance of leaf area for seedlings grown on MGRL was significantly lower than that on

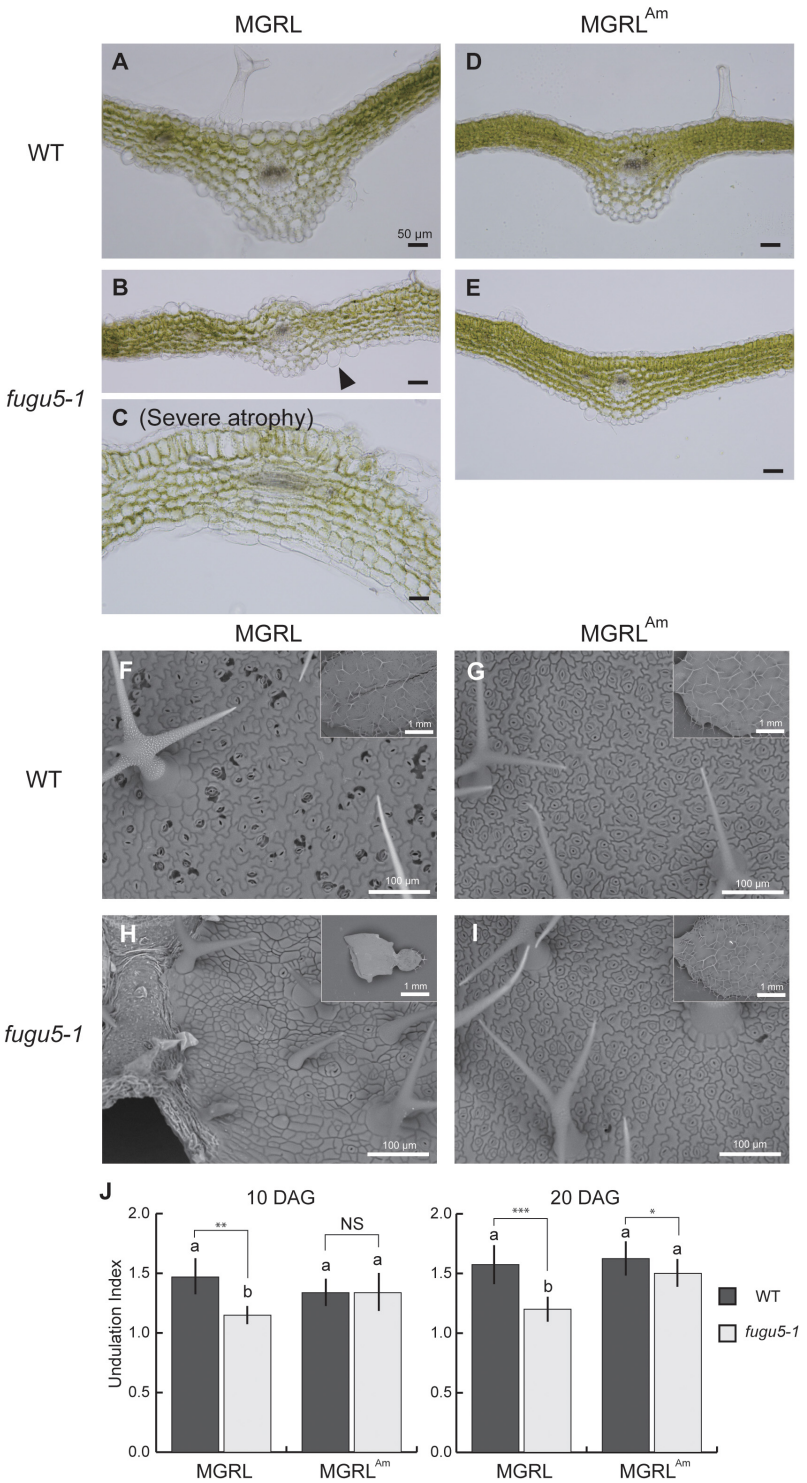


**FIGURE 2 |** Abnormal epidermal and mesophyll cells in leaves of *fugu5* grown on MGRL culture medium. WT and *fugu5-1* were grown on an MGRL or MGRL$^{Am}$ plates for 20 days. **(A–E)** Rosette leaves were fixed and sectioned for observation. Images of leaf cross sections from WT **(A)** and *fugu5-1* **(B,C)** grown on an MGRL plates, and from WT **(D)** and *fugu5-1* **(E)** grown on MGRL$^{Am}$ plates were taken using a upright microscope. Arrowheads indicate the swollen cells in epidermis. **(F–I)** SEM images of leaf adaxial side. Leaves of **(F)** WT and **(H)** *fugu5-1* grown on an MGRL plates and leaves of **(G)** WT and **(I)** *fugu5-1* grown on an MGRL$^{Am}$ plates observed. **(J)** UI of pavement cells. First leaves of 10-DAG plants and third or fourth leaves of 20-DAG plants were used for the observations above, except for severely atrophied *fugu5-1* grown on MGRL, in which the leaf stage was hardly distinguished. Different letters above each bar indicate statistically significant differences ($P < 0.05$, Tukey's HSD test), and asterisks indicate statistically significant differences at $^{*}P < 0.05$, $^{**}P < 0.01$, $^{***}P < 0.001$ (Welch two sample *t*-test, $n > 50$). Error bars indicate SD ($n > 50$).

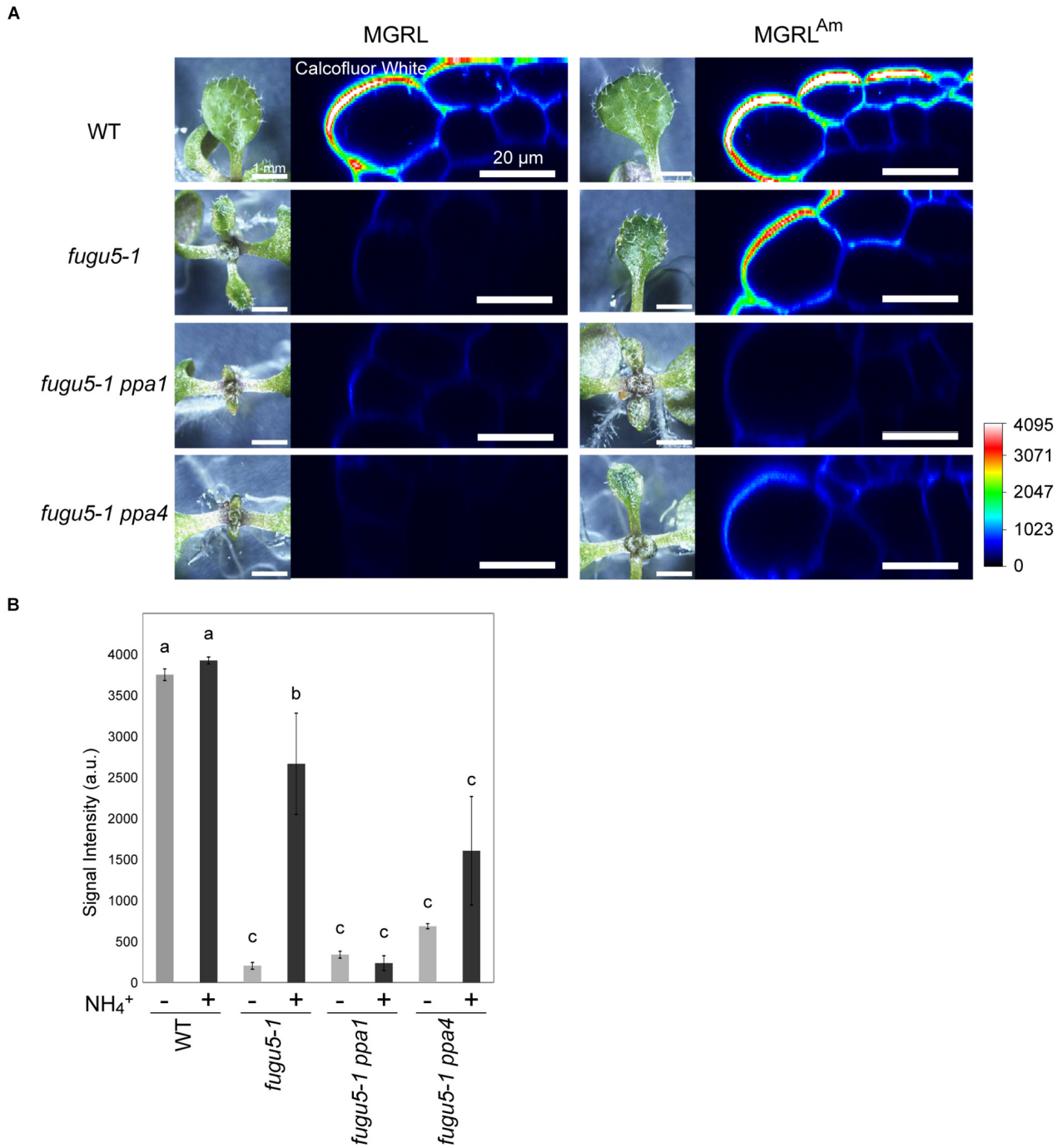


**FIGURE 3 |** Lack of β-glucan in the cell wall of leaf epidermis of mutants grown on MGRL culture medium. **(A)** X-Z section of calcofluor white-stained leaves of WT, *fugu5*, *fugu5 ppa1*, and *fugu5 ppa4*. Plantlets grown on MGRL or MGRL$^{Am}$ plates for 10 days were observed using stereomicroscopy (left panels) and CLSM (right panels). **(B)** Fluorescence intensity of calcofluor white signal at the rim of leaves. Seedlings grown on MGRL (–) or MGRL$^{Am}$ (+) plates were compared. The fluorescence of the outermost cell wall of leaf epidermis was quantified and the average signal intensities are shown. Error bars indicate standard error ($n$ = 3). Different letters above each bar indicate statistically significant differences ($P < 0.05$, Tukey's HSD test).

MGRL$^{Am}$ for each line ($F$ test; **Figure 5C**). Moreover, in 6-DAG seedlings grown with plastic sheets, which prevent direct contact of cotyledons with the growth medium, *fugu5-1 ppa1* and *fugu5-1 ppa4* grown on MGRL showed chlorosis in the emerging true leaves (**Figure 5D**, arrows). These results suggest that the phenotype exhibited by *fugu5-1 ppa1* and *fugu5-1 ppa4* grown on MGRL was independent of plant-medium contact and appeared at younger stage than that of *fugu5-1*.

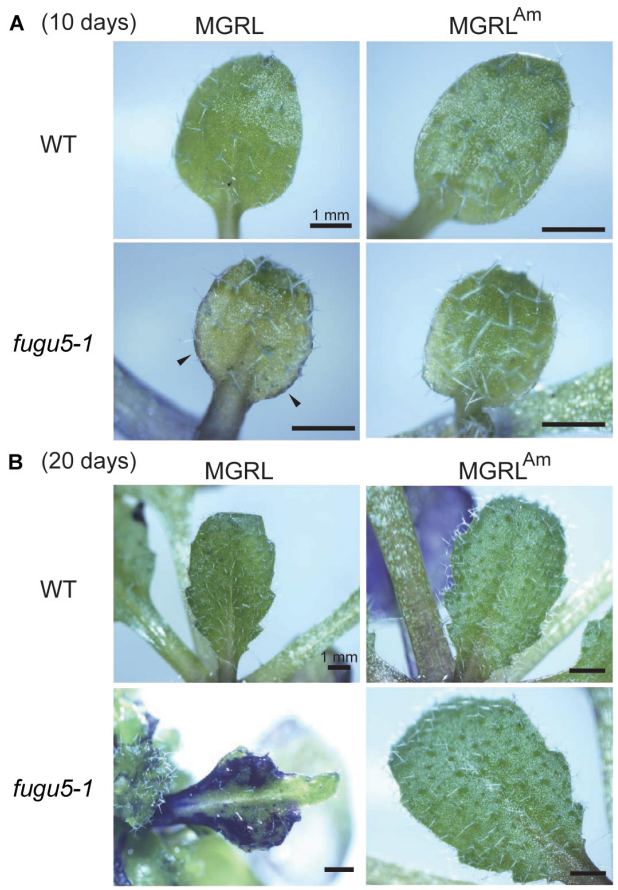


**FIGURE 4 |** Partial lack of cuticle layer of *fugu5* grown on MGRL culture medium. Whole shoots grown on MGRL or MGRL$^{Am}$ were treated with toluidine blue. **(A)** The first leaves of 10-DAG WT and *fugu5-1* grown on MGRL (left panel) or MGRL$^{Am}$ plates (right panel) were observed with a stereomicroscope. **(B)** Rosette leaves of 20-day-old WT and *fugu5-1* on MGRL (left) or MGRL$^{Am}$ plates (right) were observed. Regions stained dark blue lack a cuticle layer on the leaf surface.

## sPPase Level Was Not Affected by Supply of Ammonium Ion

A primary question of this study is how ammonium ions prevent atrophy of *fugu5* mutants. It has been shown that atrophy is triggered by excess PPi (Fukuda et al., 2016). Therefore, we postulated three possible effects of ammonium: (1) induction of sPPase expression; (2) induction of the expression of other pyrophosphatases; and/or (3) suppression of PPi generation in the mutants.

To test the first possibility, we prepared soluble fractions from WT and mutants grown on MGRL and MGRL$^{Am}$, and then performed immunoblotting using anti-sPPase, which collectively detects five sPPases, PPa1 to PPa5, to examine their protein level (Segami et al., 2018). There was no marked change in the level of sPPases between samples grown on the two types of media (**Figure 6**). In addition, we measured the mRNA levels of four sPPases and four PFPs (At1g12000, At1g20950, At1g76550, and At4g04040) and found no marked differences between MGRL and MGRL$^{Am}$ conditions (**Supplementary Figure 3** and **Supplementary Table 1**). These results suggest that ammonium does not induce the expression of sPPases or PFPs.

## Seed Viability Defects of *fugu5 ppa1 ppa2* and *fugu5 ppa1 ppa4*

To further validate the existence of other PPi-hydrolysis enzymes or PPi-removing factors, we prepared double and triple knockout mutants for various combinations of $H^+$-PPase and sPPases. If these mutants are lethal, the existence of other functional PPi removal mechanisms is unlikely. All double mutants of $H^+$-PPase and sPPase, including the most severe mutant *fugu5 ppa1*, showed normal fertility (data not shown). However, numerous shrunken seeds were observed in the triple heterozygous mutants *fugu5-1 ppa1 ppa2* and *fugu5-1 ppa1 ppa4* (**Supplementary Figure 4A**). It is worth to notice that non-shrunken seeds from *fugu5 ppa1*$^{+/-}$ *ppa2* and *fugu5 ppa1*$^{+/-}$ *ppa4* parental lines showed massive increase in size (**Supplementary Figure 4B**). The other line with shrunken seeds, *fugu5-1*$^{+/-}$ *ppa1 ppa2*, showed less size increase, suggesting that nutrient surplus due to inhibited development of 25% of seeds did not cause the size increase. Interestingly, *fugu5-1* and sPPase quadruple mutant *ppa1,2,4,5* formed larger seeds. It appears again that increased PPi somehow affected seed storage oil metabolism, in agreement with the previous report by Meyer et al. (2012), in which seed specific overexpression of PPa1 and RNAi of PPa1 or PPa4 have been analyzed.

To test the fertility of the triple mutants, we tested the genotypes of heterozygous mutant progeny. Both *fugu5-1 ppa1 ppa2* and *fugu5-1 ppa1 ppa4* germinated from freshly prepared seeds, but not from old seeds that had been stored for at least 1 year (**Tables 1**, **2**). The germination rates of *fugu5 ppa1 ppa2* and *fugu5 ppa1 ppa4* were considerably reduced. These results suggest that both *fugu5 ppa1 ppa2* and *fugu5 ppa1 ppa4* are nearly lethal and not tolerant of long-term storage.

To determine when these mutations caused seed defects, we observed ovules and embryos. At 14 DAP, when the valves turned yellow, about 75% of seeds of both *fugu5-1*$^{+/-}$ *ppa1 ppa2* and *fugu5-1 ppa1*$^{+/-}$ *ppa4* showed normal brown coloration, while the remaining 25% of seeds appeared abnormal, either green or shrunken, indicating that the ratio of these defective seeds followed Mendelian segregation (**Figures 7A,B**). In *fugu5-1 ppa1*$^{+/-}$ *ppa4*, green seeds contained green embryos with their cotyledons and hypocotyls fused together (**Figure 7A**). The genotypes of most green embryos were identified as *fugu5-1 ppa1 ppa4* homozygous (**Supplementary Figure 5**).

## Undeveloped Embryos in *fugu5 ppa1 ppa2* and *fugu5 ppa1 ppa4*

At 7–8 DAP, WT and all double mutants had green ovules, which is the normal color at this developmental stage (**Figure 7C**). The color of ovules varies during embryonic development, and WT at 5 DAP had a torpedo-stage embryo (**Figure 7D**) with yellow ovule coloration (**Figure 7C**). At 8 DAP, triple mutants

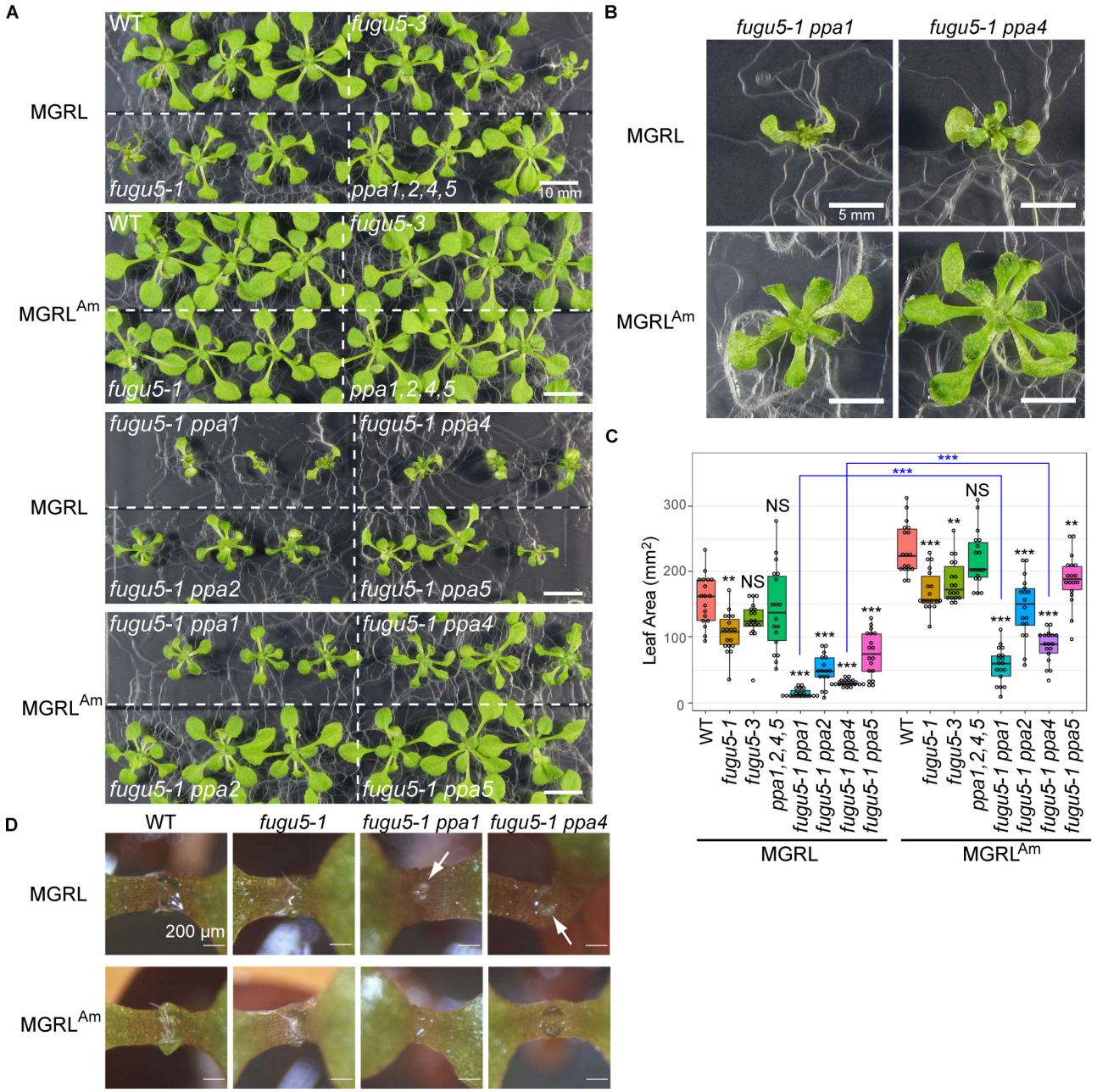


**FIGURE 5 |** Effect of $NH_4^+$ in culture medium on growth. **(A)** Growth of WT, *fugu5-1*, *fugu5-3*, *ppa1,2,4,5*, *fugu5-1 ppa1*, and *fugu5-1 ppa4* seedlings for 17 days on MGRL (without $NH_4^+$) or MGRL$^{Am}$ (3 mM $NH_4^+$) plates. **(B)** Magnified images of *fugu5-1 ppa1* and *fugu5-1 ppa4* grown on MGRL or MGRL$^{Am}$. **(C)** Leaf area was calculated using photographs and represented with boxplots and dot plots. Asterisks above the boxplots indicate statistically significant differences of mean values compared with the WT of each medium condition (**$P < 0.01$, ***$P < 0.001$, Steel test), and blue asterisks between pair indicate statistically significant differences of variances (***$P < 0.001$, $F$ test). **(D)** Seedlings were grown on MGRL or MGRL$^{Am}$ plates for 6 days using plastic sheets to prevent contact between cotyledons and medium. Arrows indicate areas of chlorosis (small true leaves).

*fugu5*$^{+/-}$ *ppa1 ppa2* and *fugu5 ppa1*$^{+/-}$ *ppa4* heterozygous, contained about 25% yellow ovules (**Figure 7C**). For further analysis of the embryos in these ovules, we observed transparent ovules cleared with Hoyer's solution (Feng and Ma, 2017). Yellow ovules of *fugu5-1*$^{+/-}$ *ppa1 ppa2* and *fugu5 ppa1*$^{+/-}$ *ppa4* heterozygous had malformed spherical embryos, whereas the embryos of green ovules exhibited bent cotyledons. The size of yellow ovule embryos was larger than that of the heart stage of the WT at 4 DAP and smaller than that of the WT torpedo stage at 5 DAP (**Figures 7D,E**, yellow ovule). In particular, *fugu5 ppa1*$^{+/-}$ *ppa4* had larger embryos than did *fugu5*$^{+/-}$ *ppa1 ppa2* heterozygous. These observations indicate that the

**TABLE 1 |** Segregation ratios of triple mutants by genotype.

| Genotype of parent | Storage[#] | Total | Genotype of seedlings | | | Ungerminated |
|---|---|---|---|---|---|---|
| | | | –/– | +/– | +/+ | |
| *fugu5-1*$^{+/-}$ *ppa1 ppa2* | 0 days | 84 | 4 | 45 | 20 | 15 |
| | 4 years | 41 | 0 | 19 | 7 | 15* |
| *fugu5-1 ppa1*$^{+/-}$ *ppa2* | 1 year | 74 | 0 | 39 | 32 | 3* |
| *fugu5-1 ppa1 ppa2*$^{+/-}$ | 1 year | 82 | 0 | 45 | 23 | 14* |
| *fugu5-1 ppa1*$^{+/-}$ *ppa4* | 0 days | 90 | 8 | 44 | 29 | 9 |
| *fugu5-3*$^{+/-}$ *ppa1 ppa4* | 2 weeks | 44 | 2 | 27 | 15 | 13 |

[#]*Storage refers to the period from seed harvest to sowing. *Some shrunken seeds were removed during the harvest process. In other cases, seeds were directly harvested from individual fruits and sowed immediately.*

**TABLE 2 |** Segregation ratios of triple mutants by phenotype.

| Genotype of parent | Storage | Seedling phenotype | | | | |
|---|---|---|---|---|---|---|
| | | Total | Dwarf | Curled | Normal | Ungerminated |
| *fugu5-1 ppa1*$^{+/-}$ *ppa4* | 1 year | 89 | 0 | 57 | 24 | 8* |
| *fugu5-3*$^{+/-}$ *ppa1 ppa4* | 1 year | 88 | 0 | 0 | 75 | 13* |

*Plants were classified by phenotype: Normal means no obvious phenotypic effects or marginal atrophy (ppa1 ppa4 or fugu5-1 ppa4-like), Curled indicates strong leaf edge atrophy (fugu5 ppa1*$^{+/-}$ *ppa4-like) and Dwarf represents severe growth defect (fugu5 ppa1 ppa4-like). See Figure 8B for morphological examples. *Some shrunken seeds were removed during the harvest process.*

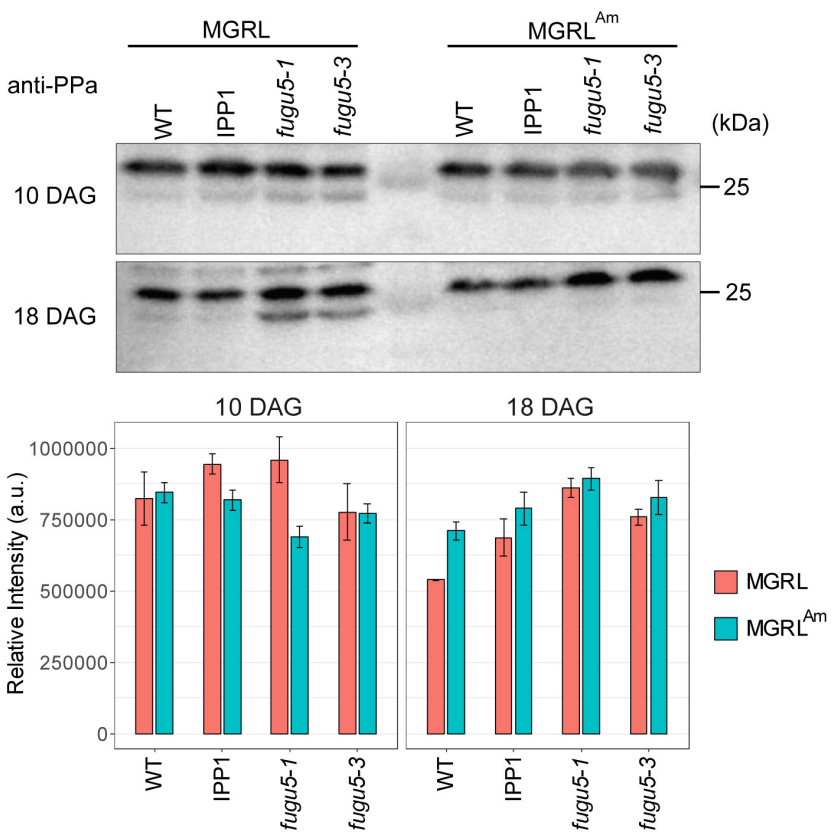


**FIGURE 6 |** Immunoblot analysis of PPases in the soluble fractions from WT and mutants. **(A)** WT, a mutant expressing yeast cytosolic PPase (IPP1), *fugu5-1*, and *fugu5-3* were grown on MGRL or MGRL$^{Am}$ plates for 10 (upper panel) or 18 days (lower panel). Soluble fractions were prepared and subjected to immunoblotting using anti-sPPase. sPPases were detected at 27 and 25 kDa. **(B)** Relative intensities of immunostained bands at 27 kDa are indicated with orange (MGRL) and blue boxes (MGRL$^{Am}$).

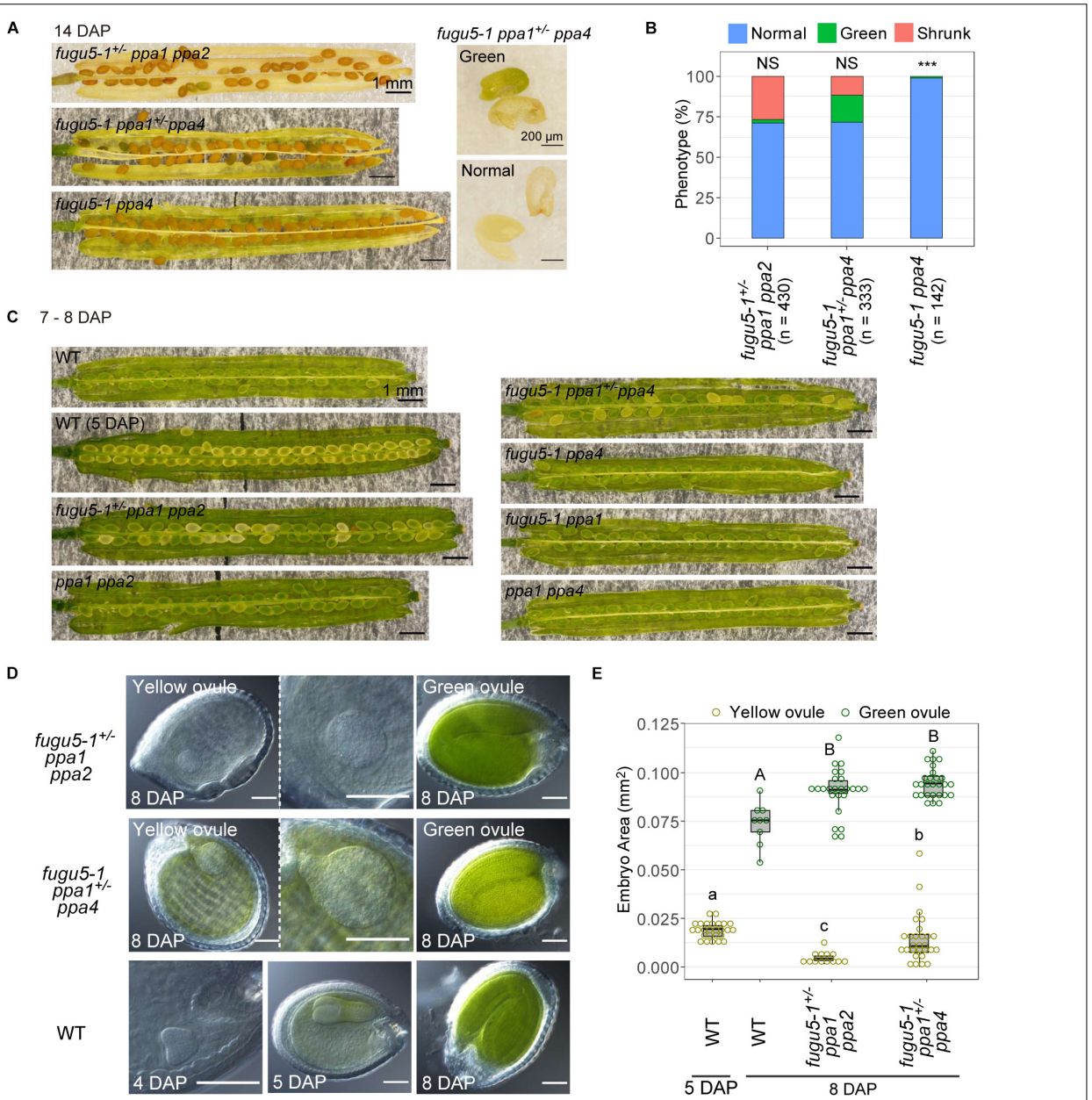


**FIGURE 7 |** Defect in seed development of *fugu5 ppa1 ppa2* and *fugu5 ppa1 ppa4*. **(A)** 14-DAP fruits of *fugu5-1*$^{+/-}$ *ppa1 ppa2, fugu5-1 ppa1*$^{+/-}$ *ppa4* and *fugu5-1 ppa4* (left). A green embryo and its seed coat of *fugu5-1 ppa1*$^{+/-}$ *ppa4* (right, green). The lower panel shows a normal embryo and its seed coat (normal). **(B)** Developmental defect of seeds in 14-DAP fruits of mutant lines. Ratios of normal (light blue), greenish (green), and shrunken seeds (orange) are shown for each line. Asterisks indicate significant differences in the proportion of normal seeds compared with 0.75 (Mendelian segregation) (*** $P < 0.001$, prop test). NS, not significant. **(C)** Images of fruits of WT and mutants at 7–8 DAP. **(D)** Ovules were treated with Hoyer's solution to achieve organ transparency and then photographed. **(E)** Embryo sizes of WT and mutants were calculated as their area in photographic images and represented by boxplots and dot plots. Different letters above each bar indicate statistically significant differences ($P < 0.01$, Steel-Dwass test).

embryos were not simply delayed in development but also grew abnormally.

## Indispensability of H$^+$-PPase and sPPases for Shoot Development

Both triple mutants *fugu5-1 ppa1 ppa2* and *fugu5-1 ppa1 ppa4* showed extremely reduced shoot growth (**Figures 8A–C**). On the other hand, the heterozygous mutant *fugu5-1*$^{+/-}$ *ppa1 ppa2* showed normal morphology and no significant differences from *ppa1 ppa2* (**Figures 8A,B**), suggesting that a single copy of the VHP1 gene is sufficient to compensate for lack of PPa1 and PPa2. Another heterozygous mutant, *fugu5-1 ppa1*$^{+/-}$ *ppa4,* showed decreased leaf area compared with *fugu5-1 ppa4* (**Figure 8C**) and a strong leaf edge curling phenotype, even when grown

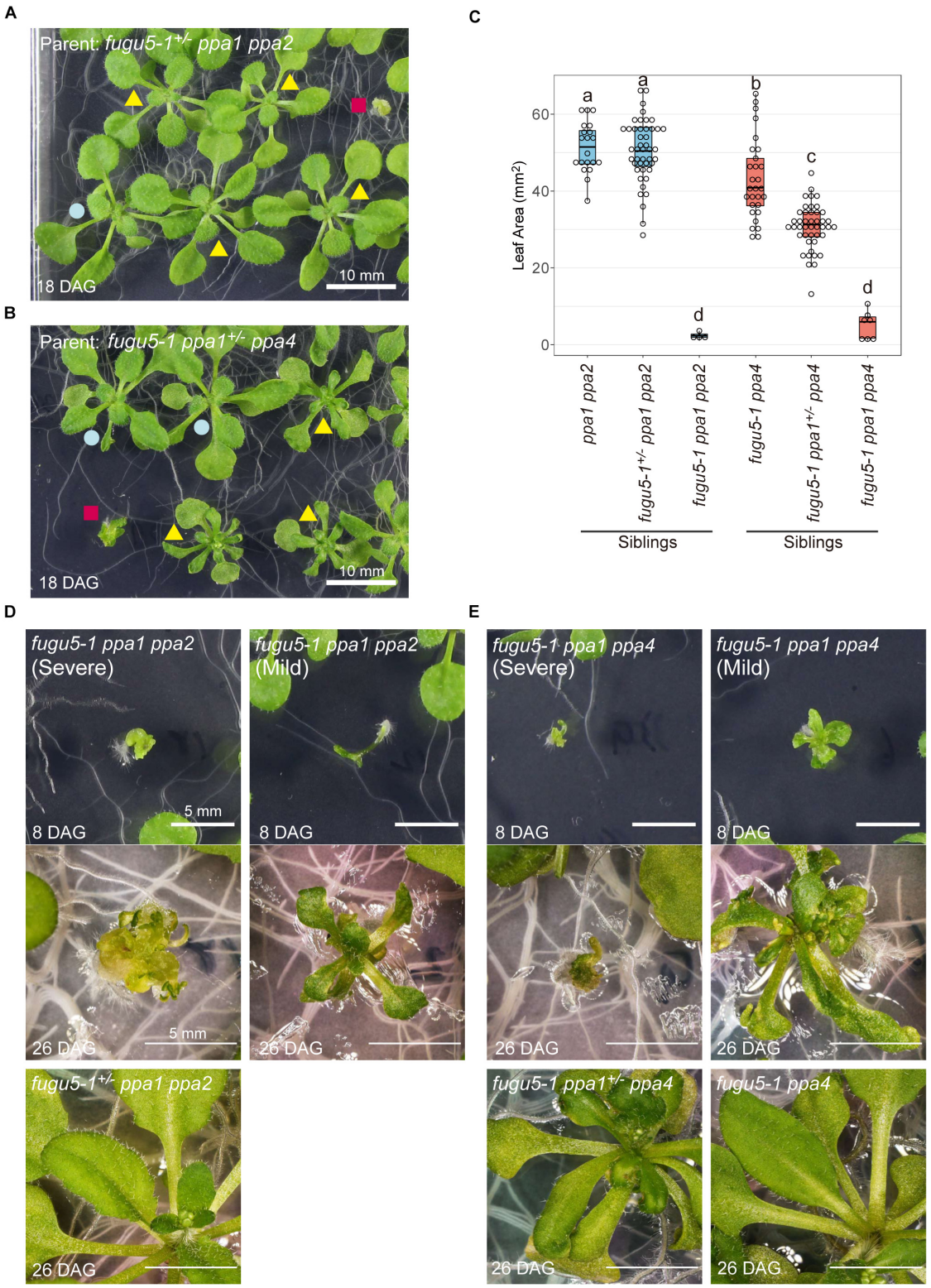


**FIGURE 8 |** Defect in development of the triple mutants *fugu5-1 ppa1 ppa2* and *fugu5 ppa1 ppa4*. **(A)** 18-DAG plants germinated from *fugu5-1*$^{+/-}$ *ppa1 ppa2* seeds. Red square indicates *fugu5-1 ppa1 ppa2*, yellow triangles indicate *fugu5-1*$^{+/-}$ *ppa1 ppa2* and blue circle indicates *ppa1 ppa2*. **(B)** 18-DAG plants germinated from *fugu5-1 ppa1*$^{+/-}$ *ppa4* seeds. Red square indicates *fugu5-1 ppa1 ppa4*, yellow triangles indicate *fugu5-1*$^{+/-}$ *ppa1 ppa4* and blue circle indicates *ppa1 ppa4*. **(C)** Comparison of leaf area of 12-DAG plants. Different letters above each plot indicate statistically significant differences ($P < 0.05$, Tukey's HSD test). **(D)** Phenotype of plant from *fugu5-1 ppa1 ppa2*. **(E)** Phenotype of *fugu5-1 ppa1 ppa4*. Plants were grown on half-strength MS plates with sucrose.

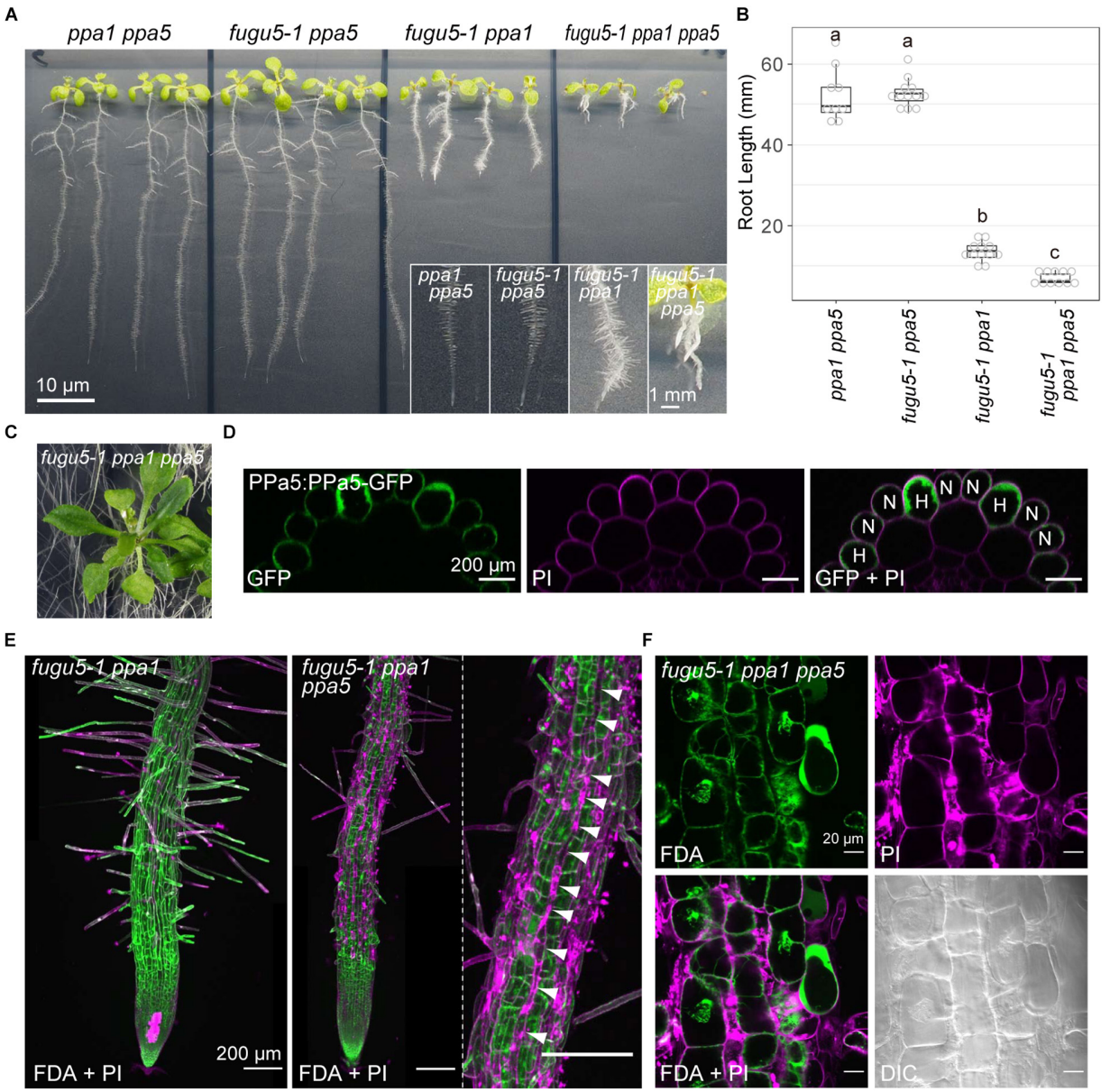


**FIGURE 9 |** Severe phenotype of the triple mutant *fugu5-1 ppa1 ppa5*. **(A)** Loss-of-function mutants (*ppa1 ppa5*, *fugu5-1 ppa5*, *fugu5-1 ppa1*, and *fugu5-1 ppa1 ppa5*) were grown on half-strength MS plates with 1% sucrose for 9 days. Lower insets show enlarged images of roots. **(B)** Root lengths of the WT and mutants were measured and visualized as boxplots and circles ($n = 3$). Different letters above each plot indicate statistically significant differences ($P < 0.05$, Tukey's HSD test). **(C)** Aboveground organs of 30-DAG *fugu5-1 ppa1 ppa5* plants. **(D)** X-Z images constructed from Z-stack images of PPa5-GFP stained with PI. Left, GFP image; middle, PI image; and right, a merged image of GFP and PI. H, root hair cell; N, non-root hair cell. **(E)** Live/dead-cell staining of roots collected from the seedlings shown in **(A)**. Roots were stained with fluorescein diacetate (FDA, green) and propidium iodide (PI, light purple). Z-stack images were captured using CLSM and then reconstructed. Arrowheads indicate a dead root hair cell line (light purple). **(F)** Enlarged images of root epidermis stained with FDA and PI.

on MS plates, on which *fugu5* showed no atrophic symptoms (**Figure 8B**; yellow triangle). At 8-DAG, both *fugu5-1 ppa1 ppa2* and *fugu5-1 ppa1 ppa4* showed extremely abnormal shapes including apparent lack of cotyledons, short roots, and distorted leaves (**Figures 8D,E**). At 26-DAG, several individuals of *fugu5-1 ppa1 ppa2* and *fugu5-1 ppa1 ppa4* successfully developed leaves, but they remained very small compared with heterozygous or double mutant plants (**Figures 8D,E**; right and lower panels), and were especially damaged in *fugu5-1 ppa1 ppa4* (**Figure 8E**; right panel). In severe cases, individuals of *fugu5-1 ppa1 ppa2* and *fugu5-1 ppa1 ppa4* had no expanded leaves (**Figures 8D,E**; left panels). These results indicate that PPa1, PPa2, and PPa4 are active in the true leaves and contribute to PPi homeostasis in the *fugu5* background.

In MGRL medium, the double mutants *fugu5-1 ppa2* and *fugu5-1 ppa5* exhibited reduced leaf area but not severe atrophy

**TABLE 3 |** Tissue-specific phenotypes of single and multiple mutants of $H^+$-PPase and sPPases.

| Organ | Mutant line | References |
|---|---|---|
| **Leaf** | | |
| Decreased size | *fugu5-3* | Asaoka et al. (2016) |
| Stomatal closure delay | *fugu5s* | Asaoka et al. (2019) |
| Altered pavement cell morphology | *fugu5-1* | This study |
| Leaf severe deformity | *fugu5-1 ppa1 ppa2* | This study |
| | *fugu5-1 ppa1 ppa4* | This study |
| Leaf edge atrophy (strong) | *fugu5-1 ppa1*$^{+/-}$ *ppa4* | This study |
| Leaf edge atrophy (mild) | *fugu5-1 ppa4* | Segami et al. (2018) |
| Leaf damage (mild) | *fugu5-1 ppa1* | Segami et al. (2018) |
| **Root** | | |
| Root tip swelling (Severe) | *fugu5-1 ppa1 ppa5* | This study |
| (Strong) | *fugu5-1 ppa1* | Segami et al. (2018) |
| (Strong) | *fugu5-1 ppa1*$^{+/-}$ *ppa2* | This study |
| (Mild) | *fugu5-1 ppa2* | Segami et al. (2018) |
| Root epidermal cell death | *fugu5-1 ppa1 ppa5* | This study |
| **Cotyledon** | | |
| Impaired cotyledon | *fugu5-1 ppa1 ppa2* | This study |
| | *fugu5-1 ppa1 ppa4* | This study |
| | *fugu5-3 ppa2 ppa4* | This study |
| Altered pavement cell morphology and microtubule dynamics | *fugu5-1, fugu5-3* | Gunji et al. (2020) |
| Elliptical shape | *fugu5s*, *vhp1-1* | Ferjani et al. (2011) |
| **Hypocotyl** | | |
| Short hypocotyl (strong) | *fugu5-1 ppa1* | Segami et al. (2018) |
| Short hypocotyl (mild) | *fugu5-1*, *fugu5-3*, *vhp1-1* | Ferjani et al. (2011) |
| **Flower** | | |
| Sterile pistil | *fugu5-3 ppa2 ppa4* | This study |
| Jaggy petal | *fugu5-3 ppa2 ppa4* | This study |
| **Embryo, seed** | | |
| Nearly lethal | *fugu5-1 ppa1 ppa2* | This study |
| | *fugu5-1 ppa1 ppa4* | This study |
| Enlargement (strong) | *fugu5-1 ppa1*$^{+/-}$ *ppa2* | This study |
| | *fugu5-1 ppa1*$^{+/-}$ *ppa4* | This study |
| Enlargement (mild) | *ppa1 ppa2 ppa4 ppa5* | This study |
| | *fugu5-1* | This study |

(**Figures 5A,C**). In addition, *fugu5-1 ppa1*$^{+/-}$ *ppa2* showed no leaf atrophy on MS medium (**Supplementary Figure 6A**), despite significantly reduced leaf area and root length (**Supplementary Figures 6B–E**), suggesting that PPa2 does not contribute to preventing leaf atrophy.

Another triple mutant *fugu5-3 ppa2 ppa4* had full viability but retarded cotyledon development compared with its heterozygous siblings *fugu5-3 ppa2*$^{+/-}$ *ppa4* and *fugu5-3 ppa2 ppa4*$^{+/-}$ (**Supplementary Figures 7A,B**). Their cotyledon shape was distorted, and more than half of the plants formed single cotyledons. Six out of 26 seedlings of this triple mutant failed to form true leaves and their growth was prematurely arrested (**Supplementary Figures 7A,C**). These observations indicate that VHP1, PPa2, and PPa4 are essential for normal development of the cotyledons and shoot apical meristem at an early developmental stage, and that PPa1 alone can maintain PPase activity at a sufficient level for viability.

In addition, *fugu5-3 ppa2 ppa4* showed severe floral phenotypic changes, including enlarged and distorted pistils (**Supplementary Figure 7D**). Although few seeds were obtained from the mutant plant, hand pollination using WT pollen was not successful. In contrast, *fugu5-3 ppa2 ppa4* pollen succeeded in pollinating WT pistils (data not shown), suggesting that the pistil of *fugu5-3 ppa2 ppa4* is impaired. The petals and sepals of the mutant also showed morphological abnormalities (**Supplementary Figure 7D**).

## Root Hair Cell-Specific Necrosis in *fugu5 ppa1 ppa5*

*fugu5-1 ppa1 ppa5* triple mutants showed normal fertility, but their phenotype was more severely affected than that of *fugu5-1 ppa1*, even on MS plates (**Figures 9A,B**). The cotyledons and true leaves of *fugu5-1 ppa1 ppa5* developed without adhesion or strong atrophy, which was also observed in the triple mutants *fugu5-1 ppa1 ppa2*, *fugu5-1 ppa1 ppa4*, and *fugu5-3 ppa2 ppa4*, suggesting negligible contribution of PPa5 to the development of cotyledons and leaves (**Figures 9A,C**). In contrast to shoots, the roots of *fugu5 ppa1 ppa5* were significantly shortened and had fewer root hairs (**Figures 9A,B**). The PPa5-GFP signal was observed only in root epidermis cells, and was particularly strong in root hair cells (**Figure 9D**). Staining of roots with FDA and PI, which visualized live/dead cells, indicated death of root epidermal cells in the root hair lines of *fugu5-1 ppa1 ppa5* (**Figures 9E,F**). Furthermore, root cells of the triple mutant were markedly shortened, even in the mature region, compared with those of *fugu5-1 ppa1* (**Figure 9E**). These observations suggest that PPa5 functions as active PPase in the mature root epidermis, mainly in root hair line cells where it acts in combination with $H^+$-PPase and PPa1. By combining the phenotypes of triple mutants described above, the physiological importance of individual sPPase in various tissues could be determined, and is summarized in **Table 3**.

# DISCUSSION

## Physiological Mechanism of Leaf Atrophy

Leaf atrophy was observed in *fugu5* mutants when grown on ammonium-free medium. This phenotype has been shown to be triggered by excessive PPi, and thus could be rescued through heterologous expression of the yeast sPPase IPP1 in *fugu5* mutants (Fukuda et al., 2016). In this study, we focused on two questions: why the atrophic phenotype depends on direct contact of shoots with medium, and the mechanism through which ammonium ions prevent leaf atrophy. To address the first question, we analyzed mutant leaves and observed several new phenotypes: irregular and disconnected leaf veins

(**Figure 1**), abnormal mesophyll tissue organization, cell swelling and severely simplified pavement cells (**Figure 2**), decrement of β-glucans (**Figure 3**), and partial lack of cuticle layer in the rosette leaves (**Figure 4**). These observations led us to consider dysfunctional biosynthesis of cell wall components and cutin. During biosynthesis of these macromolecules, PPi is generated (Heinonen, 2001). The increased level of PPi may suppress biosynthesis of these macromolecules and thus cause defects in cell wall construction and strength in growing leaves.

In the case of disconnected veins (**Figure 1**), a similar phenotype was reported in a triple mutant of glycosyltransferases in the cellulose synthase-like D (CSLD) family, *csld2 csld3 csld5*, which transfer mannose from GDP-mannose onto an endogenous acceptor (Yin et al., 2011). GDP-mannose is a nucleotide-sugar that releases PPi from its synthesis reaction, and PPi accumulation likely inhibits this reaction, as recently reported for UDP-glucose (Ferjani et al., 2018). Indeed, the etiolated hypocotyl of *fugu5-1 ppa1* contained a reduced level of mannose (Segami et al., 2018). Along with the decreased level of β-glucans in the leaf surface (**Figure 3**), cell wall synthesis was markedly inhibited in *fugu5-1* leaves grown on ammonium-free medium.

The cuticle, which acts as plant skin, is essential for the protection of leaves and structural support of tissues. Therefore, the lack of cuticle layer in *fugu5* grown on MGRL medium may result in serious damage to its tissues. In the early pathway of cuticle synthesis, ligation of CoA with long chain fatty acid by acyl-CoA synthetase (EC6.2.1.3) releases PPi into the cytosol (Pulsifer et al., 2012; Fich et al., 2016). This finding strongly suggests that the lack of VHP1 increases the PPi level in leaf epidermal cells and suppresses the formation of cuticle. Cells with immature cell walls (**Figure 3**) lacking the cuticle layer (**Figure 4**) might be physically weak and sensitive to osmotic fluctuations in the extracellular environment. Taken together, these findings indicate that leaf atrophy in *fugu5* might be caused by cell death due to external stresses, such as infiltration of solutes from the growth medium.

## The Importance of $H^+$-PPase and sPPases in Leaf Development

To address the second question regarding the physiological mechanism through which ammonium ion prevents the atrophy in *fugu5* and other mutants, we hypothesized three possible effects of ammonium in the mutants: induction of sPPases, induction of other pyrophosphatases, and suppression of PPi generation. The first hypothesis was clearly contradicted by the results of immunoblotting (**Figure 6**) and quantitative real-time polymerase chain reaction (RT-qPCR) (**Supplementary Figure 3**). We investigated the second possibility based on RT-qPCR and the lethality of multiple knockout mutants, which provides insight into the shared system of several PPases. Accumulation of PPi in cells is known to cause critical growth arrest and cell death through inhibition of fundamental metabolic reactions involving DNA and NAD (Chen et al., 1990; Serrano-Bueno et al., 2013). If ammonium induced other PPi remover(s), multiple knockout mutants of $H^+$-PPase and sPPases would survive on ammonium-containing medium.

We constructed four triple mutants, *fugu5-1 ppa1 ppa2*, *fugu5-1 ppa1 ppa4*, *fugu5-1 ppa1 ppa5*, and *fugu5-3 ppa2 ppa4*, and tested their growth on half-strength MS plates, which contained 10 mM $NH_4^+$. *fugu5-1 ppa1 ppa2* and *fugu5-1 ppa1 ppa4* showed the severest phenotypic effects, which were nearly lethal (**Tables 1**, **2** and **Figure 8**). Among their heterozygous counterparts, *fugu5-1 ppa1*$^{+/-}$ *ppa4* showed significant leaf edge atrophy (**Figures 8A,B**), whereas *fugu5-1 ppa1*$^{+/-}$ *ppa2* showed no atrophic leaf symptoms (**Supplementary Figure 6A**). These results indicate that PPa4 is more important than PPa2 for preventing leaf atrophy (**Supplementary Figures 6B,C**). The other triple mutant, *fugu5-3 ppa2 ppa4*, showed no additional effects on leaf phenotype compared to the former two mutants (**Supplementary Figure 7**). Comparison of *fugu5-3 ppa2 ppa4* with *fugu5-1 ppa1 ppa2* and *fugu5-1 ppa1 ppa4* clearly indicates the importance of PPa1 to leaf development. In GFP localization analysis for our previous study (Segami et al., 2018), VHP1-GFP and PPa1-GFP were expressed in all leaf cell types, whereas PPa2-GFP and PPa4-GFP were preferentially expressed in mesophyll and epidermis cells, respectively. Therefore, the severe phenotype of *fugu5-1 ppa1 ppa2* (**Figure 8D**) may be related to mesophyll dysfunction, whereas *fugu5-1 ppa1 ppa4* (**Figure 8E**) suffers from defects in epidermal development. PPa5-GFP is also expressed in leaf epidermis, but is limited to mature leaves, whereas PPa4-GFP is highly expressed during the early stages of leaf development. Combined with the result that *fugu5-1 ppa1 ppa5* and *fugu5 ppa5* did not exhibit strong leaf atrophy (**Figures 5A**, **9C**), this shows that the atrophic phenotype is associated with young leaves, in agreement with the notion that PPi is abundantly released in proliferating young tissues. Therefore, the combination of VHP1, PPa1, PPa2, and PPa4 might be essential for proper leaf development. The present observations of nearly lethal phenotypic effects in multiple mutants of VHP1 and PPases strongly suggest that other PPi utilizing enzymes or PPi hydrolyzing enzymes, if any exist, are not involved in PPi homeostasis.

## Phenotypes of Embryos and Root Hairs in Triple Mutants

The triple mutants *fugu5-1 ppa1 ppa2* and *fugu5-1 ppa1 ppa4* both showed nearly lethal phenotypes. Their embryos exhibited retarded growth and developed without showing the typical heart-stage and torpedo-stage shapes, becoming round in shape at 8 DAP. Finally, *fugu5-1 ppa1 ppa4* made green embryos lacking differentiation into cotyledons and hypocotyls in seeds at 14 DAP (**Figure 7A** and **Supplementary Figure 5**). In this study, we could not obtain triple homozygous mutants from seeds stored that were over 1 year (**Tables 1**, **2**). In combination with the observation that *fugu5-1 ppa1 ppa4* embryos remained green in color until 14 DAP (**Figure 7A** and **Supplementary Figure 5**), this result suggests that seed maturation in the mutant is insufficient for maintaining seed longevity during long-term storage. The high ratio of shrunken seeds to normal-sized ones (**Figure 7B**) and low germination rate suggest that PPa2 is more important than PPa4 during embryogenesis.

*fugu5-1 ppa1 ppa5* showed phenotypes of short roots, short root cells, fewer root hairs, and necrosis of the root epidermis (**Figures 9A,B,E,F**). Root epidermis is divided into two types: root hair cells and non-root hair cells (Galway et al., 1994; Berger et al., 1998). Notably, root epidermis is normally viable at an early developmental stage, before root-hair formation (**Figure 9E**). PPa5-GFP was expressed primarily in root hairs in the root elongation zone (**Figure 9D**) and PPa3-GFP was also expressed in root hair cells, whereas PPa4-GFP was mainly detected in non-root hair cells and PPa2-GFP was expressed only during the early developmental stage (Segami et al., 2018). These observations coincide with the defective root hair phenotype of *fugu5-1 ppa1 ppa5*, in which root hair line cells died (**Figure 9E**). In this triple mutant, most root hairs died, but several elongated hairs were observed (**Figures 9A,E**), suggesting that the formation and elongation of root hairs require precise regulation of PPi at a critical level and the remaining PPa3 activity was insufficient to maintain viability.

### Possible Mechanism for Rescue of Mutant Phenotype by Ammonium

To explore the relationship between PPi production and absence of ammonium supply, here we considered organ-specific nitrogen metabolism. Most plants incorporate and utilize ammonium preferentially over nitrate (Howitt and Udvardi, 2000; Konishi et al., 2017). Thus, *A. thaliana* incorporates $NH_4^+$ preferentially from $MGRL^{Am}$ medium and converts $NH_4^+$ to amino acids in roots to reduce the toxic $NH_4^+$ levels (Hachiya and Sakakibara, 2017). The amino acids thus generated are transported from the roots to shoots (Konishi et al., 2017). In contrast, $NO_3^-$ is incorporated by roots, and then transported directly from roots to shoots because $NO_3^-$ has no toxicity to plant cells. In shoots, $NO_3^-$ is reduced to $NH_4^+$ via NAD(P)H reducing equivalents that are mainly supplied by photosynthesis and is subsequently incorporated into glutamine. The assimilation of nitrate is assumed to act as a strong consumer of reducing power, and therefore ammonium utilization greatly decreases the energy consumption required to synthesize organic N compounds (Williams et al., 1987; Hachiya and Sakakibara, 2017; Gakière et al., 2018).

Considering the differences in nitrogen metabolism between roots and shoots, metabolism of $NO_3^-$ into amino acids occurs preferentially in shoots grown on MGRL medium. Although $NO_3^-$ reduction itself includes no PPi-generating reactions, for example, the biosynthesis of NAD, which is involved in $NO_3^-$ reduction, generates PPi (Heinonen, 2001; Gakière et al., 2018). We predict that the elevated level of PPi formed from $NO_3^-$ reduction related pathway in shoots causes cellular dysfunction and atrophy in *fugu5* plants grown on MGRL medium. The addition of ammonium to the medium might reduce the generation of PPi in shoots by promoting amino acid synthesis in roots. This organ-specific nitrogen metabolism for synthesis of amino acids rescues the phenotype of *fugu5*. To further test this hypothesis, we will analyze transcriptomic and metabolomic data and then identify the pathways generating high PPi levels under ammonium-free conditions.

## DATA AVAILABILITY STATEMENT

All datasets generated for this study are included in the article/**Supplementary Material**.

## AUTHOR CONTRIBUTIONS

MF co-coordinated the project, contributed to phenotyping, analyzed the data, and drafted the manuscript. MMi conducted microscopy and calcofluor white staining. MMa conceived of and initiated the project, obtained funding, and contributed to the manuscript. SS conducted association analysis, constructed multiple mutants, wrote and finalized the manuscript. AF provided the *fugu5* mutants, $AVP1_{pro}$::*IPP1* transgenic lines and contributed to the manuscript. SK conducted image analysis. RS conducted RT-qPCR analysis. TT contributed to seed phenotype analysis. All authors read and approved the final manuscript.

## FUNDING

This work was supported by JSPS KAKENHI Grants 26252011, 26113506, and 19H03177 to MMa, and 16K18687 to SS; Grant-in-Aid for Scientific Research (B) (16H04803 to AF); Grant-in-Aid for Scientific Research on Innovative Areas (25113002 and 18H05487 to AF); and MF received a Research Fellowship for Young Scientists.

## ACKNOWLEDGMENTS

We are grateful to Drs. Yoichi Nakanishi and Miki Kawachi (Nagoya University) for their valuable advice, Mr. Yuta Kato and Dr. Takao Oi (Nagoya University) for their technical advice on SEM and leaf sectioning, and Dr. Hitoshi Sakakibara (Nagoya University) and Dr. Takushi Hachiya (Shimane University) for their valuable advice and for providing experimental equipment.

## SUPPLEMENTARY MATERIAL

The Supplementary Material for this article can be found online at: https://www.frontiersin.org/articles/10.3389/fpls.2020.00655/full#supplementary-material

## REFERENCES

Amthor, J. S., Bar-Even, A., Hanson, A. D., Millar, A. H., Stitt, M., Sweetlove, L. J., et al. (2019). Engineering strategies to boost crop productivity by cutting respiratory carbon loss. *Plant Cell* 31, 297–314. doi: 10.1105/tpc.18.00743

Anderson, C. T., Carroll, A., Akhmetova, L., and Somerville, C. (2010). Real-time imaging of cellulose reorientation during cell wall expansion

in *Arabidopsis* roots. *Plant Physiol.* 152, 787–796. doi: 10.1104/pp.109.150128

Asaoka, M., Inoue, S. I., Gunji, S., Kinoshita, T., Maeshima, M., Tsukaya, H., et al. (2019). Excess pyrophosphate within guard cells delays stomatal closure. *Plant Cell Physiol.* 60, 875–887. doi: 10.1093/pcp/pcz002

Asaoka, M., Segami, S., Ferjani, A., and Maeshima, M. (2016). Contribution of PPi-hydrolyzing function of vacuolar $H^+$-pyrophosphatase in vegetative growth of *Arabidopsis* : evidenced by expression of uncoupling mutated enzymes. *Front. Plant Sci.* 7:415. doi: 10.3389/fpls.2016.00415

Baltscheffsky, M., Schultz, A., and Baltscheffsky, H. (1999). $H^+$-proton-pumping inorganic pyrophosphatase: A tightly membrane-bound family. *FEBS Lett.* 452, 121–127. doi: 10.1016/S0014-5793(99)00617-611

Berger, F., Haseloff, J., Schiefelbein, J., and Dolan, L. (1998). Positional information in root epidermis is defined during embryogenesis and acts in domains with strict boundaries. *Curr. Biol.* 8, 421–430. doi: 10.1016/S0960-9822(98)70176-70179

Chastain, C. J., Failing, C. J., Manandhar, L., Zimmerman, M. A., Lakner, M. M., and Nguyen, T. H. T. (2011). Functional evolution of C4 pyruvate, orthophosphate dikinase. *J. Exp. Bot.* 62, 3083–3091. doi: 10.1093/jxb/err058

Chen, J., Brevet, A., Fromant, M., Leveque, F., Schmitter, J. M., Blanquet, S., et al. (1990). Pyrophosphatase is essential for growth of *Escherichia coli*. *J. Bacteriol.* 172, 5686–5689. doi: 10.1128/jb.172.10.5686-5689.1990

Feng, J., and Ma, L. (2017). A method for characterizing embryogenesis in *Arabidopsis*. *J. Vis. Exp.* 2017, 1–7. doi: 10.3791/55969

Ferjani, A., Horiguchi, G., Yano, S., and Tsukaya, H. (2007). Analysis of leaf development in *fugu* mutants of *Arabidopsis* reveals three compensation modes that modulate cell expansion in determinate organs. *Plant Physiol.* 144, 988–999. doi: 10.1104/pp.107.099325

Ferjani, A., Kawade, K., Asaoka, M., Oikawa, A., Okada, T., Mochizuki, A., et al. (2018). Pyrophosphate inhibits gluconeogenesis by restricting UDP-glucose formation *in vivo*. *Sci. Rep.* 8, 1–10. doi: 10.1038/s41598-018-32894-32891

Ferjani, A., Segami, S., Horiguchi, G., Muto, Y., Maeshima, M., and Tsukayad, H. (2011). Keep an eye on PPi: the vacuolar-type $H^+$-pyrophosphatase regulates postgerminative development in *Arabidopsis*. *Plant Cell* 23, 2895–2908. doi: 10.1105/tpc.111.085415

Fich, E. A., Segerson, N. A., and Rose, J. K. C. (2016). The plant polyester cutin: biosynthesis, structure, and biological roles. *Annu. Rev. Plant Biol.* 67, 207–233. doi: 10.1146/annurev-arplant-043015-111929

Fujiwara, T., Hirai, M. Y., Chino, M., Komeda, Y., and Naito, S. (1992). Effects of sulfur nutrition on expression of the soybean seed storage protein genes in transgenic petunia. *Plant Physiol.* 99, 263–268. doi: 10.1104/pp.99.1.263

Fukuda, M., Segami, S., Tomoyama, T., Asaoka, M., Nakanishi, Y., Gunji, S., et al. (2016). Lack of $H^+$-pyrophosphatase prompts developmental damage in *Arabidopsis* leaves on ammonia-free culture medium. *Front. Plant Sci.* 7:819. doi: 10.3389/fpls.2016.00819

Gakière, B., Hao, J., de Bont, L., Pétriacq, P., Nunes-Nesi, A., and Fernie, A. R. (2018). $NAD^+$ biosynthesis and signaling in plants. *CRC. Crit. Rev. Plant Sci.* 37, 259–307. doi: 10.1080/07352689.2018.1505591

Galway, M. E., Masucci, J. D., Lloyd, A. M., Walbot, V., Davis, R. W., and Schiefelbein, J. W. (1994). The TTG gene is required to specify epidermal cell fate and cell patterning in the *Arabidopsis* root. *Dev. Biol.* 166, 740–754. doi: 10.1006/dbio.1994.1352

Gunji, S., Oda, Y., Takigawa-Imamura, H., Tsukaya, H., and Ferjani, A. (2020). Excess pyrophosphate restrains pavement cell morphogenesis and alters organ flatness in *Arabidopsis thaliana*. *Front. Plant Sci.* 11:13. doi: 10.3389/flps.2020.00031

Hachiya, T., and Sakakibara, H. (2017). Interactions between nitrate and ammonium in their uptake, allocation, assimilation, and signaling in plants. *J. Exp. Bot.* 68, 2501–2512. doi: 10.1093/jxb/erw449

Hajirezaei, M., Sonnewald, U., Viola, R., Carlisle, S., Dennis, D., and Stitt, M. (1993). Transgenic potato plants with strongly decreased expression of pyrophosphate:fructose-6-phosphate phosphotransferase show no visible phenotype and only minor changes in metabolic fluxes in their tubers. *Planta* 192, 16–30. doi: 10.1007/BF00198688

Heinonen, J. K. (2001). *Biological Role of Inorganic Pyrophosphate*. Boston, MA: Springer, doi: 10.1007/978-1-4615-1433-1436

Hirono, M., Nakanishi, Y., and Maeshima, M. (2007). Identification of amino acid residues participating in the energy coupling and proton transport of *Streptomyces coelicolor* A3(2) $H^+$-pyrophosphatase. *Biochim. Biophys. Acta Bioenerg.* 1767, 1401–1411. doi: 10.1016/j.bbabio.2007.09.007

Howitt, S. M., and Udvardi, M. K. (2000). Structure, function and regulation of ammonium transporters in plants. *Biochim. Biophys. Acta Biomembr.* 1465, 152–170. doi: 10.1016/S0005-2736(00)00136-X

Khadilkar, A. S., Yadav, U. P., Salazar, C., Shulaev, V., Paez-Valencia, J., Pizzio, G. A., et al. (2016). Constitutive and companion cell-specific overexpression of AVP1, encoding a proton-pumping pyrophosphatase, enhances biomass accumulation, phloem loading, and long-distance transport. *Plant Physiol.* 170, 401–414. doi: 10.1104/pp.15.01409

Konishi, N., Ishiyama, K., Beier, M. P., Inoue, E., Kanno, K., Yamaya, T., et al. (2017). Contributions of two cytosolic glutamine synthetase isozymes to ammonium assimilation in *Arabidopsis* roots. *J. Exp. Bot.* 68, 613–625. doi: 10.1093/jxb/erw454

Krebs, M., Beyhl, D., Görlich, E., Al-Rasheid, K. A. S., Marten, I., Stierhof, Y. D., et al. (2010). Arabidopsis V-ATPase activity at the tonoplast is required for efficient nutrient storage but not for sodium accumulation. *Proc. Natl. Acad. Sci. U.S.A.* 107, 3251–3256. doi: 10.1073/pnas.0913035107

Kriegel, A., Andrés, Z., Medzihradszky, A., Krüger, F., Scholl, S., Delang, S., et al. (2015). Job sharing in the endomembrane system: vacuolar acidification requires the combined activity of V-ATPase and V-PPase. *Plant Cell* 27, 3383–3396. doi: 10.1105/tpc.15.00733

Kurihara, D., Mizuta, Y., Sato, Y., and Higashiyama, T. (2015). ClearSee: a rapid optical clearing reagent for whole-plant fluorescence imaging. *Development* 142, 4168–4179. doi: 10.1242/dev.127613

Kürschner, W. M. (1997). The anatomical diversity of recent and fossil leaves of the durmast oak (*Quercus petraea* Lieblein/ *Q.* pseudocastanea Goeppert)—implications for their use as biosensors of palaeoatmospheric CO2 levels. *Rev. Palaeobot. Palynol.* 96, 1–30. doi: 10.1016/S0034-6667(96)00051-6

Li, J., Yang, H., Peer, W. A., Richter, G., Blakeslee, J., Bandyopadhyay, A., et al. (2005). Plant Science: *Arabidopsis* $H^+$-PPase AVP1 regulates auxin-mediated organ development. *Science* 310, 121–125. doi: 10.1126/science.1115711

Maeshima, M. (2000). Vacuolar $H^+$-pyrophosphatase. *Biochim. Biophys. Acta* 1465, 37–51.

Maeshima, M. (2001). Tonoplast transporters: organization and function. *Annu. Rev. Plant Physiol. Plant Mol. Biol.* 52, 469–497. doi: 10.1146/annurev.arplant.52.1.469

Maeshima, M., and Yoshida, S. (1989). Purification and properties of vacuolar membrane proton-translocating inorganic pyrophosphatase from mung bean. *J. Biol. Chem.* 264, 20068–20073.

Meyer, K., Stecca, K. L., Ewell-Hicks, K., Allen, S. M., and Everard, J. D. (2012). Oil and protein accumulation in developing seeds is influenced by the expression of a cytosolic pyrophosphatase in *Arabidopsis*. *Plant Physiol.* 159, 1221–1234.

Naito, S., Hirai, M. Y., Chino, M., and Komeda, Y. (1994). Expression of a soybean (*Glycine max* [L.] Merr.) seed storage protein gene in transgenic *Arabidopsis thaliana* and its response to nutritional stress and to abscisic acid mutations. *Plant Physiol.* 104, 497–503. doi: 10.1104/pp.104.2.497

Nakanishi, Y., Yabe, I., and Maeshima, M. (2003). Patch clamp analysis of a $H^+$ pump heterologously expressed in giant yeast vacuoles. *J. Biochem.* 134, 615–623. doi: 10.1093/jb/mvg184

Park, J. I., Ishimizu, T., Suwabe, K., Sudo, K., Masuko, H., Hakozaki, H., et al. (2010). UDP-glucose pyrophosphorylase is rate limiting in vegetative and reproductive phases in *Arabidopsis thaliana*. *Plant Cell Physiol.* 51, 981–996. doi: 10.1093/pcp/pcq057

Pérez-Castiñeira, J. R., López-Marqués, R. L., Losada, M., and Serrano, A. (2001). A thermostable $K^+$-stimulated vacuolar-type pyrophosphatase from the hyperthermophilic bacterium *Thermotoga maritima*. *FEBS Lett.* 496, 6–11. doi: 10.1016/S0014-5793(01)02390-2390

Pérez-Castiñeira, J. R., López-Marqués, R. L., Villalba, J. M., Losada, M., and Serrano, A. (2002). Functional complementation of yeast cytosolic pyrophosphatase by bacterial and plant $H^+$-translocating pyrophosphatases. *Proc. Natl. Acad. Sci. U.S.A.* 99, 15914–15919. doi: 10.1073/pnas.242625399

Pizzio, G. A., Paez-Valencia, J., Khadilkar, A. S., Regmi, K., Patron-Soberano, A., Zhang, S., et al. (2015). Arabidopsis type I proton-pumping pyrophosphatase expresses strongly in phloem, where it is required for pyrophosphate metabolism and photosynthate partitioning. *Plant Physiol.* 167, 1541–1553. doi: 10.1104/pp.114.254342

Pulsifer, I. P., Kluge, S., and Rowland, O. (2012). *Arabidopsisi* LONG-CHAIN ACYL-COA SYNTHETASE 1 (LACS1), LACS2, and LACS3 facilitate fatty acid uptake in yeast. *Plant Physiol. Biochem.* 51, 31–39. doi: 10.1016/j.plaphy.2011.10.003

Schindelin, J., Arganda-Carreras, I., Frise, E., Kaynig, V., Longair, M., Pietzsch, T., et al. (2012). Fiji: an open-source platform for biological-image analysis. *Nat. Methods* 9, 676–682. doi: 10.1038/nmeth.2019

Scholz-Starke, J., Primo, C., Yang, J., Kandel, R., Gaxiola, R. A., and Hirschi, K. D. (2019). The flip side of the *Arabidopsis* type I proton-pumping pyrophosphatase (AVP1): using a transmembrane $H^+$ gradient to synthesize pyrophosphate. *J. Biol. Chem.* 294, 1290–1299. doi: 10.1074/jbc.RA118.006315

Segami, S., Tomoyama, T., Sakamoto, S., Gunji, S., Fukuda, M., Kinoshita, S., et al. (2018). Vacuolar $H^+$-pyrophosphatase and cytosolic soluble pyrophosphatases cooperatively regulate pyrophosphate levels in *Arabidopsis thaliana*. *Plant Cell* 30, 1040–1061. doi: 10.1105/tpc.17.00911

Serrano-Bueno, G., Hernández, A., López-Lluch, G., Pérez-Castiñeira, J. R., Navas, P., and Serrano, A. (2013). Inorganic pyrophosphatase defects lead to cell cycle arrest and autophagic cell death through $NAD^+$ depletion in fermenting yeast. *J. Biol. Chem.* 288, 13082–13092. doi: 10.1074/jbc.M112.439349

Seufferheld, M., Vieira, M. C. F., Ruiz, F. A., Rodrigues, C. O., Moreno, S. N. J., and Docampo, R. (2003). Identification of organelles in bacteria similar to acidocalcisomes of unicellular eukaryotes. *J. Biol. Chem.* 278, 29971–29978. doi: 10.1074/jbc.M304548200

Stitt, M. (1998). Pyrophosphate as an energy donor in the cytosol of plant cells: an enigmatic alternative to ATP. *Bot. Acta* 111, 167–175. doi: 10.1111/j.1438-8677.1998.tb00692.x

Takahashi, K., Morimoto, R., Tabeta, H., Asaoka, M., Ishida, M., Maeshima, M., et al. (2017). Compensated cell enlargement in *fugu5* is specifically triggered by lowered sucrose production from seed storage lipids. *Plant Cell Physiol.* 58, 668–678. doi: 10.1093/pcp/pcx021

Tanaka, T., Tanaka, H., Machida, C., Watanabe, M., and Machida, Y. (2004). A new method for rapid visualization of defects in leaf cuticle reveals five intrinsic patterns of surface defects in *Arabidopsis*. *Plant J.* 37, 139–146. doi: 10.1046/j.1365-313X.2003.01946.x

Thomas, P. W., Woodward, F. I., and Quick, W. P. (2003). Systematic irradiance signalling in tobacco. *New Phytol.* 161, 193–198. doi: 10.1046/j.1469-8137.2003.00954.x

Williams, K., Percival, F., Merino, J., and Mooney, H. A. (1987). Estimation of tissue construction cost from heat of combustion and organic nitrogen content. *Plant, Cell Environ.* 10, 725–734. doi: 10.1111/1365-3040.ep11604754

Yin, L., Verhertbruggen, Y., Oikawa, A., Manisseri, C., Knierim, B., Prak, L., et al. (2011). The cooperative activities of CSLD2, CSLD3, and CSLD5 are required for normal *Arabidopsis* development. *Mol. Plant* 4, 1024–1037. doi: 10.1093/mp/ssr026

**Conflict of Interest:** The authors declare that the research was conducted in the absence of any commercial or financial relationships that could be construed as a potential conflict of interest.

frontiers in Plant Science

REVIEW
published: 26 June 2020
doi: 10.3389/fpls.2020.00938

# Polyphosphate: A Multifunctional Metabolite in Cyanobacteria and Algae

*Emanuel Sanz-Luque*[1,2]*, *Devaki Bhaya*[1] and *Arthur R. Grossman*[1]

[1] Department of Plant Biology, The Carnegie Institution for Science, Stanford, CA, United States, [2] Department of Biochemistry and Molecular Biology, University of Cordoba, Cordoba, Spain

Polyphosphate (polyP), a polymer of orthophosphate ($PO_4^{3-}$) of varying lengths, has been identified in all kingdoms of life. It can serve as a source of chemical bond energy (phosphoanhydride bond) that may have been used by biological systems prior to the evolution of ATP. Intracellular polyP is mainly stored as granules in specific vacuoles called acidocalcisomes, and its synthesis and accumulation appear to impact a myriad of cellular functions. It serves as a reservoir for inorganic $PO_4^{3-}$ and an energy source for fueling cellular metabolism, participates in maintaining adenylate and metal cation homeostasis, functions as a scaffold for sequestering cations, exhibits chaperone function, covalently binds to proteins to modify their activity, and enables normal acclimation of cells to stress conditions. PolyP also appears to have a role in symbiotic and parasitic associations, and in higher eukaryotes, low polyP levels seem to impact cancerous proliferation, apoptosis, procoagulant and proinflammatory responses and cause defects in TOR signaling. In this review, we discuss the metabolism, storage, and function of polyP in photosynthetic microbes, which mostly includes research on green algae and cyanobacteria. We focus on factors that impact polyP synthesis, specific enzymes required for its synthesis and degradation, sequestration of polyP in acidocalcisomes, its role in cellular energetics, acclimation processes, and metal homeostasis, and then transition to its potential applications for bioremediation and medical purposes.

**Keywords: polyphosphate, microalgae, cyanobacteria, acidocalcisome, stress responses, phosphate metabolism, metal toxicity, bioremediation**

OPEN ACCESS

***Edited by:***
*Tatsuhiro Ezawa, Graduate School of Agriculture, Hokkaido University, Japan*

***Reviewed by:***
*Katsuharu Saito, Shinshu University, Japan*
*Adolfo Saiardi, University College London, United Kingdom*

***Correspondence:**
*Emanuel Sanz-Luque*
*q92salue@uco.es*

***Specialty section:***
*This article was submitted to Plant Metabolism and Chemodiversity, a section of the journal Frontiers in Plant Science*

***Received:*** *29 April 2020*
***Accepted:*** *09 June 2020*
***Published:*** *26 June 2020*

***Citation:***
*Sanz-Luque E, Bhaya D and Grossman AR (2020) Polyphosphate: A Multifunctional Metabolite in Cyanobacteria and Algae. Front. Plant Sci. 11:938. doi: 10.3389/fpls.2020.00938*

## INTRODUCTION. A BRIEF OVERVIEW OF POLYPHOSPHATE BIOLOGY

### Orthophosphates, the Building Blocks of Polyphosphate

Phosphorus (P), mostly in the form of inorganic or orthophosphate ($PO_4^{3-}$), is integral to metabolic processes as a functional component of many molecules in the cell; these molecules include nucleic acids, phospholipids, phosphoproteins, and metabolites in most catabolic and anabolic pathways and signaling molecules. $PO_4^{3-}$ is the dominant form of P in the Earth's crust with levels in the soils often between 0.5 and 1.5 mM, although much of it may be insoluble and limiting to the growth of

organisms in both ecological and agricultural environments. Soil P is mostly derived from the weathering of $PO_4^{3-}$-containing minerals, primarily apatite ($Ca_5(PO_4)_3OH$). While often found associated with $Ca^{2+}$ salts, $PO_4^{3-}$ is also occluded in insoluble $Fe^{2+/3+}$ and $Al^{3+}$ salts and adsorbs onto surfaces of soil particles or becomes esterified to organic molecules, many that cannot be directly assimilated by most organisms. Bioavailable $PO_4^{3-}$ can be rapidly taken up by microbes, algae, and plants, which in turn can be consumed by grazers. This P is often returned to the environment as organic phosphates upon excretion and as the organisms die and decay. $PO_4^{3-}$ can also form phosphonyl bonds (carbon-phosphorus) generating a group of compounds called phosphonates that are present in marine invertebrates and can be metabolized (and synthesized) by bacteria, both in the oceans and freshwater environments (Dyhrman et al., 2006; Adams et al., 2008; Ilikchyan et al., 2009; Villarreal-Chiu et al., 2012).

Many organisms can also polymerize $PO_4^{3-}$ into polyphosphate (polyP) chains, that are composed of three to hundreds of $PO_4^{3-}$ groups linked by the high-energy phosphoanhydride bonds, the same bond that allows ATP to assume the role of the energy currency in cells. These polymers are present in all kingdoms of life, from tiny prokaryotic organisms and archaebacteria to large mammals, (Kornberg et al., 1999; Rao et al., 2009), although plants do not appear to synthesize polyP (Zhu et al., 2020) and mostly store $PO_4^{3-}$ in phytate (inositol hexakisphosphate, InsP6) (Raboy, 2003; Kolozsvari et al., 2015; Lorenzo-Orts et al., 2020), a six-fold dihydrogenphosphate ester of inositol. PolyP was likely a significant component of the pre-biological Earth as it can be spontaneously formed as a consequence of volcanic and hydrothermal vent activities (Rao et al., 2009; Achbergerova and Nahalka, 2011). It can accumulate to very high intracellular concentrations in microbes, ranging from μM to mM, especially under stress conditions when $PO_4^{3-}$ is abundant.

## Detection and Quantification

There are several ways to monitor polyP: these include visualization by transmission electron microscopy (Jensen, 1968) that can be coupled with spatially resolved elemental analysis (Eixler et al., 2005; Shebanova et al., 2017); phase contrast or bright-field microscopy after staining the cells with basic dyes including toluidine blue, methylene blue, and neutral red (Kulaev et al., 2004); binding polyP to the fluorochrome 4′,6-diamidino-2-phenylindole (DAPI); $^{31}$P nuclear magnetic resonance spectroscopy and determination of released $PO_4^{3}$ from polyP by the malachite green assay, which involve extraction and hydrolysis of the polyP (Beauvoit et al., 1989; Castro et al., 1995; Chen, 1999; Diaz et al., 2008; Khoshmanesh et al., 2012); and 2-dimensional Raman microscopy (Moudrikova et al., 2017). In photosynthetic organisms, some of these techniques can be difficult to optimize. For example, visualization of polyP can be obscured by pigmentation in photosynthetic cells; basic dyes can also bind nucleic acids and polyhydroxybutyrate (common components in cyanobacterial and algal cells) (Martinez, 1963; Kulaev et al., 2004), and $^{31}$P NMR (Hupfer et al., 2004; Hupfer et al., 2008; Kizewski et al., 2011) only detects P-containing molecules on the basis of bond class, the presence of other molecules with phosphoanhydride bonds (*e.g.* nucleotides) may cause inaccuracies in measurements, especially if these molecules are abundant. DAPI is one of the most commonly used reagents to identify polyP (polyP binding to the fluorophore alters its peak of fluorescence) (Tijssen et al., 1982; Aschar-Sobbi et al., 2008). It is a simple, inexpensive molecule that allows visualization and quantification of polyP in cells (Gomes et al., 2013; Martin and Van Mooy, 2013), although DAPI can also bind nucleic acids and inositol polyphosphate (Kolozsvari et al., 2014), making treatment with RNase and DNase (Martin and Van Mooy, 2013; Martin and Van Mooy, 2015) and optimization of protocols necessary to increase the quantification accuracy (Bru et al., 2016).

## Metabolism and Storage

In prokaryotes and some eukaryotes, including *Dyctiostelium discoideum*, the synthesis of polyP is mediated by PolyP Kinase (PPK) (Brown and Kornberg, 2004; Brown and Kornberg, 2008; Hooley et al., 2008; Livermore et al., 2016a; Weerasekara et al., 2016; Blaby-Haas and Merchant, 2017), while in most eukaryotes (fungi, protists, and algae) its synthesis requires polyP polymerase activity of VTC4. This enzyme, which is part of the Vacuolar Transporter Chaperone (VTC) complex (Hothorn et al., 2009; Aksoy et al., 2014; Ulrich et al., 2014; Desfougeres et al., 2016; Gerasimaite and Mayer, 2016; Blaby-Haas and Merchant, 2017; Gomes-Vieira et al., 2018), has no evolutionary relationship to PPK. Protein(s) responsible for the synthesis of polyP in animals has not, at this point, been identified. The catalytic reaction for both the prokaryotic and eukaryotic polyP synthesizing enzymes involves the transfer of the terminal $PO_4^{3-}$ of ATP to the growing polyP chain (although PPK can also use 1,3-diphosphoglycerate). The synthesis of polyP in prokaryotes is under *pho* regulatory control (Santos-Beneit, 2015), while, in eukaryotic organisms, polyP synthesis is linked to inositol phosphate (InsP) metabolism (Auesukaree et al., 2005; Lonetti et al., 2011; Ghosh et al., 2013; Wild et al., 2016; Cordeiro et al., 2017; Gerasimaite et al., 2017). Inositol phosphates are signaling molecules synthesized from glucose through a pathway that is conserved from Archaea to humans. These molecules perform a wide variety of functions and are linked to P and ATP cellular homeostasis (Saiardi, 2012; Azevedo and Saiardi, 2017).

$PO_4^{3-}$ can be mobilized from polyP through the catalytic activity of enzymes that degrade the polymer, including both endo- and exo-polyphosphatases (Akiyama et al., 1993; Kornberg et al., 1999; Rodrigues et al., 2002; Fang et al., 2007b; Lichko et al., 2010). Pyrophosphate generated during polyP degradation can be used as a source of energy (like polyP and

**Abbreviations:** polyP, Polyphosphate; TOR, Target of Rapamycin; PPK, Polyphosphate Kinase; VTC, Vacuolar Transporter Chaperone; Pho (regulon), Phosphate (regulon); V-type ATPase, Vacuolar-type ATPase; H+-PPase, H+-Pyrophosphatase; PPB, Polyphosphate bodies; PPX, Exo-polyphosphatase; TEM, Transmission electron microscopy; SPX domain, Domain conserved in SYG1, Pho81, and XPR11; SdR, Sulfur deprivation responses; PPGK, Polyphosphate glucokinase; InsP, Inositol phosphate; BPNP, Biogenic phosphate nanoparticles.

ATP) by various organisms (Lahti, 1983), but can also be further hydrolyzed by a vacuolar/acidocalcisome soluble pyrophosphatase without conserving the phosphoanhydride bond energy (Lemercier et al., 2004; Huang et al., 2018).

The main site of synthesis and storage of polyP is the acidic vacuole designated the acidocalcisome, discovered more than 100 years ago (Meyer, 1904; Vercesi et al., 1994) based on their visual prominence because they house densely stained polyP granules (Docampo et al., 2005; Miranda et al., 2008; Docampo, 2016; Docampo and Huang, 2016). These vacuoles have been characterized in disease causing trypanosomatids and apicomplexan parasites (Luo et al., 2004; Ruiz et al., 2004b; Fang et al., 2007a; Moreno and Docampo, 2009; Madeira da Silva and Beverley, 2010; Li and He, 2014; Kohl et al., 2018) and algae (Aksoy et al., 2014; Goodenough et al., 2019), and have similar characteristics to vacuoles in fungi (Gerasimaite et al., 2017) and animal cells (Ruiz et al., 2004a; Huizing et al., 2008; Muller et al., 2009; Moreno-Sanchez et al., 2012; Morrissey, 2012). However, there may also be acid-soluble polyP pools in other cellular locations (*e.g.* bacterial cell walls). Acidocalcisomes can attain polyP levels of 3–8 M (Moreno et al., 2002), accumulate $Ca^{2+}$ and other divalent cations, as well as some organic molecules (Kaska et al., 1985; Vercesi et al., 1994; Siderius et al., 1996; Komine et al., 2000; Ruiz et al., 2001; Docampo and Moreno, 2011; Hong-Hermesdorf et al., 2014; Penen et al., 2016; Klompmaker et al., 2017; Penen et al., 2017; Steinmann et al., 2017; Tsednee et al., 2019). In trypanosomes, these vacuoles acidify the lumen down to pH ~5.0 using both the ubiquitous V-type ATPase and the $H^+$-PPase proton pump (Scott and Docampo, 2000), although the latter may not be present in animal and yeast "acidocalcisomes." In lower eukaryotes, the VTC complex (Cohen et al., 1999; Hothorn et al., 2009; Gerasimaite et al., 2014) is located on the acidocalcisome membrane, anchored by a region of the VTC subunits containing three transmembrane domains (designated VTC domain).

## Overview of Functions

A lack of appreciation of the importance of polyP metabolism over the last several decades has caused some researchers to refer to this polymer as a "molecular fossil" (Kornberg and Fraley, 2000; Manganelli, 2007), although, an increasing number of studies implicate polyP in a variety of processes. It can either directly or indirectly buffer changes in cellular $PO_4^{3-}$ and adenylate levels, which are critical since elevated intracellular $PO_4^{3-}$ and ATP levels can inhibit many cellular reactions (*e.g.* reversible reactions in which $PO_4^{3-}$ is an end-product). PolyP also provides a reservoir of chemical bond energy for driving biological processes, although it may not be the most efficient source of energy because of its slow metabolic turnover rate relative to ATP (Van Mooy et al., 2009). The anionic nature of polyP enables it to bind and sequester cations, which can contribute to the tolerance of cells to heavy metals, preventing metabolic aberrations resulting from elevated intracellular cation concentrations (van Groenestijn et al., 1988; Rao and Kornberg, 1999; Andreeva et al., 2014), serve as a chaperone (Gray et al., 2014; Xie and Jakob, 2018) and a structural/functional component in membrane ion channels (Reusch, 1999; Reusch, 2000). In some cases, polyP can also modify protein function through post-translational attachment to lysine residues in a process known as polyphosphorylation (Azevedo et al., 2015). Organisms/cells with defects in the synthesis of polyP exhibit a range of abnormalities including cancerous proliferations, defects in cellular signaling (including TOR signaling), an inability to normally perform certain cellular processes such as autophagy and apoptosis, biofilm formation, sporulation, quorum sensing, pathogen virulence, and acclimation to both biotic and abiotic stresses, including stationary phase survival and nutrient deprivation (Kornberg et al., 1999; Rao and Kornberg, 1999; Rashid et al., 2000; Shi et al., 2004; Fraley et al., 2007; Diaz-Troya et al., 2008; Rao et al., 2009; Aksoy et al., 2014; Li and He, 2014). PolyP can also be released from acidocalcisomes of human platelets to modulate clotting and fibrinolysis (Ruiz et al., 2004a; Smith et al., 2006). Moreover, there is a growing realization of the importance of polyP with respect to cell physiology and biogeochemical cycling in marine ecosystems, as indicated by both large scale environmental analyses (Diaz et al., 2008; Orchard et al., 2010; Martin et al., 2014; Diaz et al., 2016; Dijkstra et al., 2018; Martin et al., 2018) and laboratory studies (Rhee, 1973; Jensen and Sicko-Goad, 1976; Jacobson et al., 1982; Orchard et al., 2010; Martin et al., 2014; Diaz et al., 2016). Even though the precise mechanisms by which polyP synthesis and accumulation impact cellular processes may sometimes be uncertain, it is clearly a functional giant with an impressive resume!

In this review, we highlight major aspects of polyP metabolism, storage, and function in photosynthetic organisms. However, throughout the text we refer the reader to several other recent reviews that cover the biology of polyP (Kornberg, 1995; Kornberg et al., 1999; Kulaev et al., 2004; Docampo et al., 2005; Rao et al., 2009; Docampo and Moreno, 2011; Kulakovskaya et al., 2012; Docampo, 2016; Livermore et al., 2016b; Jimenez et al., 2017; Xie and Jakob, 2018).

# POLYP SYNTHESIS, LOCALIZATION, AND STORAGE IN PHOTOSYNTHETIC MICROBES

Cyanobacteria and algae are photosynthetic organisms that serve as primary producers in terrestrial, marine, and freshwater habitats (Waterbury et al., 1979; Weisse, 1993; Sliwinska-Wilczewska et al., 2018). These organisms can survive very harsh environmental conditions, including those of the hot spring microbial mats (Ward et al., 1998) and the biofilms that form the sand crusts of deserts (Treves et al., 2013; Treves et al., 2016; Oren et al., 2019). Cyanobacteria and algae are also prominent components in dense bacterial blooms that can cause eutrophication of water bodies and release toxins into the environment (Wang, 2008; Anderson et al., 2012; Jasser and Callieri, 2017; Sliwinska-Wilczewska et al., 2018; Syed Hasnain et al., 2019), potentially compromising potable water resources. The productivity of photosynthetic microbes is often constrained by the availability of nutrients, including $PO_4^{3-}$, and like other unicellular organisms they can store large amount of polyP in granules called polyP bodies (PPBs) which are often found in acidocalcisomes (Jensen and Sicko-Goad, 1976; Grillo and Gibson,

1979; Gomez-Garcia et al., 2003; Gomez-Garcia et al., 2013; Aksoy et al., 2014; Goodenough et al., 2019).

## Regulation of PolyP Metabolism

Cyanobacterial genes encoding enzymes involved in the synthesis (polyphosphate kinase, *ppk*) and degradation (exopolyphosphatase, *ppx*) of polyP have been identified through the generation of mutants (Gomez-Garcia et al., 2003; Gomez-Garcia et al., 2013). However, there is still limited knowledge concerning the mechanisms involved in regulating polyP metabolism in cyanobacteria (Jensen and Sicko-Goad, 1976; Grillo and Gibson, 1979). Levels of *ppk* and *ppx* transcripts have been measured for a strain of *Synechococcus* present in hot spring microbial mats (growing at 50–60°C) of Yellowstone National Park. *In situ* measurements demonstrated that the *ppk* and *ppx* transcript and polypeptide levels varied over the diel cycle (Gomez-Garcia et al., 2003), as was also noted for components of other pathways including those associated with photosynthesis, respiration, nitrogen fixation, fermentation, and oxidative stress (Steunou et al., 2006; Steunou et al., 2008). While the level of the *ppk* mRNA peaked at night, *ppx* mRNA accumulation was highest during the early morning. It was hypothesized that the pattern of diel accumulation observed for these transcripts/enzymes could account for polyP storage and accumulation in cyanobacteria of the hot springs and participate in coordinating daily growth and energy demands during the light period with $PO_4^{3-}$ utilization. While we still have little detailed knowledge of regulatory factors impacting *ppk* transcription and/or PPK activity, mutants of *Anacystis nidulans* (now *Synechococcus*) with decreased $PO_4^{3-}$ assimilation and polyP accumulation were generated by treating cells with ethyl methanesulfonate (EMS) or *N*-methyl nitrosoguanidine (NTG); based on TEM, these mutants often exhibited a loss of polyP granules and were impacted in their level of PPK activity, either because of a change in the activity of the enzyme or because of altered *ppk* expression (Vaillancourt et al., 1978). On the other hand, transcripts encoding Ppx and Ppa (inorganic pyrophosphatase) proteins, involved in polyP and pyrophosphate degradation, respectively, increased upon long term $PO_4^{3-}$ deprivation of the cyanobacterium *Synechocystis* PCC6803 (Gomez-Garcia et al., 2003).

The Pho regulon controls most genes associated with the acclimation to $PO_4^{3-}$ deprivation in bacteria. In *Synechocystis* PCC6803, the major controlling elements of this regulon are SphS (sll0337; histidine kinase; analogous to *E. coli* PhoR) and SphR (slr0081; response regulator; analogous to *E. coli* PhoB) (Hirani et al., 2001; Suzuki et al., 2004; Juntarajumnong et al., 2007). The regulation of genes encoding the enzymes that degrade polyP appear to be under the control of PhoU, a negative regulator of the Pho regulon (causes suppression of the Pho regulon activity under P-replete conditions) (Wanner, 1993; Morohoshi et al., 2002). There are also some works suggesting that the concentrations of (p)ppGpp, a stringent response second messenger, can stimulate polyP accumulation in *E. coli* (Kuroda et al., 1997) and is potentially also involved in polyP accumulation in *Synechococcus* in the dark (Seki et al., 2014; Hood et al., 2016). Hence, while some specific elements have been shown to contribute to the control of the synthesis and degradation of polyP in cyanobacteria, the details of this control have not been examined.

In unicellular algae, the synthesis of polyP has not been characterized in detail, although VTC proteins are conserved in a variety of algal species. In the green, unicellular alga *Chlamydomonas reinhardtii* (*C. reinhardtii* throughout), a mutant lacking VTC1 is unable to accumulate polyP (Aksoy et al., 2014), which indicates that the VTC complex is likely required for the synthesis of polyP in this alga. The VTC4 protein, the subunit that catalyzes polyP synthesis and its translocation into the acidocalcisomes in yeast, has not yet been studied in photosynthetic organisms, but the gene encoding this protein is present in the genome of many algal species. As in budding yeast and *Trypanosoma*, the algal VTC4 proteins have the SPX, PolyP Polymerase, and VTC domains, and all of the key residues related to VTC4 functionality are conserved (**Figure 1**). Therefore, it seems reasonable to hypothesize that these VTC4 proteins catalyze polyP synthesis and are activated by the binding of inositol pyrophosphates (most phosphorylated forms of inositol) to their SPX domains, as in other eukaryotes (Wild et al., 2016; Gerasimaite et al., 2017).

## Acidocalcisomes and the Synthesis and Storage of Polyphosphate

Generally, polyP accumulates in acidocalcisomes in unicellular eukaryotes, although it can be present in other cellular compartments including the nucleus, mitochondria, cytoplasm, cell wall, and endoplasmic reticulum. In cyanobacteria, polyP granules have been observed in the center of the cell and in close proximity to carboxysomes (Nierzwicki-Bauer et al., 1983; Liberton et al., 2011), the cellular organelle that houses ribulose-1,5-bisphosphate carboxylase which is critical for the fixation of inorganic carbon. Cyanobacteria have also been observed to have polyP in regions of the cell containing ribosomes, in close association with DNA, and in the intrathylakoid space (Jensen and Sicko, 1974). In algae, several studies report polyP accumulation in acidocalcisomes (Komine et al., 2000; Ruiz et al., 2001; Aksoy et al., 2014; Goodenough et al., 2019). *C. reinhardtii* acidocalcisomes have been examined by TEM (Heuser, 2011) and in detail after freeze-fracture, deep-etching, and platinum rotary-replication (Goodenough et al., 2019). Algal acidocalcisomes have been described as *de novo* assembled vacuoles in the trans-Golgi that show diverse variants according to their disposition, composition, and consistency (Goodenough et al., 2019). However, very little is known about the physiological relevance of these observed variations. The number and size of polyP bodies in cyanobacterial and algal cells can vary greatly, but they generally increase under stress conditions (Stevens et al., 1985; Jensen, 1993; Docampo et al., 2010; Aksoy et al., 2014; Tsednee et al., 2019). As in other single-cell eukaryotes, the acidocalcisome membranes in *C. reinhardtii* harbor the VTC complex, which is responsible for the polyP polymerase and $H^+$-PPase activities (acidocalcisome membranes also harbor a V-type ATPase driven proton pump); the $H^+$-PPases, with homologues in three eukaryotic clades (not present in opisthokonts and Amoebozoa), are activated by pyrophosphate (Rea et al., 1992; Kim et al., 1994; Rodrigues et al., 1999; McIntosh

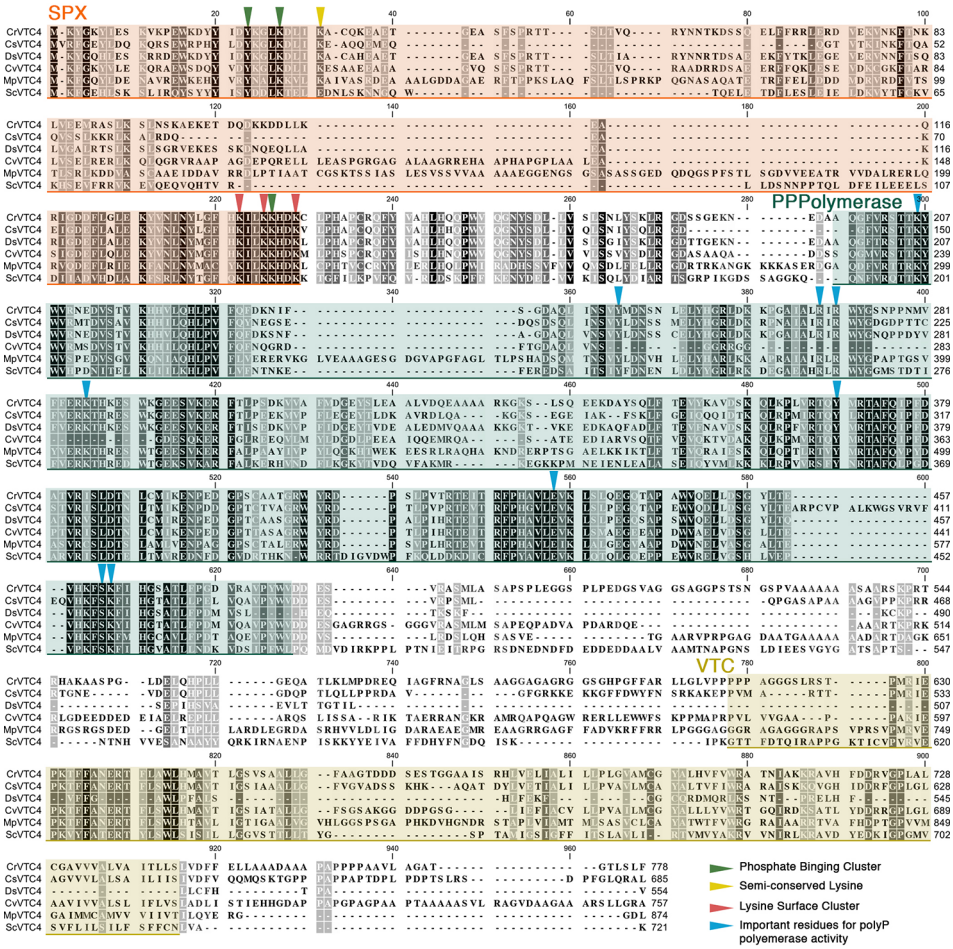


**FIGURE 1 |** Alignment of microalgal VTC4 proteins. Protein sequences of *Chlamydomonas reinhardtii* (CrVTC4, PNW79162.1), *Coccomyxa subellipsoidea* (CsVTC4, XP_005646401.1), *Dunaliella salina* (DsVTC4, Dusal.0567s00005.1), *Chlorella variabilis* (CvVTC4, XP_005844713.1), *Micromonas pusilla* (MpVTC4, XP_003055174.1), and *Saccharomyces cerevisiae* (ScVTC4, NP_012522.2) were aligned using the CLC Sequence Viewer software. SPX, polyP polymerase, and VTC domains are highlighted in orange, green, and yellow shaded boxes, respectively. Inverted triangles indicate functional residues previously described in yeast.

and Vaidya, 2002; Drozdowicz et al., 2003; Au et al., 2006; Serrano et al., 2007; Hsu et al., 2009; Tsai et al., 2014; Schilling et al., 2017; Shah et al., 2017; Segami et al., 2018a; Segami et al., 2018b) and also function in acidification of the lumen of vacuoles in land plants (Venter et al., 2006; Kajander et al., 2013; Asaoka et al., 2014).

Acidocalcisomes have been isolated from the red alga *Cyanidioschyzon merolae* and kinetoplastids and their proteome has been characterized (Yagisawa et al., 2009; Huang et al., 2014). They harbor hydrolytic enzymes, components of vesicular trafficking pathways (Rabs, SNAREs) that are associated with their biogenesis (Besteiro et al., 2008; Huang et al., 2011; Li and He, 2014; Niyogi et al., 2015) and aquaporins (Montalvetti et al., 2004). Additionally, it was recently shown that inositol pyrophosphates regulation (Cordeiro et al., 2017) plays an important role in acidocalcisome function (Huang et al., 2013; Lander et al., 2013), participating in $Ca^{2+}$ homeostasis through activation of $Ca^{2+}$ channels based on work with trypanosomatids [reviewed in (Ramakrishnan and Docampo, 2018)].

PolyP has also been localized in the cell wall of different algal species (*C. reinhardtii*, *Volvox aureus*, and *Coleochaete scutata*) (Werner et al., 2007). This was determined based on binding to a polyP binding protein (*E. coli* exopolyphosphatase, EcPPX) coupled with detection by immunofluorescence using antibodies against a maltose-binding protein fused to the EcPPX. PolyP accumulation was observed during mitosis, with a strong signal at the end of cytokinesis, and in *C. reinhardtii*, accumulation appeared highest in the mother cell envelope following mitosis and just before the release of the daughter cells. These daughter cells maintained the polyP in their cell wall for a short time after being released. The role of cell wall polyP is not clear, but it may have a protective function during cytokinesis when the daughter cell walls are not fully formed and serve as a barrier to toxic agents (*e.g.* pathogens or heavy metals;

see section 3.4) during this 'vulnerable' period (Werner et al., 2007; Penen et al., 2017).

## POLYP FUNCTIONS AND REGULATION IN PHOTOSYNTHETIC MICROBES

### PolyP as $PO_4^{3-}$ Reservoir During P Deprivation

Various functions and cellular responses are impacted by the presence/synthesis of polyP (**Figure 2**). Several studies have suggested that when the supply of $PO_4^{3-}$ is limiting in the environment, including in the sparse nutrient environments of the subtropical gyres (Perry, 1976), polyP functions as a dynamic $PO_4^{3-}$ reservoir (Kornberg et al., 1956; Harold, 1966)). "Sparing" (limiting the use of a molecule in cellular processes when it is not readily available) and internal scavenging of $PO_4^{3-}$ from polyP, nucleic acids, and phospholipids allow $PO_4^{3-}$ redistribution to accommodate processes that may extend survival during P deprivation. The presence/absence of polyP granules are indicators of the P status of organisms, but other indicators such as high affinity $PO_4^{3-}$ uptake, extracellular alkaline phosphatase activity, and the replacement of phospholipids with sulfolipids in cyanobacteria and eukaryotic algae have been reported (Dyhrman and Palenik, 1999; Riegman et al., 2000; Karl and Bjorkman, 2002; Hoppe, 2003; Dyhrman and Ruttenberg, 2006; Moseley and Grossman, 2009; Van Mooy et al., 2009; Bar-Yosef et al., 2010; Harke et al., 2012; Reistetter et al., 2013; Munoz-Martin et al., 2014; Wan et al., 2019).

In both prokaryotic and eukaryotic microbes, the role of polyP as a $PO_4^{3-}$ reservoir depends on the organism's capacity to take up $PO_4^{3-}$, synthesize and store polyP, especially when $PO_4^{3-}$ is more abundant than is required for growth, and degrade it when the level of available $PO_4^{3-}$ in the environment becomes limiting (Orchard et al., 2010). This accumulation dramatically increases when organisms are preconditioned in medium deficient for P. Exposure to excess $PO_4^{3-}$ after this preconditioning leads to the "luxury uptake" of $PO_4^{3-}$, enhanced polyP synthesis and accumulation in acidocalcisomes, which can serve as P and energy reservoirs. This phenomenon has been designated the "overplus" or over-compensation response and has been extensively studied in cyanobacteria (phytoplankton) and algae in ocean, lake, and river habitats (Liss and Langen, 1962; Harold, 1963; Harold, 1964; Voelz et al., 1966; Aitchison and Butt, 1973; Sicko-Goad and Jensen, 1976; Grillo and Gibson, 1979; Tyrell, 1999; Karl and Bjorkman, 2002; Hoppe, 2003; Kulaev et al., 2004; Hupfer et al., 2007; Falkner and Falkner, 2011). The accumulation of polyP during luxury uptake is considered important for protection of aquatic organisms against future exposure to P limitation (Hupfer et al., 2004; McMahon and Read, 2013). For *Synechocystis* PCC6803, $PO_4^{3-}$ uptake and polyP accumulation by cells exposed to overplus conditions resulted in the initial detection of polyP granules in most cells within 3 min of replenishing the medium with $PO_4^{3-}$, with the number of cells containing these granules sustained for about 1 h (Voronkov and Sinetova, 2019) followed by degradation and redistributed of the polyP within the cell over a period of a few to several days. Additionally, polyP accumulation in *Synechocystis* occurred to a lesser extent in the dark than in the light and did not appear to be very sensitive to temperature changes. The overplus response and accumulation of polyP may be an adaptation to fluctuations of $PO_4^{3-}$ in the natural environment, where the levels of polyP can vary dramatically over short time periods; such a response would help sustain growth and viability even under periods of low $PO_4^{3-}$ availability (Droop, 1973; Falkner and Falkner, 2003; Hupfer et al., 2004; Falkner and Falkner, 2011; McMahon and Read, 2013).

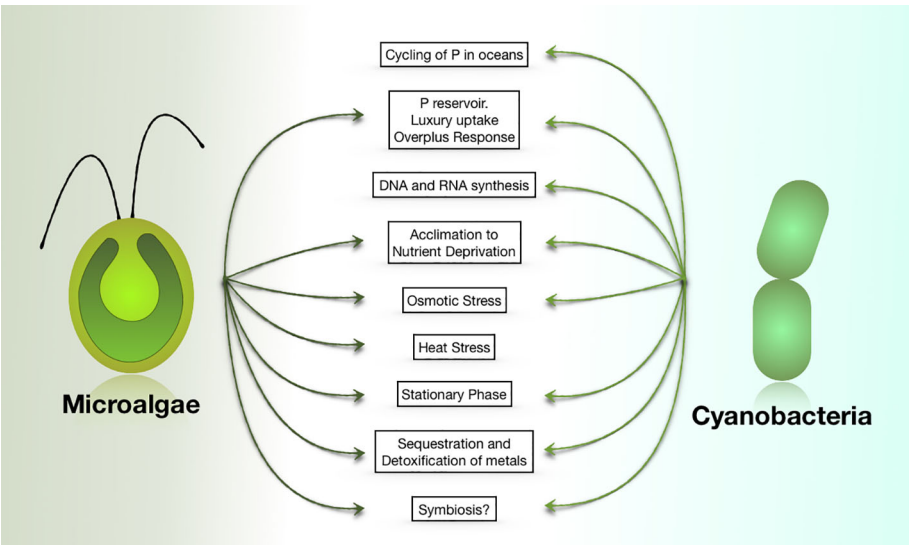


**FIGURE 2 |** PolyP functions in cyanobacteria and eukaryotic microalgae. Most of these functions have also been ascribed to polyP in non-photosynthetic organisms.

However, there is variability in the capabilities of cyanobacteria to accumulate polyP and reach a $PO_4^{3-}$ threshold at which polyP reserves are preferentially degraded, which may reflect the environment in which they evolved. In the filamentous bloom forming cyanobacterium *Nodularia spumigena*, vegetative cells exhibited different polyP levels than heterocysts (Braun et al., 2018). When $PO_4^{3-}$ is added back to P-depleted cultures, the $PO_4^{3-}$ is taken up from the medium and polyP accumulates preferentially in the vegetative cells. However, intracellular P in heterocysts remained low, highlighting functional differences between heterocysts and vegetative cells, in addition to their ability to fix molecular nitrogen.

Algae also exhibit the over-plus phenomenon. Two species of *Chlamydomonas* (*C. acidophila* KT-1 and *C. reinhardtii* C-9) exhibited the same pattern of polyP degradation when deprived of P, and the over-plus response was observed when the medium of the P-deprived cells was supplemented with an abundance of $PO_4^{3-}$. However, the levels of total polyP that accumulated varied between these species (Nishikawa et al., 2006). The overplus effect in the green alga *Chlorella vulgaris* depended on the duration of the starvation period and the $PO_4^{3-}$ concentration used during re-supply of the nutrient, with maximum accumulation after more than 8 h of deprivation and with $PO_4^{3-}$ resupply concentrations above 0.3 mM (Aitchison and Butt, 1973). So far, the specific factors that control the "overplus" response are not well understood. However, in eukaryotic algae, where the VTC complex is responsible for the synthesis of polyP, the binding of inositol pyrophosphates to the SPX domain of VTC4 must be considered since it is required to induce polyP polymerase activity in yeast (Wild et al., 2016; Gerasimaite et al., 2017). Following $PO_4^{3-}$ replenishment, accumulation of inositol pyrophosphates may be the first strategy for storing $PO_4^{3-}$ and polyP would be synthesized only when the cellular P or ATP concentrations are elevated to a level that triggers increased inositol pyrophosphate synthesis and binding to the SPX domains of the VTC polypeptides. A better understanding of this process, which has the potential to impact biotechnological strategies being developed for improved recovery of $PO_4^{3-}$ from wastewater, is needed (see *PolyP and Biotechnological Applications*).

The over-compensation phenomenon has also been studied in the red macroalga *Chondrus crispus*. After starving this alga for 2 weeks, it was resupplied with $PO_4^{3-}$ at a concentration that was greater than twice the concentration required to saturate the alga's P requirement (15 μM) (Chopin et al., 1997), however polyP accumulation was not observed. This finding suggests that over-compensation works differently or occurs under more extreme $PO_4^{3-}$conditions (*e.g.* more extended starvation, higher $PO_4^{3-}$ concentration during resupply) or that different acclimation processes in response to changes in environmental $PO_4^{3-}$ concenrations occur in multicellular photosynthetic organisms.

The presence of stored polyP in cells usually indicates a high $PO_4^{3-}$ concentration in the environment and the occurrence of luxury uptake, or a spike in the level of intracellular nutrients resulting from over-plus uptake (Karl, 2002; Karl and Bjorkman, 2002; Karl, 2014). However, the use of more sensitive methods for detection indicated that polyP was common in some marine environments, even when extracellular levels of P were low (Diaz et al., 2008; Diaz and Ingall, 2010; Orchard et al., 2010; Martin and Van Mooy, 2013). In phytoplankton populations extending from the western North Atlantic, the Gulf Stream, and into the severely P limited Sargasso Sea, it was demonstrated that P pools declined and two bio-indicators of low P conditions, alkaline phosphatase activity and the sulfolipid:phospholipid ratio, were both elevated in the biota. The lowest P concentration was measured in surface waters where the absorption of sunlight stimulated phytoplankton productivity. Surprisingly, as the level of inorganic P declined, the proportion of polyP with respect to total particulate P increased, indicating that a greater proportion of the P pool in the cell was maintained as polyP under conditions in which the level of inorganic P was at its lowest. This result was also noted specifically for cultures of marine *Synechococcus*, an abundant taxon in the oligotrophic oceans (Bjorkman, 2014; Martin et al., 2014). Overall, studies of Sargasso Sea phytoplankton conflict with the notion that polyP only serves as a luxury P reservoir that is rapidly mobilized when inorganic P levels in the environment decline. Furthermore, in the Sargasso Sea polyP was released from cells preferentially over bulk P, helping to sustain P levels in shallow waters, the zone of greatest metabolic activity. This suggests that polyP cycling in the environment may form a feedback loop that attenuates P export when environmental P becomes scarce and allows for the gradual contribution of bioavailable P to the ecosystem for sustaining primary production and supporting the use of exported carbon and nitrogen (Martin et al., 2014).

Studies with the diatom *Thallasiossira pseudonana* also demonstrated a preference for maintaining polyP even when the cells experience P deprivation. Gene expression and protein abundance patterns supported the observation that P deprivation of *T. pseudonana* resulted in an increased proportion of cellular P stored as polyP (Dyhrman et al., 2012). This observation is also in agreement with the general idea that not all polyP allocation is driven by luxury uptake and that controlled polyP cycling could be a key adaptation in low P ecosystems (Karl and Bjorkman, 2002). Similarly, the cyanobacterium *Microcystis aeruginosa,* is able to take up and store $PO_4^{3-}$ as polyP even when the concentration of external $PO_4^{3-}$ is low, which would enable it to compete with other phytoplankton when P becomes limiting (Wan et al., 2019). Taken together, these observations suggest that not all polyP allocation is driven by luxury uptake and that controlled polyP cycling could be a key component of the adaptation process in low P ecosystems (Karl and Bjorkman, 2002).

Although polyP is mainly stored in acidocalcisomes, as mentioned above, it can also be found in the cell wall, and associated with the cytoplasmic membrane and other macromolecules in the cell, which may reflect its varied functionalities. For example, it has been suggested that polyP can serve as a $PO_4^{3-}$ reservoir for the synthesis of DNA and RNA. *Synechococcus* sp. cells can contain multiple copies of genomic DNA (Binder and Chisholm, 1990; Binder and Chisholm, 1995; Mori et al., 1996). Some reports have noted an association of the fibrous structures in the nucleoid region of cyanobacterial cells with the PPBs (Voelz et al., 1966; Lawry and Jensen, 1979). There

also appears to be a link between PPBs dynamics and chromosomal DNA behavior related to day-night cycling of cells. Cyanobacterial DNA synthesis occurs in the light and is dependent on photosynthetic electron transport (Binder and Chisholm, 1990; Watanabe et al., 2012; Ohbayashi et al., 2013; Seki et al., 2014), with cell elongation and division occurring for most cells toward the end of the light period (Seki et al., 2014). In cultures of the unicellular cyanobacterium *Synechococcus* that were synchronized to a light-dark cycle, DNA appeared diffuse during the dark period and exhibited transient compaction (based on fluorescence microscopy) at the end of the light period (Smith and Williams, 2006). This compacted DNA, observed by high-voltage cryo-electron tomography (Murata et al., 2016), forms structures visually similar to condensed eukaryotic chromosomes and appears to be associated with small, paired PPBs. Additionally, phase contrast transmission electron microscopy of *Synechococcus elongatus* PCC 7942 cells showed that newly synthesized BrdU (5-bromo-2'-deoxyuridine) labeled DNA was in close proximity to the PPBs (Nitta et al., 2009). The coordinated dynamics of PPBs/polyP levels, DNA morphology, and the observed interactions between these molecules over the period when DNA is being replicated, suggest that the PPBs supply $PO_4^{3-}$ for DNA replication in the light, and may participate in regulating DNA synthesis (Murata et al., 2016).

Another potential connection between polyP and DNA synthesis has been revealed by analyses of akinetes, spore-like cells that develop in some cyanobacteria that are specialized to survive adverse environmental conditions. The akinetes are generally larger than vegetative cells and differentiate from vegetative cells within the cyanobacterial filaments. They develop a thick cell wall as they mature and are dormant under harsh environmental conditions. When conditions improve, the akinetes divide and give rise to a new population of vegetative cells that can disperse in the environment (Hori et al., 2003; Karlsson-Elfgren and Brunberg, 2004; Karlsson-Elfgren et al., 2004). Akinetes accumulate glycogen, a storage polysaccharide, and cyanophycin, a nitrogen (N) storage polymer composed of aspartic acid residues with arginine side groups. The DNA content of akinetes can be several times higher than that of vegetative cells. For example, vegetative cells of the filamentous cyanobacterium *Aphanizomenon ovalisporum* were shown to be polyploid with an average of eight copies of the genome per cell while the average number of genome copies in the akinetes of this organism was 119; some of the akinetes had in excess of 400 copies of the genome. Ribosome levels in akinetes were also elevated relative to that of vegetative cells (Sukenik et al., 2012). Akinetes of *Anabaena cylindrica* were also enriched for DNA relative to vegetative cells (Simon, 1977). Interestingly, PPBs were not observed in akinetes but were abundant in vegetative cells, suggesting that polyP in akinetes is used for generating the multiple copies of genomic DNA associated with development, maturation and fruiting of akinetes, and ultimately, the formation of numerous vegetative cells (Sukenik et al., 2012).

## PolyP Accumulation During Sulfur and Nitrogen Deprivation

High levels of polyP can build up in cyanobacteria and algae exposed to stress conditions, including nutrient deprivation and metal ion toxicity (Harold, 1966; Lawry and Jensen, 1979; Lawry and Jensen, 1986; Siderius et al., 1996; Aksoy et al., 2014; Hong-Hermesdorf et al., 2014; Goodenough et al., 2019). In *C. reinhardtii*, polyP accumulation occurs in sulfur (S)-deprived cells and is crucial to allow proper acclimation (Aksoy et al., 2014). In this alga, a mutant lacking one of the subunits of the VTC complex (VTC1) exhibited an aberrant S deprivation response (SdR) with reduced expression of some of S-deprivation-responsive genes. Although the role of polyP in this transcriptional regulation is not well understood, it is known that the inability to synthesize polyP impacts the expression of SdR genes to different degrees. Cells experiencing S starvation induce acclimation in a two-tiered response (Aksoy et al., 2013). Mutants in VTC1 that are unable to accumulate polyP are altered in their abilities to induce genes from both tiers of regulation, with a more significant impact on genes induced during the second tier (*ARSs*, *ECPs*, and *HAPs*) (Aksoy et al., 2014). PolyP accumulation as a consequence of S deprivation has also been described in the green alga *Parachlorella kessleri*, which accumulates polyP during the early stages of starvation, before starch and lipids accumulate (Ota et al., 2016).

PolyP also accumulates in N-deprived algae (Goodenough et al., 2019). An inability to synthesize polyP in the *C. reinhardtii vtc1* mutant impairs accumulation of the L-amino oxidase (LAO1) (Aksoy et al., 2014), a protein that becomes prominent during N deprivation which functions in scavenging ammonium from amino acids. This again highlights a role of the synthesis/accumulation of polyP for normal acclimation to nutrient limitation conditions. The polyP that accumulates during N starvation is degraded and acidocalcisomes resorbed upon exposure of the cells to N replete conditions (Goodenough et al., 2019). PolyP also accumulates in various *Chlorella* strains when they are deprived of N, and becomes the major $PO_4^{3-}$ source following the addition of N to the cultures (Kuesel et al., 1989; Chu et al., 2013; Chu et al., 2015). When N deprived cells are transferred to N replete medium, polyP is depleted over the first 3 days, even prior to using the $PO_4^{3-}$ present in the medium. However, when polyP-accumulating cells are exposed to both N and P starvation, they do not use the polyP as a source of $PO_4^{3-}$. The reason why N is required to use polyP is not clear, but indicates that the absence of extracellular P is not enough to trigger the degradation of polyP and that there is a regulatory hierarchy controlling the induction of nutrient acclimation responses. When cells are deprived only for one nutrient, they induce energy-consuming acclimation responses to optimize the acquisition of that nutrient, facilitate intracellular mobilization, and metabolic adjustment to promote survival. However, if cells experience deprivation for two nutrients, the heirarchy of the evolved cellular responses could favor initiation of only one of the two "programs." Examining the impact of imposing a

limitation for N either prior to or as the cells are exposed to P deprivation (and other multideprivation combinations) may reveal heirarchical responses that reflect the environments in which the organisms evolved.

## PolyP During Stationary Phase and Other Abiotic Stresses

PolyP accumulation has also been linked to osmotic stress and the entrance of specific microbes and phytoplankton into stationary phase (Feuillade et al., 1995; Kornberg et al., 1999; Diaz et al., 2008; Cade-Menun and Paytan, 2010). In *C. reinhardtii*, polyP-filled acidocalcisomes are also generated during stationary phase (Goodenough et al., 2019). Early work with *C. reinhardtii* on polyP showed that one-week-old cultures (stationary phase) grown under mixotrophic conditions generated PPBs that can be released from the cells by exocytosis (Komine et al., 2000). It is not clear whether the accumulation of polyP in stationary phase cells is a consequence of a deficiency for a specific nutrient or to other factors related to the status of the cultures. Similarly, *Chlorella vulgaris* cultures contained little polyP during exponential growth, accumulating it as cells approached stationary phase (Aitchison and Butt, 1973).

PolyP has also been suggested to function in the neutralization of microalgal cells that become alkalinized when incubated in high concentrations of ammonium (Pick et al., 1990). In *Dunaliella salina,* the addition of 20 mM ammonium increased the cytosolic pH and reduced cellular ATP levels. High intracellular pH can dramatically affect photosynthetic and respiratory activities, inhibiting ATP production. When *Dunaliella* cultures experienced high ammonium levels, polyP was degraded and the cells were able to maintain ATP levels and neutralize their cytoplasm; polyP hydrolysis results in $H^+$ release, which could compensate for cytsolic alkalinization. In support of these ideas, when algal cells are cultured under conditions of P deprivation and accumulate less polyP, it takes a longer time for them to recover from ammonium "shock."

Osmotic shock impacts the length of polyP polymers in *Dunaliella salina* and *Phaeodactylum tricornotum* (Bental et al., 1990; Leitao et al., 1995). Hyperosmotic shock promoted the synthesis of longer polymers with concomitant ATP hydrolysis, while the opposite effect, smaller polymer synthesis with an increase in ATP levels, was elicited in cells exposed to hypoosmotic stress. Whether polyP solely functions to maintain the chemical balance in the cell or could have an additional role in the acclimation to omotic stress is unclear.

Some algae accumulate polyP upon exposure to elevated temperatures, but very little is known about this phenomenon in photosynthetic organisms. A *Cylindrocystis*-like alga isolated from the High Arctic, where temperatures oscillate from −12 to +5°C, showed elevated polyP accumulation when cultivated at 20°C (Barcyte et al., 2020). However, another *Cylindrocystis*-like strain that inhabits the desert and grows at elevated temperatures did not accumulate polyP under the same conditions. The different responses of these strains suggest that, as in bacteria, polyP is being synthesized in response to heat stress, and that higher temperatures may be required to elicit its accumulation in the desert alga.

## PolyP as a Chelator of Cations

Several metal ions are critical for growth but become toxic when in excess (*e.g.* Fe, Cu, Zn, Mn, etc.), while other toxic metals ions are nonessential (*e.g.* Cd, Pb, or Hg). Both prokaryotic and eukaryotic photosynthetic organisms have evolved different and sometimes synergistic mechanisms for dealing with toxic levels of metal ions (Twiss and Nalewajko, 1992; Baptista and Vasconcelos, 2006). They can remove the ions from solution by adsorbing them onto their surfaces, import them and sequester them on molecular surfaces within the cell, make functional use of them through biotransformations (*e.g.* incorporation into proteins), increase the activities of efflux pumps, and store them in subcellular compartments (Darnall et al., 1986; Swift and Forciniti, 1997; Baptista and Vasconcelos, 2006).

Several studies have shown that metal ions are bound to the PPBs and sequestered in acidocalcisomes (Baxter and Jensen, 1980; Pettersson et al., 1988; Fiore and Trevors, 1994; Swift and Forciniti, 1997; Docampo et al., 2005; Docampo and Moreno, 2011; Goodenough et al., 2019; Tsednee et al., 2019), with $Mg^{2+}$ and $Ca^{2+}$ being abundant polyP-chelated cations (Siderius et al., 1996; Komine et al., 2000). The presence of $Ca^{2+}$ channels in trypanosomatid acidocalcisome membranes also suggests a possible role of these vacuoles in $Ca^{2+}$ sequestration and exchange, which in turn could impact various signaling pathways (Ramakrishnan and Docampo, 2018). In addition to $Ca^{2+}$ and $Mg^{2+}$, polyP can bind $Zn^{2+}$ $Mn^{2+}$, $Al^{3+}$, and $K^+$ and play a role in detoxifying heavy metals such as $Cd^{2+}$ and $Pb^{2+}$. Positive correlations between high levels of polyP and tolerance to cation toxicity have been observed (Sicko-Goad et al., 1975; Baxter and Jensen, 1980; Jensen et al., 1982; Sicko-Goad and Lazinsky, 1986; Torres et al., 1998; Rangsayator et al., 2002; Andrade et al., 2004; Moura et al., 2019), with some cyanobacteria and microalgae also showing increased polyP accumulation during the $PO_4^{3-}$ overplus reaction when high external metal ion concentrations are included in the medium (Sicko-Goad et al., 1978; Siderius et al., 1996). PolyP levels in the cyanobacteria *Anabaena flos-aquae* and *A. variabilis* increased when the cells experienced elevated $Zn^{2+}$ concentrations (Rachlin et al., 1985); a similar increase in polyP was observed when *Spirulina* (*Arthrospira*) *platensis* was exposed to high levels of $Cd^{2+}$ (Rangsayator et al., 2002), when *Plectonema boryanum* was exposed to high levels of $Mg^{2+}$, $Sr^{2+}$, $Ba^{2+}$, and $Mn^{2+}$ redundant (Baxter and Jensen, 1980) and when *Microcystis novacekii* BA005 or *Nostoc paludosum* BA033 were exposed to high $Mn^{2+}$ concentrations (Moura et al., 2019). However, it was also observed that exposure of *C. reinhardtii* to $Cd^{2+}$ and $Hg^{2+}$ elicit polyP degradation and an increase in the amount of short chain polyP and orthophosphate in the vacuoles as the metal ion is being sequestered (Nishikawa et al., 2003; Samadani and Dewez, 2018a; Samadani and Dewez, 2018b), suggesting that the energy in the phosphoanhydride bond and/or the polymer length might contribute to more effective sequestration.

$PO_4^{3-}$ levels can not only impact cation accumulation, but also the tolerance of photosynthetic microbes to toxic metals. When *C. reinhartii* and *Scenedesmus obliquus* were administered elevated levels of $PO_4^{3-}$ they accumulated more $Cd^{2+}$ and $Zn^{2+}$ (Yu and Wang, 2004a; Yu and Wang, 2004b) and increases in accumulation of $Cu^{2+}$ and $Cd^{2+}$ in *C. reinhardtii* cells exposed to elevated $PO_4^{3-}$ concentrations have been correlated with an increase in the tolerance of the cells to the potentially toxic effects of these metal ions (the intracellular stoichiometry of metal ion to $PO_4^{3-}$ was most important in assessing toxicity) (Wang and Dei, 2006). In the cyanobacterium *M. aeruginosa*, $Cd^{2+}$ and $Zn^{2+}$ uptake was promoted by elevated cellular $PO_4^{3-}$ concentrations, with short term $Cd^{2+}$ and $Zn^{2+}$ uptake rates increased by 40- and 16-fold, respectively, when the cellular $PO_4^{3-}$ concentration was increased from 66 to 118 μmol/g dry weight. P-enriched cells also exhibited greater tolerance to $Cd^{2+}$ and $Zn^{2+}$ than cells deprived of P (Zeng and Wang, 2009; Zeng et al., 2009). A mutant of *Nostoc muscorum* that was resistant to $Ni^{2+}$ exhibited a two fold increase in $Ni^{2+}$ uptake relative to the wild type strain, with a concomitant increase in the level of cellular polyP (Singh, 2012). These results all strongly support the idea that many photosynthetic microbes, both prokaryotic and eukaryotic, in an environment with sufficient P can synthesize polyP, mostly as PPBs, that serves as scaffolds for metal binding and detoxification and potentially also as a source of energy for maintaining metal homeostasis.

A similar situation may also occur in some macroalgae. For example, the macroalga *Macrocystis pyrifera* accumulated more $Cd^{2+}$ when it was induced to synthesize high levels of PPBs (Walsh and Hunter, 1992). Elevated capacities to tolerate and sequester metal ions that are potentially toxic, including $Pb^{2+}$ and $Cu^{2+}$, have also been described for organisms of the photosynthetic microbial mat communities of the Ebro Delta in Catalonia (Esteve et al., 1992; Guerrero et al., 1999; Manosa et al., 2001; Burgos et al., 2013). Specific cyanobacteria that live in these microbial communities, including *Oscillatoria* sp. PCC 7515, *Chroococcus* sp. PCC 9106 and *Spirulina* sp. PCC 6313, have high tolerances for $Pb^{2+}$ (Mateo et al., 1997; Maldonado et al., 2010; Maldonado et al., 2011) and have been shown to take up this metal and accumulate it in association with extracellular polymers and intracellular PPBs (Maldonado et al., 2011). A marine *Synechococcus* strain has been shown to sequester radionuclides, including uranium, with much of it bound to polysaccharides on the surface of the cells (Sakaguchi et al., 1978; Acharya et al., 2009). However, an acid soluble polyP may also function in uranium sequestration. Based on energy dispersive X-ray (EDX) spectroscopy and spectrophotometric analyses it was determined that PPBs can form on the surface of the cells of the nitrogen-fixing filamentous cyanobacterium *Anabaena torulosa* and bind uranium (Acharya et al., 2012; Acharya and Apte, 2013).

*C. reinhardtii* represents a robust model microalgal system that is relatively easy to maniputlate at the genetic and molecular levels and has been used to dissect some molecular aspects of metal chelation and toxicity (Hanikenne, 2003). Recent studies have shown that this alga can accumulate $Mn^{2+}$, which colocalizes with polyP and $Ca^{2+}$ in acidocalcisomes (Tsednee et al., 2019). The capacity of *C. reinhardtii* to store $Mn^{2+}$ was also shown to depend on its ability to accumulate polyP. The *vtc1* mutant, which is unable to synthesize polyP, does not accumulate $Mn^{2+}$; the same inability to accumulate $Mn^{2+}$ occurs in wild type cells when they are deprived of P (and cannot make polyP). Interestingly, little of the sequestered $Mn^{2+}$ was chelated directly to polyP, which has led to the suggestion that polyP serves as an intermediate in the binding of $Mn^{2+}$ to a ligand that has not yet been defined. Algal cells, like cyanobacteria (mentioned above), may also exploit extracellular polymers, including polyP (located in the cell wall), as a first line of defense against metal toxicity (Penen et al., 2017). *C. reinhardtii* cell wall-less mutants exhibited reduced growth in the presence of various metals, including $Cd^{2+}$, $Co^{2+}$, $Ni^{2+}$, and $Cu^{2+}$ (Macfie and Welbourne, 2014). This sensitivity could reflect reduced chelation of these metal ions in the absence of extracellular polyP (Werner et al., 2007). Interestingly, both *C. reinhardtii* and *C. acidophila* growing in the presence of heavy metals (*e.g.* $Cd^{2+}$, $Hg^{2+}$) degrades polyP (Nishikawa et al., 2003; Nishikawa et al., 2009; Samadani and Dewez, 2018a; Samadani and Dewez, 2018b), which promotes an increase in the concentration of shorter chains of polyP, free $PO_4^{3-}$ and ultimately a decrease in intracellular $PO_4^{3-}$. The mechanism for metal tolerance associated with these changes in polyP features/levels may involve the initial chelation of the toxic metals to polyP which is required for some other form of sequestration that ameliorates metal toxicity; this may relate to the ultimate use of another cation chelator as well as excretion of the ion from the cells. The formation of palmelloid cell aggregates of *C. reinhardtii* cells may also contribute to the cell's ability to withstand metal toxicity (Samadani and Dewez, 2018a; Samadani et al., 2020). In summary, it seems like there are multiple methods for algal and cyanobacterial cells to cope with metal cation toxicity, with some that require chelation by polyP and others for which the mechanism(s) appear to be more complex.

## PolyP as Substrate for Kinases

Specific enzymes that use polyP to phosphorylate sugars have been identified in bacteria, including cyanobacteria, and belong to the family of proteins designated polyP glucokinases (PPGK, polyphosphate–glucose phosphotransferase, EC 2.7.1.63). These proteins use glucose and polyP (and often nucleotides such as ATP) as substrates to catalyze glucose phosphorylation, generating glucose 6-phosphate. PPGKs were first observed in *Mycobacterium phlei* (Szymona, 1957) and in Gram-positive bacteria in the order *Actinomycetales* (Szymona and Ostrowski, 1964; Szymona and Widomski, 1974; Szymona and Szymona, 1978; Szymona and Szymona, 1979; Pepin and Wood, 1986; Mukai et al., 2003; Tanaka et al., 2003; Lindner et al., 2010; Liao et al., 2012; Koide et al., 2013). Although many PPGK enzymes can use a range of nucleotide triphosphates as substrates, the enzymes of the most ancient *Actinomycetales* species have a preference for polyP. In contrast, the more recently evolved bacterial species use ATP and are unable to use polyP, similar to

strictly ATP dependent fungal and mammalian hexokinases (Rao et al., 2009). Currently it is thought that the early phosphoryl donor for glucose phosphorylation was polyP and as ATP became the dominant energy donor of the cells, glucokinases evolved into isoforms more specific for ATP, although many of the PPGKs that have been characterized can use both polyP and nucleotide triphosphates as substrates.

A novel subfamily of PPGK proteins have so far, been identified only in $N_2$-fixing, filamentous cyanobacteria. Glucokinases from the filamentous nitrogen fixers *Nostoc* sp. PCC7120 (formerly *Anabaena* sp. PCC 7120) and *Nostoc punctiforme* PCC73102 (Klemke et al., 2014; Albi and Serrano, 2015) have been shown to catalyze *in vitro* phosphorylation of glucose using polyP as the phosphoryl donor. These PPGKs have a higher affinity for polyP with more than 10 phosphoryl residues, exhibit moderate activity using mannose as a substrate and, unlike most other glucokinases, appear to be specific for polyP and unable to use nucleoside triphosphates (*e.g.* ATP or GTP) as phosphoryl donors. The gene encoding this enzyme in *Anabaena* sp. PCC 7120 is expressed under conditions of N deprivation and a strain with a null mutation in the gene is compromised under $N_2$-fixing conditions (Klemke et al., 2014). It was hypothesized that this glucokinase is part of a response to N deprivation in which "N sparing" reactions (*e.g.* limiting the use of N-containing nucleotides) are elicited.

## Integration of PolyP and Inositol Phosphate Metabolism in Microalgae

PolyP has been associated with active metabolism in various microbes, including algae (Aitchison and Butt, 1973), and can be used as a substrate for the generation of ATP and, in some cases, can phosphorylate other cellular metabolites. As discussed above, its synthesis and degradation are sensitive to environmental conditions and critical for microbes to acclimation to various stress conditions. Therefore, polyP metabolism is linked to the energetics of cells, integral to various cellular processes and likely highly controlled. A link between inositol pyrophosphate metabolism and polyP synthesis has been reported for *Trypanosoma brucei* (Cordeiro et al., 2017) and budding yeast (Wild et al., 2016; Gerasimaite et al., 2017). Mutants in these organisms that are unable to synthesize inositol pyrophosphates (InsP7 and InsP8) exhibited impaired polyP accumulation. In yeast, polyP synthesis has been shown to be activated by the binding of inositol pyrophosphates to the SPX domain of the VTC4 subunit of the VTC complex (Wild et al., 2016). Although the VTC4 protein is currently uncharacterized in algae, based on the genome sequences of various algae, it appears to be conserved in many Chlorophyceae species (e.g., *C. reinhardtii, Chlorella variabilis, Micromonas pusilla, Dunaliella salina,* and *Coccomyxa subellipsoidea,* among others). The VTC4 proteins of the algae contain SPX and polyP polymerase domains, with conservation of specific amino acid residues required for activity (**Figure 1**). These findings suggest that activation of polyP synthesis in microalgae will also respond to inositol pyrophosphates.

Interestingly, a connection between the accumulation of inositol pyrophosphates and TOR signaling has been established in *C. reinhardtii* (Couso et al., 2016). The *vip1* mutant, which is unable to synthesize the highly phosphorylated forms of inositol, exhibited a hypersensitive response to rapamycin (a TOR inhibitor) and more pronounced lipid (triacylglycerol, TAG) synthesis than the wild type strain. Although the precise interactions that link these two pathways and how that link might integrate with polyP metabolism are not understood, the results suggest a connection between polyP and control of cellular energetics, growth, and acclimation through the TOR pathway. Furthermore, the increase in TAG synthesis in inositol pyrophosphate deficient strains indicates that inositol pyrophosphate synthesis and possibly polyP accumulation can impact lipid synthesis and storage. Close interactions between acidocalcisomes and mitochondria observed in *Trypanosoma* and *C. reinhardtii* cells (Docampo and Huang, 2016; Goodenough et al., 2019) also suggests a role (although speculative) for acidocalcisomes and polyP in regulating cellular energetics. The potential integration of polyP metabolism into the central metabolic networks of the cell is an exciting field and may provide new insights into the diversity of phenotypes observed in cells impaired for the synthesis of this polymer.

# POLYP AND BIOTECHNOLOGICAL APPLICATIONS

Various uses have been proposed for polyP with respect to human health, agricultural practices, and the remediation of ecosystems. PPBs, also recently called "biogenic phosphate nanoparticles" (BPNP), in addition to having roles in $PO_4^{3-}$ storage, cellular energetics, and metal sequestration, may function in reducing inflammation and protecting mammalian cells from various forms of damage, including oxidative damage (Segawa et al., 2011; Kashima et al., 2015). High levels of BPNPs were synthesized in *Synechococcus* sp PCC7002 overexpressing the the *ppk* gene. The isolated BPNPs from this cyanobacterium were shown to be taken up by polarized human intestinal epithelial (Caco-2) cells (Gao et al., 2018) where they inhibited the induction of nitric oxide synthase and the production of proinflammatory mediators in mouse cell cultures (Feng et al., 2018). This work on potential "health impacts" and uses of polyP for medical applications is intriguing, although it would benefit from further studies of the efficacy and scope of polyP in these processes.

The PPK enzyme can also be used to catalyze ATP production for the synthesis of various compounds. For example, the high temperature resistant PPK from *Thermosynechococcus elongatus* BP-1 was used to generate ATP from ADP and polyP for the production of D-amino acid dipeptide (Sato et al., 2007).

In agriculture, $PO_4^{3-}$ is an essential nutrient, but its bioavailability in the soil often limits crop productivity. The requirement of $PO_4^{3-}$ for achieving optimal agricultural yields makes it a critical resource for maintaining food security for future generations. To increase crop yields, high levels of $PO_4^{3-}$ are often included in fertilizers, although only a small proportion of the applied $PO_4^{3-}$ may be recovered in the biomass (Pathak et al., 2010); more than 80% of the

applied $PO_4^{3-}$ can be lost in wastewater (*e.g.* parboiled rice mill effluents) or to surface waters as runoff. Hence, in addition to the inefficient economic aspects of applying large amounts of $PO_4^{3-}$ fertilizer to boost crop productivity, high levels of this nutrient can contaminate agricultural soils, while its runoff into nearby water bodies can cause eutrophication and create toxic habitats (Hupfer et al., 2004; McMahon and Read, 2013). According to several predictions, continued production of high $PO_4^{3-}$ fertilizers may also become challenging for future generations as the Earth's $PO_4^{3-}$ reserves might be exhausted in less than 100 years (Cordell and White, 2014; Mukherjee et al., 2015). Furthermore, $PO_4^{3-}$ containing rocks are not equally distributed over the Earth, creating a need for most countries to import this vital nutrient. Indeed, the negative socio-economic impact of limitations in $PO_4^{3-}$ availability and how, based on current agricultural practices, it can cause environmental degradation, creates a need to reassess the ways in which $PO_4^{3-}$ is delivered and recycled for the establishment of sustainable agricultural practices (Solovchenko et al., 2016).

To ameliorate the negative impact of amending soils with excess $PO_4^{3-}$, several studies using cyanobacteria and algae have explored ways to direct polyP metabolism toward bioremediation/water treatment and the production of biofertilizers (Kulakovskaya et al., 2012; Mukherjee et al., 2015; Solovchenko et al., 2016; Siebers et al., 2019). Various cyanobacteria including *Aphanothece* sp., *Spirulina* sp., *Arthrospira* sp., *Lyngbya* sp., *Anabaena* sp., and *Phormidium* sp., as well as eukaryotic microalgae such as *Chlorella* sp. and *Scenedesmus* sp., have been used for removal of nutrients from wastewater (Ray et al., 2013; Mukherjee et al., 2015); much of the excess $PO_4^{3-}$ that is assimilated by these organisms is polymerized into polyP. Cyanobacteria and microalgae that accumulate high levels of polyP could potentially be integrated into strategies for economical, commercial-scale removal of $PO_4^{3-}$ from wastewaters and the generation of $PO_4^{3-}$-rich bacterial/algal biomass that could be incorporated into fertilizers for agricultural applications. The rate at which the $PO_4^{3-}$ is mobilized from these biofertilizers would depend on its degradation/hydrolysis by enzymes released to the soil by microorganisms, with potential slow/moderate release favoring sustained plant growth with reduced $PO_4^{3-}$ runoff.

The development of polyP-based biological systems for bioremediation and the generation of biofertilizers would benefit from engineered bacterial/algal strains that accumulate excess polyP. The feasibility of developing such strains has been demonstrated for both heterotrophic and photosynthetic bacteria. A high polyP accumulating bacterium was constructed by introducing the *ppk* gene from the cyanobacterium *Microcystis aeruginosa* NIES-843 into *Pseudomonas putida* that was already efficient in removing $PO_4^{3-}$ from its environment. This strain, grown in a sequencing batch biofilm reactor, had a much higher capacity to remove $PO_4^{3-}$ from the medium than the control strain (no introduced *ppk* gene) (Du et al., 2012). An alternative approach exploited the finding that mutants in a gene encoding a negative regulatory element of the Pho regulon, PhoU, also accumulated high levels of polyP. Inactivation of the *phoU* gene in *Synechococcus* sp. PCC6803 resulted in elevated intracellular polyP accumulation and a 4-fold increase in the ability of the cells to remove $PO_4^{3-}$ from the medium relative to the wild type cells (Morohoshi et al., 2002). Furthermore, such strains may also become integral to biostrategies for removing toxic metals from contaminated waters. A more holistic, integrated understanding of how, when, and where polyP is synthesized, as well as the ways in which it interacts with the metabolic and regulatory circuits in the cells, will facilitate the exploitation of its synthesis and accumulation for biotechnological applications.

## FUTURE PERSPECTIVE

Since the discovery of polyP more than 100 years ago, various functions have been ascribed to this polymer in organisms from all kingdoms of life. PolyP could modulate functionalities of proteins by sequestering cations and influencing the biosynthesis of metalloenzyme and metal toxicity, serve as a scaffold to facilitate protein folding, promote protein degradation, modify proteins through covalent binding (polyphosphorylation), and potentially provide substrate for nucleic acids synthesis. Additionally, polyP can impact $Ca^{2+}$ signaling, contribute to the energy currency of the cell, and impact adenylate homeostasis; these functions can have potential multifactorial effects on a wide variety of cellular processes. Aspects of these functions may guide experimentation toward elucidation of the ways in which this simple molecule assists organisms in coping with environmental challenges.

While our knowledge has slowly accrued over the past half century concerning the synthesis and functions of polyP, there is still little known about the acidocalcisome, which houses polyP, with many questions to be answered. What are the steps in acidocalcisome biogenesis and what makes it different from other vacuoles in the cell? What are the consequences of acidocalcisome interactions with contractile vacuoles and mitochondria and do they interact with other organelles (*e.g.* chloroplasts)? How do acidocalcisomes release their contents (*e.g.* $Ca^{2+}$, polyP, $PO_4^{3-}$) into the cytoplasm or extracellular space, what signals trigger the release, and how does the release serve ecosystem functions? What role does polyP play in symbiotic interactions between photosynthetic microbes and sponges of the Caribbean coral reef (Zhang et al., 2015), between plants and arbuscular mycorrhiza (Kuga et al., 2008; Tani et al., 2009; Hijikata et al., 2010; Kikuchi et al., 2014; Ferrol et al., 2019), and between algae and animals (Cobb, 1978)? Unraveling the signaling networks that promote release or retainment of polyP granules in phytoplankton will provide a more complete understanding of P cycling and nutrient balancing in nature.

Molecular connections linking the acclimation of cells to stress conditions with polyP metabolism and its impact on cellular energetics and central metabolism, and both the extracellular factors and intracellular regulatory elements that control polyP synthesis, degradation, distribution, and secretion are crucial for elucidating mechanisms by which this ancient molecule modulates cellular processes. This information will also provide the foundational knowledge to foster biotechnological applications that rely on polyP metabolism and to potentially engineer organisms to better cope with adverse environmental conditions, serve in

remediation of contaminated ecosystems, and help ameliorate the often detrimental consequences of human activities on our planet.

## AUTHOR CONTRIBUTIONS

ES-L, DB, and AG discussed and wrote the manuscript.

## FUNDING

This work was funded by the European Union's Horizon 2020 research and innovation programme under the Marie Sklodowska-Curie grant agreement No. 751039 (to ES-L) and in part by DOE grant DE-SC0008806, which was awarded to AG. DB and AG also acknowledge NSF grant # 1921429.

## REFERENCES

Acharya, C., and Apte, S. K. (2013). Novel surface associated polyphosphate bodies sequester uranium in the filamentous, marine cyanobacterium, *Anabaena torulosa*. *Metallomics* 5, 1595–1598. doi: 10.1039/c3mt00139c

Acharya, C., Joseph, D., and Apte, S. K. (2009). Uranium sequestration by a marine cyanobacterium, *Synechococcus elongatus* strain BDU/75042. *Bioresour. Technol.* 100, 2176–2181. doi: 10.1016/j.biortech.2008.10.047

Acharya, C., Chandwadkar, P., and Apte, S. K. (2012). Interaction of uranium with a filamentous, heterocystous, nitrogen-fixing cyanobacterium, *Anabaena torulosa*. *Bioresour. Technol.* 116, 290–294. doi: 10.1016/j.biortech.2012.03.068

Achbergerova, L., and Nahalka, J. (2011). Polyphosphate–an ancient energy source and active metabolic regulator. *Microb. Cell Fact* 10, 63. doi: 10.1186/1475-2859-10-63

Adams, M. M., Gomez-Garcia, M. R., Grossman, A. R., and Bhaya, D. (2008). Phosphorus deprivation responses and phosphonate utilization in a thermophilic *Synechococcus* sp. from microbial mats. *J. Bacteriol.* 190, 8171–8184. doi: 10.1128/JB.01011-08

Aitchison, P. A., and Butt, V. S. (1973). The relation between the synthesis of inorganic polyphosphate and phosphate uptake by *Chlorella vulgaris*. *J. Exp. Bot.* 24, 497–510. doi: 10.1093/jxb/24.3.497

Akiyama, M., Crooke, E., and Kornberg, A. (1993). An exopolyphosphatase of *Escherichia coli*. The enzyme and its ppx gene in a polyphosphate operon. *J. Biol. Chem.* 268, 633–639.

Aksoy, M., Pootakham, W., Pollock, S. V., Moseley, J. L., Gonzalez-Ballester, D., and Grossman, A. R. (2013). Tiered regulation of sulfur deprivation responses in *Chlamydomonas reinhardtii* and identification of an associated regulatory factor. *Plant Physiol.* 162, 195–211. doi: 10.1104/pp.113.214593

Aksoy, M., Pootakham, W., and Grossman, A. R. (2014). Critical function of a *Chlamydomonas reinhardtii* putative polyphosphate polymerase subunit during nutrient deprivation. *Plant Cell* 26, 4214–4229. doi: 10.1105/tpc.114.129270

Albi, T., and Serrano, A. (2015). Two strictly polyphosphate-dependent gluco (manno)kinases from diazotrophic cyanobacteria with potential to phosphorylate hexoses from polyphosphates. *Appl. Microbiol. Biotechnol.* 99, 3887–3900. doi: 10.1007/s00253-014-6184-7

Anderson, D. M., Cembella, A. D., and Hallegraeff, G. M. (2012). Progress in understanding harmful algal blooms: paradigm shifts and new technologies for research, monitoring, and management. *Ann. Rev. Mar. Sci.* 4, 143–176. doi: 10.1146/annurev-marine-120308-081121

Andrade, L., Keim, C. N., Farina, M., and Pfeiffer, W. C. (2004). Zinc detoxification by a cyanobacterium from a metal contaminated bay in Brazil. *Braz. Arch. Biol. Biotechnol.* 47, 147–152. doi: 10.1590/S1516-89132004000100020

Andreeva, N., Ryazanova, L., Dmitriev, V., Kulakovskaya, T., and Kulaev, I. (2014). Cytoplasmic inorganic polyphosphate participates in the heavy metal tolerance of *Cryptococcus humicola*. *Folia Microbiol. (Praha)* 59, 381–389. doi: 10.1007/s12223-014-0310-x

Asaoka, M., Segami, S., and Maeshima, M. (2014). Identification of the critical residues for the function of vacuolar H(+)-pyrophosphatase by mutational analysis based on the 3D structure. *J. Biochem.* 156, 333–344. doi: 10.1093/jb/mvu046

Aschar-Sobbi, R., Abramov, A. Y., Diao, C., Kargacin, M. E., Kargacin, G. J., French, R. J., et al. (2008). High sensitivity, quantitative measurements of polyphosphate using a new DAPI-based approach. *J. Fluoresc.* 18, 859–866. doi: 10.1007/s10895-008-0315-4

Au, K. M., Barabote, R. D., Hu, K. Y., and Saier, M. H.Jr. (2006). Evolutionary appearance of H+-translocating pyrophosphatases. *Microbiology* 152, 1243–1247. doi: 10.1099/mic.0.28581-0

Auesukaree, C., Tochio, H., Shirakawa, M., Kaneko, Y., and Harashima, S. (2005). Plc1p, Arg82p, and Kcs1p, enzymes involved in inositol pyrophosphate synthesis, are essential for phosphate regulation and polyphosphate accumulation in Saccharomyces cerevisiae. *J. Biol. Chem.* 280, 25127–25133. doi: 10.1074/jbc.M414579200

Azevedo, C., and Saiardi, A. (2017). Eukaryotic Phosphate Homeostasis: The Inositol Pyrophosphate Perspective. *Trends Biochem. Sci.* 42, 219–231. doi: 10.1016/j.tibs.2016.10.008

Azevedo, C., Livermore, T., and Saiardi, A. (2015). Protein polyphosphorylation of lysine residues by inorganic polyphosphate. *Mol. Cell* 58, 71–82. doi: 10.1016/j.molcel.2015.02.010

Baptista, M. S., and Vasconcelos, M. T. (2006). Cyanobacteria metal interactions: Requirements, toxicity and ecological implications. *Crit. Rev. Microbiol.* 32, 127–137. doi: 10.1080/10408410600822934

Barcyte, D., Pilatova, J., Mojzes, P., and Nedbalova, L. (2020). The Arctic *Cylindrocystis* (Zygnematophyceae, Streptophyta) Green Algae are Genetically and Morphologically Diverse and Exhibit Effective Accumulation of Polyphosphate. *J. Phycol.* 56, 217–232. doi: 10.1111/jpy.12931

Bar-Yosef, Y., Sukenik, A., Hadas, O., Viner-Mozzini, Y., and Kaplan, A. (2010). Enslavement in the water body by toxic *Aphanizomenon ovalisporum*, inducing alkaline phosphatase in phytoplanktons. *Curr. Biol.* 20, 1557–1561. doi: 10.1016/j.cub.2010.07.032

Baxter, M., and Jensen, T. (1980). Uptake of magnesium, strontium, barium and manganese by *Plectonema boryanum* with special reference to polyphosphate bodies. *Protoplasma* 104, 81–89. doi: 10.1007/BF01279371

Beauvoit, B., Rigoulet, M., Guerin, B., and Canioni, P. (1989). Polyphosphates as a source of high energy phosphates in yeast mitochondria: A $^{31}$P NMR study. *FEBS Lett.* 252, 17–21. doi: 10.1016/0014-5793(89)80882-8

Bental, M., Pick, U., Avron, M., and Degani, H. (1990). Metabolic studies with NMR spectroscopy of the alga *Dunaliella salina* trapped within agarose beads. *Eur. J. Biochem.* 188, 111–116. doi: 10.1111/j.1432-1033.1990.tb15377.x

Besteiro, S., Tonn, D., Tetley, L., Coombs, G. H., and Mottram, J. C. (2008). The AP3 adaptor is involved in the transport of membrane proteins to acidocalcisomes of *Leishmania*. *J. Cell Sci.* 121, 561–570. doi: 10.1242/jcs.022574

Binder, B. J., and Chisholm, S. W. (1990). Relationship between DNA cycle and growth rate in *Synechococcus* sp. strain PCC 6301. *J. Bacteriol.* 172, 2313–2319. doi: 10.1128/jb.172.5.2313-2319.1990

Binder, B. J., and Chisholm, S. W. (1995). Cell Cycle Regulation in Marine *Synechococcus* sp. Strains. *Appl. Environ. Microbiol.* 61, 708–717. doi: 10.1128/AEM.61.2.708-717.1995

Bjorkman, K. M. (2014). Polyphosphate goes from pedestrian to prominent in the marine P-cycle. *Proc. Natl. Acad. Sci. U. S. A* 111, 7890–7891. doi: 10.1073/pnas.1407195111

Blaby-Haas, C. E., and Merchant, S. S. (2017). Regulating cellular trace metal economy in algae. *Curr. Opin. Plant Biol.* 39, 88–96. doi: 10.1016/j.pbi.2017.06.005

Braun, P. D., Schulz-Vogt, H. N., Vogts, A., and Nausch, M. (2018). Differences in the accumulation of phosphorus between vegetative cells and heterocysts in the cyanobacterium *Nodularia spumigena*. *Sci. Rep.* 8, 5651. doi: 10.1038/s41598-018-23992-1

Brown, M. R., and Kornberg, A. (2004). Inorganic polyphosphate in the origin and survival of species. *Proc. Natl. Acad. Sci. U. S. A* 101, 16085–16087. doi: 10.1073/pnas.0406909101

Brown, M. R., and Kornberg, A. (2008). The long and short of it - polyphosphate, PPK and bacterial survival. *Trends Biochem. Sci.* 33, 284–290. doi: 10.1016/j.tibs.2008.04.005

Bru, S., Jimenez, J., Canadell, D., Arino, J., and Clotet, J. (2016). Improvement of biochemical methods of polyP quantification. *Microb. Cell* 4, 6–15. doi: 10.15698/mic2017.01.551

Burgos, A., Maldonado, J., De Los Rios, A., Sole, A., and Esteve, I. (2013). Effect of copper and lead on two consortia of phototrophic microorganisms and their capacity to sequester metals. *Aquat. Toxicol.* 140-141, 324–336. doi: 10.1016/j.aquatox.2013.06.022

Cade-Menun, B. J., and Paytan, B. (2010). Nutrient temperature and light stress alter phosphorus and carbon forms in culture-grown algae. *Marine Chem.* 121, 27–36. doi: 10.1016/j.marchem.2010.03.002

Castro, C. D., Meehan, A. J., Koretsky, A. P., and Domach, M. M. (1995). In situ 31P nuclear magnetic resonance for observation of polyphosphate and catabolite responses of chemostat-cultivated *Saccharomyces cerevisiae* after alkalinization. *Appl. Environ. Microbiol.* 61, 4448–4453. doi: 10.1128/AEM.61.12.4448-4453.1995

Chen, K. Y. (1999). *Study of polyphosphate metabolism in intact cells by 31-P nuclear magnetic resonance spectroscopy* Vol. 23. Eds. H. C. Schroder and W. E. G. Muller (Berlin, Heidelberg, New York: Springer-Verlag), 241–252.

Chopin, C., Lehmal, H., and Halcrow, K. (1997). Polyphosphates in the red macroalga *Chondrus crispus* (Rhodophyceae). *New Phytol.* 135, 587–594. doi: 10.1046/j.1469-8137.1997.00690.x

Chu, F. F., Chu, P. N., Cai, P. J., Li, W. W., Lam, P. K., and Zeng, R. J. (2013). Phosphorus plays an important role in enhancing biodiesel productivity of *Chlorella vulgaris* under nitrogen deficiency. *Bioresour. Technol.* 134, 341–346. doi: 10.1016/j.biortech.2013.01.131

Chu, F. F., Shen, X. F., Lam, P. K., and Zeng, R. J. (2015). Polyphosphate during the Regreening of *Chlorella vulgaris* under Nitrogen Deficiency. *Int. J. Mol. Sci.* 16, 23355–23368. doi: 10.3390/ijms161023355

Cobb, A. H. (1978). Inorganic polyphosphate involved in the symbiosis between chloroplasts of alga *Codium fragile* and mollusc *Elysia viridis*. *Nature* 55, 554–555. doi: 10.1038/272554a0

Cohen, A., Perzov, N., Nelson, H., and Nelson, N. (1999). A novel family of yeast chaperons involved in the distribution of V-ATPase and other membrane proteins. *J. Biol. Chem.* 274, 26885–26893. doi: 10.1074/jbc.274.38.26885

Cordeiro, C. D., Saiardi, A., and Docampo, R. (2017). The inositol pyrophosphate synthesis pathway in *Trypanosoma brucei is* linked to polyphosphate synthesis in acidocalcisomes. *Mol. Microbiol.* 106, 319–333. doi: 10.1111/mmi.13766

Cordell, D., and White, S. (2014). Life's Bottleneck: Sustaining the World's Phosphorus for a Food Secure Future. *Annu. Rev. Environ. Resour.* 39, 161–188. doi: 10.1146/annurev-environ-010213-113300

Couso, I., Evans, B. S., Li, J., Liu, Y., Ma, F., Diamond, S., et al. (2016). Synergism between Inositol Polyphosphates and TOR Kinase Signaling in Nutrient Sensing, Growth Control, and Lipid Metabolism in Chlamydomonas. *Plant Cell* 28, 2026–2042. doi: 10.1105/tpc.16.00351

Darnall, D. W., Greene, B., Henzl, M. T., Hosea, J. M., McPherson, R. A., Sneddon, J., et al. (1986). Selective recovery of gold and other metal ions from an algal biomass. *Environ. Sci. Technol.* 20, 206–208. doi: 10.1021/es00144a018

Desfougeres, Y., Gerasimaite, R. U., Jessen, H. J., and Mayer, A. (2016). Vtc5, a Novel Subunit of the Vacuolar Transporter Chaperone Complex, Regulates Polyphosphate Synthesis and Phosphate Homeostasis in Yeast. *J. Biol. Chem.* 291, 22262–22275. doi: 10.1074/jbc.M116.746784

Diaz, J. M., and Ingall, E. D. (2010). Fluorometric quantification of natural inorganic polyphosphate. *Environ. Sci. Technol.* 44, 4665–4671. doi: 10.1021/es100191h

Diaz, J., Ingall, E., Benitez-Nelson, C., Paterson, D., de Jonge, M. D., McNulty, I., et al. (2008). Marine polyphosphate: a key player in geologic phosphorus sequestration. *Science* 320, 652–655. doi: 10.1126/science.1151751

Diaz, J. M., Björkman, K. M., Haley, S. T., Ingall, E. D., Karl, D. M., Longo, A. F., et al. (2016). Polyphosphate dynamics at Station ALOHA, North Pacific subtropical gyre. *Limnol. Oceanogr.* 61, 227–239. doi: 10.1002/lno.10206

Diaz-Troya, S., Perez-Perez, M. E., Florencio, F. J., and Crespo, J. L. (2008). The role of TOR in autophagy regulation from yeast to plants and mammals. *Autophagy* 4, 851–865. doi: 10.4161/auto.6555

Dijkstra, N., Kraal, P., Séguret, M. J. M., Flores, M. R., Gonzalez, S., Rijkenberg, M. J. A., et al. (2018). Phosphorus dynamics in and below the redoxcline in the Black Sea and implications for phosphorus burial. *Geochim. Cosmochim. Acta* 222, 685–703. doi: 10.1016/j.gca.2017.11.016

Docampo, R., and Huang, G. (2016). Acidocalcisomes of eukaryotes. *Curr. Opin. Cell Biol.* 41, 66–72. doi: 10.1016/j.ceb.2016.04.007

Docampo, R., and Moreno, S. N. (2011). Acidocalcisomes. *Cell Calcium* 50, 113–119. doi: 10.1016/j.ceca.2011.05.012

Docampo, R., de Souza, W., Miranda, K., Rohloff, P., and Moreno, S. N. (2005). Acidocalcisomes - conserved from bacteria to man. *Nat. Rev. Microbiol.* 3, 251–261. doi: 10.1038/nrmicro1097

Docampo, R., Ulrich, P., and Moreno, S. N. (2010). Evolution of acidocalcisomes and their role in polyphosphate storage and osmoregulation in eukaryotic microbes. *Philos. Trans. R. Soc. Lond. B. Biol. Sci.* 365, 775–784. doi: 10.1098/rstb.2009.0179

Docampo, R. (2016). The origin and evolution of the acidocalcisome and its interactions with other organelles. *Mol. Biochem. Parasitol.* 209, 3–9. doi: 10.1016/j.molbiopara.2015.10.003

Droop, M. R. (1973). Some thoughts on nutrient limitation in algae. *J. Phycol.* 9, 264–273. doi: 10.1111/j.1529-8817.1973.tb04092.x

Drozdowicz, Y. M., Shaw, M., Nishi, M., Striepen, B., Liwinski, H. A., Roos, D. S., et al. (2003). Isolation and characterization of TgVP1, a type I vacuolar H +-translocating pyrophosphatase from *Toxoplasma gondii*. The dynamics of its subcellular localization and the cellular effects of a diphosphonate inhibitor. *J. Biol. Chem.* 278, 1075–1085. doi: 10.1074/jbc.M209436200

Du, H., Yang, L., Wu, J., Xiao, L., Wang, X., and Jiang, L. (2012). Simultaneous removal of phosphorus and nitrogen in a sequencing batch biofilm reactor with transgenic bacteria expressing polyphosphate kinase. *Appl. Microbiol. Biotechnol.* 96, 265–272. doi: 10.1007/s00253-011-3839-5

Dyhrman, S. T., and Palenik, B. (1999). Phosphate stress in cultures and field populations of the dinoflagellate *Prorocentrum minimum* detected by a single-cell alkaline phosphatase assay. *Appl. Environ. Microbiol.* 65, 3205–3212. doi: 10.1128/AEM.65.7.3205-3212.1999

Dyhrman, S. T., and Ruttenberg, K. C. (2006). Presence and regulation of alkaline phosphatase activity in eukaryotic phytoplankton from the coastal ocean: Implications for dissolved organic phosphorus remineralization. *Limnol. Oceanogr.* 51, 1381–1390. doi: 10.4319/lo.2006.51.3.1381

Dyhrman, S. T., Chappell, P. D., Haley, S. T., Moffett, J. W., Orchard, E. D., Waterbury, J. B., et al. (2006). Phosphonate utilization by the globally important marine diazotroph *Trichodesmium*. *Nature* 439, 68–71. doi: 10.1038/nature04203

Dyhrman, S. T., Jenkins, B. D., Rynearson, T. A., Saito, M. A., Mercier, M. L., Alexander, H., et al. (2012). The transcriptome and proteome of the diatom *Thalassiosira pseudonana* reveal a diverse phosphorus stress response. *PloS One* 7, e33768. doi: 10.1371/journal.pone.0033768

Eixler, S., Selig, U., and Karsten, U. (2005). Extraction and detection methods for polyphosphate storage in autotrophic planktonic organisms. *Hydrobiologia* 533, 135–143. doi: 10.1007/s10750-004-2406-9

Esteve, I., Martinez-Alonso, M., and Mir, J. (1992). Distribution, topology and structure of microbial mat communties in Spain. Preliminary studies. *Limnetica* 8, 185–195.

Falkner, R., and Falkner, G. (2003). Distinct adaptivity during phosphate uptake by the Cyanobacterium *Anabaena variabilis* reflects information processing about preceding phosphate supply. *J. Trace Microprobe Techniques* 21, 363–375. doi: 10.1081/TMA-120020271

Falkner, G., and Falkner, G. (2011). "The Complex Regulation of the Phosphate Uptake System of Cyanobacteria," in *Bioenergetic Processes of Cyanobacteria: From Evolutionary Singularity to Ecological Diversity*. Eds. G. A. P, C. Obinger and G. Renger (Berlin/Heidelberg: Springer), 109–130.

Fang, J., Rohloff, P., Miranda, K., and Docampo, R. (2007a). Ablation of a small transmembrane protein of *Trypanosoma brucei* (TbVTC1) involved in the synthesis of polyphosphate alters acidocalcisome biogenesis and function, and leads to a cytokinesis defect. *Biochem. J.* 407, 161–170. doi: 10.1042/BJ20070612

Fang, J., Ruiz, F. A., Docampo, M., Luo, S., Rodrigues, J. C., Motta, L. S., et al. (2007b). Overexpression of a $Zn^{2+}$-sensitive soluble exopolyphosphatase from *Trypanosoma cruzi* depletes polyphosphate and affects osmoregulation. *J. Biol. Chem.* 282, 32501–32510. doi: 10.1074/jbc.M704841200

Feng, G., Dong, S., Huang, M., Zeng, M., Liu, Z., Zhao, Y., et al. (2018). Biogenic Polyphosphate Nanoparticles from a Marine Cyanobacterium *Synechococcus* sp. PCC 7002: Production, Characterization, and Anti-Inflammatory Properties In Vitro. *Mar. Drugs* 16, 322–337. doi: 10.3390/md16090322

Ferrol, N., C, A.-A., and Pérez-Tienda, J. (2019). Review: Arbuscular mycorrhizas as key players in sustainable plant phosphorus acquisition: An overview on the

mechanisms involved. *Plant Sci.* 280, 441–447. doi: 10.1016/j.plantsci.2018.11.011

Feuillade, J., Bielicki, G., and J.-P. Renou, J.-P. (1995). $^{31}$P-NMR study of natural phytoplankton samples. *Hydrobiologia* 300/301, 391–398. doi: 10.1007/BF00024480

Fiore, M. F., and Trevors, J. T. (1994). Cell composition and metal tolerance in cyanobacteria. *Biometals* 7, 83–103. doi: 10.1007/BF00140478

Fraley, C. D., Rashid, M. H., Lee, S. S., Gottschalk, R., Harrison, J., Wood, P. J., et al. (2007). A polyphosphate kinase 1 (ppk1) mutant of *Pseudomonas aeruginosa* exhibits multiple ultrastructural and functional defects. *Proc. Natl. Acad. Sci. U. S. A* 104, 3526–3531. doi: 10.1073/pnas.0609733104

Gao, F., Wu, H., Zeng, M., Huang, M., and Feng, G. (2018). Overproduction, purification, and characterization of nanosized polyphosphate bodies from *Synechococcus* sp. PCC 7002. *Microb. Cell Fact* 17, 27. doi: 10.1186/s12934-018-0870-6

Gerasimaite, R., and Mayer, A. (2016). Enzymes of yeast polyphosphate metabolism: structure, enzymology and biological roles. *Biochem. Soc. Trans.* 44, 234–239. doi: 10.1042/BST20150213

Gerasimaite, R., Sharma, S., Desfougeres, Y., Schmidt, A., and Mayer, A. (2014). Coupled synthesis and translocation restrains polyphosphate to acidocalcisome-like vacuoles and prevents its toxicity. *J. Cell Sci.* 127, 5093–5104. doi: 10.1242/jcs.159772

Gerasimaite, R., Pavlovic, I., Capolicchio, S., Hofer, A., Schmidt, A., Jessen, H. J., et al. (2017). Inositol Pyrophosphate Specificity of the SPX-Dependent Polyphosphate Polymerase VTC. *ACS Chem. Biol.* 12, 648–653. doi: 10.1021/acschembio.7b00026

Ghosh, S., Shukla, D., Suman, K., Lakshmi, B. J., Manorama, R., Kumar, S., et al. (2013). Inositol hexakisphosphate kinase 1 maintains hemostasis in mice by regulating platelet polyphosphate levels. *Blood* 122, 1478–1486. doi: 10.1182/blood-2013-01-481549

Gomes, F. M., Ramos, I. B., Wendt, C., Girard-Dias, W., De Souza, W., Machado, E. A., et al. (2013). New insights into the in situ microscopic visualization and quantification of inorganic polyphosphate stores by 4',6-diamidino-2-phenylindole (DAPI)-staining. *Eur. J. Histochem.* 57, e34. doi: 10.4081/ejh.2013.e34

Gomes-Vieira, A. L., Wideman, J. G., Paes-Vieira, L., Gomes, S. L., Richards, T. A., and Meyer-Fernandes, J. R. (2018). Evolutionary conservation of a core fungal phosphate homeostasis pathway coupled to development in *Blastocladiella emersonii*. *Fungal Genet. Biol.* 115, 20–32. doi: 10.1016/j.fgb.2018.04.004

Gomez-Garcia, M. R., Losada, M., and Serrano, A. (2003). Concurrent transcriptional activation of *ppa* and *ppx* genes by phosphate deprivation in the cyanobacterium *Synechocystis* sp. strain PCC 6803. *Biochem. Biophys. Res. Commun.* 302, 601–609. doi: 10.1016/S0006-291X(03)00162-1

Gomez-Garcia, M. R., Fazeli, F., Grote, A., Grossman, A. R., and Bhaya, D. (2013). Role of polyphosphate in thermophilic *Synechococcus* sp. from microbial mats. *J. Bacteriol.* 195, 3309–3319. doi: 10.1128/JB.00207-13

Goodenough, U., Heiss, A. A., Roth, R., Rusch, J., and Lee, J. H. (2019). Acidocalcisomes: Ultrastructure, biogenesis, and distribution in microbial eukaryotes. *Protist* 170, 287–313. doi: 10.1016/j.protis.2019.05.001

Gray, M. J., Wholey, W. Y., Wagner, N. O., Cremers, C. M., Mueller-Schickert, A., Hock, N. T., et al. (2014). Polyphosphate is a primordial chaperone. *Mol. Cell* 53, 689–699. doi: 10.1016/j.molcel.2014.01.012

Grillo, J. F., and Gibson, J. (1979). Regulation of phosphate accumulation in the unicellular cyanobacterium *Synechococcus*. *J. Bacteriol.* 140, 508–517. doi: 10.1128/JB.140.2.508-517.1979

Guerrero, R., Haselton, A., Sole, M., and Margulis, L. (1999). *Titanospirillum velox*: A huge, speedy sulfur storing spirillum from Ebro Delta microbial mats. *Proc. Natl. Acad. Sci. U.S.A.* 96, 11584–11588. doi: 10.1073/pnas.96.20.11584

Hanikenne, M. (2003). *Chlamydomonas reinhardtii* as a eukaryotic photosynthetic model for studies of heavy metal homeostasis and tolerance. *New Phytol.* 159, 331–340. doi: 10.1046/j.1469-8137.2003.00788.x

Harke, M. J., Berry, D. L., Ammerman, J. W., and Gobler, C. J. (2012). Molecular response of the bloom-forming cyanobacterium, *Microcystis aeruginosa*, to phosphorus limitation. *Microb. Ecol.* 63, 188–198. doi: 10.1007/s00248-011-9894-8

Harold, F. M. (1963). Accumulation of inorganic polyphosphate in *Aerobacter aerogenes*. I. Relationship to growth and nucleic acid synthesis. *J. Bacteriol.* 86, 216–221. doi: 10.1128/JB.86.2.216-221.1963

Harold, F. M. (1964). Enzymatic and genetic control of polyphosphate accumulation in *Aerobacter aerogenes*. *J. Gen. Microbiol.* 35, 81–90. doi: 10.1099/00221287-35-1-81

Harold, F. M. (1966). Inorganic polyphosphates in biology: structure, metabolism, and function. *Bacteriol. Rev.* 30, 772–794. doi: 10.1128/MMBR.30.4.772-794.1966

Heuser, J. E. (2011). The origins and evolution of freeze-etch electron microscopy. *J. Electron Microsc.* 60, S3–S29. doi: 10.1093/jmicro/dfr044

Hijikata, N., Murase, M., Tani, C., Ohtomo, R., Osaki, M., and Ezawa, T. (2010). Polyphosphate has a central role in the rapid and massive accumulation of phosphorus in extraradical mycelium of an arbuscular mycorrhizal fungus. *New Phytol.* 186, 285–289. doi: 10.1111/j.1469-8137.2009.03168.x

Hirani, T. A., Suzuki, I., Murata, N., Hayashi, H., and Eaton-Rye, J. J. (2001). Characterization of a two-component signal transduction system involved in the induction of alkaline phosphatase under phosphate-limiting conditions in *Synechocystis* sp. PCC 6803. *Plant Mol. Biol.* 45, 133–144. doi: 10.1023/a:1006425214168

Hong-Hermesdorf, A., Miethke, M., Gallaher, S. D., Kropat, J., Dodani, S. C., Chan, J., et al. (2014). Subcellular metal imaging identifies dynamic sites of Cu accumulation in Chlamydomonas. *Nat. Chem. Biol.* 10, 1034–1042. doi: 10.1038/nchembio.1662

Hood, R. D., Higgins, S. A., Flamholz, A., Nichols, R. J., and Savage, D. F. (2016). The stringent response regulates adaptation to darkness in the cyanobacterium *Synechococcus elongatus*. *Proc. Natl. Acad. Sci. U. S. A* 113, E4867–E4876. doi: 10.1073/pnas.1524915113

Hooley, P., Whitehead, M. P., and Brown, M. R. (2008). Eukaryote polyphosphate kinases: is the 'Kornberg' complex ubiquitous? *Trends Biochem. Sci.* 33, 577–582. doi: 10.1016/j.tibs.2008.09.007

Hoppe, H.-G. (2003). Phosphatase activity in the sea. *Hydrobiologia* 493, 187–200. doi: 10.1023/A:1025453918247

Hori, K., Okamoto, J., Tanji, Y., and Unno, H. (2003). Formation, sedimentation and germination properties of *Anabaena* akinetes. *Biochem. Eng. J.* 14, 67–73. doi: 10.1016/S1369-703X(02)00136-5

Hothorn, M., Neumann, H., Lenherr, E. D., Wehner, M., Rybin, V., Hassa, P. O., et al. (2009). Catalytic core of a membrane-associated eukaryotic polyphosphate polymerase. *Science* 324, 513–516. doi: 10.1126/science.1168120

Hsu, S-H., Hsiao, Y.-Y., Liu, P.-F., Lin, S.-M., Luo, Y.-Y., and Pan, R.-L. (2009). Purification, characterization, and spectral analyses of histidine-tagged vacuolar $H^+$-pyrophosphatase expressed in yeast. *Bot. Stud.* 50, 291–301.

Huang, G., Fang, J., Sant'Anna, C., Li, Z. H., Wellems, D. L., Rohloff, P., et al. (2011). Adaptor protein-3 (AP-3) complex mediates the biogenesis of acidocalcisomes and is essential for growth and virulence of *Trypanosoma brucei*. *J. Biol. Chem.* 286, 36619–36630. doi: 10.1074/jbc.M111.284661

Huang, G., Bartlett, P. J., Thomas, A. P., Moreno, S. N., and Docampo, R. (2013). Acidocalcisomes of *Trypanosoma brucei* have an inositol 1,4,5-trisphosphate receptor that is required for growth and infectivity. *Proc. Natl. Acad. Sci. U. S. A* 110, 1887–1892. doi: 10.1073/pnas.1216955110

Huang, G., Ulrich, P. N., Storey, M., Johnson, D., Tischer, J., Tovar, J. A., et al. (2014). Proteomic analysis of the acidocalcisome, an organelle conserved from bacteria to human cells. *PloS Pathog.* 10, e1004555. doi: 10.1371/journal.ppat.1004555

Huang, R., Wan, B., Hultz, M., Diaz, J. M., and Tang, Y. (2018). Phosphatase-Mediated Hydrolysis of Linear Polyphosphates. *Environ. Sci. Technol.* 52, 1183–1190. doi: 10.1021/acs.est.7b04553

Huizing, M., Helip-Wooley, A., Westbroek, W., Gunay-Aygun, M., and Gahl, W. A. (2008). Disorders of lysosome-related organelle biogenesis: clinical and molecular genetics. *Annu. Rev. Genomics Hum. Genet.* 9, 359–386. doi: 10.1146/annurev.genom.9.081307.164303

Hupfer, M., Rube, B., and Schmieder, P. (2004). Origin and diagenesis of polyphosphate in lake sediments: A $^{31}$P-NMR study. *Limnol. Oceanogr.* 49, 1–10. doi: 10.4319/lo.2004.49.1.0001

Hupfer, M., Gloess, S., and Grossart, H.-P. (2007). Polyphosphate-accumulating microorganisms in aquatic sediments. *Aquat. Microbial Ecol. AQUAT MICROB. Ecol.* 47, 299–311. doi: 10.3354/ame047299

Hupfer, M., Glöss, S., Schmieder, P., and Grossart, H.-P. (2008). Methods for detection and quantification of polyphosphate and polyphosphate accumulating microorganisms in aquatic sediments. *Int. Rev. Hydrobiol.* 93, 1–30. doi: 10.1002/iroh.200610935

Ilikchyan, I. N., McKay, R. M., Zehr, J. P., Dyhrman, S. T., and Bullerjahn, G. S. (2009). Detection and expression of the phosphonate transporter gene *phnD in* marine and freshwater picocyanobacteria. *Environ. Microbiol.* 11, 1314–1324. doi: 10.1111/j.1462-2920.2009.01869.x

Jacobson, L., Halmann, M., and Yariv, J. (1982). The molecular composition of the volutin granule of yeast. *Biochem. J.* 201, 473–479. doi: 10.1042/bj2010473

Jasser, I., and Callieri, C. (2017). "Picocyanobacteria: The smallest cell size cyanobacteria," in *Handbook on Cyanobacterial Monitoring and Cytotoxin Analysis*. Eds. J. Meriluoto, L. Spoof and G. A. Codd (Chickester, UK: John Wiley & Son), 19–27.

Jensen, T. E., and Sicko, L. M. (1974). Phosphate metabolism in blue-green algae. I. Fine structure of the "polyphosphate overplus" phenomenon in *Plectonema boryanum*. *Can. J. Microbiol.* 20, 1235–1239. doi: 10.1139/m74-190

Jensen, T. E., and Sicko-Goad, L. (1976). *Aspects of Phosphate Utilization by Blue-Green Algae*. p.^pp. USA: US Environmental Protection Agency, Office of Research and Development, Corvallis Environmental Research Laboratory, Corvallis, Oregon.

Jensen, T. E., Baxter, M. J., Rachlin, M., and Jani, V. (1982). Uptake of heavy metals by Plectonema boryanum (Cyanophyceae) into cellular components, especially polyphosphate bodies; an X-ray energy dispersive study. *Envinron. Poll* A27, 119–127. doi: 10.1016/0143-1471(82)90104-0

Jensen, T. E. (1968). Electron microscopy of polyphosphate bodies in a blue-green alga. *Nostoc. Pruniforme Arch. Mikrobiol.* 62, 144–152. doi: 10.1007/BF00410400

Jensen, T. E. (1993). "Cyanobacterial ultrastructure," in *Ultrastructure of microalgae*. Ed. T. Berne (Florida: CRC Press), 8–51.

Jimenez, J., Bru, S., Ribeiro, M. P. C., and Clotet, J. (2017). Polyphosphate: popping up from oblivion. *Curr. Genet.* 63, 15–18. doi: 10.1007/s00294-016-0611-5

Juntarajumnong, W., Hirani, T. A., Simpson, J. M., Incharoensakdi, A., and Eaton-Rye, J. J. (2007). Phosphate sensing in *Synechocystis* sp. PCC 6803: SphU and the SphS-SphR two-component regulatory system. *Arch. Microbiol.* 188, 389–402. doi: 10.1007/s00203-007-0259-0

Kajander, T., Kellosalo, J., and Goldman, A. (2013). Inorganic pyrophosphatases: One substrate, three mechanisms. *FEBS Lett.* 587, 1863–1869. doi: 10.1016/j.febslet.2013.05.003

Karl, D. M., and Bjorkman, K. M. (2002). "Dynamics of DOP," in *Biochemistry of Marine Dissolved Organic Matter*. Eds. D. A. Hansell and C. A. Carlson (New York: Elsevier Science), 249–266.

Karl, D. M. (2002). Nutrient dynamics in the deep blue sea. *Trends Microbiol.* 10, 410–418. doi: 10.1016/S0966-842X(02)02430-7

Karl, D. M. (2014). Microbially mediated transformations of phosphorus in the sea: New views of an old cycle. *Ann. Rev. Mar. Sci.* 6, 279–337. doi: 10.1146/annurev-marine-010213-135046

Karlsson-Elfgren, I., and Brunberg, A.-K. (2004). The importance of shallow sediments in the recruitmentof *Anabaena* and *Aphanizomenon* (Cyanophyceae). *J. Phycol.* 40, 831–836. doi: 10.1111/j.1529-8817.2004.04070.x

Karlsson-Elfgren, I., Rengefors, K., and Gustafsson, S. (2004). Factors regulating recruitment from the sediment to the water column in the bloom-forming cyanobacterium *Gleotrichia echinulata*. *Freshwater Biol.* 49, 265–273. doi: 10.1111/j.1365-2427.2004.01182.x

Kashima, S., Fujiya, M., Konishi, H., Ueno, N., Inaba, Y., Moriichi, K., et al. (2015). Polyphosphate, an active molecule derived from probiotic *Lactobacillus brevis*, improves the fibrosis in murine colitis. *Transl. Res.* 166, 163–175. doi: 10.1016/j.trsl.2015.02.002

Kaska, D. D., Piscopo, I. C., and Gibor, A. (1985). Intracellular calcium redistribution during mating in *Chlamydomonas reinhardii*. *Exp. Cell Res.* 160, 371–379. doi: 10.1016/0014-4827(85)90183-1

Khoshmanesh, A., Cook, P. L., and Wood, B. R. (2012). Quantitative determination of polyphosphate in sediments using Attenuated Total Reflectance-Fourier Transform Infrared (ATR-FTIR) spectroscopy and partial least squares regression. *Analyst* 137, 3704–3709. doi: 10.1039/c2an35289c

Kikuchi, Y., Hijikata, N., Yokoyama, K., Ohtomo, R., Handa, Y., Kawaguchi, M., et al. (2014). Polyphosphate accumulation is driven by transcriptome alterations that lead to near-synchronous and near-equivalent uptake of inorganic cations in an arbuscular mycorrhizal fungus. *New Phytol.* 204, 638–649. doi: 10.1111/nph.12937

Kim, E. J., Zhen, R. G., and Rea, P. A. (1994). Heterologous expression of plant vacuolar pyrophosphatase in yeast demonstrates sufficiency of the substrate-binding subunit for proton transport. *Proc. Natl. Acad. Sci. U. S. A* 91, 6128–6132. doi: 10.1073/pnas.91.13.6128

Kizewski, F., Liu, Y. T., Morris, A., and Hesterberg, D. (2011). Spectroscopic approaches for phosphorus speciation in soils and other environmental systems. *J. Environ. Qual.* 40, 751–766. doi: 10.2134/jeq2010.0169

Klemke, F., Beyer, G., Sawade, L., Saitov, A., Korte, T., Maldener, I., et al. (2014). All1371 is a polyphosphate-dependent glucokinase in *Anabaena* sp. PCC 7120. *Microbiology* 160, 2807–2819. doi: 10.1099/mic.0.081836-0

Klompmaker, S. H., Kohl, K., Fasel, N., and Mayer, A. (2017). Magnesium uptake by connecting fluid-phase endocytosis to an intracellular inorganic cation filter. *Nat. Commun.* 8, 1879. doi: 10.1038/s41467-017-01930-5

Kohl, K., Zangger, H., Rossi, M., Isorce, N., Lye, L. F., Owens, K. L., et al. (2018). Importance of polyphosphate in the Leishmania life cycle. *Microb. Cell* 5, 371–384. doi: 10.15698/mic2018.08.642

Koide, M., Miyanaga, A., Kudo, F., and Eguchi, T. (2013). Characterization of polyphosphate glucokinase SCO5059 from *Streptomyces coelicolor* A3(2). *Biosci. Biotechnol. Biochem.* 77, 2322–2324. doi: 10.1271/bbb.130498

Kolozsvari, B., Parisi, F., and Saiardi, A. (2014). Inositol phosphates induce DAPI fluorescence shift. *Biochem. J.* 460, 377–385. doi: 10.1042/BJ20140237

Kolozsvari, B., Firth, S., and Saiardi, A. (2015). Raman Spectroscopy Detection of Phytic Acid in Plant Seeds Reveals the Absence of Inorganic Polyphosphate. *Mol. Plant* 8, 826–828. doi: 10.1016/j.molp.2015.01.015

Komine, Y., Eggink, L. L., Park, H., and Hoober, J. K. (2000). Vacuolar granules in *Chlamydomonas reinhardtii*: polyphosphate and a 70-kDa polypeptide as major components. *Planta* 210, 897–905. doi: 10.1007/s004250050695

Kornberg, A., and Fraley, C. D. (2000). Inorganic polyphosphate. A molecular fossil come to light. *ASM News* 66, 275–280.

Kornberg, A., Kornberg, S. R., and Simms, E. S. (1956). Metaphosphate synthesis by an enzyme from *Escherichia coli*. *Biochim. Biophys. Acta* 20, 215–227. doi: 10.1016/0006-3002(56)90280-3

Kornberg, A., Rao, N. N., and Ault-Riche, D. (1999). Inorganic polyphosphate: a molecule of many functions. *Annu. Rev. Biochem.* 68, 89–125. doi: 10.1146/annurev.biochem.68.1.89

Kornberg, A. (1995). Inorganic polyphosphate: toward making a forgotten polymer unforgettable. *J. Bacteriol.* 177, 491–496. doi: 10.1128/JB.177.3.491-496.1995

Kuesel, A. C., Sianoudis, J., Leibfritz, D., Grimme, L. H., and Mayer, A. (1989). P-31 in-vivo NMR investigation on the function of polyphosphates as phosphate- and energysource during the regreening of the green alga *Chlorella fusca*. *Arch. Microbiol.* 152, 167–171. doi: 10.1007/BF00456096

Kuga, Y., Saito, K., Nayuki, K., Peterson, R. L., and Saito, M. (2008). Ultrastructure of rapidly frozen and freeze-substituted germ tubes of an arbuscular mycorrhizal fungus and localization of polyphosphate. *New Phytol.* 178, 189–200. doi: 10.1111/j.1469-8137.2007.02345.x

Kulaev, I. S., Vagabov, V. M., and Kulakovskaya, T. V. (2004). *The biochemistry of inorganic polyphosphates*. (Chinchester, West Sussex, England: Jon Wiley & Sons, Ltd).

Kulakovskaya, T., Vagabov, V., and Kulaev, I. (2012). Inorganic Polyphosphate in Industry, Agriculture and Medicine: Modern State and Outlook. *Process Biochem.* 47, 1–10. doi: 10.1016/j.procbio.2011.10.028

Kuroda, A., Murphy, H., Cashel, M., and Kornberg, A. (1997). Guanosine tetra- and pentaphosphate promote accumulation of inorganic polyphosphate in *Escherichia coli*. *J. Biol. Chem.* 272, 21240–21243. doi: 10.1074/jbc.272.34.21240

Lahti, R. (1983). Microbial inorganic pyrophosphatases. *Microbiol. Rev.* 47, 169–178. doi: 10.1128/MMBR.47.2.169-178.1983

Lander, N., Ulrich, P. N., and Docampo, R. (2013). *Trypanosoma brucei* vacuolar transporter chaperone 4 (TbVtc4) is an acidocalcisome polyphosphate kinase required for in vivo infection. *J. Biol. Chem.* 288, 34205–34216. doi: 10.1074/jbc.M113.518993

Lawry, N. H., and Jensen, T. E. (1979). Deposition of condensed phosphate as an effect of varying sulfur deficiency in the cyanobacterium *Synechococcus* sp. (*Anacystis nidulans*). *Arch. Microbiol.* 120, 1–7. doi: 10.1007/BF00413264

Lawry, N. H., and Jensen, T. E. (1986). Condensed phosphate deposition, sulfur amino acid use, and unidirectional transsulfuration in *Synechococcus leopoliensis*. *Arch. Microbiol.* 144, 317–323. doi: 10.1007/BF00409879

Leitao, J. M., Lorenz, B., Bachinski, N., Wilhelm, C., Muller, W., and Schroder, H. C. (1995). Osmotic stress-induced synthesis and degradation of inorganic polyphosphates in the alga *Phaeodactylum tricornutum*. *Mar. Ecol. Prog. Ser.* 121, 279–288. doi: 10.3354/meps121279

Lemercier, G., Espiau, B., Ruiz, F. A., Vieira, M., Luo, S., Baltz, T., et al. (2004). A pyrophosphatase regulating polyphosphate metabolism in acidocalcisomes is essential for *Trypanosoma brucei* virulence in mice. *J. Biol. Chem.* 279, 3420–3425. doi: 10.1074/jbc.M309974200

Li, F. J., and He, C. Y. (2014). Acidocalcisome is required for autophagy in *Trypanosoma brucei*. *Autophagy* 10, 1978–1988. doi: 10.4161/auto.36183

Liao, H., Myung, S., and Zhang, Y.-H. P. (2012). One-step purification and immobilization of thermophilic polyphosphate glucokinase from *Thermobifida fusca* YX: glucose-6-phosphate generation without ATP. *Appl. Microbiol. Biotechnol.* 93, 1109–1117. doi: 10.1007/s00253-011-3458-1

Liberton, M., Austin, J., Berg, R. H., and Pakrasi, H. B. (2011). Unique thylakoid membrane architecture of a unicellular $N_2$-fixing cyanobacterium revealed by electron tomography. *Plant Physiol.* 155, 1656–1666. doi: 10.1104/pp.110.165332

Lichko, L. P., Kulakovskaya, T. V., and Kulaev, I. S. (2010). Properties of partially purified endopolyphosphatase of the yeast *Saccharomyces cerevisiae*. *Biochem. (Mosc)* 75, 1404–1407. doi: 10.1134/S0006297910110131

Lindner, S. N., Niederholtmeyer, H., Schmitz, K., Schoberth, S. M., and Wendisch, V. F. (2010). Polyphosphate/ATP-dependent NAD kinase of *Corynebacterium glutamicum*: biochemical properties and impact of ppnK overexpression on lysine production. *Appl. Microbiol. Biotechnol.* 87, 583–593. doi: 10.1007/s00253-010-2481-y

Liss, E., and Langen, P. (1962). Experiments on polyphosphate overcompensation in yeast cells after phosphate deficiency. *Arch. Mikrobiol.* 41, 383–392. doi: 10.1007/BF00422195

Livermore, T. M., Chubb, J. R., and Saiardi, A. (2016a). Developmental accumulation of inorganic polyphosphate affects germination and energetic metabolism in *Dictyostelium discoideum*. *Proc. Natl. Acad. Sci. U. S. A* 113, 996–1001. doi: 10.1073/pnas.1519440113

Livermore, T. M., Azevedo, C., Kolozsvari, B., Wilson, M. S. C., and Saiardi, A. (2016). Phosphate, inositol and polyphosphates. *Biochem. Soc. Trans.* 44, 253–259. doi: 10.1042/BST20150215

Lonetti, A., Szijgyarto, Z., Bosch, D., Loss, O., Azevedo, C., and Saiardi, A. (2011). Identication of an Evolutionarily Conserved Family of Inorganic Polyphosphate Endophosphatases. *J. Biol. Chem.* 286, 31966–31974. doi: 10.1074/jbc.M111.266320

Lorenzo-Orts, L., Couto, D., and Hothorn, M. (2020). Identity and functions of inorganic and inositol polyphosphates in plants. *New Phytol.* 225, 637–652. doi: 10.1111/nph.16129

Luo, S., Rohloff, P., Cox, J., Uyemura, S. A., and Docampo, R. (2004). *Trypanosoma brucei* plasma membrane-type $Ca^{2+}$-ATPase 1 (TbPMC1) and 2 (TbPMC2) genes encode functional $Ca^{2+}$-ATPases localized to the acidocalcisomes and plasma membrane, and essential for $Ca^{2+}$ homeostasis and growth. *J. Biol. Chem.* 279, 14427–14439. doi: 10.1074/jbc.M309978200

Macfie, S. M., and Welbourne, P. M. (2014). The cell wall as a barrier to the uptake of metal ions in the unicellular green alga *Chlamydomonas reinhardtii*. *Arch. Environ. Contam. Toxicol.* 39, 413–419. doi: 10.1007/s002440010122

Madeira da Silva, L., and Beverley, S. M. (2010). Expansion of the target of rapamycin (TOR) kinase family and function in Leishmania shows that TOR3 is required for acidocalcisome biogenesis and animal infectivity. *Proc. Natl. Acad. Sci. U.S.A.* 107, 11965–11970. doi: 10.1073/pnas.1004599107

Maldonado, J., de los Rios, A., Esteve, I., Ascaso, C., Puyen, Z. M., Brambilla, C., et al. (2010). Sequestration and in vivo effect of lead on DE2009 microalga, using high-resolution microscopic techniques. *J. Hazard Mater.* 183, 44–50. doi: 10.1016/j.jhazmat.2010.06.085

Maldonado, J., Sole, A., Puyen, Z. M., and Esteve, I. (2011). Selection of bioindicators to detect lead pollution in Ebro delta microbial mats, using high-resolution microscopic techniques. *Aquat. Toxicol.* 104, 135–144. doi: 10.1016/j.aquatox.2011.04.009

Manganelli, R. (2007). Polyphosphate and stress response in mycobacteria. *Mol. Microbiol.* 65, 258–260. doi: 10.1111/j.1365-2958.2007.05819.x

Manosa, S., Mateo, R., and Guitart, R. (2001). A review of the effects of agricultural and industrial contamination in the Ebro delta biota and wildlife. *Envinron. Monit. Assess.* 71, 187–205. doi: 10.1023/A:1017545932219

Martin, P., and Van Mooy, B. A. (2013). Fluorometric quantification of polyphosphate in environmental plankton samples: extraction protocols, matrix effects, and nucleic acid interference. *Appl. Environ. Microbiol.* 79, 273–281. doi: 10.1128/AEM.02592-12

Martin, P., and Van Mooy, B. A. (2015). Correction for martin and van mooy, fluorometric quantification of polyphosphate in environmental plankton samples: extraction protocols, matrix effects, and nucleic acid interference. *Appl. Environ. Microbiol.* 81, 461. doi: 10.1128/AEM.03436-14

Martin, P., Dyhrman, S. T., Lomas, M. W., Poulton, N. J., and Van Mooy, B. A. (2014). Accumulation and enhanced cycling of polyphosphate by Sargasso Sea plankton in response to low phosphorus. *Proc. Natl. Acad. Sci. U. S. A* 111, 8089–8094. doi: 10.1073/pnas.1321719111

Martin, P., Lauro, F. M., Sarkar, A., Goodkin, N., Prakash, P. N., and Vinayachandran, P. N. (2018). Particulate polyphosphate and alkaline phosphatase activity across a latitudinal transect in the tropical Indian Ocean. *Limnol. Oceanogr.* 63, 1395–1406. doi: 10.1002/lno.10780

Martinez, R. J. (1963). On the nature of the granules of the genus *Spirillum*. *Archiv. Fur Mikrobiol.* 4, 334–343. doi: 10.1007/BF00509002

Mateo, R., Martinez-Vilalta, A., and Guitart, R. (1997). Lead shot pellets in the Ebro delta Spain: densities in sediments and prevalence of exposure in waterflow. *Environ. Pollut.* 96, 335–341. doi: 10.1016/S0269-7491(97)00046-8

McIntosh, M. T., and Vaidya, A. B. (2002). Vacuolar type H+ pumping pyrophosphatases of parasitic protozoa. *Int. J. Parasitol.* 32, 1–14. doi: 10.1016/S0020-7519(01)00325-3

McMahon, K. D., and Read, E. K. (2013). Microbial contributions to phosphorus cycling in eutrophic lakes and wastewater. *Annu. Rev. Microbiol.* 67, 199–219. doi: 10.1146/annurev-micro-092412-155713

Meyer, A. (1904). Orientierende untersuchungen ueber verbreitung. morphologie, und chemie des volutins. *Bot. Zeit* 62, 113–152.

Miranda, K., de Souza, W., Plattner, H., Hentschel, J., Kawazoe, U., Fang, J., et al. (2008). Acidocalcisomes in Apicomplexan parasites. *Exp. Parasitol.* 118, 2–9. doi: 10.1016/j.exppara.2007.07.009

Montalvetti, A., Rohloff, P., and Docampo, R. (2004). A functional aquaporin co-localizes with the vacuolar proton pyrophosphatase to acidocalcisomes and the contractile vacuole complex of *Trypanosoma cruzi*. *J. Biol. Chem.* 279, 38673–38682. doi: 10.1074/jbc.M406304200

Moreno, S. N., and Docampo, R. (2009). The role of acidocalcisomes in parasitic protists. *J. Eukaryot. Microbiol.* 56, 208–213. doi: 10.1111/j.1550-7408.2009.00404.x

Moreno, B., Rodrigues, C. O., Bailey, B. N., Urbina, J. A., Moreno, S. N., Docampo, R., et al. (2002). Magic-angle spinning (31)P NMR spectroscopy of condensed phosphates in parasitic protozoa: visualizing the invisible. *FEBS Lett.* 523, 207–212. doi: 10.1016/S0014-5793(02)02977-0

Moreno-Sanchez, D., Hernandez-Ruiz, L., Ruiz, F. A., and Docampo, R. (2012). Polyphosphate is a novel pro-inflammatory regulator of mast cells and is located in acidocalcisomes. *J. Biol. Chem.* 287, 28435–28444. doi: 10.1074/jbc.M112.385823

Mori, T., Binder, B., and Johnson, C. H. (1996). Circadian gating of cell division in cyanobacteria growing with average doubling times of less than 24 hours. *Proc. Natl. Acad. Sci. U. S. A* 93, 10183–10188. doi: 10.1073/pnas.93.19.10183

Morohoshi, T., Maruo, T., Shirai, Y., Kato, J., Ikeda, T., Takiguchi, N., et al. (2002). Accumulation of inorganic polyphosphate in phoU mutants of *Escherichia coli* and *Synechocystis* sp. strain PCC6803. *Appl. Environ. Microbiol.* 68, 4107–4110. doi: 10.1128/AEM.68.8.4107-4110.2002

Morrissey, J. H. (2012). Polyphosphate multi-tasks. *J. Thromb. Haemostasis* 10, 2313–2314. doi: 10.1111/jth.12001

Moseley, J., and Grossman, A. R. (2009). "Phosphorus limitation from the physiological to the genomic," in *The Chlamydomonas Sourcebook*, vol. 2 . Eds. E. Harris, D. Stern and G. B. Witman (Elsevier: Academic Press), 189–216.

Moudrikova, S., Sadowsky, A., Metzger, S., Nedbal, L., Mettler-Altmann, T., and Mojzes, P. (2017). Quantification of Polyphosphate in Microalgae by Raman Microscopy and by a Reference Enzymatic Assay. *Anal. Chem.* 89, 12006–12013. doi: 10.1021/acs.analchem.7b02393

Moura, K., Lizieri, C., Franco, M., Vaz, M., Araujo, W., Convey, P., et al. (2019). Physiological and thylakoid ultrastructural changes in cyanobacteria in response to toxic manganese concentrations. *Ecotoxicology* 28 (8), 1009–1021. doi: 10.1007/s10646-019-02098-y

Mukai, T., Kawai, S., Matsukawa, H., Matuo, Y., and Murata, K. (2003). Characterization and molecular cloning of a novel enzyme, inorganic polyphosphate/ATP-glucomannokinase, of *Arthrobacter* sp. strain KM. *Appl. Environ. Microbiol.* 69, 3849–3857. doi: 10.1128/AEM.69.7.3849-3857.2003

Mukherjee, C., Chowdhury, R., and Ray, K. (2015). Phosphorus Recycling from an Unexplored Source by Polyphosphate Accumulating Microalgae and

Cyanobacteria-A Step to Phosphorus Security in Agriculture. *Front. Microbiol.* 6, 1421. doi: 10.3389/fmicb.2015.01421

Muller, F., Mutch, N. J., Schenk, W. A., Smith, S. A., Esterl, L., Spronk, H. M., et al. (2009). Platelet polyphosphates are proinflammatory and procoagulant mediators in vivo. *Cell* 139, 1143–1156. doi: 10.1016/j.cell.2009.11.001

Munoz-Martin, M. A., Martinez-Rosell, A., Perona, E., Fernandez-Pinas, F., and Mateo, P. (2014). Monitoring bioavailable phosphorus in lotic systems: a polyphasic approach based on cyanobacteria. *Sci. Total Environ.* 475, 158–168. doi: 10.1016/j.scitotenv.2013.06.076

Murata, K., Hagiwara, S., Kimori, Y., and Kaneko, Y. (2016). Ultrastructure of compacted DNA in cyanobacteria by high-voltage cryo-electron tomography. *Sci. Rep.* 6, 34934. doi: 10.1038/srep34934

Nierzwicki-Bauer, S. A., Balkwill, D. L., and Stevens, S. E.Jr. (1983). Three-dimensional ultrastructure of a unicellular cyanobacterium. *J. Cell Biol.* 97, 713–722. doi: 10.1083/jcb.97.3.713

Nishikawa, K., Yamakoshi, Y., Uemura, I., and Tominaga, N. (2003). Ultrastructural changes in *Chlamydomonas acidophila* (Chlorophyta) induced by heavy metals and polyphosphate metabolism. *FEMS Microbiol. Ecol.* 44, 253–259. doi: 10.1016/S0168-6496(03)00049-7

Nishikawa, K., Machida, H., Yamakoshi, Y., Ohtomo, R., Saito, K., Saito, M., et al. (2006). Polyphosphate metabolism in an acidophilic alga *Chlamydomonas acidophilia* KT-1 (Chlorophyte) under phosphate stress. *Plant Sci.* 170, 307–313. doi: 10.1016/j.plantsci.2005.08.025

Nishikawa, K., Tominaga, N., Uchino, T., Oikawa, A., and Tokunaga, H. (2009). "Polyphosphate contributes to CD tolerance in *Chlamydomonas Acidophila* KT-1," in *Algae: Nutrition, Pollution Control and Energy Sources*. Ed. K. N. Hagen (Hauppauge, NY: Nova Science Publishers), 13–21.

Nitta, K., Nagayama, K., Danev, R., and Kaneko, Y. (2009). Visualization of BrdU-labelled DNA in cyanobacterial cells by Hilbert differential contrast transmission electron microscopy. *J. Microsc.* 234, 118–123. doi: 10.1111/j.1365-2818.2009.03162.x

Niyogi, S., Jimenez, V., Girard-Dias, W., de Souza, W., Miranda, K., and Docampo, R. (2015). Rab32 is essential for maintaining functional acidocalcisomes, and for growth and infectivity of *Trypanosoma cruzi*. *J. Cell Sci.* 128, 2363–2373. doi: 10.1242/jcs.169466

Ohbayashi, R., Watanabe, S., Kanesaki, Y., Narikawa, R., Chibazakura, T., Ikeuchi, M., et al. (2013). DNA replication depends on photosynthetic electron transport in cyanobacteria. *FEMS Microbiol. Lett.* 344, 138–144. doi: 10.1111/1574-6968.12166

Orchard, E. D., Benitez-Nelson, C. R., Pellechia, P. J., Lomas, M. W., and Dyhrman, S. T. (2010). Polyphosphate in *Trichodesmium* from the low-phosphorus Sargasso Sea. *Limnol. Oceanogr.* 55, 2161–2169. doi: 10.4319/lo.2010.55.5.2161

Oren, N., Raanan, H., Kedem, I., Turjeman, A., Bronstein, M., Kaplan, A., et al. (2019). Desert cyanobacteria prepare in advance for dehydration and rewetting: The role of light and temperature sensing. *Mol. Ecol.* 28, 2305–2320. doi: 10.1111/mec.15074

Ota, S., Yoshihara, M., Yamazaki, T., Takeshita, T., Hirata, A., Konomi, M., et al. (2016). Deciphering the relationship among phosphate dynamics, electron-dense body and lipid accumulation in the green alga *Parachlorella kessleri*. *Sci. Rep.* 6, 25731. doi: 10.1038/srep25731

Pathak, H., Mohanty, S., Jain, N., and Bhatia, A. (2010). Nitrogen, phosphorus, and potassium budgets in Indian agriculture. *Nutr. Cycling Agroecosyst* 86, 287–299. doi: 10.1007/s10705-009-9292-5

Penen, F., Malherbe, J., Isaure, M. P., Dobritzsch, D., Bertalan, I., Gontier, E., et al. (2016). Chemical bioimaging for the subcellular localization of trace elements by high contrast TEM, TEM/X-EDS, and NanoSIMS. *J. Trace Elem. Med. Biol.* 37, 62–68. doi: 10.1016/j.jtemb.2016.04.014

Penen, F., Isaure, M. P., Dobritzsch, D., Bertalan, I., Castillo-Michel, H., Proux, O., et al. (2017). Pools of cadmium in *Chlamydomonas reinhardtii* revealed by chemical imaging and XAS spectroscopy. *Metallomics* 9, 910–923. doi: 10.1039/C7MT00029D

Pepin, C. A., and Wood, H. G. (1986). Polyphosphate glucokinase from *Propionibacterium shermanii*. Kinetics and demonstration that the mechanism involves both processive and nonprocessive type reactions. *J. Biol. Chem.* 261, 4476–4480.

Perry, M. J. (1976). Phosphate utilization by an oceanic diatom in phosphorus limited chemostat culture and in oligotrophic waters of the central North Pacific. *Limnol. Oceanogr.* 21, 88–107. doi: 10.4319/lo.1976.21.1.0088

Pettersson, A., Hallbom, L., and Bergman, B. (1988). Aluminum Effects on Uptake and Metabolism of Phosphorus by the Cyanobacterium *Anabaena cylindrica*. *Plant Physiol.* 86, 112–116. doi: 10.1104/pp.86.1.112

Pick, U., Bental, M., Chitlaru, E., and Weiss, M. (1990). Polyphosphate-hydrolysis - a protective mechanism against alkaline stress. *FEBS Lett.* 274, 15–18. doi: 10.1016/0014-5793(90)81318-I

Raboy, V. (2003). myo-Inositol-1,2,3,4,5,6-hexakisphosphate. *Phytochemistry* 64, 1033–1043. doi: 10.1016/S0031-9422(03)00446-1

Rachlin, J. W., Jensen, T. E., and Warkentine, B. E. (1985). Morphometric analysis of the response of Anabaena flos-aquae and *Anabaena variabilis* (Cyanophyceae) to selected concentrations of zinc. *Arch. Environ. Contam. Toxicol.* 14, 395–402. doi: 10.1007/BF01055524

Ramakrishnan, S., and Docampo, M. (2018). Membrane proteins in trypanosomatids involved in $Ca^{2+}$ homeostasis and signaling. *Genes* 9, 304. doi: 10.3390/genes9060304

Rangsayator, N., Upatham, E. S., Kruatrachue, M., Pokethitiyook, P., and Lanza, G. R. (2002). Phytoremediation potential of *Spirulina* (Arthrospira) *platensis*: biosorption and toxicity studies of cadmium. *Environ. Pollut.* 119, 45–53. doi: 10.1016/S0269-7491(01)00324-4

Rao, N. N., and Kornberg, A. (1999). Inorganic polyphosphate regulates responses of *Escherichia coli to* nutritional stringencies, environmental stresses and survival in the stationary phase. *Prog. Mol. Subcell Biol.* 23, 183–195. doi: 10.1007/978-3-642-58444-2_9

Rao, N. N., Gomez-Garcia, M. R., and Kornberg, A. (2009). Inorganic polyphosphate: essential for growth and survival. *Annu. Rev. Biochem.* 78, 605–647. doi: 10.1146/annurev.biochem.77.083007.093039

Rashid, M. H., Rumbaugh, K., Passador, L., Davies, D. G., Hamood, A. N., Iglewski, B. H., et al. (2000). Polyphosphate kinase is essential for biofilm development, quorum sensing, and virulence of *Pseudomonas aeruginosa*. *Proc. Natl. Acad. Sci. U. S. A* 97, 9636–9641. doi: 10.1073/pnas.170283397

Ray, K., Mukherjee, C., and Ghosh, A. N. (2013). A way to curb phosphorus toxicity in the environment: use of polyphosphate reservoir of cyanobacteria and microalga as a safe alternative phosphorus biofertilizer for Indian agriculture. *Environ. Sci. Technol.* 47, 11378–11379. doi: 10.1021/es403057c

Rea, P. A., Kim, Y., Sarafian, V., Poole, R. J., Davies, J. M., and Sanders, D. (1992). Vacuolar H(+)-translocating pyrophosphatases: a new category of ion translocase. *Trends Biochem. Sci.* 17, 348–353. doi: 10.1016/0968-0004(92)90313-X

Reistetter, E. N., Krumhardt, K., Callnan, K., Roache-Johnson, K., Saunders, J. K., Moore, L. R., et al. (2013). Effects of phosphorus starvation versus limitation on the marine cyanobacterium *Prochlorococcus* MED4 II: gene expression. *Environ. Microbiol.* 15, 2129–2143. doi: 10.1111/1462-2920.12129

Reusch, R. N. (1999). Polyphosphate/poly-(R)-3-hydroxybutyrate) ion channels in cell membranes. *Prog. Mol. Subcell Biol.* 23, 151–182. doi: 10.1007/978-3-642-58444-2_8

Reusch, R. N. (2000). Transmembrane ion transport by polyphosphate/poly-(R)-3-hydroxybutyrate complexes. *Biochem. (Mosc)* 65, 280–295.

Rhee, G.-Y. (1973). A continuous culture study of phosphate uptake, growth rate and polyphosphate in *Scenedesmus* sp. *J. Phycol.* 9, 495–506.

Riegman, R., Stolte, W., Noordeloos, A. A. M., and Slezak, D. (2000). Nutrient uptake, and alkaline phosphate (EC 3 : 1 : 3 : 1) activity of *Emiliania huxleyi* (Prymnesiophyceae) during growth under N and P limitation in continuous cultures. *J. Phycol.* 36, 87–96. doi: 10.1046/j.1529-8817.2000.99023.x

Rodrigues, C. O., Scott, D. A., and Docampo, R. (1999). Characterization of a vacuolar pyrophosphatase in *Trypanosoma brucei* and its localization to acidocalcisomes. *Mol. Cell Biol.* 19, 7712–7723. doi: 10.1128/MCB.19.11.7712

Rodrigues, C. O., Ruiz, F. A., Vieira, M., Hill, J. E., and Docampo, R. (2002). An acidocalcisomal exopolyphosphatase from *Leishmania major* with high affinity for short chain polyphosphate. *J. Biol. Chem.* 277, 50899–50906. doi: 10.1074/jbc.M208940200

Ruiz, F. A., Marchesini, N., Seufferheld, M., Govindjee,, and Docampo, R. (2001). The polyphosphate bodies of *Chlamydomonas reinhardtii* possess a proton-pumping pyrophosphatase and are similar to acidocalcisomes. *J. Biol. Chem.* 276, 46196–46203. doi: 10.1074/jbc.M105268200

Ruiz, F. A., Lea, C. R., Oldfield, E., and Docampo, R. (2004a). Human platelet dense granules contain polyphosphate and are similar to acidocalcisomes of bacteria and unicellular eukaryotes. *J. Biol. Chem.* 279, 44250–44257. doi: 10.1074/jbc.M406261200

Ruiz, F. A., Luo, S., Moreno, S. N., and Docampo, R. (2004b). Polyphosphate content and fine structure of acidocalcisomes of *Plasmodium falciparum*. *Microsc. Microanal.* 10, 563–567. doi: 10.1017/S1431927604040875

Saiardi, A. (2012). How inositol pyrophosphates control cellular phosphate homeostasis? *Adv. Biol. Regul.* 52, 351–359. doi: 10.1016/j.jbior.2012.03.002

Sakaguchi, T., Horikoshi, T., and Nakajima, A. (1978). Uptake of uranium from sea water by microalgae. *J. Fermentation Technol.* 56, 561–565.

Samadani, M., and Dewez, D. (2018a). Effect of mercury on the polyphosphate level of alga *Chlamydomonas reinhardtii*. *Environ. Pollut.* 240, 506–513. doi: 10.1016/j.envpol.2018.04.141

Samadani, M., and Dewez, D. (2018b). Cadmium accumulation and toxicity affect the extracytoplasmic polyphosphate level in *Chlamydomonas reinhardtii*. *Ecotoxicol. Environ. Saf.* 166, 200–206. doi: 10.1016/j.ecoenv.2018.09.094

Samadani, M., El-Khoury, J., and Dewez, D. (2020). Tolerance Capacity of Chlamydomonas VHLR Mutants for the Toxicity of Mercury. *Water Air Soil Pollut.* 231, 167–178. doi: 10.1007/s11270-020-04543-9

Santos-Beneit, F. (2015). The Pho regulon: a huge regulatory network in bacteria. *Front. Microbiol.* 6, 402. doi: 10.3389/fmicb.2015.00402

Sato, M., Masuda, Y., Kirimura, K., and Kino, K. (2007). Thermostable ATP regeneration system using polyphosphate kinase from *Thermosynechococcus elongatus* BP-1 for D-amino acid dipeptide synthesis. *J. Biosci. Bioeng.* 103, 179–184. doi: 10.1263/jbb.103.179

Schilling, R. K., Tester, M., Marschner, P., Plett, D. C., and Roy, S. J. (2017). AVP1: One Protein, Many Roles. *Trends Plant Sci.* 22, 154–162. doi: 10.1016/j.tplants.2016.11.012

Scott, D. A., and Docampo, R. (2000). Characterization of isolated acidocalcisomes of *Trypanosoma cruzi*. *J. Biol. Chem.* 275, 24215–24221. doi: 10.1074/jbc.M002454200

Segami, S., Asaoka, M., Kinoshita, S., Fukuda, M., Nakanishi, Y., and Maeshima, M. (2018a). Biochemical, Structural and Physiological Characteristics of Vacuolar H+-Pyrophosphatase. *Plant Cell Physiol.* 59, 1300–1308. doi: 10.1093/pcp/pcy054

Segami, S., Tomoyama, T., Sakamoto, S., Gunji, S., Fukuda, M., Kinoshita, S., et al. (2018b). Vacuolar H(+)-Pyrophosphatase and Cytosolic Soluble Pyrophosphatases Cooperatively Regulate Pyrophosphate Levels in Arabidopsis thaliana. *Plant Cell* 30, 1040–1061. doi: 10.1105/tpc.17.00911

Segawa, S., Fujiya, M., Konishi, H., Ueno, N., Kobayashi, N., Shigyo, T., et al. (2011). Probiotic-derived polyphosphate enhances the epithelial barrier function and maintains intestinal homeostasis through integrin-p38 MAPK pathway. *PloS One* 6, e23278. doi: 10.1371/journal.pone.0023278

Seki, Y., Nitta, K., and Kaneko, Y. (2014). Observation of polyphosphate bodies and DNA during the cell division cycle of *Synechococcus elongatus* PCC 7942. *Plant Biol. (Stuttg)* 16, 258–263. doi: 10.1111/plb.12008

Serrano, A., Perez-Castineira, J. R., Baltscheffsky, M., and Baltscheffsky, H. (2007). H+-PPases: yesterday, today and tomorrow. *IUBMB Life* 59, 76–83. doi: 10.1080/15216540701258132

Shah, N. R., Wilkinson, C., Harborne, S. P., Turku, A., Li, K. M., Sun, Y. J., et al. (2017). Insights into the mechanism of membrane pyrophosphatases by combining experiment and computer simulation. *Struct. Dyn* 4, 032105. doi: 10.1063/1.4978038

Shebanova, A., Ismagulova, T., Solovchenko, A., Baulina, O., Lobakova, E., Ivanova, A., et al. (2017). Versatility of the green microalga cell vacuole function as revealed by analytical transmission electron microscopy. *Protoplasma* 254, 1323–1340. doi: 10.1007/s00709-016-1024-5

Shi, X., Rao, N. N., and Kornberg, A. (2004). Inorganic polyphosphate in *Bacillus cereus*: motility, biofilm formation, and sporulation. *Proc. Natl. Acad. Sci. U. S. A* 101, 17061–17065. doi: 10.1073/pnas.0407787101

Sicko-Goad, L., and Jensen, T. E. (1976). Phosphate metabolism in blue-green algae. II. Changes in phosphate distribution during starvation and the "polyphosphate overplus" phenomenon in *Plectonema boryanum*. *Am. J. Bot.* 63, 183–188. doi: 10.1002/j.1537-2197.1976.tb11800.x

Sicko-Goad, L., and Lazinsky, D. (1986). Quantitative ultrastructural changes associated with lead-coupled luxury phosphate uptake and polyphosphate utilization. *Arch. Environ. Contamination Toxicol.* 15, 617–627. doi: 10.1007/BF01054908

Sicko-Goad, L., Crang, R. E., and Jensen, T. E. (1975). Phosphate metabolism in blue–green algae. IV.In situ analysis of polyphosphate bodies by X-ray energy dispersive analysis. *Cytobiology* 11, 430–437.

Sicko-Goad, L., Jensen, T. E., and Ayala, R. P. (1978). Phosphate metabolism in blue-green bacteria. V. Factors affecting phosphate uptake in *Plectonema boryanum*. *Can. J. Microbiol.* 24, 105–108. doi: 10.1139/m78-019

Siderius, M., Musgrave, A., van den Ende, H., Koerten, H., Cambier, P., and van der Meer, P. (1996). *Chlamydomonas eugametos* (Chlorophyta) stores phosphate in polyphosphate bodies together with calcium. *J. Phycol.* 32, 402–409. doi: 10.1111/j.0022-3646.1996.00402.x

Siebers, N., Musgrave, A., Van den Ende, H., Koerten, H., Cambier, P., and Van der Meer, P. (2019). Towards phosphorus recycling for agriculture by algae: soil incubation and rhizotron path toward involving microalgae. *Algal Res.* 43, 101634–101639. doi: 10.1016/j.algal.2019.101634

Simon, R. D. (1977). Macromolecular composition of spores from the filamentous cyanobacterium *Anabaena cylindrica*. *J. Bacteriol.* 129, 1154–1155. doi: 10.1128/JB.129.2.1154-1155.1977

Singh, A. L. (2012). Study of Ni uptake and its compartmentalization in Ni(r), Pd (r) and Ni(s)/ Pd(s) strain of *Nostoc muscorum*. *J. Environ. Sci. Eng.* 54, 104–106.

Sliwinska-Wilczewska, S., Maculewicz, J., Barreiro Felpeto, A., and Latala, A. (2018). Allelopathic and Bloom-Forming Picocyanobacteria in a Changing World. *Toxins (Basel)* 10, 48–67. doi: 10.3390/toxins10010048

Smith, R. M., and Williams, S. B. (2006). Circadian rhythms in gene transcription imparted by chromosome compaction in the cyanobacterium *Synechococcus elongatus*. *Proc. Natl. Acad. Sci. U. S. A* 103, 8564–8569. doi: 10.1073/pnas.0508696103

Smith, S. A., Mutch, N. J., Baskar, D., Rohloff, P., Docampo, R., and Morrissey, J. H. (2006). Polyphosphate modulates blood coagulation and fibrinolysis. *Proc. Natl. Acad. Sci. U. S. A* 103, 903–908. doi: 10.1073/pnas.0507195103

Solovchenko, A., Verschoor, A. M., Jablonowski, N. D., and Nebdal, L. (2016). Phosphorus from wastewater to crops: An alternative path involving microalgae. *Biotechnol. Adv.* 34, 550–564. doi: 10.1016/j.biotechadv.2016.01.002

Steinmann, M. E., Schmidt, R. S., Butikofer, P., Maser, P., and Sigel, E. (2017). TbIRK is a signature sequence free potassium channel from *Trypanosoma brucei* locating to acidocalcisomes. *Sci. Rep.* 7, 656. doi: 10.1038/s41598-017-00752-1

Steunou, A. S., Bhaya, D., Bateson, M. M., Melendrez, M. C., Ward, D. M., Brecht, E., et al. (2006). In situ analysis of nitrogen fixation and metabolic switching in unicellular thermophilic cyanobacteria inhabiting hot spring microbial mats. *Proc. Natl. Acad. Sci. U. S. A* 103, 2398–2403. doi: 10.1073/pnas.0507513103

Steunou, A. S., Jensen, S. I., Brecht, E., Becraft, E. D., Bateson, M. M., Kilian, O., et al. (2008). Regulation of *nif* gene expression and the energetics of $N_2$ fixation over the diel cycle in a hot spring microbial mat. *ISME J.* 2, 364–378. doi: 10.1038/ismej.2007.117

Stevens, S. E.Jr., Nierzwicki-Bauer, S. A., and Balkwill, D. L. (1985). Effect of nitrogen starvation on the morphology and ultrastructure of the cyanobacterium *Mastigocladus laminosus*. *J. Bacteriol.* 161, 1215–1218. doi: 10.1128/JB.161.3.1215-1218.1985

Sukenik, A., Kaplan-Levy, R. N., Welch, J. M., and Post, A. F. (2012). Massive multiplication of genome and ribosomes in dormant cells (akinetes) of *Aphanizomenon ovalisporum* (Cyanobacteria). *ISME J.* 6, 670–679. doi: 10.1038/ismej.2011.128

Suzuki, S., Ferjani, A., Suzuki, I., and Murata, N. (2004). The SphS-SphR two component system is the exclusive sensor for the induction of gene expression in response to phosphate limitation in *Synechocystis*. *J. Biol. Chem.* 279, 13234–13240. doi: 10.1074/jbc.M313358200

Swift, D. T., and Forciniti, D. (1997). Accumulation of lead by *Anabaena cylindrica* : mathematical modeling and an energy dispersive X-ray study. *Biotechnol. Bioeng.* 55, 408–418. doi: 10.1002/(SICI)1097-0290(19970720)55:2<408::AID-BIT18>3.0.CO;2-C

Syed Hasnain, S., Tanzeelur, R., Ghulam Mujtaba, S., Syeda Tayyaba, B., and Saqib, Z. (2019). Toxic Algae and Their Environmental Consequences. *Trends Telemed. E-Health* 1 (4), 1–3. TTEH.000519.002019.

Szymona, M., and Ostrowski, W. (1964). Inorganic Polyphosphate Glucokinase of *Mycobacterium Phlei*. *Biochim. Biophys. Acta* 85, 283–295. doi: 10.1016/0926-6569(64)90249-4

Szymona, O., and Szymona, M. (1978). Multiple forms of polyphosphate-glucose phosphotransferase in various *Micobacterium* strains. *Acta Microbiol. Pol.* 27, 73–78.

Szymona, O., and Szymona, M. (1979). Polyphosphate and ATP-glucose phosphotransferase activities of *Novocardia minima*. *Acta Microbiol. Pol.* 28, 153–160.

Szymona, M., and Widomski, J. (1974). A kinetic study on inorganic polyphosphate glucokinase from *Mycobacterium tuberculosis* H37RA. *Physiol. Chem. Phys.* 6, 393–404.

Szymona, M. (1957). Utilization of inorganic polyphosphates for phosphorylation of glucose in *Micobacterium phlei*. *Bull. Acad. Pol. Sci. Ser. Sci. Biol.* 5, 379–381.

Tanaka, S., Lee, S. O., Hamaoka, K., Kato, J., Takiguchi, N., Nakamura, K., et al. (2003). Strictly polyphosphate-dependent glucokinase in a polyphosphate-accumulating bacterium, *Microlunatus phosphovorus*. *J. Bacteriol.* 185, 5654–5656. doi: 10.1128/JB.185.18.5654-5656.2003

Tani, C., Ohtomo, R., Osaki, M., Kuga, Y., and Ezawa, T. (2009). ATP-dependent but proton gradient-independent polyphosphate-synthesizing activity in extraradical hyphae of an arbuscular mycorrhizal fungus. *Appl. Environ. Microbiol.* 75, 7044–7050. doi: 10.1128/AEM.01519-09

Tijssen, J. P., Beekes, H. W., and Van Steveninck, J. (1982). Localization of polyphosphates in Saccharomyces fragilis, as revealed by 4',6-diamidino-2-phenylindole fluorescence. *Biochim. Biophys. Acta* 721, 394–398. doi: 10.1016/0167-4889(82)90094-5

Torres, M., Goldberg, J., and Jensen, T. E. (1998). Heavy metal uptake by polyphosphate bodies in living and killed cells of *Plectonema boryanum* (cyanophycae). *Microbios* 96, 141–147.

Treves, H., Raanan, H., Finkel, O. M., Berkowicz, S. M., Keren, N., Shotland, Y., et al. (2013). A newly isolated Chlorella sp. from desert sand crusts exhibits a unique resistance to excess light intensity. *FEMS Microbiol. Ecol.* 86, 373–380. doi: 10.1111/1574-6941.12162

Treves, H., Raanan, H., Kedem, I., Murik, O., Keren, N., Zer, H., et al. (2016). The mechanisms whereby the green alga Chlorella ohadii, isolated from desert soil crust, exhibits unparalleled photodamage resistance. *New Phytol.* 210, 1229–1243. doi: 10.1111/nph.13870

Tsai, J. Y., Kellosalo, J., Sun, Y. J., and Goldman, A. (2014). Proton/sodium pumping pyrophosphatases: the last of the primary ion pumps. *Curr. Opin. Struct. Biol.* 27, 38–47. doi: 10.1016/j.sbi.2014.03.007

Tsednee, M., Castruita, M., Salome, P. A., Sharma, A., Lewis, B. E., Schmollinger, S. R., et al. (2019). Manganese co-localizes with calcium and phosphorus in Chlamydomonas acidocalcisomes and is mobilized in manganese-deficient conditions. *J. Biol. Chem.* 294, 17626–17641. doi: 10.1074/jbc.RA119.009130

Twiss, M. R., and Nalewajko, C. (1992). Influence of phosphorus nutrition on copper toxicity to three strains of *Scenedesmus acuta* (Chlorophyceae). *J. Phycol.* 28, 291–298. doi: 10.1111/j.0022-3646.1992.00291.x

Tyrell, T. (1999). The influence of nitrogen and phosphorus on oceanic primary production. *Nature* 400, 525–531. doi: 10.1038/22941

Ulrich, P. N., Lander, N., Kurup, S. P., Reiss, L., Brewer, J., Soares Medeiros, L. C., et al. (2014). The acidocalcisome vacuolar transporter chaperone 4 catalyzes the synthesis of polyphosphate in insect-stages of *Trypanosoma brucei* and *T. cruzi*. *J. Eukaryot. Microbiol.* 61, 155–165. doi: 10.1111/jeu.12093

Vaillancourt, S., Beuchemin-Newhouse, N., and Cedergren, R. J. (1978). Polyphosphate-deficient mutants of *Anacystis nidulans*. *Can. J. Microbiol.* 24, 112–116. doi: 10.1139/m78-021

van Groenestijn, J. W., Vlekke, G. J., Anink, D. M., Deinema, M. H., and Zehnder, A. J. (1988). Role of Cations in Accumulation and Release of Phosphate by Acinetobacter Strain 210A. *Appl. Environ. Microbiol.* 54, 2894–2901. doi: 10.1128/AEM.54.12.2894-2901.1988

Van Mooy, B. A., Fredricks, H. F., Pedler, B. E., Dyhrman, S. T.., Karl, D. M., Koblízek, M., et al. (2009). Phytoplankton in the ocean use non-phosphorus lipids in response to phosphorus scarcity. *Nature* 458, 69–72. doi: 10.1038/nature07659

Venter, M., Groenewald, J. H., and Botha, F. C. (2006). Sequence analysis and transcriptional profiling of two vacuolar H+ -pyrophosphatase isoforms in *Vitis vinifera*. *J. Plant Res.* 119, 469–478. doi: 10.1007/s10265-006-0009-4

Vercesi, A. E., Moreno, S. N., and Docampo, R. (1994). $Ca^{2+}/^{H+}$ exchange in acidic vacuoles of *Trypanosoma brucei*. *Biochem. J.* 304 ( Pt 1), 227–233. doi: 10.1042/bj3040227

Villarreal-Chiu, J. F., Quinn, J. P., and McGrath, J. W. (2012). The genes and enzymes of phosphonate metabolism by bacteria, and their distribution in the marine environment. *Front. Microbiol.* 3, 19. doi: 10.3389/fmicb.2012.00019

Voelz, H., Voelz, U., and Ortigoza, R. O. (1966). The "polyphosphate overplus" phenomenon in *Myxococcus xanthus* and its influence on the architecture of the cell. *Arch. Mikrobiol.* 53, 371–388. doi: 10.1007/BF00409874

Voronkov, A., and Sinetova, M. (2019). Polyphosphate accumulation dynamics in a population of *Synechocystis* sp. PCC 6803 cells under phosphate overplus. *Protoplasma* 256, 1153–1164. doi: 10.1007/s00709-019-01374-2

Walsh, R. S., and Hunter, K. A. (1992). Influence of phosphorus storage on the uptake of cadmium by the marine alga *Macrocystis pyrifera*. *Limnol. Oceanogr.* 37, 1361–1369. doi: 10.4319/lo.1992.37.7.1361

Wan, L., Chen, X., Deng, Q., Yang, L., Li, X., Zhang, J., et al. (2019). Phosphorus strategy in bloom-forming cyanobacteria (*Dolichospermum* and *Microcystis*) and its role in their succession. *Harmful Algae* 84, 46–55. doi: 10.1016/j.hal.2019.02.007

Wang, W.-X., and Dei, R. C. H. (2006). Metal stoichiometry in predicting Cd and Cu toxicity to a freshwater green alga *Chlamydomonas reinhardtii*. *Envinron. Poll* 142, 303–312. doi: 10.1016/j.envpol.2005.10.005

Wang, D.-Z. (2008). Neurotoxins from Marine Dinoflagellates: A Brief Review. *Mar. Drugs* 6, 349–371. doi: 10.3390/md6020349

Wanner, B. L. (1993). Gene regulation by phosphate in enteric bacteria. *J. Cell Biochem.* 51, 47–54. doi: 10.1002/jcb.240510110

Ward, D. M., Ferris, M. J., Nold, S. C., and Bateson, M. M. (1998). A natural view of microbial biodiversity within hot spring cyanobacterial mat communities. *Microbiol. Mol. Biol. Rev.* 62, 1353–1370. doi: 10.1128/MMBR.62.4.1353-1370.1998

Watanabe, S., Ohbayashi, R., Shiwa, Y., Noda, A., Kanesaki, Y., Chibazakura, T., et al. (2012). Light-dependent and asynchronous replication of cyanobacterial multi-copy chromosomes. *Mol. Microbiol.* 83, 856–865. doi: 10.1111/j.1365-2958.2012.07971.x

Waterbury, J. B., Watson, S. W., Guillard, R. R. L., and Brand, L. E. (1979). Widespread occurrence of a unicellular, marine, planktonic, cyanobacterium. *Nature*, 277, 293–294. doi: 10.1038/277293a0

Weerasekara, A. W., Jenkins, S., Abbott, L. K., Waite, I., McGrath, J. W., Larma, I., et al. (2016). Microbial phylogenetic and functional responses within acidified wastewater communities exhibiting enhanced phosphate uptake. *Bioresour. Technol.* 220, 55–61. doi: 10.1016/j.biortech.2016.08.037

Weisse, T. (1993). Dynamics of autotrophic phytoplankton in marine and freshwater ecosystems. *Adv. Microbial Ecol.*, 13, 327–370. doi: 10.1007/978-1-4615-2858-6_8

Werner, T. P., Amrhein, N., and Freimoser, F. M. (2007). Inorganic polyphosphate occurs in the cell wall of *Chlamydomonas reinhardtii* and accumulates during cytokinesis. *BMC Plant Biol.* 7, 51. doi: 10.1186/1471-2229-7-51

Wild, R., Gerasimaite, R., Jung, J. Y., Truffault, V., Pavlovic, I., Schmidt, A., et al. (2016). Control of eukaryotic phosphate homeostasis by inositol polyphosphate sensor domains. *Science* 352, 986–990. doi: 10.1126/science.aad9858

Xie, L., and Jakob, U. (2018). Inorganic polyphosphate, a multifunctional polyanionic protein scaffold. *J. Biol. Chem.* 294, 2180–2190. doi: 10.1074/jbc.REV118.002808

Yagisawa, F., Nishida, K., Yoshida, M., Ohnuma, M., Shimada, T., Fujiwara, T., et al. (2009). Identification of novel proteins in isolated polyphosphate vacuoles in the primitive red alga *Cyanidioschyzon merolae*. *Plant J.* 60, 882–893. doi: 10.1111/j.1365-313X.2009.04008.x

Yu, R. Q., and Wang, X.-W. (2004a). Biological uptake of Cd, Se(IV) and Zn by *Chlamydomonas reinhardtii in* response to different phosphate and nitrate additions. *Aquat. Microb. Ecol.* 35, 163–173. doi: 10.3354/ame035163

Yu, R. Q., and Wang, X.-W. (2004b). Biokinetics of cadmium, selenium and zinc in freshwater algae *Scenedesmus obliquus* under different phosphorus and nitrogen conditions and metal transfer to *Dafnia magna*. *Environ. Pollut.* 129, 443–456. doi: 10.1016/j.envpol.2003.11.013

Zeng, J., and Wang, W. X. (2009). The importance of cellular phosphorus in controlling the uptake and toxicity of cadmium and zinc in *Microcystis aeruginosa*, a freshwater cyanobacterium. *Environ. Toxicol. Chem.* 28, 1618–1626. doi: 10.1897/08-639.1

Zeng, J., Yang, L., and Wang, W. X. (2009). Acclimation to and recovery from cadmium and zinc exposure by a freshwater cyanobacterium, *Microcystis aeruginosa*. *Aquat. Toxicol.* 93, 1–10. doi: 10.1016/j.aquatox.2009.02.013

Zhang, F., Blasiak, L. C., Karolin, J. O., Powell, R. J., Geddes, C. D., and Hill, R. T. (2015). Phosphorus sequestration in the form of polyphosphate by microbial symbionts in marine sponges. *Proc. Natl. Acad. Sci. U. S. A* 112, 4381–4386. doi: 10.1073/pnas.1423768112

Zhu, J., Loubery, S., Broger, L., Zhang, Y., Lorenzo-Orts, L., Utz-Pugin, A., et al. (2020). A genetically validated approach for detecting inorganic polyphosphates in plants. *Plant J.* 102, 507–576. doi: 10.1111/tpj.14642

**Conflict of Interest:** The authors declare that the research was conducted in the absence of any commercial or financial relationships that could be construed as a potential conflict of interest.

frontiers in Plant Science

REVIEW
published: 30 June 2020
doi: 10.3389/fpls.2020.00982

# Fixing the Broken Phosphorus Cycle: Wastewater Remediation by Microalgal Polyphosphates

*Stephen P. Slocombe[1]*, Tatiana Zúñiga-Burgos[1,2], Lili Chu[1], Nicola J. Wood[1,3], Miller Alonso Camargo-Valero[2,4] and Alison Baker[1]*

*[1] Centre for Plant Sciences and Astbury Centre for Structural Molecular Biology, Faculty of Biological Sciences, School of Molecular and Cellular Biology, University of Leeds, Leeds, United Kingdom, [2] BioResource Systems Research Group, School of Civil Engineering, University of Leeds, Leeds, United Kingdom, [3] Centre for Doctoral Training in Bioenergy, School of Chemical and Process Engineering, University of Leeds, Leeds, United Kingdom, [4] Departamento de Ingeniería Química, Universidad Nacional de Colombia, Manizales, Colombia*

Phosphorus (P), in the form of phosphate derived from either inorganic ($P_i$) or organic ($P_o$) forms is an essential macronutrient for all life. P undergoes a biogeochemical cycle within the environment, but anthropogenic redistribution through inefficient agricultural practice and inadequate nutrient recovery at wastewater treatment works have resulted in a sustained transfer of P from rock deposits to land and aquatic environments. Our present and near future supply of P is primarily mined from rock P reserves in a limited number of geographical regions. To help ensure that this resource is adequate for humanity's food security, an energy-efficient means of recovering P from waste and recycling it for agriculture is required. This will also help to address excess discharge to water bodies and the resulting eutrophication. Microalgae possess the advantage of polymeric inorganic polyphosphate (PolyP) storage which can potentially operate simultaneously with remediation of waste nitrogen and phosphorus streams and flue gases ($CO_2$, $SO_x$, and $NO_x$). Having high productivity in photoautotrophic, mixotrophic or heterotrophic growth modes, they can be harnessed in wastewater remediation strategies for biofuel production either directly (biodiesel) or in conjunction with anaerobic digestion (biogas) or dark fermentation (biohydrogen). Regulation of algal P uptake, storage, and mobilization is intertwined with the cellular status of other macronutrients (e.g., nitrogen and sulphur) in addition to the manufacture of other storage products (e.g., carbohydrate and lipids) or macromolecules (e.g., cell wall). A greater understanding of controlling factors in this complex interaction is required to facilitate and improve P control, recovery, and reuse from waste streams. The best understood algal genetic model is *Chlamydomonas reinhardtii* in terms of utility and shared resources. It also displays mixotrophic growth and advantageously, species of this genus are often found growing in wastewater treatment plants. In this review, we focus primarily on the molecular and genetic aspects of PolyP production or turnover and place this knowledge in the context of wastewater remediation and highlight developments and challenges in this field.

**Keywords: acidocalcisomes, biofuel, biomass, biogas, phosphorus, polyphosphate, wastewater**

OPEN ACCESS

***Edited by:***
*Jose Roman Perez-Castineira, Universidad de Sevilla, Spain*

***Reviewed by:***
*Nishikant Wase, University of Virginia, United States*
*Alexei E. Solovchenko, Lomonosov Moscow State University, Russia*

****Correspondence:***
*Stephen P. Slocombe*
*S.P.Slocombe@leeds.ac.uk*

***Specialty section:***
*This article was submitted to Plant Metabolism and Chemodiversity, a section of the journal Frontiers in Plant Science*

***Received:*** *31 March 2020*
***Accepted:*** *16 June 2020*
***Published:*** *30 June 2020*

***Citation:***
*Slocombe SP, Zúñiga-Burgos T, Chu L, Wood NJ, Camargo-Valero MA and Baker A (2020) Fixing the Broken Phosphorus Cycle: Wastewater Remediation by Microalgal Polyphosphates. Front. Plant Sci. 11:982. doi: 10.3389/fpls.2020.00982*

# INTRODUCTION

## The Problem

Compared with the other macronutrients (carbon, sulphur, and nitrogen: C, S, and N), the biogeochemical cycle of Phosphorus (P) lacks a gaseous atmospheric component to assist with cyclic replenishment of soils (e.g., for N: lightning, biological N-fixation, and the Haber-Bosch process). This has led to the P cycle being described as "broken," consequently modern agriculture largely depends on non-renewable inorganic Phosphate ($P_i$)-based fertilizers derived from geological sources (Elser and Bennett, 2011). High grade $P_i$ rock reserves are projected to last for only 50 to 150 years as mined products already show diminished $P_i$ content and greater levels of heavy metal contamination. Additionally, global distribution of rock phosphate is uneven with most reserves present in just a handful of countries; Morocco and Western Sahara alone hold over 70% of total global reserves (Van Kauwenberg, 2010; U.S. Geological Survey, 2017). As such, much of the world is vulnerable to volatile prices and supply insecurity. An estimated 80% of extracted $P_i$ is being lost due to runoff, which in addition to $P_i$ present in sewage discharges is detrimental for the environment (Schröder et al., 2011). In addition, P (and other nutrients) are not being effectively recycled back to agriculture from wastes under the current system. Although livestock manure is often returned to soil, this can be polluting whereas the spreading of sewage and/or sewage sludge is restricted by regulations (Schröder et al., 2011). Current wastewater treatment methods are also affected by regulatory concerns and economic cost, therefore alternative approaches for P-remediation that recycle back to agriculture are needed (Baker et al., 2015). In Europe for instance, an analysis of P stores and flows showed that a higher demand for P fertilizer was mainly driven by poor P efficiency (i.e., useful P output as a function of total system P input: 38% overall). Here, regional P imbalance (P surplus) and system P losses were well correlated to total system P inputs ($P_i$ fertilizer, manure, sewage sludge, digestate, etc.) and livestock densities, causing unnecessary P accumulation in soils and rivers (Withers et al., 2020).

## A Potential Solution

Microalgae have long been studied for sustainable wastewater treatment (Baker et al., 2015; Li et al., 2019b) and have the added advantage of accumulating polyphosphate granules (PolyP). This means that they could be used to return $P_i$ back to soil in slow-release form and help to close the P-cycle (Siebers et al., 2019); although this approach has been indirectly adopted by reusing alga-rich effluents from wastewater treatment systems in crop irrigation (i.e., reuse of effluents from wastewater pond systems), the actual mechanisms controlling algal P uptake from wastewaters are not well understood. In recent years, the genetic model *Chlamydomonas reinhardtii* has become the foremost species for understanding the molecular biology underpinning P-metabolism and the production of PolyP in microalgae. Although other micro-algal species have been better investigated for wastewater treatment (Li et al., 2019b), *Chlamydomonas* sp. are often identified in sewage treatment works (STW) worldwide (see *Microalgal Research Models*). Therefore, the *Chlamydomonas* genus provides a good option for facilitating research and development, from the laboratory to engineered wastewater treatment systems.

In this review we first evaluate the remediation potential of microalgae in closing the P-cycle, focusing on wastewater treatment. Second, we explore PolyP in relation to its structure, P-starvation responses, synthesis, and turnover in microalgae. We focus principally on *Chlamydomonas* as a genetic and laboratory model. Our working hypothesis is that better understanding of the cellular regulatory factors governing PolyP metabolism would enable the development of species and strains that are more efficient at P recovery from wastewater, as well as shedding light on key environmental variables controlling luxury P uptake by microalgae that can inform engineering design.

# MICROALGAL POLYPHOSPHATES AND WASTEWATER REMEDIATION

In this section, we examine algal PolyP and how their production might be integrated into wastewater remediation and the return of recycled-$P_i$ to soils and crops.

## Microalgal Biomass and Wastewater Remediation

Small-scale microalgal biomass cultivation has been traditionally used for human consumption, particularly *Spirulina* in highly alkaline lakes of Africa (Habib et al., 2008; Slocombe and Benemann, 2016). Today, this cyanobacterium, along with *Chlorella*, comprises the bulk of algae biomass harvested (~30,000 tons dry weight per annum) mostly for dietary supplements (Slocombe and Benemann, 2016). With regards to wastewater remediation, microalgae have been extensively used for the treatment of domestic wastewater worldwide for over a century, particularly in combination with naturally occurring bacteria in wastewater treatment pond systems (Tarayre et al., 2016). Wastewater treatment ponds are very effective at removing organic matter, pathogens, and nutrients (N and P), but overall performance is seasonal and climate dependent. From the late 1950s, large-scale, high-rate algal ponds (HRAP) were developed in California to improve conventional pond performance by optimizing algal biomass growth and predominance over bacteria; nowadays, there are many HRAP systems currently in operation elsewhere, in both tropical and temperate climate countries (Park et al., 2011). To avoid C limitation and elevation of pH, $CO_2$ provision is desirable, and this can come from bacterial activity, $CO_2$ solubilization from the atmosphere by induced mixing or more effectively, from the injection of flue gases from power plants and industry, or even from combined heat and power (CHP) units burning anaerobically generated biogas at STWs (Acién et al., 2016). Flue gas heat recovery systems can also supply energy to increase reactor temperature as low-grade heat from CHP units, usually at around 40°C, which could be used to extend the growth season

and raise productivity for micro-algae at cooler temperate latitudes, but this has not been fully explored.

During the 1970s and 1980s, the focus of research into large-scale algal cultivation shifted away from sewage remediation towards the generation of biofuels (Borowitzka, 2013a). Ironically, waste-water inputs into algal biomass cultivation are now considered necessary to render algal biofuel production economic, therefore a combination of the two processes is seen as a way forward (Park et al., 2011). Downstream processes, including harvesting, dewatering, algal lipid extraction, and esterification, are still bottlenecks contributing much to the total biodiesel production cost (Mata et al., 2010), which leaves anaerobic (co-) digestion of sewage sludge (and algal biomass) as the current most feasible option for biofuel (biogas) production at STWs; however, the resulting nutrient rich digestate liquor (concentrate) is still an economic burden despite its potential for nutrient recycling in agriculture. Further economic benefits arising from co-production of high-value algal side-products, such as the keto-carotenoids or pro-vitamin A are feasible (Borowitzka, 2013b), but restrictions in the use of wastewater as a nutrient source for pharmaceutical or nutraceutical production lines is a major hurdle.

## Wastewater Treatment and Phosphate Recycling

The historical provision of sanitation and sewerage was driven by the need to reduce transmission of waterborne diseases (Public Health protection). Off-site/centralized wastewater treatment and disposal later emerged as an effective strategy to control the presence of nutrients (C, N, and P) in surface waters (Environmental protection) (Lofrano and Brown, 2010). On average, high-income countries treat about 70% of their domestic and industrial wastewater, whereas this drops to 38%, 28%, and 8% in upper middle-income, lower middle-income, and low-income countries, respectively. Globally, over 80% of all wastewater and fecal sludge is disposed of without treatment (WWAP, 2017). Large centralized STWs have introduced on site energy generation *via* anaerobic digestion of sewage sludge as a measure to reduce net greenhouse gas (GHG) emissions and energy bills, with Western Europe ahead of this trend in industrialized regions, and India and China as leaders in developing countries (Abbasi et al., 2012). Comparatively little progress has been made to achieve similar efficiencies in the N and P cycles at STWs however, where nutrient control is prioritized over recovery and reuse.

In the UK, nutrient losses to surface waters are estimated at 980 kt N $year^{-1}$ of total dissolved N and 16 kt P $year^{-1}$ of total phosphorus, with a 60% contribution from urban areas despite the introduction of the EU Urban Waste Water Directive in 1991 (Worrall et al., 2009; Worrall et al., 2016). Current STWs efficiently remove organic matter using heterotrophic bacteria but rely on nitrification/denitrification to remove N compounds, a process that is energy intensive and wastefully returns $N_2$ (and greenhouses gases, e.g., $N_2O$) to the atmosphere. In fact, the estimated $N_2O$ emission rate at STWs is 4.9 tonnes of $CO_2$-e per tonne of N removed (Johnson and Schroepfer, 1964; Camargo Valero et al., 2010a; NGER, 2016). Some of the C and N is also taken up by bacteria and is removed as harvested biomass at secondary sedimentation units (**Figure 1A**).

On the other hand, P control at small STWs is often achieved by chemical precipitation and adsorption, but these processes usually impede reuse (Tarayre et al., 2016). At large STWs, the bacterial route is usually preferred *via* Enhanced Biological Phosphorus Removal (EBPR). This was first implemented in the 1970s where a group of heterotrophic bacteria, called PolyP-accumulating organisms (PAO) are enriched within the activated sludge process with extended aeration. $P_i$ removal by PAO bacteria is achieved *via* aerobic, in-cell accumulation of large quantities of Poly-P (Melia et al., 2017) but this process is limited by organic C, so an expensive acetate supplement is often added as part of the treatment (Manyumba et al., 2009).

The C, N, and P taken up by bacteria are removed from wastewaters as surplus activated sludge and sent to anaerobic digesters (AD) for biogas production, where the C uptake is valorized as biomethane and the N and P are released either as reactive inorganic species (ammonium and $P_i$) into the aqueous phase (digestate liquor that returns to the head of the treatment works) or as biomass in a solid phase (digestate cake that is preferably spread on land). Complementary processes recovering both N and P from digestate liquors as struvite precipitates ($NH_4MgPO_4{\bullet}6H_2O$) have been implemented at industrial scale but are limited by the costs associated with Mg salts and alkali needed to optimize the precipitation (Campos et al., 2019; Gonzales-Morales et al., 2019).

In contrast, sustainable removal of all inorganic and organic N along with P could be achieved using photosynthetic organisms such as microalgae. Microalgae have been identified as a viable option for meeting energy and nutrient recovery goals in STWs, as they comfortably grow in sewage under either heterotrophic or phototrophic conditions, without the need for supplemental nutrient sources, and the resulting algal biomass can be used to enhance biogas production in existing AD digesters or applied directly as a slow-release fertilizer (Usher et al., 2014; Schreiber et al., 2018).

Research conducted in wastewater treatment ponds reports that *Chlamydomonas, Chlorella, Euglena*, and *Scenedesmus* spp. are the most commonly occurring microalgal species in tropical, subtropical, and temperate climates (Abis and Mara, 2005; Ahmadi et al., 2005; Crimp et al., 2018; Florentino et al., 2019), with effective capacity to meet ammonium and P removal targets. Nutrient control and recovery from sewage is achieved *via* algal uptake, which offers a significant benefit over bacteria in that algae accumulate both N and P. Under some environmental/operational conditions the microalgae perform "luxury P uptake," defined as the uptake of P beyond that required for growth and storage of phosphate within the biomass as PolyP (>1% P dry weight) (Powell et al., 2008). Also, algae preserve their poly PolyP granules for several days, whereas bacteria tend to rapidly re-release their stored P making any scaled-up PolyP storage and processing through to fertilizer far more difficult (Li et al., 2019b).

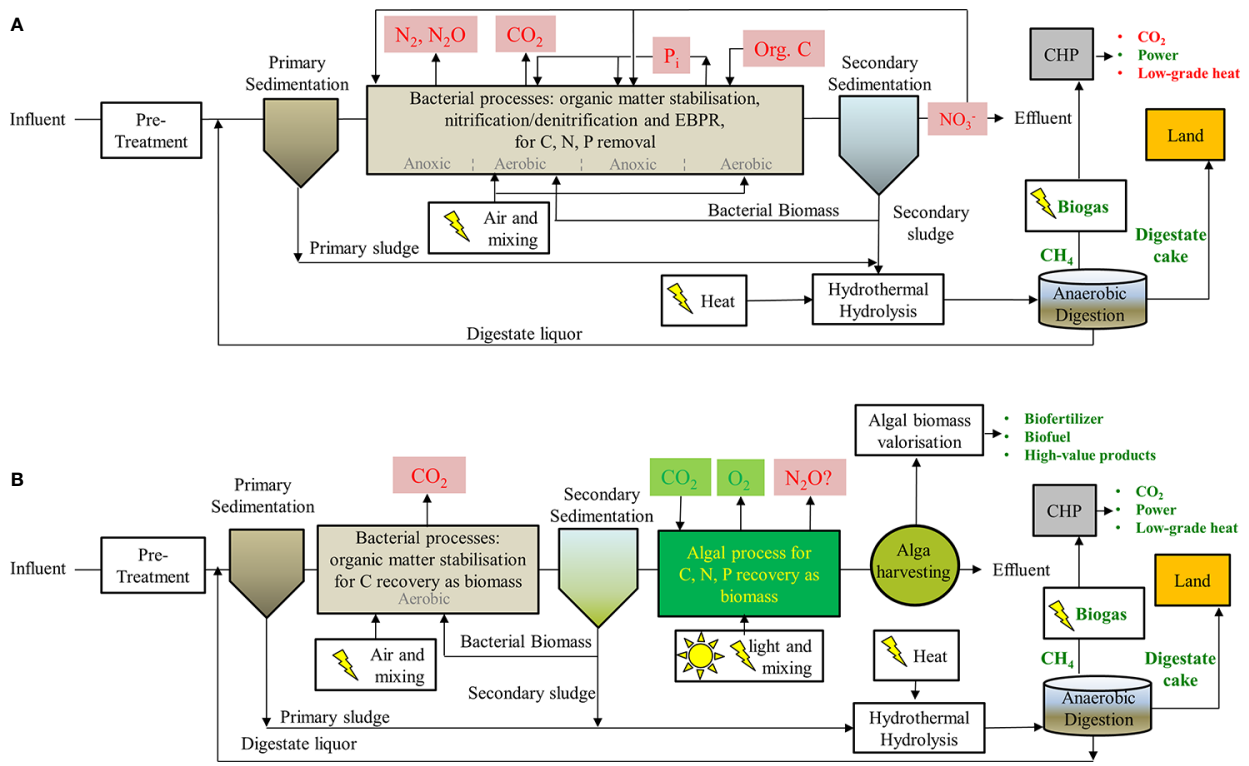


**FIGURE 1 |** Diagram showing wastewater processing steps for **(A)** conventional STW combining denitrification and EPBR treatments downstream of primary sedimentation and **(B)** proposed substitution of these steps with a microalgae/bacteria consortium. Undesirable products such as important greenhouse gases (e.g., $CO_2$, $N_2O$), energetically wasteful steps and costly/non-renewable inputs (e.g., supplements: organic C) or wasteful outputs (e.g., $N_2$, $NO_3^-$) are shown in red. Products or steps that are beneficial or that can be potentially renewable are shown in green along with biogas, biofuels, and value products. Downstream anaerobic digestions steps are indicated for both processes resulting in the production of methane and fertilizers.

## Scale-Up of P Uptake in Algal Treatment Plants

Alga-based STWs have proven their ability to effectively recover both N (from ammonium) and P even under outdoor conditions in temperate climate countries (up to 10% N and 3% P in dry algal biomass), as reported in wastewater treatment pond systems in the UK (Camargo-Valero et al., 2010b) and New Zealand (Powell et al., 2011), therefore removing altogether the need for nitrification/de-nitrification and bacterial P removal processes. However, they have a large footprint, and their performance is still seasonal, heavily dependent on weather conditions, and unpredictable (Powell et al., 2008). Full-scale microalgal ponds for waste-water remediation are associated with losses of biomass and remedial productivity, largely down to issues of maintaining effective mixing and the absence of sedimentation units to recover and recycle algal biomass (Sutherland et al., 2020).

Further research is also needed to improve our understanding on luxury P uptake by microalgae and potential negative impacts arising from large scale microalgae cultivation on wastewaters (Usher et al., 2014), including any potential release of harmful greenhouse gases into the atmosphere such as $N_2O$ (Plouviez et al., 2019). Grazers and algal pathogens are also an issue (McBride et al., 2016), nevertheless, there is evidence that mixtures of different algal species and bacterial in ecosystem consortia can increase robustness against predation and maintain productivity in large-scale HRAP wastewater treatments (Sutherland et al., 2017).

In future, STWs can be developed/retrofitted in places where space is not at a premium. For instance, freshwater algae can be cultivated in floating modules adjacent to coastal cities for sewage treatment (Novoveská et al., 2016). In the meantime, development and implementation of microalgae-based treatment processes at existing large STWs will require additional considerations as they should fit within existing current process layouts. Proposed schemes where access to land is available often involve standard preliminary treatment (screens, grit, sand removal, etc.) and primary clarification. This is followed by anaerobic digestion (e.g., Upflow Anaerobic Sludge Blanket -UASB reactors) and aerobic stabilization, where a microalgae/bacterial consortium benefits from algal oxygen production and nutrient uptake in symbiosis with bacterial stabilization of organic carbon compounds (e.g., HRAP). Next, potential downstream processes for the valorization of algal biomass (biofuel/fertilizer production) and treated wastewater have been suggested in existing literature (Li

et al., 2019b). However, the immediate challenge is benefiting from existing assets at large STWs and finding a feasible alternative for intensive algal cultivation (i.e., small footprint and hydraulic retention times in the order of hours), that take advantage of existing well-known activated sludge processes for the stabilization of organic matter and anaerobic digestion of sludge with thermal hydrolysis for enhanced bioenergy production *in situ* (**Figure 1B**).

## Algal Polyphosphates as Slow-Release Fertilizer

PolyPs of biological origin are unbranched linear polymers of inorganic phosphate ($P_i$) linked by phospho-anhydride bonds and of variable chain length, ranging from 10s to 100s. These tend to accumulate in vacuoles or acidocalcisomes as granules (Albi and Serrano, 2016). Although higher plants produce organic phosphate ($P_o$) in the form of phytate (inositol hexakisphosphate) there is no strong evidence to support the presence of actual PolyP granules in higher plants, despite a recent and extensive search (Zhu et al., 2020). Instead, these can be found in bacteria, fungi, and lower plants, such as algae and the mosses (Seufferheld and Curzi, 2010).

Given the polluting nature of organic manure (Schröder et al., 2011) it is notable that its P-composition consists largely of orthophosphate ($P_i$). Particularly piggery manure (Liang et al., 2017) and to a lesser extent dairy (He and Dou, 2010), where phytate (10% of total $P_i$) is also present along with pyrophosphate (6%) and PolyP (3%). The expectation is that algal biomass containing remediated $P_i$ in the form of PolyP can be returned to soil in a form that can be taken up by crops with minimal wastage. Hence, PolyP in the form of triphosphate (TPP) has been shown to act as a slow-release P-fertilizer, a desirable characteristic that favors utilization by crops and delays leaching into agricultural runoff (McBeath et al., 2007). Evidence suggests that $P_i$ from algal biomass applied to soil can be taken up by plants (Siebers et al., 2019). Furthermore, algal biomass is practical for return-to-soil, not requiring tilling or exhibiting N-volatilization or fugitive methane emissions like manures, sludge or digestate (Mulbry et al., 2005).

Manufacturing a purified form of slow-release P fertilizer from algal biomass has not yet been explored. Laboratory extraction methods of PolyP involve a straightforward aqueous boiling step (Martin and Van Mooy, 2013), therefore it might be possible to incorporate this step into procedures for isolating other algal products such as lipids or carotenoids at a cost-effective commercial level. There is evidence that algal PolyP can be taken up in mammalian gut cell lines, so there could be the option of using biomass for bespoke feeds (Gao et al., 2018).

## Microalgal Research Models

As noted, multiple algal species have been found in STWs, including species known for high biomass productivity and species diversity could be a prerequisite for success. *Chlamydomonas reinhardtii* is the best studied species to date however, in terms of photosynthesis, genetics, and molecular biology (Salomé and Merchant, 2019). Heterologous protein expression has been successful in this alga (although there are others), which shows effective protein folding in the plastid (Gong et al., 2011; Tran et al., 2013) as well as protein secretion (Molino et al., 2018). Therefore, there is much potential for biotechnology and high-value side-products in tandem with wastewater remediation.

A practical advantage of *Chlamydomonas reinhardtii* (and other *Chlamydomonas* sp.) is its rapid propagation under mixotrophic conditions, using acetate. For instance, colonies on agar plates can grow within days facilitating the genetics. Growth rate in mixotrophic mode generally exceeds the sum of the heterotrophic and autotrophic rates (Laliberté and de la Noüe, 1993; Smith et al., 2015). Hence, mixotrophic capability can also boost growth on wastewater, e.g., *C. debaryana* shows potential for wastewater treatment in temperate regions subject to annual fluctuations in light supply (Park et al., 2012). In addition, a *Chlamydomonas* sp. was found growing in palm oil mill effluent, indicating further the utility of this genus (Ding et al., 2016). *Chlamydomonas* sp. are widespread and often found in STWs (Thomas and Burger, 1933; Haughey, 1968; Abo-Shehada and Sallal, 1996; Crimp et al., 2018) whereas the natural occurrence of *C. reinhardtii* is limited to a few lacustrine environments in NE US (Pröschold et al., 2005). Whether or not this species can be used for wastewater treatment is debatable, although mutant strains can be found that demonstrate improved potential for remediation (Zhou et al., 2015). It should be noted that *C. reinhardtii* is unlikely to be mated to other species of the genus (Pröschold et al., 2005) but related species would be relatively easy to replicate mutations in.

Although the genetic model *C. reinhardtii*, has not been considered as a natural biofuel species due to its preference for producing carbohydrate, genetic alterations that reduce flux to carbohydrates in favor of oil such as the *sta6* mutation have been found (Blaby et al., 2013; Goodenough et al., 2014). In addition, certain conditions have been shown to produce "liporotunds" which are large cells containing many lipid bodies (Goodson et al., 2011; Ngan et al., 2015). The appearance of these cells appears to be dependent on acetate provision. This is thought to alter the expression of specific pathways (e.g., increasing the glyoxylate cycle) that favor flux to oil production.

# MICROALGAL POLYPHOSPHATES

In this section, we summarize the microalgal PolyP literature in relation to structure, cell biology, P-starvation responses, synthesis, and turnover. Understanding these factors better would enable the development of species and strains that are more efficient at P recovery from wastewater.

## PolyP Structure and Function

PolyP polymers in pure form exist in various physical states such as sols, gels or glass, although it is not known to what extent these

dictate the final structure of PolyP of biological origin. For instance, PolyP adopts a very ordered structure in granules found in the vacuoles of yeast and some green algal species (Shebanova et al., 2017). Interactions of PolyP with metal cations such as $Ca^{2+}$ and $Mg^{2+}$ allow the chains to adopt conformations dependent on their metal ion-coordination preferences (Reusch, 2000). Complexes of PolyP with actin and the cell wall have been noted, and recently, proposed for yeast and microalgae in the case of polyhydroxybutyrate (PHB) (Solovchenko et al., 2019). PolyP interacts with PHB to form channels in bacteria for instance (Reusch, 2000) but we could find no evidence for gene homologs of the bacterial PHB synthase in any eukaryotic genome. The presence of a nitrogenous component in purified *Chlorella* PolyP granules was reported in the 1960s (Correll, 1966) but has never been confirmed. In yeast, arginine accumulates alongside PolyP in vacuoles with some evidence reported for an association although these reserves can also act independently (Dürr et al., 1979; Westenberg et al., 1989). Recently, separate nitrogenous granules containing guanine have been identified in *Chlamydomonas* acidocalcisomes (Moudříková et al., 2017) and distinct granule forms have been visualized in these organelles (Goodenough et al., 2019). Therefore, it is possible that accidental co-purification of separate N-stores might account for some earlier reports of direct PolyP interactions with organic or nitrogenous compounds.

The principal role for PolyP appears to be dynamic P-storage in microalgae. In *Chlamydomonas*, the majority of $P_i$ taken up by pre-P-starved cells is incorporated into PolyP. Whereas, during P-starvation PolyP is removed below detection levels along with declines in $P_i$, ATP, and sugar phosphates (Hebeler et al., 1992). PolyP appears to be stored in granules in vacuole-like acidocalcisomes in this species (see *Storage in Acidocalcisomes*) but has also been reported in cell walls where it might play a role in cytokinesis (Werner et al., 2007). Increases in P-storage as PolyP are elicited by limitation of other nutrients or with P-resupply following P-starvation—so-called luxury storage (see *Regulation of Phosphate Metabolism in Microalgae*). Other forms of stress that are unrelated to nutrient supply can also have an impact on microalgal PolyP levels and chain lengths, however. For instance, synthesis and mobilization of PolyP appear to be involved in the response to changes in pH and osmoregulation in halotolerant microalgae (Weiss et al., 1991; Leitão et al., 1995). In *Chlamydomonas* species, PolyP mobilization appears to play a role in detoxification and export of Cd and Hg (Nishikawa et al., 2003; Samadani et al., 2008). On the other hand, there is evidence for sequestration of essential and/or toxic metals with PolyP or in acidocalcisomes (see *Sequestration of Heavy Metals by PolyP*).

Other roles for PolyP have been identified in prokaryotes for energy storage, stress response, virulence, motility, quorum sensing and in yeast, antioxidant stress response and protein phosphorylation (Rao et al., 2009; Albi and Serrano, 2016; Docampo, 2020). In future, some of these might be found to operate in microalgae. This can be elucidated by examining mutants defective in genes for PolyP synthesis, turnover, and regulation (see *Storage in Acidocalcisomes*, *Synthesis and Turnover*, and *Regulation of Phosphate Metabolism in Microalgae*).

### Quantification

Free $P_i$ in the microalgal medium is commonly assayed by Molybdate assay (Strickland and Parsons, 1968) and alternatives have been compared (Cogan et al., 1999). Total biomass P can be measured after oxidation and re-mineralization (Solorzano and Sharp, 1980). PolyP granules were originally identified through metachromatic staining (Albi and Serrano, 2016). Today, DAPI staining is often used to visualize PolyP granules in conjunction with confocal microscopy, for example in *Chlamydomonas* (**Figure 2**). Quantification of PolyP was originally achieved by isolating acid-soluble (lower MW) and acid-insoluble fractions (higher MW) using trichloracetic acid (TCA), followed by hydrolysis and assay for P (Aitchison and Butt, 1973). PolyP-DAPI can be used for measurement in plate assays but there is much spectral overlap with DNA-DAPI fluorescence (Shebanova et al., 2017). A PolyP-specific dye has been identified for both microscopy and quantitative plate assays (Angelova et al., 2014) but has only recently been exploited (Zhu et al., 2020)[1]. PolyP can also be separated by chain length by electrophoresis in DNA-sequencing gels or commercial mini-gels (Smith et al., 2018). Enzyme assays can reportedly be used to both quantify PolyP and size chain lengths (Christ et al., 2019).

## Storage in Acidocalcisomes

The principal repositories for PolyP in both eukaryotes and prokaryotes are membrane-bound organelles called acidocalcisomes (Seufferheld et al., 2003; Lander et al., 2016). Five non-exclusive features have been defined for the eukaryotic organelles: i) presence of a single PolyP granule; ii) an acidic lumen; iii) a characteristic complement of trans-membrane

[1] Only available by synthesis to order, at the time of writing.

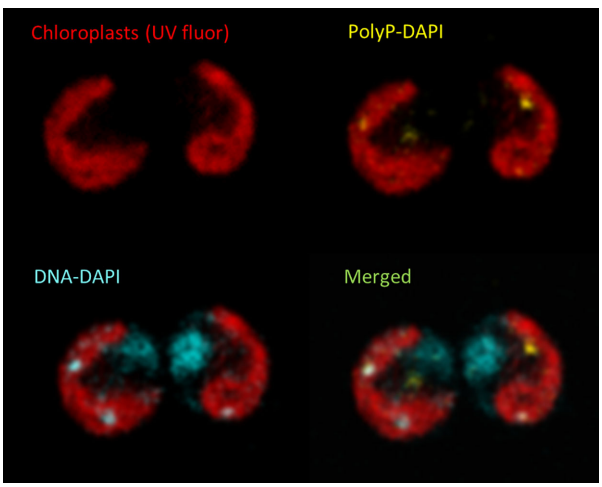


**FIGURE 2 |** Confocal image of typical live DAPI-stained *Chlamydomonas* cells showing the cup-shaped chloroplast revealed by chlorophyll autofluorescence (red). PolyP granules (yellow) and DNA (blue) were distinguished by the distinct fluorescence of their respective DAPI conjugates. Separate and merged images are shown for the same pair of cells.

transporters ($H^+$-PPase and V-type ATPases; metal cation exchangers); iv) a trans-membrane complex responsible for PolyP synthesis (e.g., VTC) and v) a distinctive membrane ultrastructure under TEM which presumably relates to its individual protein/lipid composition (Goodenough et al., 2019). Acidocalcisomes and their PolyP play additional roles beyond storage. For instance, they are required for pathogenicity in eukaryotic parasites, and in *Chlamydomonas* they are central in many stress responses (Docampo et al., 2010). They also have the capacity for Ca-storage (e.g., in *Chlamydomonas* sp., where $P_i$ uptake was shown to be Ca-dependent (Siderius et al., 1996)) and this is important for coccolithophore formation in marine Haptophyte algae (Gal et al., 2018). Taken together, functional acidocalcisomes appear to be important for delivering a robust response towards environmental change, with ramifications for outdoor algal cultivation and for micro-organism containment.

In *Chlamydomonas* and Trypanosomes, the organelles are generated at the trans-face of the Golgi (Goodenough et al., 2019). Under N-stress in *Chlamydomonas*, acidocalcisomes generate a single PolyP granule and appear to fuse with autophagous vacuoles (Goodenough et al., 2019). This process could transfer PolyP synthesis capacity to the resultant "hybrid" and account for autophagous vacuoles with multiple granules (Goodenough et al., 2019). It seems the process is also part of a delivery mechanism for periplasmic proteins (Komine et al., 2000; Aksoy et al., 2014) and in Trypanosomes, acidocalcisomes are required for autophagy (Li and He, 2014). PolyP is also likely to be trafficked to the cell wall by this route, where it has a role in retention of some of the periplasmic proteins (Werner et al., 2007). In *Chlamydomonas* the autophagous vacuoles are important in the S deprivation response for macromolecular turnover of S-amino acids and sulfolipids (Aksoy et al., 2014) and seem to be required for TAG synthesis and protein turnover (Couso et al., 2018). A similar process might be occurring in P deprivation where sulfolipids replace phospholipids (see *P-Sparing Measures*). Certain P deprivation–specific periplasmic proteins are delivered by other means however and this route is relatively unimportant during nutrient-repletion (Aksoy et al., 2014). In N deprivation, membrane fragments have been observed in the autophagous vacuoles implying turnover (Goodenough et al., 2019). The autophagy route is dependent on the vacuolar transporter chaperone (VTC) complex which is located at the acidocalcisome membrane and responsible for PolyP synthesis (see *Synthesis and Turnover*) (Aksoy et al., 2014). Together these observations underline the subtle interdependency and partial overlap of responses to the various nutrient-stresses experienced by algae.

### Sequestration of Heavy Metals by PolyP

Although PolyP/acidocalcisomes are the principal store for $Ca^{2+}$ in *Chlamydomonas* (Siderius et al., 1996) they have been shown to sequester enzyme co-factor cations ($Ca^{2+}$, $Mg^{2+}$, $Fe^{3+}$, $Zn^{2+}$, $Mn^{2+}$) and toxic metals ($Al^{3+}$, $Cu^{2+}$, $Cd^{2+}$ etc.) in a range of organisms (Albi and Serrano, 2016). In *Chlamydomonas*, Cd and Cu toxicity depends on the cellular metal/P ratio, underlining the importance of P-availability in metal-remediation (Wang and Dei, 2006). In this alga, $Cu^{2+}$ co-localizes with PolyP during $Zn^{2+}$ deprivation (Hong-Hermesdorf et al., 2014; Liu et al., 2016) suggesting complex regulation. In some cases, PolyP appear to be necessary for metal uptake in *Chlamydomonas* but are not the final ligand (e.g., for Mn) (Tsednee et al., 2019). This metal-uptake faculty is potentially important for municipal wastewater treatment works receiving industrial inputs that may be contaminated with heavy metals but can affect P recycling for agriculture (Babel and del Mundo Dacera, 2006). This ability might not be universal among microalgae however, since bodies accumulating large amounts of PolyP in another green alga, *Parachlorella kessleri*, were found not to contain the major metals (Ca or Fe) (Ota et al., 2016). Clearly the use of microalgae for both P recovery for agriculture and removal of heavy metals might require separate processes, with some consideration required of the microalgal species.

## Synthesis and Turnover

The pathways for accumulation and mobilization of PolyP in the eukaryotic algal cell are very poorly characterised. *Chlamydomonas reinhardtii* is an attractive model system for addressing this knowledge gap as it is the most intensively studied species. Genetic analysis is facilitated by the existence of 2 mating types, analogous to yeast, and the advanced stages of genome sequence annotation (Salomé and Merchant, 2019). There are extensive collections of point and insertional mutants and gene modification by CRISPR-cas has also been reported (Guzmán-Zapata et al., 2019; Shin et al., 2019) thereby facilitating testing of gene function.

Synthesis of microbial PolyP is carried out principally by reversible ATP-specific kinases PPK1 and to a lesser degree PPK2, which utilizes GTP (Rao et al., 2009). Over-expression of PPK1 in Synechococcus, a cyanobacterium (prokaryotic alga) led to a doubling of PolyP levels (Gao et al., 2018). The occurrence of these genes is very limited in eukaryotes however (Rao et al., 2009) and no orthologues of these genes could be detected in the *Chlamydomonas* genome. Over-expression of *E.coli* Ppk1 in yeast (Gerasimaite et al., 2014) and Arabidopsis (Zhu et al., 2020) has led to toxicity (possibly due to cytosolic PolyP accumulation) and in the latter case, ectopic PolyP granules were identified.

In place of PPK, a VTC complex located at the vacuole or acidocalcisomes appears to be responsible for PolyP synthesis in yeast (Hothorn et al., 2009) and *Chlamydomonas* (Aksoy et al., 2014). In higher plants the existence of the VTC complex is uncertain, and the presence of large stores of PolyP has been questioned (Zhu et al., 2020).

**Figure 3** shows a schematic of poly P synthesis based on the yeast model (with putative or known *Chlamydomonas* orthologues indicated). Two VTC complexes are evident in yeast where one relocates to the acidocalcisomes under P deprivation (**Figure 3**). Electron microscopy (TEMs) in microalgae suggest that a complex at the membrane of this organelle generates strands of PolyP that are injected into the organelle (Shebanova et al., 2017). In yeast, synthesis and translocation by VTC into the organelle probably ensures that PolyP is targeted exclusively to this organelle, given that it appears to be toxic in the cytosol (Gerasimaite et al., 2014).

The acidity of the acidocalcisome lumen is controlled by the proton-pump activity of the membrane-bound $H^+$-PPase and the V-type ATPase, where the acidic lumen facilitates cation import by proton-exchangers (Ruiz et al., 2001; Docampo et al., 2010). Lumen acidity could potentially be regulated by stresses such as starvation leading to alterations in acidocalcisome proton-pump activity or expression levels; possibly influencing PolyP synthesis and turnover, and the autophagy process (Li and He, 2014).

Mobilization of $P_i$ from PolyP reserves occurs in response to P-starvation in *Chlamydomonas* species (Hebeler et al., 1992; Nishikawa et al., 2006). The key enzymes responsible for PolyP degradation are exopolyphosphatases (PPX) where the prokaryote and eukaryote PPX classes are unrelated. Endopolyphosphatases (PPN) have also been identified in yeast (Albi and Serrano, 2016). The enzymes involved in the mobilization of PolyP have yet to be fully studied in microalgae, although various polyphosphatases have been identified in higher plants (Zhu et al., 2020). Understanding these factors will help target genes for increasing PolyP levels in microalgae for P-remediation.

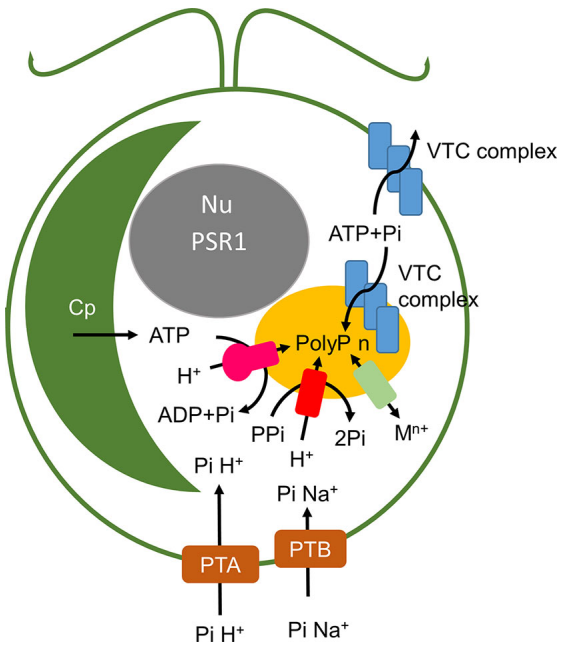


**FIGURE 3 |** Schematic of polyphosphate synthesis in *Chlamydomonas*. PTA and PTB phosphate transporters are orthologues of the *S. cerevisiae* Pho81 and Pho 89 proton- and sodium-linked transporters and are under *PSR1* regulation as described in the text and **Figure 6**. These are presumed to take up environmental $P_i$ under different nutrient and pH levels. The acidocalcisome (yellow) contains a V-type H+ ATPase (pink) and a pyrophosphatase dependent ATPase (red) which energize the membrane. Polyphosphate is synthesized from ATP and $P_i$ by the VTC complex. VTC complex and PolyP have also been reported in the cell wall. Metal transporters (pale green) provide metal ion homeostasis. Cp chloroplast, Nu nucleus.

## REGULATION OF PHOSPHATE METABOLISM IN MICROALGAE

In the natural environment, microalgae continually adapt to changing levels of light and nutrients in order to compete for survival, and in doing so change the local environment. For instance, growth on nitrates leads to higher external pH; ammonium to lower pH whereas urea has no effect. Unlike higher plants, algae cannot select N-source to regulate pH but are compelled to utilize ammonium first (Scherholz and Curtis, 2013), which will have the benefit to remove the need for ammonia nitrification at STWs. Microalgae additionally cause diurnal variations in culture pH owing to the uptake and release of $CO_2$ dependent on the availability of solar energy for photosynthesis and water temperature, which creates a distinctive variation in dissolved oxygen resulting in direct changes of redox potential (**Figure 4**) and hence, process conditions must be fully understood and monitored at full-scale wastewater treatment systems. Provision of $CO_2$ (e.g., from flue gases) or from bicarbonate can regulate culture pH, with the additional aim of removing C-limitation and boosting productivity (Acién et al., 2016). Culture pH can in turn influence $P_i$ availability and uptake (Kube et al., 2018). Therefore, the regulation of $P_i$ is intertwined with that of other macro- and micro-nutrients.

The regulation of microalgal P-metabolism itself is particularly complex, possibly because PolyP can be exploited both as a P-reserve and an energy store (**Figure 5**). Early research led to fundamental discoveries and concepts in P storage, particularly in relation to "luxury uptake" which refers to acquisition beyond the immediate cellular requirements (Droop, 1974; Elrifi and Turpin, 1985), with significant ramifications for the nascent fields of ecology and algal biotechnology. Under nutrient-replete conditions (hence light-limited), many microalgae do not accumulate extensive PolyP reserves, in the absence of prior stresses. For instance, in *Chlamydomonas*, PolyP granules are very rarely reported in acidocalcisomes in these circumstances (Goodenough et al., 2019), and in *Chlorella*, measured PolyP levels were low (Aitchison and Butt, 1973). Under active growth, $P_i$ must be assimilated in the form of phospholipids and nucleic acids in preparation for cell division (Zachleder et al., 2016). Synthesis of PolyP under replete conditions might thus be expected to compete with growth and cell division, due to the energetics of Pi-uptake and PolyP synthesis (Rao et al., 2009). Diurnal accumulation of PolyP might occur however, particularly where there are diurnal variations in acquisition or availability (Watanabe et al., 1988; Kimura et al., 1999).

As nutrients are consumed, growth often becomes nutrient-limited and ultimately subject to nutrient-stress, particularly in stationary phase (**Figure 5**). Under these circumstances, in *Chlamydomonas* and in other microalgae, such stressors can be drivers of PolyP accumulation as part of the "luxury-phosphate" response. This accumulation is generally observed in stationary phase and is also triggered by experimental depletion of N, S, Zn, amino-acids (in auxotrophic mutants)

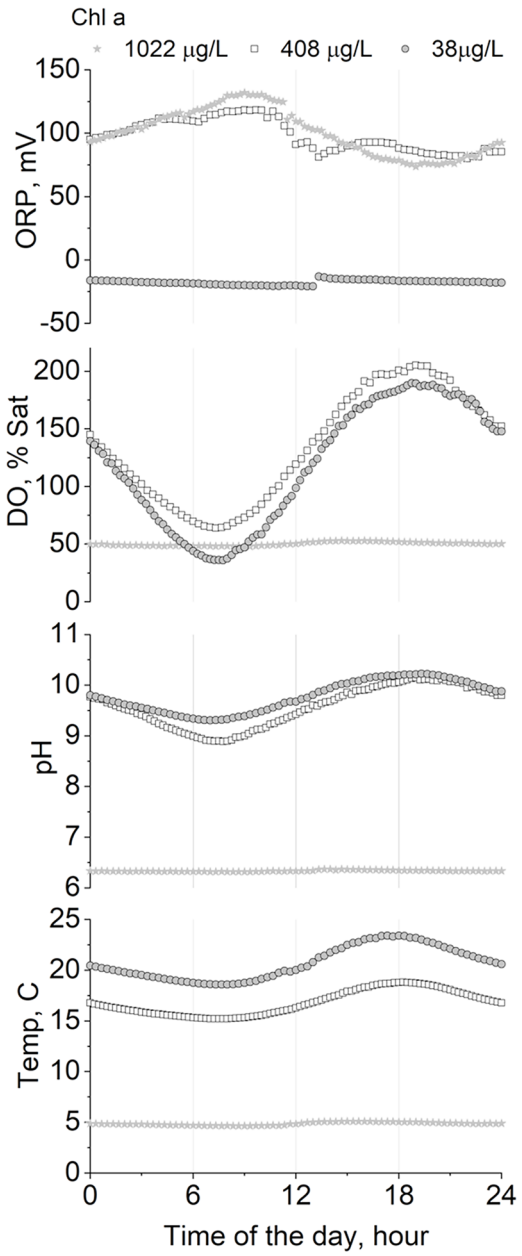


**FIGURE 4 |** Diurnal variation of pH, oxygen saturation (%), and redox potential (ORP) as a function of algal biomass concentration (reported as Chlorophyll *a* in ug/L) in outdoor algal ponds treating real wastewater in a mix alga-bacteria culture in the UK. Diurnal water temperature variation is also reported for reference (original data from Camargo-Valero, 2009). Published with permission from Miller Alonso Camargo-Valero (co-author) under Creative Commons License (University of Leeds).

or alterations in pH in many micro-organisms (Harold, 1966). In the case of *Chlamydomonas*, transfer to N-depleted medium (or S/Zn-deprived) with adequate P supply triggers the formation of PolyP granules which accumulate in acidocalcisomes (Goodenough et al., 2019). This process appears to be analogous to the accumulation of TAG in response to various stresses that slow growth, given that a multiplicity of nutrient-stresses also triggers PolyP synthesis (in the presence of $P_i$) (Bajhaiya et al., 2016). In fact, the two processes are likely to compete in some species and in certain circumstances (particularly if enough $P_i$ is present).

In the case of P-limitation or starvation (**Figure 5**), depletion leads to a series of regulatory steps to i) conserve P, ii) accelerate uptake, iii) exploit further external $P_o$ resources, iv) allow continued growth, and v) prime the cell for $P_i$ hyper-accumulation if $P_i$ is resupplied (Wykoff et al., 1999). The capacity to produce some PolyP (or turnover) could be important during P deprivation since a knockout of *VTC1* in *Chlamydomonas* was detrimental to growth under these conditions but not under replete conditions (Mahmoud-Aly et al., 2018). The starvation processes appear to be coordinated by a signal-transduction pathway leading to induction of a "Phosphate Starvation Response" myb-type transcription factor *PSR1*. Hyper-accumulation of PolyP or "overplus" was first studied in *Chlorella*, where it was dependent on the duration of starvation before resupply of $P_i$ (Aitchison and Butt, 1973). This priming for hyper-accumulation, through induction of PolyP synthesis and P-uptake is presumably a strategic adaptation in the face of fluctuating supplies (Nishikawa et al., 2006; Moseley and Grossman, 2009). This phenomenon is important for P-remediation purposes because it implies that uptake can be accelerated through genetic or physiological means.

## Global Regulatory Networks and *PSR1*

The regulatory response pathways for P deprivation are summarized for *Chlamydomonas* in **Figure 6**. These are shown in relation to N and S deprivation, indicating that a degree of overlap exists in terms of gene activation and the putative signal transduction networks. The nature of a sensor that can detect reduced external $P_i$ levels is not known but its existence is plausible because the starvation response can be blocked by the $P_i$ analog phosphite (Yehudai-Resheff et al., 2007). In yeast and plants, SPX domain proteins (we note that several are encoded in the *Chlamydomonas* genome) bind to pyrophosphorylated inositol phosphates (PPInsPs) which appear to signal intracellular $P_i$ levels and influence the P-starvation response and PolyP synthesis (Wild et al., 2016). VIP1 is one such kinase that generates PPInsPs but has been linked to the TOR kinase complex in relation to TAG accumulation and N-deprivation responses (Couso et al., 2018) (**Figure 6**). The LST8 subunit of TOR is down-regulated under P-starvation in a *PSR1*-dependent fashion. This pathway appears to link P-stress to TOR-mediated de-repression of TAG synthesis and autophagy, along with repression of translation (Couso et al., 2020). Investigation of the signal transduction pathway in S deprivation in *Chlamydomonas* has clearly identified SNRK-family involvement (Gonzalez-Ballester et al., 2008; González-Ballester et al., 2010) but this kinase group have also been implicated more widely in other stress responses in this alga (Colina et al., 2019) (**Figure 6**).

The *PSR1* gene was originally found to be instrumental in the "phosphate starvation response" through the phenotypes of its allelic mutants (*psr1-1, 1-2*) which were identified in screens for defects in $P_i$ uptake and exophosphatase production

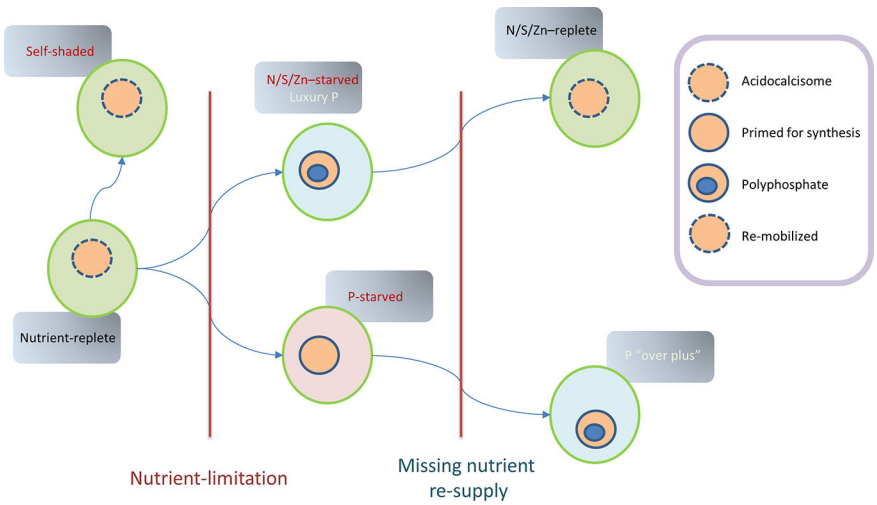


**FIGURE 5 |** Theoretical model summarizing *Chlamydomonas* P-status during various states that could follow an established period of nutrient-replete growth. In this original state, polyphosphate granules are rare although acidocalcisomes are present. Non-limited growth can lead to self-shading in the presence of abundant nutrients, with nutrient storage perhaps compromised by low light availability. Limited nutrients (N/S/Zn) with replete P lead to luxury P-uptake and PolyP production which can be remobilized if nutrient repletion is restored. In contrast, P-limitation can lead to P-starvation, with measures implemented (e.g., *via PSR1*) to both conserve phosphate and maintain growth leading to a lowering of total P-content. Subsequent P-resupply leads to P "overplus" due to priming for P-accumulation.

(Shimogawara et al., 1999). The mutants showed an inability to divide more than once after imposition of P-stress and a reduction in photosynthesis but were not impeded in their survival of P-stress, suggesting that *PSR1* was responsible for adaptive responses for maintaining growth. When exposed to P-stress, *Chlamydomonas* exhibits a *PSR1*-dependent increase in $P_i$-uptake capacity (10-fold increase in the $V_{max}$ with a shift in $K_m$ from 10 μM to 0.1–0.3 μM) (Shimogawara et al., 1999). Hence there is an alteration of P importer gene profile (repression of *PTA1,3* and elevation of *PTB 2-5,8*) and increased capacity for PolyP synthesis (*VTC1, VCX1*: encoding respectively a subunit of the transmembrane PolyP synthesis complex and vacuolar Ca-importer). In addition, there is an induction of peri-plasmic phosphatase activity (*PHOX*) to release $P_i$ from external $P_o$ sources (such as glucose-1-P) (Moseley et al., 2006).

Complementation of this specific phosphatase defect in the *psr1-1* mutant was used to identify the *PSR1* gene as encoding a myb class of transcription factor (Wykoff et al., 1999). Subsequent studies of the phenotypic and transcriptomic responses of the *psr1-1* mutant determined that the *PSR1* gene is required for a wide range of cellular responses to P deprivation and is necessary for many of the gene expression changes associated with these responses (Wykoff et al., 1999; Moseley et al., 2006; Bajhaiya et al., 2016).

## P-Sparing Measures

Gene expression changes associated with P deprivation include those that directly lead to P-sparing, e.g., turnover and replacement of phospholipids (e.g., phosphodiesterase *GDP1*) with sulfolipids (*SQD1,3*). In addition, there appears to be global *PSR1*-dependent measures hypothesized to reduce $P_i$ usage by dialing down the production and consumption of ATP and phosphorylated intermediates (Moseley et al., 2006). For instance, transcriptional repression of genes leading to diminished pentose-phosphate pathway activity along with reductions in chloroplast and cytoplasmic protein translation concomitant with an induction of certain glycolytic steps, suggesting possible regulatory controls (GAP1, 2) (Moseley et al., 2006).

In the chloroplast, DNA levels are reduced in a *PSR1*-independent fashion as a P-conservation measure whereas cpRNA is increased *via PSR1*-mediated repression of a polynucleotide phosphorylase (PNPase) which is phosphorolytic and consumes $P_i$ (Yehudai-Resheff et al., 2007).

## Adaptation to P-Starvation

*PSR1* was also found to be responsible for a range of adaptive responses to lessen the deleterious effects of P deprivation. For instance, retarded cell division and growth due to starvation heralds a greater sensitivity to high light due to photoinhibition through excessive photosynthetic electron energy flux. This is combatted by diminishing photosynthetic function, and photosystem I (PSI) and II abundance. The greatest genetic reductions were seen in Light harvesting complex proteins (LHCs) of PSI (*LHCAs*) and PSI itself (*PSAE, K*), along with chlorophyll synthesis (*CHL27*). Induction of certain LHCs appear to be generally stress-associated (LHCSR2, 3) (Moseley et al., 2006; Greenwell et al., 2010; Ngan et al., 2015; Bajhaiya et al., 2016; Guo et al., 2018). Evidence suggests that the novel LHCSRs dissipate excess light during P-limitation, allowing continued growth (Guo et al., 2018). Many of these changes present an alternative amino-acid composition which might have evolved to enable "sparing" of the elements reduced by stress (e.g., LHCBM9 for S-sparing) (González-Ballester et al., 2010).

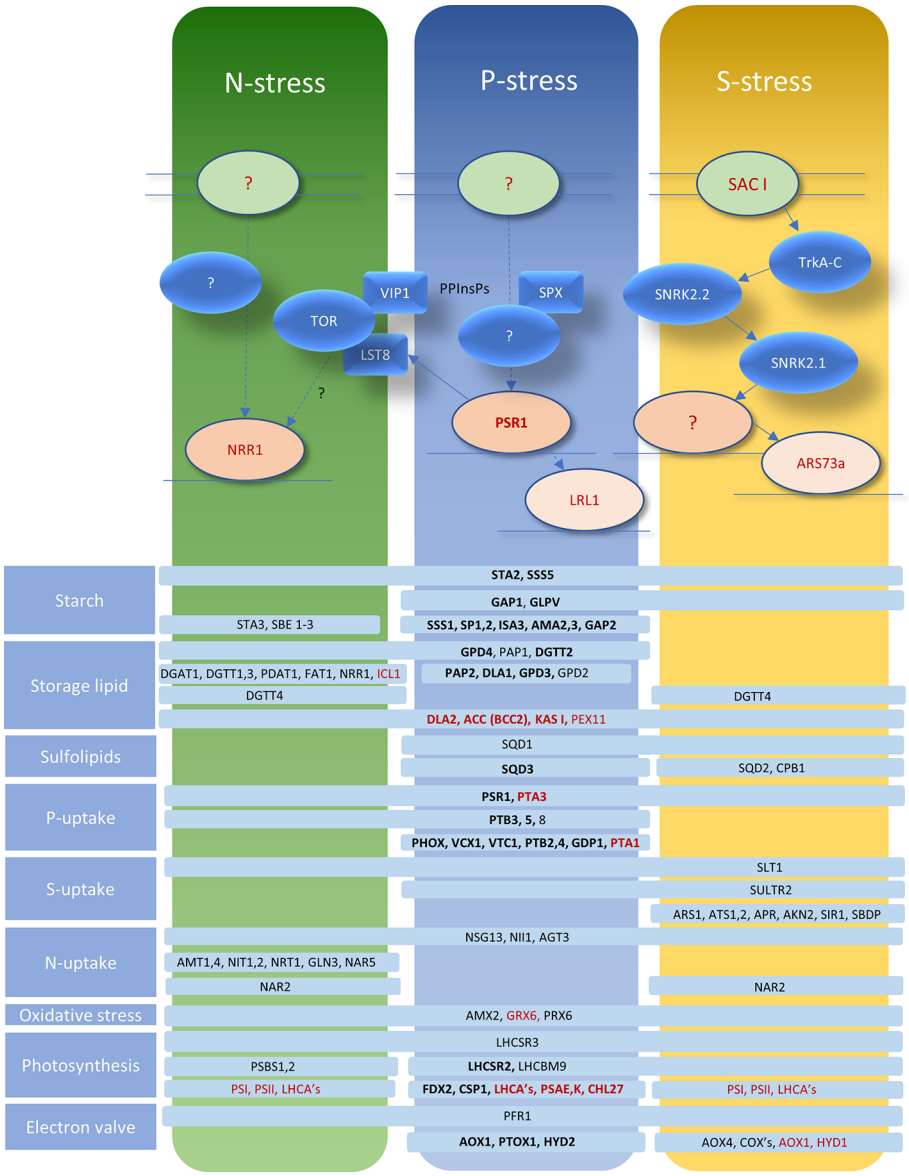


**FIGURE 6 |** Representation of signal transduction networks for P/S/N deprivation responses in relation to the global regulator *PSR1*. Putative relationships are shown by dotted lines, epistatic relationships by complete arrows. Sensors are indicated by pale green ovals; protein kinases by blue ovals; other signal-transduction factors/domains by blue lozenges, transcription factors are indicated in shades of red and PPInsPs are pyrophosphorylated inositol phosphates. Representative genes showing alterations in expression are indicated in pale blue bars conveying which stress elicits the changes (black: upregulated; red: downregulated; bold: change dependent on *PSR1* for P deprivation). Functional gene categories are indicated to the left. The information and models shown are a collation of transcriptomic data and molecular work from published sources: (Moseley et al., 2006; Gonzalez-Ballester et al., 2008; González-Ballester et al., 2010; Toepel et al., 2011; Schmollinger et al., 2014; Bajhaiya et al., 2016; Wild et al., 2016; Couso et al., 2018; Couso et al., 2020).

Likewise, induction of "electron valve" pathways (*AOX1, PTOX1, HYD2*) provides, respectively, alternative mitochondrial, plastid oxidases, and PSI electron acceptor (Moseley et al., 2006; Bajhaiya et al., 2016), along with alterations in genes associated with oxidative stress (AMX2, PRX6, GRX6) (González-Ballester et al., 2010; Bajhaiya et al., 2016). Diversion of reduced carbon away from growth and into storage reserves also creates a sink for surplus photosynthetic energy. In *Chlamydomonas*, this is mainly achieved through starch production although storage lipids are also induced by P deprivation; where both processes are dependent on *PSR1* (Wykoff et al., 1999; Moseley et al., 2006; Bajhaiya et al., 2016). Here a multiplicity of starch-synthesis genes is induced, principally *STA2* (**Figure 6**) along with a more muted response for the storage-lipid related genes, including a type 2 *DGAT* (*DGTT2*). Upregulation of gene activity is associated primarily with the terminal TAG synthesis steps, rather than the genes for fatty acid biosynthesis,

which are either repressed or do not change (**Figure 6**). This is probably an indication that rates of fatty acid synthesis under nutrient-replete conditions are adequate to support the level of TAG synthesis seen with nutrient-stress in this species; either with or without the *sta6* mutation, which prevents starch synthesis and boosts flux to TAG (Blaby et al., 2013). A further MYB TF gene, *LRL1* appears to be influential for maximizing some of the late-response P-deprivation responses (**Figure 6**) (Hidayati et al., 2019).

### Integration of *PSR1* With Other Networks

Despite the greater research focus on P deprivation, in keeping with the way *PSR1* was initially discovered, its global significance and involvement in other forms of nutrient stresses has been established, suggesting a degree of integration for signal-transduction pathways as a network of "hubs" as proposed in *Chlamydomonas* (Gargouri et al., 2015). For instance, the gene appears to be necessary for storage lipid synthesis associated with S and N deprivation (Ngan et al., 2015) as well as for P deprivation (Bajhaiya et al., 2016). In fact, rapid and transient upregulation of the *PSR1* transcript itself is well-documented for all 3 stresses (Wykoff et al., 1999; Ngan et al., 2015; Bajhaiya et al., 2016). For instance, under P deprivation, *PSR1* peaks at 8 h post-stress, preceding a prolonged induction of exo-phosphatase activity (Wykoff et al., 1999). This is consistent with a likely "classical" negative feedback regulation mechanism, as reviewed (Ueda and Yanagisawa, 2019), for PSR1 but the nature of this has yet to be fully resolved. A comparative transcriptomic study reported that only a small minority of transcriptionally altered genes (96 out of 6930 in total) were affected in all 3 stresses (Schmollinger et al., 2014). Nevertheless, many of the genes falling into this category (**Figure 6**) are major actors in the various biochemical pathways affected by stresses, e.g., *NII1* (Nitrite Reductase), *STA2* (starch synthesis), *LHCSR3, PFR1*, (photosynthetic and "electron valve" adaptation to excess light energy transduction) and the major sulfate transporter gene *SLT1*. Conversely down-regulation of *KASI* and *ACC (BCC2)* (fatty acid biosynthesis) is seen along with *PEX11* (peroxisome biogenesis/beta-oxidation) and *PTA3*, a putative low-affinity/high-rate P-transporter (**Figure 6**).

## Over-Expression of Regulatory Factors

In waste remediation of $P_i$, it is desirable to prioritize $P_i$-uptake and PolyP production. One option is to hijack or enhance the P-starvation response. The easiest way to achieve this is to target regulatory networks, requiring less gene manipulation (Sang et al., 2005). Alterations to a single transcription factor can effect multiple changes to metabolic or regulatory pathways simultaneously (Bajhaiya et al., 2017; Li et al., 2019a). Since *PSR1* has been identified as global regulator of P deprivation and other nutrient stresses, over-expression of this factor has much potential for wastewater remediation by enhancing a suite of genes that could accelerate uptake of $P_i$ and perhaps other nutrients and contaminants (Bajhaiya et al., 2016). For instance, biomass total P levels are increased by 5-fold in *PSR1* over-expressing *Chlamydomonas* lines relative to background control (*cw15*) irrespective of the $P_i$-supply conditions (Bajhaiya et al., 2016).

Gene over-expression studies indicated that artificial *PSR1* upregulation elicits an increase in biomass P-content along with a number of P deprivation–specific gene-expression responses under nutrient-replete conditions, such as elevated *PHOX* (exophosphatase) and putative high-affinity $P_i$-transporters (PBT2, 4) (Bajhaiya et al., 2016). Although the experiments suggest that *PSR1* upregulation alone might be sufficient to elicit the Pi-starvation response, there was still an additional boost with P-starvation, either in the wild-type backgrounds or in the *psr1* mutant (Bajhaiya et al., 2016). Since over-expressed *PSR1* transcript was also elevated further under P-starvation (despite the use of a constitutive gene promoter) it was arguable that the *PSR1* transcript level was still of key importance, although other factors cannot be ruled out.

In addition to PolyP accumulation, *PSR1* also regulates C-storage products that, in the case of oil, could be useful by-products of wastewater remediation, e.g., for biofuels or other purposes. Accumulation of starch and associated synthesis gene transcripts are greatly induced by PSR1-everexpression, along with increased cell size (Bajhaiya et al., 2016). This particular study was unable to show *PSR1*-directed over-expression of storage lipid in *Chlamydomonas* (backgrounds CC125 or *cw15*: cell-wall deficient) nevertheless, a second over-expression study (Ngan et al., 2015) demonstrated a mean 2-fold increase among multiple transformants (relative to the background, 4a+). Here, a sub-population of transformants was comprised of large-celled "liporotunds." The appearance of "liporotunds" in *Chlamydomonas* generally appears to require provision of acetate; that is, dependent on mixotrophic/photoheterotrophic growth (commonly provided for in *Chlamydomonas* culture) (Goodenough et al., 2014). The presence of the *sta6* mutation is also recognized as another factor for generating "liporotunds" (Goodson et al., 2011).

It has not been established in any of the over-expression studies whether biomass increase in $P_i$ involves increases in PolyP granule production – these are largely absent from wild-type nutrient-replete cells (Goodenough et al., 2019). Accumulation of PolyP under replete conditions would be advantageous for wastewater remediation envisaging a return of biomass to agricultural land in potentially "slow-release" form. Likewise, it is unknown if $P_i$-uptake, either from $P_i$ or release from $P_o$ sources, can be accelerated in wastewater, e.g., given the increased secretion of exophosphatases. Furthermore, it is possible that uptake of other nutrients and trace elements are increased relative to wild-type, given the various gene stress-responses indicated in **Figure 6**. Uncertainty was raised if rates of biomass production would be compromised by *PSR1*-overespression, considering the increases seen in storage products and cell size (Ngan et al., 2015) but this was not noted in a similar study (Bajhaiya et al., 2016).

A further potential advantage of *PSR1*-overexpression, or alteration of any other relevant transcription factor, is to gain a greater influence over nutrient remediation rates when C:N:P ratios of wastewater influent fluctuate. Responses to this ratio are highly complex and species-dependent, having led to much research on which algal strain might be best suited for a certain

wastewater stream (Kube et al., 2018). The complexity likely arises from differences in the responses to limitation or starvation of specific nutrients, such as luxury uptake and how their signal-transduction responses might impinge on each other. In addition, C-storage energetics are likely to compete with energy-intensive uptake and storage of N and P. For instance, TAG is a more concentrated and calorific C-reserve than starch therefore, preference for TAG over starch might leave less energy for PolyP accumulation, and this systematic choice varies greatly across the Phyla (Slocombe et al., 2015). Therefore, imposing control over global transcription factors could address a key limitation over the current apparent need to match species to wastewater type (Kube et al., 2018; Li et al., 2019b).

## CONCLUSIONS AND OUTLOOK

Although global P reserves and the environment are currently under pressure from unsustainable use, much can be gained from improvements in agricultural practice and wastewater management. PolyP-containing microalgal biomass appears to be practical as a slow-release fertilizer, therefore microalgae could be used to recycle P from STWs back to agriculture. This provides an opportunity to improve the energetics, effluent purity, and circular economy of STWs combined with outputs such as P-fertilizer, biofuel, and value products.

Central to this aim is a better understanding of PolyP production and its regulation, particularly in the microalgal research tool *Chlamydomonas reinhardtii*. It is uncertain if this species can be used extensively in STWs but it is likely that other species of the genus can be utilized. Algae from other genera must also be studied, since a species mix appears to protect against biotic and abiotic challenges, particularly in open ponds. There is also a wider need to understand the various cellular and metabolic functions of PolyP given that the field has often been neglected. The regulation of P-metabolism appears to be closely integrated into a network of regulatory "hubs" including other forms of metabolic regulation such as S deprivation. One such factor is the *PSR1* gene which can be manipulated to increase $P_i$-uptake and biomass PolyP levels.

Remediation of P from STWs is likely to involve large-scale open ponds, whereas waste-streams for high-value products can be envisaged in closed-circulation systems where novel engineered strains might be permitted. Wastewater inputs have been envisaged as a means of rendering algal biofuels sustainable and economic. For instance, co-localization of sewage treatment plants and flue gas sources (e.g., from power stations or cement works) along with suitable terrain for algal ponds are likely to be increasingly explored. At conventional STWs, existing activated sludge processes can focus on the stabilization of organic matter (no nitrification), while secondary effluents can be used to feed intensive algal-based processes aimed at N and P control and recovery *via* biological algal uptake. The resulting algal biomass can be harvested and valorized as a fertilizer (if remaining pathogen content allows) or as a feedstock for biogas production *via* anaerobic co-digestion with surplus activated sludge, taking advantage of thermal hydrolysis processes already available to increase biomethane production and produce a nutrient-rich, pathogen-free digestate cake for reuse in agriculture.

Overall, improving our understanding on how and why luxury P uptake occurs in microalgae is crucial to fill current knowledge gaps on the regulation of algal phosphate uptake and its effective use in the development of effective P recovery strategies. Removal of nutrients from wastewater to meet regulatory limits is also a major benefit arising from the integration of microalgae into STWs, providing added value, that could help drive economic biofuel and biofertilizer production.

## AUTHOR CONTRIBUTIONS

SS, TZ-B, LC, NW, MC-V, AB: Literature search, writing, image design, proofing.

## ACKNOWLEDGMENTS

This work was supported by UK Research and Innovation (UKRI) through a grant award from the Biotechnology and Biological Sciences Research Council – BBSRC (BB/N016033/1). Further recognition to the EPSRC Centre for Doctoral Training in Bioenergy (EP/L014912/1) and to the ESRC funded GCRF Water Security and Sustainable Development Hub (ES/S008179/1) for the financial support provided to NW and TZ-B, respectively.

## REFERENCES

Abbasi, T., Tauseef, S. M., and Abbasi, S. A. (2012). Biogas energy. *Springer Briefs Environ. Sci.* 2, 11–23. doi: 10.1007/978-1-4614-1040-9

Abis, K. L., and Mara, D. D. (2005). Primary facultative ponds in the UK: the effect of operational parameters on performance and algal populations. *Water Sci. Technol.* 51 (12), 61–67. doi: 10.2166/wst.2005.0427

Abo-Shehada, M. N., and Sallal, A. K. J. (1996). Preliminary studies on the bacterial and parasitic microflora and microfauna of domestic sewage in northern Jordan. *Int. J. Environ. Health Res.* 6, 31–38. doi: 10.1080/09603129609356870

Acién, F., Fernández-Sevilla, J., and Grima, E. (2016). "Supply of CO2 to Closed and Open Photobioreactors," in *Microalgal Production for Biomass and High-Value Products*. Eds. S. P. Slocombe and J. R. Benemann (Boca Raton, FL: Taylor & Francis Group), 225–252. doi: 10.1201/b19464-11

Ahmadi, A., Riahi, H., and Noori, M. (2005). Studies of the effects of environmental factors on the seasonal change of phytoplankton population in municipal waste water stabilization ponds. *Toxicol. Environ. Chem.* 87 (4), 543–550. doi: 10.1080/02772240500315456

Aitchison, P. A., and Butt, V. S. (1973). The relation between the synthesis of inorganic polyphosphate and phosphate uptake by *Chlorella vulgaris*. *J. Exp. Bot.* 24, 497–510. doi: 10.1093/jxb/24.3.497

Aksoy, M., Pootakham, W., and Grossman, A. R. (2014). Critical function of a *Chlamydomonas reinhardtii* putative polyphosphate polymerase subunit during nutrient deprivation. *Plant Cell* 26, 4214–4229. doi: 10.1105/tpc.114.129270

Albi, T., and Serrano, A. (2016). Inorganic polyphosphate in the microbial world. Emerging roles for a multifaceted biopolymer. *World J. Microbiol. Biotechnol.* 32, 1–12. doi: 10.1007/s11274-015-1983-2

Angelova, P. R., Agrawalla, B. K., Elustondo, P. A., Gordon, J., Shiba, T., Abramov, A. Y., et al. (2014). In situ investigation of mammalian inorganic polyphosphate localization using novel selective fluorescent probes JC-D7 and JC-D8. *ACS Chem. Biol.* 9, 2101–2110. doi: 10.1021/cb5000696

Babel, S., and del Mundo Dacera, D. (2006). Heavy metal removal from contaminated sludge for land application: A review. *Waste Manage.* 9, 988–1004. doi: 10.1016/j.wasman.2005.09.017

Bajhaiya, A. K., Dean, A. P., Zeef, L. A. H., Webster, R. E., and Pittman, J. K. (2016). PSR1 is a global transcriptional regulator of phosphorus deficiency responses and carbon storage metabolism in *Chlamydomonas reinhardtii*. *Plant Physiol.* 170, 1216–1234. doi: 10.1104/pp.15.01907

Bajhaiya, A. K., Ziehe Moreira, J., and Pittman, J. K. (2017). Transcriptional Engineering of Microalgae: Prospects for High-Value Chemicals. *Trends Biotechnol.* 35, 95–99. doi: 10.1016/j.tibtech.2016.06.001

Baker, A., Ceasar, S. A., Palmer, A. J., Paterson, J. B., Qi, W., Muench, S. P., et al. (2015). Replace, reuse, recycle: Improving the sustainable use of phosphorus by plants. *J. Exp. Bot.* 66, 3523–3540. doi: 10.1093/jxb/erv210

Blaby, I. K., Glaesener, A. G., Mettler, T., Fitz-Gibbon, S. T., Gallaher, S. D., Liu, B., et al. (2013). Systems-level analysis of nitrogen starvation-induced modifications of carbon metabolism in a *Chlamydomonas reinhardtii* starchless mutant. *Plant Cell* 25, 4305–4323. doi: 10.1105/tpc.113.117580

Borowitzka, M. (2013a). "Energy from Microalgae: A Short History," in *Algae for Biofuels and Energy SE - 1 Developments in Applied Phycology*. Eds. M. A. Borowitzka and N. R. Moheimani (Netherlands: Springer), 1–15. doi: 10.1007/978-94-007-5479-9_1

Borowitzka, M. A. (2013b). High-value products from microalgae—their development and commercialisation. *J. Appl. Phycol.* 25, 743–756. doi: 10.1007/s10811-013-9983-9

Camargo Valero, M. A., Read, L. F., Mara, D. D., Newton, R. J., Curtis, T. P., and Davenport, R. J. (2010a). Nitrification-denitrification in waste stabilisation ponds: A mechanism for permanent nitrogen removal in maturation ponds. *Water Sci. Technol.* 61, 1137–1146. doi: 10.2166/wst.2010.963

Camargo-Valero, M. A., Mara, D. D., and Newton, R. J. (2010b). Nitrogen removal in maturation WSP ponds via biological uptake and sedimentation of dead biomass. *Water Sci. Technol.* 61 (4), 1027–1034. doi: 10.2166/wst.2010.952

Camargo-Valero, M. A. (2009). *Nitrogen transformations pathways and removal mechanisms in domestic wastewater treatment by maturation ponds* (Leeds, UK: PhD Thesis, School of Civil Engineering, University of Leeds). http://www.sleigh-munoz.co.uk/wash/Mara/ThesisMiller.html.

Campos, J. L., Crutchik, D., Franchi, O., Pavissich, J. P., Belmonte, M., Pedrouso, A., et al. (2019). Nitrogen and Phosphorus Recovery From Anaerobically Pretreated Agro-Food Wastes: A Review. *Front. Sustain. Food Syst.* 2, Art. 91. doi: 10.3389/fsufs.2018.00091

Christ, J. J., Willbold, S., and Blank, L. M. (2019). Polyphosphate Chain Length Determination in the Range of Two to Several Hundred P-Subunits with a New Enzyme Assay and 31P NMR. *Anal. Chem.* 91, 7654–7661. doi: 10.1021/acs.analchem.9b00567

Cogan, E. B., Birrell, G. B., and Griffith, O. H. (1999). A robotics-based automated assay for inorganic and organic phosphates. *Anal. Biochem.* 271, 29–35. doi: 10.1006/abio.1999.4100

Colina, F., Amaral, J., Carbó, M., Pinto, G., Soares, A., Cañal, M. J., et al. (2019). Genome-wide identification and characterization of CKIN/SnRK gene family in *Chlamydomonas reinhardtii*. *Sci. Rep.* 9, 350. doi: 10.1038/s41598-018-35625-8

Correll, D. L. (1966). Imidonitrogen in chlorella "polyphosphate". *Science* 151, 819–821. doi: 10.1126/science.151.3712.819

Couso, I., Pérez-Pérez, M. E., Martínez-Force, E., Kim, H. S., He, Y., Umen, J. G., et al. (2018). Autophagic flux is required for the synthesis of triacylglycerols and ribosomal protein turnover in *Chlamydomonas*. *J. Exp. Bot.* 69, 1355–1367. doi: 10.1093/jxb/erx372

Couso, I., Pérez-Pérez, M. E., Ford, M. M., Martínez-Force, E., Hicks, L. M., Umen, J. G., et al. (2020). Phosphorus Availability Regulates TORC1 Signaling via LST8 in Chlamydomonas. *Plant Cell* 32, 69–80. doi: 10.1105/tpc.19.00179

Crimp, A., Brown, N., and Shilton, A. (2018). Microalgal luxury uptake of phosphorus in waste stabilization ponds - frequency of occurrence and high performing genera. *Water Sci. Technol.* 78, 165–173. doi: 10.2166/wst.2017.632

Dürr, M., Urech, K., Boller, T., Wiemken, A., Schwencke, J., and Nagy, M. (1979). Sequestration of arginine by polyphosphate in vacuoles of yeast (*Saccharomyces cerevisiae*). *Arch. Microbiol.* 121, 169–175. doi: 10.1007/BF00689982

Ding, G. T., Yaakob, Z., Takriff, M. S., Salihon, J., and Abd Rahaman, M. S. (2016). Biomass production and nutrients removal by a newly-isolated microalgal strain *Chlamydomonas* sp in palm oil mill effluent (POME). *Int. J. Hydrogen Energy* 41, 4888–4895. doi: 10.1016/j.ijhydene.2015.12.010

Docampo, R., Ulrich, P., and Moreno, S. N. J. (2010). Evolution of acidocalcisomes and their role in polyphosphate storage and osmoregulation in eukaryotic microbes. *Philos. Trans. R. Soc B Biol. Sci.* 365, 775–784. doi: 10.1098/rstb.2009.0179

Docampo, R. (2020). Catching protein polyphosphorylation in the act. *J. Biol. Chem.* 295, 1452–1453. doi: 10.1074/jbc.H120.012632

Droop, M. R. (1974). The nutrient status of algal cells in continuous culture. *J. Mar. Biol. Assoc. United Kingdom* 54, 825–855. doi: 10.1017/S002531540005760X

Elrifi, I. R., and Turpin, D. H. (1985). Steadystate luxury consumption and the concept of optimum nutrient ratios: a study with phosphate and nitrate limited *Selenastrum minutum* (chlorophyta). *J. Phycol.* 21, 592–602. doi: 10.1111/j.0022-3646.1985.00592.x

Elser, J., and Bennett, E. (2011). Phosphorus cycle: A broken biogeochemical cycle. *Nature* 478, 29031. doi: 10.1038/478029a

Florentino, A. P., Costa, M. C., Nascimento, J. G. S., Abdala-Neto, E. F., Mota, C. R., and Santos, A. B. (2019). Identification of microalgae from waste stabilization ponds and evaluation of electroflotation by alternate current for simultaneous biomass separation and cell disruption. *Engenharia Sanitaria Ambiental* 24, 177–186. doi: 10.1590/s1413-41522019193972

Gal, A., Sorrentino, A., Kahil, K., Pereiro, E., Faivre, D., and Scheffel, A. (2018). Native-state imaging of calcifying and noncalcifying microalgae reveals similarities in their calcium storage organelles. *Proc. Natl. Acad. Sci. U. S. A.* 115, 11000–11005. doi: 10.1073/pnas.1804139115

Gao, F., Wu, H., Zeng, M., Huang, M., and Feng, G. (2018). Overproduction, purification, and characterization of nanosized polyphosphate bodies from *Synechococcus* sp. PCC 7002. *Microb. Cell Fact.* 17, 27. doi: 10.1186/s12934-018-0870-6

Gargouri, M., Park, J. J., Holguin, F. O., Kim, M. J., Wang, H., Deshpande, R. R., et al. (2015). Identification of regulatory network hubs that control lipid metabolism in *Chlamydomonas reinhardtii*. *J. Exp. Bot.* 66, 4551–4566. doi: 10.1093/jxb/erv217

Gerasimaite, R., Sharma, S., Desfougères, Y., Schmidt, A., and Mayer, A. (2014). Coupled synthesis and translocation restrains polyphosphate to acidocalcisome-like vacuoles and prevents its toxicity. *J. Cell Sci.* 127, 5093–5104. doi: 10.1242/jcs.159772

Gong, Y., Hu, H., Gao, Y., Xu, X., and Gao, H. (2011). Microalgae as platforms for production of recombinant proteins and valuable compounds: Progress and prospects. *J. Ind. Microbiol. Biotechnol.* 38, 1879–1890. doi: 10.1007/s10295-011-1032-6

González-Ballester, D., Casero, D., Cokus, S., Pellegrini, M., Merchant, S. S., and Grossman, A. R. (2010). RNA-Seq analysis of sulfur-deprived chlamydomonas cells reveals aspects of acclimation critical for cell survival. *Plant Cell* 22, 2058–2084. doi: 10.1105/tpc.109.071167

Gonzales-Morales, C., Camargo-Valero, M. A., Molina Perez, F. J., and Fernández, B. (2019). Effect of the stirring speed on the struvite formation using the centrate from a WWTP. *Rev. Facultad Ingeniería* 92, 42–50. doi: 10.17533/udea.redin.20190518

Gonzalez-Ballester, D., Pollock, S. V., Pootakham, W., and Grossman, A. R. (2008). The central role of a SNRK2 kinase in sulfur deprivation responses. *Plant Physiol.* 147, 216–277. doi: 10.1104/pp.108.116137

Goodenough, U., Blaby, I., Casero, D., Gallaher, S. D., Goodson, C., Johnson, S., et al. (2014). The path to triacylglyceride obesity in the sta6 strain of *Chlamydomonas reinhardtii*. *Eukaryot. Cell* 13, 591–613. doi: 10.1128/EC.00013-14

Goodenough, U., Heiss, A. A., Roth, R., Rusch, J., and Lee, J. H. (2019). Acidocalcisomes: Ultrastructure, Biogenesis, and Distribution in Microbial Eukaryotes. *Protist* 170, 287–313. doi: 10.1016/j.protis.2019.05.001

Goodson, C., Roth, R., Wang, Z. T., and Goodenough, U. (2011). Structural correlates of cytoplasmic and chloroplast lipid body synthesis in *Chlamydomonas reinhardtii* and stimulation of lipid body production with acetate boost. *Eukaryot. Cell* 10, 1592–1606. doi: 10.1128/EC.05242-11

Greenwell, H. C., Laurens, L. M. L., Shields, R. J., Lovitt, R. W., Flynn, K. J., Anderson, R. A., et al. (2010). Placing microalgae on the biofuels priority list: a review of the technological challenges. *J. R. Soc Interface* 7, 703–726. doi: 10.1098/rsif.2009.0322

Guo, J., Wilken, S., Jimenez, V., Choi, C. J., Ansong, C., Dannebaum, R., et al. (2018). Specialized proteomic responses and an ancient photoprotection mechanism sustain marine green algal growth during phosphate limitation. *Nat. Microbiol.* 3, 781–790. doi: 10.1038/s41564-018-0178-7

Guzmán-Zapata, D., Sandoval-Vargas, J. M., Macedo-Osorio, K. S., Salgado-Manjarrez, E., Castrejón-Flores, J. L., Oliver-Salvador, M. D. C., et al. (2019). Efficient editing of the nuclear APT reporter gene in *Chlamydomonas reinhardtii* via expression of a CRISPR-Cas9 module. *Int. J. Mol. Sci.* 20, 1247. doi: 10.3390/ijms20051247

Habib, M. A. B., Parvin, M., Huntington, T. C., and Hasan, M. R. (2008). "A review on culture, production and use of spirulina as food for humans and feeds for domestic animals and fish," in *FAO Fisheries and Aquaculture Circular*, ISBN: No. 1034. (Rome: FAO).

Harold, F. M. (1966). Inorganic polyphosphates in biology: structure, metabolism, and function. *Bacteriol. Rev.* 30, 772–794. doi: 10.1128/MMBR.30.4.772-794.1966

Haughey, A. (1968). The planktonic algae of Auckland sewage treatment ponds. *New Zeal. J. Mar. Freshw. Res.* 2, 721–766. doi: 10.1080/00288330.1968.9515271

He, Z., and Dou, Z. (2010). "Phosphorus forms in animal manure and the impact on soil P status," in *Manure: Management, Uses and Environmental Impacts*. Ed. C. S. Dellaguardia (New York, NY: Nova Science Publishers), 83–114.

Hebeler, M., Hentrich, S., Mayer, A., Leibfritz, D., and Grimme, L. H. (1992). "Phosphate regulation and compartmentation in Chlamydomonas reinhardtii studied by in vivo 31 P-NMR," in *Research in Photosynthesis*, vol. 3. Ed. N. Murata (Dordrecht: Kluwer Academic Publishers), 717 – 720.

Hidayati, N. A., Yamada-Oshima, Y., Iwai, M., Yamano, T., Kajikawa, M., Sakurai, N., et al. (2019). Lipid remodeling regulator 1 (LRL1) is differently involved in the phosphorus-depletion response from PSR1 in *Chlamydomonas reinhardtii*. *Plant J.* 100, 610–626. doi: 10.1111/tpj.14473

Hong-Hermesdorf, A., Miethke, M., Gallaher, S. D., Kropat, J., Dodani, S. C., Chan, J., et al. (2014). Subcellular metal imaging identifies dynamic sites of Cu accumulation in *Chlamydomonas*. *Nat. Chem. Biol.* 10, 1034–1042. doi: 10.1038/nchembio.1662

Hothorn, M., Neumann, H., Lenherr, E. D., Wehner, M., Rybin, V., Hassa, P. O., et al. (2009). Catalytic core of a membrane-associated eukaryotic polyphosphate polymerase. *Science* 324, 513–516. doi: 10.1126/science.1168120

Johnson, W. K., and Schroepfer, G. J. (1964). Nitrogen Removal by Nitrification and Denitrification. *J. Water Pollut. Control Fed.* 36, 1015–1036.

Kimura, T., Watanabe, M., Kohata, K., and Sudo, R. (1999). Phosphate metabolism during diel vertical migration in the raphidophycean alga, *Chattonella antiqua*. *J. Appl. Phycol.* 11, 301–311. doi: 10.1023/A:1008196308564

Komine, Y., Eggink, L. L., Park, H., and Hoober, J. K. (2000). Vacuolar granules in *Chlamydomonas reinhardtii*: Polyphosphate and a 70-kDa polypeptide as major components. *Planta* 210, 897–905. doi: 10.1007/s004250050695

Kube, M., Jefferson, B., Fan, L., and Roddick, F. (2018). The impact of wastewater characteristics, algal species selection and immobilisation on simultaneous nitrogen and phosphorus removal. *Algal Res.* 31, 478–488. doi: 10.1016/j.algal.2018.01.009

Laliberté, G., and de la Noüe, J. (1993). Autotrophic, heterotrophic, and mixotrophic growth of *Chlamydomonas-humicola* (chlorophyceae) on acetate. *J. Phycol.* 29, 612–620. doi: 10.1111/j.0022-3646.1993.00612.x

Lander, N., Cordeiro, C., Huang, G., and Docampo, R. (2016). Inorganic polyphosphate (polyP) physiology: Polyphosphate and acidocalcisomes. *Biochem. Soc Trans.* 44, 1–6. doi: 10.1042/BST20150193

Leitão, J. M., Lorenz, B., Bachinski, N., Wilhelm, C., Muller, W. E. G., and Schroder, H. C. (1995). Osmotic-stress-induced synthesis and degradation of inorganic polyphosphates in the alga *Phaeodactylum tricornutum*. *Mar. Ecol. Prog. Ser.* 121, 279–288. doi: 10.3354/meps121279

Li, F. J., and He, C. Y. (2014). Acidocalcisome is required for autophagy in *Trypanosoma brucei*. *Autophagy* 10, 1978–1988. doi: 10.4161/auto.36183

Li, D.-W., Balamurugan, S., Yang, Y.-F., Zheng, J.-W., Huang, D., Zou, L.-G., et al. (2019a). Transcriptional regulation of microalgae for concurrent lipid overproduction and secretion. *Sci. Adv.* 5, eaau3795. doi: 10.1126/sciadv.aau3795

Li, K., Liu, Q., Fang, F., Luo, R., Lu, Q., Zhou, W., et al. (2019b). Microalgae-based wastewater treatment for nutrients recovery: A review. *Bioresour. Technol.* 291, 121934. doi: 10.1016/j.biortech.2019.121934

Liang, X., Jin, Y., He, M., Liu, Y., Hua, G., Wang, S., et al. (2017). Composition of phosphorus species and phosphatase activities in a paddy soil treated with manure at varying rates. *Agric. Ecosyst. Environ.* 237, 173–180. doi: 10.1016/j.agee.2016.12.033

Liu, T. Y., Huang, T. K., Yang, S. Y., Hong, Y. T., Huang, S. M., Wang, F. N., et al. (2016). Identification of plant vacuolar transporters mediating phosphate storage. *Nat. Commun.* 7, 11095. doi: 10.1038/ncomms11095

Lofrano, G., and Brown, J. (2010). Wastewater management through the ages: A history of mankind. *Sci. Total Environ.* 408, 5254–5264. doi: 10.1016/j.scitotenv.2010.07.062

Mahmoud-Aly, M., Li, Y., Shanab, S. M. M., Amin, A. Y., and Hanafy Ahmed, A. H. (2018). Physiological characterization of a chlamydomonas reinhardtii vacuolar transporter chaperon1 mutant under phosphorus deprivation condition. *Biosci. Res.* 15, 4532–4539.

Manyumba, F., Wood, E., and Horan, N. (2009). Meeting the phosphorus consent with biological nutrient removal under UK winter conditions. *Water Environ. J.* 23, 83–90. doi: 10.1111/j.1747-6593.2008.00110.x

Martin, P., and Van Mooy, B. A. S. (2013). Fluorometric Quantification of Polyphosphate in Environmental Plankton Samples: Extraction Protocols, Matrix Effects, and Nucleic Acid Interference. *Appl. Environ. Microbiol.* 79, 273–281. doi: 10.1128/AEM.02592-12

Mata, T. M., Martins, A. A., and Caetano, N. S. (2010). Microalgae for biodiesel production and other applications: A review. *Renewable Sustain. Energy Rev. Eng.* 14, 217–232. doi: 10.1016/j.rser.2009.07.020

McBeath, T. M., Lombi, E., McLaughlin, M. J., and Bünemann, E. K. (2007). Polyphosphate-fertilizer solution stability with time, temperature, and pH. *J. Plant Nutr. Soil Sci.* 170, 387–391. doi: 10.1002/jpln.200625166

McBride, R. C., Smith, V. H., Carney, L. T., and Lane, T. W. (2016). "Crop Protection in Open Ponds," in *Microalgal Production for Biomass and High-Value Products*. Eds. S. P. Slocombe and J. R. Benemann (Boca Raton, FL: Taylor & Francis Group), 165–182. doi: 10.1201/b19464-11

Melia, P. M., Cundy, A. B., Sohi, S. P., Hooda, P. S., and Busquets, R. (2017). Trends in the recovery of phosphorus in bioavailable forms from wastewater. *Chemosphere* 186, 381–395. doi: 10.1016/j.chemosphere.2017.07.089

Molino, J. V. D., de Carvalho, J. C. M., and Mayfield, S. P. (2018). Comparison of secretory signal peptides for heterologous protein expression in microalgae: Expanding the secretion portfolio for Chlamydomonas reinhardtii. *PloS One* 13, e0192433. doi: 10.1371/journal.pone.0192433

Moseley, J., and Grossman, A. R. (2009). Phosphate Metabolism and Responses to Phosphorus Deficiency. *Chlamydomonas Sourceb. 3-Vol set* 2, 189–215. doi: 10.1016/B978-0-12-370873-1.00014-9

Moseley, J. L., Chang, C. W., and Grossman, A. R. (2006). Genome-based approaches to understanding phosphorus deprivation responses and PSR1 control in *Chlamydomonas reinhardtii*. *Eukaryot. Cell* 5, 26–44. doi: 10.1128/EC.5.1.26-44.2006

Moudříková, S., Nedbal, N., Solovchenko, A., and Mojzeš, P. (2017). Raman microscopy shows that nitrogen-rich cellular inclusions in microalgae are microcrystalline guanine. *Algal Res.* 23, 216–222. doi: 10.1016/j.algal.2017.02.009

Mulbry, W., Westhead, E. K., Pizarro, C., and Sikora, L. (2005). Recycling of manure nutrients: Use of algal biomass from dairy manure treatment as a slow release fertilizer. *Bioresour. Technol.* 96, 451–458. doi: 10.1016/j.biortech.2004.05.026

Ngan, C. Y., Wong, C. H., Choi, C., Yoshinaga, Y., Louie, K., Jia, J., et al. (2015). Lineage-specific chromatin signatures reveal a regulator of lipid metabolism in microalgae. *Nat. Plants* 1, 1–12. doi: 10.1038/nplants.2015.107

NGER (2016). *National Greenhouse and Energy Reporting Scheme Measurement – Technical Guidelines for the estimation of emissions by facilities in Australia (August 2016)* (Canberra, Australia: Dept. of the Environment and Energy, Australian Government). http://www.environment.gov.au/.

Nishikawa, K., Yamakoshi, Y., Uemura, I., and Tominaga, N. (2003). Ultrastructural changes in Chlamydomonas acidophila (Chlorophyta) induced by heavy metals and polyphosphate metabolism. *FEMS Microbiol. Ecol.* 44, 253–259. doi: 10.1016/S0168-6496(03)00049-7

Nishikawa, K., Machida, H., Yamakoshi, Y., Ohtomo, R., Saito, K., Saito, M., et al. (2006). Polyphosphate metabolism in an acidophilic alga *Chlamydomonas acidophila* KT-1 (Chlorophyta) under phosphate stress. *Plant Sci.* 170, 307–313. doi: 10.1016/j.plantsci.2005.08.025

Novoveská, L., Zapataa, A. K. M., Zabolotney, J. B., Atwood, M. C., and Sundstrom, E. R. (2016). Optimizing microalgae cultivation and wastewater treatment in large-scale offshore photobioreactors. *Algal Res.* 18, 86–94. doi: 10.1016/j.algal.2016.05.033

Ota, S., Yoshihara, M., Yamazaki, T., Takeshita, T., Hirata, A., Konomi, M., et al. (2016). Deciphering the relationship among phosphate dynamics, electron-dense body and lipid accumulation in the green alga *Parachlorella kessleri*. *Sci. Rep.* 6, 1–11. doi: 10.1038/srep25731

Park, J. B. K., Craggs, R. J., and Shilton, A. N. (2011). Wastewater treatment high rate algal ponds for biofuel production. *Bioresour. Technol.* 102, 35–42. doi: 10.1016/j.biortech.2010.06.158

Park, K. C., Whitney, C., McNichol, J. C., Dickinson, K. E., MacQuarrie, S., Skrupski, B. P., et al. (2012). Mixotrophic and photoautotrophic cultivation of 14 microalgae isolates from Saskatchewan, Canada: Potential applications for wastewater remediation for biofuel production. *J. Appl. Phycol.* 24, 339–348. doi: 10.1007/s10811-011-9772-2

Plouviez, M., Shilton, A., Packer, M. A., and Guieysse, B. (2019). Nitrous oxide emissions from microalgae: potential pathways and significance. *J. Appl. Phycol.* 31, 1–8. doi: 10.1007/s10811-018-1531-1

Powell, N., Shilton, A. N., Pratt, S., and Chisti, Y. (2008). Factors Influencing Luxury Uptake of Phosphorus by Microalgae in Waste Stabilization Ponds. *Environ. Sci. Tech.* 16, 5958–5962. doi: 10.1021/es703118s

Powell, N., Shilton, A., Pratt, S., and Chisti, Y. (2011). Luxury uptake of phosphorus by microalgae in full-scale waste stabilisation ponds. *Water Sci. Technol.* 63 (4), 704–709. doi: 10.2166/wst.2011.116

Pröschold, T., Harris, E. H., and Coleman, A. W. (2005). Portrait of a species: *Chlamydonomas reinhardtii*. *Genetics* 170, 1601–1610. doi: 10.1534/genetics.105.044503

Rao, N. N., Gómez-García, M. R., and Kornberg, A. (2009). Inorganic Polyphosphate: Essential for Growth and Survival. *Annu. Rev. Biochem.* 78, 605–647. doi: 10.1146/annurev.biochem.77.083007.093039

Reusch, R. N. (2000). Transmembrane Ion Transport by Polyphosphate/ Poly-(R)-3-hydroxybutyrate Complexes. *Biochem* 65, 280–295.

Ruiz, F. A., Marchesini, N., Seufferheld, M., Govindjee,, and Docampo, R. (2001). The Polyphosphate Bodies of *Chlamydomonas reinhardtii* Possess a Proton-pumping Pyrophosphatase and Are Similar to Acidocalcisomes. *J. Biol. Chem.* 276, 46196–46203. doi: 10.1074/jbc.M105268200

Salomé, P. A., and Merchant, S. S. (2019). A series of fortunate events: Introducing *Chlamydomonas* as a reference organism. *Plant Cell* 31, 1682–1707. doi: 10.1105/tpc.18.00952

Samadani, M., and Dewez, D. (2018). Cadmium accumulation and toxicity affect the extracytoplasmic polyphosphate level in *Chlamydomonas reinhardtii*. *Ecotoxicol. Environ. Saf.* 166, 200–206. doi: 10.1016/j.ecoenv.2018.09.094

Sang, Y. L., Lee, D. Y., and Tae, Y. K. (2005). Systems biotechnology for strain improvement. *Trends Biotechnol.* 23, 349–358. doi: 10.1016/j.tibtech.2005.05.003

Scherholz, M. L., and Curtis, W. R. (2013). Achieving pH control in microalgal cultures through fed-batch addition of stoichiometrically-balanced growth media. *BMC Biotechnol.* 13, 39. doi: 10.1186/1472-6750-13-39

Schmollinger, S., Mühlhaus, T., Boyle, N. R., Blaby, I. K., Casero, D., Mettler, T., et al. (2014). Nitrogen-sparing mechanisms in *Chlamydomonas* affect the transcriptome, the proteome, and photosynthetic metabolism. *Plant Cell* 26, 1410–1435. doi: 10.1105/tpc.113.122523

Schröder, J. J., Smit, A. L., Cordell, D., and Rosemarin, A. (2011). Improved phosphorus use efficiency in agriculture: A key requirement for its sustainable use. *Chemosphere* 84, 822–831. doi: 10.1016/j.chemosphere.2011.01.065

Schreiber, C., Schiedung, H., Harrison, L., Briese, C., Ackermann, B., Kant, J., et al. (2018). Evaluating potential of green alga *Chlorella vulgaris* to accumulate phosphorus and to fertilize nutrient-poor soil substrates for crop plants. *J. Appl. Phycol.* 30, 2827–2836. doi: 10.1007/s10811-018-1390-9

Seufferheld, M. J., and Curzi, M. J. (2010). Recent discoveries on the roles of polyphosphates in plants. *Plant Mol. Biol. Rep.* 28, 549–559. doi: 10.1007/s11105-010-0187-z

Seufferheld, M., Vieira, M. C. F., Ruiz, F. A., Rodrigues, C. O., Moreno, S. N. J., and Docampo, R. (2003). Identification of organelles in bacteria similar to acidocalcisomes of unicellular eukaryotes. *J. Biol. Chem.* 278, 29971–29978. doi: 10.1074/jbc.M304548200

Shebanova, A., Ismagulova, T., Solovchenko, A., Baulina, O., Lobakova, E., Ivanova, A., et al. (2017). Versatility of the green microalga cell vacuole function as revealed by analytical transmission electron microscopy. *Protoplasma* 254, 1323–1340. doi: 10.1007/s00709-016-1024-5

Shimogawara, K., Wykoff, D. D., Usuda, H., and Grossman, A. R. (1999). *Chlamydomonas reinhardtii* mutants abnormal in their responses to phosphorus deprivation. *Plant Physiol.* 120, 685–693. doi: 10.1104/pp.120.3.685

Shin, Y. S., Jeong, J., Nguyen, T. H. T., Kim, J. Y. H., Jin, E. S., and Sim, S. J. (2019). Targeted knockout of phospholipase A 2 to increase lipid productivity in *Chlamydomonas reinhardtii* for biodiesel production. *Bioresour. Technol.* 271, 368–374. doi: 10.1016/j.biortech.2018.09.121

Siderius, M., Musgrave, A., Van Den Ende, H., Koerten, H., Cambier, P., and Van Der Meer, P. (1996). *Chlamydomonas eugametos* (Chlorophyta) stores phosphate in polyphosphate bodies together with calcium. *J. Phycol.* 32, 402–409. doi: 10.1111/j.0022-3646.1996.00402.x

Siebers, N., Hofmann, D., Schiedung, H., Landsrath, A., Ackermann, B., Gao, L., et al. (2019). Towards phosphorus recycling for agriculture by algae: Soil incubation and rhizotron studies using 33P-labeled microalgal biomass. *Algal Res.* 43, 101634. doi: 10.1016/j.algal.2019.101634

Slocombe, S. P., and Benemann, J. R. (2016). "Introduction," in *Microalgal production for biomass and high-value products*. Eds. S. P. Slocombe and J. R. Benemann (Boca Raton, FL: CRC press), xvii–xxxx. Available at: http://www.crcnetbase.com/isbn/978-1-4822-1970-8.

Slocombe, S. P., Zhang, Q., Ross, M., Anderson, A., Thomas, N. J., Lapresa, Á., et al. (2015). Unlocking nature's treasure-chest: screening for oleaginous algae. *Sci. Rep.* 5, 9844. doi: 10.1038/srep09844

Smith, R. T., Bangert, K., Wilkinson, S. J., and Gilmour, D. J. (2015). Synergistic carbon metabolism in a fast growing mixotrophic freshwater microalgal species *Micractinium inermum*. *Biomass Bioenergy* 82, 73–86. doi: 10.1016/j.biombioe.2015.04.023

Smith, S. A., Wang, Y., and Morrissey, J. H. (2018). DNA ladders can be used to size polyphosphate resolved by polyacrylamide gel electrophoresis. *Electrophoresis* 39, 2454–2459. doi: 10.1002/elps.201800227

Solorzano, L., and Sharp, J. H. (1980). Determination of total dissolved phosphorus particulate phosphorus in natural water. *Limnol. Ocean.* 25, 754–758. doi: 10.4319/lo.1980.25.4.0754

Solovchenko, A. E., Ismagulova, T. T., Lukyanov, A. A., Vasilieva, S. G., Konyukhov, I. V., Pogosyan, S.II, et al. (2019). Luxury phosphorus uptake in microalgae. *J. Appl. Phycol.* 31, 2755–2770. doi: 10.1007/s10811-019-01831-8

Strickland, J. D. H., and Parsons, T. R. (1968). A manual for sea water analysis. *Bull. Fish. Res. Bd. Canada* 167, 49–64.

Sutherland, D. L., Turnbull, M. H., and Craggs, R. J. (2017). Environmental drivers that influence microalgal species in fullscale wastewater treatment high rate algal ponds. *Water Res.* 124, 504–512. doi: 10.1016/j.watres.2017.08.012

Sutherland, D. L., Park, J., Heubeck, S., Ralph, P. J., and Craggs, R. J. (2020). Size matters – Microalgae production and nutrient removal in wastewater treatment high rate algal ponds of three different sizes. *Algal Res.* 45, 101734. doi: 10.1016/j.algal.2019.101734

Tarayre, C., De Clercq, L., Charlier, R., Michels, E., Meers, E., Camargo-Valero, M., et al. (2016). New perspectives for the design of sustainable bioprocesses for phosphorus recovery from waste. *Bioresour. Technol.* 206, 264–274. doi: 10.1016/j.biortech.2016.01.091

Thomas, S., and Burger, J. W. (1933). *Chlamydomonas* in Storage Reservoirs. *J. Am. Water Works Assoc.* 25, 991–999. doi: 10.1002/j.1551-8833.1933.tb14722.x

Toepel, J., Albaum, S. P., Arvidsson, S., Goesmann, A., la Russa, M., Rogge, K., et al. (2011). Construction and evaluation of a whole genome microarray of *Chlamydomonas reinhardtii*. *BMC Genomics* 12, 579. doi: 10.1186/1471-2164-12-579

Tran, M., Henry, R. E., Siefker, D., Van, C., Newkirk, G., Kim, J., et al. (2013). Production of anti-cancer immunotoxins in algae: Ribosome inactivating proteins as fusion partners. *Biotechnol. Bioeng.* 110, 2826–2835. doi: 10.1002/bit.24966

Tsednee, M., Castruita, M., Salomé, P. A., Sharma, A., Lewis, B. E., Schmollinger, S. R., et al. (2019). Manganese co-localizes with calcium and phosphorus in *Chlamydomonas* acidocalcisomes and is mobilized in Mn-deficient conditions. *J. Biol. Chem.* 294, 17626–17641. doi: 10.1074/jbc.ra119.009130

U.S. Geological Survey. (2017). *Mineral Commodity Summaries, January 2017. Phosphate Rock*. (Reston, VA: USGS). Available at https://minerals.usgs.gov/minerals/pubs/commodity/phosphate_rock/mcs-2017-phosp.pdf.

Ueda, Y., and Yanagisawa, S. (2019). Perception, transduction, and integration of nitrogen and phosphorus nutritional signals in the transcriptional regulatory network in plants. *J. Exp. Bot.* 70, 3709–3717. doi: 10.1093/jxb/erz148

Usher, P., Ross, A. B., Camargo-Valero, M. A., Tomlin, A. S., and Gale, W. F. (2014). An Overview of the Environmental Impacts of Large Scale Microalgae Cultivation. *Biofuels* 5 (3), 331–349. doi: 10.1080/17597269.2014.913925

Van Kauwenberg, S. J. (2010). *World Phosphate Rock Reserves and Resources* (Alabama, USA: Technical Bulletin IFDCT-75. Muscle Shoals).

Wang, W. X., and Dei, R. C. H. (2006). Metal stoichiometry in predicting Cd and Cu toxicity to a freshwater green alga *Chlamydomonas reinhardtii*. *Environ. Pollut.* 142, 303–312. doi: 10.1016/j.envpol.2005.10.005

Watanabe, M., Kohata, K., and Kunugi, M. (1988). Phosphate accumulation and metabolism by *Heterosigma akashiwo* (raphidophyceae) during diel vertical migration in a stratified microcosm. *J. Phycol.* 24, 22–28. doi: 10.1111/j.1529-8817.1988.tb04452.x

Weiss, M., Bental, M., and Pick, U. (1991). Hydrolysis of polyphosphates and permeability changes in response to osmotic shocks in cells of the halotolerant alga *Dunaliella*. *Plant Physiol.* 97, 1241–1248. doi: 10.1104/pp.97.3.1241

Werner, T. P., Amrhein, N., and Freimoser, F. M. (2007). Inorganic polyphosphate occurs in the cell wall of *Chlamydomonas reinhardtii* and accumulates during cytokinesis. *BMC Plant Biol.* 7, 1–11. doi: 10.1186/1471-2229-7-51

Westenberg, B., Boller, T., and Wiemken, A. (1989). Lack of arginine- and polyphosphate-storage pools in a vacuole-deficient mutant (end1) of *Saccharomyces cerevisiae*. *FEBS Lett.* 254, 133–136. doi: 10.1016/0014-5793(89)81024-5

Wild, R., Gerasimaite, R., Jung, J. Y., Truffault, V., Pavlovic, I., Schmidt, A., et al. (2016). Control of eukaryotic phosphate homeostasis by inositol polyphosphate sensor domains. *Science* 352, 986–990. doi: 10.1126/science.aad9858

Withers, P. J. A., Forber, K. G., Lyon, C., Rothwell, S., Doody, D. G., Jarvie, H. P., et al. (2020). Towards resolving the phosphorus chaos created by food systems. *Ambio* 49, 1076–1089. doi: 10.1007/s13280-019-01255-1

Worrall, F., Burt, T. P., Howden, N. J. K., and Whelan, M. J. (2009). Fluvial flux of nitrogen from Great Britain 1974–2005 in the context of the terrestrial nitrogen budget of Great Britain. *Global Biochem. Cycles* 23, GB3017. doi: 10.1029/2008GB003351

Worrall, F., Jarvie, H. P., Howden, N. J. K., and Burt, T. P. (2016). The fluvial flux of total reactive and total phosphorus from the UK in the context of a national phosphorus budget: comparing UK river fluxes with phosphorus trade imports and exports. *Biogeochemistry* 130, 31–51. doi: 10.1007/s10533-016-0238-0

WWAP (United Nations World Water Assessment Programme) (2017). *The United Nations World Water Development Report 2017. Wastewater: The Untapped Resource* (Paris: UNESCO).

Wykoff, D. D., Grossman, A. R., Weeks, D. P., Usuda, H., and Shimogawara, K. (1999). Psr1, a nuclear localized protein that regulates phosphorus metabolism in *Chlamydomonas*. *Proc. Natl. Acad. Sci.* 96, 15336–15341. doi: 10.1073/pnas.96.26.15336

Yehudai-Resheff, S., Zimmer, S. L., Komine, Y., and Stern, D. B. (2007). Integration of chloroplast nucleic acid metabolism into the phosphate deprivation response in *Chlamydomonas reinhardtii*. *Plant Cell* 19, 1023–1038. doi: 10.1105/tpc.106.045427

Zachleder, V., Bisova, K., and Vitova, M. (2016). "The Cell Cycle of Microalgae," in *The Physiology of Microalgae*. Eds. M. A. Borowitzka, J. Beardall and J. A. Raven (New York: Springer), 3–46. doi: 10.1007/978-3-319-24945-2

Zhou, Y., Schideman, L. C., Park, D. S., Stirbet, A., Govindjee, Rupassara, S.II, et al. (2015). Characterization of a *Chlamydomonas reinhardtii* mutant strain with improved biomass production under low light and mixotrophic conditions. *Algal Res.* 11, 134–147. doi: 10.1016/j.algal.2015.06.001

Zhu, J., Loubéry, S., Broger, L., Lorenzo-Orts, L., Utz-Pugin, A., Young-Tae, C., et al. (2020). A genetically validated approach to detect inorganic polyphosphates in plants. *Plant J.* 102, 507–516. doi: 10.1101/630129

**Conflict of Interest:** The authors declare that the research was conducted in the absence of any commercial or financial relationships that could be construed as a potential conflict of interest.

frontiers in Microbiology

REVIEW
published: 14 July 2020
doi: 10.3389/fmicb.2020.01367

# Phosphate Homeostasis – A Vital Metabolic Equilibrium Maintained Through the INPHORS Signaling Pathway

*Sisley Austin and Andreas Mayer**

*Département de Biochimie, Université de Lausanne, Lausanne, Switzerland*

Cells face major changes in demand for and supply of inorganic phosphate ($P_i$). $P_i$ is often a limiting nutrient in the environment, particularly for plants and microorganisms. At the same time, the need for phosphate varies, establishing conflicts of goals. Cells experience strong peaks of $P_i$ demand, e.g., during the S-phase, when DNA, a highly abundant and phosphate-rich compound, is duplicated. While cells must satisfy these $P_i$ demands, they must safeguard themselves against an excess of $P_i$ in the cytosol. This is necessary because $P_i$ is a product of all nucleotide-hydrolyzing reactions. An accumulation of $P_i$ shifts the equilibria of these reactions and reduces the free energy that they can provide to drive endergonic metabolic reactions. Thus, while $P_i$ starvation may simply retard growth and division, an elevated cytosolic $P_i$ concentration is potentially dangerous for cells because it might stall metabolism. Accordingly, the consequences of perturbed cellular $P_i$ homeostasis are severe. In eukaryotes, they range from lethality in microorganisms such as yeast (Sethuraman et al., 2001; Hürlimann, 2009), severe growth retardation and dwarfism in plants (Puga et al., 2014; Liu et al., 2015; Wild et al., 2016) to neurodegeneration or renal Fanconi syndrome in humans (Legati et al., 2015; Ansermet et al., 2017). Intracellular $P_i$ homeostasis is thus not only a fundamental topic of cell biology but also of growing interest for medicine and agriculture.

**Keywords: nutrient signaling, phosphate, acidocalcisome, SPX, polyphosphate, inositol pyrophosphate, Tor, PKA**

OPEN ACCESS

***Edited by:***
*Jose Roman Perez-Castineira, Universidad de Sevilla, Spain*

***Reviewed by:***
*Silvia N. J. Moreno, University of Georgia, United States*
*Dennis D. Wykoff, Villanova University, United States*

***Correspondence:**
*Andreas Mayer*
*andreas.mayer@unil.ch*

***Specialty section:***
*This article was submitted to Microbiological Chemistry and Geomicrobiology, a section of the journal Frontiers in Microbiology*

***Received:*** *23 March 2020*
***Accepted:*** *27 May 2020*
***Published:*** *14 July 2020*

***Citation:***
*Austin S and Mayer A (2020) Phosphate Homeostasis – A Vital Metabolic Equilibrium Maintained Through the INPHORS Signaling Pathway. Front. Microbiol. 11:1367. doi: 10.3389/fmicb.2020.01367*

## PHOSPHATE CONTROL IS A CHALLENGE FOR CELLS

Cells should coordinate their systems for the uptake, export, and storage of $P_i$ in order to strike a delicate balance between the biosynthetic requirements for $P_i$ and the risks of an excessive cytoplasmic $P_i$ concentration. To achieve this, they may use signaling networks that sense extra- and intracellular $P_i$ and a buffering system for cytosolic $P_i$. In this review, we do not provide a global overview of phosphate homeostasis in all model organisms studied in this respect because this adds significant complexity and detail, resulting for example from multicellularity, tissue differentiation, or the complexity of their life cycles. We will rather focus on the yeast *Saccharomyces cerevisiae* because it is a unicellular model and the eukaryotic model system in which relevant pathways and mechanisms have been best characterized. Focusing on a single well-characterized and simple

model provides the best basis for our effort to develop a conceptual framework for intracellular phosphate homeostasis, which may provide leads to dissect this crucial homeostatic system also in other eukaryotic organisms (**Table 1**). We therefore add information from other models only where it is necessary to provide information that is not available for *S. cerevisiae*.

## STRATEGIES FOR PHOSPHATE HOMEOSTASIS

Multicellular organisms can regulate $P_i$ concentration at the organismal level. Humans, for example, maintain $P_i$ concentration in circulating body fluids through filtration at the level of the kidneys and controlled reabsorption (Biber et al., 2013; Sabbagh, 2013). They can access the apatite in bones as a huge $P_i$ reserve. These well-studied mechanisms provide the individual cells with a relatively constant environment of extracellular $P_i$, alleviating the need for complex $P_i$-foraging programs at the cellular level. Nevertheless, human tissues widely express a regulated $P_i$ exporter in the plasma membrane (XPR1) (Giovannini et al., 2013), which suggests that they might also maintain a safeguard against peaks of cytosolic $P_i$. Dysregulation of XPR1 leads to neurodegeneration and brain calcification, suggesting that XPR1 might dampen the significant changes of $P_i$ concentration in brain cells that can occur depending on its metabolic state (McIlwain et al., 1951). Interestingly, XPR1 is even important for $P_i$ homeostasis at the organismal level because it is implicated in the reabsorption of $P_i$ across the renal tubules of the kidney (Ansermet et al., 2017).

Whereas $P_i$ regulation at the organismal level has been intensely studied, particularly in humans (Biber et al., 2013; Sabbagh, 2013), it is poorly understood how cytosolic $P_i$ concentration is measured and regulated at the level of individual cells. Unicellular organisms can experience rapid changes in $P_i$ availability. They use multiple systems to maintain $P_i$ homeostasis, which allow the cell to mount a graded response that is tuned to the degree of $P_i$ availability and consumption (Bostian et al., 1983). Cells respond to $P_i$ scarcity with various foraging strategies (Conrad et al., 2014; Puga et al., 2017), in which they try to liberate $P_i$ from a variety of extracellular substrates. They can express $P_i$ importers of low and high affinity, which allow them to acquire $P_i$ under a wide range of external concentrations. They maintain important $P_i$ stores in acidocalcisome-like organelles, which, in case of sudden $P_i$ starvation, can guarantee them sufficient reserves to finish the next cell cycle and make an ordered transition into a robust quiescent state. Finally, cells can also "recycle" and liberate $P_i$ from internal sources, such as nucleotides and phospholipids. While such recycling appears senseless for a growing cell—because it will need those compounds to grow—it may become critical for cells that have already arrested growth. They may choose to reallocate their internal $P_i$ pool in order to perform new biosyntheses that are critical to survive in the non-dividing, starved state. Since $P_i$ scarcity retards growth but as such does not seem to be lethal, mounting starvation responses can rely on (relatively slow) transcriptional $P_i$ starvation programs. But cells may also experience a sudden excess of $P_i$ and may need highly reactive mechanisms to protect themselves against the potentially lethal consequences. In this situation, posttranslational signaling becomes important, allowing to rapidly and simultaneously regulate multiple systems for import, export, and storage of $P_i$ and to thus dampen cytosolic $P_i$ peaks.

## ACIDOCALCISOMES: A CONSERVED ORGANELLE WITH A ROLE IN PHOSPHATE BUFFERING?

Acidocalcisomes are membrane-bound organelles that are conserved from bacteria to mammals (Docampo and Huang, 2016), but their functions are poorly understood. Yeast cells have an acidocalcisome-like compartment, the vacuole, which carries transporters for all compounds that are typically concentrated in acidocalcisomes (**Figure 1**). Typical acidocalcisome features comprise high concentrations of divalent cations, an acidic pH, and several hundred millimolars of the basic amino acids arginine as lysine. $P_i$ is accumulated to similarly high concentrations in the form of polyphosphate (polyP), a polymer of up to a thousand $P_i$ units linked through phosphoric anhydride bonds. PolyP is stored in the acidocalcisome lumen, where polyphosphatases are also located. It is assumed that these enzymes can hydrolyze polyP, which may allow re-export of the liberated $P_i$ into the cytosol (Gerasimaite and Mayer, 2016, 2017). Thereby, acidocalcisome-like organelles might be important buffering devices for cytosolic $P_i$. In line with this, cells lacking polyP show an accelerated activation of the transcriptional phosphate starvation response on low-$P_i$ media (Neef and Kladde, 2003; Thomas and O'Shea, 2005). They also show delays in the S-phase and slower dNTP synthesis, probably because a rapid duplication of nucleic acids and phospholipids generates a $P_i$ requirement that transiently exceeds the uptake capacity of the cell and necessitates the engagement of internal $P_i$ reserves (Neef and Kladde, 2003; Bru et al., 2016). A major open question is whether and how acidocalcisome-like vacuoles behave in these situations, i.e., how the turnover and release of $P_i$ back into the cytosol are triggered, such that futile cycles of polyP synthesis and hydrolysis are avoided. This is a pre-condition for acidocalcisome-like vacuoles to constitute an efficient regulated $P_i$ buffer.

While acidocalcisomes store high concentrations of phosphate and are, hence, prime candidates for a $P_i$-buffering system, it must be kept in mind that other organelles also use and/or liberate $P_i$ as part of their metabolic functions. For example, the endoplasmic reticulum (ER) lumen contains many chaperones that hydrolyze ATP (Depaoli et al., 2019). The Golgi liberates $P_i$ as a by-product of the glycosylation reactions in this compartment, and it is likely that this $P_i$ is recycled back to the cytosol through a dedicated channel, Erd1 (Snyder et al., 2017). Likewise, the mitochondria permanently import large quantities of $P_i$ in order to regenerate ATP from ADP (Palmieri and Monné, 2016). Phosphate homeostasis in the cytosol will be influenced by these different processes, but their impact has yet remained essentially unaddressed.

**TABLE 1 |** Proteins and terms repeatedly used in the review.

| | |
|---|---|
| Arg82 | Inositol polyphosphate multikinase (IPMK); sequentially phosphorylates $InsP_3$ to form $InsP_5$ |
| Ddp1 | Member of the Nudix hydrolase family; displays di-phosphoinositol polyphosphate hydrolase activity; hydrolyzes the ß-phosphates of $InsP_8$ and $InsP_7$ |
| Gde1 | Glycerophosphocholine (GroPCho) phosphodiesterase; carries an SPX domain |
| INPHORS | Acronym for intracellular phosphate reception and signaling |
| InsPP | Inositol pyrophosphate |
| Ipk1 | Nuclear inositol pentakisphosphate 2-kinase; converts $InsP_5$ to $InsP_6$ |
| Kcs1 | Inositol hexakisphosphate kinase; phosphorylates $InsP_6$ or Ins(1,3,4,5,6)$P_5$, creating 5-$InsP_7$ or 5PP-$InsP_4$, respectively |
| Phm8 | Lysophosphatidic acid phosphatase |
| PHO pathway | Phosphate-responsive signaling pathway regulating transcription in *Saccharomyces cerevisiae* |
| Pho11 | Cell wall-associated acid phosphatase |
| Pho12 | Cell wall-associated acid phosphatase |
| Pho2 | Transcription factor for the PHO pathway; cooperates with Pho4 |
| Pho4 | Transcription factor for the PHO pathway; cooperates with Pho2 |
| Pho5 | Repressible secreted acid phosphatase |
| Pho8 | Repressible alkaline phosphatase located in the vacuole |
| Pho80 | Cyclin subunit of the cyclin-dependent Pho85/80/81 kinase |
| Pho81 | Cyclin-dependent kinase inhibitor (CKI); regulatory subunit of the Pho85/80/81 kinase; possesses an SPX domain |
| Pho84 | High-affinity inorganic phosphate plasma membrane transporter |
| Pho85 | Catalytic subunit of the cyclin-dependent Pho85/80/81 kinase; Pho85 associates with at least 10 different cyclins to regulate a wide spectrum of target proteins involved in many cellular processes |
| Pho87 | Low-affinity inorganic phosphate plasma membrane transporter; carries an SPX domain |
| Pho89 | High-affinity inorganic phosphate plasma membrane transporter |
| Pho90 | Low-affinity inorganic phosphate plasma membrane transporter; carries an SPX domain |
| Pho91 | Low-affinity inorganic phosphate transporter in the vacuolar membrane; possesses an SPX domain; homologs are rice OsSPX-MFS3 and *Trypanosoma brucei* TbPho91 |
| Pho92 | Posttranscriptional regulator of phosphate metabolism; regulates the degradation of Pho4 mRNA by binding to its 3'-UTR in a $P_i$-dependent manner |
| $P_i$ | Inorganic phosphate |
| PKA | cAMP-dependent protein kinase; controls a variety of cellular processes, including metabolism |
| Plc1 | Phospholipase C; hydrolyzes phosphatidylinositol 4,5-biphosphate ($PIP_2$) to generate the signaling molecules $InsP_3$ and 1,2-diacylglycerol (DAG) |
| polyP | Polymer of up to a thousand $P_i$ units linked through phosphoric anhydride bonds |
| Ppn1 | Endo- and exopolyphosphatase in vacuoles |
| Ppn2 | $Zn^{2+}$-dependent endopolyphosphatase in vacuoles |
| Ppx1 | Soluble exopolyphosphatase in the cytosol |
| Rim15 | Serine/threonine protein kinase; regulates cell proliferation in response to nutrients |
| Siw14 | Member of the dual-specificity phosphatase family; hydrolyzes the ß-phosphates of 5-$InsP_7$ and $InsP_8$ |
| Spl2 | Regulator of low-affinity phosphate transporter |
| SPX domain | Domain binding inositol pyrophosphates and Pi; involved in the regulation of phosphate homeostasis |
| Syg1 | Plasma membrane protein presumed to export inorganic phosphate; possesses an SPX domain; similarities with human XPR1 |
| Vip1 | Diphosphoinositol pentakisphosphate kinases (PPIP5K); contains both a kinase and a histidine acid phosphatase domain; the kinase domain phosphorylates $InsP_6$ and 5-$InsP_7$ to generate 1-$InsP_7$ and 1,5-$InsP_8$, respectively |
| VTC complex | Polyphosphate polymerase complex; synthesizes polyP from nucleotide triphosphates and translocates it across the vacuolar membrane; composed of four subunits: Vtc4, the catalytically active subunit; Vtc1/2 or Vtc1/3, mainly localized in the ER or in vacuoles, respectively; and the regulatory subunit Vtc5. Vtc2, Vtc3, Vtc4, and Vtc5 possess an SPX domain |

## BASIC SETUP FOR $P_i$ REGULATION IN YEAST

$P_i$ homeostasis can be achieved by controlling a variety of processes in a synergistic manner, such as the import and export of $P_i$, its intracellular storage and re-mobilization, active foraging for $P_i$ in the environment, and $P_i$ recycling within the cell. In yeast, many components contributing to these processes are known. At least 25 out of the approximately 6,000 genes in yeast are directly implicated in $P_i$ homeostasis, illustrating the crucial importance of this parameter for the cells. They comprise secreted acid phosphatases to liberate $P_i$ from a variety of substrates in the environment (Oshima, 1997): $P_i$ importers of high (Pho84 and Pho89) and low (Pho87 and Pho90) affinity and

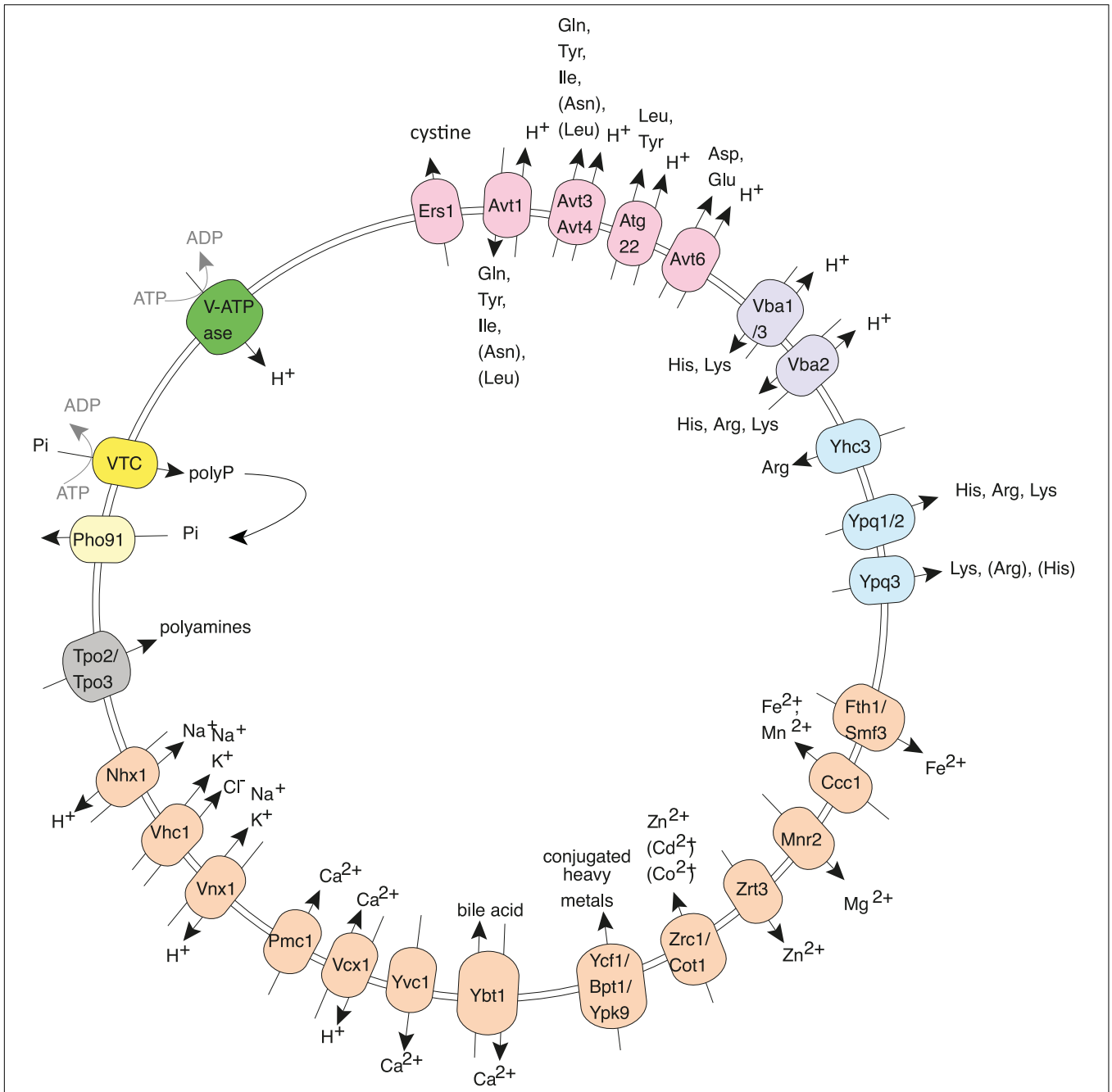


**FIGURE 1 |** Yeast vacuoles as an example of an acidocalcisome-like organelle. The polyphosphate polymerase VTC transfers inorganic phosphate ($P_i$) into vacuoles by converting it into polyphosphate (polyP) and translocating it across the membrane. Here, the lumenal polyphosphatases can convert polyP back into $P_i$, which can be re-exported into the cytosol through Pho91. Apart from polyP, yeast vacuoles actively accumulate many other compounds that are typical of acidocalcisomes, such as $Ca^{2+}$, $Mn^{2+}$, $Zn^{2+}$, and basic amino acids. Examples of the involved transporters are shown in the illustration.

a putative $P_i$ exporter in the plasma membrane (Syg1; **Figure 2**) (Persson et al., 2003). Cells can also recycle $P_i$ from internal sources, e.g., by liberating it from nucleotides or phospholipids (Phm8 and Gde1) (Patton-Vogt, 2007; Xu et al., 2013). An ATP-driven protein complex (VTC complex) exists for storing and concentrating $P_i$ as an osmotically inactive polyphosphate and depositing it inside the vacuole, from where it can be re-mobilized by polyphosphatases (Ppn1 and Ppn2) (Sethuraman et al., 2001; Gerasimaite and Mayer, 2016, 2017). The vacuolar membrane carries a $P_i$ transporter (Pho91) (Hürlimann et al., 2009), which might participate in the re-mobilization of polyP and export $P_i$ resulting from polyP hydrolysis into the cytoplasm.

Many genes involved in $P_i$ homeostasis are expressed through a transcriptional control mechanism, the phosphate-responsive

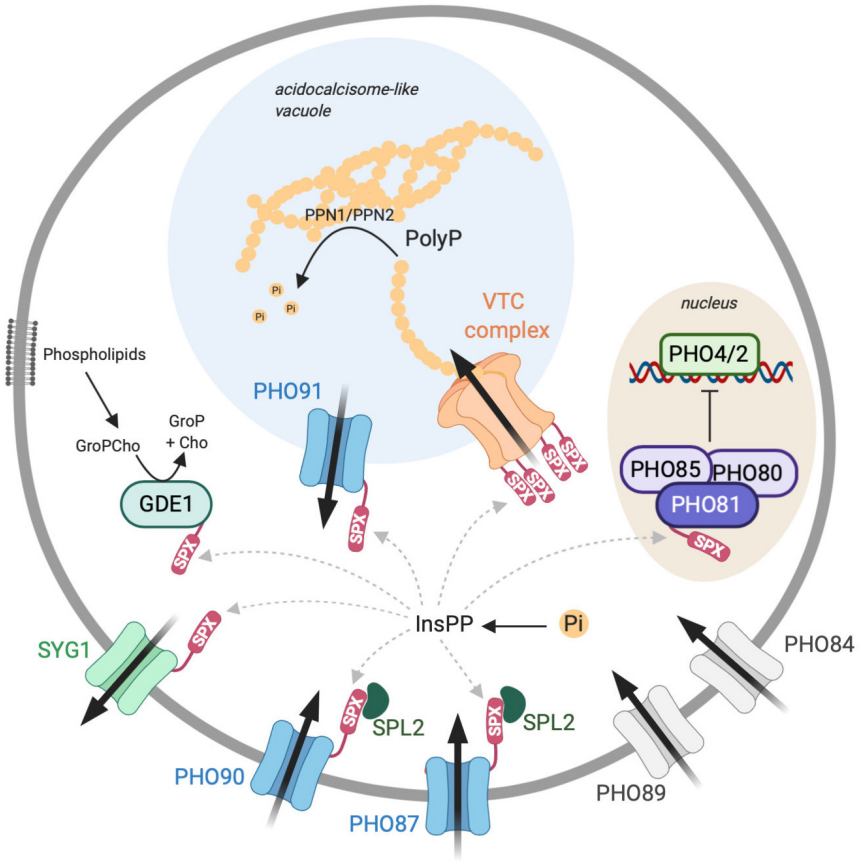


**FIGURE 2 |** The INPHORS (intracellular phosphate reception and signaling) pathway for inorganic phosphate ($P_i$) homeostasis in the cytosol, based on known components from *Saccharomyces cerevisiae*. $P_i$ can be imported into the cytosol by high-affinity (*Pho89/84*) and low-affinity importers (*Pho87/90*) and by a $P_i$-permeable vacuolar channel (*Pho91*). It can be exported from the cytosol by secretion into the extracellular space (*Syg1*) or by conversion into polyphosphate (polyP) and transferred into the acidocalcisome-like vacuole (*VTC*). Inside this organelle, polyphosphatases can reconvert polyP into $P_i$ to make it available for export into the cytosol. A $P_i$-regulated kinase (*Pho80/85/81*) phosphorylates transcription factors (*Pho4/2*) for the transcriptional phosphate starvation response. A sensor for cytosolic $P_i$ might regulate the levels of inositol pyrophosphates (InsPPs; e.g., 5-InsP$_7$), which then act on SPX domains. These should, when bound to InsPPs, inactivate proteins importing $P_i$ and activate proteins exporting $P_i$ from the cytosol.

signal transduction (PHO) pathway (Yoshida et al., 1989b). The PHO pathway is regulated through a $P_i$-responsive kinase (Pho80/Pho85/Pho81), which phosphorylates the transcription factor Pho4, thereby keeping it inactive. $P_i$ starvation favors the dephosphorylation of Pho4 and allows it to activate a wide spectrum of genes dedicated not only to $P_i$ import and storage but also to foraging for extracellular $P_i$ and the recycling of intracellular phosphate (Carroll and O'Shea, 2002). The response is graded: Upon moderate phosphate starvation, high-affinity $P_i$ importers (Pho84) and the polyP polymerase VTC are induced, whereas proteins for $P_i$ foraging are upregulated only upon further $P_i$ limitation (Vardi et al., 2014). This includes phosphatases that are secreted from the cells in order to recover $P_i$ from phosphorylated substrates in their environment (Oshima, 1997). In addition, phosphate starvation leads to the enhanced production of proteins for $P_i$ recycling, which allows the cell to recover $P_i$ from internal molecules (Ogawa et al., 2000). Examples are the glycerophosphodiesterase Gde1 (Fisher et al., 2005; Patton-Vogt, 2007), which can remove $P_i$ from intermediates of lipid metabolism, or Phm8, which dephosphorylates nucleoside monophosphates (Xu et al., 2013). For all of these systems, it has remained enigmatic how $P_i$ availability is measured in order to regulate them.

Yeast cells thus use multiple systems and mechanisms to control cytosolic $P_i$. We can expect that this results in a high degree of redundancy, which can be taken as an indication that $P_i$ homeostasis is of critical importance for the cells. For the exploration of $P_i$ homeostasis, this comes as a blessing and a curse at the same time: On the one hand, mutants in a single compound of this complex system will usually be viable and amenable to investigation, but, on the other hand, redundancy renders it more difficult to generate clear phenotypes that are necessary to analyze its function.

Cells should benefit from information about the concentrations of free $P_i$ in their environment, within the cytoplasm, and within the subcellular compartments. How cells perceive or measure these important parameters is not well understood at this point. Available evidence suggests a

transceptor for extracellular $P_i$. A transceptor is a transporter that senses an external substrate independently of its transport activity. Pho84 was (together with the low-affinity transporter Pho87) proposed to sense extracellular $P_i$ in this manner and to regulate intracellular responses, such as the protein kinase A (PKA) pathway (Giots et al., 2003; Mouillon and Persson, 2005, 2006; Popova et al., 2010). The transceptor does not appear to address all $P_i$-regulated events because a major $P_i$-dependent response, the transcriptional starvation response (PHO pathway), reacts to intracellular rather than extracellular $P_i$, arguing against a general role of Pho84 or Pho87 in $P_i$ sensing (Wykoff and O'Shea, 2001; Auesukaree et al., 2004; Desfougères et al., 2016). We thus face the possibility that cells may use at least two different signaling mechanisms that distinguish between cytosolic and extracellular $P_i$. Such a differentiation might be useful because the PKA pathway is particularly important when cells exit a growth arrest resulting from nutrient limitation (Conrad et al., 2014). In this situation—of a non-dividing cell—cytosolic $P_i$ is not a useful readout because there is no $P_i$ consumption and, hence, the cytosolic concentration may easily be sufficient. The decision to reenter the cell cycle can more reliably be instructed by information about the external $P_i$ supply, which will be necessary to support the next S-phase. Hence, the interest of a transceptor. In contrast, the measurement of cytosolic $P_i$ is highly relevant in an actively growing and dividing cell because, here, the duplication of all cellular components requires the uptake of enormous amounts of $P_i$. In this situation, the exhaustion of an existing external $P_i$ resource usually occurs gradually, calling for the activation of additional $P_i$ foraging, which is one of the main purposes of the phosphate starvation response. However, the consumption of cytosolic $P_i$ changes drastically in the different phases of the cell cycle, being by far the highest in the S-phase. A dividing cell will therefore have to closely monitor and regulate its cytosolic $P_i$ in order to avoid large changes in this critical parameter. The sensing mechanism for intracellular $P_i$ should hence address multiple proteins for the mobilization, transport, and storage of $P_i$ in order to stabilize the $P_i$ concentration in the cytosol in the face of a grossly fluctuating demand.

## INPHORS: A CONSERVED PHOSPHATE SIGNALING PATHWAY FOR INTRACELLULAR $P_i$

A yeast cell thus uses multiple and potentially redundant systems to supply $P_i$ to the cytoplasm or withdraw it from there. A key question is how the activities of these systems are coordinated. An important hint in this respect comes from the sequences of these proteins since many of them carry an SPX (*S*yg1/*P*ho81/*X*PR1) domain. The fact that all of the 10 yeast proteins that contain an SPX domain are involved in $P_i$ homeostasis strongly suggests a role of this domain in coordinating $P_i$ signaling (Secco et al., 2012a,b). SPX appears to act in conjunction with inositol pyrophosphates (InsPPs), molecules which are also critical for $P_i$ homeostasis (Auesukaree et al., 2005; Wild et al., 2016).

InsPPs are highly phosphorylated inositol species with at least one pyrophosphate moiety. Their abundance increases in correlation with the availability of $P_i$ in the media (and hence presumably in response to the resulting changes in cytosolic $P_i$) (Lee et al., 2007; Lonetti et al., 2011; Wild et al., 2016; Gu et al., 2017). They bind to the SPX domains, through which they modulate the activity of the target proteins associated with these domains, such as polyP polymerases, $P_i$ transporters, or $P_i$-dependent plant transcription factors (Wild et al., 2016; Puga et al., 2017). A variety of InsPP isomers exist in cells (**Figure 3**), but it is unclear whether different isomers assume different signaling functions, and might represent an inositol pyrophosphate "code" (Azevedo and Saiardi, 2017; Gerasimaite et al., 2017; Shears, 2017). Available data do not provide a consistent picture. Whereas studies on the transcriptional phosphate starvation response (PHO pathway) concluded that phosphate starvation is signaled through increasing the 1-$InsP_7$ concentration (Lee et al., 2007, 2008), later studies on the VTC complex indicated that phosphate starvation is signaled by a decline of 5-$InsP_7$ (Lonetti et al., 2011; Wild et al., 2016; Gerasimaite et al., 2017). In contrast, studies on the mammalian $P_i$ exporter XPR1 provided strong evidence for its exclusive regulation through 1,5-$InsP_8$ (Li et al., 2020). Further work will be necessary to clarify whether the transcriptional phosphate starvation response and the transport and storage of $P_i$ through SPX-containing proteins are indeed regulated by different inositol pyrophosphate isomers or whether these isomers might serve as signals to integrate different physiological parameters with $P_i$ signaling (Azevedo and Saiardi, 2017; Shears, 2017).

SPX domains and InsPPs were found in many eukaryotes, and mutations affecting them give corresponding phenotypes (Secco et al., 2012a; Wilson et al., 2013; Shears, 2015; Wild et al., 2016; Puga et al., 2017). Since, in addition, SPX domains are frequently associated with proteins that mediate the uptake, export, storage, or foraging for $P_i$, we can postulate an evolutionarily conserved signaling pathway in which cytosolic $P_i$ is measured, translated into a corresponding change of InsPPs, and thereby communicated to a multitude of SPX-containing proteins (**Figure 2**). We term this pathway INPHORS (intracellular phosphate reception and signaling). We postulate that InsPPs address these proteins in a coordinated fashion in order to maintain cytosolic $P_i$ in a suitable range. Then, we must expect that SPX domains bound to inositol pyrophosphates can have either activating or inactivating effects, depending on the proteins that they associate with. Since the levels of inositol pyrophosphates increase with the level of available $P_i$, proteins exporting $P_i$, either across the plasma membrane or into intracellular storage places such as the acidocalcisome-like vacuole, should be activated by inositol pyrophosphate-bound SPX. Likewise, we should expect that the activation of the transcriptional phosphate starvation response, the PHO pathway, should be repressed by InsPPs. This scheme is partially consistent with existing data because the SPX-containing polyP polymerase VTC is activated through the interaction between its SPX domains and the inositol pyrophosphate 5-$InsP_7$ (Auesukaree et al., 2005; Lonetti et al., 2011; Wild et al., 2016; Gerasimaite et al., 2017) and because the low-affinity $P_i$

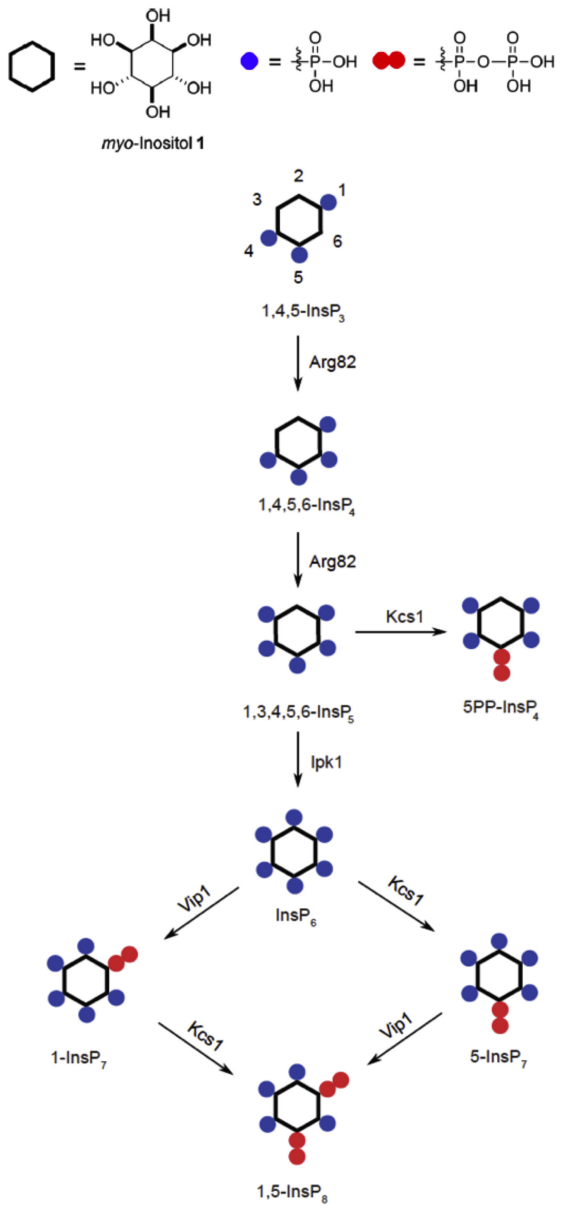


**FIGURE 3 |** Synthesis of inositol pyrophosphates (InsPPs) in yeast cells, starting from $InsP_3$. Responsible enzymes are indicated for each step. *Blue dots* indicate a phosphoryl group and *pairs of red dots* a pyrophosphoryl group on the inositol ring.

importers Pho87 and Pho90 are inhibited by their respective SPX domains (Hürlimann et al., 2009). In contrast, conflicting data exist on other SPX proteins. The SPX-containing kinase Pho85/80/81, which represses the PHO pathway, was reported to be silenced by the inositol pyrophosphate 1-$InsP_7$ (Lee et al., 2007). Furthermore, patch-clamp experiments suggested that the vacuolar $P_i$ exporter Pho91 is activated by 5-$InsP_7$ (Potapenko et al., 2018), although we would expect the inverse. It has also been suggested that inorganic pyrophosphate (PPi) can stimulate Pho91 (Potapenko et al., 2019). An argument against this hypothesis is that stimulation was observed with a high concentration of this compound, which is toxic in yeast and maintained at very low cytosolic levels by the essential enzyme Ipp1 (Serrano-Bueno et al., 2013). Further analyses will be needed in order to elucidate the reasons for the inconsistencies mentioned above and/or to allow us to revise our working hypothesis.

## THE $P_i$ TRANSPORTERS OF YEAST

Yeast cells can take up $P_i$ through five transporters (Pho84, Pho87, Pho89, Pho90, and Pho91). The deletion of all five transporters together is lethal, but the quintuple mutant can be rescued by the overexpression of any one of these five importers (Wykoff and O'Shea, 2001) or by the overexpression of *GIT1*, a glycerophosphoinositol permease that also transports $P_i$ and glycerol-3-phosphate (Wykoff and O'Shea, 2001; Popova et al., 2010). A further transporter in the plasma membrane, Syg1, is presumed to export $P_i$ due to its homology to the mammalian $P_i$ exporter XPR1 (Giovannini et al., 2013).

### High-Affinity $P_i$ Transporters: Pho84 and Pho89

Pho84 and Pho89 are high-affinity transporters since they permit the uptake of $P_i$ from low-$P_i$ media (<0.2 mM) with a $K_m$ of 8–40 μM (Bun-ya et al., 1991; Wykoff and O'Shea, 2001; Auesukaree et al., 2003; Levy et al., 2011). While Pho84 is a $H^+$ symporter with a pH optimum in the acidic range (Bun-ya et al., 1991; Pérez-Sampietro et al., 2016), Pho89 is active at alkaline pH and driven by $Na^+$ (Martinez and Persson, 1998; Zvyagilskaya et al., 2008; Serra-Cardona et al., 2014). In addition to $P_i$, Pho84 serves also for the low-affinity co-transport of manganese ions (Jensen et al., 2003) and for the import of selenite (Lazard et al., 2010). Pho84 is highly expressed at intermediate concentrations of $P_i$ (<0.5 mM), but becomes transferred to the vacuole for degradation in the absence of $P_i$ or at high excess of $P_i$ (Petersson et al., 1999; Pratt et al., 2004; Lundh et al., 2009). Pho84 allows the cells to exploit very low $P_i$ concentrations, and their growth arrests only below a threshold of 5 μM. In standard $P_i$-rich media, Pho84 is required for the maintenance of normal polyP levels (Hürlimann et al., 2007) and for repressing transcription through the PHO pathway (Wykoff et al., 2007). However, constitutive activation of the PHO pathway in cells lacking Pho84 does not reflect a major contribution of this high-affinity transporter to $P_i$ uptake under $P_i$-replete conditions. It is rather the consequence of the downregulation of the low-affinity transporters, which results from the deletion of PHO84 due to feedback regulation (Wykoff et al., 2007; Vardi et al., 2013). This feedback regulation creates a bistable, Spl2-dependent switch, which dedicates cells either to the $P_i$-starved regulatory state (downregulating the low-affinity $P_i$ transporters and inducing the PHO pathway) or to the $P_i$-replete state (stabilizing the low-affinity transporters and repressing the PHO pathway). 14-3-3 proteins (Bmh1 and Bmh2, which also interact with the inositol hexakisphosphate kinase Kcs1) were proposed to influence this commitment (Teunissen et al., 2017), but the nature of their influence has not yet been

resolved. The decision between the two states may depend on small differences in the cytosolic $P_i$ concentration, i.e., on the degree to which cells experience $P_i$ limitation, or on stochastic fluctuations. The bistable switch allows a fraction of the cells in a population to stably maintain their commitment to the phosphate starvation response for multiple generations—even after phosphate has been replenished. This can be seen as a potential advantage because these cells would be best prepared for a sudden drop in $P_i$ availability and facilitate the survival of the population under such conditions.

As mentioned above, Pho84 has also been proposed to act as a $P_i$ transceptor, which could provide an alternative explanation how it represses the PHO pathway under phosphate-replete conditions. Obtaining clear evidence for an activity as a transceptor is difficult because it requires maintaining signaling while suppressing the transporter function entirely. In the case of Pho84, one caveat is that the substrates that were used to induce putative transceptor signaling in the absence of transport, such as glycerol-3-phosphate, might be hydrolyzed extracellularly by yeast and the released $P_i$ taken up by Pho84 (Popova et al., 2010). Also, transport-deficient point mutants retain low-capacity transport, which, in a $P_i$-starved, non-dividing cell, may nevertheless suffice to satisfy the needs. Finally, the complex feedback regulation mentioned above complicates the interpretation of the experiments that suggested Pho84 as a transceptor (Giots et al., 2003; Mouillon and Persson, 2005; Popova et al., 2010; Samyn et al., 2012).

## SPX-Containing Low-Affinity $P_i$ Transporters: Pho87 and Pho90

Pho87 and Pho90 are two low-affinity plasma membrane transporters which mediate the uptake of $P_i$ from the environment with $K_m$ values of 200–800 μM (Tamai et al., 1985; Wykoff and O'Shea, 2001; Auesukaree et al., 2003; Giots et al., 2003; Pinson et al., 2004; Hürlimann et al., 2007, 2009). They belong to the divalent anion:$Na^+$ symporter (DASS) family. Both Pho87 and Pho90 harbor an SPX domain at their N-terminus. Removal of this SPX domain leads to phenotypes suggesting an enhanced, unrestricted flux of $P_i$ across these transporters: up to an eightfold increased $P_i$ uptake activity, higher total phosphate, and higher polyP content. Cells expressing Pho90 without an SPX domain also become sensitive to high $P_i$ concentrations in the media, and they show an enhanced leakage of cellular $P_i$ on low-$P_i$ media (Hürlimann et al., 2009). Together, these observations indicate that the SPX domain has a restrictive function on Pho87 and Pho90, which is necessary to close these transporters at excessively high and low concentrations of $P_i$.

The transcription of the *PHO87* and *PHO90* genes is independent of $P_i$ availability, but the transporters are targeted to the vacuole and degraded in response to $P_i$ limitation (Auesukaree et al., 2003; Wykoff et al., 2007; Hürlimann et al., 2009; Ghillebert et al., 2011). This targeting requires their SPX domain and, for Pho87, also Spl2. But why do cells have low-affinity transporters in addition to a high-affinity system? When the low-affinity importers are ablated, the cells compensate by expressing more Pho84, and this largely rescues their $P_i$ uptake activity. While this demonstrates that a high-affinity transporter can substitute for the low-affinity system, even under high-$P_i$ conditions (Wykoff and O'Shea, 2001; Pinson et al., 2004; Ghillebert et al., 2011), it brings up the question what benefit a cell draws from expressing low-affinity transporters when it has high-affinity transporters available. An advantage becomes apparent in situations where Pi gradually becomes limiting, for example in a culture that is exhausting the available Pi as it grows. At an intermediate $P_i$ concentration, both high- and low-affinity transporters are expressed. The decrease in $P_i$ availability can be detected earlier and over a much larger range of external $P_i$ concentrations when the cells use low-affinity transporters as long as $P_i$ is abundant and begin to express high-affinity transporters only once $P_i$ becomes scarcer. In an environment of gradually depleting $P_i$, this provides for a longer transition phase from $P_i$-replete conditions to full $P_i$ starvation, giving the cells much more time to adapt and prepare for $P_i$ starvation (Levy et al., 2011). This leads to enhanced recovery from growth arrest once $P_i$ becomes available again.

## SPX-Controlled Vacuolar $P_i$ Transporter: Pho91

Pho91 is a low-affinity $P_i$ transporter. Like the low-affinity $P_i$ transporters Pho90 and Pho87, it belongs to the DASS family and its expression is independent of $P_i$ supply (Auesukaree et al., 2003). However, a green fluorescent protein (GFP) fusion of Pho91 is localized to vacuoles (Hürlimann et al., 2007). When overexpressed in a mutant lacking all other $P_i$ importers, Pho91 can nevertheless support the growth and $P_i$ uptake of cells with a $K_m$ of around 200 μM (Wykoff and O'Shea, 2001). Initially, this was taken as an indication that it operates at the plasma membrane. However, yeast cells can take up nutrients also by other routes—as shown for magnesium, which can be acquired by endocytic transfer to the vacuole lumen and subsequent transport across the vacuolar membrane into the cytosol (Klompmaker et al., 2017). Such an uptake route *via* vacuoles might also allow $P_i$ acquisition through Pho91. In further support of a function at the vacuolar membrane, the ablation of Pho91 leads to an overaccumulation of phosphate in vacuoles, whereas its overexpression depletes this vacuolar pool. This led to the proposal that Pho91 transfers $P_i$ from vacuoles to the cytosol (Hürlimann et al., 2007).

This view could be confirmed by electrophysiological analysis of Pho91 and of its homologs from rice OsSPX-MFS3 and *Trypanosoma brucei* TbPho91 (Wang et al., 2015; Potapenko et al., 2018), where a $Na^+$-dependent transport of $P_i$ into the cytosol with $K_m$ values of 1–10 mM could be demonstrated. The transport activity is highly pH-dependent, as demonstrated for OsSPX-MFS3 (Wang et al., 2015). Whereas net charge transport occurs at neutral pH, the protein does not mediate significant $P_i$ transport under these conditions. $P_i$ is only transported in the presence of a pH gradient, when the extra-cytosolic face of the protein is exposed to acidic pH. This pH dependency corresponds to the natural condition under which these Pho91-like transporters operate because the lumen of the vacuoles in which they reside is much more acidic than the cytosol. In the

absence of a pH gradient, OsSPX-MFS3 mediates $P_i$ efflux from the cytosol (Wang et al., 2015). For TbPho91 and Pho91, it was shown that charge transport depends on their SPX domain and on 5-$InsP_7$. Other inositol polyphosphates, such as 1-$InsP_7$ or $InsP_6$, do not activate the channel (Potapenko et al., 2018). However, these experiments have been conducted in the absence of a proton gradient across the membrane. Thus, while they demonstrate a regulatory impact of SPX and 5-$InsP_7$ on the transporter, their effects on $P_i$ transport under a pH gradient remain to be determined.

Overall, these observations suggest that Pho91 transports $P_i$ from the vacuole into the cytosol (Hürlimann et al., 2007), which might be necessary to allow the degradation of vacuolar polyP. It might then be a critical element of the system to buffer cytosolic $P_i$ *via* polyP (Neef and Kladde, 2003; Thomas and O'Shea, 2005). However, direct evidence for an impact of Pho91 on cytosolic $P_i$ and a coherent model for the functioning of a vacuolar, polyP-based $P_i$ buffer is still missing.

### The SPX-Containing Putative $P_i$ Exporter Syg1

Syg1 was identified as a genetic suppressor of defects in pheromone signaling and predicted to be on the plasma membrane (Spain et al., 1995). Syg1, the mammalian transporter XPR1, and the related PHO1 from *Arabidopsis* share around 30% of sequence identity and some common features, such as an N-terminal SPX and a C-terminal EXS (for ERD1/XPR1/SYG1) domain. The function of the EXS domain is still unknown. Although the transport activity for Syg1 itself has not yet been shown, its human homolog XPR1 does facilitate $P_i$ export across the plasma membrane (Giovannini et al., 2013; Wilson et al., 2019; Li et al., 2020). Export depends on its SPX domain and on 1,5-$InsP_8$. Thus, Syg1 likely acts as a $P_i$ exporter in yeast.

## POLYPHOSPHATE METABOLISM AND PHOSPHATE HOMEOSTASIS

Inorganic polyphosphate is a polymer of dozens to hundreds of orthophosphate ($P_i$) linked by energy-rich phosphoric anhydride bonds. PolyP efficiently chelates ions such as $Ca^{2+}$, $Mg^{2+}$, and $Mn^{2+}$. Yeast cells can accumulate up to a quarter of their dry weight in the form of polyphosphate (Langen and Liss, 1958), located mostly in their acidocalcisome-like vacuole (Saito et al., 2005). Minor amounts have also been associated with other organelles, such as mitochondria, the ER, or the periplasmic space (Pestov et al., 2004; Lichko L. et al., 2006; Kulakovskaya et al., 2010). The sequestered polyP is not an immobile aggregate. Instead, it appears to be highly mobilizable (Wiame, 1947; Urech et al., 1978). PolyP is necessary to rapidly buffer changes in the cytosolic phosphate levels that can result from sudden changes in $P_i$ availability or consumption (Neef and Kladde, 2003; Thomas and O'Shea, 2005). The polyP in the acidocalcisomes of other organisms can also be mobilized, for example upon osmotic challenges or changes in nutrient supply (Docampo and Huang, 2016). The accumulation of polyP has a strong impact on cytosolic $P_i$ homeostasis and should hence be carefully controlled by the cell (Desfougères et al., 2016). However, it remains a major unsolved question how the synthesis and degradation of polyP are coordinated to achieve this goal. While we have some insights into the synthesis of polyP, it remains an enigma how the cells can store polyP in a compartment that contains considerable polyphosphatase activities and how the conversion of polyP back into cytosolic $P_i$ is regulated (Gerasimaite and Mayer, 2016).

### PolyP Synthesis by the VTC Complex

The VTC proteins form complexes which all contain Vtc1, a 14-kDa integral membrane protein that spans the membrane three times, and Vtc4, the catalytically active subunit that synthesizes polyP from nucleotide triphosphates (Müller et al., 2002, 2003; Hothorn et al., 2009). Catalytic activity requires $Mn^{2+}$, which is located in the active site. All VTC proteins have a transmembrane region similar to Vtc1. In contrast to Vtc1, the other VTC proteins contain an additional SPX domain at the N-terminus and a hydrophilic central domain, both facing the cytosolic side of the membrane (Müller et al., 2003). The central domain accommodates the catalytic center in Vtc4, whereas it is assumed to have only regulatory, non-catalytic function in Vtc2, Vtc3, and Vtc5 (Hothorn et al., 2009; Desfougères et al., 2016). VTC complexes exist in different isoforms, which contain Vtc1 and Vtc4, plus either Vtc2 or Vtc3. Vtc5 can associate with VTC to increase its activity, but VTC functions at a lower basal activity without it (Desfougères et al., 2016). Vtc1/2/4 is mainly localized in the ER, whereas Vtc1/3/4 concentrates on the vacuoles, when the cells are cultivated in $P_i$-replete media. Under $P_i$ limitation, both complexes localize to the vacuoles (Hothorn et al., 2009).

VTC acts not only as a polyP polymerase but at the same time as a polyP translocase. It couples the synthesis of polyP at the cytosolic face of the membrane with its translocation into the lumen of the organelle (Gerasimaite et al., 2014). Continued synthesis of polyP by VTC requires the electrochemical gradient across the vacuolar membrane, which is established by V-ATPase. This gradient is assumed to provide the driving force translocating the negatively charged polyP chain (Wurst et al., 1995; Gerasimaite et al., 2014).

The activity of VTC can be assayed on isolated yeast vacuoles (Gerasimaite et al., 2014). This *in vitro* system allowed the discovery of the regulation of SPX domains through inositol pyrophosphates (Wild et al., 2016). While SPX domains bind various inositol polyphosphates and pyrophosphates with $K_d$ values in the low micromolar or even sub-micromolar range (Wild et al., 2016), these different isomers show strikingly different agonist properties on VTC. Only InsPPs stimulate the enzyme at low micromolar concentrations, with 5-$InsP_7$ being the isomer that appears to regulate VTC *in vivo* (Gerasimaite et al., 2017). Since $InsP_7$ increases when cells are in $P_i$-replete conditions and decreases under $P_i$ starvation (Lonetti et al., 2011; Wild et al., 2016), VTC should synthesize polyP when cytosolic $P_i$ is sufficiently high, but it should be switched off when this parameter is too low. This reflects the *in vivo* situation because cells accumulate polyP stocks when sufficient $P_i$ is still available and they deplete this stock under $P_i$ starvation or upon a transient excessive consumption of $P_i$ during the S-phase (Langen and Liss, 1960;

Bru et al., 2016). That VTC must be carefully controlled by the cells is also suggested by the fact that it has a major impact on cytosolic $P_i$. Inappropriate overactivation of VTC can lead to $P_i$ depletion from the cytosol and activate the PHO starvation pathway even on $P_i$-rich media, whereas its silencing can suppress the PHO pathway on media with limiting $P_i$ (Desfougères et al., 2016). PolyP storage is a major function of yeast vacuoles, which is probably the reason why polyP production also activates the vacuolar membrane fusion machinery. The resulting fusion of several vacuoles together increases the volume of the compartment, thereby accommodating the need for increasing storage space in a rapid and efficient manner (Müller et al., 2002; Desfougères et al., 2016).

## Polyphosphatases

### The Exopolyphosphatase Ppx1

Ppx1 is a member of the DHH phosphoesterase superfamily, together with h-prune, a mammalian exopolyphosphatase (Tammenkoski et al., 2008). Ppx1 is a soluble enzyme which hydrolyzes polyP to release $P_i$ and $PP_i$ (Wurst and Kornberg, 1994). Hydrolysis is processive, i.e., the enzyme does not leave the polyP chain after having hydrolyzed its terminal $P_i$ residue. Ppx1 hydrolyzes polyP chains as short as three $P_i$ residues, but cannot degrade $PP_i$ and ATP. The enzyme is metal-dependent, with a preference for $Mg^{2+}$, and active from pH 5.5 to 9 (Tammenkoski et al., 2007).

Ppx1 is expressed irrespective of $P_i$ availability (Ogawa et al., 2000). Initial studies ascribed it to the cytosol, but exopolyphosphatase activities in the plasma membrane and mitochondrial fractions were also related to Ppx1 (Lichko et al., 2003; Lichko L.P. et al., 2006). High-throughput localization studies through GFP fusion proteins suggested localization in the cytosol, but also some enrichment in the nucleus (Huh et al., 2003). In any case, Ppx1 appears to be localized outside the vacuoles, where the major polyP stores are kept. In line with this, its deletion affects neither the chain length nor the abundance of polyP in the cell (Lonetti et al., 2011). It was hence proposed that Ppx1 might counteract an the accumulation of polyP in the cytosol, which is toxic for cells (Gerasimaite et al., 2014). A further attractive possibility is that Ppx1 might trim polyP from proteins that are covalently modified with this polymer (Azevedo et al., 2015, 2018, 2019).

### The Vacuolar Endopolyphosphatases Ppn1 and Ppn2

In its active, homo-tetrameric state, Ppn1 is a non-processive endopolyphosphatase which preferentially hydrolyzes long polyP in the midst of the chain rather than at its terminal phosphate residues. Depending on the conditions, however, it was also reported to have exopolyphosphatase activity *in vitro* (Kumble and Kornberg, 1996; Andreeva et al., 2015). Ppn1 activity requires $Mn^{2+}$ or $Mg^{2+}$. The enzyme can hydrolyze polyP down to $P_i$ and tripolyphosphate, whereas pyrophosphate and ATP are potent inhibitors (Kumble and Kornberg, 1996). PPN1 gene expression is induced under $P_i$ limitation, i.e., when vacuolar polyP pools are consumed (Kumble and Kornberg, 1996). PPN1 knockouts retain polyP in similar amounts as wild types, but their polyP is of higher chain length.

Ppn2 is a member of the phospoprotein phosphatase (PPP) superfamily of metallophosphatases that resides in the vacuolar lumen. The enzyme depends on $Zn^{2+}$ and exclusively shows endopolyphosphatase activity (Gerasimaite and Mayer, 2017). Ppn1 and Ppn2 together constitute the major part of the vacuolar polyphosphatase activity. They are necessary to mobilize polyP stores under $P_i$ starvation. In their absence, the cells accumulate polyP of excessively high chain length and they virtually show no short-chain polyP anymore.

# PHOSPHATE "RECYCLING"

When $P_i$ becomes limiting, the cells use the PHO pathway to induce first the high-affinity transporter Pho84. They secrete phosphatases to recover $P_i$ from external sources and induce VTC expression to maximize their polyP stores (Ogawa et al., 2000; Springer et al., 2003; Thomas and O'Shea, 2005; Wykoff et al., 2007; Vardi et al., 2014). When the cells really starve for $P_i$, the polyP stores are hydrolyzed (Langen and Liss, 1958; Sethuraman et al., 2001; Neef and Kladde, 2003; Thomas and O'Shea, 2005; Gerasimaite and Mayer, 2017). Using this strategy might be helpful to allow redifferentiation and ordered transition into the quiescent state (the $G_0$ phase of the cell cycle), in which cells arrest growth and become more resistant to stresses (De Virgilio, 2011). This important transition often coincides with the induction of autophagy, which transfers large amounts of cytosolic material, including RNA and organelles, into vacuoles for degradation (De Virgilio, 2011). Their hydrolysis provides the cells with a source of degradable nucleotides and phospholipids. Profound $P_i$ starvation induces the expression of enzymes that release $P_i$ from these internal molecules. It appears likely that this represents a "last resort" because it makes little sense for a cell to deplete its pools of nucleotides or phospholipids, which are indispensable for the next cell division, unless it is the only means to survive. In line with this, cells in which these recycling pathways have been ablated show poor long-term survival on $P_i$-free media (Xu et al., 2013).

Gde1 is a glycerophosphocholine phosphodiesterase which hydrolyzes glycerophosphocholine to glycerol-3-phosphate and choline (Fisher et al., 2005). Glycerol-3-phosphate can either be channeled into the synthesis of new phospholipids, into glycolysis, or it can be hydrolyzed by the glycerol-3-phosphatases Gpp1 and Gpp2 (Patton-Vogt, 2007). All these pathways effectively lead to the recycling of internal $P_i$. They are of sufficiently high capacity to allow the cells to grow on glycerophosphocholine as the sole source of phosphate. That the recycling activity of Gde1 may be relevant to the maintenance of cytosolic $P_i$ homeostasis is suggested by the fact that GDE1 gene expression is regulated by the PHO pathway and strongly induced in low-$P_i$ conditions (Ogawa et al., 2000; Almaguer et al., 2004). Furthermore, Gde1 carries an N-terminal SPX domain, which is expected to subject the enzyme to regulation by the INPHORS pathway. However, the regulatory role of this SPX domain has not yet been experimentally confirmed.

Interestingly, Gde1 shares its glycerophosphodiesterase domain with Pho81, a key regulator of the PHO pathway. Whether the glycerophosphodiesterase domain of Pho81 is catalytically active is also unknown.

Phm8 has originally been identified as a lysophosphatidic acid phosphatase (Reddy et al., 2008). Its expression is strongly induced by $P_i$ starvation (Ogawa et al., 2000). Under $P_i$ starvation, yeast cells show a significant reduction in lysophosphatidic acid, and this reduction has been ascribed to Phm8 (Reddy et al., 2008). The enzyme might thus participate in the recycling of phosphate from degraded phospholipids. Phm8 has also been identified as a nucleotide monophosphate phosphatase (Xu et al., 2013). The enzyme allows liberating $P_i$ from a wide variety of nucleoside monophosphates. In its absence, cells cannot survive $P_i$ starvation for prolonged periods of time, underscoring the relevance of its $P_i$ recycling activities in this situation.

The repressible "alkaline" phosphatase Pho8 (Kaneko et al., 1982) shows maximal activity on artificial chromogenic substrates, such as *p*-nitrophenyl phosphate, at alkaline pH. However, the enzyme is membrane-anchored and resides within the vacuole, which is an acidic compartment with a pH ranging from 5 to 6. At this pH, Pho8 exhibits maximal activity toward phosphoserine and phosphothreonine, and it has therefore been proposed that it may serve to dephosphorylate peptides (Donella-Deana et al., 1993), which are imported into vacuoles through autophagy. The expression of the enzyme is induced upon $P_i$ starvation through the PHO pathway (Kaneko et al., 1985). Pho8 can also dephosphorylate fructose-2,6-bisphosphate, which is generated in the cytosol, but the physiological relevance of this activity has remained unexplored, and it remains unclear how fructose-2,6-bisphosphate could be translocated into vacuoles, where Pho8 is located (Plankert et al., 1991). Pho8 may also participate in the recuperation of $P_i$ from $NAD^+$. Upon $P_i$ starvation, part of the nicotinamide nucleotide pool may be converted into nicotinamide riboside, liberating $P_i$ (Lu and Lin, 2011). This conversion requires Pho8 and the vacuolar nucleoside transporter Fun26. Yeast cells with a constitutively activated PHO pathway show increased production and secretion of nicotinamide riboside.

# ELEMENTS OF THE INPHORS PATHWAY

## The PIPP5 Kinase Vip1

Vip1 belongs to a conserved family of diphosphoinositol pentakisphosphate kinases (PPIP5Ks) (Randall et al., 2019). These enzymes contain both a kinase and a histidine acid phosphatase domain, which compete with each other (Mulugu et al., 2007). Their enzymatic and structural properties have mainly been uncovered through studies of the mammalian enzymes (Wang et al., 2012; Weaver et al., 2013; Gu et al., 2017; Nair et al., 2018; Randall et al., 2019), but the essential features could be confirmed for the plant and yeast members of the family (Pöhlmann et al., 2014; Dong et al., 2019; Zhu et al., 2019). The kinase domain phosphorylates $InsP_6$ and 5-$InsP_7$ to generate 1-$InsP_7$ and 1,5-$InsP_8$, respectively, whereby 5-$InsP_7$ appears to be the preferred substrate over $InsP_6$ (Wang et al., 2012; Weaver et al., 2013). The simultaneous presence of competing kinase and phosphatase domains, which, in addition, appear to be coordinated by allosteric effects (Yousaf et al., 2018), has important consequences. It can translate small changes in the concentration of the substrates into much larger changes of product concentration, i.e., it can amplify the response in a signaling cascade. Under suitable conditions (for PIPP5Ks, when only the phosphatase but not the kinase domain is substrate-limited), it can also make the net kinase activity quite insensitive to changes in substrate concentrations (Gu et al., 2017). This property would allow the cell to modulate 5-$InsP_7$ without an immediate impact on the level of 1,5-$InsP_8$, providing an important prerequisite to use these inositol pyrophosphates to communicate different cellular parameters, which might then be integrated by proteins that can "read" several different inositol pyrophosphates, such as SPX domains.

Importantly, the phosphatase activity of PIPP5Ks is inhibitable by $P_i$ in the low millimolar range—a concentration range that is commonly found in the cytosol—and their kinase activity is boosted by an increasing ATP concentration (Gu et al., 2017; Zhu et al., 2019). Since cellular ATP concentration diminishes with cellular $P_i$ availability (Boer et al., 2003), $P_i$ limitation in the cytosol should tip the equilibrium between the kinase and phosphatase activities in favor of dephosphorylation, decreasing the pools of 1,5-$InsP_8$ and 1-$InsP_7$. PIPP5Ks might thus provide an important link between the $P_i$ concentration and the corresponding changes in the inositol pyrophosphate levels. However, whether PIPP5Ks represent the critical $P_i$ sensor is not yet clear. Also, the physiological implications of the sensitivity of PIPP5K to phosphoinositides, such as $PI(4,5)P_2$ (Nair et al., 2018), are not yet understood.

## The $InsP_6$ Kinase Kcs1

Kcs1 is a member of the inositol hexakisphosphate kinase family and phosphorylates the phosphate on carbon 5 of $InsP_6$ or $Ins(1,3,4,5,6)P_5$, creating 5-$InsP_7$ or 5PP-$InsP_4$, respectively (Saiardi et al., 1999, 2000; **Figure 3**). The physiological relevance of 5PP-$InsP_4$ is uncertain because it accumulates to appreciable levels only in a mutant lacking IPK1, which cannot convert $Ins(1,3,4,5,6)P_5$ into $InsP_6$ and, hence, does not offer $InsP_6$, which is the far more abundant substrate of Kcs1 in a wild-type cell, where it probably outcompetes $Ins(1,3,4,5,6)P_5$. Kcs1 shares a PxxxDxKxG motif in its catalytic site with other members of the family. The ablation of Kcs1 activity leads to the constitutive activation of the PHO transcription pathway even on high-$P_i$ media, to an overaccumulation of $P_i$ and ATP, and to a complete absence of polyP synthesis (Auesukaree et al., 2005; Lonetti et al., 2011; Szijgyarto et al., 2011; Wild et al., 2016). In contrast, KCS1 overexpression represses the PHO pathway even under $P_i$ limitation, where it would normally be maximally active (Auesukaree et al., 2005). The inactivation of this enzyme thus produces the effects that we would expect if its product 5-$InsP_7$ was a negative regulator of the phosphate starvation response. Erroneous activation of the phosphate starvation program in

a kcs1Δ cell under high-$P_i$ conditions should then lead to an overaccumulation of $P_i$. Although the synthesis of polyP normally occurs under high-$P_i$ conditions (Langen and Liss, 1958), this requires the activation of the VTC complex by 5-$InsP_7$, which is not present in kcs1Δ cells (Lonetti et al., 2011; Wild et al., 2016). Therefore, kcs1Δ mutants cannot accumulate polyP.

Kcs1 has a $K_m$ for $InsP_6$ of 0.6 μM and an exceptionally high $K_m$ for ATP of around 1 mM (Saiardi et al., 1999). By consequence, its activity should be sensitive to the fluctuations of cytosolic ATP concentrations that normally occur in living yeast cells (Saiardi et al., 1999). This may be one reason why mutants in nucleotide metabolism that show constitutively lower cellular ATP levels—and thereby probably lower production of 5-$InsP_7$ and 1,5-$InsP_8$—lead to a constitutive activation of the PHO pathway (Choi et al., 2017). The cellular ATP concentration in wild-type cells declines as a result of $P_i$ limitation (Boer et al., 2010). This opens the possibility that $P_i$ limitation might be translated into a reduction of 5-$InsP_7$ and 1,5-$InsP_8$ through a reduced ATP production.

## The Inositol Pyrophosphatases Ddp1 and Siw14

Inositol pyrophosphates can be turned over by two dedicated phosphatases, which selectively hydrolyze the phosphoric anhydride bonds in these molecules. They have considerable influence on the steady-state levels of inositol pyrophosphates, but it is unknown whether their activity is constitutive or regulated.

Ddp1 belongs to the Nudix hydrolase family. In cells lacking the *DDP1* gene, the abundance of $InsP_7$ increases up to sixfold (Lonetti et al., 2011; Steidle et al., 2016). Ddp1 displays diphosphoinositol polyphosphate hydrolase activity (Safrany et al., 1999). It also exhibits di-adenosine polyphosphate hydrolase activity (Cartwright and McLennan, 1999; Safrany et al., 1999), which is of unclear physiological significance in yeast. Ddp1 can hydrolyze polyP (Lonetti et al., 2011). However, the enzyme is localizing to the cytosol and the nucleus, i.e., out of reach of the major polyP reserves, which are localized in the vacuole (Saito et al., 2005). This makes it unlikely that Ddp1 influences $P_i$ homeostasis through polyP turnover. In line with this, its deletion has no significant impact on the polyP pool (Lonetti et al., 2011). Cells lacking Ddp1 show a 20% reduction of polyP rather than an increase. This reduction might be a secondary consequence of the deregulation of the INPHORS pathway and of an altered cellular $P_i$ homeostasis due to the influence of Ddp1 on inositol pyrophosphates. The polyphosphatase activity of Ddp1 might, however, serve to modify the polyphosphorylation of proteins in the nucleus (Azevedo et al., 2015).

Siw14 belongs to the atypical dual-specificity phosphatase family and hydrolyzes the ß-phosphate of 5-$InsP_7$ with high specificity (Steidle et al., 2016; Wang et al., 2018). Mutants lacking *SIW14* display a sixfold increase in $InsP_7$ content. This effect is synergistic with the simultaneous deletion of *DDP1* and the double mutants display a 20-fold increase in $InsP_7$ (Steidle et al., 2016). Overexpression of *SIW14* depletes the $InsP_7$ pool.

## Inositol Pyrophosphate Receptors: SPX Domains

SPX domains are found in all eukaryotic kingdoms and share common sequence features, most notably clusters of positively charged amino acids. These conserved arginine and lysine residues cluster in a surface patch which forms a high-affinity (sub-micromolar) binding site for inositol polyphosphates and pyrophosphates. Purified SPX domains show a relatively low discrimination in binding different inositol polyphosphates or pyrophosphate isomers, and their affinity decreases in parallel to the net charge of the compound ($InsP_8$ > $InsP_7$ > $InsP_6$). In marked contrast to the low selectivity in binding, the agonist properties of different isomers vary considerably. The VTC complex, for example, is strongly activated by 1,5-$InsP_8$, but very poorly by 5-PPP-$InsP_5$, which carries the same number of phosphate groups (Gerasimaite et al., 2017). Likewise, 5-$InsP_7$ activates VTC, whereas $InsP_6$ has virtually no effect. Thus, despite the extremely high charge density of the inositol polyphosphates and their similar binding affinities, the SPX domain must decode precise structural features of the ligands and translate them into different degrees of activation.

Neither the binding affinity nor the $EC_{50}$ values of inositol pyrophosphate isomers seem to faithfully reflect their physiological relevance for controlling an SPX domain. This could be illustrated with VTC, which has an $EC_{50}$ for 5-$InsP_7$ that is similar to that of 1-$InsP_7$ and is 20-fold higher than that of 1,5-$InsP_8$. Nevertheless, genetic ablation of the enzyme synthesizing 1-$InsP_7$ and 1,5-$InsP_8$ (Vip1) has no significant impact on polyP synthesis *in vivo*. The ablation of 5-$InsP_7$ synthesis (Kcs1), in contrast, eliminates polyP synthesis, strongly suggesting this isomer as the relevant controller of the SPX domains of VTC *in vivo*. Whether 5-$InsP_7$ is the principal regulator also for the other SPX-controlled proteins in the cell is an important issue that remains to be explored. The mammalian $P_i$ exporter XPR1 provides an important example in this respect because this SPX-controlled transporter is opened by 1,5-$InsP_8$ rather than by 1-$InsP_7$ or 5-$InsP_7$ (Li et al., 2020).

## Spl2

Spl2 interacts with the SPX domains of Pho90 and Pho87 and restrains the flux of $P_i$ through Pho90 (Wykoff et al., 2007; Hürlimann et al., 2009). It is transcribed at a basal constitutive level, but it becomes further induced through the PHO pathway upon $P_i$ limitation (Ogawa et al., 1995; Flick and Thorner, 1998). Together with the PHO81 gene, SPL2 was originally identified as a multicopy suppressor of the growth defect resulting from the ablation of the phospholipase C Plc1 (Flick and Thorner, 1998). Plc1 hydrolyzes phosphatidylinositol 4,5-biphosphate into 1,2-diacylglycerol and inositol 1,4,5-triphosphate, which is the precursor for the synthesis of inositol pyrophosphates (Saiardi et al., 2000). The genetic interactions of Spl2, Pho81, and Plc1 can thus be rationalized based on the premise that low cytosolic $P_i$ is signaled by low levels of inositol pyrophosphates. The absence of Plc1 activity impairs the synthesis of inositol pyrophosphates and

induces the phosphate starvation response (Auesukaree et al., 2005). When such cells are cultivated on $P_i$-rich standard yeast media, one should expect that they behave incorrectly, i.e., they are maximizing their efforts for $P_i$ uptake although this nutrient is abundant. A resulting excessive $P_i$ concentration in the cytosol is the likely reason for their growth defect. This inappropriate regulation can be mitigated by the overexpression of Spl2, which limits $P_i$ transporter activity (Hürlimann et al., 2009), or by the overexpression of Pho81 (Creasy et al., 1993; Ogawa et al., 1995), which inactivates the transcriptional phosphate starvation response. This sets cells back into the high-$P_i$ mode, which then corresponds again to the $P_i$-rich conditions of standard media, which had been used for these experiments (Flick and Thorner, 1998).

Upon $P_i$ starvation, the low-affinity phosphate transporters Pho87 and Pho90 are endocytosed and targeted to the vacuole. For Pho87 and Pho90, this process depends on their SPX domains. Although the SPX domains of both transporters interact with Spl2, Spl2 is only necessary for the vacuolar targeting of Pho87, which occurs rapidly upon phosphate limitation. The degradation of Pho90, which occurs only after prolonged $P_i$ limitation, is independent of Spl2 (Ghillebert et al., 2011; Pérez-Sampietro et al., 2016). Thus, Spl2 may allow the cells to differentially degrade their low-affinity transporters as a function of declining $P_i$ availability.

The deletion of *SPL2* does not produce a striking growth phenotype on $P_i$-rich standard yeast media (Flick and Thorner, 1998), but it results in an exacerbated sensitivity to selenite, probably due to the resulting hyperactivation of the low-affinity transporter Pho90, which is involved in selenite toxicity (Lazard et al., 2010).

## THE PHO PATHWAY: A TRANSCRIPTIONAL PHOSPHATE STARVATION RESPONSE

The PHO pathway is a transcriptional response pathway that regulates the expression of a wide variety of genes (Ogawa et al., 2000), many of which have been proven beneficial or essential for growth and survival under $P_i$ limitation. The PHO pathway has been studied extensively, providing us with detailed insights into its regulation and with numerous tools to manipulate it. A key element is the nuclear Pho80/85/81 kinase, which is inactivated through its Pho81 regulatory subunit when $P_i$ becomes limiting (Schneider et al., 1994). The kinase subunit Pho85 phosphorylates the transcription factor Pho4 and thereby shifts its localization toward the cytosol (Kaffman et al., 1994; O'Neill et al., 1996). Pho4 localization is hence defined through an equilibrium of Pho85-controlled import and export across the nuclear membrane. The removal of Pho4 from the nucleus under $P_i$-replete conditions represses the expressions of genes controlled by the PHO pathway. In the following, we describe the key regulatory factors, but we will discuss only the most important PHO-regulated target genes.

### The PHO Regulon: Phosphate-Responsive Genes (the PHO Genes)

The transcription factors Pho4 and Pho2 co-regulate the expressions of dozens of genes (Bun-ya et al., 1991; Oshima, 1997; Ogawa et al., 2000). Among these genes are the $P_i$ transporters Pho84 (Bun-ya et al., 1991), Pho89 (Martinez and Persson, 1998), and the ER protein Pho86, which is involved in the targeting and exit of Pho84 from the ER (Yompakdee et al., 1996). PHO genes also encode several phosphatases (Persson et al., 2003): the repressible secreted acid phosphatase Pho5 and the cell wall-associated acid phosphatases Pho11 and Pho12 (Toh-e and Kakimoto, 1975; Arima et al., 1983; Bostian et al., 1983), which liberate $P_i$ from phosphoester substrates; the vacuolar "alkaline" phosphatase Pho8 (Kaneko et al., 1985); and the glycerophosphocholine (GroPCho) phosphodiesterase Gde1 (Ogawa et al., 2000). All genes for the synthesis and degradation of vacuolar polyphosphate (*VTC1* through *VTC5*, *PPN1*, and *PPN2*) are also controlled by the PHO pathway (Ogawa et al., 2000).

The genes of some regulators of the PHO pathway are themselves transcribed under the control of this pathway, such as *PHO81* and *SPL2* (Wykoff et al., 2007; Hürlimann et al., 2009; Ghillebert et al., 2011). As described above, this generates the possibility of positive and negative feedback loops, which can lead to heterogeneity in a yeast population, e.g., with a fraction of cells remaining stably committed to the $P_i$ starvation program even under $P_i$-replete conditions (Wykoff et al., 2007; Vardi et al., 2013, 2014; Estill et al., 2015).

Besides the genes mentioned above, the PHO pathway regulates numerous other genes, among them many open reading frames of unknown function, for which the relationship to $P_i$ homeostasis has not yet been understood (Ogawa et al., 2000). A similar complexity of $P_i$-regulated transcription has been found in other fungi, e.g., in *Cryptococcus neoformans* and *Schizosaccaromyces pombe*, where the number of PHO genes has been determined to be in the range of 130–160 (Henry et al., 2011; Carter-O'Connell et al., 2012; Lev and Djordjevic, 2018). They suggest links of the PHO signaling pathway to cellular transport, carbohydrate and lipid metabolism, and the responses to stress and to chemicals.

### Regulation of PHO Genes During $P_i$ Limitation and Serious $P_i$ Starvation

The transition of *S. cerevisiae* into phosphate starvation is a complex process in which the cells show a graded adaptation to the declining $P_i$ availability and temporally separate waves of gene induction. When $P_i$ gradually becomes limiting, the activity of Pho85 kinase declines, leading first to a partial dephosphorylation of the Pho4 transcription factor. The partially dephosphorylated Pho4 induces only part of the PHO genes, such as the high-affinity transporter Pho84. Others, such as the secreted acid phosphatase Pho5, follow only upon more profound $P_i$ starvation, leading to the inactivation of Pho85 kinase and the full dephosphorylation of Pho4 (O'Neill et al., 1996; Springer et al., 2003; Thomas and O'Shea, 2005). This establishes a

graded response, which first maximizes phosphate acquisition and, upon more serious starvation, activates the recycling of $P_i$ from internal resources.

The activation of the PHO pathway is also influenced by a metabolic intermediate of purine biosynthesis, 5-aminoimidazole-4-carboxamide ribonucleotide (AICAR) (Pinson et al., 2009). AICAR binds Pho2 and Pho4 *in vitro* and promotes their interaction *in vivo*, suggesting a direct effect on these transcription factors. Since AICAR also transcriptionally regulates purine biosynthesis, it may coordinate phosphate acquisition with nucleotide synthesis. Nucleotide synthesis is a major sink for $P_i$, and such coordination might be useful for this reason. Importantly, the activation of the PHO pathway through AICAR does not coincide with a major accumulation of Pho4 in the nucleus, in striking contrast to the induction through Pho85/80/81. AICAR thus represents an alternative pathway to activate the transcription of PHO pathway genes.

Detailed analyses of the temporal pattern of PHO gene activation revealed further features that stabilize the transcriptional response and keep the cells from erroneously self-inactivating the PHO pathway (Vardi et al., 2014). This is relevant under moderate $P_i$ limitation, where such self-inactivation might occur, because the measures by which the cells seek to improve $P_i$ acquisition may completely rectify the initial decline in cytosolic $P_i$ that triggered the starvation response, thereby leading to an oscillation of the PHO pathway activation and inactivation. This cannot happen upon complete depletion of $P_i$ from the media. A decisive difference is thus whether the cells experience only moderate $P_i$ limitation or profound $P_i$ starvation. Upon moderate limitation of $P_i$, a first wave of transcription induces a subset of genes: for the high-affinity $P_i$ importer Pho84; Pho86, which is involved in its biogenesis; the secreted acid phosphatases Pho12 and Pho11 (Vardi et al., 2014); the genes for the VTC complex, which depletes cytosolic $P_i$ and transfers it as polyP into vacuoles; Spl2, which shuts down the low-affinity $P_i$ transporters; and Pho81, which reduces Pho85 kinase activity and promotes Pho4-dependent transcription. This wave of gene induction enhances global $P_i$ absorption and storage by the cells and, at the same time, establishes a positive feedback loop that stabilizes the induction of Pho4-dependent gene expression (Wykoff et al., 2007; Vardi et al., 2013, 2014). This feedback loop maintains the activation of the PHO pathway for several generations, even after the cells have been transferred back into high-$P_i$ media.

Cells experiencing profound $P_i$ starvation (no $P_i$ in the medium) reveal other features. They induce the same set of immediately activated genes as cells in intermediate $P_i$. However, due to the absence of $P_i$ in the media, the induction of these genes cannot suffice to stabilize their cytosolic $P_i$. The more pronounced and stable decline in cytosolic $P_i$ is believed to trigger a second wave of gene inductions 2 h after the first wave (Vardi et al., 2014). This second wave additionally activates genes for the intracellular recuperation of $P_i$ from nucleotides, lipids, and other substrates (Phm8 and Pho8); the high-affinity $P_i$ importer Pho89; and the secreted phosphatase Pho5. This second wave of transcription coincides with the induction of the environmental stress response and a decline in the growth rate. The partial dephosphorylation of the transcription factor Pho4 may be the trigger for the first transcriptional wave (Springer et al., 2003; Vardi et al., 2014), whereas full dephosphorylation of Pho4 might trigger the second wave of induction. Furthermore, the promoter regions of the genes induced in these two waves show characteristic differences that may support this differential activation through their impact on the chromatin structure (Lam et al., 2008), which is also influenced by inositol polyphosphates (Steger et al., 2003).

Upon serious $P_i$ starvation, the cells finally arrest their cell cycle after two further divisions, and they enter into the quiescent $G_0$ phase of the cell cycle. Pho85/80/81 kinase influences the entry and exit into quiescence in at least two ways: It phosphorylates and thereby inhibits the Rim15 kinase, which is a key factor for $G_0$ entry (Wanke et al., 2005). Under $P_i$-replete conditions, Pho85/80/81 is active and phosphorylates Rim15, which then concentrates in the cytosol, where it is sequestered from its nuclear targets that initiate the $G_0$ program. The residue that becomes phosphorylated on Rim15 is the same as the one phosphorylated through the TOR pathway, suggesting that $P_i$ availability is integrated with information about the availability of other nutrients, such as amino acids, at the level of Rim15. Pho85/80/81 also phosphorylates and thereby destabilizes the cyclin Cln3, which is necessary for the exit from $G_0$ (Menoyo et al., 2013). Both activities may synergize to favor an entry into $G_0$ when $P_i$ and, hence, Pho85/80/81 activities are low.

## ELEMENTS OF THE PHO PATHWAY

### Pho85, Pho80, and the Regulation of Transcription Through Pho4 and Pho2

Pho4 is a transcription factor which is expressed independently of the $P_i$ concentration in the medium (Yoshida et al., 1989a). It carries a transactivation domain and a basic helix–loop–helix motif. Pho2 is a transcriptional activator bearing a homeobox (Bürglin, 1988). It interacts with Pho4 (controlling the PHO pathway), but also with a variety of transcription factors, such as Swi5 (controlling mating type switching) and Bas1 (controlling purine and histidine biosynthesis) (Bhoite et al., 2002). Its interaction with Pho4 increases the affinity for Pho4 binding sites in the promoter region of the PHO genes and allows them to recruit the general transcription machinery (Shao et al., 1996; Magbanua et al., 1997a,b).

Pho85 is a cyclin-dependent kinase subunit that associates with at least 10 different cyclins to regulate a wide spectrum of target proteins involved in many cellular processes, such as cell cycle control, storage and metabolism of carbohydrates, amino acid metabolism, and calcium signaling (Toh-E et al., 1988; Toh-E and Nishizawa, 2001; Huang et al., 2007). The cyclins confer target specificity to Pho85. Virtually all Pho85 effects that are directly relevant to phosphate homeostasis are mediated through its association with the cyclin Pho80. Pho80, and by consequence also the Pho85/80 kinase, are localized in the nucleus. This localization is independent of $P_i$ availability (Hirst et al., 1994; Schneider et al., 1994). Pho85/80 is constitutively associated with Pho81, which inhibits its kinase activity under $P_i$ limitation. Nuclear Pho85/80/81 phosphorylates the transcription factor

Pho4 at five sites (O'Neill et al., 1996; Komeili and O'Shea, 1999). One of these phosphorylations blocks the association of Pho4 with the transcription factor Pho2; others promote the interaction of Pho4 with the nuclear export receptor Msn5 (Kaffman et al., 1998a) and impair its interaction with the nuclear import receptor Pse1 (Kaffman et al., 1998b). By means of these phosphorylations, Pho85/80 hinders the transcription of PHO genes in two ways: by impairing the interaction of Pho4 with the second necessary transcription factor Pho2 and by favoring the export of Pho4 into the cytosol.

## Pho81

Pho81 is a cyclin-dependent kinase inhibitor (CKI) and the major regulator of Pho85/80 kinase and the PHO pathway (Schneider et al., 1994). Pho81 binds the Pho80 subunit of the Pho85/80 complex independently of Pi availability, but it inhibits the kinase only in low-$P_i$ conditions (Schneider et al., 1994; Ogawa et al., 1995; O'Neill et al., 1996; Huang et al., 2001). Pho81 can also regulate the Pho85/Pcl7 cyclin-CDK complex in a $P_i$-dependent manner, which controls glycogen metabolism (Lee et al., 2000). PHO81 gene expression is induced by Pho4 upon $P_i$ limitation (Bun-ya et al., 1991; Creasy et al., 1993, 1996; Ogawa et al., 2000), and Pho81 itself is also a substrate for Pho85/80 kinase (Knight et al., 2004; Waters et al., 2004). This creates a possibility for feedback regulation.

Pho81 is a large protein of almost 1,200 amino acids, which can be dissected into three functional domains (Ogawa et al., 1995). An N-terminal SPX domain and a C-terminal part, both of which influence the degree to which $P_i$ starvation can induce the PHO pathway. The central part of the protein contains six ankyrin repeats. Part of these repeats and an adjacent region form a 141-amino acid piece that is sufficient to maintain some $P_i$-dependent regulation of the PHO pathway *in vivo*. The resulting inducibility is limited, however, because this central domain yields only a fivefold induction of the *PHO5* gene on $P_i$-free media, and this only upon overexpression, whereas full-length Pho81, expressed at normal levels from its native promoter, yields an almost 200-fold induction (Ogawa et al., 1995). This central region was later trimmed further to remove the remaining ankyrin repeats, resulting in an 80-amino acid region, termed "minimum domain." Also, the minimum domain allows only a less than 10-fold induction of PHO5 when overexpressed (Huang et al., 2001). Nevertheless, the minimum domain was ascribed a key function in the regulation of the PHO pathway through Pho81 (Lee et al., 2007, 2008). That the other parts of Pho81 may as well play a crucial role in regulation is suggested by the observation that the minimum domain is not sufficient to allow Pho85/80 to regulate the stress response pathway in a $P_i$-dependent manner (Swinnen et al., 2005), which full-length Pho81 does. Furthermore, several mutations leading to the constitutive activation of the PHO pathway lie in the N-terminal part of Pho81 (Creasy et al., 1993; Ogawa et al., 1995), underlining the physiological relevance of this region.

It has been reported that Pho81 requires the PIPP5K Vip1 and its product 1-$InsP_7$ to inhibit Pho85/80 kinase and that $InsP_7$ shows a corresponding increase under $P_i$ starvation (Lee et al., 2007). Although this model has been widely accepted, several observations cannot easily be reconciled with it: Firstly, the $InsP_7$ concentration actually decreases with decreasing $P_i$ availability and Vip1 makes only a minor contribution to the $InsP_7$ pool in rich media (Lonetti et al., 2011; Steidle et al., 2016; Wild et al., 2016). Secondly, the inactivation of the enzymes Plc1, Ipk1, and Arg82, which ablates the synthesis of 1-$InsP_7$ and its precursor $InsP_6$, inhibits Pho85/80 (Auesukaree et al., 2005) instead of showing the activation that one should expect if $InsP_7$ inhibited the enzyme. Thirdly, vip1Δ mutants can also activate the PHO pathway, though with a moderate delay relative to wild-type cells (Choi et al., 2017). Thus, it is currently unclear how the PHO pathway is regulated through inositol pyrophosphates and the availability of $P_i$.

## Control of the PHO Pathway Through Other Parameters Than Pho4 Activation

Besides phosphate limitation, several other conditions can activate PHO genes. Potassium starvation upregulates the *PHO* genes *PHO84*, *PHO5*, and *SPL2* using the *PHO* signaling pathway (Anemaet and van Heusden, 2014; Canadell et al., 2015). Also, growth on acidic or alkaline pH, or the activation of calcineurin, can trigger the PHO pathway (Causton et al., 2001; Serrano et al., 2002; Ruiz et al., 2003; Luan and Li, 2004). The cell cycle activates PHO genes transiently and in a cyclic manner through Pho4 (Spellman et al., 1998), but also through the transcription factor Fkh2 (Pondugula et al., 2009; Korber and Barbaric, 2014; Bru et al., 2016).

While some activation of the PHO pathway may be related to secondary effects of the tested conditions on cytosolic $P_i$ concentration, it is clear that Pho4/Pho2 are not the only transcription factors inducing PHO gene expression. These genes are embedded into a complex network of transcriptional control, which engages many other players, including the SAGA complex (Nishimura et al., 1999), the SWI-SNF complex (Gregory et al., 1999), the nucleosome spacing factor Ino80 (Barbaric et al., 2007), the arginine methyl transferase Hmt1 (Chia et al., 2018), or the transcriptional activator Crz1 (Serra-Cardona et al., 2014). These factors can either directly activate transcription or they may regulate promoter activity through the chromatin structure (Steger et al., 2003; Lam et al., 2008; Korber and Barbaric, 2014).

Yeast cells also perform pervasive transcription, which produces non-coding RNAs (Xu et al., 2009). Antisense transcripts for *PHO5* and *PHO84* mediate an exosome-dependent reduction in the abundance of messenger RNA (mRNA) from these two genes (Camblong et al., 2007) and affect chromatin remodeling during the activation of *PHO5* transcription (Uhler et al., 2007). On the *PHO84* promoter, it recruits the histone deacetylase Hda1, which downregulates transcription (Camblong et al., 2007). At the *KCS1* locus, antisense and intragenic transcripts are produced, and their production depends on the transcription factor Pho4 and on $P_i$ starvation (Nishizawa et al., 2008). These transcripts lead to the synthesis of truncated Kcs1, which is presumed to show lower activity.

Phosphate-dependent regulation of gene expression appears to act also on steps subsequent to the initiation of transcription. For example, Pho92 regulates the degradation of Pho4 mRNA

by binding to its 3′-UTR in a $P_i$-dependent manner (Kang et al., 2014). The nonsense-mediated decay pathway is probably involved in this mRNA degradation reaction through Pop2 and the Ccr4-NOT complex.

## Outlook

$P_i$ homeostasis is an essential and complex aspect of metabolism. Even a simple unicellular organism such as yeast dedicates a significant percentage of its only 6,000 genes on it, underlining its fundamental importance. Many components involved in the $P_i$ homeostasis in yeast are conserved in other organisms, suggesting that there are common approaches to the problem. Others appear functionally conserved, but realized in a quite organism-specific manner. For example, $P_i$-dependent transcriptional control is a widespread phenomenon which is conserved in that it employs SPX domains and InsPPs, and we expect that the way in which SPX domains interact with their target proteins may reveal common features. However, in other organisms, the mediators transmitting this control to the transcription factors can differ from the PHO pathway components acting in yeast. Work in a variety of different model organisms will thus contribute essential information necessary to grasp the full spectrum of strategies underlying $P_i$ homeostasis.

Yeast cells are a prime model to study phosphate homeostasis in a eukaryotic cell system because many of the proteins immediately implicated in stabilizing cytosolic $P_i$ are known and important elements of the signaling cascades regulating their expression and activity have begun to emerge. A major challenge lies in the high degree of redundancy that cells use in order to regulate their internal phosphate store. In order to study the regulatory mechanisms behind $P_i$ homeostasis, it will therefore be necessary to establish reduced and simplified systems, both *in vivo* and *in vitro*, which will allow isolating individual aspects of the complex regulatory network and exploring them without too much interference by redundant mechanisms. The potent and convenient methods for manipulating the yeast genome provide the necessary tools to tackle this task.

## AUTHOR CONTRIBUTIONS

Both authors wrote all parts of the review together.

## FUNDING

This work was supported by grants from the SNSF (CRSII5_170925) and the ERC (788442) to AM.

## ACKNOWLEDGMENTS

We thank Geun-Don Kim, Andrea Schmidt, Valentin Chabert, and Juan Francisco Bada for their comments on our manuscript.

## REFERENCES

Almaguer, C., Cheng, W., Nolder, C., and Patton-Vogt, J. (2004). Glycerophosphoinositol, a novel phosphate source whose transport is regulated by multiple factors in *Saccharomyces cerevisiae*. *J. Biol. Chem.* 279, 31937–31942. doi: 10.1074/jbc.M403648200

Andreeva, N., Trilisenko, L., Eldarov, M., and Kulakovskaya, T. (2015). Polyphosphatase PPN1 of *Saccharomyces cerevisiae*: switching of exopolyphosphatase and endopolyphosphatase activities. *PLoS One* 10:e0119594. doi: 10.1371/journal.pone.0119594

Anemaet, I. G., and van Heusden, G. P. H. (2014). Transcriptional response of *Saccharomyces cerevisiae* to potassium starvation. *BMC Genomics* 15:1040. doi: 10.1186/1471-2164-15-1040

Ansermet, C., Moor, M. B., Centeno, G., Auberson, M., Hu, D. Z., Baron, R., et al. (2017). Renal fanconi syndrome and hypophosphatemic rickets in the absence of xenotropic and polytropic retroviral receptor in the nephron. *J. Am. Soc. Nephrol.* 28, 1073–1078. doi: 10.1681/ASN.2016070726

Arima, K., Oshima, T., Kubota, I., Nakamura, N., Mizunaga, T., and Toh-e, A. (1983). The nucleotide sequence of the yeast PHO5 gene: a putative precursor of repressible acid phosphatase contains a signal peptide. *Nucleic Acids Res.* 11, 1657–1672. doi: 10.1093/nar/11.6.1657

Auesukaree, C., Homma, T., Kaneko, Y., and Harashima, S. (2003). Transcriptional regulation of phosphate-responsive genes in low-affinity phosphate-transporter-defective mutants in *Saccharomyces cerevisiae*. *Biochem. Biophys. Res. Commun.* 306, 843–850. doi: 10.1016/s0006-291x(03)01068-4

Auesukaree, C., Homma, T., Tochio, H., Shirakawa, M., Kaneko, Y., and Harashima, S. (2004). Intracellular phosphate serves as a signal for the regulation of the PHO pathway in *Saccharomyces cerevisiae*. *J. Biol. Chem.* 279, 17289–17294. doi: 10.1074/jbc.M312202200

Auesukaree, C., Tochio, H., Shirakawa, M., Kaneko, Y., and Harashima, S. (2005). Plc1p, Arg82p, and Kcs1p, enzymes involved in inositol pyrophosphate synthesis, are essential for phosphate regulation and polyphosphate accumulation in *Saccharomyces cerevisiae*. *J. Biol. Chem.* 280, 25127–25133. doi: 10.1074/jbc.M414579200

Azevedo, C., Desfougères, Y., Jiramongkol, Y., Partington, H., Trakansuebkul, S., Singh, J., et al. (2019). Development of a yeast model to study the contribution of vacuolar polyphosphate metabolism to lysine polyphosphorylation. *J. Biol. Chem.* 295, 1439–1451. doi: 10.1074/jbc.RA119.011680

Azevedo, C., Livermore, T., and Saiardi, A. (2015). Protein polyphosphorylation of lysine residues by inorganic polyphosphate. *Mol. Cell* 58, 71–82. doi: 10.1016/j.molcel.2015.02.010

Azevedo, C., and Saiardi, A. (2017). Eukaryotic phosphate homeostasis: the inositol pyrophosphate perspective. *Trends Biochem. Sci.* 42, 219–231. doi: 10.1016/j.tibs.2016.10.008

Azevedo, C., Singh, J., Steck, N., Hofer, A., Ruiz, F. A., Singh, T., et al. (2018). Screening a protein array with synthetic biotinylated inorganic polyphosphate to define the human polyP-ome. *ACS Chem. Biol.* 13, 1958–1963. doi: 10.1021/acschembio.8b00357

Barbaric, S., Luckenbach, T., Schmid, A., Blaschke, D., Hörz, W., and Korber, P. (2007). Redundancy of chromatin remodeling pathways for the induction of the yeast PHO5 promoter in vivo. *J. Biol. Chem.* 282, 27610–27621. doi: 10.1074/jbc.M700623200

Bhoite, L. T., Allen, J. M., Garcia, E., Thomas, L. R., Gregory, I. D., Voth, W. P., et al. (2002). Mutations in the pho2 (bas2) transcription factor that differentially affect activation with its partner proteins bas1, pho4, and swi5. *J. Biol. Chem.* 277, 37612–37618. doi: 10.1074/jbc.M206125200

Biber, J., Hernando, N., and Forster, I. (2013). Phosphate transporters and their function. *Annu. Rev. Physiol.* 75, 535–550. doi: 10.1146/annurev-physiol-030212-183748

Boer, V. M., Crutchfield, C. A., Bradley, P. H., Botstein, D., and Rabinowitz, J. D. (2010). Growth-limiting intracellular metabolites in yeast growing under diverse nutrient limitations. *Mol. Biol. Cell* 21, 198–211. doi: 10.1091/mbc.e09-07-0597

Boer, V. M., de Winde, J. H., Pronk, J. T., and Piper, M. D. W. (2003). The genome-wide transcriptional responses of *Saccharomyces cerevisiae* grown on glucose in

aerobic chemostat cultures limited for carbon, nitrogen, phosphorus, or sulfur. *J. Biol. Chem.* 278, 3265–3274. doi: 10.1074/jbc.M209759200

Bostian, K. A., Lemire, J. M., and Halvorson, H. O. (1983). Physiological control of repressible acid phosphatase gene transcripts in *Saccharomyces cerevisiae*. *Mol. Cell Biol.* 3, 839–853. doi: 10.1128/mcb.3.5.839

Bru, S., Martínez-Laínez, J. M., Hernández-Ortega, S., Quandt, E., Torres-Torronteras, J., Martí, R., et al. (2016). Polyphosphate is involved in cell cycle progression and genomic stability in *Saccharomyces cerevisiae*. *Mol. Microbiol.* 101, 367–380. doi: 10.1111/mmi.13396

Bun-ya, M., Nishimura, M., Harashima, S., and Oshima, Y. (1991). The PHO84 gene of *Saccharomyces cerevisiae* encodes an inorganic phosphate transporter. *Mol. Cell Biol.* 11, 3229–3238. doi: 10.1128/mcb.11.6.3229

Bürglin, T. R. (1988). The yeast regulatory gene PHO2 encodes a homeo box. *Cell* 53, 339–340. doi: 10.1016/0092-8674(88)90153-5

Camblong, J., Iglesias, N., Fickentscher, C., Dieppois, G., and Stutz, F. (2007). Antisense RNA stabilization induces transcriptional gene silencing via histone deacetylation in *S. cerevisiae*. *Cell* 131, 706–717. doi: 10.1016/j.cell.2007.09.014

Canadell, D., González, A., Casado, C., and Ariño, J. (2015). Functional interactions between potassium and phosphate homeostasis in *Saccharomyces cerevisiae*. *Mol. Microbiol.* 95, 555–572. doi: 10.1111/mmi.12886

Carroll, A. S., and O'Shea, E. K. (2002). Pho85 and signaling environmental conditions. *Trends Biochem. Sci.* 27, 87–93. doi: 10.1016/s0968-0004(01)02040-0

Carter-O'Connell, I., Peel, M. T., Wykoff, D. D., and O'Shea, E. K. (2012). Genome-wide characterization of the phosphate starvation response in *Schizosaccharomyces pombe*. *BMC Genomics* 13:697. doi: 10.1186/1471-2164-13-697

Cartwright, J. L., and McLennan, A. G. (1999). The *Saccharomyces cerevisiae* YOR163w gene encodes a diadenosine 5′, 5‴-$P^1$,$P^6$-Hexaphosphate (Ap6A) hydrolase member of the MutT motif (Nudix hydrolase) family. *J. Biol. Chem.* 274, 8604–8610. doi: 10.1074/jbc.274.13.8604

Causton, H. C., Ren, B., Koh, S. S., Harbison, C. T., Kanin, E., Jennings, E. G., et al. (2001). Remodeling of yeast genome expression in response to environmental changes. *Mol. Biol. Cell* 12, 323–337. doi: 10.1091/mbc.12.2.323

Chia, S. Z., Lai, Y.-W., Yagoub, D., Lev, S., Hamey, J. J., Pang, C. N. I., et al. (2018). Knockout of the Hmt1p arginine methyltransferase in *Saccharomyces cerevisiae* leads to the dysregulation of phosphate-associated genes and processes. *Mol. Cell. Proteomics* 17, 2462–2479. doi: 10.1074/mcp.RA117.000214

Choi, J., Rajagopal, A., Xu, Y.-F., Rabinowitz, J. D., and O'Shea, E. K. (2017). A systematic genetic screen for genes involved in sensing inorganic phosphate availability in *Saccharomyces cerevisiae*. *PLoS One* 12:e0176085. doi: 10.1371/journal.pone.0176085

Conrad, M., Schothorst, J., Kankipati, H. N., Van Zeebroeck, G., Rubio-Texeira, M., and Thevelein, J. M. (2014). Nutrient sensing and signaling in the yeast *Saccharomyces cerevisiae*. *FEMS Microbiol. Rev.* 38, 254–299. doi: 10.1111/1574-6976.12065

Creasy, C. L., Madden, S. L., and Bergman, L. W. (1993). Molecular analysis of the PHO81 gene of *Saccharomyces cerevisiae*. *Nucleic Acids Res.* 21, 1975–1982. doi: 10.1093/nar/21.8.1975

Creasy, C. L., Shao, D., and Begman, L. W. (1996). Negative transcriptional regulation of PH081 expression in *Saccharomyces cerevisiae*. *Gene* 168, 23–29. doi: 10.1016/0378-1119(95)00737-7

De Virgilio, C. (2011). The essence of yeast quiescence. *FEMS Microbiol. Rev.* 36, 306–339. doi: 10.1111/j.1574-6976.2011.00287.x

Depaoli, M. R., Hay, J. C., Graier, W. F., and Malli, R. (2019). The enigmatic ATP supply of the endoplasmic reticulum. *Biol. Rev. Camb. Philos. Soc.* 94, 610–628. doi: 10.1111/brv.12469

Desfougères, Y., Gerasimaitë, R. U., Jessen, H. J., and Mayer, A. (2016). Vtc5, a novel subunit of the vacuolar transporter chaperone complex, regulates polyphosphate synthesis and phosphate homeostasis in yeast. *J. Biol. Chem.* 291, 22262–22275. doi: 10.1074/jbc.M116.746784

Docampo, R., and Huang, G. (2016). Acidocalcisomes of eukaryotes. *Curr. Opin. Cell Biol.* 41, 66–72. doi: 10.1016/j.ceb.2016.04.007

Donella-Deana, A., Ostojić, S., Pinna, L. A., and Barbarić, S. (1993). Specific dephosphorylation of phosphopeptides by the yeast alkaline phosphatase encoded by PHO8 gene. *Biochim. Biophys. Acta* 1177, 221–228. doi: 10.1016/0167-4889(93)90044-p

Dong, J., Ma, G., Sui, L., Wei, M., Satheesh, V., Zhang, R., et al. (2019). Inositol pyrophosphate InsP8 acts as an intracellular phosphate signal in *Arabidopsis*. *Mol. Plant* 12, 1463–1473. doi: 10.1016/j.molp.2019.08.002

Estill, M., Kerwin-Iosue, C. L., and Wykoff, D. D. (2015). Dissection of the PHO pathway in *Schizosaccharomyces pombe* using epistasis and the alternate repressor adenine. *Curr. Genet.* 61, 175–183. doi: 10.1007/s00294-014-0466-6

Fisher, E., Almaguer, C., Holic, R., Griac, P., and Patton-Vogt, J. (2005). Glycerophosphocholine-dependent growth requires Gde1p (YPL110c) and Git1p in *Saccharomyces cerevisiae*. *J. Biol. Chem.* 280, 36110–36117. doi: 10.1074/jbc.M507051200

Flick, J. S., and Thorner, J. (1998). An essential function of a phosphoinositide-specific phospholipase C is relieved by inhibition of a cyclin-dependent protein kinase in the yeast *Saccharomyces cerevisiae*. *Genetics* 148, 33–47.

Gerasimaite, R., and Mayer, A. (2016). Enzymes of yeast polyphosphate metabolism: structure, enzymology and biological roles. *Biochem. Soc. Trans.* 44, 234–239. doi: 10.1042/BST20150213

Gerasimaite, R., and Mayer, A. (2017). Ppn2, a novel Zn(2+)-dependent polyphosphatase in the acidocalcisome-like yeast vacuole. *J. Cell Sci.* 130, 1625–1636. doi: 10.1242/jcs.201061

Gerasimaite, R., Pavlovic, I., Capolicchio, S., Hofer, A., Schmidt, A., Jessen, H. J., et al. (2017). Inositol pyrophosphate specificity of the SPX-dependent polyphosphate polymerase VTC. *ACS Chem. Biol.* 12, 648–653. doi: 10.1021/acschembio.7b00026

Gerasimaite, R., Sharma, S., Desfougères, Y., Schmidt, A., and Mayer, A. (2014). Coupled synthesis and translocation restrains polyphosphate to acidocalcisome-like vacuoles and prevents its toxicity. *J. Cell Sci.* 127, 5093–5104. doi: 10.1242/jcs.159772

Ghillebert, R., Swinnen, E., De Snijder, P., Smets, B., and Winderickx, J. (2011). Differential roles for the low-affinity phosphate transporters Pho87 and Pho90 in *Saccharomyces cerevisiae*. *Biochem. J.* 434, 243–251. doi: 10.1042/BJ20101118

Giots, F., Donaton, M., and Thevelein, J. M. (2003). Inorganic phosphate is sensed by specific phosphate carriers and acts in concert with glucose as a nutrient signal for activation of the protein kinase A pathway in the yeast *Saccharomyces cerevisiae*. *Mol. Microbiol.* 47, 1163–1181. doi: 10.1046/j.1365-2958.2003.03365.x

Giovannini, D., Touhami, J., Charnet, P., Sitbon, M., and Battini, J.-L. (2013). Inorganic phosphate export by the retrovirus receptor XPR1 in metazoans. *Cell Rep.* 3, 1866–1873. doi: 10.1016/j.celrep.2013.05.035

Gregory, P. D., Schmid, A., Zavari, M., Münsterkötter, M., and Hörz, W. (1999). Chromatin remodelling at the PHO8 promoter requires SWI-SNF and SAGA at a step subsequent to activator binding. *EMBO J.* 18, 6407–6414. doi: 10.1093/emboj/18.22.6407

Gu, C., Nguyen, H.-N., Hofer, A., Jessen, H. J., Dai, X., Wang, H., et al. (2017). The significance of the bifunctional kinase/phosphatase activities of PPIP5Ks for coupling inositol pyrophosphate cell-signaling to cellular phosphate homeostasis. *J. Biol. Chem.* 292, 4544–4555. doi: 10.1074/jbc.M116.765743

Henry, T. C., Power, J. E., Kerwin, C. L., Mohammed, A., Weissman, J. S., Cameron, D. M., et al. (2011). Systematic screen of *Schizosaccharomyces pombe* deletion collection uncovers parallel evolution of the phosphate signal transduction pathway in yeasts. *Eukaryot. Cell* 10, 198–206. doi: 10.1128/ec.00216-10

Hirst, K., Fisher, F., McAndrew, P. C., and Goding, C. R. (1994). The transcription factor, the Cdk, its cyclin and their regulator: directing the transcriptional response to a nutritional signal. *EMBO J.* 13, 5410–5420. doi: 10.1002/j.1460-2075.1994.tb06876.x

Hothorn, M., Neumann, H., Lenherr, E. D., Wehner, M., Rybin, V., Hassa, P. O., et al. (2009). Catalytic core of a membrane-associated eukaryotic polyphosphate polymerase. *Science* 324, 513–516. doi: 10.1126/science.1168120

Huang, D., Friesen, H., and Andrews, B. (2007). Pho85, a multifunctional cyclin-dependent protein kinase in budding yeast. *Mol. Microbiol.* 66, 303–314. doi: 10.1111/j.1365-2958.2007.05914.x

Huang, S., Jeffery, D. A., Anthony, M. D., and O'Shea, E. K. (2001). Functional analysis of the cyclin-dependent kinase inhibitor Pho81 identifies a novel inhibitory domain. *Mol. Cell Biol.* 21, 6695–6705. doi: 10.1128/mcb.21.19.6695-6705.2001

Huh, W.-K., Falvo, J. V., Gerke, L. C., Carroll, A. S., Howson, R. W., Weissman, J. S., et al. (2003). Global analysis of protein localization in budding yeast. *Nature* 425, 686–691. doi: 10.1038/nature02026

Hürlimann, H. C. (2009). *Investigations on the Physiology and Molecular Basis of Polyphosphate Hyper- and Hypo-Accumulation in Saccharomyces cerevisiae*. Zurich: ETH.

Hürlimann, H. C., Pinson, B., Stadler-Waibel, M., Zeeman, S. C., and Freimoser, F. M. (2009). The SPX domain of the yeast low-affinity phosphate transporter Pho90 regulates transport activity. *EMBO Rep.* 10, 1003–1008. doi: 10.1038/embor.2009.105

Hürlimann, H. C., Stadler-Waibel, M., Werner, T. P., and Freimoser, F. M. (2007). Pho91 is a vacuolar phosphate transporter that regulates phosphate and polyphosphate metabolism in *Saccharomyces cerevisiae*. *Mol. Biol. Cell* 18, 4438–4445. doi: 10.1091/mbc.e07-05-0457

Jensen, L. T., Ajua-Alemanji, M., and Culotta, V. C. (2003). The *Saccharomyces cerevisiae* high affinity phosphate transporter encoded by PHO84 also functions in manganese homeostasis. *J. Biol. Chem.* 278, 42036–42040. doi: 10.1074/jbc.M307413200

Kaffman, A., Herskowitz, I., Tjian, R., and O'Shea, E. K. (1994). Phosphorylation of the transcription factor-Pho4 by a cyclin-Cdk complex, Pho80-Pho85. *Science* 263, 1153–1156. doi: 10.1126/science.8108735

Kaffman, A., Rank, N. M., O'Neill, E. M., Huang, L. S., and O'Shea, E. K. (1998a). The receptor Msn5 exports the phosphorylated transcription factor Pho4 out of the nucleus. *Nature* 396, 482–486. doi: 10.1038/24898

Kaffman, A., Rank, N. M., and O'Shea, E. K. (1998b). Phosphorylation regulates association of the transcription factor Pho4 with its import receptor Pse1/Kap121. *Genes Dev.* 12, 2673–2683. doi: 10.1101/gad.12.17.2673

Kaneko, Y., Tamai, Y., Toh-e, A., and Oshima, Y. (1985). Transcriptional and post-transcriptional control of PHO8 expression by PHO regulatory genes in *Saccharomyces cerevisiae*. *Mol. Cell Biol.* 5, 248–252. doi: 10.1128/mcb.5.1.248

Kaneko, Y., Toh-e, A., and Oshima, Y. (1982). Identification of the genetic locus for the structural gene and a new regulatory gene for the synthesis of repressible alkaline phosphatase in *Saccharomyces cerevisiae*. *Mol. Cell Biol.* 2, 127–137. doi: 10.1128/mcb.2.2.127

Kang, H.-J., Jeong, S.-J., Kim, K.-N., Baek, I.-J., Chang, M., Kang, C.-M., et al. (2014). A novel protein, Pho92, has a conserved YTH domain and regulates phosphate metabolism by decreasing the mRNA stability of PHO4 in *Saccharomyces cerevisiae*. *Biochem. J.* 457, 391–400. doi: 10.1042/BJ20130862

Klompmaker, S. H., Kohl, K., Fasel, N., and Mayer, A. (2017). Magnesium uptake by connecting fluid-phase endocytosis to an intracellular inorganic cation filter. *Nat. Commun.* 8:1879.

Knight, J. P., Daly, T. M., and Bergman, L. W. (2004). Regulation by phosphorylation of Pho81p, a cyclin-dependent kinase inhibitor in *Saccharomyces cerevisiae*. *Curr. Genet.* 46, 10–19. doi: 10.1007/s00294-004-0502-z

Komeili, A., and O'Shea, E. K. (1999). Roles of phosphorylation sites in regulating activity of the transcription factor Pho4. *Science* 284, 977–980. doi: 10.1126/science.284.5416.977

Korber, P., and Barbaric, S. (2014). The yeast PHO5 promoter: from single locus to systems biology of a paradigm for gene regulation through chromatin. *Nucleic Acids Res.* 42, 10888–10902. doi: 10.1093/nar/gku784

Kulakovskaya, T. V., Lichko, L. P., Vagabov, V. M., and Kulaev, I. S. (2010). Inorganic polyphosphates in mitochondria. *Biochem. Mosc.* 75, 825–831.

Kumble, K. D., and Kornberg, A. (1996). Endopolyphosphatases for long chain inorganic polyphosphate in yeast and mammals. *J. Biol. Chem.* 271, 27146–27151. doi: 10.1074/jbc.271.43.27146

Lam, F. H., Steger, D. J., and O'Shea, E. K. (2008). Chromatin decouples promoter threshold from dynamic range. *Nature* 453, 246–250. doi: 10.1038/nature06867

Langen, P., and Liss, E. (1958). [Formation and conversion of yeast polyphosphates]. *Biochem. Z.* 330, 455–466.

Langen, P., and Liss, E. (1960). [Differentiation of orthophosphates of yeast cells]. *Biochem. Z.* 332, 403–406.

Lazard, M., Blanquet, S., Fisicaro, P., Labarraque, G., and Plateau, P. (2010). Uptake of selenite by *Saccharomyces cerevisiae* involves the high and low affinity orthophosphate transporters. *J. Biol. Chem.* 285, 32029–32037. doi: 10.1074/jbc.M110.139865

Lee, M., O'Regan, S., Moreau, J. L., Johnson, A. L., Johnston, L. H., and Goding, C. R. (2000). Regulation of the Pcl7-Pho85 cyclin-Cdk complex by Pho81. *Mol. Microbiol.* 38, 411–422. doi: 10.1046/j.1365-2958.2000.02140.x

Lee, Y.-S., Huang, K., Quiocho, F. A., and O'Shea, E. K. (2008). Molecular basis of cyclin-CDK-CKI regulation by reversible binding of an inositol pyrophosphate. *Nat. Chem. Biol.* 4, 25–32. doi: 10.1038/nchembio.2007.52

Lee, Y. S., Mulugu, S., York, J. D., and O'Shea, E. K. (2007). Regulation of a cyclin-CDK-CDK inhibitor complex by inositol pyrophosphates. *Science* 316, 109–112. doi: 10.1126/science.1139080

Legati, A., Giovannini, D., Nicolas, G., López-Sánchez, U., Quintáns, B., Oliveira, J. R. M., et al. (2015). Mutations in XPR1 cause primary familial brain calcification associated with altered phosphate export. *Nat. Genet.* 47, 579–581. doi: 10.1038/ng.3289

Lev, S., and Djordjevic, J. T. (2018). Why is a functional PHO pathway required by fungal pathogens to disseminate within a phosphate-rich host: a paradox explained by alkaline pH-simulated nutrient deprivation and expanded PHO pathway function. *PLoS Pathog.* 14:e1007021. doi: 10.1371/journal.ppat.1007021

Levy, S., Kafri, M., Carmi, M., and Barkai, N. (2011). The competitive advantage of a dual-transporter system. *Science* 334, 1408–1412. doi: 10.1126/science.1207154

Li, X., Gu, C., Hostachy, S., Sahu, S., Wittwer, C., Jessen, H. J., et al. (2020). Control of XPR1-dependent cellular phosphate efflux by InsP8 is an exemplar for functionally-exclusive inositol pyrophosphate signaling. *Proc. Natl. Acad. Sci. U.S.A.* 14:201908830. doi: 10.1073/pnas.1908830117

Lichko, L., Kulakovskaya, T., Pestov, N., and Kulaev, I. (2006). Inorganic polyphosphates and exopolyphosphatases in cell compartments of the yeast *Saccharomyces cerevisiae* under inactivation of PPX1 and PPN1 genes. *Biosci. Rep.* 26, 45–54. doi: 10.1007/s10540-006-9003-2

Lichko, L. P., Kulakovskaya, T. V., and Kulaev, I. S. (2006). Inorganic polyphosphate and exopolyphosphatase in the nuclei of *Saccharomyces cerevisiae*: dependence on the growth phase and inactivation of the PPX1 and PPN1 genes. *Yeast* 23, 735–740. doi: 10.1002/yea.1391

Lichko, L. P., Pestov, N. A., Kulakovskaya, T. V., and Kulaev, I. S. (2003). Effect of PPX1 inactivation on the exopolyphosphatase spectra in cytosol and mitochondria of the yeast *Saccharomyces cerevisiae*. *Biochem. Mosc.* 68, 740–746.

Liu, J., Yang, L., Luan, M., Wang, Y., Zhang, C., Zhang, B., et al. (2015). A vacuolar phosphate transporter essential for phosphate homeostasis in *Arabidopsis*. *Proc. Natl. Acad. Sci. U.S.A.* 112, E6571–E6578. doi: 10.1073/pnas.1514598112

Lonetti, A., Szijgyarto, Z., Bosh, D., Loss, O., Azevedo, C., and Saiardi, A. (2011). Identification of an evolutionarily conserved family of inorganic polyphosphate endopolyphosphatases. *J. Biol. Chem.* 286, 31966–31974. doi: 10.1074/jbc.M111.266320

Lu, S.-P., and Lin, S.-J. (2011). Phosphate-responsive signaling pathway is a novel component of NAD+ metabolism in *Saccharomyces cerevisiae*. *J. Biol. Chem.* 286, 14271–14281. doi: 10.1074/jbc.M110.217885

Luan, Y., and Li, H. (2004). Model-based methods for identifying periodically expressed genes based on time course microarray gene expression data. *Bioinformatics* 20, 332–339. doi: 10.1093/bioinformatics/btg413

Lundh, F., Mouillon, J.-M., Samyn, D., Stadler, K., Popova, Y., Lagerstedt, J. O., et al. (2009). Molecular mechanisms controlling phosphate-induced downregulation of the yeast Pho84 phosphate transporter. *Biochemistry* 48, 4497–4505. doi: 10.1021/bi9001198

Magbanua, J. P., Fujisawa, K., Ogawa, N., and Oshima, Y. (1997a). The homeodomain protein Pho2p binds at an A/T-rich segment flanking the binding site of the basic-helix-loop-helix protein Pho4p in the yeast PHO promoters. *Yeast* 13, 1299–1308. doi: 10.1002/(sici)1097-0061(199711)13:14<1299::aid-yea178>3.0.co;2-a

Magbanua, J. P., Ogawa, N., Harashima, S., and Oshima, Y. (1997b). The transcriptional activators of the PHO regulon, Pho4p and Pho2p, interact directly with each other and with components of the basal transcription machinery in *Saccharomyces cerevisiae*. *J. Biochem.* 121, 1182–1189. doi: 10.1093/oxfordjournals.jbchem.a021713

Martinez, P., and Persson, B. L. (1998). Identification, cloning and characterization of a derepressible Na+-coupled phosphate transporter in *Saccharomyces cerevisiae*. *Mol. Gen. Genet.* 258, 628–638. doi: 10.1007/s004380050776

McIlwain, H., Buchel, L., and Cheshire, J. D. (1951). The inorganic phosphate and phosphocreatine of brain especially during metabolism in vitro. *Biochem. J.* 48, 12–20. doi: 10.1042/bj0480012

Menoyo, S., Ricco, N., Bru, S., Hernández-Ortega, S., Escoté, X., Aldea, M., et al. (2013). Phosphate-activated cyclin-dependent kinase stabilizes G1 cyclin to trigger cell cycle entry. *Mol. Cell Biol.* 33, 1273–1284. doi: 10.1128/mcb.01556-12

Mouillon, J.-M., and Persson, B. L. (2005). Inhibition of the protein kinase A alters the degradation of the high-affinity phosphate transporter Pho84 in *Saccharomyces cerevisiae*. *Curr. Genet.* 48, 226–234. doi: 10.1007/s00294-005-0019-0

Mouillon, J.-M., and Persson, B. L. (2006). New aspects on phosphate sensing and signalling in *Saccharomyces cerevisiae*. *FEMS Yeast Res.* 6, 171–176. doi: 10.1111/j.1567-1364.2006.00036.x

Müller, O., Bayer, M. J., Peters, C., Andersen, J. S., Mann, M., and Mayer, A. (2002). The Vtc proteins in vacuole fusion: coupling NSF activity to V(0) trans-complex formation. *EMBO J.* 21, 259–269. doi: 10.1093/emboj/21.3.259

Müller, O., Neumann, H., Bayer, M. J., and Mayer, A. (2003). Role of the Vtc proteins in V-ATPase stability and membrane trafficking. *J. Cell Sci.* 116, 1107–1115. doi: 10.1242/jcs.00328

Mulugu, S., Bai, W., Fridy, P. C., Bastidas, R. J., Otto, J. C., Dollins, D. E., et al. (2007). A conserved family of enzymes that phosphorylate inositol hexakisphosphate. *Science* 316, 106–109. doi: 10.1126/science.1139099

Nair, V. S., Gu, C., Janoshazi, A. K., Jessen, H. J., Wang, H., and Shears, S. B. (2018). Inositol pyrophosphate synthesis by diphosphoinositol pentakisphosphate kinase-1 is regulated by phosphatidylinositol(4,5)bisphosphate. *Biosci. Rep.* 38:BSR20171549. doi: 10.1042/BSR20171549

Neef, D. W., and Kladde, M. P. (2003). Polyphosphate loss promotes SNF/SWI- and Gcn5-dependent mitotic induction of PHO5. *Mol. Cell Biol.* 23, 3788–3797. doi: 10.1128/mcb.23.11.3788-3797.2003

Nishimura, K., Yasumura, K., Igarashi, K., Harashima, S., and Kakinuma, Y. (1999). Transcription of some PHO genes in *Saccharomyces cerevisiae* is regulated by spt7p. *Yeast* 15, 1711–1717. doi: 10.1002/(sici)1097-0061(199912)15:16<1711::aid-yea497>3.0.co;2-8

Nishizawa, M., Komai, T., Katou, Y., Shirahige, K., Ito, T., and Toh-E, A. (2008). Nutrient-regulated antisense and intragenic RNAs modulate a signal transduction pathway in yeast. *PLoS Biol.* 6:e326. doi: 10.1371/journal.pbio.0060326

Ogawa, N., DeRisi, J., and Brown, P. O. (2000). New components of a system for phosphate accumulation and polyphosphate metabolism in *Saccharomyces cerevisiae* revealed by genomic expression analysis. *Mol. Biol. Cell* 11, 4309–4321. doi: 10.1091/mbc.11.12.4309

Ogawa, N., Noguchi, K., Sawai, H., Yamashita, Y., Yompakdee, C., and Oshima, Y. (1995). Functional domains of Pho81p, an inhibitor of Pho85p protein kinase, in the transduction pathway of Pi signals in *Saccharomyces cerevisiae*. *Mol. Cell Biol.* 15, 997–1004. doi: 10.1128/mcb.15.2.997

O'Neill, E. M., Kaffman, A., Jolly, E. R., and O'Shea, E. K. (1996). Regulation of PHO4 nuclear localization by the PHO80-PHO85 cyclin-CDK complex. *Science* 271, 209–212. doi: 10.1126/science.271.5246.209

Oshima, Y. (1997). The phosphatase system in *Saccharomyces cerevisiae*. *Genes Genet. Syst.* 72, 323–334. doi: 10.1266/ggs.72.323

Palmieri, F., and Monné, M. (2016). Discoveries, metabolic roles and diseases of mitochondrial carriers: a review. *Biochim. Biophys. Acta* 1863, 2362–2378. doi: 10.1016/j.bbamcr.2016.03.007

Patton-Vogt, J. (2007). Transport and metabolism of glycerophosphodiesters produced through phospholipid deacylation. *Biochim. Biophys. Acta* 1771, 337–342. doi: 10.1016/j.bbalip.2006.04.013

Pérez-Sampietro, M., Serra-Cardona, A., Canadell, D., Casas, C., Ariño, J., and Herrero, E. (2016). The yeast Aft2 transcription factor determines selenite toxicity by controlling the low affinity phosphate transport system. *Sci. Rep.* 6:32836. doi: 10.1038/srep32836

Persson, B. L., Lagerstedt, J. O., Pratt, J. R., Pattison-Granberg, J., Lundh, K., Shokrollahzadeh, S., et al. (2003). Regulation of phosphate acquisition in *Saccharomyces cerevisiae*. *Curr. Genet.* 43, 225–244. doi: 10.1007/s00294-003-0400-9

Pestov, N. A., Kulakovskaya, T. V., and Kulaev, I. S. (2004). Inorganic polyphosphate in mitochondria of *Saccharomyces cerevisiae* at phosphate limitation and phosphate excess. *FEMS Yeast Res.* 4, 643–648. doi: 10.1016/j.femsyr.2003.12.008

Petersson, J., Pattison, J., Kruckeberg, A. L., Berden, J. A., and Persson, B. L. (1999). Intracellular localization of an active green fluorescent protein-tagged Pho84 phosphate permease in *Saccharomyces cerevisiae*. *FEBS Lett.* 462, 37–42. doi: 10.1016/s0014-5793(99)01471-4

Pinson, B., Merle, M., Franconi, J.-M., and Daignan-Fornier, B. (2004). Low affinity orthophosphate carriers regulate *PHO* gene expression independently of internal orthophosphate concentration in *Saccharomyces cerevisiae*. *J. Biol. Chem.* 279, 35273–35280. doi: 10.1074/jbc.M405398200

Pinson, B., Vaur, S., Sagot, I., Coulpier, F., Lemoine, S., and Daignan-Fornier, B. (2009). Metabolic intermediates selectively stimulate transcription factor interaction and modulate phosphate and purine pathways. *Genes Dev.* 23, 1399–1407. doi: 10.1101/gad.521809

Plankert, U., Purwin, C., and Holzer, H. (1991). Yeast fructose-2,6-bisphosphate 6-phosphatase is encoded by PHO8, the gene for nonspecific repressible alkaline phosphatase. *Eur. J. Biochem.* 196, 191–196. doi: 10.1111/j.1432-1033.1991.tb15803.x

Pöhlmann, J., Risse, C., Seidel, C., Pohlmann, T., Jakopec, V., Walla, E., et al. (2014). The Vip1 inositol polyphosphate kinase family regulates polarized growth and modulates the microtubule cytoskeleton in fungi. *PLoS Genet.* 10:e1004586. doi: 10.1371/journal.pgen.1004586

Pondugula, S., Neef, D. W., Voth, W. P., Darst, R. P., Dhasarathy, A., Reynolds, M. M., et al. (2009). Coupling phosphate homeostasis to cell cycle-specific transcription: mitotic activation of *Saccharomyces cerevisiae* PHO5 by Mcm1 and forkhead proteins. *Mol. Cell Biol.* 29, 4891–4905. doi: 10.1128/mcb.00222-09

Popova, Y., Thayumanavan, P., Lonati, E., Agrochão, M., and Thevelein, J. M. (2010). Transport and signaling through the phosphate-binding site of the yeast Pho84 phosphate transceptor. *Proc. Natl. Acad. Sci. U.S.A.* 107, 2890–2895. doi: 10.1073/pnas.0906546107

Potapenko, E., Cordeiro, C. D., Huang, G., and Docampo, R. (2019). Pyrophosphate stimulates the phosphate-sodium symporter of *Trypanosoma brucei* Acidocalcisomes and *Saccharomyces cerevisiae* vacuoles. *mSphere* 4:e00045-19.

Potapenko, E., Cordeiro, C. D., Huang, G., Storey, M., Wittwer, C., Dutta, A. K., et al. (2018). 5-diphosphoinositol pentakisphosphate (5-IP7) regulates phosphate release from Acidocalcisomes and yeast vacuoles. *J. Biol. Chem.* 293, 19101–19112. doi: 10.1074/jbc.RA118.005884

Pratt, J. R., Mouillon, J.-M., Lagerstedt, J. O., Pattison-Granberg, J., Lundh, K. I., and Persson, B. L. (2004). Effects of methylphosphonate, a phosphate analogue, on the expression and degradation of the high-affinity phosphate transporter Pho84, in *Saccharomyces cerevisiae*. *Biochemistry* 43, 14444–14453. doi: 10.1021/bi049327t

Puga, M. I., Mateos, I., Charukesi, R., Wang, Z., Franco-Zorrilla, J. M., de Lorenzo, L., et al. (2014). SPX1 is a phosphate-dependent inhibitor of PHOSPHATE STARVATION RESPONSE 1 in *Arabidopsis*. *Proc. Natl. Acad. Sci. U.S.A.* 111, 14947–14952. doi: 10.1073/pnas.1404654111

Puga, M. I., Rojas-Triana, M., de Lorenzo, L., Leyva, A., Rubio, V., and Paz-Ares, J. (2017). Novel signals in the regulation of Pi starvation responses in plants: facts and promises. *Curr. Opin. Plant Biol.* 39, 40–49. doi: 10.1016/j.pbi.2017.05.007

Randall, T. A., Gu, C., Li, X., Wang, H., and Shears, S. B. (2019). A two-way switch for inositol pyrophosphate signaling: evolutionary history and biological significance of a unique, bifunctional kinase/phosphatase. *Adv. Biol. Regul.* 75:100674. doi: 10.1016/j.jbior.2019.100674

Reddy, V. S., Singh, A. K., and Rajasekharan, R. (2008). The *Saccharomyces cerevisiae* PHM8 gene encodes a soluble magnesium-dependent lysophosphatidic acid phosphatase. *J. Biol. Chem.* 283, 8846–8854. doi: 10.1074/jbc.M706752200

Ruiz, A., Yenush, L., and Ariño, J. (2003). Regulation of ENA1 Na(+)-ATPase gene expression by the Ppz1 protein phosphatase is mediated by the calcineurin pathway. *Eukaryot. Cell* 2, 937–948. doi: 10.1128/ec.2.5.937-948.2003

Sabbagh, Y. (2013). Phosphate as a sensor and signaling molecule. *Clin. Nephrol.* 79, 57–65. doi: 10.5414/CN107322

Safrany, S. T., Ingram, S. W., Cartwright, J. L., Falck, J. R., McLennan, A. G., Barnes, L. D., et al. (1999). The diadenosine hexaphosphate hydrolases from *Schizosaccharomyces pombe* and *Saccharomyces cerevisiae* are homologues of the human diphosphoinositol polyphosphate phosphohydrolase. Overlapping substrate specificities in a MutT-type protein. *J. Biol. Chem.* 274, 21735–21740. doi: 10.1074/jbc.274.31.21735

Saiardi, A., Caffrey, J. J., Snyder, S. H., and Shears, S. B. (2000). The inositol hexakisphosphate kinase family. Catalytic flexibility and function in yeast

vacuole biogenesis. *J. Biol. Chem.* 275, 24686–24692. doi: 10.1074/jbc.m002750200

Saiardi, A., Erdjument-Bromage, H., Snowman, A. M., Tempst, P., and Snyder, S. H. (1999). Synthesis of diphosphoinositol pentakisphosphate by a newly identified family of higher inositol polyphosphate kinases. *Curr. Biol.* 9, 1323–1326. doi: 10.1016/s0960-9822(00)80055-x

Saito, K., Ohtomo, R., Kuga-Uetake, Y., Aono, T., and Saito, M. (2005). Direct labeling of polyphosphate at the ultrastructural level in *Saccharomyces cerevisiae* by using the affinity of the polyphosphate binding domain of *Escherichia coli* exopolyphosphatase. *Appl. Environ. Microbiol.* 71, 5692–5701. doi: 10.1128/AEM.71.10.5692-5701.2005

Samyn, D. R., Ruiz-Pávon, L., Andersson, M. R., Popova, Y., Thevelein, J. M., and Persson, B. L. (2012). Mutational analysis of putative phosphate- and proton-binding sites in the *Saccharomyces cerevisiae* Pho84 phosphate:H(+) transceptor and its effect on signalling to the PKA and PHO pathways. *Biochem. J.* 445, 413–422. doi: 10.1042/BJ20112086

Schneider, K. R., Smith, R. L., and O'Shea, E. K. (1994). Phosphate-regulated inactivation of the kinase PHO80-PHO85 by the CDK inhibitor PHO81. *Science* 266, 122–126. doi: 10.1126/science.7939631

Secco, D., Wang, C., Arpat, B. A., Wang, Z., Poirier, Y., Tyerman, S. D., et al. (2012a). The emerging importance of the SPX domain-containing proteins in phosphate homeostasis. *New Phytol.* 193, 842–851. doi: 10.1111/j.1469-8137.2011.04002.x

Secco, D., Wang, C., Shou, H., and Whelan, J. (2012b). Phosphate homeostasis in the yeast *Saccharomyces cerevisiae*, the key role of the SPX domain-containing proteins. *FEBS Lett.* 586, 289–295. doi: 10.1016/j.febslet.2012.01.036

Serra-Cardona, A., Petrezselyova, S., Canadell, D., Ramos, J., and Ariño, J. (2014). Coregulated expression of the Na+/phosphate Pho89 transporter and Ena1 Na+-ATPase allows their functional coupling under high-pH stress. *Mol. Cell Biol.* 34, 4420–4435. doi: 10.1128/mcb.01089-14

Serrano, R., Ruiz, A., Bernal, D., Chambers, J. R., and Ariño, J. (2002). The transcriptional response to alkaline pH in *Saccharomyces cerevisiae*: evidence for calcium-mediated signalling. *Mol. Microbiol.* 46, 1319–1333. doi: 10.1046/j.1365-2958.2002.03246.x

Serrano-Bueno, G., Hernández, A., López-Lluch, G., Pérez-Castiñeira, J. R., Navas, P., and Serrano, A. (2013). Inorganic pyrophosphatase defects lead to cell cycle arrest and autophagic cell death through NAD+ depletion in fermenting yeast. *J. Biol. Chem.* 288, 13082–13092. doi: 10.1074/jbc.M112.439349

Sethuraman, A., Rao, N. N., and Kornberg, A. (2001). The endopolyphosphatase gene: essential in *Saccharomyces cerevisiae*. *Proc. Natl. Acad. Sci. U.S.A.* 98, 8542–8547. doi: 10.1073/pnas.151269398

Shao, D., Creasy, C. L., and Bergman, L. W. (1996). Interaction of *Saccharomyces cerevisiae* Pho2 with Pho4 increases the accessibility of the activation domain of Pho4. *Mol. Gen. Genet.* 251, 358–364. doi: 10.1007/BF02172527

Shears, S. B. (2015). Inositol pyrophosphates: why so many phosphates? *Adv. Biol. Regul.* 57, 203–216. doi: 10.1016/j.jbior.2014.09.015

Shears, S. B. (2017). Intimate connections: inositol pyrophosphates at the interface of metabolic regulation and cell signaling. *J. Cell Physiol.* 233, 1897–1912. doi: 10.1002/jcp.26017

Snyder, N. A., Stefan, C. P., Soroudi, C. T., Kim, A., Evangelista, C., and Cunningham, K. W. (2017). H(+) and Pi byproducts of glycosylation affect Ca(2+) homeostasis and are retrieved from the golgi complex by homologs of TMEM165 and XPR1. *G3* 7, 3913–3924. doi: 10.1534/g3.117.300339

Spain, B. H., Koo, D., Ramakrishnan, M., Dzudzor, B., and Colicelli, J. (1995). Truncated forms of a novel yeast protein suppress the lethality of a G protein alpha subunit deficiency by interacting with the beta subunit. *J. Biol. Chem.* 270, 25435–25444. doi: 10.1074/jbc.270.43.25435

Spellman, P. T., Sherlock, G., Zhang, M. Q., Iyer, V. R., Anders, K., Eisen, M. B., et al. (1998). Comprehensive identification of cell cycle-regulated genes of the yeast *Saccharomyces cerevisiae* by microarray hybridization. *Mol. Biol. Cell* 9, 3273–3297. doi: 10.1091/mbc.9.12.3273

Springer, M., Wykoff, D. D., Miller, N., and O'Shea, E. K. (2003). Partially phosphorylated Pho4 activates transcription of a subset of phosphate-responsive genes. *PLoS Biol.* 1:E28. doi: 10.1371/journal.pbio.0000028

Steger, D. J., Haswell, E. S., Miller, A. L., Wente, S. R., and O'Shea, E. K. (2003). Regulation of chromatin remodeling by inositol polyphosphates. *Science* 299, 114–116. doi: 10.1126/science.1078062

Steidle, E. A., Chong, L. S., Wu, M., Crooke, E., Fiedler, D., Resnick, A. C., et al. (2016). A novel inositol pyrophosphate phosphatase in *Saccharomyces cerevisiae*: Siw14 PROTEIN SELECTIVELY CLEAVES THE β-PHOSPHATE FROM 5-DIPHOSPHOINOSITOL PENTAKISPHOSPHATE (5PP-IP5). *J. Biol. Chem.* 291, 6772–6783. doi: 10.1074/jbc.M116.714907

Swinnen, E., Rosseels, J., and Winderickx, J. (2005). The minimum domain of Pho81 is not sufficient to control the Pho85-Rim15 effector branch involved in phosphate starvation-induced stress responses. *Curr. Genet.* 48, 18–33. doi: 10.1007/s00294-005-0583-3

Szijgyarto, Z., Garedew, A., Azevedo, C., and Saiardi, A. (2011). Influence of inositol pyrophosphates on cellular energy dynamics. *Science* 334, 802–805. doi: 10.1126/science.1211908

Tamai, Y., Toh-e, A., and Oshima, Y. (1985). Regulation of inorganic phosphate transport systems in Saccharomyces cerevisiae. *J. Bacteriol.* 164, 964–968.

Tammenkoski, M., Koivula, K., Cusanelli, E., Zollo, M., Steegborn, C., Baykov, A. A., et al. (2008). Human metastasis regulator protein H-prune is a short-chain exopolyphosphatase. *Biochemistry* 47, 9707–9713. doi: 10.1021/bi8010847

Tammenkoski, M., Moiseev, V. M., Lahti, M., Ugochukwu, E., Brondijk, T. H. C., White, S. A., et al. (2007). Kinetic and mutational analyses of the major cytosolic exopolyphosphatase from *Saccharomyces cerevisiae*. *J. Biol. Chem.* 282, 9302–9311. doi: 10.1074/jbc.M609423200

Teunissen, J. H. M., Crooijmans, M. E., Teunisse, P. P. P., and van Heusden, G. P. H. (2017). Lack of 14-3-3 proteins in *Saccharomyces cerevisiae* results in cell-to-cell heterogeneity in the expression of Pho4-regulated genes *SPL2* and *PHO84*. *BMC Genomics* 18:701. doi: 10.1186/s12864-017-4105-8

Thomas, M. R., and O'Shea, E. K. (2005). An intracellular phosphate buffer filters transient fluctuations in extracellular phosphate levels. *Proc. Natl. Acad. Sci. U.S.A.* 102, 9565–9570. doi: 10.1073/pnas.0501122102

Toh-e, A., and Kakimoto, S. (1975). Genes coding for the structure of the acid phosphatases in *Saccharomyces cerevisiae*. *Mol. Gen. Genet.* 143, 65–70. doi: 10.1007/bf00269421

Toh-E, A., and Nishizawa, M. (2001). Structure and function of cyclin-dependent Pho85 kinase of *Saccharomyces cerevisiae*. *J. Gen. Appl. Microbiol.* 47, 107–117. doi: 10.2323/jgam.47.107

Toh-E, A., Tanaka, K., Uesono, Y., and Wickner, R. B. (1988). PHO85, a negative regulator of the PHO system, is a homolog of the protein kinase gene, CDC28, of *Saccharomyces cerevisiae*. *Mol. Gen. Genet.* 214, 162–164. doi: 10.1007/BF00340196

Uhler, J. P., Hertel, C., and Svejstrup, J. Q. (2007). A role for noncoding transcription in activation of the yeast PHO5 gene. *Proc. Natl. Acad. Sci. U.S.A.* 104, 8011–8016. doi: 10.1073/pnas.0702431104

Urech, K., Dürr, M., Boller, T., Wiemken, A., and Schwencke, J. (1978). Localization of polyphosphate in vacuoles of *Saccharomyces Cerevisiae*. *Arch. Microbiol.* 116, 275–278. doi: 10.1007/bf00417851

Vardi, N., Levy, S., Assaf, M., Carmi, M., and Barkai, N. (2013). Budding yeast escape commitment to the phosphate starvation program using gene expression noise. *Curr. Biol.* 23, 2051–2057. doi: 10.1016/j.cub.2013.08.043

Vardi, N., Levy, S., Gurvich, Y., Polacheck, T., Carmi, M., Jaitin, D., et al. (2014). Sequential feedback induction stabilizes the phosphate starvation response in budding yeast. *Cell Rep.* 9, 1122–1134. doi: 10.1016/j.celrep.2014.10.002

Wang, C., Yue, W., Ying, Y., Wang, S., Secco, D., Liu, Y., et al. (2015). Rice SPX-major facility superfamily3, a vacuolar phosphate efflux transporter, is involved in maintaining phosphate homeostasis in rice. *Plant Physiol.* 169, 2822–2831. doi: 10.1104/pp.15.01005

Wang, H., Falck, J. R., Hall, T. M. T., and Shears, S. B. (2012). Structural basis for an inositol pyrophosphate kinase surmounting phosphate crowding. *Nat. Chem. Biol.* 8, 111–116. doi: 10.1038/nchembio.733

Wang, H., Gu, C., Rolfes, R. J., Jessen, H. J., and Shears, S. B. (2018). Structural and biochemical characterization of Siw14: a protein-tyrosine phosphatase fold that metabolizes inositol pyrophosphates. *J. Biol. Chem.* 293, 6905–6914. doi: 10.1074/jbc.RA117.001670

Wanke, V., Pedruzzi, I., Cameroni, E., Dubouloz, F., and De Virgilio, C. (2005). Regulation of G0 entry by the Pho80-Pho85 cyclin-CDK complex. *EMBO J.* 24, 4271–4278. doi: 10.1038/sj.emboj.7600889

Waters, N. C., Knight, J. P., Creasy, C. L., and Bergman, L. W. (2004). The yeast Pho80-Pho85 cyclin-CDK complex has multiple substrates. *Curr. Genet.* 46, 1–9.

Weaver, J. D., Wang, H., and Shears, S. B. (2013). The kinetic properties of a human PPIP5K reveal that its kinase activities are protected against the consequences of a deteriorating cellular bioenergetic environment. *Biosci. Rep.* 33:e00022. doi: 10.1042/BSR20120115

Wiame, J. M. (1947). Étude d'une substance polyphosphorée, basophile et métachromatique chez les levures. *Biochim. Biophys. Acta* 1, 234–255. doi: 10.1016/0006-3002(47)90137-6

Wild, R., Gerasimaite, R., Jung, J.-Y., Truffault, V., Pavlovic, I., Schmidt, A., et al. (2016). Control of eukaryotic phosphate homeostasis by inositol polyphosphate sensor domains. *Science* 352, 986–990. doi: 10.1126/science.aad9858

Wilson, M. S., Jessen, H. J., and Saiardi, A. (2019). The inositol hexakisphosphate kinases IP6K1 and -2 regulate human cellular phosphate homeostasis, including XPR1-mediated phosphate export. *J. Biol. Chem.* 294, 11597–11608. doi: 10.1074/jbc.RA119.007848

Wilson, M. S. C., Livermore, T. M., and Saiardi, A. (2013). Inositol pyrophosphates: between signalling and metabolism. *Biochem. J.* 452, 369–379. doi: 10.1042/BJ20130118

Wurst, H., and Kornberg, A. (1994). A soluble exopolyphosphatase of *Saccharomyces cerevisiae*. *Purif. charact.* 269, 10996–11001.

Wurst, H., Shiba, T., and Kornberg, A. (1995). The gene for a major exopolyphosphatase of *Saccharomyces cerevisiae*. *J. Bacteriol.* 177, 898–906. doi: 10.1128/jb.177.4.898-906.1995

Wykoff, D. D., and O'Shea, E. K. (2001). Phosphate transport and sensing in *Saccharomyces cerevisiae*. *Genetics* 159, 1491–1499.

Wykoff, D. D., Rizvi, A. H., Raser, J. M., Margolin, B., and O'Shea, E. K. (2007). Positive feedback regulates switching of phosphate transporters in *S. cerevisiae*. *Mol. Cell* 27, 1005–1013. doi: 10.1016/j.molcel.2007.07.022

Xu, Y.-F., Létisse, F., Absalan, F., Lu, W., Kuznetsova, E., Brown, G., et al. (2013). Nucleotide degradation and ribose salvage in yeast. *Mol. Syst. Biol.* 9:665. doi: 10.1038/msb.2013.21

Xu, Z., Wei, W., Gagneur, J., Perocchi, F., Clauder-Münster, S., Camblong, J., et al. (2009). Bidirectional promoters generate pervasive transcription in yeast. *Nature* 457, 1033–1037. doi: 10.1038/nature07728

Yompakdee, C., Bun-ya, M., Shikata, K., Ogawa, N., Harashima, S., and Oshima, Y. (1996). A putative new membrane protein, Pho86p, in the inorganic phosphate uptake system of *Saccharomyces cerevisiae*. *Gene* 171, 41–47. doi: 10.1016/0378-1119(96)00079-0

Yoshida, K., Kuromitsu, Z., Ogawa, N., and Oshima, Y. (1989a). Mode of expression of the positive regulatory genes PHO2 and PHO4 of the phosphatase regulon in *Saccharomyces cerevisiae*. *Mol. Gen. Genet.* 217, 31–39. doi: 10.1007/bf00330939

Yoshida, K., Ogawa, N., and Oshima, Y. (1989b). Function of the PHO regulatory genes for repressible acid phosphatase synthesis in *Saccharomyces cerevisiae*. *Mol. Gen. Genet.* 217, 40–46. doi: 10.1007/bf00330940

Yousaf, R., Gu, C., Ahmed, Z. M., Khan, S. N., Friedman, T. B., Riazuddin, S., et al. (2018). Mutations in diphosphoinositol-pentakisphosphate kinase PPIP5K2 are associated with hearing loss in human and mouse. *PLoS Genet.* 14:e1007297. doi: 10.1371/journal.pgen.1007297

Zhu, J., Lau, K., Puschmann, R., Harmel, R. K., Zhang, Y., Pries, V., et al. (2019). Two bifunctional inositol pyrophosphate kinases/phosphatases control plant phosphate homeostasis. *eLife* 8:e43582. doi: 10.7554/eLife.43582

Zvyagilskaya, R. A., Lundh, F., Samyn, D., Pattison-Granberg, J., Mouillon, J.-M., Popova, Y., et al. (2008). Characterization of the Pho89 phosphate transporter by functional hyperexpression in *Saccharomyces cerevisiae*. *FEMS Yeast Res.* 8, 685–696. doi: 10.1111/j.1567-1364.2008.00408.x

**Conflict of Interest:** The authors declare that the research was conducted in the absence of any commercial or financial relationships that could be construed as a potential conflict of interest.

frontiers in Plant Science

ORIGINAL RESEARCH
published: 12 August 2020
doi: 10.3389/fpls.2020.01240

# The $H^+$-Translocating Inorganic Pyrophosphatase From *Arabidopsis thaliana* Is More Sensitive to Sodium Than Its $Na^+$-Translocating Counterpart From *Methanosarcina mazei*

*José R. Pérez-Castiñeira* and Aurelio Serrano*

*Instituto de Bioquímica Vegetal y Fotosíntesis, Universidad de Sevilla-CSIC, Sevilla, Spain*

OPEN ACCESS

**Edited by:**
*Gabino Ríos,*
*Instituto Valenciano de Investigaciones Agrarias, Spain*

**Reviewed by:**
*Ali Ferjani,*
*Tokyo Gakugei University, Japan*
*Roberto Adrian Gaxiola,*
*Arizona State University, United States*
*Anssi Malinen,*
*University of Turku, Finland*

***Correspondence:**
*José R. Pérez-Castiñeira*
*jroman@us.es*

**Specialty section:**
*This article was submitted to Plant Metabolism and Chemodiversity, a section of the journal Frontiers in Plant Science*

**Received:** *17 March 2020*
**Accepted:** *28 July 2020*
**Published:** *12 August 2020*

**Citation:**
*Pérez-Castiñeira JR and Serrano A (2020) The $H^+$-Translocating Inorganic Pyrophosphatase From Arabidopsis thaliana Is More Sensitive to Sodium Than Its $Na^+$-Translocating Counterpart From Methanosarcina mazei. Front. Plant Sci. 11:1240. doi: 10.3389/fpls.2020.01240*

Overexpression of membrane-bound $K^+$-dependent $H^+$-translocating inorganic pyrophosphatases ($H^+$-PPases) from higher plants has been widely used to alleviate the sensitivity toward NaCl in these organisms, a strategy that had been previously tested in *Saccharomyces cerevisiae*. On the other hand, $H^+$-PPases have been reported to functionally complement the yeast cytosolic soluble pyrophosphatase (IPP1). Here, the efficiency of the $K^+$-dependent $Na^+$-PPase from the archaeon *Methanosarcina mazei* (MVP) to functionally complement IPP1 has been compared to that of its $H^+$-pumping counterpart from *Arabidopsis thaliana* (AVP1). Both membrane-bound integral PPases (mPPases) supported yeast growth equally well under normal conditions, however, cells expressing MVP grew significantly better than those expressing AVP1 under salt stress. The subcellular distribution of the heterologously-expressed mPPases was crucial in order to observe the phenotypes associated with the complementation. *In vitro* studies showed that the PPase activity of MVP was less sensitive to $Na^+$ than that of AVP1. Consistently, when yeast cells expressing MVP were grown in the presence of NaCl only a marginal increase in their internal PPi levels was observed with respect to control cells. By contrast, yeast cells that expressed AVP1 had significantly higher levels of this metabolite under the same conditions. The $H^+$-pumping activity of AVP1 was also markedly inhibited by $Na^+$. Our results suggest that mPPases primarily act by hydrolysing the PPi generated in the cytosol when expressed in yeast, and that AVP1 is more susceptible to $Na^+$ inhibition than MVP both *in vivo* and *in vitro*. Based on this experimental evidence, we propose $Na^+$-PPases as biotechnological tools to generate salt-tolerant plants.

**Keywords: *Arabidopsis thaliana*, heterologous expression, membrane-bound ion ($H^+$- or $Na^+$)-pumping inorganic pyrophosphatases, *Methanosarcina mazei*, *Saccharomyces cerevisiae*, salt stress, soluble inorganic pyrophosphatase**

## INTRODUCTION

The membrane-bound $K^+$-dependent $H^+$-translocating inorganic pyrophosphatase ($H^+$-PPase), encoded by *AVP1*, has been reported to be the protein responsible for removing most of the inorganic pyrophosphate (PPi) generated in the cytosol of *Arabidopsis thaliana* cells (Ferjani et al., 2011; Kriegel et al., 2015; Segami et al., 2018b). The removal of PPi, a by-product of many biosynthetic reactions, is essential in all living cells because its accumulation causes the collapse of anabolism, eventually leading to cell death (Lahti, 1983; Serrano-Bueno et al., 2013). AVP1 couples the energy released by the hydrolysis of PPi to the translocation of protons into the vacuole, thus acting as a second proton pump in the plant tonoplast along with the V-type $H^+$-ATPase (Sarafian et al., 1992; Graus et al., 2018). By contrast, in the cytosol of *Saccharomyces cerevisiae* cells only one protein seems to have the capacity to hydrolyse PPi: the extremely efficient soluble inorganic pyrophosphatase (sPPase), encoded by *IPP1* (Kolakowski et al., 1988).

In a seminal paper published in 2001, Gaxiola and co-workers reported that overexpression of AVP1 alleviated the sensitivity of *A. thaliana* to NaCl (Gaxiola et al., 2001). Thereafter, several groups obtained other plants with higher tolerance to salinity and other stresses based on this approach (Park et al., 2005; Gao et al., 2006; Li et al., 2008; Lv et al., 2008; Pasapula et al., 2011; Gaxiola et al., 2012; Schilling et al., 2014; Yang et al., 2015; Lv et al., 2016; Ahire et al., 2018). This strategy had been originally tested in *S. cerevisiae* (Gaxiola et al., 1999), thus demonstrating the suitability of this yeast to study and test solutions to salt stress in plants.

Although AVP1 and its orthologs in higher plants have been used as tools to develop salt-tolerant plants, membrane-bound PPases with different biochemical properties have been characterized from other organisms. A $K^+$-independent $H^+$-PPase was identified in 1966 in the photosynthetic alphaproteobacterium *Rhodospirillum rubrum* (RVP) (Baltscheffsky and Baltscheffsky, 1995). The corresponding gene was cloned and sequenced in the 1990s (Baltscheffsky et al., 1998) and expressed both in *E. coli* (Schultz and Baltscheffsky, 2004) and *S. cerevisiae* (Drake et al., 2010). Two ortologs of RVP have been identified in *A. thaliana* (AVP2 and AVP3) and reported to be located in the Golgi membranes, however, these proteins seem to have much lower expression levels than AVP1 and their physiological importance remains to be established (Drozdowicz et al., 2000; Ferjani et al., 2011). An important breakthrough in the field of PPases was the discovery of $K^+$-dependent $Na^+$-translocating mPPases ($Na^+$-PPases) in eubacteria and archaea (Malinen et al., 2007; Baykov et al., 2013). Nowadays, genome projects of a wide variety of organisms as well as metagenomics and biochemical studies are significantly broadening the $Na^+$-PPases field (Luoto et al., 2015; Serrano A., unpublished).

Our group has previously reported the generation of several *S. cerevisiae* mutant strains whose *IPP1* genes are under the control of the glucose-repressible promoter of the *GAL1* gene. These strains cannot grow on glucose, thus demonstrating the essentiality of the sPPase encoded by *IPP1* (Serrano-Bueno et al., 2013), however, the capacity to grow on this carbon source is recovered when they are transformed with plasmids bearing genes coding for $H^+$-PPases under the control of constitutive promoters (Pérez-Castiñeira et al., 2002; Drake et al., 2010; Pérez-Castiñeira et al., 2011; Hernández et al., 2015). This system avoids the competition for the substrate between the heterologous $H^+$-PPase and the yeast cytosolic sPPase *in vivo*, a situation that resembles that of a plant cell cytosol.

In this communication, the capacity of two different mPPases to complement IPP1 under salt stress has been studied. In order to accomplish this task, several yeast mutants with different sensitivities to NaCl and conditional expression of IPP1 were generated. These mutants were transformed with plasmids bearing genes coding for AVP1 or the $K^+$-dependent $Na^+$-PPase from the salt-tolerant archaeon *Methanosarcina mazei* (MVP) (Malinen et al., 2007). MVP was more efficient than AVP1 at supporting growth of the different yeast mutants in the presence of NaCl. The addition of N-terminal signal peptides that modify the subcellular distribution of the mPPases (Drake et al., 2010) was essential for efficient complementation of IPP1. *In vitro* assays showed that AVP1 is significantly more sensitive to $Na^+$ than MVP.

Our results suggest that mPPases may be direct targets of $Na^+$ *in vivo*, a situation that might lead to a toxic accumulation of PPi in the cytosol of plant cells subjected to high concentrations of salt. Based on this evidence, we propose the heterologous expression of chimeric versions of $Na^+$-PPases with appropriate N-terminal signal peptides as a more efficient way to improve salt-tolerance in plants than the current approach, based on the use of untargeted $H^+$-PPases. In connection with this, *in silico* analyses of currently available genomes suggest that $Na^+$-PPases, originally described in bacteria and archaea (Malinen et al., 2007; Luoto et al., 2011; Luoto et al., 2015), are present in other organisms, including some of the photosynthetic lineage like certain marine microalgal groups (Prasinophyceae and diatoms). Our findings suggest new biotechnological applications for microalgae in order to improve plants of agronomical interest.

## MATERIALS AND METHODS

### Yeast Strains

The strains used in this work are shown in **Table 1**. YPC3 mutant strain was generated from *S. cerevisiae* haploid strain W303-1A (MATa, *ade2-1 can1-100 his3-11,15 leu2-3,112 trp1-1*, *ura3-1*) by the single-step transplacement procedure as previously described (Drake et al., 2010). This mutant has *IPP1*, the gene that codes for the cytosolic soluble inorganic PPase, under the control of the

**Abbreviations:** AVP1, $K^+$-dependent $H^+$-translocating inorganic pyrophosphatase from *Arabidopsis thaliana*; mPPase, membrane-bound integral ion ($H^+$- or $Na^+$) -pumping inorganic pyrophosphatase; MVP, $K^+$-dependent $Na^+$-translocating inorganic pyrophosphatase from *Methanosarcina mazei;* PPase, Inorganic pyrophosphatase; PPi, Inorganic pyrophosphate; sPPase, Soluble inorganic pyrophosphatase.

**TABLE 1** | Yeast strains used in this work.

| Name | Relevant genotype | Reference |
|---|---|---|
| W303-1A | *MATa, ade2-1 can1-100 his3-11,15 leu2-3,112 trp1-1 ura3-1* | (Thomas and Rothstein, 1989) |
| G19 | MATα, *ade2-1 can1-100 his3-11,15 leu2-3,112 trp1-1 ura3-1 ena1Δ::HIS3::ena4Δ* | (Quintero et al., 1996) |
| B31 | *MATα, ade2-1 can1-100 his3-11,15 leu2-3,112 trp1-1 ura3-1 ena1Δ::HIS3::ena4Δ nha1Δ::LEU2* | (Bañuelos et al., 1998) |
| YPC3 | W303-1A $ipp1_{UAS}$-$ipp1_{TATA}$::*HIS3*-$GAL1_{UAS}$-$GAL1_{TATA}$-*IPP1* | (Drake et al., 2010) |
| YPC5 | G19 $ipp1_{UAS}$-$ipp1_{TATA}$::*TRP1*-$GAL1_{UAS}$-$GAL1_{TATA}$-*IPP1* | This study |
| YPC6 | B31 $ipp1_{UAS}$-$ipp1_{TATA}$::*TRP1*-$GAL1_{UAS}$-$GAL1_{TATA}$-*IPP1* | This study |

yeast galactokinase gene (*GAL1*) promoter (Drake et al., 2010). YPC5 and YPC6 mutant strains were obtained from *S. cerevisiae* strains G19 and B31, respectively, by following the same strategy except that the *TRP7* cassette was used as a selection marker instead of *HIS3*. Mutant G19 had been derived from strain W303-1B by disrupting its *ENA1-4* genes with the yeast *HIS3* cassette (Quintero et al., 1996), whereas B31 was obtained from G19 by disrupting *NHA1* with the *LEU2* cassette (Bañuelos et al., 1998). Both mutants were generously provided by Professor Alonso Rodríguez Navarro (Universidad Politécnica de Madrid, Spain).

## Plasmids Construction and Yeast Transformation

YPC3, YPC5, and YPC6 cells were transformed with the plasmids shown in **Table 2** as previously described (Schiestl and Gietz, 1989). All plasmids are 2 micron-based derivatives of the *URA3*-containing *E. coli/S. cerevisiae* shuttle plasmid pRS699, that bears the yeast *PMA1* promoter for constitutive expression of inserts (Serrano and Villalba, 1995). The latter were made by in-frame fusion of the N-terminal signal peptides of *S. cerevisiae* SUC2 invertase (Inv) or the $K^+$-dependent $H^+$-PPase from *Trypanosoma cruzi* (Tc), the sequence coding for the yeast-enhanced green fluorescent protein (yEGFP) and the coding sequence of the $K^+$-dependent $H^+$-PPase from *A. thaliana* (AVP1) (Drake et al., 2010). An identical approach was followed with the coding sequence of the $K^+$-dependent $Na^+$-PPase from *M. mazei* (MVP) (Malinen et al., 2007), generously provided by Professor Reijo Lahti, University of Turku (Finland).

**TABLE 2** | Plasmids used for yeast transformation.

| Plasmid | Insertion | Reference |
|---|---|---|
| pIPP1 | Sequence coding for the cytosolic soluble PPase from *S. cerevisiae* | (Pérez-Castiñeira et al., 2002) |
| pInvGFPAVP1 | Sequence coding for the putative N-terminal signal peptide of Suc2p followed by those of yEGFP and the $H^+$-PPase from *A. thaliana* (AVP1) | (Drake et al., 2010) |
| pInvGFPMVP | Sequence coding for the putative N-terminal signal peptide of Suc2p followed by those of yEGFP and the $Na^+$-PPase from *M. mazei* (MVP) | This study |
| pTcGFPAVP1 | Sequence coding for the putative N-terminal signal peptide of the $K^+$-dependent $H^+$-PPase from *Trypanosoma cruzi* followed by those of yEGFP and AVP1 | (Drake et al., 2010) |
| pTcGFPMVP | Sequence coding for the putative N-terminal signal peptide of the $K^+$-dependent $H^+$-PPase from *T. cruzi* followed by those of yEGFP and MVP | This study |

*Original and chimeric nucleotide sequences described in the table were inserted between yeast PMA1 promoter and terminator of the URA3-containing plasmid pRS699 (Serrano and Villalba, 1995).*

For the transformation procedure, YPC3, YPC5 and YPC6 cells were initially grown at 30°C in YPGal liquid medium [1% (w/v) yeast extract, 2% (w/v) peptone, 2% (w/v) galactose], while transformants were selected on 2% agar plates made in galactose-containing synthetic medium [0,17% (w/v) yeast nitrogen base without amino acids and ammonium sulphate, 2% (w/v) galactose, 50 mM TRIS-HCl pH 6, and a mixture of nucleotides and amino acids described in (Treco and Lundblad, 2001)], devoid of histidine and uracil (YPC3); histidine, tryptophan, and uracil (YPC5); or histidine, tryptophan, leucine, and uracil (YPC6). Colonies appeared after incubating the plates for 3-4 days at 30°C.

## Phenotype Complementation Tests

Complementation studies were performed by inoculating 2 ml of galactose-containing selective medium with transformed cells from the plates and growing overnight at 30°C on an orbital shaker (150 r.p.m.). The following day, 10 µl of these cultures were used to inoculate 2 ml of YPD medium [1% (w/v) yeast extract, 2% (w/v) peptone, 2% (w/v) glucose] (1:200 dilution) and allowed to grow overnight as described above. This treatment is necessary to bring down the PPase activity associated with the chromosome-encoded IPP1, controlled by the glucose-repressible *GAL1* promoter (Pérez-Castiñeira et al., 2002). After overnight growth on glucose, ten-fold serial dilutions of the cultures were made in sterile water and 5 µl drops of each dilution were spotted onto YPD agar plates containing different NaCl concentrations and 50 mM TRIS-MES adjusted to pH 6. Plates were incubated at 30°C for several days.

## Isolation of Yeast Microsomal Membranes

Preparations of membrane fractions were obtained from YPC6 cells transformed with the different plasmids by a modification of a method previously described (Serrano and Villalba, 1995): yeast colonies were collected from a plate and grown up to stationary phase in galactose-containing selective liquid medium; then, 400 ml of YPD were inoculated with 2 ml of stationary cultures. After overnight growth, cells were collected by centrifugation at 700 x *g* for 10 min, washed thoroughly with water, resuspended in 5 ml of ice-cold buffer A (25 mM Tris-HCl, pH 8, 10% glycerol, 4 mM β-mercaptoethanol, 2 mM DTT, 1 mM benzamidine, 2 mM ϵ-aminocaproic acid, 1 mM PMSF), and homogenized by vigorous vortexing for five one-min bursts in the presence of glass beads (0.5 mm Ø) with one-min intervals on ice. From this point on, the whole procedure was carried out

at 0°C (except centrifugations, that were performed at 4°C). The homogenate was diluted up to 25 ml with buffer B (10 mM Tris-HCl, pH 7.6, 10% (w/v) glycerol, 2 mM DTT) and centrifuged for 10 min at 700 x *g* to remove beads and debris. The resulting supernatant was centrifuged for 20 min at 20,000 x *g* and the pellet [the crude mitochondrial fraction, that includes mitochondria and plasma membrane vesicles among others (Serrano and Villalba, 1995)] was discarded for PPi hydrolysis assays due to the potential interference of the mitochondrial PPase (Lundin et al., 1991). The supernatant of this step was centrifuged for 30 min at 120,000 x *g*. The pellet thus obtained, the microsomal fraction, was taken up, homogenized in stripping buffer [60 mM Tris/HCl, pH 8, 12% (w/v) glycerol, 0.72 M KCl, and 1.2 mM $CaCl_2$ (Lenoir et al., 2002)] and centrifuged for 20 min at 120,000 x *g*. Finally, the stripped microsomal fraction was washed with buffer B and centrifuged (20 min, 120,000 x *g*). The final pellet was resuspended and homogenized in 0.5–1 ml of buffer B. Microsomes were directly used for activity assays or divided into aliquots and kept at -80°C until use.

## Pyrophosphatase Activity and ACMA Quenching Assays, Western Blot, and Total Protein Estimation

Pyrophosphatase (PPase) activity was assayed at 30°C by incubation of protein preparations with $Mg_2PPi$ at pH 7.2 with the addition of KCl, NaCl and/or NaF when indicated, and colorimetrically measuring the released ortophosphate as previously described (Rathbun and Betlach, 1969). $Mg_2PPi$ was obtained by adding fixed volumes of stock solutions of appropriate concentrations of $MgCl_2$ and $Na_4PPi$ to the assay mixes. Reactions were started by the addition of the latter and stopped with a mixture of trichloroacetic acid, sodium acetate, acetic acid, and formaldehyde (final concentrations: 4% (w/v), 0,5 M, 0.5 M, and 1% (w/v), respectively) (Schultz and Baltscheffsky, 2004). Control yeast microsomal membranes devoid of PPase activity and containing the same amount of total protein were used as blanks in every assay. ACMA quenching assays and *Western blot*s were performed as described elsewhere (Perez-Castiñeira and Apps, 1990; Valverde et al., 1997). A polyclonal antibody raised against the purified $Na^+$-PPase from the marine bacterium *Thermotoga maritima* (TVP) (López-Marqués et al., 2005) and a commercial polyclonal rabbit antibody against yeast IPP1 protein (AP21326F_N, OriGene EU, Germany) were used for immunodetection of mPPases and sPPases, respectively, after SDS-PAGE and semi-dry electroblotting transfer. Antibody against TVP was affinity-purified as previously described (Pringle et al., 1991). Protein concentration was estimated using a Coomassie-blue dye binding-based assay from Bio-Rad (München, Germany) following manufacturer's instructions and using ovalbumin as a standard.

## Analysis of Enzyme Kinetics

Kinetic data obtained for AVP1 and MVP were fitted to the Hill equation and to a mathematical expression based on the concerted MWC allosteric model (see Results) by weighted non-linear least squares (nls) regression using RStudio (version 1.1.456 – © 2009–2018 RStudio, Inc.), downloaded from https://cran.cnr.berkeley.edu. This version of RStudio is an integrated development environment (IDE) for the programming language R, version 3.5.1 (2018-07-02), "Feather Spray" (© 2018 The R Foundation for Statistical Computing), and was run under Ubuntu 18.04.1 LTS ("Bionic Beaver") and Debian GNU/Linux 10 ("buster"). Averages of three to five independent experiments were used for regression calculations and each experimental data point was weighted as 1/variance.

## Determination of Internal PPi Levels in Yeast Cells

100 ml cultures of YPC6 cells transformed with the plasmids shown in **Table 2** and treated to minimize the chromosome-encoded IPP1 (see above) were grown in glucose-containing medium (YPD adjusted to pH 6) with agitation in the presence or absence of 100 mM NaCl. The initial optical densities at 660 nm ($OD_{660}$) of the cultures where individually adjusted so that all of them had an $OD_{660}$ of around 0.5 (roughly $10^9$ cells) after 8–9 h. Then, cells were collected by centrifugation, washed with ice-cold deionised water and broken as described for isolation of yeast membranes, except that a 4% (v/v) perchloric acid aqueous solution was used instead of buffer A. Beads, debris, and denatured proteins were removed by centrifugation (20 min, 20,000 × g, *4 °C*) and PPi concentrations were determined colorimetrically in the supernatants after neutralization with KOH, as previously described (Heinonen et al., 1981).

## Molecular Phylogenetic Analysis of mPPases

The amino acid sequences of selected $H^+$- and $Na^+$-translocating mPPases orthologs of bacteria, archaea, parasitic protists, microalgae and plants were aligned with the CLUSTAL X software tool (Larkin et al., 2007). Phylogenetic trees were constructed with the evolutionary distances (neighbor joining) and maximum parsimony methods using the SeaView v5.2 software (Gouy et al., 2010).

# RESULTS

## MVP Functionally Complements Yeast IPP1 More Efficiently Than AVP1 Under Salt Stress

Three yeast strains with increasing sensitivities to NaCl were generated (**Table 1**) and transformed with *E. coli/S. cerevisiae* shuttle plasmids bearing the genes coding for chimeric versions of AVP1 and MVP under the control of the yeast *PMA*1 promoter (**Table 2**). Drop tests to check for growth of transformants onto YPD plates at pH 6 containing different concentrations of NaCl were carried out.

We have previously shown that addition of certain sequences in the N-termini of the coding sequences of some mPPases altered the subcellular distribution of the resulting chimeric peptide and improved their expression levels. Among these sequences were those encoding the N-terminal signal peptides from the *S. cerevisiae* invertase SUC2 or the $K^+$-dependent $H^+$-

PPase from *Trypanosoma cruzi* (TcVP), which targeted the chimeric mPPases mainly to the plasma membrane or the internal membrane systems, respectively. Fusion with the yEGFP sequence further enhanced mPPase expression levels, especially in the case of AVP1 (Drake et al., 2010; Pérez-Castiñeira et al., 2011). This protein engineering strategy was applied to the coding sequence of the $K^+$-dependent $Na^+$-PPase from *M. mazei* with similar results (**Supplementary Figure S1**).

Initial studies of growth in the presence of NaCl were done with YPC3, a mutant derived from the strain W303-1A, which is not especially sensitive to $Na^+$ and is able to grow in the presence of NaCl concentrations in the molar range (Rios et al., 1997). **Figure 1** shows drop tests comparing growth obtained with YPC3 cells transformed with plasmids bearing different PPase genes and with the parental strain W303-1A. Cells expressing MVP grew significantly better than those expressing AVP1 in the presence of NaCl, however, no difference was observed in the absence of salt. Moreover, the chimera with the N-terminal signal peptide of yeast invertase SUC2 (InvGFPMVP) performed better than that with the N-terminal signal peptide of TcVP (TcGFPMVP). InvGFPAVP1 also supported growth more efficiently than TcGFPAVP1, albeit at lower NaCl concentrations than the MVP chimeras. None of the cells expressing mPPases grew better than those expressing their soluble counterpart from yeast (IPP1) under any of the conditions tested.

The use of YPC3 mutant and its parental strain forced the addition of very high concentrations of NaCl to observe the effects exerted by this salt (above 1 M). At such high concentrations, NaCl poses two types of stress to yeast cells, namely, osmotic stress and sodium toxicity. Although in glucose-containing medium the latter contributes more to growth inhibition than the former (Rios et al., 1997), we were interested in the specific effects of $Na^+$. It was then decided to use yeast strains that were sensitive to lower NaCl concentrations in order to minimize osmotic stress, therefore, we generated mutant strains YPC5 and YPC6. These strains have conditional expression of their respective *IPP1* genes in genetic backgrounds associated with higher sensitivities to NaCl (knock-outs of genes encoding major sodium pumps and/or transporters; **Table 1**). YPC5 and YPC6 cells were transformed with the plasmids described in **Table 2** and the results obtained are shown in **Figures 2A, B**, respectively. An identical pattern to that obtained in the case of transformed YPC3 cells was observed, the only difference being the concentrations of NaCl required to inhibit growth. YPC5 cells stopped growing at around 0.5 M NaCl,

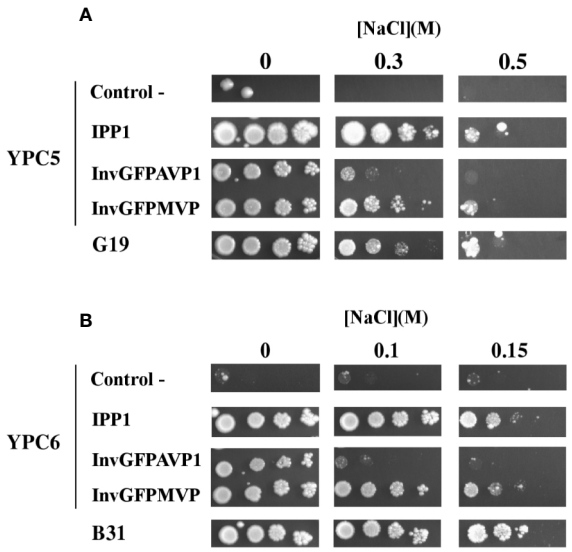


**FIGURE 2 |** Drop tests for sodium-sensitive yeast strains YPC5 **(A)**, YPC6 **(B)**, and their respective parental strains G19 and B31. Cells were transformed with plasmids pIPP1, pInvGFPAVP1 and pInvGFPMVP as described in the main text. The rest of conditions as described in . Negative controls are YPC5 **(A)** and YPC6 **(B)** cells transformed with empty plasmid.

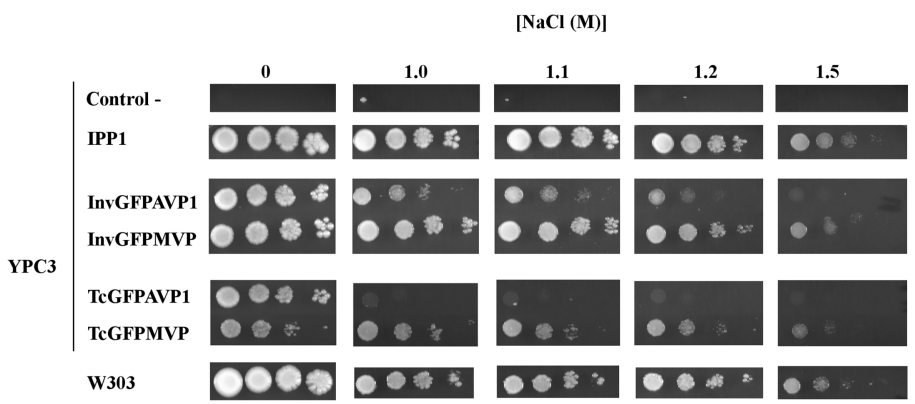


**FIGURE 1 |** Drop tests for yeast mutant YPC3 cells and parental strain W303 grown in the presence different concentrations of NaCl. Cells were transformed with plasmids shown in and grown as described in the main text. Serial dilutions of the cultures were made in sterile water and spotted on to YPD plates adjusted to pH 6 and containing the indicated concentrations of NaCl. Growth was recorded after 4 days at 30 °C. Negative controls are YPC3 cells transformed with empty plasmid.

whereas 150 mM NaCl was sufficient to obtain a similar effect in YPC6 cells. As far as mPPases are concerned, the chimera InvGFPMVP supported growth more efficiently than InvGFPAVP1, and both performed better than TcGFPMVP and TcGFPAVP1, respectively (not shown for clarity), as in the case of YPC3. YPC5 and YPC6 cells expressing IPP1 always performed better than those expressing chimeric mPPases. YPC6 cells transformed with plasmids pInvGFPMVP and pInvGFPAVP1 were selected for subsequent studies.

The results obtained with YPC3, YPC5 and YPC6 showed that the capacity of AVP1 to complement IPP1 was severely hampered by the presence of NaCl in the medium, whereas that of MVP was less sensitive to this circumstance. The fact that identical results were obtained with NaCl concentrations ranging from 1.5 M down to 150 mM suggests that the effects exerted by NaCl are actually due to $Na^+$ toxicity rather than to osmotic stress. This idea was supported by drop tests performed with transformed YPC5 and YPC6 cells in YPD plates supplemented with 1 M and 0.3 M sorbitol, that showed no difference with respect to those performed in YPD alone (not shown). Moreover, the addition of KCl instead of NaCl in the culture medium did not inhibit growth in any case (not shown), demonstrating that the phenotypes observed in the presence of NaCl were due to the toxic effects of $Na^+$.

## Membrane-Associated PPase Activity and Expression Levels of the Heterologously-Expressed mPPases Do Not Change When Yeast Cells Are Subjected to Salt Stress

In order to check whether the phenotypes observed could be due to differences in protein expression and/or PPase activity, different studies were done with microsomal membrane preparations and soluble extracts obtained from transformed YPC6 cells. The upper panel of **Figure 3A** shows fluoride-insensitive PPi hydrolysis activity associated with microsomal membranes. As expected, PPase activity could only be detected in preparations obtained from cells transformed with plasmids bearing genes coding for mPPases. These activities increased 6 to 7-fold in the presence of 100 mM KCl *in vitro*, a feature of both AVP1 and MVP (Kim et al., 1994; Malinen et al., 2007). The presence of NaCl during growth did not alter *in vitro* activity levels.

No membrane-bound PPase activity was detected in YPC6 control cells (transformed with empty plasmid pRS699), whereas in membrane preparations of cells transformed with plasmid pIPP1 some residual activity was detected in the absence of NaF (not shown). This indicates that some molecules of the yeast cytosolic sPPase remain attached to these membranes even after treatment with stripping buffer, as sensitivity to fluoride is a characteristic of this enzyme (see below).

Immunodetection carried out with microsomal membranes using an affinity-purified polyclonal antibody against the $Na^+$-PPase from *T. maritima* (TVP) confirmed the results obtained with PPase assays, that is, salt stress does not significantly alter expression levels and/or protein processing patterns in any case (**Figure 3A**, lower panel). The latter are due to partial degradation of the heterologously-expressed mPPases by yeast vacuolar proteases *in vivo* and it is a characteristic of our expression system (Pérez-Castiñeira et al., 2011).

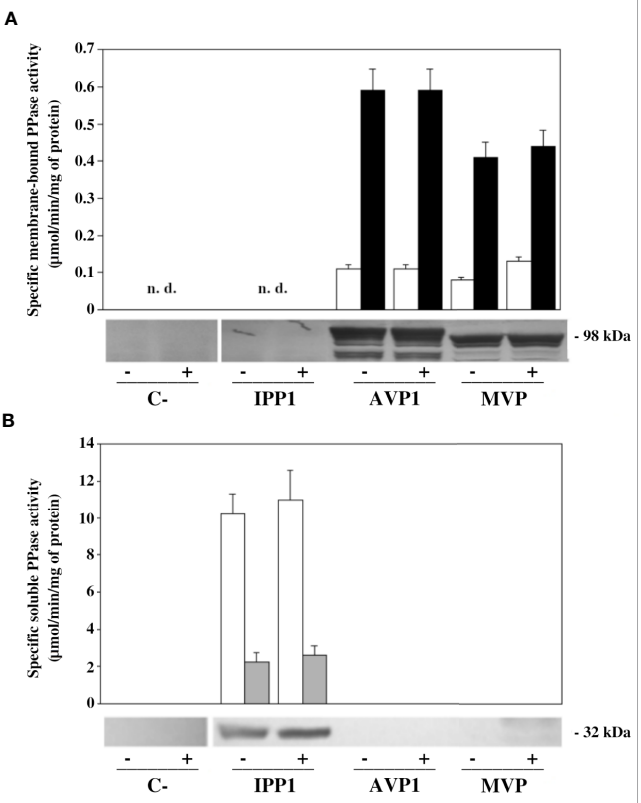


**FIGURE 3 |** Levels of PPi hydrolysis activity and immunodetection of mPPases in microsomal membranes **(A)** and sPPases in soluble extracts **(B)** of YPC6 mutant cells transformed with plasmids shown in **Table 2**. Cells were cultured in liquid YPD up to an $OD_{660nm}$ of 0.3, as described in main text, then, each culture was divided into two aliquots, one of which was subjected to a treatment with 100 mM NaCl by adding the appropriate volume of a 5 M stock solution of NaCl, whereas the same volume of deionized water was added to the other aliquot. All cultures were grown up to an $OD_{660nm}$ of 0.8-1, cells were collected and microsomal membranes and soluble crude extracts were obtained as described in Materials and Methods. An affinity purified polyclonal antibody against *Thermotoga maritima* mPPase **(A)** and a commercial antibody against IPP1 **(B)** were used for immunodetection. 70 μg of total protein were loaded per lane in all cases. Positive (+) signs denote samples obtained from cells subjected to treatment with 100 mM NaCl. Negative (-) signs denote samples obtained from control cultures with no added salt. "n. d.": not detected.

A parallel set of experiments were carried out with soluble protein extracts of YPC6 cells transformed with the same plasmids as above. Fluoride-sensitive sPPase activity could be measured only in extracts from cells transformed with plasmid pIPP1, consistently, a commercial antibody against IPP1 recognized a band of the expected size (ca. 37 kDa) in this sample (**Figure 3B**). Similar results were obtained with cells of the parental strain B31, albeit with lower levels of activity and IPP1 polypeptide (not shown). Growing cells in the presence of NaCl did not significantly alter IPP1 expression levels.

## Membrane-Bound PPases Exhibit Different Sensitivities to NaCl *In Vitro*

The effect exerted by $Na^+$ on the PPase activities of AVP1 and MVP *in vitro* was studied by performing assays in the presence of increasing concentrations (0, 50, and 100 mM) of added NaCl. It must be borne in mind that PPi is added as $Na_4PPi$ (see Materials and Methods), therefore, basal concentrations of $Na^+$ four times higher than those of PPi are always present in the assays. Both AVP1 and MVP depend on $K^+$ for full activity (Kim et al., 1994; Malinen et al., 2007), therefore, 100 mM KCl was always present in the assay mix to provide the concentration of $K^+$ usually maintained in most plant cells (Nieves-Cordones et al., 2016). $Mg_2PPi$ was used as substrate, as previously reported for diverse mPPases (Leigh et al., 1992; Gordon-Weeks et al., 1996; Tsai et al., 2014). Results obtained are shown in **Figure 4**. AVP1 seemed to be quite sensitive to NaCl, showing a decrease in $V_m$ of 20% and 50% in the presence of 50 and 100 mM NaCl, respectively; by contrast, MVP showed virtually no inhibition at 50 mM NaCl and only a 20% decrease in this parameter when the salt concentration was raised up to 100 mM.

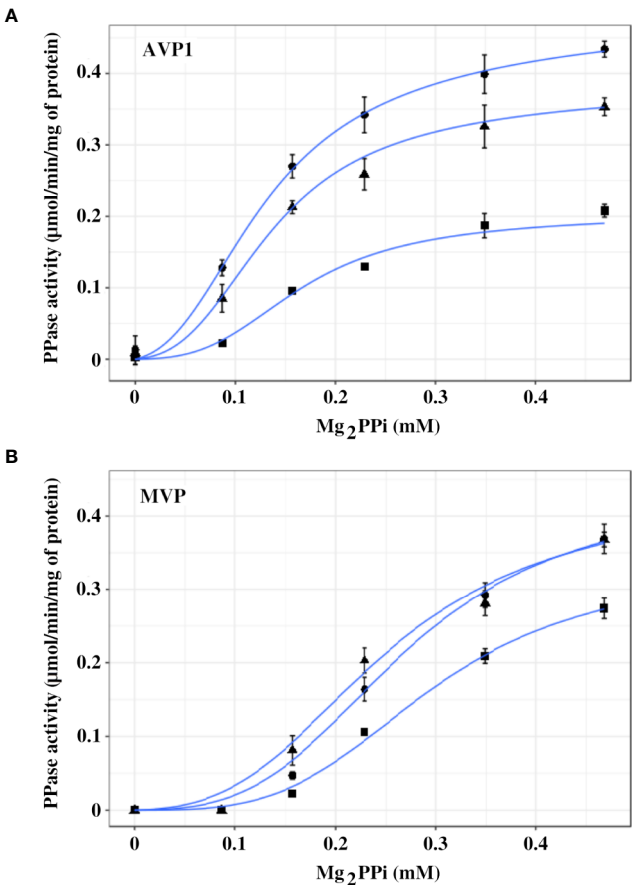


**FIGURE 4 |** Graphical representation of PPase activity versus substrate ($Mg_2PPi$) concentration for AVP1 **(A)** and MVP **(B)** in the presence of 0 mM (●), 50 mM (▲), and 100 mM (■) NaCl. Data points correspond to the averages ± standard errors (SE) of 4 independent experiments. The substrate, $Mg_2PPi$, was obtained by mixing stock solutions of $Na_4PPi$ and $MgCl_2$, as described in Materials and Methods, consequently, basal concentrations of $Na^+$ four times higher than those of PPi are present in the assays. $Mg_2PPi$ concentrations were estimated considering the dissociation constants for individual PPi complexes with $H^+$, $Na^+$, $K^+$, and $Mg^{2+}$, as previously described (Baykov et al., 1993). Graph lines were calculated with Equation 1 using RStudio, as described in Materials and Methods.

The experimental data were fitted with the empirical Hill equation (Hill, 1910) by weighted non-linear least squares regression using RStudio, yielding values of the Hill coefficient $n_H$ of 2–3 for AVP1 and 3.5–4.5 for MVP. This indicates a significant degree of positive cooperativity for both proteins, MVP showing a higher deviation from the Michaelis-Menten behaviour (that is, higher sigmoidicity) than AVP1. The $V_m$ value predicted by the Hill equation for MVP decreased somewhat with increasing concentrations of NaCl, however, neither $n_H$ nor the $K_{0.5}$ values changed significantly (**Table 3A**).

In order to model the kinetic properties of AVP1 and MVP and relate them to the structural information available for these proteins, a simplified equation was derived from the MWC concerted allosteric model (Monod et al., 1965). The following assumptions were made to obtain the equation:

1. The ratio $v/V_m$ is proportional to the saturation function ($\hat{Y}$) of the allosteric model
2. AVP1 and MVP can exist in two states, R and T, in thermodynamic equilibrium driven by the allosteric constant L= [T]/[R]. R is assumed to be active and T inactive.
3. The substrate ($Mg_2PPi$) binds only to the R state, thus defining a single dissociation constant $K_R$.
4. The number of catalytic binding sites for substrate is 2 for both mPPases functional oligomers. This assumption is based on the structural information currently available, which

**TABLE 3 |** Kinetic values obtained by fitting the Hill equation (A) and Equation 1 (B) to the experimental data shown in **Figure 4**.

| **(A)** | | | |
|---|---|---|---|
| **AVP1** | | **[NaCl] (mM)** | |
| **Parameter** | **0** | **50** | **100** |
| $V_m$ (U/mg prot.) | 0.47 ± 0.01 | 0.37 ± 0.01 | 0.23 ± 0.01 |
| $K_{0.5}$ (mM) | 0.14 ± 0.08 | 0.14 ± 0.11 | 0.19 ± 0.17 |
| $n_H$ | 2.06 ± 0.14 | 2.45 ± 0.22 | 2.63 ± 0.34 |
| **MVP** | | **[NaCl] (mM)** | |
| **Parameter** | **0** | **50** | **100** |
| $V_m$ (U/mg prot.) | 0.41 ± 0.04 | 0.35 ± 0.04 | 0.33 ± 0.01 |
| $K_{0.5}$ (mM) | 0.27 ± 0.27 | 0.20 ± 0.27 | 0.30 ± 0.25 |
| $n_H$ | 3.74 ± 0.60 | 4.27 ± 1.50 | 3.46 ± 0.3 |
| **(B)** | | | |
| **AVP1** | | **[NaCl] (mM)** | |
| **Parameter** | **0** | **50** | **100** |
| $V_m$ (U/mg prot.) | 0.51 ± 0.01 | 0.40 ± 0.01 | 0.24 ± 0.05 |
| L | 17 ± 5 | 50 ± 3 | 106 ± 14 |
| $K_R$ (µM) | 84 ± 9 | 64 ± 13 | 69 ± 30 |
| **MVP** | | **[NaCl] (mM)** | |
| **Parameter** | **0** | **50** | **100** |
| $V_m$ (U/mg prot.) | 0.46 ± 0.01 | 0.47 ± 0.09 | 0.34 ± 0.04 |
| L | 615 ± 45 | 123 ± 22 | 7 $10^3$ ± 790 |
| $K_R$ (µM) | 62 ± 8 | 90 ± 16 | 35 ± 11 |

shows that AVP1 and MVP are homodimers with one substrate binding site in each subunit (Li et al., 2016).

5. $Mg_2PPi$ may also act as an allosteric positive effector by displacing the R-T equilibrium to the R state. To account for this effect in the simplest possible way, L is divided by the factor $(1+S/K_R)^2$. This means that either $Mg_2PPi$ exerts its stabilising role by binding to the two existing catalytic sites (that is, there are no specific regulatory sites for $Mg_2PPi$), or it binds with the same affinity to regulatory and catalytic sites.

The final equation obtained was:

$$v/V_m = \frac{(S/K_R)\cdot(1+S/K_R)}{(1+S/K_R)^2 + [L/(1+S/K_R)^2]} \qquad \text{(Equation 1)}$$

Where S is the concentration of the substrate ($Mg_2PPi$), $K_R$ is the dissociation constant of the substrate toward the active R state, and L is the allosteric constant ([T]/[R]).

The experimental data were fitted with this equation (**Figure 4**), giving plots very similar to those obtained with the empirical Hill equation (data not shown).

The values of the parameters in Equation 1 calculated using RStudio illustrated the differences observed in the kinetic properties of AVP1 and MVP, thus, the allosteric constant L was one order of magnitude higher for MVP than for AVP1 (**Table 3**). This result is consistent with the higher values of the Hill parameter $n_H$ previously obtained (see above). The value of L for AVP1 increased with the concentration of NaCl, whereas the calculated dissociation constant $K_R$ did not change significantly (**Table 3B**). This suggests that NaCl displaces the allosteric equilibrium of AVP1 toward the inactive T state. By contrast, in the case of MVP, L decreases in the presence of 50 mM NaCl, while a concentration of 100 mM is necessary to increase its value one order of magnitude with respect to that obtained in the absence of salt (**Table 3B**).

In another set of experiments, PPase activities were assayed by fixing $MgCl_2$ concentrations in the assays (1 and 2.5 mM) and increasing PPi (up to 0.25 mM) in the presence of 0, 50, and 100 mM NaCl. The concentrations of PPi and $Mg^{2+}$ were chosen to ensure that a significant amount of free $Mg^{2+}$ (that is, not complexed by PPi) was always present in the assay. **Figure 5** shows that the kinetic behaviour of both AVP1 and MVP changed significantly in this situation with respect to the results shown in **Figure 4**. Fitting these data with the Hill equation produced good plots and the $V_m$ values were correctly predicted but the values of the rest of the parameters ($n_H$ and $K_{0.5}$) showed high values of standard errors and were not considered reliable (not shown).

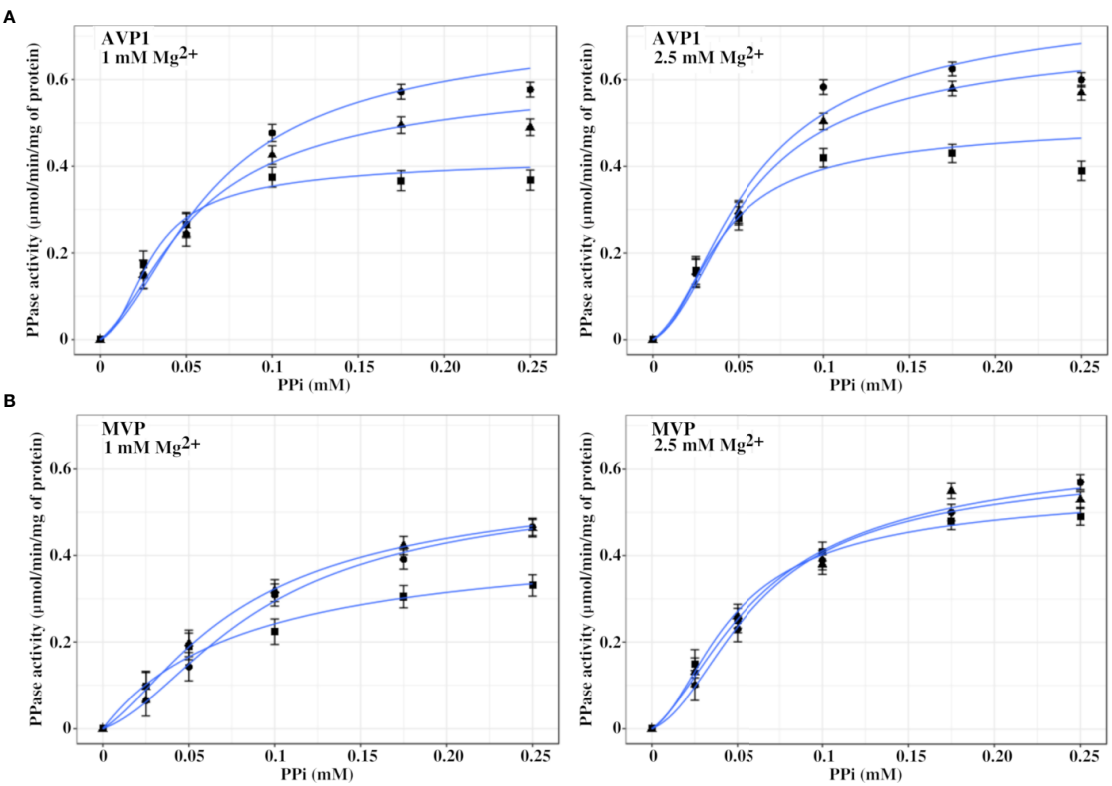


**FIGURE 5 |** Graphical representation of PPase activity versus PPi concentration for AVP1 **(A)** and MVP **(B)** in the presence of 0 mM (●), 50 mM (▲), and 100 mM (■) NaCl. $MgCl_2$ was fixed in the assays at the indicated concentrations. As in **Figure 4**, basal concentrations of $Na^+$ four times higher than those of PPi are present in the assays. Data points correspond to the averages ± SE of 3 independent experiments. Graph lines were calculated with Equation 1 using RStudio, as described in Materials and Methods.

Equation 1 predicted the kinetic behaviour of AVP1 and MVP in the presence of excess $Mg^{2+}$ and the values obtained for the different parameters are shown in **Table 4**. The values of the allosteric constant L significantly decreased with respect to those shown in **Table 3**, especially in the case of MVP; moreover, these values were not affected by the presence of increasing concentrations of NaCl, with the only exception of AVP1 when its PPase activity was assayed at 100 mM NaCl and 1 mM $MgCl_2$.

Kinetic data further show that $V_m$ values for AVP1 steadily decreased with NaCl concentration, especially in the presence of 1 mM $Mg^{2+}$, this effect being somewhat attenuated at 2.5 mM $Mg^{2+}$. PPi concentrations of 0.25 mM and higher exerted a significant inhibitory effect on AVP1 activity at the concentrations of $MgCl_2$ tested. Equation 1 could not model this effect, therefore, only data obtained with PPi concentrations up to 0.2 mM were used for curve fitting. Vm values for MVP only decreased significantly at 100 mM NaCl and 1 mM $Mg^{2+}$. Inhibition of MVP by PPi concentrations up to 0.5 mM was not observed (not shown).

An appropriate $[K^+]/[Na^+]$ ratio in the cytosol has been reported to be extremely important for cell viability in both yeast and higher plants and the presence of high external sodium concentrations may alter this ratio producing toxic effects (Gómez et al., 1996; Maathuis and Amtmann, 1999). PPase activity assays of AVP1 and MVP performed with optimal substrate concentration and decreasing $[K^+]/[Na^+]$ ratios showed that AVP1 is inhibited to a higher extent than MVP when the concentration of $Na^+$ is higher than that of $K^+$. As observed in previous experiments, the presence of excess $Mg^{2+}$ significantly protected AVP1 against inhibition by $Na^+$ (**Figure 6A**). Expectedly, the $H^+$-pumping activity of AVP1 decreased in parallel with the PPase activity (**Figure 6B**), whereas no $H^+$-translocation was detected with microsomes obtained from cells expressing MVP (not shown).

**TABLE 4** | Values of parameters obtained by fitting Equation 1 to kinetic data corresponding to AVP1 (A) and MVP (B) in the presence of fixed $Mg^{2+}$ concentrations.

| **(A)** | | | |
|---|---|---|---|
| **$[MgCl_2]$ = 1 mM** | | **[NaCl] (mM)** | |
| **Parameter** | **0** | **50** | **100** |
| **$V_m$ (U/mg prot.)** | 0.77 ± 0.11 | 0.64 ± 0.05 | 0.43 ± 0.05 |
| **L** | 4 ± 2 | 3 ± 1 | 13 ± 5 |
| **$K_R$ (μM)** | 56 ± 8 | 48 ± 2 | 20 ± 3 |
| **$[MgCl_2]$ = 2.5 mM** | | **[NaCl] (mM)** | |
| **Parameter** | **0** | **50** | **100** |
| **$V_m$ (U/mg prot.)** | 0.82 ± 0.09 | 0.73 ± 0.05 | 0.52 ± 0.04 |
| **L** | 5 ± 1 | 7 ± 2 | 9 ± 3 |
| **$K_R$ (μM)** | 50 ± 3 | 42 ± 4 | 27 ± 4 |
| **(B)** | | | |
| **$[MgCl_2]$ = 1 mM** | | **[NaCl] (mM)** | |
| **Parameter** | **0** | **50** | **100** |
| $V_m$ (U/mg prot.) | 0.62 ± 0.05 | 0.62 ± 0.02 | 0.45 ± 0.07 |
| L | 4 ± 3 | 2 ± 1 | 0 ± 1 |
| $K_R$ (μM) | 83 ± 28 | 77 ± 6 | 88 ± 47 |
| **$[MgCl_2]$ = 2.5 mM** | | **[NaCl] (mM)** | |
| **Parameter** | **0** | **50** | **100** |
| $V_m$ (U/mg prot.) | 1.07 ± 0.45 | 0.69 ± 0.11 | 0.58 ± 0.03 |
| L | 0 ± 1 | 3 ± 1 | 5 ± 2 |
| $K_R$ (μM) | 200 ± 50 | 59 ± 38 | 40 ± 4 |

*Values of specific PPase hydrolytic activity obtained with PPi concentrations up to 0.175 mM (AVP1) and 0.25 mM (MVP) were used for curve fitting and calculation of parameters. Graphical representations of experimental data and lines calculated with Equation 1 are shown in **Figure 5**.*

## Intracellular PPi Levels

In order to check whether the sensitivities of AVP1 and MVP to NaCl *in vitro* could have an effect *in vivo*, YPC6 cells transformed with plasmids pInvGFPAVP1 and pInvGFPMVP were subjected

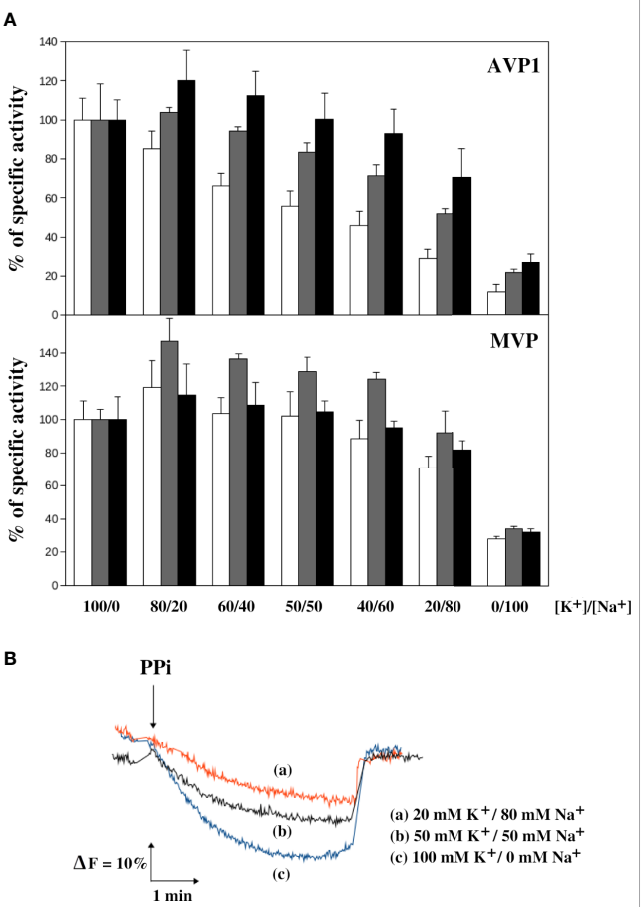


**FIGURE 6** | Sensitivity of the PPase activity of AVP1 and MVP **(A)** and the $H^+$-pumping activity of AVP1 **(B)** to the $[K^+]/[Na^+]$ ration in the presence of different concentrations of $Mg^{2+}$. PPase assays were performed with 0.25 mM PPi and 0.5 mM (white bars), 1 mM (gray bars), and 2.5 mM (black bars) $MgCl_2$. Activities are averages ± SE of 4 independent experiments and are expressed as percentages of PPase activity with respect to the average values obtained in the absence of NaCl (a tetrasodium salt of PPi was used, therefore, an extra 1 mM $Na^+$ was always present in the assays). These values, expressed as micromoles of PPi/min/mg of protein, were: 0.49 ± 0.05 (0.5 mM $Mg^{2+}$), 0.60 ± 0.11 (1 mM $Mg^{2+}$), 0.62 ± 0.06 (2.5 mM $Mg^{2+}$) for AVP1; and 0.49 ± 0.06 (0.5 mM $Mg^{2+}$), 0.50 ± 0.05 (1 mM $Mg^{2+}$), 0.60 ± 0.08 (2.5 mM $Mg^{2+}$) for MVP. $H^+$-pumping activity was assayed as described in Materials and Methods in the presence of 1 mM $MgCl_2$ at the indicated concentrations of NaCl.

to salt stress with 100 mM NaCl for several hours and cellular levels of PPi were determined. Yeast cells transformed with pInvGFPAVP1 showed significantly higher levels of PPi with respect to control cells expressing IPP1, this effect being milder in those cells transformed with pInvGFPMVP. PPi levels were virtually unchanged in YPC6 cells transformed with plasmid pIPP1 when they were subjected to salt stress (**Figure 7**).

## Addition of Extracellular Magnesium

*In vitro* kinetic studies suggested that magnesium cations can protect mPPases against inhibition by $Na^+$ (see above). In order to study a possible protective effect exerted by $Mg^{2+}$ *in vivo*, different concentrations of $MgCl_2$ were added to agar plates made with YPD at pH 6, and growth of YPC6 mutants transformed with plasmids pIPP1, pInvGFPAVP1, and pInvGFPMVP was checked in the presence of 100 mM NaCl. There was an improvement of growth in all cases when $MgCl_2$ concentration in the medium was raised up to 25 mM (**Supplementary Figure S2**). This suggests a general enhancement of yeast metabolism under salt stress regardless of the enzyme responsible for the removal of cytosolic PPi. This protective effect was not observed at 10 mM $MgCl_2$ (not shown).

# DISCUSSION

## Yeast Strains With Conditional Expression of IPP1 Allow Comparative Studies Between Different Heterologously-Expressed PPases

In a paper published in 1999, Gaxiola and co-workers reported that overexpression of AVP1, the major $H^+$-PPase from *A. thaliana*, alleviated the sensitivity of yeast toward NaCl. The authors proposed that AVP1 acted by enhancing $Na^+$ transport from the cytosol into the vacuole (Gaxiola et al., 1999). These experiments were carried out with a yeast mutant devoid of the P-type $Na^+$-ATPases located at the plasma membrane, encoded by the *ENA* genes. In *S. cerevisiae*, these genes are located in chromosome IV in tandem repeats with a variable number of copies (four in the case of strain W303-1A/B, used in that study). Disruption of *ENA* genes results in mutant cells (*ena1-4Δ*) with a higher sensitivity toward $Na^+$ than the parental strain (Quintero et al., 1996). This mutant strain was transformed with a plasmid bearing the coding sequence of AVP1 under the control of the *GAL1* promoter and the effect of salt on the transformants was studied. Several aspects of this experimental system are worth considering: first, a version of AVP1 with a point mutation that increased its capacity to pump protons (Zhen et al., 1997) was used. This was probably needed in order to observe phenotypes in yeast, due to the presence of a highly efficient cytosolic sPPase (IPP1) that competes with AVP1 for their common substrate, inorganic pyrophosphate (PPi). Second, the sensitivity to NaCl was checked on galactose because expression of AVP1 would be repressed by glucose, because of the *GAL1* promoter. The use of galactose for studies of $Na^+$ toxicity in *S. cerevisiae* must be taken with caution because osmotic adjustment through glycerol synthesis has been reported to be the limiting factor for growth on this carbon source under salt stress (Rios et al., 1997).

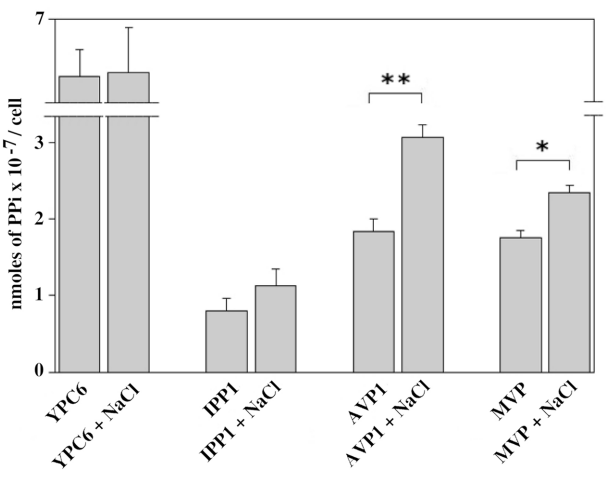


**FIGURE 7 |** Internal levels of PPi measured in YPC6 cells transformed with the indicated plasmids and grown in the presence of 100 mM NaCl. Experiments were performed as described in Materials and Methods. Values are averages ± SE corresponding to 5 independent experiments. Student's unpaired *t* tests were done by using webpage http://www.graphpad.com/quickcalcs/ttest1.cfm: (**) Extremely statistically significant difference (P = 0.0006). (*) Very statistically significant difference (P = 0.0026).

In this work, a different experimental approach has been followed. We have previously shown that the glucose-repressible *GAL1* promoter can be inserted immediately upstream the coding sequence of *IPP1* gene in the yeast haploid strain W303-1A. This manipulation generates a strain, YPC3, that is unable to grow on glucose due to the negligible levels of cytosolic sPPase (IPP1) in the presence of this carbon source. This demonstrates the essentiality of cytosolic PPi removal for cell viability (Drake et al., 2010; Serrano-Bueno et al., 2013). Here, the same strategy was applied to an *ena1-4Δ* mutant (G19) and a double *ena1-4Δ nha1Δ* mutant (B31) in order to generate strains YPC5 and YPC6, respectively. Mutant B31 lacks not only *ENA1-4*, but also *NHA1*, that encodes a $K^+(Na^+)/H^+$ antiporter located at the plasma membrane; expectedly, this strain exhibits a higher sensitivity to sodium than the *ena1-4Δ* mutant G19 (Bañuelos et al., 1998). The derived strains YPC5 and YPC6 maintained their sensitivities toward $Na^+$ but they could not grow on glucose due to the repression of *IPP1* transcription (**Figure 2**).

Transformation of YPC3, YPC5, and YPC6 with plasmids bearing genes coding for mPPases under the control of a constitutive promoter restored growth on glucose, as expected from previous reports (Pérez-Castiñeira et al., 2002; Drake et al., 2010; Pérez-Castiñeira et al., 2011; Hernández et al., 2015; Hernández et al., 2016). This experimental approach has several advantages: (a) it reproduces in yeast a situation similar to that of the plant cell, where most of the PPi generated in the cytosol is removed by AVP1 (Ferjani et al., 2011; Kriegel et al., 2015; Segami et al., 2018b); (b) the use of yeast strains that depend on the expression of fully functional mPPases for growth allows comparative studies on how salt stress may affect these

proteins *in vivo* in the same cellular environment; (c) the use of glucose, the preferred carbon source of yeast, ensures that the inhibitory effects exerted by NaCl on growth are mainly due to sodium toxicity rather than to osmotic stress (Rios et al., 1997).

## The PPase Activity of AVP1 Is More Sensitive to $Na^+$ Than That of MVP

Our results show that yeast cells expressing AVP1 always grew worse in the presence of NaCl than those expressing MVP or the yeast cytosolic sPPase (IPP1). Moreover, the fact that none of the mPPases tested was able to support growth on NaCl better than IPP1 hinted that the former were not able to reduce significantly the concentration of $Na^+$ in the cytosol. Moreover, the chimera TcGFPAVP1, that is predominantly located in internal yeast membranes and complements the vacuolar $H^+$-ATPase (Pérez-Castiñeira et al., 2011; Hernández et al., 2015; Hernández et al., 2016), supports growth under salt stress less efficiently than InvGFPAVP1, that preferentially locates at the plasma membrane (Drake et al., 2010). This suggests that, in our system, AVP1 is not increasing the proton gradient across the vacuole membrane, that would result in an enhancement of secondary $Na^+$ transport into this compartment. Altogether, these results indicate that the observed phenotypes depend on the PPase activities rather than on the ion pumping capacity of the mPPases.

Total intracellular concentrations of $Na^+$ and $K^+$ were measured, as previously reported (Gaxiola et al., 1999), showing that the $[K^+]/[Na^+]$ ratio significantly decreased when transformed YPC6 cells were grown in the presence of 100 mM NaCl regardless of the PPase (soluble or membrane-bound) they expressed. Moreover, analyses of $Na^+$ and $K^+$ concentrations in the cytosol, performed by selectively making the plasma membrane permeable (Ohsumi et al., 1988), yielded similar results (not shown). These results discarded a significant extrusion of $Na^+$ ions from the cytosol mediated either by AVP1 [coupled to $H^+/Na^+$ antiporters (Nass et al., 1997)] or by MVP (directly).

Other experiments aimed at establishing possible mechanisms of AVP1 inhibition by $Na^+$ *in vivo* were performed with negative results. These included studies of trypsin digestion patterns, to check for conformational changes produced by salt stress in AVP1, or immunoprecipitation, to look for possible interactions between AVP1 and proteins involved in stress response (data not shown). Finally, the direct effect of $Na^+$ on the two activities presented by AVP1 (PPi hydrolysis and proton pumping) was tested. The possible effects on the $Na^+$ sensitivity of AVP1 and MVP exerted by $Mg^{2+}$ was also studied, as previous evidence points out the importance of this divalent cation not only for the kinetic and catalytic properties but also for the structures of all types of PPases (Heikinheimo et al., 1996; Kellosalo et al., 2012; Lin et al., 2012; Tsai et al., 2014).

**Figure 4** shows that AVP1 is more sensitive to NaCl than MVP when the concentration of $Mg^{2+}$ exactly doubles that of PPi. AVP1 and MVP showed different degrees of cooperativity, the deviation of the latter from the Michaelian behaviour being more pronounced than that of AVP1. This was illustrated by the higher values of $n_H$ and the allosteric constant L obtained for MVP when the experimental data were fitted with the Hill equation and an expression derived from the concerted allosteric model, respectively. Moreover, the degree of cooperativity (and hence the value of L) of AVP1 increased with NaCl concentration, whereas, in the case of MVP, this effect was significant only at high concentrations of salt (100 mM). Therefore, according to our simplified allosteric model, $Na^+$ is displacing the equilibrium between the active R state and the inactive L state toward the latter, that is, it acts as a negative allosteric effector, mainly for AVP1.

The presence of free $Mg^{2+}$ significantly decreases the value of the predicted allosteric constant, which suggests that this cation stabilizes the active R state of both AVP1 and MVP. Addition of 100 mM NaCl in the assays under these conditions results in a more modest increase of L with respect to previous experiments, that were performed with no excess of $Mg^{2+}$.

In summary, a simplified version of the allosteric model supports the idea that mPPases have at least two conformational states with different catalytic activities, with $Mg^{2+}$ acting both as a co-substrate and as a positive allosteric effector; by contrast, $Na^+$ is a negative allosteric effector, especially for AVP1. These results are consistent with previous reports published by other groups for this type of proteins (Takeshige and Hager, 1988; Luo et al., 1999; Hsiao et al., 2004). Interestingly, exhaustive kinetic studies done with the $Na^+$-regulated $H^+$-PPase from the green sulphur bacteria *Chlorobium limicola* expressed in *E. coli* indicate the $Na^+$ can displace $Mg^{2+}$ from the enzyme, thereby arresting substrate conversion (Luoto et al., 2015).

## Limitations of the Kinetic Studies

Our results differ from those previously reported by Malinen et al. (2008), that thoroughly studied the kinetic behaviour of MVP and found that the dependence of the hydrolysis rate on substrate concentration obeyed the Michaelis-Menten equation. In this study, MVP was heterologously expressed in *E. coli*, that may imply significant changes in the protein (folding, interaction with biomembranes, and/or post-translational modifications, among others) with respect to our approach, based on the expression of chimeric versions of mPPases in yeast. Moreover, the use of different PPase activity assays (Rathbun and Betlach, 1969; Baykov and Avaeva, 1981) might also contribute to the differences observed by the two groups in the kinetic properties of MVP.

We are aware of the limitations of our experimental approach to study kinetic properties and that many more data, as well as a more elaborated model, are needed in order to establish with precision the mechanistic differences between AVP1 and MVP. In any case, our aim was not to perform exhaustive kinetic studies of AVP1 and MVP, but to compare the properties of both mPPases in the same cellular environment in order to find a correlation between the observed phenotypes and the enzymatic activities measured *in vitro*. The evidence presented here shows that the PPase activity of MVP is less sensitive to salt stress than AVP1 when both proteins are embedded in membranes of a eukaryotic organism such as yeast. This is further supported by the results shown in **Figure 6**, that indicate that low free $Mg^{2+}$

concentrations and $[K^+]/[Na^+]$ ratios significantly inhibit both the hydrolytic and the proton pumping activities of AVP1 at optimal PPi concentration. Moreover, intracellular PPi levels *in vivo* are significantly increased in yeast YPC6 cells expressing InvGFPAVP1 grown in the presence of 100 mM NaCl with respect to cells grown in culture medium without added salt. The increase was lower in cells expressing InvGFPMVP, which might explain why these cells are more resistant to salt stress, since PPi accumulation collapses anabolism (Lahti, 1983; Serrano-Bueno et al., 2013).

## A Possible Role of $Mg^{2+}$ in Salt Tolerance

Addition of external magnesium in the culture medium alleviated the sensitivity to NaCl in all the transformants obtained using the YPC6 mutant, even in cells expressing IPP1 (**Supplementary Figure S2**). This suggests that $Mg^{2+}$ exerts a general beneficial effect under conditions of salt stress, which is not surprising, as $Na^+$ has been reported to inhibit other enzymes, such as Hal2 nucleotidase and the RNase MRP, by displacement of $Mg^{2+}$ from its binding sites (Serrano et al., 1999).

Homeostasis of $Mg^{2+}$ in yeast is mechanistically complex and several transporters and internal reservoirs seem to be implicated (Klompmaker et al., 2017), moreover, this cation has been reported to influence the $K^+/Na^+$ exchange rate in this organism (Rodríguez-Navarro and Sancho, 1979). This evidence suggests that introducing $Mg^{2+}$ to study mechanisms of salt stress complicates the overall picture and deserves more experimental work. In any case, it might be interesting to study if the toxic effects exerted by $Na^+$ in yeast and other organisms might be linked to depletion of free $Mg^{2+}$ levels in the cytosol.

## Controversy About the Mechanisms by Which $H^+$-PPases Alleviate Salt Stress

The results presented here suggest that $Na^+$ can directly inhibit AVP1 *in vivo*, which can explain why an overexpression of this protein increases salt tolerance in plants. AVP1 inhibition would result in an accumulation of PPi, that might alter the reactions catalysed by the PPi-dependent phosphofructokinase and the UDP-glucose pyrophosphorylase, along with other anabolic reactions (Ferjani et al., 2018). Moreover, higher PPi concentrations could also decrease the concentration of free divalent cations such as $Mg^{2+}$ and $Ca^{2+}$ by chelation, thereby altering the activity of multiple proteins and cellular systems (Segami et al., 2018a).

There is a certain controversy about the mechanism by which overexpression of AVP1 and its ortologs increases tolerance to abiotic stresses in *A. thaliana* and other crops. It is often considered that $H^+$-PPase overexpression increases the pH gradient across the tonoplast thus promoting the removal of $Na^+$ from the cytosol *via* proton-coupled $Na^+$-$K^+$ transporters. This view was reinforced by a recent report showing that transient overexpression of the $H^+$-PPase in *Nicotiana benthamiana* leads to higher vacuolar proton currents and vacuolar acidification (Graus et al., 2018). This results in a drop in photosynthetic capacity, plasma membrane depolarization and eventual leaf necrosis under non-stressed conditions; paradoxically, salt rescued leaf cells from cell death. Moreover, in non-transformed plants, a rise in V-PPase but not of V-ATPase pump currents was detected in the presence of salt. These results indicate, on the one hand, that plants need to regulate the $H^+$-PPase pump activity very carefully and, on the other, that $H^+$-PPase proton pump function becomes increasingly important under salt stress (Graus et al., 2018). However, there are some points to be considered in this communication, thus, a 300% higher $H^+$-PPase proton pump activity with respect to control plants was obtained by transient overexpression. This is much higher than the values obtained by stable overexpression of $H^+$-PPases in other plants and definitely becomes detrimental under non-stressed conditions. The latter is probably due to the impairment of cellular pH homeostasis, therefore, salt-stress is likely to alleviate this phenotype by readjusting cellular pH *via* $H^+/Na^+$-$K^+$ antiporters. Another interesting result that appears in this article is that *N. benthamiana* plants overexpressing IPP1 showed no detrimental effects in the absence of salt but presented similar maximum photochemical quantum yields of photosystem II to those overexpressing $H^+$-PPases in the presence of 200 mM NaCl (Graus et al., 2018). This shows that very high expressions levels of $H^+$-PPases may not give any advantage to the plant compared with the overexpression of a soluble PPase, such as IPP1. In a way, this resembles the results presented here.

Several groups have reported that stable overexpression of $H^+$-PPases stimulates growth and increases tolerance to biotic and abiotic stresses of *A. thaliana* and many other plants, however, in these reports plants overexpressing other types of PPases were never used as controls (Gaxiola et al., 2001; Park et al., 2005; Gao et al., 2006; Li et al., 2008; Lv et al., 2008; Pasapula et al., 2011; Schilling et al., 2014; Yang et al., 2015; Lv et al., 2016; Ahire et al., 2018). This makes difficult to ascertain the degree of involvement of the two activities exhibited by $H^+$-PPases (PPi hydrolysis and $H^+$-pumping) in stress tolerance. On the other hand, it has been reported that salt tolerance in *A. thaliana* is positively correlated with the expression of *AVP1* and *AtNHX1*, the gene coding for a vacuolar $Na^+/H^+$ antiporter, in both roots and shoots. However, no measures of protein levels or enzymatic and ion transport activities were performed in this study, therefore, the physiological implications of these results were not established (Jha et al., 2010).

Our results are consistent with experiments performed in *A. thaliana* that suggest that the hydrolysis of cytosolic PPi, rather than vacuolar acidification, is the major function of AVP1 *in planta* (Ferjani et al., 2011; Kriegel et al., 2015; Segami et al., 2018b). In any case, the cytosolic concentration of PPi may have many implications for metabolism, especially in plant cells (Segami et al., 2018a). This must be taken into consideration when using PPases to develop plants with increased tolerance to different stresses.

## Phylogenetics Analysis

Based on molecular phylogenetic analysis and biochemical evidences, mPPases can be classified into three major classes: $K^+$-dependent $H^+$- and $Na^+$-PPases, and $K^+$-independent $H^+$-PPases (Serrano et al., 2007; Baykov et al., 2013). Phylogenetic analyses suggest that these ancestral ionic pumps are broadly distributed among prokaryotes (bacteria and archaea), protists, and the

photosynthetic lineage (algae and plants), being more widespread than previously thought (**Figure 8**). The mPPases studied in this work, AVP1, from a land plant, and MVP, from a salt-tolerant archaeon, are well characterized archetypical representatives of their respective mPPase classes and are evolutionarily rather distant (**Figure 8**), which would be consistent with their different sensitivities to sodium. Although the physiological significance of $Na^+$-PPases and their involvement in salt tolerance are still to be clarified, the higher tolerance of MVP to sodium inhibition reported in this work strongly support a role in such scenario. Since molecular phylogenetic studies carried out by our group (A. Serrano, in preparation) indicate that orthologs of these prokaryotic $Na^+$-PPases appear in several groups of marine salt-tolerant photosynthetic protists (e.g., Prasinophytes) (**Figure 8**), the generation of transmembrane $Na^+$-gradients at the expense of PPi could be a mechanism of energy transduction common to prokaryotic and eukaryotic microorganisms. The biochemical and functional validation of these eukaryotic $Na^+$-PPases, as well as their physiological significance and evolutionary origin, are currently under study by our group.

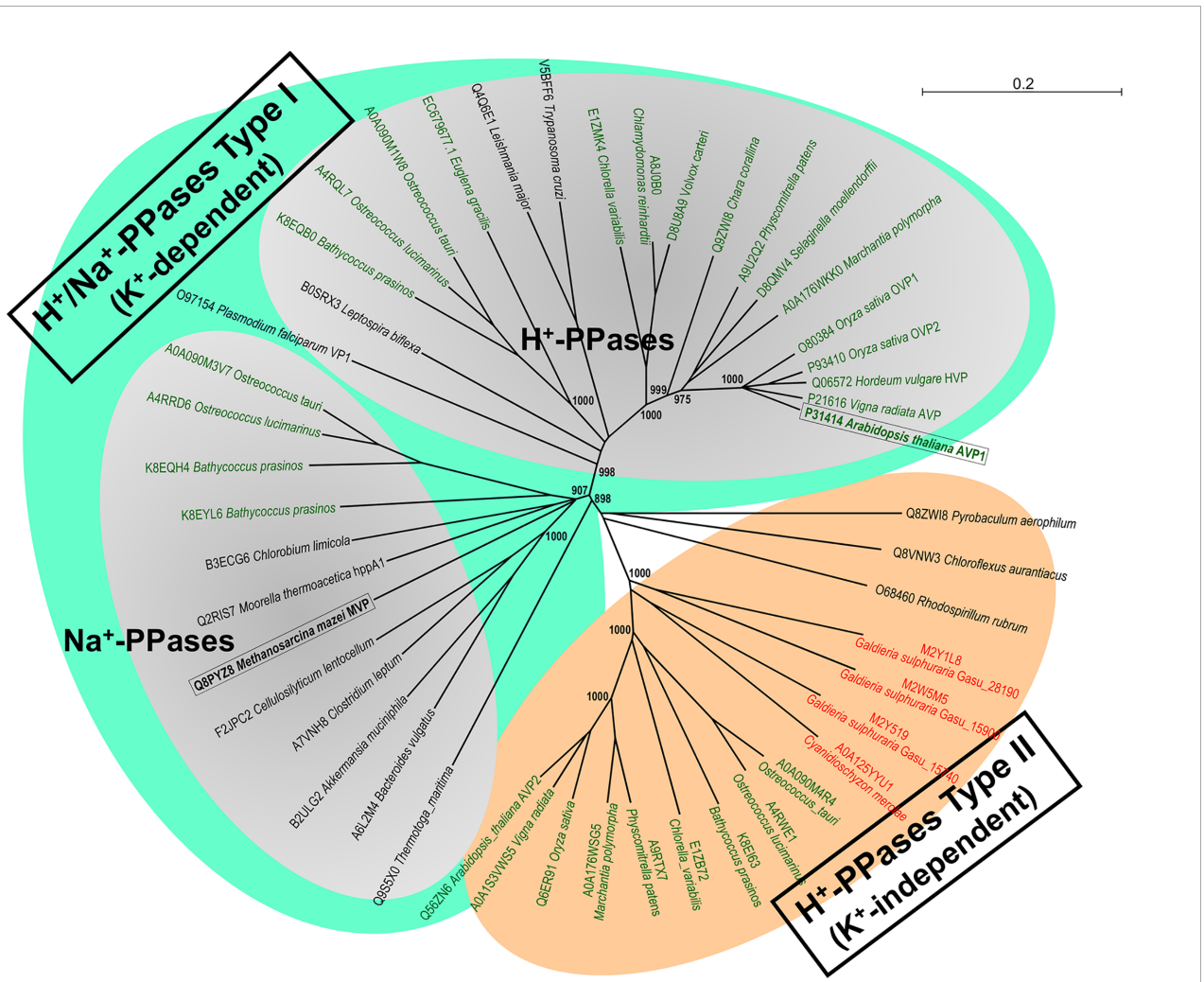


**FIGURE 8 |** Molecular phylogenetic analysis of the three major classes of mPPases, $K^+$-dependent $H^+$- and $Na^+$-PPases and $K^+$-independent $H^+$-PPases, broadly distributed among prokaryotes, protists and the photosynthetic lineage (algae and plants). A Neighbor-Joining phylogenetic tree obtained from a multiple sequence alignment of selected protein orthologs from prokaryotes, microalgae, parasitic protists and higher plants (generated by CLUSTAL X and Sea View v5.2 software packages) is shown. Note the well-defined and robust clusters of the three main classes of $H^+$- and $Na^+$-PPases, which are clearly divergent, and the probable $Na^+$-PPase orthologs of marine prasinophycean microalgae (*Ostreococcus* spp.; *Bathycoccus* spp.) that clearly cluster with *bona fide* $Na^+$-PPases of bacteria and archaea. A similar topology was obtained for a Maximum Likelihood tree (not shown). The two mPPases studied in this work are shown boxed in bold. Those of land plants and Chlorophyta microalgae are shown in green types and those of Rhodophyta microalgae in red types. Sequences are identified by their species names and UniProtKB accession numbers or genome/transcriptome sequencing projects numbers. The numbers in selected nodes are bootstrap values based on 1,000 replicates. Scale bar indicates number of changes per amino acid site.

## CONCLUSIONS

Our results not only point at $Na^+$-PPases as potential powerful biotechnological tools to obtain salt-resistant plants, but also suggest that altering the subcellular distribution of heterologously-expressed membrane-bound proteins, like mPPases, may also be crucial to obtain the desired phenotypes.

## DATA AVAILABILITY STATEMENT

All datasets generated for this study are included in the article/ **Supplementary Material**.

## AUTHOR CONTRIBUTIONS

Both authors jointly designed the experimental approach. JP-C performed laboratory work and wrote the first version of manuscript. AS performed in silico phylogenetic analyses and corrected and supervised the manuscript.

## FUNDING

Regional Andalusian Government (Junta de Andalucía) and Spanish Ministry of Science and Innovation for financial support to PAIDI group BIO-261 (grants P07-CVI-03082 and BFU2010-15622 to AS), partially funded by the EU-FEDER program (Fondo Europeo de Desarrollo Regional). PAIDI group BIO-261 belongs to the CeiA3 and AndaluciaTECH University Campuses of International Excellence.

## SUPPLEMENTARY MATERIAL

The Supplementary Material for this article can be found online at: https://www.frontiersin.org/articles/10.3389/fpls.2020.01240/full#supplementary-material

## REFERENCES

Ahire, M. L., Anil Kumar, S., Punita, D. L., Mundada, P. S., Kavi Kishor, P. B., and Nikam, T. D. (2018). The vacuolar proton pyrophosphatase gene (SbVPPase) from the Sorghum bicolor confers salt tolerance in transgenic Brahmi [Bacopa monnieri (L.) Pennell]. *Physiol. Mol. Biol. Plants Int. J. Funct. Plant Biol.* 24, 809–819. doi: 10.1007/s12298-018-0586-4

Baltscheffsky, M., and Baltscheffsky, H. (1995). Alternative photophosphorylation, inorganic pyrophosphate synthase and inorganic pyrophosphate. *Photosynth. Res.* 46, 87–91. doi: 10.1007/BF00020419

Baltscheffsky, M., Nadanaciva, S., and Schultz, A. (1998). A pyrophosphate synthase gene: molecular cloning and sequencing of the cDNA encoding the inorganic pyrophosphate synthase from Rhodospirillum rubrum. *Biochim. Biophys. Acta* 1364, 301–306. doi: 10.1016/S0005-2728(98)00062-0

Bañuelos, M. A., Sychrová, H., Bleykasten-Grosshans, C., Souciet, J. L., and Potier, S. (1998). The Nha1 antiporter of Saccharomyces cerevisiae mediates sodium and potassium efflux. *Microbiol. Read. Engl.* 144 (Pt 10), 2749–2758. doi: 10.1099/00221287-144-10-2749

Baykov, A. A., and Avaeva, S. M. (1981). A simple and sensitive apparatus for continuous monitoring of orthophosphate in the presence of acid-labile compounds. *Anal. Biochem.* 116, 1–4. doi: 10.1016/0003-2697(81)90313-4

Baykov, A. A., Bakuleva, N. P., and Rea, P. A. (1993). Steady-state kinetics of substrate hydrolysis by vacuolar $H^+$-pyrophosphatase: A simple three-state model. *Eur. J. Biochem.* 217, 755–762. doi: 10.1111/j.1432-1033.1993.tb18303.x

Baykov, A. A., Malinen, A. M., Luoto, H. H., and Lahti, R. (2013). Pyrophosphate-fueled Na+ and H+ transport in prokaryotes. *Microbiol. Mol. Biol. Rev. MMBR* 77, 267–276. doi: 10.1128/MMBR.00003-13

Drake, R., Serrano, A., and Pérez-Castiñeira, J. R. (2010). N-terminal chimaeras with signal sequences enhance the functional expression and alter the subcellular localization of heterologous membrane-bound inorganic pyrophosphatases in yeast. *Biochem. J.* 426, 147–157. doi: 10.1042/BJ20091491

Drozdowicz, Y. M., Kissinger, J. C., and Rea, P. A. (2000). AVP2, a Sequence-Divergent, K+-Insensitive H+-Translocating Inorganic Pyrophosphatase from Arabidopsis. *Plant Physiol.* 123, 353–362. doi: 10.1104/pp.123.1.353

Ferjani, A., Segami, S., Horiguchi, G., Muto, Y., Maeshima, M., and Tsukaya, H. (2011). Keep an eye on PPi: the vacuolar-type H+-pyrophosphatase regulates postgerminative development in Arabidopsis. *Plant Cell* 23, 2895–2908. doi: 10.1105/tpc.111.085415

Ferjani, A., Kawade, K., Asaoka, M., Oikawa, A., Okada, T., Mochizuki, A., et al. (2018). Pyrophosphate inhibits gluconeogenesis by restricting UDP-glucose formation in vivo. *Sci. Rep.* 8 (1), 14696. doi: 10.1038/s41598-018-32894-1

Gao, F., Gao, Q., Duan, X., Yue, G., Yang, A., and Zhang, J. (2006). Cloning of an $H^+$-PPase gene from *Thellungiella halophila* and its heterologous expression to improve tobacco salt tolerance. *J. Exp. Bot.* 57, 3259–3270. doi: 10.1093/jxb/erl090

Gaxiola, R. A., Rao, R., Sherman, A., Grisafi, P., Alper, S. L., and Fink, G. R. (1999). The Arabidopsis thaliana proton transporters, AtNhx1 and Avp1, can function in cation detoxification in yeast. *Proc. Natl. Acad. Sci. U. S. A.* 96, 1480–1485. doi: 10.1073/pnas.96.4.1480

Gaxiola, R. A., Li, J., Undurraga, S., Dang, L. M., Allen, G. J., Alper, S. L., et al. (2001). Drought- and salt-tolerant plants result from overexpression of the AVP1 H+-pump. *Proc. Natl. Acad. Sci. U. S. A.* 98, 11444–11449. doi: 10.1073/pnas.191389398

Gaxiola, R. A., Sanchez, C. A., Paez-Valencia, J., Ayre, B. G., and Elser, J. J. (2012). Genetic manipulation of a "vacuolar" H(+)-PPase: from salt tolerance to yield enhancement under phosphorus-deficient soils. *Plant Physiol.* 159, 3–11. doi: 10.1104/pp.112.195701

Gómez, M. J., Luyten, K., and Ramos, J. (1996). The capacity to transport potassium influences sodium tolerance in Saccharomyces cerevisiae. *FEMS Microbiol. Lett.* 135, 157–160. doi: 10.1111/j.1574-6968.1996.tb07982.x

Gordon-Weeks, R., Steele, S. H., and Leigh, R. A. (1996). The Role of Magnesium, Pyrophosphate, and Their Complexes as Substrates and Activators of the Vacuolar H+-Pumping Inorganic Pyrophosphatase (Studies Using Ligand Protection from Covalent Inhibitors). *Plant Physiol.* 111, 195–202. doi: 10.1104/pp.111.1.195

Gouy, M., Guindon, S., and Gascuel, O. (2010). SeaView version 4: A multiplatform graphical user interface for sequence alignment and phylogenetic tree building. *Mol. Biol. Evol.* 27, 221–224. doi: 10.1093/molbev/msp259

Graus, D., Konrad, K. R., Bemm, F., Patir Nebioglu, M. G., Lorey, C., Duscha, K., et al. (2018). High V-PPase activity is beneficial under high salt loads, but detrimental without salinity. *New Phytol.* 219, 1421–1432. doi: 10.1111/nph.15280

Heikinheimo, P., Lehtonen, J., Baykov, A., Lahti, R., Cooperman, B. S., and Goldman, A. (1996). The structural basis for pyrophosphatase catalysis. *Struct. Lond. Engl.* 1993 4, 1491–1508. doi: 10.1016/S0969-2126(96)00155-4

Heinonen, J. K., Honkasalo, S. H., and Kukko, E. I. (1981). A method for the concentration and for the colorimetric determination of nanomoles of inorganic pyrophosphate. *Anal. Biochem.* 117, 293–300. doi: 10.1016/0003-2697(81)90725-9

Hernández, A., Serrano-Bueno, G., Perez-Castiñeira, J. R., and Serrano, A. (2015). 8-Dehydrosterols induce membrane traffic and autophagy defects through V-

ATPase dysfunction in Saccharomyces cerevisae. *Biochim. Biophys. Acta BBA - Mol. Cell Res.* 1853, 2945–2956. doi: 10.1016/j.bbamcr.2015.09.001

Hernández, A., Herrera-Palau, R., Madroñal, J. M., Albi, T., López-Lluch, G., Perez-Castiñeira, J. R., et al. (2016). Vacuolar H(+)-Pyrophosphatase AVP1 is Involved in Amine Fungicide Tolerance in Arabidopsis thaliana and Provides Tridemorph Resistance in Yeast. *Front. Plant Sci.* 7, 85. doi: 10.3389/fpls.2016.00085

Hill, A. V. (1910). The possible effects of the aggregation of the molecules of hemoglobin on its dissociation curves. Proceedings of the Physiological Society, p. iv–vii. *J. Physiol.* 40, iv–vii. doi: 10.1113/jphysiol.1910.sp001386

Hsiao, Y. Y., Van, R. C., Hung, S. H., Lin, H. H., and Pan, R. L. (2004). Roles of histidine residues in plant vacuolar H(+)-pyrophosphatase. *Biochim. Biophys. Acta* 1608, 190–199. doi: 10.1016/j.bbabio.2004.01.001

Jha, D., Shirley, N., Tester, M., and Roy, S. J. (2010). Variation in salinity tolerance and shoot sodium accumulation in Arabidopsis ecotypes linked to differences in the natural expression levels of transporters involved in sodium transport. *Plant Cell Environ.* 33, 793–804. doi: 10.1111/j.1365-3040.2009.02105.x

Kellosalo, J., Kajander, T., Kogan, K., Pokharel, K., and Goldman, A. (2012). The structure and catalytic cycle of a sodium-pumping pyrophosphatase. *Science* 337, 473–476. doi: 10.1126/science.1222505

Kim, E. J., Zhen, R. G., and Rea, P. A. (1994). Heterologous expression of plant vacuolar pyrophosphatase in yeast demonstrates sufficiency of the substrate-binding subunit for proton transport. *Proc. Natl. Acad. Sci. U. S. A.* 91, 6128–6132. doi: 10.1073/pnas.91.13.6128

Klompmaker, S. H., Kohl, K., Fasel, N., and Mayer, A. (2017). Magnesium uptake by connecting fluid-phase endocytosis to an intracellular inorganic cation filter. *Nat. Commun.* 8, 1879. doi: 10.1038/s41467-017-01930-5

Kolakowski, L. F., Schloesser, M., and Cooperman, B. S. (1988). Cloning, molecular characterization and chromosome localization of the inorganic pyrophosphatase (PPA) gene from S. cerevisiae. *Nucleic Acids Res.* 16, 10441–10452. doi: 10.1093/nar/16.22.10441

Kriegel, A., Andrés, Z., Medzihradszky, A., Krüger, F., Scholl, S., Delang, S., et al. (2015). Job Sharing in the Endomembrane System: Vacuolar Acidification Requires the Combined Activity of V-ATPase and V-PPase. *Plant Cell* 27, 3383–3396. doi: 10.1105/tpc.15.00733

Lahti, R. (1983). Microbial inorganic pyrophosphatases. *Microbiol. Rev.* 47, 169–178. doi: 10.1128/MMBR.47.2.169-178.1983

Larkin, M. A., Blackshields, G., Brown, N. P., Chenna, R., McGettigan, P. A., McWilliam, H., et al. (2007). Clustal W and Clustal X version 2.0. *Bioinform. Oxf. Engl.* 23, 2947–2948. doi: 10.1093/bioinformatics/btm404

Leigh, R. A., Pope, A. J., Jennings, I. R., and Sanders, D. (1992). Kinetics of the Vacuolar H+-Pyrophosphatase : The Roles of Magnesium, Pyrophosphate, and their Complexes as Substrates, Activators, and Inhibitors. *Plant Physiol.* 100, 1698–1705. doi: 10.1104/pp.100.4.1698

Lenoir, G., Menguy, T., Corre, F., Montigny, C., Pedersen, P. A., Thinès, D., et al. (2002). Overproduction in yeast and rapid and efficient purification of the rabbit SERCA1a Ca(2+)-ATPase. *Biochim. Biophys. Acta* 1560, 67–83. doi: 10.1016/S0005-2736(01)00458-8

Li, B., Wei, A., Song, C., Li, N., and Zhang, J. (2008). Heterologous expression of the TsVP gene improves the drought resistance of maize. *Plant Biotechnol. J.* 6, 146–159. doi: 10.1111/j.1467-7652.2007.00301.x

Li, K.-M., Wilkinson, C., Kellosalo, J., Tsai, J.-Y., Kajander, T., Jeuken, L. J. C., et al. (2016). Membrane pyrophosphatases from Thermotoga maritima and Vigna radiata suggest a conserved coupling mechanism. *Nat. Commun.* 7, 13596. doi: 10.1038/ncomms13596

Lin, S.-M., Tsai, J.-Y., Hsiao, C.-D., Huang, Y.-T., Chiu, C.-L., Liu, M.-H., et al. (2012). Crystal structure of a membrane-embedded H+-translocating pyrophosphatase. *Nature* 484, 399–403. doi: 10.1038/nature10963

López-Marqués, R. L., Pérez-Castiñeira, J. R., Buch-Pedersen, M. J., Marco, S., Rigaud, J.-L., Palmgren, M. G., et al. (2005). Large-scale purification of the proton pumping pyrophosphatase from Thermotoga maritima: A "Hot-Solve" method for isolation of recombinant thermophilic membrane proteins. *Biochim. Biophys. Acta BBA - Biomembr.* 1716, 69–76. doi: 10.1016/j.bbamem.2005.08.004

Lundin, M., Baltscheffsky, H., and Ronne, H. (1991). Yeast PPA2 gene encodes a mitochondrial inorganic pyrophosphatase that is essential for mitochondrial function. *J. Biol. Chem.* 266, 12168–12172.

Luo, S., Marchesini, N., Moreno, S. N., and Docampo, R. (1999). A plant-like vacuolar H(+)-pyrophosphatase in Plasmodium falciparum. *FEBS Lett.* 460, 217–220. doi: 10.1016/S0014-5793(99)01353-8

Luoto, H. H., Belogurov, G. A., Baykov, A. A., Lahti, R., and Malinen, A. M. (2011). Na+-translocating membrane pyrophosphatases are widespread in the microbial world and evolutionarily precede H+-translocating pyrophosphatases. *J. Biol. Chem.* 286, 21633–21642. doi: 10.1074/jbc.M111.244483

Luoto, H. H., Nordbo, E., Malinen, A. M., Baykov, A. A., and Lahti, R. (2015). Evolutionarily divergent, Na+-regulated H+-transporting membrane-bound pyrophosphatases. *Biochem. J.* 467, 281–291. doi: 10.1042/BJ20141434

Lv, S., Zhang, K., Gao, Q., Lian, L., Song, Y., and Zhang, J. (2008). Overexpression of an H+-PPase gene from Thellungiella halophila in cotton enhances salt tolerance and improves growth and photosynthetic performance. *Plant Cell Physiol.* 49, 1150–1164. doi: 10.1093/pcp/pcn090

Lv, S., Jiang, P., Wang, D., and Li, Y. (2015). H+-pyrophosphatase from Salicornia europaea enhances tolerance to low phosphate under salinity in Arabidopsis. *Plant Signal. Behav.* 11 (1), e1128615. doi: 10.1080/15592324.2015.1128615

Maathuis, F. J. M., and Amtmann, A. (1999). K + Nutrition and Na + Toxicity: The Basis of Cellular K + /Na + Ratios. *Ann. Bot.* 84, 123–133. doi: 10.1006/anbo.1999.0912

Malinen, A. M., Belogurov, G. A., Baykov, A. A., and Lahti, R. (2007). Na +-pyrophosphatase: a novel primary sodium pump. *Biochemistry* 46, 8872–8878. doi: 10.1021/bi700564b

Malinen, A. M., Baykov, A. A., and Lahti, R. (2008). Mutual Effects of Cationic Ligands and Substrate on Activity of the $Na^+$-Transporting Pyrophosphatase of *Methanosarcina mazei* †. *Biochemistry* 47, 13447–13454. doi: 10.1021/bi801803b

Monod, J., Wyman, J., and Changeux, J. P. (1965). On the nature of allosteric transitions: A plausible model. *J. Mol. Biol.* 12, 88–118. doi: 10.1016/S0022-2836(65)80285-6

Nass, R., Cunningham, K. W., and Rao, R. (1997). Intracellular sequestration of sodium by a novel Na+/H+ exchanger in yeast is enhanced by mutations in the plasma membrane H+-ATPase. *Insights into Mech. Sodium Tolerance J. Biol. Chem.* 272, 26145–26152. doi: 10.1074/jbc.272.42.26145

Nieves-Cordones, M., Martínez, V., Benito, B., and Rubio, F. (2016). Comparison between Arabidopsis and Rice for Main Pathways of K+ and Na+ Uptake by Roots. *Front. Plant Sci.* 7, 992. doi: 10.3389/fpls.2016.00992

Ohsumi, Y., Kitamoto, K., and Anraku, Y. (1988). Changes induced in the permeability barrier of the yeast plasma membrane by cupric ion. *J. Bacteriol.* 170, 2676–2682. doi: 10.1128/JB.170.6.2676-2682.1988

Park, S., Li, J., Pittman, J. K., Berkowitz, G. A., Yang, H., Undurraga, S., et al. (2005). Up-regulation of a $H^+$-pyrophosphatase ($H^+$- PPase) as a strategy to engineer drought-resistant crop plants. *Proc. Natl. Acad. Sci. U.S.A.* 102, 18830–18835. doi: 10.1073/pnas.0509512102

Pasapula, V., Shen, G., Kuppu, S., Paez-Valencia, J., Mendoza, M., Hou, P., et al. (2011). Expression of an Arabidopsis vacuolar H+-pyrophosphatase gene (AVP1) in cotton improves drought- and salt tolerance and increases fibre yield in the field conditions. *Plant Biotechnol. J.* 9, 88–99. doi: 10.1111/j.1467-7652.2010.00535.x

Perez-Castiñeira, J. R., and Apps, D. K. (1990). Vacuolar H(+)-ATPase of adrenal secretory granules. Rapid partial purification and reconstitution into proteoliposomes. *Biochem. J.* 271, 127–131. doi: 10.1042/bj2710127

Pérez-Castiñeira, J. R., López-Marqués, R. L., Villalba, J. M., Losada, M., and Serrano, A. (2002). Functional complementation of yeast cytosolic pyrophosphatase by bacterial and plant H+-translocating pyrophosphatases. *Proc. Natl. Acad. Sci.* 99, 15914–15919. doi: 10.1073/pnas.242625399

Pérez-Castiñeira, J. R., Hernández, A., Drake, R., and Serrano, A. (2011). A plant proton-pumping inorganic pyrophosphatase functionally complements the vacuolar ATPase transport activity and confers bafilomycin resistance in yeast. *Biochem. J.* 437, 269–278. doi: 10.1042/BJ20110447

Pringle, J. R., Adams, A. E. M., Drubin, D. G., and Haarer, B. K. (1991). "[40] Immunofluorescence methods for yeast," in *Methods in Enzymology* (Academic Press), 565–602. doi: 10.1016/0076-6879(91)94043-C

Quintero, F. J., Garciadeblás, B., and Rodríguez-Navarro, A. (1996). The SAL1 gene of Arabidopsis, encoding an enzyme with 3'(2'),5'-bisphosphate nucleotidase and inositol polyphosphate 1-phosphatase activities, increases salt tolerance in yeast. *Plant Cell* 8, 529–537. doi: 10.1105/tpc.8.3.529

Rathbun, W. B., and Betlach, M. V. (1969). Estimation of enzymically produced orthophosphate in the presence of cysteine and adenosine triphosphate. *Anal. Biochem.* 28, 436–445. doi: 10.1016/0003-2697(69)90198-5

Rios, G., Ferrando, A., and Serrano, R. (1997). Mechanisms of salt tolerance conferred by overexpression of the HAL1 gene in Saccharomyces cerevisiae. *Yeast Chichester Engl.* 13, 515–528. doi: 10.1002/(SICI)1097-0061(199705)13:6<515::AID-YEA102>3.0.CO;2-X

Rodríguez-Navarro, A., and Sancho, E. D. (1979). Cation exchanges of yeast in the absence of magnesium. *Biochim. Biophys. Acta BBA - Biomembr.* 552, 322–330. doi: 10.1016/0005-2736(79)90286-4

Sarafian, V., Kim, Y., Poole, R. J., and Rea, P. A. (1992). Molecular cloning and sequence of cDNA encoding the pyrophosphate-energized vacuolar membrane proton pump of Arabidopsis thaliana. *Proc. Natl. Acad. Sci. U. S. A.* 89, 1775–1779. doi: 10.1073/pnas.89.5.1775

Schiestl, R. H., and Gietz, R. D. (1989). High efficiency transformation of intact yeast cells using single stranded nucleic acids as a carrier. *Curr. Genet.* 16, 339–346. doi: 10.1007/BF00340712

Schilling, R. K., Marschner, P., Shavrukov, Y., Berger, B., Tester, M., Roy, S. J., et al. (2014). Expression of the *Arabidopsis* vacuolar $H^+$-pyrophosphatase gene (AVP1) improves the shoot biomass of transgenic barley and increases grain yield in a saline field. *Plant Biotechnol. J.* 12, 378–386. doi: 10.1111/pbi.12145

Schultz, A., and Baltscheffsky, M. (2004). Inhibition studies on Rhodospirillum rubrum H(+)-pyrophosphatase expressed in Escherichia coli. *Biochim. Biophys. Acta* 1656, 156–165. doi: 10.1016/j.bbabio.2004.03.005

Segami, S., Asaoka, M., Kinoshita, S., Fukuda, M., Nakanishi, Y., and Maeshima, M. (2018a). Biochemical, structural and physiological characteristics of vacuolar H +-pyrophosphatase. *Plant Cell Physiol.* 59 (7), 1300–1308. doi: 10.1093/pcp/pcy054

Segami, S., Tomoyama, T., Sakamoto, S., Gunji, S., Fukuda, M., Kinoshita, S., et al. (2018b). Vacuolar $H^+$-Pyrophosphatase and Cytosolic Soluble Pyrophosphatases Cooperatively Regulate Pyrophosphate Levels in *Arabidopsis thaliana*. *Plant Cell* 30, 1040–1061. doi: 10.1105/tpc.17.00911

Serrano, R., and Villalba, J.-M. (1995). "Chapter 35 Expression and Localization of Plant Membrane Proteins in Saccharomyces," in *Methods in Cell Biology*. Eds. D. W. Galbraith, D. P. Bourque and H. J. Bohnert (Academic Press), 481–496. doi: 10.1016/S0091-679X(08)61052-3

Serrano, R., Mulet, J. M., Rios, G., Marquez, J. A., de Larrinoa, I. F., Leube, M. P., et al. (1999). A glimpse of the mechanisms of ion homeostasis during salt stress. *J. Exp. Bot.* 50, 1023–1036. doi: 10.1093/jxb/50.Special_Issue.1023

Serrano, A., Pérez-Castiñeira, J., Baltscheffsky, M., and Baltscheffsky, H. (2007). H+-PPases: yesterday, today and tomorrow. *IUBMB Life* 59, 76–83. doi: 10.1080/15216540701258132

Serrano-Bueno, G., Hernández, A., López-Lluch, G., Pérez-Castiñeira, J. R., Navas, P., and Serrano, A. (2013). Inorganic pyrophosphatase defects lead to cell cycle arrest and autophagic cell death through NAD+ depletion in fermenting yeast. *J. Biol. Chem.* 288, 13082–13092. doi: 10.1074/jbc.M112.439349

Takeshige, K., and Hager, A. (1988). Ion Effects on the H+-Translocating Adenosine Triphosphatase and Pyrophosphatase Associated with the Tonoplast of Chora corallina. *Plant Cell Physiol.* 29, 649–657. doi: 10.1093/oxfordjournals.pcp.a077542

Thomas, B. J., and Rothstein, R. (1989). Elevated recombination rates in transcriptionally active DNA. *Cell* 56, 619–630. doi: 10.1016/0092-8674(89)90584-9

Treco, D. A., and Lundblad, V. (2001). Preparation of Yeast Media. *Curr. Protoc. Mol. Biol.* 23, 13.1.1–13.1.7. doi: 10.1002/0471142727.mb1301s23

Tsai, J.-Y., Kellosalo, J., Sun, Y.-J., and Goldman, A. (2014). Proton/sodium pumping pyrophosphatases: the last of the primary ion pumps. *Curr. Opin. Struct. Biol.* 27, 38–47. doi: 10.1016/j.sbi.2014.03.007

Valverde, F., Losada, M., and Serrano, A. (1997). Functional complementation of an Escherichia coli gap mutant supports an amphibolic role for NAD(P)-dependent glyceraldehyde-3-phosphate dehydrogenase of Synechocystis sp. strain PCC 6803. *J. Bacteriol.* 179, 4513–4522. doi: 10.1128/jb.179.14.4513-4522.1997

Yang, Y., Tang, R. J., Li, B., Wang, H. H., Jin, Y. L., Jiang, C. M., et al. (2015). Overexpression of a *Populus trichocarpa* $H^+$- pyrophosphatase gene PtVP1.1 confers salt tolerance on transgenic poplar. *Tree Physiol.* 35, 663–677. doi: 10.1093/treephys/tpv027

Zhen, R. G., Kim, E. J., and Rea, P. A. (1997). Acidic residues necessary for pyrophosphate-energized pumping and inhibition of the vacuolar H +-pyrophosphatase by N,N'-dicyclohexylcarbodiimide. *J. Biol. Chem.* 272, 22340–22348. doi: 10.1074/jbc.272.35.22340

**Conflict of Interest:** The authors declare that the research was conducted in the absence of any commercial or financial relationships that could be construed as a potential conflict of interest.

# Advantages of publishing in Frontiers

**OPEN ACCESS**
Articles are free to read for greatest visibility and readership

**FAST PUBLICATION**
Around 90 days from submission to decision

**HIGH QUALITY PEER-REVIEW**
Rigorous, collaborative, and constructive peer-review

**TRANSPARENT PEER-REVIEW**
Editors and reviewers acknowledged by name on published articles

**Frontiers**
Avenue du Tribunal-Fédéral 34
1005 Lausanne | Switzerland

**Visit us:** www.frontiersin.org
**Contact us:** frontiersin.org/about/contact

**REPRODUCIBILITY OF RESEARCH**
Support open data and methods to enhance research reproducibility

**DIGITAL PUBLISHING**
Articles designed for optimal readership across devices

**FOLLOW US**
@frontiersin

**IMPACT METRICS**
Advanced article metrics track visibility across digital media

**EXTENSIVE PROMOTION**
Marketing and promotion of impactful research

**LOOP RESEARCH NETWORK**
Our network increases your article's readership